

Defining the transcriptional landscapes of human developing and aged tendons: insights into the signalling pathways and cellular contributions to regenerative tendon formation

Alina Kurjan

August 2024

Defining the transcriptional landscapes of human developing and aged tendons: insights into the signalling pathways and cellular contributions to regenerative tendon formation

Alina Kurjan

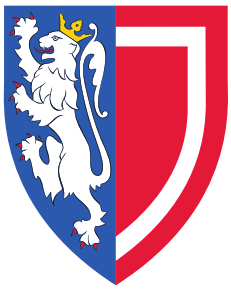
Supervisors: Associate Professor Sarah Snelling, Dr. Mathew Baldwin, Associate Professor Adam Cribbs, Professor Christopher Buckley

August 2024

A thesis submitted in fulfilment for the award of
Doctor of Philosophy in Molecular and Cellular Medicine

Nuffield Department of Orthopaedics, Rheumatology and Musculoskeletal Sciences

Balliol College, University of Oxford



Abstract

Tendon diseases present a significant global health challenge, affecting individuals of all ages and leading to substantial socioeconomic impacts, often necessitating surgical interventions with high failure rates. While tendons can regenerate without scarring during development, this ability diminishes with age, increasing susceptibility to injuries and impairing healing. Understanding the mechanisms underlying tendon regeneration and its decline is essential for developing treatments that enhance tendon repair. This thesis advances this understanding by identifying and describing the transcriptomes at the single-cell level in both regenerative, developing tendons and non-regenerative, aged tendons. Using single-nucleus and spatial RNA-sequencing techniques, it identifies 14 distinct cell types within foetal Achilles and quadriceps tendons, including diverse fibroblast populations essential for extracellular matrix (ECM) synthesis and organisation, support of attachment sites, and tissue remodelling. Analysis of tendon development from embryonic to foetal stages reveals 7 states of embryonic progenitors contributing to the formation of tendon main body fibroblasts, loose connective tissue fibroblasts, and chondrocytes, with lineage trajectories mapped into foetal stages. Comparative histological and transcriptomic analyses between developing and adult tendons highlight structural and molecular differences, including variations in cellular densities and compositions, morphologies, and ECM organisation. Notably, adult tendons exhibit a complex immune cell repertoire and distinct fibroblast populations focused on maintaining homeostasis. Furthermore, fibroblasts in ruptured aged tendons display a limited reactivation of developmental programs associated with repair. These findings provide insights into the cellular mechanisms underpinning tendon development, ageing, and repair, identifying key cell types and their functions. This work lays a foundation for future research aimed at validating these findings and translating them into clinical applications to enhance tendon repair and improve patient outcomes.

Acknowledgements

…Through thesis madness,
Coffee, hugs, and all you folks,
Crycat emoji…

This thesis wouldn't have been possible without the support and encouragement from so many individuals and organisations.

First, a huge thank you to my soon-to-be husband, Máté. Your immense patience, support, encouragement, and love have been my (sh)rock, and I would not dare to be here without you. Likewise, a massive thank you to my wonderful parents – your support and sacrifices made my dream of studying abroad a reality. None of this would have happened without your endless work, encouragement, and belief in me.

I also extend my heartfelt thanks to my fantastic supervisors, Sarah, Mat, Adam, and Chris. Your wisdom and guidance have been pivotal in shaping this research and helping me grow, and I appreciate all the support and kind words over those fantastic 4 years. You were amazing, and I am lucky to have been supervised by such a caring and knowledgeable team!

I am especially grateful to all my wonderful colleagues over the years for your friendship and support. Specifically, thank you the for the coffee breaks, putting up with my bluntness and terrible jokes, and making office life so enjoyable. Jolet, Cenk, Lorenzo, Mat, Chinemerem, Claudia – your extra efforts with experiments and analysis were lifesavers. Jolet, Cenk, Lorenzo – your constant availability, support, and sense of humour were my biggest support pillars throughout this experience. Working with you all was an absolute blast.

To my dearest friends, thank you for your understanding, encouragement, and the moments of joy and laughter that kept me sane. Brunett, our unforgettable moments in Oxford, especially the matriculation edamame incident, will never be forgotten. Kat, Chris, and Eleanor, your immense support and friendship made this journey so much easier and more enjoyable, and I will always be grateful for that.

And of course, a big thank you to the wonderful folks at the NDORMS for giving me this opportunity and to the funders – Archimedes Foundation, MRC DTP, Snell Scholarship, and CZI – for your financial support over the years.

Table of contents

ABSTRACT ..... **II**

ACKNOWLEDGEMENTS ..... **III**

TABLE OF CONTENTS ..... **IV**

LIST OF FIGURES ..... **VIII**

LIST OF TABLES ..... **XII**

CHAPTER 1: INTRODUCTION **1**

1.1 Tendon Biology and Pathology ***1***

1.2 Clinical Significance ***4***

1.3 Research Gaps and Thesis Structure ***5***

CHAPTER 2: LITERATURE REVIEW **7**

2.1 Introduction ***7***

2.2 Healthy Tendon Structure and Function ***7***

2.2.1 Attachment sites 10

2.2.2 Nutrient supply and innervation 15

2.2.3 Cellular composition 18

2.3 Tendon ECM Composition and Organisation ***26***

2.3.1 Collagens 26

2.3.2 Non-collagenous ECM 34

2.4 Tendon Development ***44***

2.4.1 Vertebrate limb development 44

2.4.2 Limb musculoskeletal tissue development 47

2.4.3 Stages of embryonic tendon morphogenesis 50

2.4.4 Embryonic tendon attachment 51

2.4.5 Tendon foetal and postnatal maturation 53

2.4.6 Foetal and postnatal maturation of the enthesis and the MTJ 58

2.4.7 Key developmental regulators 59

2.5 Tendon Injury Repair ***60***

2.5.1 Stages of tendon repair 60

2.5.2 Differences in repair of developing and aged tendons 63

2.5.3 Cellular contributions to scarless and scarred repair 65

2.5.4 Tissue niche contributions to scarless and scarred tendon repair 70

2.6 High-resolution Transcriptomics in the Study of Tendon Biology ***72***

2.7 Conclusions ***75***

CHAPTER 3: METHODS 77

3.1 Declaration 77

3.2 Ethics 77

3.2.1 Human developmental tissue samples 77

3.2.2 Human adult tissue samples 78

3.3 Human Tendon Tissue Acquisition and Processing 78

3.4 10X Chromium Single-Nucleus RNA-Sequencing 78

3.4.1 Nuclei isolation 78

3.4.2 Library preparation and sequencing 79

3.4.3 Data pre-processing, quality control, normalisation, and dimensionality reduction 79

3.5 10X Visium Spatial RNA-Sequencing 82

3.6 Data from Embryonic Whole Limbs 82

3.7 Data from Adult Tendons 83

3.8 Data and Code Availability 84

CHAPTER 4: TRANSCRIPTOMIC ANALYSIS OF HUMAN FOETAL ACHILLES AND QUADRICEPS TENDONS 85

4.1 Introduction 85

4.2 Methods 86

4.2.1 Challenges of analysing generated datasets 86

4.2.2 Single-nucleus RNA-sequencing data analysis 86

4.2.3 Spatial RNA-sequencing data analysis 94

4.3 Results 96

4.3.1 Single-nuclei resolution characterisation of foetal tendon cell types 96

4.3.2 Spatial transcriptomic analysis of gene expression patterns in human 20 pcw foetal Achilles and quadriceps tendons 107

4.3.3 Spatial mapping of foetal single-nuclei cell types 109

4.3.4 Matrisomal gene expression profiling of foetal tendon fibroblasts 121

4.3.5 Temporal dynamics of tendon cell type gene expression across foetal development 124

4.4 Discussion 133

4.4.1 Foetal tendon fibroblasts 134

4.4.2 Foetal tendon non-fibroblast cell populations 137

4.4.3 Limitations and significance 139

CHAPTER 5: EXPANSION OF TENDON DEVELOPMENT STUDY USING SINGLE-CELL AND SPATIAL RNA-SEQUENCING DATA FROM EMBRYONIC WHOLE LIMBS 142

5.1 Introduction 142

5.2 Methods ***143***
5.2.1 Embryonic Visium spatial RNA-seq data analysis and reference dataset preparation 143
5.2.2 Embryonic scRNA-seq data integration and batch correction 144
5.2.3 Visium spatial RNA-seq data-based random forest classifier training and tendon cell prediction in embryonic whole limb scRNA-seq data 145
5.2.4 Embryonic tendon cell annotation 147
5.2.5 RNA Velocity 149
5.2.6 Embryonic data trajectory and fate analysis with Harmony, Palantir, and CellRank 149
5.2.7 Embryonic scRNA-seq and foetal snRNA-seq data integration with scGen and trajectory inference with Moscot and CellRank 150
5.2.8 Single-cell regulatory network inference and clustering analysis 151

5.3 Results ***152***
5.3.1 A needle in a haystack: identifying tendon cells in embryonic limbs using multicell-resolution spatial transcriptomics 152
5.3.2 Characterisation of embryonic tendon cell types 155
5.3.3 Delineation of tendon cell differentiation trajectories and lineage-specific drivers in embryonic development 164
5.3.4 Probabilistic modelling of tendon cell fates in embryonic and foetal development 177

5.4 Discussion ***185***
5.4.1 Embryonic tendon cell types and developmental trajectories 185
5.4.2 Limitations and significance 190

CHAPTER 6: COMPARATIVE ANALYSIS OF DEVELOPING AND AGED HUMAN TENDONS 193

6.1 Introduction ***193***

6.2 Methods ***194***
6.2.1 Histology, Bonar scoring, image data quantification, and statistical analysis 194
6.2.2 Data integration with scVI-scANVI 195
6.2.3 Scanpy-based differential gene expression analysis 196
6.2.4 Cell type harmonisation with CellHint 196
6.2.5 DESeq2-based pseudobulk differential gene expression analysis 196
6.2.6 SCENIC analysis 197

6.3 Results ***198***
6.3.1 Histological examination of foetal and aged tendons 198
6.3.2 Comparison of developing and aged tendon cell types 207
6.3.3 Comparison of foetal and adult fibroblast transcriptomic profiles 217

6.4 Discussion ***234***

6.4.1 Developing and aged tendon tissue comparisons 235
6.4.2 Developing and aged tendon cellular compositions and fibroblast transcriptomic profiles..... 237
6.4.3 Limitations and significance 241

CHAPTER 7: DISCUSSION AND CONCLUSIONS 244
7.1 Introduction 244
7.2 Summary of Findings 245
7.2.1 Cellular heterogeneity and functional specialisation in foetal tendon development. 245
7.2.2 Differentiation pathways and lineage commitments in embryonic and foetal tendon development 247
7.2.3 Comparative analysis of structural and molecular changes in developing and aged tendons 249
7.3 Implications of the Findings and Directions for Future Research 253
7.3.1 Tendon development 253
7.3.2 Potential influence of non-fibroblast populations on repair outcomes in injured aged and developing tendons 255
7.3.3 Potential influence of fibroblast populations on repair outcomes in injured aged and developing tendons 256
7.4 Strengths and Limitations of the Study 259
7.5 Conclusion 260

APPENDIX: TABLES AND FIGURES 262

REFERENCES 317

List of figures

Figure 1. Schematic representations of tendon structural organisation. 10
Figure 2. Schematic representation of the myotendinous junction structure. 12
Figure 3. Schematic representation of the fibrocartilaginous enthesis structure. 14
Figure 4. Cellular morphologies and distributions within tendon structure. 18
Figure 5. Schematic diagram of fibril-forming collagens and heterotypic fibrils. 27
Figure 6. Transmission electron microscopy images of cross-sectional views of mouse flexor digitorum longus tendon collagen fibrils from wild-type and mutant mice at 30 days post-natal. 28
Figure 7. Schematic diagram of fibril-associated collagens containing interrupted triple helices (FACIT). 29
Figure 8. Schematic diagram of beaded filament- and network-forming collagens VI and IV. .. 31
Figure 9. Brightfield and polarized light microscopy images of picrosirius red-stained foetal patellar tendon. 34
Figure 10. Schematic of early embryonic limb bud development. 46
Figure 11. Timeline summary of mouse embryonic and early foetal musculoskeletal tissue development. 48
Figure 12. Schematic diagrams of tendon ECM development: collagen fibril and cellular morphology changes over time. 54
Figure 13. Schematic diagram and transmission electron micrographs of fibril expansion in murine postnatal tendon development. 56
Figure 14. Stages of adult tendon repair. 61
Figure 15. Comparison of adult and foetal tendon repair outcomes following injury. 64
Figure 16. UMAP projections of foetal tendon samples before (A) and after integration and batch correction using scVI (B). 88
Figure 17. Leiden clustering and between-cluster differential gene expression analysis of foetal tendon cell data. 90
Figure 18. UMAP plots of foetal tendon samples after label refining using scANVI. 92
Figure 19. Expression of early developmental tendon ECM markers in foetal tendon snRNA-seq data. 97
Figure 20. Expression patterns of general and type-specific fibroblast genes in foetal tendon snRNA-seq data. 99
Figure 21. Expression of endotenon and interfascicular matrix-associated genes in foetal tendon snRNA-seq data. 100
Figure 22. Expression of tendon attachment site-associated genes in foetal tendon snRNA-seq data. 102
Figure 23. Distribution of foetal snRNA-seq samples across Leiden clusters. 103
Figure 24. Expression of immune cell markers in foetal tendon snRNA-seq data. 104
Figure 25. Foetal tendon cell type annotation before and after scANVI label prediction. 106
Figure 26. H&E images of snap-frozen 10μm-thick Achilles and quadriceps tendon sections used for spatial RNA-sequencing. 108

Figure 27. Pearson correlation matrix of inferred foetal tendon single-nuclei RNA-sequencing cell type abundances per single 10X Visium sequencing spot. 110
Figure 28. Abundance of cell types within each manually annotated region of spatially-resolved 20 post-conception week human foetal quadriceps and Achilles tendons. 112
Figure 29. Cell2location mapping of Achilles and quadriceps tendon snRNA-seq cell type transcriptomic profiles from five 20 post-conception week samples. 113
Figure 30. Unsupervised non-negative matrix factorisation (NMF) analysis of Visium ST cell2location results for 5 factors across the three 20 post-conception week tendon spatial RNA-sequencing samples. 116
Figure 31. Unsupervised non-negative matrix factorisation (NMF) analysis of Visium ST cell2location results for 12 factors across the three 20 post-conception week tendon samples 118
Figure 32. Fibroblast type-specific gene expression of established early tendon cell markers in Visium spatial transcriptomics data of 20 post-conception week foetal quadriceps tendon. 120
Figure 33. Foetal 12-20 post-conception week tendon proteoglycan and collagen gene expression profiles. 122
Figure 34. Venn diagrams of intersecting gene ontology biological process (GO:BP) terms in tendon fibroblasts for each of the four clustered gene expression change patterns in 12 to 20 post-conception weeks of human foetal development. 125
Figure 35. tascCODA-estimated compositional changes in developing tendons from 12 to 20 post-conception weeks (pcw). 133
Figure 36. Tendon tissue demarcation in spatial RNA-seq data from a whole 8 post-conception week human embryonic hindlimb. 144
Figure 37. Comparison of random forest classifier and gene scoring methods for tendon cell identification within whole limb embryonic scRNA-seq data. 147
Figure 38. Embryonic tendon scRNA-seq Leiden clustering and marker gene analysis. 148
Figure 39. Expression of early tendon markers in human embryonic single-cell RNA-sequencing data from fore- and hindlimbs of 11 human embryonic donors. 153
Figure 40. Tendon cell marker expression in a whole 8 post-conception week embryonic human leg. 154
Figure 41. Expression of mesenchymal and tendon stem/progenitor cell markers in embryonic tendon cells. 156
Figure 42. Characterisation of gene expression profiles in human embryonic tendon cells from 6.5 to 9.3 post-conception weeks. 158
Figure 43. Human embryonic 6.5 to 9.3 post-conception week tendon collagen and proteoglycan gene expression profiles. 161
Figure 44. Differentially expressed genes in human 6.5-9.3 post-conception week (pcw) embryonic tendon cell types and comparison with foetal tendon cell signatures. 163
Figure 45. Visualisation of cell differentiation during embryonic tendon development using Harmony-enhanced force-directed layouts and multiscale diffusion maps. 165
Figure 46. RNA Velocity analysis of embryonic limb tendon cells. 167

Figure 47. Palantir pseudotime trajectory analysis of human 6.5-9.3 post-conception week embryonic tendon cells. 168
Figure 48. Analysis of differentiation branch probabilities across Palantir pseudotime. 170
Figure 49. MAGIC-imputed gene expression trends across Palantir pseudotime for the three major embryonic tendon cell lineages 173
Figure 50. CellRank fate mapping of embryonic tendon cell differentiation. 174
Figure 51. Gene expression correlation of CellRank lineage drivers. 175
Figure 52. CellRank directed partition-based graph abstraction (PAGA) map of embryonic tendon cell fate probabilities. 176
Figure 53. Force-directed layout of scGen-integrated embryonic single-cell RNA-seq and foetal single-nucleus RNA-seq datasets 178
Figure 54. Moscot-CellRank analysis of human embryonic and foetal tendon cell transitions. 180
Figure 55. Force-directed layout illustrating selected developmental tendon initial and terminal state cells used in CellRank-Moscot analysis. 181
Figure 56. CellRank cell fate probability distributions for embryonic and foetal tendon fibroblast lineages 182
Figure 57. SCENIC analysis of cell type-specific regulon activity. 184
Figure 58. Photomicrographs of foetal and adult Achilles, patellar, and quadriceps tendon tissues stained with haematoxylin and eosin. 200
Figure 59. Photomicrographs of foetal and adult tendon tissues stained with masson's trichrome, alcian blue, and picrosirius red. 202
Figure 60. Results of StarDist quantification of nuclear properties in haematoxylin-stained tissues 204
Figure 61. Examples of foetal and adult tendon sample tiles used for StarDist nuclei segmentation. 206
Figure 62. Original cell type annotations of scANVI-integrated embryonic, foetal, and adult tendon data. 208
Figure 63. Marker gene overlap between foetal and adult tendon cell types. 210
Figure 64. CellHint harmonisation of annotated cell types across different tendon datasets. . 212
Figure 65. Embryonic, foetal, and adult tendon fibroblast proteoglycan and collagen gene expression profiles. 216
Figure 66. Venn diagrams of intersecting upregulated or downregulated gene ontology biological process (GO:BP) pathways in CellHint-paired foetal and adult cell types. 218
Figure 67. Analysis of significantly up- and downregulated genes and pathways in adult ruptured COL3A1hi Fibroblasts vs foetal COL6A6 FNDC1 fibroblasts 222
Figure 68. Analysis of significantly up- and downregulated genes and pathways in adult ruptured COL3A1hi Fibroblasts vs foetal Chondrocytes 225
Figure 69. Analysis of significantly up- and downregulated genes and pathways in adult healthy FBLNhi Fibroblasts vs foetal ABI3BP GAS2 fibroblasts. 228
Figure 70. Analysis of significantly up- and downregulated genes and pathways in adult healthy ABCA10 fibroblasts vs foetal COL3A1 PI16 fibroblasts 231

Figure 71. Comparative analysis of shared SCENIC regulon activation patterns in specific fibroblast cell types across developing and adult datasets. 233
Figure 72. Timeline summary of identified embryonic, foetal, and adult tendon cell lineages. 253

Appendix Figure 1. Analysis of spatial RNA-seq data of human foetal 20 pcw Achilles and quadriceps tendons tendons. 281
Appendix Figure 2. Unsupervised non-negative matrix factorisation (NMF) analysis of Visium ST cell2location results for 12 and 5 factors across the three tendon samples. 285
Appendix Figure 3. Cell2location discrete mapping of quadriceps tendon scRNA-seq cell type transcriptomic profiles from five 20 pcw single-nuclei RNA-sequencing samples. 287
Appendix Figure 4. Fibroblast type-specific expression of fascicular and sheath TSPC markers. 288
Appendix Figure 5. Foetal 12-20 pcw tendon matrisomal gene expression profiles. 290
Appendix Figure 6. DESeq2 LRT and Wald differential gene expression analysis of transcriptomic changes in 12, 17, and 20 pcw human foetal Achilles and quadriceps tendon fibrillar and loose connective tissue fibroblasts. 293
Appendix Figure 7. Embryonic sample UMAPs before (left) and after (right) integration and batch correction with scVI. 299
Appendix Figure 8. Embryonic tendon cell type annotation. 300
Appendix Figure 9. Embryonic 6-9pcw tendon matrisomal gene expression profiles. 303
Appendix Figure 10. Selection of initial and terminal states using multiscale space embedding components for Palantir pseudotime calculation. 304
Appendix Figure 11. MAGIC-imputed gene expression trends across Palantir pseudotime for the three lineages identified in 6.5-9.3 pcw embryonic tendon cells. 307
Appendix Figure 12. Moscot sankey diagram plot showing developing tendon fibroblast lineage cell type transitions from 7.2 pcw to 20 pcw. 308
Appendix Figure 13. UMAPs showing embryonic, foetal and adult Achilles and quadriceps tendon data before (left) and after (right) integration with scANVI. 310
Appendix Figure 14. Embryonic, foetal, and adult tendon fibroblast matrisomal gene expression profiles. 315
Appendix Figure 15. Comparative analysis of shared SCENIC regulon activation patterns in specific fibroblast cell types across developing and adult datasets. 316

List of tables

Table 1. Comparative summary of tendon cell type annotations across different human and murine spatial, single-cell, and single-nucleus RNA sequencing studies. 22
Table 2. Summary of select murine studies on neonatal and adult tendon repair. 66
Table 3. Foetal sample cell and gene counts following individual quality control and filtering steps. 81
Table 4. Summary of significant shared and unique gene ontology biological process (GO:BP) functions for each tendon fibroblast type. 131
Table 5. Bonar scores of individual foetal and adult healthy control tendon tissues. 198

Appendix Table 1. Overview of tendon collagens. 262
Appendix Table 2. Overview of tendon non-collagenous ECM proteins. 268
Appendix Table 3. Sample metadata for single-cell (sc), single-nucleus (sn), and spatial RNA sequencing experiments. 278
Appendix Table 4. Summary of data collection, processing, and analysis contributions for Chapters 4–6. 280
Appendix Table 5. Data cell type counts by study. 311

Chapter 1: Introduction

1.1 Tendon Biology and Pathology

Tendons are fundamental connective tissues in the musculoskeletal system, serving as intermediaries between muscles and bones to facilitate movement and maintain joint stability. Found throughout the body, these complex viscoelastic and mechanoresponsive tissues are comprised of small yet heterogeneous populations of cells embedded within a densely packed, collagen-rich extracellular matrix (ECM) aligned parallel to the tissue's long axis. This specialised molecular structure and composition enable tendons to bear and transmit high tensile forces, store elastic energy, and absorb shocks during movement. Consequently, maintaining the structural and functional integrity of tendons is crucial for preserving musculoskeletal health and overall mobility.

Despite their robustness and resilience, tendons are susceptible to a range of injuries and degenerative conditions, collectively referred to as tendinopathies. These disorders are characterised by pain, swelling, and impaired function, which can significantly affect an individual's ability to perform daily activities and engage in physical exercise (Magnusson, Langberg and Kjaer, 2010; Malliaras *et al.*, 2013; Simpson, Rio and Cook, 2016). The prevalence of tendinopathies is considerable, affecting individuals across various age groups and lifestyles, from elite athletes to those with sedentary habits (reviewed in Millar *et al*., 2021). The most common tendinopathies are observed in the lower and upper extremities of the body, affecting the tibial, Achilles, patellar, and gluteal tendons in the legs (Albers *et al.*, 2016; Riel *et al.*, 2019), as well as the rotator cuff, and elbow flexor and extensor tendons in the hands (Luime *et al.*, 2004; Miranda *et al.*, 2005; Shiri *et al.*, 2007; Littlewood, May and Walters, 2013; Sanders *et al.*, 2015). The impact of these conditions extends beyond the physiological domain, imposing a significant socioeconomic burden due to healthcare costs, lost productivity, and long-term disability in severe cases (Walker-Bone *et al.*, 2012; Hopkins *et al.*, 2016; James *et al.*, 2018).

Tendinopathies pose a complex challenge in clinical management, primarily due to their aetiology involving both extrinsic and intrinsic factors. Extrinsically, mechanical overload, improper training techniques, medication side effects, and

environmental conditions play significant roles, while intrinsically, age, genetics, and underlying metabolic conditions contribute to their development (reviewed in Millar *et al*., 2021). Several models have been proposed for the pathogenesis of tendinopathy, encompassing both non-inflammatory and inflammatory mechanisms, with the latter typically suggested to be transient (Dakin *et al.*, 2015; Jomaa *et al.*, 2020).

In general, there is strong evidence that microtears resulting from mechanical overload or compression lead to changes in tendon structure, initiating a cycle of inadequate repair and consequent degeneration (Selvanetti, Cipolla and Puddu, 1997; Cook and Purdam, 2009; Guerquin *et al.*, 2013; Tang *et al.*, 2018; Chen *et al.*, 2024). Specifically, mechanical overload disrupts the homeostasis of tendon fibroblasts (generically referred to as “tenocytes”), causing their differentiation as well as altered collagen synthesis and matrix remodelling (Zhang and Wang, 2013; Nie *et al.*, 2021). Such overload also triggers tenocytes to release extracellular particles, promoting macrophage infiltration and cytokine release, thereby instigating inflammation (Chen *et al.*, 2024). The model proposed by Cook and Purdam (2009) suggests that initial responses to mechanical overload are potentially reversible adaptations if the load is removed. However, persistent or chronic overload perpetuates these adaptations, leading to failed healing responses and irreversible degeneration characterised by extensive ECM breakdown and cellular changes, including apoptosis and exhaustion. Additionally, prolonged inflammation may cause the growth of new, non-functional hyperpermeable blood vessels into the tendon that are theorised to further contribute to pain and degeneration (Pufe *et al.*, 2001, 2005; Alfredson, 2005; Järvinen, 2020). Of course, other causes such as age-driven degeneration and accumulation of advanced glycation end-products (AGEs), genetic predispositions, epigenetic modifications, and changes in biochemical environment or cellular behaviour, such as the accumulation of reactive oxygen species, also contribute to tendon pathology (Bestwick and Maffulli, 2000; Bailey, 2001; Kohler *et al.*, 2013; Delabastita, Bogaerts and Vanwanseele, 2019; Thankam *et al.*, 2019; Riasat *et al.*, 2020).

Tendinopathies therefore manifest through a spectrum of microstructural and cellular changes within the tendon tissue, including observable abnormalities such as variations in tendon thickness, changes in stiffness, altered cellularity,

scattered neovascularisation, and hypoechogenicity on imaging modalities (Åström and Rausing, 1995; Khan *et al.*, 1999; Maffulli, Barrass and Ewen, 2000; Maffulli, Sharma and Luscombe, 2004; Longo, Ronga and Maffulli, 2018; Millar *et al.*, 2021; Sharif, Ahmad and Shabbir, 2023). The latter is a consequence of deviation from the normal tendon architecture, attributable to factors like tears, disorganised collagen fibres (more diffuse, with coalesced bundles and reduced birefringence to polarized light), increased ground substance (non-collagenous ECM), and fluid accumulation.

Notably, the increase in ground substance varies across tendon types and within different microanatomical regions (Khan *et al.*, 1999). For example, proteoglycan or glycosaminoglycan accumulation, referred to as mucoid degeneration, is commonly found in different tendinopathies and appears histologically as large mucoid patches and vacuoles between fibres, causing collagen thinning, increased tendon softness and diminution of colour (e.g. from glistening white to grey or brown) (Khan *et al.*, 1999). In other cases, lipoid, hyaline, fibrinoid and hypoxic degeneration as well as calcification have also been observed (Khan *et al.*, 1999; Maffulli, Barrass and Ewen, 2000; Maffulli, Sharma and Luscombe, 2004).

At the cellular level, tendinopathic tendons exhibit regions of both hypercellularity, with cells showing round nuclei and increased metabolic activity focused on proteoglycan and protein production, and hypocellularity, with cells displaying pyknotic nuclei indicative of apoptosis or necrosis (Åström and Rausing, 1995; Järvinen *et al.*, 1997). The degree of these changes, assessable via histopathological methods, can be quantitatively evaluated using scoring systems like the Bonar or Movin scores, offering insights into the severity and progression of tendinopathy (Cook *et al.*, 2004; Maffulli *et al.*, 2008; Zabrzyńska *et al.*, 2021).

Interestingly, these structural and cellular changes can occur without symptomatic manifestation, a phenomenon known as asymptomatic tendinopathy. In such cases, significant degeneration can progress unnoticed, potentially leading to spontaneous tendon rupture (Kannus and Józsa, 1991). Asymptomatic tendinopathy has been frequently observed in both athletic and elderly populations, most commonly affecting tendons of the shoulders, knees,

feet, and ankles (Gaida *et al.*, 2010; Rio *et al.*, 2014; Noback *et al.*, 2018; Lieberthal *et al.*, 2019; Splittgerber and Ihm, 2019; Mills *et al.*, 2020). The underlying reasons for the absence of symptoms, potentially including higher pain thresholds (Rio *et al.*, 2018), remain incompletely understood, presenting an additional clinical challenge in the management and prevention of tendon injuries.

1.2 Clinical Significance

Due to the spectrum of aetiologies underpinning tendinopathy and tendon ruptures, the prognosis varies significantly, influenced by injury severity, specific tendon involvement, patient age and health, and the timing and suitability of treatment. Treatment modalities range from conservative approaches – physical therapy, pharmacological intervention, and lifestyle modifications – to surgical repair (Park *et al.*, 2020; Myhrvold *et al.*, 2022). Some conservative treatments, such as eccentric loading exercises for lower limb tendinopathies, have demonstrated efficacy in reducing pain and improving tendon functionality (Theodorou, Komnos and Hantes, 2023). However, conservative treatments often require prolonged periods to achieve noticeable improvements, and the outcomes can be inconsistent, not benefiting all patients uniformly. The persistent and recurring nature of tendinopathy makes it notoriously difficult to manage effectively. Surgical options, while available for refractory cases, carry risks of complications such as infection, adhesions, and re-rupture, all of which negatively impact patient outcomes.

Prognostic factors for poor outcomes for tendinopathy and surgical treatment include patient age, pain severity at onset, delay in treatment initiation, and comorbid conditions such as diabetes mellitus or obesity. Additionally, individuals in professions or sports demanding repetitive tendon use are at a heightened risk of compromised recovery. For instance, athletes are particularly susceptible to Achilles and patellar tendinopathies. The latter, also called “jumper’s knee”, exhibits a variable reported prevalence of 11-45% and necessitates surgical intervention in about 10% of cases due to conservative treatment failure, with complication rates ranging from 18-50% and a reoperation rate near 10% (Lian, Engebretsen and Bahr, 2005; Durcan *et al.*, 2014; Nutarelli *et al.*, 2023; Theodorou, Komnos and Hantes, 2023). Ultimately,

only a quarter of patients return to their pre-injury sports performance level (Panni, Tartarone and Maffulli, 2000; Maffulli, Giai Via and Oliva, 2017; Maffulli *et al.*, 2021; Cognetti *et al.*, 2023). Rotator cuff tendon tears also represent a significant challenge, especially in older adults, with prevalence reaching up to 80% in those over 80 years (Minagawa *et al.*, 2013; Meng *et al.*, 2023) and about 20% among athletes (McMahon, Prasad and Francis, 2014). Despite surgical intervention offering symptomatic relief, full functional restoration is rare, and re-ruptures occur in about 31–51% of cases (Park *et al.*, 2020; Myhrvold *et al.*, 2022; Meng *et al.*, 2023; Wang *et al.*, 2024). These examples highlight the necessity for effective tailored treatments and their timely application.

1.3 Research Gaps and Thesis Structure

Current therapeutic strategies for tendinopathies and tendon injuries are primarily palliative, focusing on symptom management rather than addressing the underlying cellular and molecular causes or promoting effective tissue regeneration. Despite advances in biologics and biomaterials, progress is hampered by incomplete understanding of the fundamental aspects of tendon biology, namely development and ageing. While the former is essential for uncovering how tendons are initially formed and how they can fully regenerate up until early post-natal stages, the latter is crucial for identifying how tendons change over time and become susceptible to degeneration and injury. Critical gaps persist, especially in cellular and molecular profiling of tendons, compounded by a marked deficiency in research analysing human tissues.

This thesis aims to address these research gaps by delineating the transcriptional landscapes of human embryonic, foetal, and aged tendons. First, the existing literature on the anatomy and physiology of healthy tendons, encompassing aspects of tendon development, repair mechanisms, and the implications of ageing and disease, is reviewed (Chapter 2). Then, following the outlining of methods used throughout the study (Chapter 3), key cell type transcriptomic profiles and spatial distributions are described using single-nucleus and spatial RNA sequencing of maturing foetal tendons (Chapter 4). The origins of those cells are then traced back to embryonic stages of development (Chapter 5), and, finally, a comparative analysis between the

histological and transcriptional profiles of aged and developing tendons is conducted, spotlighting critical disparities (Chapter 6). Through this investigation, I aspire to inform the discovery of novel therapeutic targets, development of biomaterials, and strategies for enhancing tendon repair and mitigating the progression of tendinopathies.

Chapter 2: Literature Review

2.1 Introduction

Tendons are critical connective tissues that transmit forces from muscle to bone, ensuring locomotion and joint stability. These structures exhibit remarkable adaptability across different life stages, enabling them to maintain function under varying physiological conditions. However, the regenerative capacity of tendons diminishes with age, predisposing them to a spectrum of tendinopathies that impair function and diminish quality of life. Despite the clinical significance of tendinopathies, our understanding of the transcriptional dynamics that govern tendon development, maturation, and aging remains incomplete.

This chapter aims to critically review the current literature on the detailed structure and cellular composition of healthy tendons, exploring their development from embryonic to postnatal stages as well as mechanisms of repair following injury. By synthesising insights from histological, cellular, and molecular studies, this review endeavours to highlight the knowns and unknowns within the field, facilitating better understanding and contextualisation of the research presented in this thesis.

2.2 Healthy Tendon Structure and Function

Within the human body, tendons assume a myriad of functional roles, often reflected in their distinct morphological features. This specialisation enables tendons to perform tasks ranging from stability and anchoring to the precise coordination of fine movements and the efficient transmission of force. For example, **energy-storing tendons** like the Achilles store energy when loaded and release it during recoil, thereby conserving energy and enhancing propulsion during locomotion (Benjamin *et al*., 2008; Thorpe *et al*., 2013). In contrast, **positional tendons**, such as those in the hands and feet, are designed for maintaining posture and stabilizing joints. They prioritise force transmission over energy storage, thus playing a crucial role in fine motor control (Benjamin, Kaiser and Milz, 2008).

These unique tendon functionalities are underpinned by their differing biomechanical properties arising from their molecular compositions, active signalling pathways, and ECM organisation. Compared with positional tendons, energy-storing tendons have higher water, sulphated glycosaminoglycan (GAG), and DNA content, and possess more tightly crosslinked collagen fibres and helical fascicles (Birch, 2007; Quigley *et al*., 2018; Thorpe *et al*., 2013). Those features specifically optimise them for heavy mechanical loads and recoil, making them able to endure higher tensile stresses and be more resilient to injuries and collagen denaturation (Kondratko-Mittnacht *et al.*, 2015; Choi *et al.*, 2018; Quigley *et al.*, 2018; Lin *et al.*, 2020). In contrast, positional tendons are more viscoelastic and possess cells with higher proliferation and collagen production capacity as well as more rapid collagen turnover (Goodman *et al.*, 2004; Thornton *et al.*, 2010; Choi *et al.*, 2018), enabling them to better absorb and dissipate forces over a range of velocities and facilitate repair processes.

Macroscopically, healthy tendons present as tough, fibrous cords with an opaque white appearance attributable to the dense concentration of collagen fibres that make up the bulk of their structure. Specifically, about 65-80% of the tendon's dry mass is composed of type I collagen, with the remainder comprising other collagens (e.g., types III, V, VI, XI, XII, XIV etc.), elastin, and different proteoglycans and glycoproteins such as decorin (DCN), biglycan (BGN), and fibromodulin (FMOD) (Kannus, 2000; Wu, Nerlich and Docheva, 2017).

The predominance of fibrillar collagens is a key factor in establishing the tendon's hierarchical organisation (Figure 1A). The triple-helical tropocollagen fibrils aggregate together in a head-to-tail and side-by-side quarter-staggered array to form **microfibrils**, which then coalesce into **fibrils** (Exposito *et al.*, 2010). These fibrils undergo further aggregation and crosslinking to form **fibres**, stabilising the fibril network and enhancing tensile strength. The crosslinked collagen fibres group into **fascicles** and become encased in the **endotenon**, also known as the **interfascicular matrix** (**IFM**) (Figure 1A). This thin connective tissue layer carries blood vessels and nerves, providing metabolic support through nutrient delivery and waste removal in addition to facilitating the sliding of fibre bundles (Benjamin *et al*., 2008; Fallon, 2002). The fascicles, collectively sheathed by the endotenon, are further enveloped by the **epitenon**,

which spans the length of the tendon to protect it, supply nutrients, maintain structural integrity, and minimise friction against surrounding tissues (Figure 1A). **Synovial sheaths**, comprising an inner synovial membrane that produces lubricating synovial fluid and an outer fibrous layer for structural support (Figure 1B-b), are specifically present in regions of tendons exposed to high friction, such as those in the hands and feet. Conversely, tendons less exposed to friction (e.g., Achilles tendons) are surrounded by a **paratenon** (Figure 1B-a), a looser connective tissue sheath that, while not producing synovial fluid, can facilitate movement and vascular supply (Benjamin *et al*., 2008; Wu *et al*., 2017). This complex hierarchical arrangement can be likened to muscle structure and ensures that the tendon can resist tensile forces while also mitigating potential consequences of fibril damage.

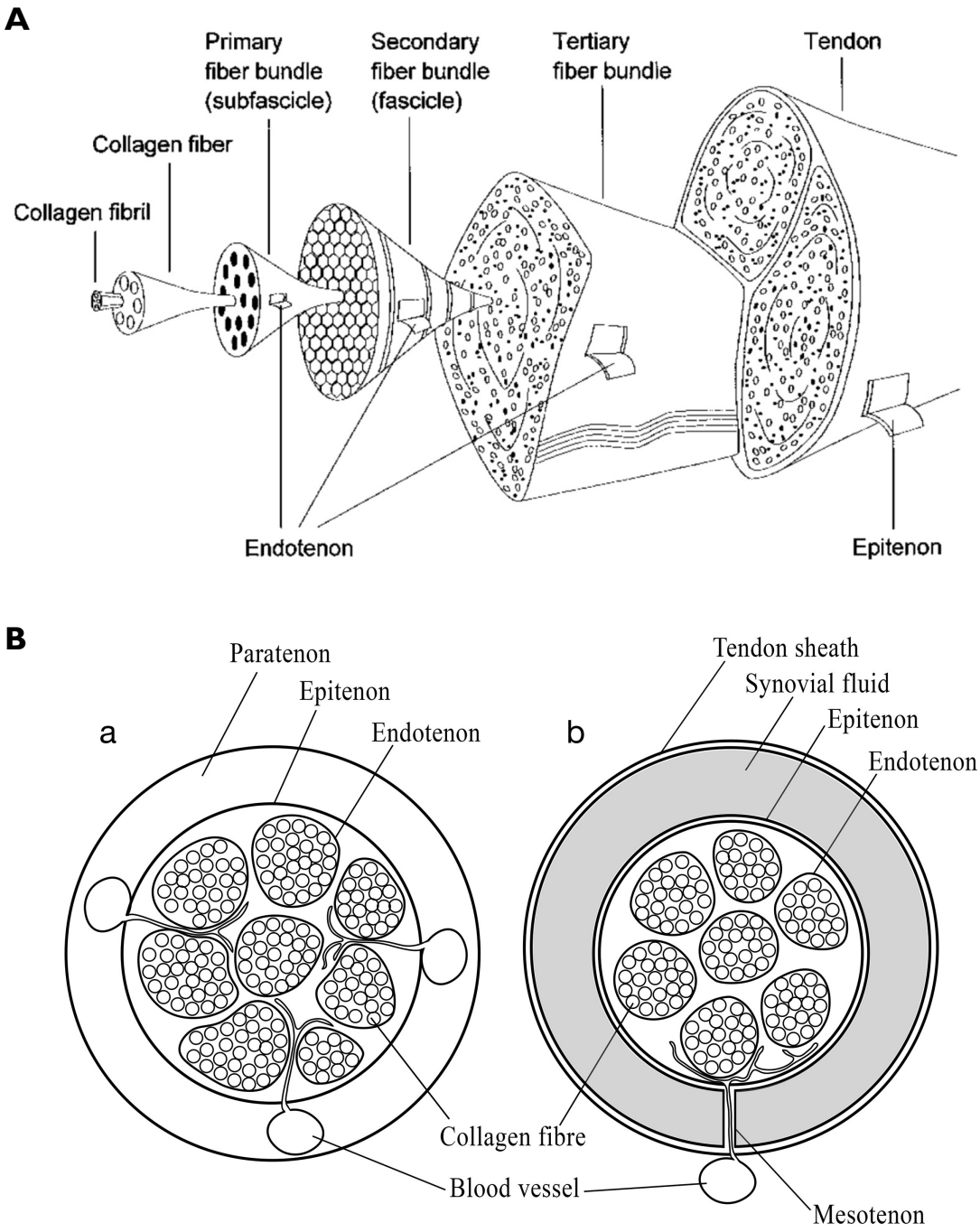


Figure 1. Schematic representations of tendon structural organisation. *(A) Longitudinal view, reproduced, with permission, from Kannus (2000). (B) Transverse view of a paratenon-covered (a) or synovial sheath-covered (b) tendon. Reproduced, with permission, from Lee (2021).*

2.2.1 Attachment sites

The architectural integrity and functional efficacy of tendons critically depend on their specialised attachment structures – the **myotendinous junction** (**MTJ**) at the muscle and the **enthesis** at the bone. Far from being just anatomical demarcations, these sites are complex, highly organised tissues that enable

effective force transfer and avoid stress concentration between mechanically and biochemically distinct tissue types. Their role in integrating muscle, tendon and bone tissues makes them particularly susceptible to injuries and ruptures: in humans, the MTJ frequently experiences strain injuries and tears, especially in athletes (Orchard and Seward, 2002; Jakobsen and Krogsgaard, 2021), while the enthesis is prone to larger ruptures, which present significant challenges in orthopaedic interventions like rotator cuff repair (Galatz *et al.*, 2004; Wang *et al.*, 2024). Understanding the complex architecture and composition of these attachment sites is essential for developing effective repair strategies and reducing injury risks.

2.2.1.1 Myotendinous junction

The myotendinous junction is a complex structure, commonly characterised by the presence of evaginations and invaginations of the muscle cell membrane, called sarcolemma, that resemble finger-like processes in longitudinal sections (Knudsen *et al.*, 2015). When viewed in 3D, this structure is more accurately described through “furrow-like indentations” in the muscle tissue and “ridge-like protrusions” within the tendon (Knudsen *et al.*, 2015). Collagen fibres at this junction are precisely oriented – multidirectionally adjacent to the muscle for force dissipation and longitudinally within the tendon to optimise force transmission (Knudsen *et al.*, 2015), thus mitigating stress at the junction (Tidball, 1984; Noonan and Garrett, 1992; Knudsen *et al.*, 2015). This interface is further enhanced by exercise-induced increases in sarcolemma protrusions into the tendon, a clear adaptation to distribute the additional load more effectively and minimise stress (reviewed in Jakobsen and Krogsgaard, 2021).

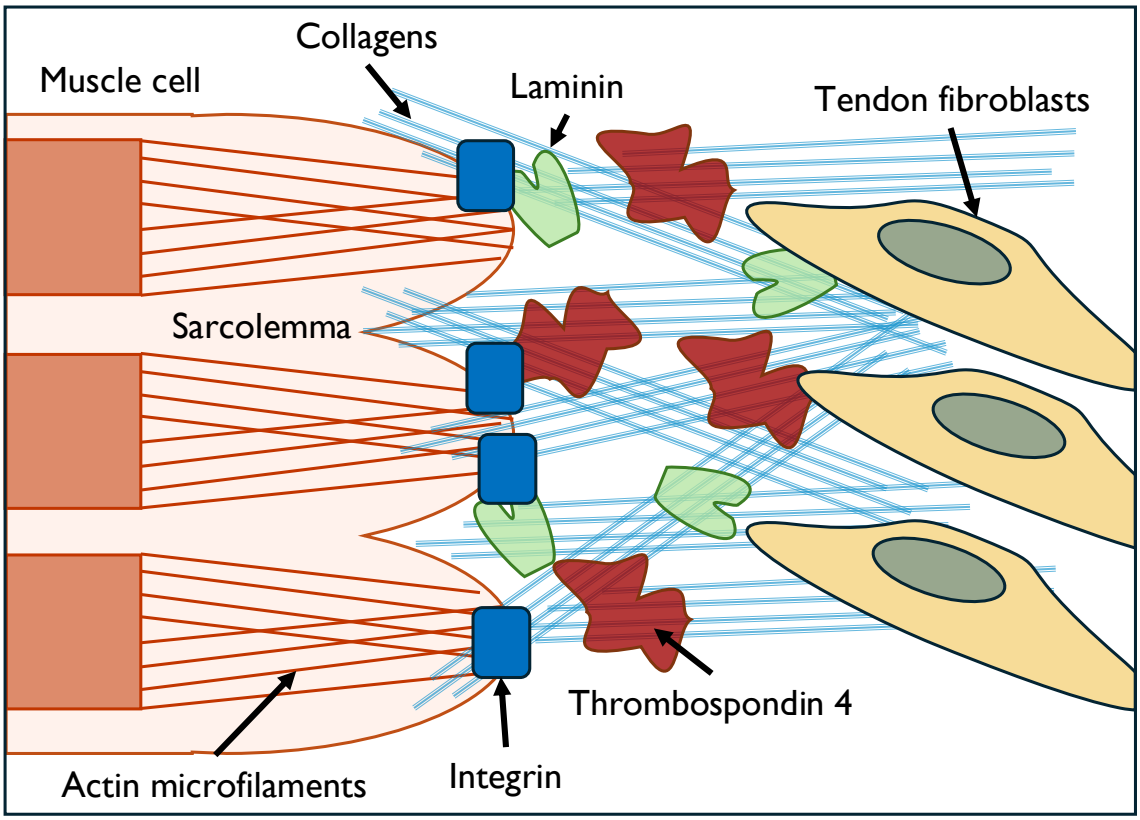


Figure 2. Schematic representation of the myotendinous junction structure. *The transmembrane integrins of muscle cells connect the actin cytoskeletal filaments to laminins and thrombospondins within the tendon extracellular matrix. Tendon fibroblasts also bind to these components, establishing a direct linkage between the tendon and muscle cells.*

At the molecular level, the MTJ is formed by transmembrane complexes within the sarcolemma (primarily involving various integrins) linking the muscle cell cytoskeleton to basement membrane components like laminins, which in turn connect to the tendon's collagen-rich matrix (reviewed in Charvet *et al.*, 2012; Tong *et al.*, 2024) (Figure 2). This junction is further stabilised and reinforced by an array of proteins including collagens and glycoproteins that connect myofibres or cellular components to the tendon ECM. Among these, the MTJ-specific collagen type XXII (COL22A1), a distinct fibril-associated collagen with interrupted triple helices (FACIT) produced by myocytes and located in the basement membrane, is crucial for preventing muscle fibre detachment during contractions (Koch *et al.*, 2004; Charvet *et al.*, 2013; Jakobsen *et al.*, 2021). Muscle cells also contribute other key molecules such as nestin (NES) and neural cell adhesion molecule-1 (NCAM1 or CD56). While NES acts as a structural scaffold, maintaining the integrity of the MTJ even in the absence of typical muscle proteins like desmin (DES) (Carlsson *et al.*, 1999), NCAM1

modulates cell adhesions and possibly signal transduction at the neuromuscular junction and the MTJ, promoting stability and coordination between muscular and tendinous tissues (Langhauser *et al.*, 2012). On the tendon side, glycoproteins and proteoglycans produced by tenocytes such as thrombospondin-4 (THBS4), BGN, and FMOD are crucial for correct ECM organisation and regulation of cell-ECM interactions (Can *et al.*, 2014; Frolova *et al.*, 2014; Subramanian and Schilling, 2014; Narayanan and Calve, 2021; Karlsen *et al.*, 2022). Additionally, a variety of proteins including tetraspanin-24 (CD151), kindlin-2 (FERMT2), cartilage intermediate layer protein (CILP), integrin-α10 (ITGA10), agrin (AGRN), vitrin (VIT), metalloproteinase inhibitor 3 (TIMP3), annexins-A3 and -A4 (ANXA3, ANXA4), plexin-A1 (PLXNA1), and syndecan-2 (SDC2) have been identified as abundant in the human MTJ (Karlsen *et al.*, 2022). These proteins are implicated in several functions, including force transmission, membrane folding, and the binding of ECM and cells.

2.2.1.2 Enthesis

The area of tendon attachment to bone is called the enthesis. It serves as another transitional zone bridging the soft, flexible tendon and the hard, mineralised bone, easing the stress and strain between these two structurally different tissues (Blitz *et al.*, 2009; Zelzer *et al.*, 2014; Killian, 2022). Entheses are broadly categorised into fibrous (e.g., periosteal, osseous) and fibrocartilaginous types based on their attachment type and the mechanical demands they withstand (Apostolakos *et al.*, 2014). **Fibrous entheses** are marked by the direct incorporation of dense fibrous tissue similar to tendon mid-substance from the tendon into the bone or periosteum (Apostolakos *et al.*, 2014). Typically occurring over large surface areas at sites where the angle of attachment does not significantly alter and the mechanical stress is comparatively low (e.g., deltoid muscle attachment to the humerus and adductor magnus to the linea aspera of the femur), these entheses are characterised by perforating collagen fibres called Sharpey's fibres (Aaron, 2012; Apostolakos *et al.*, 2014). In contrast, **fibrocartilaginous entheses**, which are subject to greater mechanical stress and frequent changes in the angle of attachment, attach to the epiphyses and apophyses of bones and have

a more complex structure characterised by a gradient of four histological zones: the aligned tendon, unmineralised fibrocartilage, mineralised fibrocartilage, and the underlying subchondral bone (Apostolakos *et al.*, 2014; Killian, 2022). There is a distinctive basophilic tidemark marking the interface between the unmineralised and mineralised fibrocartilage, which characterises a healthy enthesis but may appear disrupted in cases of enthesopathy. The latter is common, as fibrocartilaginous entheses are more numerous and prone to overuse injuries such as those of the rotator cuff and Achilles tendons (Apostolakos *et al.*, 2014; Killian, 2022).

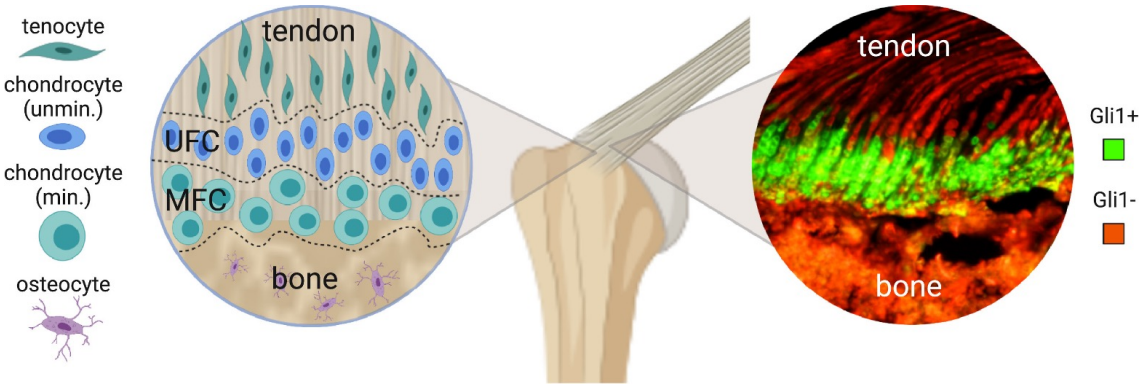


Figure 3. Schematic representation of the fibrocartilaginous enthesis structure. *This type of tendon-to-bone attachment site is characterised by spatial gradients in structure, composition, and cell phenotypes. The tendon region transitions into the unmineralised (unmin.) fibrocartilage (UFC) zone containing aggrecan- and collagen II-producing fibrochondrocytes. In turn, this zone transitions into the mineralised (min.) fibrocartilage (MFC), distinguished by its more differentiated chondrocytes that synthesise collagen types I and X. The final transition is into bone, predominantly composed of mineralised collagen type I. Additionally, the distribution of Gli1-lineage cells (Gli1+) and cells not derived from the Gli1 lineage (Gli-) is shown. Reproduced, with permission, from Fang, Sup, et al. (2022).*

Fibrocartilaginous entheses have significant variations along their length in viscoelastic properties, collagen structure, and cellular and ECM composition (Thomopoulos *et al.*, 2003; Apostolakos *et al.*, 2014) (Figure 3). The tendon end is comprised primarily of tenocytes in an ECM composed of highly aligned collagen types I and III, elastin, and proteoglycans, with tissue biomechanical properties similar to those of the tendon mid-substance. The unmineralised fibrocartilage zone is avascular, primarily occupied by specialised fibrochondrocytes that contribute collagen type II and aggrecan (ACAN) to the niche. The properties of this zone allow efficient stress dissipation and force

dampening. Transition to the hard, mineralised (calcified) fibrocartilage is indicated by the tidemark. Here, the ECM consists primarily of collagen type II, ACAN, and collagen types I and X, interlocking irregularly with the bone, thus providing mechanical integrity and strength (Apostolakos *et al.*, 2014; Schwartz, Long and Thomopoulos, 2015). Finally, the attached bone region contains collagen type I and osteocytes.

2.2.2 Nutrient supply and innervation

Vascular perfusion and the diffusion of synovial fluid are the principal mechanisms for nutrient delivery, though they vary in predominance based on the tendon's anatomical and functional characteristics. Mature tendons are hypovascular compared to other tissues, with some regions entirely devoid of vascular structures. Tendons receive vascular supply intrinsically from the MTJ and the enthesis, and extrinsically from the surrounding connective tissues including paratenon and synovial sheath (Ahmed *et al.*, 1998; Fenwick, Hazleman and Riley, 2002; Sharma and Maffulli, 2006). At the MTJ, perimyseal vessels from the muscle extend between tendon fascicles, typically not reaching beyond the proximal third of the tendon (Sharma and Maffulli, 2006). Conversely, at the enthesis, a sparse confined blood supply is obtained from vessels that anastomose with those of the periosteum (Fenwick, Hazleman and Riley, 2002; Sharma and Maffulli, 2006).

Vascular perfusion differs depending on the type of tendon and its surrounding connective tissues. It is particularly prominent in extrasynovial tendons, which are not encased in synovial sheaths and are typically subjected to higher mechanical loads (Fenwick, Hazleman and Riley, 2002; Shen *et al.*, 2021). These tendons feature more extensive vascular networks, where vessels entering the paratenon travel transversely and branch extensively, penetrating the epitenon and navigating within the endotenon septae, forming an intratendinous network rich in anastomoses (Sharma and Maffulli, 2006; Shen *et al.*, 2021). This extensive vascularisation enhances nutrient delivery, significantly influencing the outcomes of healing and repair processes (Shen *et al.*, 2021).

In contrast to extrasynovial tendons, intrasynovial tendons, such as the flexor tendons in the hands and feet, show a different vascularisation pattern, with blood vessels entering the tendon only at specific locations (Fenwick, Hazleman and Riley, 2002; Shen *et al.*, 2021). These vessels originate from the synovial sheath's outer lining and pass into the tendon through a specialised connective tissue called the mesotenon (Figure 1B-b). The mesotenon manifests as vinculae – cord-like structures in the fingers – or as broader sheet-like folds in areas such as the ankles. Upon entry through the mesotenon, these vessels branch out to form a vascular plexus on the tendon's surface. A subset of these vessels penetrates further into the epitenon and extends along the endotenon septae, creating a bridge between the external and internal blood supplies of the tendon (Sharma and Maffulli, 2006; Lee, 2021). Given their sparse points of entry, these vessels are relatively few, necessitating a reliance on the diffusion of nutrients from the synovial fluid – a process greatly augmented by mechanical loading (Manske *et al.*, 1978; Lundborg, Holm and Myrhage, 1980; Manske and Lesker, 1983). Active movement and exercise are essential as they promote synovial fluid circulation, enhancing nutrient distribution and waste removal within the tendon. In contrast, without the stimulus of movement (as seen in passive mobilisation), the fluid dynamics are impaired, which can slow injury recovery and potentially worsen degenerative changes (Lundborg, Holm and Myrhage, 1980).

Similarly to the vasculature, tendon innervation is sparse in both density and distribution. It consists of a network of sensory and autonomic nerve fibres originating primarily from nerve trunks from adjacent muscles, skin, and connective tissues enveloping the tendon (Ackermann, Salo and Hart, 2016; Sager *et al.*, 2019). These fibres are distributed throughout tendon structure, extending through endo-, epi- and paratenon without penetrating tendon fascicles under normal physiological conditions (Ackermann, 2015; Ackermann, Salo and Hart, 2016). The sensory nerve endings, including Ruffini and Vater-Pacini corpuscles as well as Golgi tendon organs, are primarily located at the MTJs and entheses, where they detect mechanical changes and tension (Jozsa *et al.*, 1996; Ackermann, Salo and Hart, 2016; Sager *et al.*, 2019). Additionally, other nerve endings act as nociceptors involved in pain perception, and some

are involved in controlling blood flow within the vascular system of the tendon (Rajpar and Tomlinson, 2022).

The low oxygen, sparsely cellular, and poorly vascularised and innervated nature of tendons contributes to their low metabolic turnover and suboptimal healing capacity, particularly in aged individuals. This condition leads to an inefficient and protracted repair process. Age-related changes in tendon vascularity and innervation (which vary by study methodology, tendon type, and individual age) typically manifest as reduced blood flow and vessel density, alongside a diminished capacity for vascular endothelial cell proliferation and differentiation in uninjured elderly tendons (Langberg *et al.*, 2001; Márquez-Arabia *et al.*, 2017; Riggin *et al.*, 2022). In contrast, tendinopathy and tendon injuries are characterised by hypervascularisation and nerve ingrowth into the tendon fascicles (reviewed in Ackermann *et al*., 2016; Tempfer and Traweger, 2015). Additionally, neovascularisation, primarily driven by vascular endothelial growth factor (VEGF), is a critical aspect of the tendinopathy response and pivotal in the early stages of healing. Under normal conditions, VEGF expression remains low in asymptomatic tendons; however, it significantly increases in response to chronic overuse, promoting neovascularisation in both early and late stages of tendinopathy (Vasta *et al.*, 2016; Riggin *et al.*, 2019, 2022).

2.2.3 Cellular composition

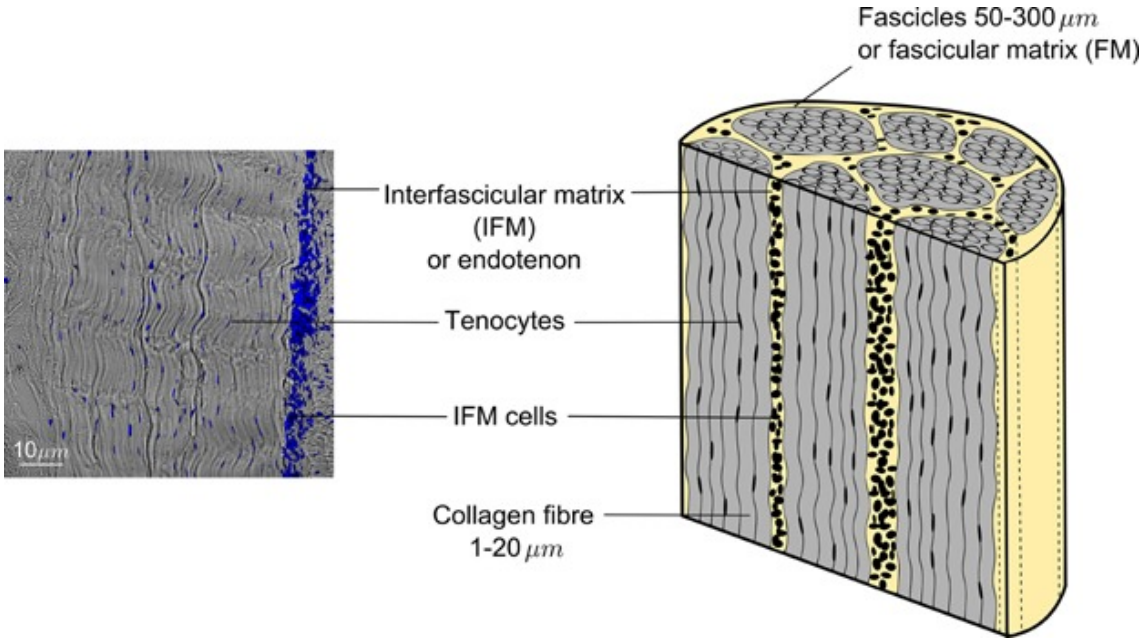


Figure 4. Cellular morphologies and distributions within tendon structure. *A histological section of a longitudinally cut bovine flexor tendon highlights differences in cell distribution and morphology between the fascicular and interfascicular (endotenon) regions. The accompanying schematic illustrates these distinct regions, providing both longitudinal and transverse views. Reproduced from Spiesz et al. (2015) (CC BY 4.0).*

Contrary to the earlier notions of tendons as homogenous structures populated solely by tenocytes, it is now acknowledged that tendon cell populations are varied and specialised, underscoring their complex biology. Despite the increasing recognition of this complexity, the precise identities and functions of these cell types remain incompletely defined. **Intrafascicular** cells embedded within the fascicular matrix of tendons orchestrate the assembly of a dense and organised ECM, depositing and sustaining collagens and other matrix components that are essential for tendon strength and function. These fibroblasts are commonly characterised by expression of markers such as *SCX*, *MKX*, *COL1A1*, and *TNMD*, and are identifiable by their elongated, spindle-like morphology (Figure 4). They align in rows along collagen fibres and form connexin-mediated gap junctions, which are critical for intercellular communication that governs tendon tissue homeostasis and facilitates repair mechanisms (McNeilly *et al.*, 1996; Kannus, 2000; Franchi *et al.*, 2007; Kalson *et al.*, 2015).

In contrast, the **interfascicular** matrix and connective tissues, including the epitenon, paratenon, and synovial sheaths, contain more varied and abundant

cell populations (Figure 4). Spatial and single-cell/nucleus RNA-sequencing studies of human and animal tendons have revealed the presence of diverse cell types, though not consistently across all research. These include fibroblasts with elevated expression of collagen type III (Steffen *et al.*, 2023), and, in certain studies, populations of *PTPRC*$^+$ (protein tyrosine phosphatase receptor type C, or CD45) immune cells, *PECAM1*$^+$ (platelet and endothelial cell adhesion molecule 1, or CD31) endothelial cells, *MCAM*$^+$ (melanoma cell adhesion molecule, or CD146) pericytes or mural cells, and cells expressing *ACTA2* (alpha smooth muscle actin, α-SMA) and *MYH11* (myosin heavy chain-11), indicative of smooth muscle (summarised in Table 1). Further, muscle cells, nervous system cells, adipocytes, and fibro-adipogenic progenitors (FAPs) were also reported in select studies (Table 1). This cellular diversity, documented across different tendons and conditions, underscores their highly complex and heterogeneous cellular environment.

Tendon attachment sites add yet another layer of complexity. During embryonic, foetal and postnatal development, MTJs and entheses harbour cells expressing markers characteristic of both tenogenic and myogenic or chondrogenic fates, respectively (Blitz *et al.*, 2013; Sugimoto *et al.*, 2013; Esteves de Lima *et al.*, 2021; Yaseen *et al.*, 2021). The persistence of these cell populations into adulthood remains uncertain, although single-cell analysis carried out by Yan *et al*. (2022) reported the presence of such cells in what was assumed to be MTJs from mature patients. Based on the developmental tendon literature, adult MTJs may contain cells from somitic *PAX3*$^+$ (*paired box 3*) and/or lateral plate mesoderm *SCX*$^+$/*OSR1*$^+$ (*odd-skipped related 1*) lineage *PAX7*$^+$*MYOG*$^+$ (*myogenin*) muscle cells, along with *SCX*$^+$ lineage tenocytes (Esteves de Lima *et al.*, 2021). Entheses, on the other hand, are known to harbour *SCX*$^+$ lineage tenocytes, *SOX9*$^+$ (*sex determining region Y-box 9*) lineage chondrocytes, and *GLI1*$^+$ (*GLI family zinc finger 1*) lineage fibrochondrocytes (Blitz *et al.*, 2009, 2013; Schwartz, Long and Thomopoulos, 2015; Felsenthal *et al.*, 2018; Eyal *et al.*, 2019). Recent single-cell analysis of murine early postnatal mineralising entheses identified populations of muscle and synoviocytes, immune cells (e.g., macrophages and B/T cells), and mesenchymal lineage cells such as clonogenic *Gli1*$^+$*Cd34*$^+$*Cd44*$^+$*Ly6a*$^+$ (*lymphocyte antigen 6 family member A*) enthesis progenitors, pre-enthesoblasts, *Scx*$^+$*Tnmd*$^+$*Sox9*$^+$*Acan*$^+$ enthesoblasts,

Sox9^{+}*Acan*$^{+}$*Runx2*$^{+}$ (*runt-related transcription factor 2*) mineralising chondrocytes, *Scx*$^{+}$*Tnmd*$^{+}$*Spp1*$^{+}$ (*osteopontin*) tenocytes, and *Bglap*$^{+}$ *(osteocalcin) Dmp1*$^{+}$ (*dentin matrix acidic phosphoprotein 1*) osteocytes (Fang, Xiao, *et al.*, 2022). Interestingly, IL-17 producing γδT-cells have been identified in mature entheseal tissues of ligaments (Cuthbert *et al.*, 2019), though their presence in tendon entheses remains to be confirmed.

In addition to these differentiated and specialised cells, multiple studies have identified MSC-like tendon stem/progenitor cells (TSPCs) in both developing and adult tendons. Initial findings by Bi and colleagues (2007) showed that a small subset of cells isolated from 8-12-year-old human tendons exhibited self-renewal, clonogenic, and multipotent characteristics. These cells expressed a range of markers typical of bone marrow stem cells, pericytes and tendon cells, including *STRO-1*, *MCAM* (*CD146*), *ENG* (*endoglin, or CD105*), *THY1 (Thy-1 cell surface antigen, or CD90)*, *CD44*, *SCX*, *TNMD*, *COMP (cartilage oligomeric matrix protein)*, and *TNC (tenascin-C)* (Bi *et al.*, 2007; Lui and Chan, 2011). Subsequent research corroborated the presence of these TSPCs in various tendon locations, including fascicles, the peritenon, and the enthesis (Tan, Lui and Lee, 2013), and highlighted that tendons from younger individuals contained more TSPCs with enhanced self-renewal capabilities (Kohler *et al.*, 2013; Ruzzini *et al.*, 2014). Yin *et al.* (2016) further refined the understanding of TSPCs by identifying the role of NES in the tenogenic capacity and reparative functions of TSPCs located specifically in the peritenon and endotenon of adult tendons.

Building on this foundational knowledge, more recent studies have identified what appear to be distinct, injury-responsive populations of tendon sheath progenitors that can differentiate into tenocytes, implicating these cells in tendon regeneration. Specifically, TPPP3 has previously been identified as a marker for murine embryonic tendon sheath cells (Staverosky *et al.*, 2009), and Harvey *et al*. (2019) showed that TPPP3-lineage cells expressing *PDGFRA* (and *CD34* but not *SCX*) were located in the paratenon layers of human adult patellar tendons. These cells migrated to the sites of injury, subsequently differentiating into tenocytes that integrated within the tendon's mid-substance and contributed to its repair. Additionally, Grinstein *et al.* (2022) and Walia *et al.* (2022) identified yet another population of sheath injury-responsive quiescent

progenitors expressing *AXIN2* distinct from the *TPPP3*-expressing cells. Collectively, these findings delineate at least three diverse TSPC populations within adult tendons, each with distinct roles in tendon maintenance and repair. The reader is referred to Huang *et al.* (2021) for a more comprehensive review of the different reported TSPCs and their niches.

While high-resolution transcriptomic analyses have advanced our understanding of the cellular composition of tendons, they have also highlighted substantial challenges in unifying this body of knowledge. Table 1 summarises tendon cell type annotations, the markers used, and populations assumed to be TSPCs across the different high-resolution studies. Despite some commonalities, particularly among established cell types like endothelial cells, it is evident that there is considerable biological and technical variation in the reported populations. The technical variation is, of course, attributable to the differences in tissue processing, cell dissociation, isolation, and sequencing protocols used by different groups. This is further complicated by studies sequencing only specific populations following fluorescence-activated cell sorting or cell culture, both of which are known to affect transcriptional programmes (Perucca Orfei *et al.*, 2021). However, the most pertinent challenge remains in the consensus surrounding the nomenclature and definition of markers for key tendon cells, especially fibroblasts. Each study (including the one in this thesis) presents unique fibroblast categorisations, usually differentiated by their marker expression profiles, with or without validation. Consequently, cross-study comparisons are limited unless raw data are accessed and accurately anchored. This situation underscores the necessity for a more collaborative approach towards the comprehensive atlas of both healthy and pathological tendons, a sentiment echoed by recent calls to action from the Human Cell Atlas (Baldwin *et al.*, 2021, 2023).

Table 1. Comparative summary of tendon cell type annotations across different human and murine spatial, single-cell, and single-nucleus RNA sequencing studies. *Columns show study descriptions, cell type annotations, their defining and reported markers, and any references to tendon stem/progenitor cells (TSPCs), with key markers for these cells summarised at the top of the table. ? – no markers reported.*

Fascicular TSPC markers:	STRO-1, CD105 (ENG), CD146 (MCAM), CD90 (THY1), CD44, NES, SCX, TNMD, COMP, TNC. (Bi *et al.*, 2007; Lui and Chan, 2011).
Loose connective tissue (IFM, epitenon, paratenon) TSPC markers:	TPPP3, PDGFRA, CD34. No SCX (Harvey, Flamenco and Fan, 2019); ACTA2, FMOD, TNC cells with capacity to turn on SCX (Dyment *et al.*, 2013); AXIN2 (Grinstein *et al.*, 2022; Walia *et al.*, 2022).

Study	Identified cells, markers used for their definition and other reported expressed genes	Tendon stem/progenitor cells?
Yin *et al*., 2016: C1 Fluidigm single-cell analysis of passage 1 cells from 71 human adult (Achilles?) tendon cells.	**Cluster I (endothelial/haematopoietic):** NES(high), CD146 (high), CD34(high), CD31(high), TNC(low), COL1(low), MKX(low). **Cluster II (nestin+ tspcs):** CD146 (medium), NES(medium), CD34(medium), CD31(medium), TNC(high), COL1(high), MKX(low), THBS4(low). **Cluster III (tenocytes):** SCX, COL14, ELN, NES(low), CD146(low), CD34(low), CD31(low), TNC(high), COL1(high), MKX(high), THBS4(high).	Authors liken cluster II to TSPCs based on its expression of nestin and tendon-associated genes. Nestin+ cells were shown to reside in endotenon/peritenon. CD34−CD18−CD44+CD90+CD105+ cells were split into NES+ and NES- TSPCs. NES+ had more CD146, CD105, CD90, CD51, CD44, CD29, higher self-renewal and tenogenic capacities. Based on additional experiments, authors conclude that NES is essential for TSPC tenogenic capacity, injury repair and self-renewal.
Harvey *et al*., 2019: single-cell analysis of mouse adult (3 months old) patellar tendons.	**Tenocytes:** Fmod, Tnmd, Thbs4. **Red Blood Cells:** ? **Osteoblasts:** ? **Endothelial Cells:** ?; Stained for PECAM1. **Macrophages & Antigen-Presenting Cells:** ?; Stained for F4/80. **Tendon fibro-adipogenic progenitors (T-FAPs):** Pdgfra, Ly6a. **Tppp3+ Sheath Cells:** Tppp3, Prg4.	Tppp3+Pdgfra+ subset of Tppp3+ patatenon sheath cells act as injury-responsive tendon stem cells capable of becoming tenocytes. Those cells are localised entirely within the sheaths, express CD34, and do not express Scx. They penetrate the injury site, migrating into the tendon fascicles, and giving rise to Tppp3-lineage tenocytes that remain in the tendon midsubstance. PDGFRa signalling is essential for this process, driving both tenogenesis and fibrosis.

De Micheli *et al*., 2020: single-cell analysis of mouse young adult (6-week-old) Achilles tendons.	**Tendon fibroblasts 1:** Col1a1, Mkx(high), Scx(high), Tnmd. Also express Sox9, Spp1, Tppp3, Pdgfra(middle), Cilp, Chad, Plod2, Clu, Fibin, S100a4 **Tendon fibroblasts 2:** Col1a1, Mkx(low), Scx(low), Tnmd. Also express CD34, Dpt, Pdgfra(high), Bicc1, Apod, Svep1, Smoc2, S100a4. **Junctional Fibroblasts:** Col22a1. Also express Pcsk6, Tspan15, Matn4, Chst2, Zfp385b, Pdgfra(high), Tppp3. **Pericytes:** CD146 (Mcam). Also express Acta2, Myh11, Tpm2, Pde3a, Lmod1, Tppp3, Tnmd. **Endothelial Cells:** CD31 (Pecam1) + absence of CD45 (Ptprc). **Red Blood Cells:** Hba-a1, Alas2 **Immune Cells:** Tppp3, CD45, CD206 (Mrc1), Ncf1, Lyz2, Plek, Pf4, S100a4. **Schwann nerve cells:** Plp1, Prx, Cnp, Ncmap. **Glial Nerve Cells:** Ncam1, Cadm1, Cdh2, Lgi4.	Point out the presence of small Tppp3+Pdgfra+ subsets that also express Col1a1, calling into question whether or not those represent the progenitor populations. Cells annotated as pericytes express the CD146 and Acta2 and are mostly negative for endothelial markers CD34 and CD31. Do not express any Scx or Mkx, but do express Tnmd and Tppp3.
Kendal *et al*., 2020: single-cell analysis of human adult (21-70yr old) healthy and diseased tendons (Healthy: Hamstring, Tibialis posterior, Flexor hallucis longus; Diseased: Achilles, 2nd and 3rd toe extensors, peroneus long).	**Endothelial:** CD34, PECAM1, VWF **Monocyte:** MS4A7, CD14, CD68 **T cells:** CD3E, IL7R **Tenocyte A:** CD10, CD26, CD54, FBN1, MFAP5, VCAN, EMILIN1, SCX, COL1A1, COL3A1, POSTN, ACAN, COL5A1, COL11A1 **Tenocyte B:** CD105, CD146, CD90, FBN1, MFAP5, VCAN, EMILIN1, SCX, COL1A1, COL3A1, POSTN, ACAN, COL5A1, COL11A1 **Tenocyte C (smooth muscle mesenchymal cells):** CD146, CD90, CD105(low), ACTA2, RGS5, ITGA7, TAGLN, MYL9, COL4A1, TNC, MYH11, TPPP3 (low) **Tenocyte D (fibro–adipogenic progenitors):** COL6A1/2/3, BGN, FBLN2, FMOD, COL3A1, GSN, LUM, DCN, LY6E, CXCL14, LY6E, TPPP3, PDGFRA, CD34, CD90, CD146(low), CD105(low). **Tenocyte E:** COL6A1/2/3, BGN, FBLN2, FMOD, COL3A1, GSN, LUM, DCN, LY6E, CXCL14, TPPP3, PDGFRA, CD26, CD90(low), CD54(low).	Authors liken Tenocytes E to paratenon TSPCs based on expression of TPPP3 and PRG4. Tenocytes C have high expression of ACTA2, RGS5, ITGA7, TAGLN, MYL9, COL4A1, TNC, MYH11. Almost no SCX expression, low expression of TPPP3, and no PDGFRA. Proteomics found CD90, CD105, CD146 at the surface. Mostly found in diseased samples, with very few cells in healthy. Tenocytes E and D were similar to each other and expressed TPPP3 and PDGFRA, though at low levels. But D cells were positive for endothelial marker CD34, and E cells did not have any CD105 or CD146.

Akbar *et al*., 2021: single-cell and spatial RNA-seq analysis of adult human healthy hamstring and diseased supraspinatus tendons.	**Normal Tenocytes (nT1, nT2):** SCX, TNMD, FBLN1, GSN, CFD, CXCL14. **Diseased Tenocytes (dT1, dT2, dT3, dTc):** Upregulated COL1A1, COL3A1, and FN1. SERPINE, LOXL1, LOXL2, CD55, PRG4, CRTAC1, STMN1, PTTG1, CENPF, POSTN, MMP2, CTHRC1. **Mural Cells (mT):** NOTCH3, ACTA2, RGS5. **Dendritic Cells (DC):** CLEC10A, HLA-DQA1, INSIG1, C1QA. **Macrophages (Macro1, Macro2, Macro-C):** CCL3, CXCL2, SEPP1, CD9, LGALS1, PTTG1, STMN1. **T Cells (T-Cell1, T-Cell2):** CD52, CCL5, LTB, IL7R. **Endothelial Cells (7 subtypes):** PECAM1/CD31, CD36, CLDN5, CLEC14A, LYVE1, CCL21, HLA-DRA, COL4A1, SEMA3G, CD36, ACKR1, SELE, FABP4 etc. **Muscle Cells:** MYF5, DLK1, APOC1	Mural cells mentioned as possible progenitors in reference to literature.
Steffen *et al*., 2022: spatial RNA-seq analysis of rat adult (3 months old) patellar tendons.	The data were annotated by anchoring to the de Micheli 2020 annotated dataset. The following subsets were mapped: **Tendon Fibroblasts 1 (located at Midsubstance):** differentially expressed Chad, Comp, Cilp2, Clu, Ecrg4, Mfge8, Fmod, Cst3, Dcn, Col1a1, Sparc. **Tendon Fibroblasts 2 (located at Tendon periphery):** differentially expressed Apoe1, Ccl21, Col3a11, Cfd2, Tmsb4x2, Gsn1, CD74. **Red Blood Cells, Pericytes, Immune Cells, Endothelial Cells (all located in the outer Sheath).** There were possible enthesis cells expressing high levels of Col2a1, Spp1, Lbp etc., however the authors did not proceed with annotating based on the initial clustering of the spatial data.	No mention.
Ackerman *et al*., 2022: spatial RNA-seq analysis of uninjured and injured (14, 21, and 28 post-surgery) adult (10–12 weeks old) mouse tendons.	**Cluster 0 (C0synthetic):** Found in less reactive areas. High expression of Tnmd, Col1a1, and Fmod. **Cluster 1 (C1native_tendon):** Resembles normal tendons. High Coch, Chad, and Car3 expression. **Cluster 2 (C2reactive):** Represents reactive tissue adjacent to the repair site. High expression of Mmp13, Lox, and Fbln2. **Cluster 3 (C3fibrotic):** At the peripheral shell of healing tendon. High expression of Col3a1, Postn, and Thbs3. **Cluster 4 (C4inflammatory):** High expression of Saa3, S100a8, S100a9, and markers for immune cells like neutrophils and monocytes. **Cluster 5 (C5muscle-assoc):** Exhibits features of both muscle and native tendon tissue, indicative of a muscle-tendon interface. Only clusters 5 and 1 were found in uninjured tendon.	No mention.

Mimpen *et al*., 2022: single-nucleus and spatial RNA-seq analysis of human adult (18-37yr old) healthy hamstring tendons.	**MKX+ Fibroblasts (throughout tendon):** MKX, TNMD, THBS4, THSD4, COMP, PIEZO2, COL11A1, COL11A2, COL12A1, COL14A1, FMOD, ITGA10, MET, CPXM2, CADM1, COL1A1, COL3A1, DCN. **PDGFRA+ Fibroblasts (close to skeletal muscle):** PDGFRA, NEGR1, NOVA1, FBN1, FBLN1, FBLN2, FBLN5, ELN, CD55, ABCA8, COL15A1, DCLK1, KCND2, VIT, COL1A1, COL3A1, DCN. **Mural Cells:** NOTCH3, PDGFRB, MYO1B, ADAMTS12, PDE1C, PDE3A, PDGFRB, RERG. **Vascular Endothelial Cells:** PECAM1/CD31, PTPRB, VWF, CDH5, FLT1, CD34, NOTCH4, ADGRL4, TEK. **Lymphatic Endothelial Cells:** PECAM1/CD31, PTPRB, VWF, CDH5, MMRN1, PROX1, KDR, FLT4, EPHB4, LYVE1, MMRN1, NRG3, PKHD1L1. **Adipocytes:** GPAM, TMEM132C, PLIN1, PLIN4, AQP7, ADIPOQ. **Macrophages:** CD14, CD163, MERTK, MRC1, MSR1. **T cells:** CD247, IL7R, CD69, THEMIS. **Dendritic Cells:** HLA-DQA1, CD74, GPAT3, CIITA, HLA-DRB1. **Nervous System Cells:** NTRK3, TENM2, KANK4, SLC2A1, SLC22A3, CLDN1 **Satellite Cells:** PAX7, CALCR, CDH4, CLCN5, CTNND2, GREM1. **Fast-twitch Skeletal Muscle Cells:** TNNC2, TNNT3, TNNI2, HOMER1, ACTN3, KCNQ5, MYH1, MYH3, MYLK4, MYBPC2, TRDN, DES. **Transitional Skeletal Muscle Cells:** COL22A1, ADAMTSL1, CPM, CSMD1, FRAS1, PZP, RALYL, SAMD5, SORBS2, SPAG16, TRDN, DES. **Slow-twitch Skeletal Muscle Cells:** TNNC1, TNNI1, TNNT1, ATP2A2, CCR3, LGR5, MYH7, MYH7B, NEK10, TECRL, TRDN, DES.	A small subset of PDGFRA+ fibroblasts expressed TPPP3. Further investigation needed to confirm. MCAM/CD146 was nearly undetectable in all tendon populations.
Fu *et al*., 2023: single-cell analysis of human healthy and diseased tendons.	**TSPCs:** ACTA2, RGS5, THY1, and MCAM. **TC1-6 (tendon fibroblasts):** Expressing tendon-related genes like DCN, TNC, FBLN2, COL1A1, COL3A1, FMOD. **TC7 (pathological repair-related fibroblasts):** Expressing scar healing-related markers TPPP3, COL3A1, COL5A1, DPT. **TC8 (pre-hypertrophic chondrocytes):** CD55, CRLF1, SMOC1. **TC9 (hypertrophic chondrocytes):** OGN, SOX9, SCRG1. **TC10 (osteocytes):** IBSP, SPP1, SOX9, RUNX2. **Endothelial Cells (EC1-5):** VWF, PECAM1, PLVAP. **T cells, Dendritic Cells (DC), Macrophages (Mac):** CD3D, CD68, CD14. **Smooth Muscle Cells (SMC1, SMC2):** MYL9, MYH11	Specifically define a cluster of TSPCs that express ACTA2, RGS5, THY1 (CD90), and MCAM (CD146). However, tSNE plots reveal very limited overlap in the expression of ACTA2 and the TSPC cluster (Fig1J), necessitating caution with interpretation.

2.3 Tendon ECM Composition and Organisation

2.3.1 Collagens

Collagens are essential in forming the structural and functional properties of tendons through their organisation into complex macromolecular assemblies, called suprastructures**,** within the ECM (reviewed in Birk and Brückner, 2011). The organisation and function of these suprastructures are profoundly influenced by their composite nature: while a single type of collagen may be predominant, the overall suprastructure invariably incorporates a mix of other collagen types and non-collagenous components. These additional macromolecules may be present in significant or trace amounts, yet they are crucial in determining the specific architectural and functional attributes of the tissue.

Tendon collagens can be categorised based on their functions and supramolecular structures into the fibril-forming, network-forming, beaded filament-forming, and FACIT (fibril-associated collagens containing interrupted triple helices) types. The roles these collagens play, along with the consequences of their mutations, are outlined in Appendix Table 1.

2.3.1.1 Fibril-forming collagens

Fibril-forming collagens (types I, II, III, V, XI, and XXVII) form the bulk of tendon's ECM and impart tensile strength and flexibility. Collagens I, II, and III, which form striated fibrils (Figure 5A), constitute the core components of tendon fibres. **Collagen I**, encoded by *COL1A1* and *COL1A2*, forms over 95% of tendon collagenous ECM. Its densely packed, parallel-aligned fibril bundles are essential for tendon functionality, providing the requisite tensile strength (Riley, 2004). Defects in collagen I can disrupt tenocyte activity, impair fibril growth, and reduce tendon thickness, thus increasing rupture risk and destabilising attachments (Marini *et al.*, 2007; Buckley *et al.*, 2013; Park *et al.*, 2020).

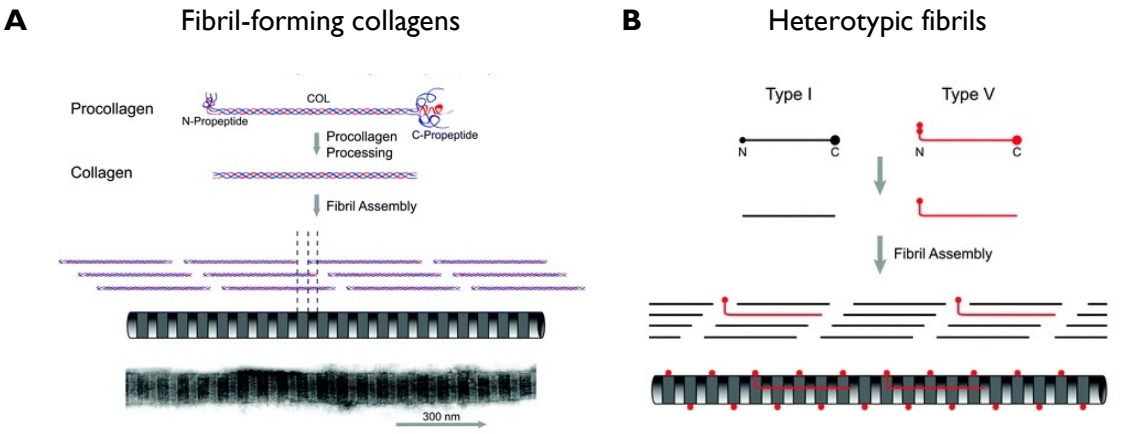


Figure 5. Schematic diagram of fibril-forming collagens and heterotypic fibrils. *Panel (A) shows the synthesis, processing, and assembly of collagen into fibrils. Panel (B) illustrates a fibril composed of type I fibrillar collagen and a regulatory, fibril-forming type V collagen within a heterotypic structure. This configuration is used for the nucleation of fibril assembly. COL: collagenous domain. Adapted, with permission, from Birk and Brückner (2011).*

Collagen III, encoded by *COL3A1*, is the second most abundant collagen in tendon, accounting for ~1-3% of the mature tendon's collagenous ECM (Riley, 2004; S. Zhang *et al.*, 2021). During embryonic development, when fibrils are small and disconnected, collagen III is produced at higher levels and co-distributed with collagen I across the fascicles and connective tissue layers. Although collagen III's prevalence declines as tendons mature, it remains concentrated in the outer sheaths. Concurrently, the fibril diameter in the fascicles increases while the one in the outer sheaths remains small, reflecting collagen III's important role in initial tendon ECM formation and the regulation of fibril diameter and tendon elasticity (Birk and Mayne, 1997; Kuo, Petersen and Tuan, 2008; Buckley *et al.*, 2013). Collagen III levels also increase transiently during early stages of tendon repair, highlighting its role in wound healing (Maffulli *et al.*, 2000; Dahlgren, Brower-Toland and Nixon, 2005). Importantly, elevated collagen III expression is sustained in chronic tendinopathy (Lui *et al.*, 2010; Jelinsky *et al.*, 2011).

Collagen II (*COL2A1*) predominates in the fibrocartilaginous zones of the enthesis, facilitating stress absorption at attachment points by providing a gradient of mechanical properties (Fukuta *et al.*, 1998; Nourissat *et al.*, 2010; Buckley *et al.*, 2013). **Collagen XXVII** (*COL27A1*) forms unusually small, thin, non-striated fibrils and is also found in the enthesis (Alcaide-Ruggiero *et al.*,

2021). Not much is known about its roles in tendons, however studies show that it contributes to structural support and is linked to developmental skeletal disorders via potential associations with *SOX9* (Pace *et al.*, 2003; Jenkins *et al.*, 2005; Kotabagi *et al.*, 2017; Kim *et al.*, 2021).

Collagens V (*COL5A1*, *COL5A2*, *COL5A3*) and **XI** (*COL11A1*, *COL11A2*) represent a quantitatively minor regulatory collagen type essential in fibrillogenesis and fibre organisation. During foetal development, these collagens are anchored to the fibroblast surface and determine the number and diameter of protofibrils (Watanabe *et al.*, 2007; Wenstrup *et al.*, 2011; Smith, Zhang and Birk, 2014). They initiate the assembly of major collagen I, II, or III protofibrils, and are subsequently incorporated into the fibrils themselves (Figure 5B). This incorporation is marked by the protrusion of their globular N-terminal domains outside the fibril structure, effectively regulating fibre diameter through steric hindrance (Wenstrup *et al.*, 2004, 2011; Sun *et al.*, 2011, 2020; Smith, Zhang and Birk, 2014; Connizzo *et al.*, 2015). Consequently, a reduction in collagens V and XI correlates with the formation of fewer, larger diameter, and irregularly shaped fibres (Figure 6), diminishing mechanical properties such as maximum load, modulus, and stiffness (Malfait *et al.*, 2005; Wenstrup *et al.*, 2011; Johnston *et al.*, 2017; Sun *et al.*, 2020; R. J. Leiphart *et al.*, 2022).

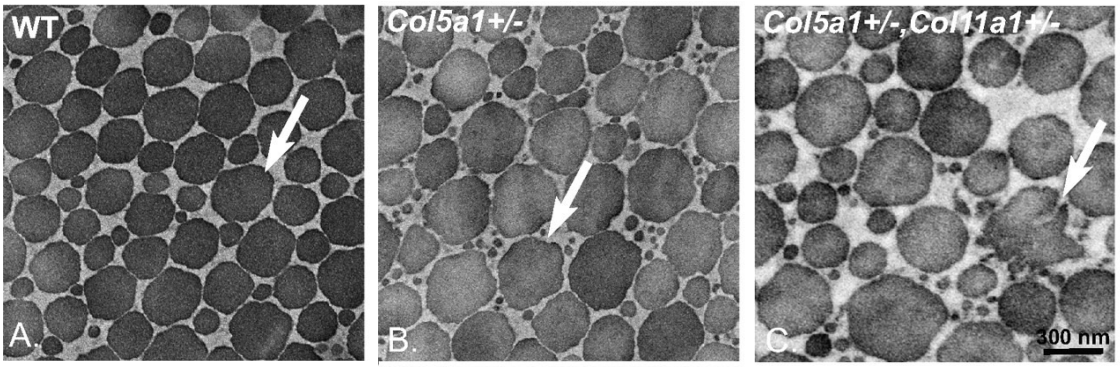


Figure 6. Transmission electron microscopy images of cross-sectional views of mouse flexor digitorum longus tendon collagen fibrils from wild-type and mutant mice at 30 days post-natal. *Panel (A) shows structurally normal fibrils in WT mice. Panels (B) and (C) display irregular fibrils in heterozygous mutants for Col5a1 and double mutants for Col5a1 and Col11a1, respectively. The size bar represents 300 nm. Arrows indicate normal fibres in WT (A) and irregular fibres in the mutants (B, C). Adapted from Wenstrup et al. (2011) (CC-BY 4.0).*

2.3.1.2 Fibril-associated collagens containing interrupted triple helices

FACIT collagens (types IX, XII, XIV, XXII) serve a wide array of functions. These collagens modulate the surface properties of fibrils (Figure 7), assist in the packing of fibril-forming collagens during assembly, and facilitate the integration of tendon cells with the ECM. Additionally, they play a crucial role in regulating mechanical properties by influencing tenocyte collagen synthesis through feedback mechanisms (Birk and Brückner, 2011).

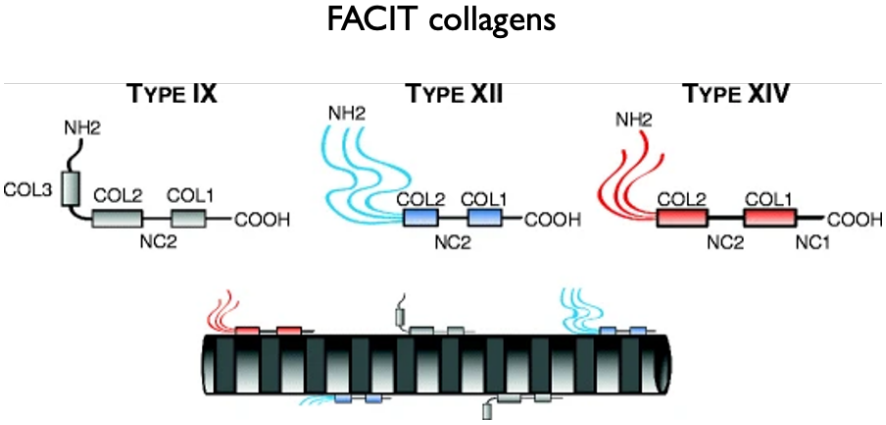


Figure 7. Schematic diagram of fibril-associated collagens containing interrupted triple helices (FACIT). *FACIT collagens associate with collagen fibrils to modulate their properties. One possible collagenous (COL) and non-collagenous (NC) domain configuration within different FACIT types is shown. Adapted, with permission, from Birk and Brückner (2011).*

Collagens XII and XIV are integral during the formative stages of tendon development, playing distinct roles in the organisation and maturation of the tendon matrix. **Collagen XII** (*COL12A1*), through its regulation of intercellular communication and collagen type I synthesis, is essential for integrating the developing tendon matrix and fascicle structure. It orchestrates fibril alignment and tenocyte organisation, underpinning the stabilisation of fibrils preceding crosslinking (Izu *et al.*, 2021). While collagen XII expression is ubiquitous in early tendon development (e.g., in E6-E14 of chicks), it becomes more targeted as development proceeds, concentrating in the fascicular and interfascicular ECM and on tenocyte surfaces by the time of birth to facilitate cellular connectivity (Wälchli *et al.*, 1994; Zhang, Young and Birk, 2003). Deficiencies in collagen XII expression can lead to altered tenocyte morphology and impaired cellular communication, which may manifest as decreased tissue resilience and a reduction in type I collagen levels (Tzortzaki *et al.*, 2003; Fung *et al.*, 2022).

In parallel, **collagen XIV** (COL14A1) is important in the early stages of collagen type I fibrillogenesis. Expressed highly during embryonic development, it regulates the timing and pattern of fibril growth (Wälchli *et al.*, 1994; Young, Gordon and Birk, 2000; Ansorge *et al.*, 2009). This expression declines as tendons mature, becoming sparse in adult tissues. Mutations in the COL14A1 gene can cause premature fibril formation and alter the mechanical properties of tendons in early postnatal stages (Ansorge *et al.*, 2009). However, these phenotypic deviations tend to normalise, and functionality is typically restored as tendon maturation completes, underscoring this collagen's role in early structural development rather than in ongoing tendon maintenance (Ansorge *et al.*, 2009).

Two key FACIT collagens play vital roles in tendon attachment regions. **Type IX collagen** (*COL9A1*, *COL9A2*, *COL9A3*), situated on the surfaces of type II collagen fibrils in cartilaginous enthesis tissues, serves as a molecular bridge to the matrix, enhancing the mechanical resilience and flexibility of the tendon while also reinforcing the tissue's resistance to compression (Fässler *et al.*, 1994; Fukuta *et al.*, 1998; Czarny-Ratajczak *et al.*, 2001; Posey *et al.*, 2008). Conversely, **type XXII collagen** (*COL22A1*) is essential for the attachment of tendons to muscles. It functions as a fibroblast adhesion factor at the MTJ, reinforcing the connection between skeletal muscles and tendons. Its expression, initiated in response to early embryonic muscle contractions, increases with organismal development and remains localised to the MTJ, distinct from other FACIT collagens (Koch *et al.*, 2004; Jakobsen *et al.*, 2017; Lipp *et al.*, 2023). Dysfunction in type XXII collagen is associated with muscular dystrophy, marked by weakened muscle-to-tendon force transmission and fibre detachment (Charvet *et al.*, 2013).

2.3.1.3 Filament- and network-forming collagens

In addition to major groups of fibrillar and FACIT collagens, the tendon is supported by various other structural collagens. **Collagen type VI** (*COL6A1-COL6A6*) is a non-fibrillar, **beaded filament-forming** collagen that is particularly concentrated in the pericellular matrix around fibroblasts. It modulates the size of fibrillar collagens and is crucial during developmental stages. Initially expressed broadly, its presence later localises to areas vital for

force transmission, such as the enthesis (Thakkar *et al.*, 2014; Liu *et al.*, 2015). Here, collagen VI collaborates with proteoglycans like biglycan to ensure correct alignment and distribution of collagen fibrils (Ryan J. Leiphart *et al.*, 2022). Deficiency in collagen VI leads to disorganised ECM with higher density of smaller diameter fibrils that compromise the biomechanical properties of tendons, including stiffness and load capacity. Additionally, the absence of collagen VI is associated with increased activity of matrix metalloproteinases, suggesting a disruption in cell-matrix interactions and fibrillogenesis (Izu *et al.*, 2011; Thakkar *et al.*, 2014). Therefore, collagen VI is integral to maintaining both the microstructural environment needed by tenocytes and the tendon's macrostructural integrity essential for mechanical performance.

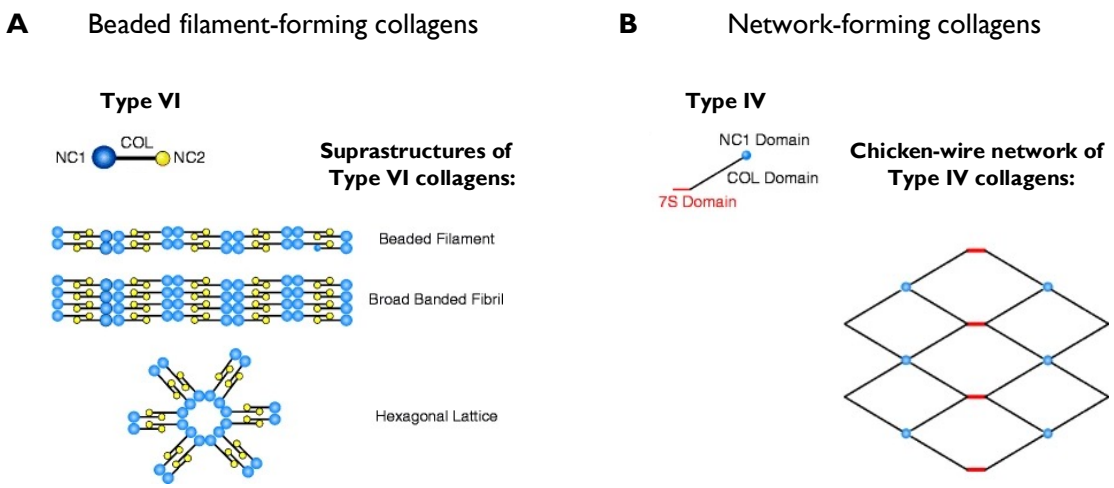


Figure 8. Schematic diagram of beaded filament- and network-forming collagens VI and IV. (A) *Collagen VI monomers consist of a collagenous (COL) domain flanked by two non-collagenous (NC) domains. These monomers assemble from their N-terminal to C-terminal ends to form dimers, which then combine into tetramers. These tetramers aggregate into three different suprastructures: beaded filaments, broad-banded fibrils, and hexagonal lattices.* ***(B)*** *Collagen IV monomers consist of a COL domain flanked by a C-terminal NC domain and an N-terminal 7S domain. These monomers assemble into dimers and tetramers, which then aggregate into a chicken wire-shaped network. Adapted, with permission, from Birk and Brückner (2011).*

Finally, **network-forming collagens** (types IV and X) are found in specific regions of the tendon. **Collagen IV** (*COL4A1-COL4A6*) forms a robust "chicken-wire" network within the basement membranes, which are essential for tissue compartmentalisation as well as cellular and structural support. This meshwork permeates the vasculature and is found in the endotenon, epitenon, and paratenon layers (J. Zhang *et al.*, 2021). Mutations in the *COL4A1* gene lead to incomplete and irregular basement membranes, causing defects in vascular

function as well as adhesion formation and impaired tendon movement (Van Agtmael *et al.*, 2010; Taylor *et al.*, 2011). On the other hand, **Collagen X** (*COL10A1*) forms hexagonal lattices and is found in the mineralised fibrocartilage zone of the enthesis. Expressed by hypertrophic chondrocytes, it is likely involved in mineralisation and ossification (Fukuta *et al.*, 1998; Apostolakos *et al.*, 2014).

2.3.1.4 Post-translational modifications and crosslinking of collagens

The functionality and tissue-specific roles of collagens are significantly influenced by intracellular and extracellular **post-translational modifications**. Intracellularly, newly synthesised collagens undergo proline and lysine residue modifications that are necessary for the formation of collagen's triple-helix structure. For example, the synthesis of type I collagen involves a variety of hydroxylations (e.g., 4-hydroxyproline, 3-hydroxyproline, and 5-hydroxylysine) alongside targeted glycosylations, such as the addition of galactose and glucose to hydroxylysine (Salo and Myllyharju, 2021). While collagen I of bone and skin is rich in hydroxylysine glycoside, they have fewer sites of 3-hydroxyproline compared to the collagen found in tendons (Weis *et al.*, 2010; Pokidysheva *et al.*, 2013; Hudson *et al.*, 2017). At the same time, foetal tendons and ligaments have only minimal levels of prolyl 3-hydroxylation in type I collagen sites compared to adult tissues (Hudson *et al.*, 2021). Additionally, tendons show high glycosylation at a specific lysine site (K87) that is significant for cross-link formation (Pokidysheva *et al.*, 2013; Hudson *et al.*, 2017).

Once secreted into the extracellular space, collagen molecules undergo further processing, including the cleavage of terminal propeptides and assembly into the suprastructures through **crosslinking**. The former is carried out by collagen type-specific **metalloproteinases** (**MMPs**) of the tolloid family (e.g., BMP1, TLL) as well as **a disintegrin and metalloproteinase with thrombospondin motifs** (**ADAMTS**) peptidases (Canty-Laird, Lu and Kadler, 2012), while the latter is facilitated by both enzymatic and non-enzymatic mechanisms. Collagen crosslinking is carefully modulated by mechanical stimuli, hormonal status, TGF-β signalling, and hypoxia, as well as ECM proteins such as *FMOD*, fibulin-4 (FBLN4 encoded by *EFEMP2*), and thrombospondin 1 (*THBS1*) (Sethi *et al.*,

2011; Makris *et al.*, 2014; Kalamajski *et al.*, 2016; Sasaki *et al.*, 2016; Rosini *et al.*, 2018; Ellingson, Pancheri and Schiele, 2022).

Enzymatic crosslinking primarily involves the action of **lysyl oxidase** (**LOX**), LOX-like isoforms (LOXL) and transglutaminases. LOX catalyses the conversion of lysine residues in collagen molecules into reactive aldehydes. These aldehydes can then form covalent bonds with other lysine or hydroxylysine residues. These immature, reducible crosslinks can then react further with another oxidised lysine to form mature, irreversible pyridinoline crosslinks (Kagan and Li, 2003; Avery and Bailey, 2005; Eyre, Weis and Wu, 2008). Specifically, hydroxylysyl pyridinoline (HP) crosslinks are prevalent in tissues subjected to significant mechanical loads, with corresponding higher densities of those links observed in load-bearing flexor than positional extensor tendons (Herod, Chambers and Veres, 2016; Svensson *et al.*, 2018; Hudson *et al.*, 2021). Interestingly, the ratio of HP to collagen increases with age and injury, with a corresponding decrease in immature crosslinks and an increase in tendon elastic modulus (i.e., stiffening) (Bank *et al.*, 1999; Couppé *et al.*, 2009; Stammers *et al.*, 2020).

In addition to the above, non-enzymatic crosslinking occurs through glycation and glycoxidation reactions, where sugars react with lysine residues to form **advanced glycation end-products** (**AGEs**) (Sajithlal, Chithra and Chandrakasan, 1998). These AGEs, such as pentosidine, can irreversibly crosslink collagen molecules, further contributing to the resistance of the collagen fibres to enzymatic breakdown. Consequently, excessive AGE cross-linking has been noted in ageing and diseases such as diabetes (Chaudhuri *et al.*, 2018) and is strongly associated with collagen damage as it decreases tendon elasticity and impairs tissue remodelling and repair due to the inflammation and oxidative stress-promoting effects on the surrounding cells (Zhou, Li and Cai, 2004; Fessel *et al.*, 2014; Suzuki, Yabu and Nakamura, 2022).

2.3.1.5 Collagen crimping

Under the microscope, healthy collagen networks appear in a sinusoidal pattern called **crimps**, which permit longitudinal fibril elongation and contribute to the

strength of the tendon (Jarvinen *et al.*, 2004; Herchenhan *et al.*, 2012; Legerlotz *et al.*, 2014). Acting as a functional adaptation to mechanical load, the crimps have larger angles and fibre bundles in energy-storing rather than positional tendons (Jarvinen *et al.*, 2004; Spiesz *et al.*, 2018). Generally, training, stress relaxation, ageing, and injuries reduce the crimp angle, leading to increased tendon stiffness and predisposition to overstretching and damage (Jarvinen *et al.*, 2004; Franchi *et al.*, 2013; Spiesz *et al.*, 2018; Lee *et al.*, 2023).

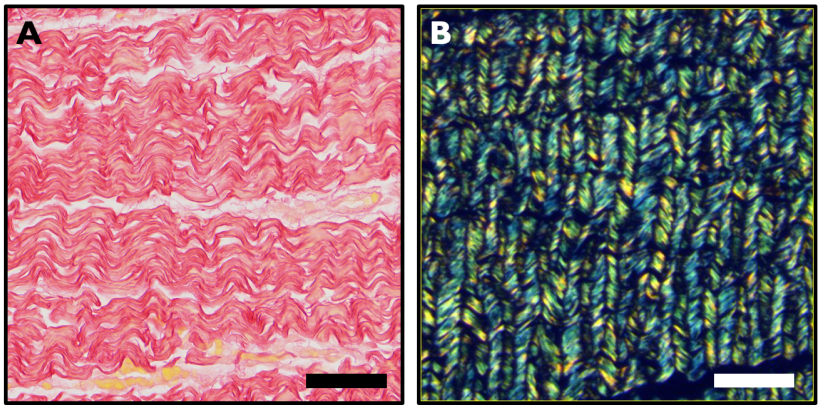


Figure 9. Brightfield and polarized light microscopy images of picrosirius red-stained foetal patellar tendon. *Panel **A** shows a brightfield microscopy image of a 19 post-conception week patellar tendon section, and Panel **B** displays a similar tissue region from the same tendon under polarized light. The images illustrate collagen crimping and birefringence in developing tendon (see section 6.3.1 for more details). Size bar corresponds to 50 µm.*

2.3.2 Non-collagenous ECM

The non-collagenous components of tendon ECM, often termed "***ground substance***", occupy the interstitial spaces between cells and collagen fibres, thereby reinforcing structural integrity and enhancing biomechanical properties. Water, the most abundant component of this gel-like matrix, typically accounts for ~70-91% of the total weight of the tendon, varying with health and mechanical loading conditions. Mechanically loaded tendons generally have a reduced water content compared to healthy, unloaded tendons, which in turn display lower water levels than tendinopathic tendons (Hannafin and Arnoczky, 1994; Ho and Kulig, 2016; Griffith *et al.*, 2017). These variations in water content significantly impact the physical properties of the tendons and are directly influenced by the protein and sugar composition of the ground substance, particularly the glycoproteins such as **glycosaminoglycans** (**GAGs**) and **proteoglycans** (**PGs**) (summarised in Appendix Table 2).

2.3.2.1 Glycosaminoglycans

Glycosaminoglycans are complex polysaccharides that function to organise the ECM and regulate cellular behaviour and signalling. Structurally, GAGs are enriched with carboxylate groups, imparting a strong negative charge that enables them to attract and retain water within interstitial spaces (Rozario and DeSimone, 2010). This capacity not only facilitates lubrication and contributes to the overall viscosity of the tissue, but also ensures cellular organisation and resilience to mechanical stress.

Hyaluronic acid (**HA**), otherwise called **hyaluronan**, is synthesised by hyaluronan synthases (HAS1 to HAS4) at the plasma membrane. HA predominates in the early embryonic ECM, forming pericellular matrices by binding to cell surface receptors like CD44 (hyaluronan receptor) and RHAMM (receptor for hyaluronic acid-mediated motility). These highly hydrated matrices enable and regulate cell migration, proliferation, and differentiation (Toole, 2001; Li *et al.*, 2007; Maharjan, Pilling and Gomer, 2011), influencing tissue development, healing, and pathological events such as metastasis (Toole, 2001). For example, during embryogenesis, HA acts as a chemoattractant and inhibits cell differentiation; downregulation of HA is therefore necessary for the initiation of chondrogenic differentiation in embryonic limbs (Krenn, Brand-Saberi and Wachtler, 1991; Toole, 2001; Tzircotis, Thorne and Isacke, 2005; Li *et al.*, 2007). Additionally, in wound healing, the regenerative capacity of foetal tendons characterised by scarless repair correlates with high sustained levels of HA, promoting regenerative cellular activities and mitigating the inflammation and fibrosis typical of aged tendon repair (Longaker *et al.*, 1989, 1991; Beredjiklian *et al.*, 2003; Favata *et al.*, 2006).

The molecular weight of HA, reflective of its polymeric integrity, influences its cellular effects. Tissue damage and inflammation often yield fragmented HA, which promotes inflammation and inhibits fibroblast differentiation, contrary to high molecular weight HA's anti-inflammatory properties (Scheibner *et al.*, 2006; Jiang, Liang and Noble, 2007; Maharjan, Pilling and Gomer, 2011; Rayahin *et al.*, 2015). Nonetheless, both low and high molecular weight HA supplementation have demonstrated efficacy in adult tendon repair, diminishing inflammation, encouraging cell proliferation and collagen synthesis, and

providing lubrication to prevent adhesions (Abate, Schiavone and Salini, 2014; Honda *et al.*, 2017; Mohebbi *et al.*, 2021; Oliva *et al.*, 2021; Frizziero *et al.*, 2022; Costa *et al.*, 2023).

In contrast to HA, which remains non-sulfated, other GAGs undergo enzymatic post-synthetic modifications that result in highly varied structures and functions. Enzymes such as CHST11 and UST sulfotransferases catalyse sulfation, increasing the GAGs' negative charge and thereby enhancing their capacity for molecular interactions (Soares da Costa, Reis and Pashkuleva, 2017; Mizumoto and Yamada, 2021, 2023). Further, epimerisation, largely mediated by dermatan sulfate epimerase (DSE), modulates the stereochemistry of sugar units within the GAG chains, influencing their interactions with proteins (Mizumoto and Yamada, 2021, 2023).

These biochemical diversifications lead to the classification of GAGs into four major types: **chondroitin sulfate** (**CS**), **dermatan sulfate** (**DS**), **heparan sulfate** (**HS**)/**heparin** (**Hep**), and **keratan sulfate** (**KS**), each distinguished by unique disaccharide units and varying degrees of sulfation (Soares da Costa, Reis and Pashkuleva, 2017). Once modified, these GAGs are covalently linked to core proteins, forming **proteoglycans** (**PG**) (Iozzo and Schaefer, 2015; Puri *et al.*, 2020). While the protein core determines the PG's intracellular, secretory or ECM localisation, the GAG components maintain the interfibrillar space, contribute to hydration, and mediate interactions with a variety of extracellular ligands, including growth factors and adhesion molecules (Soares da Costa, Reis and Pashkuleva, 2017).

2.3.2.2 Small leucine-rich proteoglycans

Within tendons, several classes of PGs and their associated GAGs can be identified. Among these are the extracellular **small leucine-rich proteoglycans** (**SLRPs**) – specifically classes I (BGN, DCN, asporin (ASPN)), II (FMOD, lumican (LUM), keratocan (KERA)), and III (osteoglycin (OGN), otherwise called mimecan) – which modulate collagen fibrillogenesis and interact with a wide range of growth factors, thereby influencing ECM assembly and cellular behaviour (Iozzo and Schaefer, 2015) (Appendix Table 2). In general, both the PG and the sulfated GAG components of SLRPs are involved in non-covalent

binding to various types of fibrillar collagens (Iozzo and Schaefer, 2015). By doing so, they control the lateral assembly of collagen molecules into fibrils while also limiting access to their cleavage and linkage points, protecting them from enzymatic breakdown and preventing excessive crosslinking (Zhang *et al.*, 2005; Iozzo and Schaefer, 2015; Robinson *et al.*, 2017). Consequently, SLRPs are highly expressed in developing tissues and are necessary for organ morphogenesis and mature tissue homeostasis (Iozzo and Schaefer, 2015; Beach *et al.*, 2022).

Biglycan (BGN) and **decorin (DCN)** are class I CS/DS GAG-containing SLRPs sharing structural and functional similarities, including key collagen fibril binding sites, the ability to bind and limit TGF-β activity, and the capacity to modulate pro-inflammatory signalling pathways (Hildebrand *et al.*, 1994; Kolb *et al.*, 2001; Moreth, Iozzo and Schaefer, 2012; Anders and Schaefer, 2014; Abbah *et al.*, 2016). Despite this, BGN and DCN display distinct temporal and spatial expression patterns within tendon tissues. For instance, in mice, the expression of *BGN* peaks immediately after birth and declines sharply over the following month, whereas *DCN* shows highest expression in the first two weeks post-birth, then stabilises at a lower level even as the protein content continues to increase (Zhang *et al.*, 2006). Initially distributed throughout the tendon ECM, both proteins eventually become concentrated within the pericellular matrices during early postnatal development (Zhang *et al.*, 2006), with DCN found in both the fibrillar and surrounding loose connective tissue regions (Svensson *et al.*, 1999). During tendon maturation and ageing (from postnatal day (P) 21 to P56), there is twice as much DCN as BGN, both the CS/DS GAG and PG contents decrease, and the GAG chains become shorter in mouse positional (tail) tendons (Derwin *et al.*, 2001).

Determining the precise contributions of DCN and BGN to tendon biology is challenging due to the variability in effects reported across different studies, which highlight age- and tendon-specific roles for each proteoglycan. For example, mice completely lacking DCN (*Dcn*$^{-/-}$) exhibit abnormally large and irregularly shaped collagen fibrils, resulting in weaker mature tendons 150 days post-birth (P150) (Zhang *et al.*, 2006). This phenotype manifests within 1-2 weeks after birth, coinciding with the onset of early postnatal tendon linear and lateral fibril expansion (Ezura *et al.*, 2000; Zhang *et al.*, 2006). Interestingly, it is

more pronounced in positional than load-bearing flexor tendons, where a compensatory increase in BGN synthesis is observed, suggesting an adaptive response that partially offsets the structural deficiencies caused by the absence of DCN (Zhang *et al.*, 2006). Similarly, *Bgn*$^{-/-}$ mice display comparable phenotypes, yet collagen fibril diameters remain normal in flexor tendons and only slightly decrease in positional tendons (Corsi *et al.*, 2002; Dourte *et al.*, 2013). Further, studies on injured tendons indicate that both *Bgn*$^{-/-}$ and *Dcn*$^{-/-}$ P120 adult tendons show diminished mechanical properties post-injury, underscoring the importance of these proteoglycans in tendon repair and healing (Dunkman *et al.*, 2014).

While informative, these studies confound the developmental and homeostatic effects. Consequently, inducible knockdown models have been employed to clarify their roles in tissue maintenance and healing. In P7 neonates, simultaneous knockdown of BGN and DCN (I-*Dcn*$^{-/-}$*Bgn*$^{-/-}$) results in compromised tendon properties, such as reduced cross-sectional areas and smaller fibril diameters (Beach *et al.*, 2024). In contrast, in P150 adult tendons, this knockdown mimics the *Dcn*$^{-/-}$ phenotype with larger fibril diameters and mechanical vulnerabilities like decreased stiffness and increased tissue viscosity (Robinson *et al.*, 2005, 2017). Remarkably, while inducible knockdown of DCN alone (I-*Dcn*$^{-/-}$) shows minimal effect on P150 adult tendon mechanics and injury healing responses (Leahy *et al.*, 2023; Beach *et al.*, 2024), BGN knockdown (I-*Bgn*$^{-/-}$) significantly influences quasistatic and viscoelastic properties (Beach *et al.*, 2022) as well as improves tendon injury healing outcomes (Leahy *et al.*, 2023).

These observations illustrate the complex and synergistic roles of DCN and BGN in tendon structure and function across different life stages. Overall, DCN is essential during early postnatal development for structuring the tendon ECM and regulating growth, whereas BGN plays a crucial role in adult tendon maintenance and repair. The significant impact of BGN on healing outcomes, particularly in improving late-stage tendon mechanical properties and gene expression related to healing, highlights its vital role in regulating late-stage fibrillogenesis during both development and healing processes.

Unlike other class I SLRPs, **asporin** (**ASPN**) lacks GAG chains and instead features a calcium-binding aspartic acid sequence (Lorenzo *et al.*, 2001). ASPN's role in tendon biology remains underexplored; it is known to be highly expressed in tendons during early foetal development (from E15.5 onwards) (Henry *et al.*, 2001). However, its gene expression and protein levels diminish in older human and equine tendons, respectively (Peffers *et al.*, 2014, 2015). Generally, ASPN is known to compete with DCN for collagen binding sites, modulate chondrogenic differentiation through TGF-β signalling, and participate in collagen calcium mineralisation (Kalamajski *et al.*, 2009; Fan, Yan and Zhang, 2022). Knockout mice lacking ASPN (*Aspn*$^{-/-}$) exhibit altered GAG compositions and an upregulation of several key genes related to tendon function (e.g., *BGN*, *DCN*, *COL1A1*, *COL1A2*, *COL3A1*, *LUM*, and *LOX*) in skin (Maccarana *et al.*, 2017). These changes indicate a regulatory role rather than a direct involvement in collagen fibrillogenesis, highlighting the need for further investigation and validation of ASPN's functions in tendons.

Fibromodulin (**FMOD**), **lumican** (**LUM**), and **keratocan** (**KERA**) are Class II SLRPs with poorly sulfated KS GAGs, sharing structural similarities and protein binding sites (Rees *et al.*, 2009). These proteins have different temporal and spatial expression patterns. In mice, *FMOD* expression peaks around two weeks after birth (P14) and declines significantly after two months (P56), although its protein levels continue to build up gradually (Ezura *et al.*, 2000). In contrast, *LUM*'s expression peaks earlier, around P8-10, and then steadily decreases into adulthood, with a significant reduction in protein levels by P30 (Ezura *et al.*, 2000). While less is known about KERA in tendons, it is reported to be highly differentially expressed during embryonic tendon development (B. Zhang *et al.*, 2023). Both FMOD and LUM initially localise throughout the tendon matrix but later exhibit distinct localisations reflecting their specific roles in tendon architecture. During maturation, FMOD becomes increasingly concentrated within the tendon fibre bundles, LUM localises primarily to connective tissue regions (e.g., endotenon), and KERA becomes co-localised with both the fibrillar collagens in fascicles and in the surrounding loose connective tissues, similarly to DCN (Svensson *et al.*, 1999; Rees *et al.*, 2009).

When studying murine tendon structure across genetic mutations, a clear gradient in the severity of structural abnormalities is observed among LUM

(*Lum*$^{-/-}$), FMOD (*Fmod*$^{-/-}$), and double-null (*Lum*$^{-/-}$*Fmod*$^{-/-}$) mutants. Initially, at P4, all three have larger than normal diameter collagen fibrils (Ezura *et al.*, 2000). By P10, a higher ratio of smaller to larger diameter fibrils is observed across all deficient phenotypes, indicating ongoing disruptions in fibril maturation processes (Ezura *et al.*, 2000). By the 1-3 month' mark, LUM-deficient tendons show slight irregularities in fibril cross-section contours but recover back to normal fibril diameter distributions (Ezura *et al.*, 2000). In contrast, FMOD-null and double-deficient tendons continue to exhibit smaller, more irregular fibril diameters as well as a reduction in total fibre bundles and endotenon tissue, leading to disorganised cell distribution and increased stiffness (Svensson *et al.*, 1999; Ezura *et al.*, 2000; Jepsen *et al.*, 2002). FMOD-null mice display increased compensatory LUM deposition (Svensson *et al.*, 1999; Jepsen *et al.*, 2002), leading to a less severe presentation than observed it double-mutant mice.

Overall, the critical roles of LUM and FMOD in tendon development and maintenance are evident from their complementary but distinct regulatory effects on fibril maturation and tendon stiffness. While LUM modulates the early stages of postnatal fibril assembly, ensuring proper fibril alignment and spacing, FMOD takes over in later stages to facilitate the fusion and growth of these fibrils into mature, large-diameter structures critical for tendon strength.

KERA shares structural similarities with LUM, suggesting a potentially similar role in the regulatory process of collagen fibrillogenesis (Carlson *et al.*, 2005). While KERA's specific function in tendons is yet to be fully understood, its deficiency in mice (*Kera*$^{-/-}$) leads to increased collagen fibril diameters in the cornea (Liu *et al.*, 2003), indicating its influence on fibril structure. However, corneal keratocan is highly glycosylated and abundant compared to tendon keratocan (Funderburgh, Caterson and Conrad, 1987; Rees *et al.*, 2009; Puri *et al.*, 2020), suggesting that its biochemical properties and functions can vary significantly. This is supported by the studies where mice lacking a specific KS sulfotransferase, CHST5 (*Chst5*$^{-/-}$), which results in low levels of KS sulfation, exhibit tightly packed, smaller diameter fibrils in the corneas (Hayashida *et al.*, 2006), hinting at the poorly sulfated KERA function in the organisation and restriction of fibril diameters. Overall, KERA may have a role in tendon collagen

fibre organisation to that akin of LUM with which is shares spatial expression patterns.

In addition to the class I and II SLRPs, tendons express a class III KS-containing **osteoglycin** (**OGN**), also known as mimecan. Mice lacking OGN (*Ogn*$^{-/-}$) exhibit mild collagen disruption phenotypes, with reduced tensile strength reported in skin, cornea, and cardiac tissues (Iozzo and Schaefer, 2015; Moncayo-Arlandi *et al*., 2014; Tasheva *et al*., 2002). In the context of tendons, deficiency in OGN leads to slightly weaker and more compliant tail tendons, with reduced resilience specifically noted at 4 months postnatal, although not evident at 1 or 8 months (Boote *et al*., 2023). Similarly to ASPN, aged equine tendons exhibit significantly lower levels of OGN protein compared to young tendons (Peffers *et al*., 2014).

2.3.2.3 Large aggregating proteoglycans

In addition to abundant SLRPs, extracellular HA- and lectin-binding **large aggregating proteoglycans** called **hyalectans** form dense, hydrated gel-like meshes that enhance tendon viscoelastic properties and provide resistance to tensile forces (Iozzo and Schaefer, 2015). These hyalectans not only contribute to the mechanical resilience of tendons, but also stabilise other matrisomal components (Iozzo and Schaefer, 2015), affecting tendon development, function, and repair. Among those, **aggrecan** (**ACAN**) and **versican** (**VCAN**) are critical, playing distinct yet complementary roles within the tendon ECM.

ACAN is highly expressed and deposited in tendon areas exposed to significant mechanical loading, such as the fibrocartilaginous regions of the enthesis, providing critical resistance to compressive forces (Waggett *et al*., 1998). It is upregulated following injury and in tendinopathies (Berglund *et al*., 2006; Corps *et al*., 2006), supporting tissue organisation and stabilisation during the initial phases of repair by modulating fibroblast differentiation and collagen deposition (Plaas *et al*., 2011; Velasco *et al*., 2011; V. M. Wang *et al*., 2012). However, for optimal healing, aggrecan must be degraded by specific enzymes such as ADAMTS5, facilitated by interactions with the CD44 receptor. Murine studies indicate that disrupting the normal accumulation of ACAN (and other HA-binding entities) by knocking out CD44 can enhance tendon wound healing (H. Ansorge

et al., 2009; Velasco *et al*., 2011), suggesting that while ACAN is beneficial early on, its timely removal is crucial for effective tissue repair and functionality.

Interestingly, excessive ACAN accumulation, as seen in mice lacking ADAMTS5 (Adamts5-/-), results in increased pericellular deposition of ACAN in both the entheseal regions and the main body of tendons (V. M. Wang *et al*., 2012). This accumulation causes irregularities in collagen fibril diameters, impairing the structural integrity of the enthesis and elevating the risk of ruptures (V. M. Wang *et al*., 2012). Interestingly, the effects on positional versus load-bearing tendons vary: positional tendons in the knockout mice display larger cross-sectional areas and reduced tensile modulus, leading to decreased stiffness and potentially less effective function in activities requiring precise movements and stability (V. M. Wang *et al*., 2012). In contrast, load-bearing tendons exhibit increased stiffness, indicated by a higher tensile modulus compared to wild-type tendons (V. M. Wang *et al*., 2012). This increased stiffness reduces the likelihood of deformation under normal loads but could make the tendons more brittle and susceptible to injury under excessive or abnormal strains. Thus, careful regulation of ACAN levels is essential for maintaining proper collagen structure, mechanical properties, and secure tendon attachments to prevent damage and ensure optimal tendon function.

VCAN is the most abundant CS-containing PG in tendons (Yoon and Halper, 2005), primarily localised within the loose connective tissues around blood vessels and the pericellular ECM around tenocytes in the mid-tendon (Bode-Lesniewska *et al*., 1996; Corps *et al*., 2004). It is highly expressed during the perinatal period (Higuchi *et al*., 2021; Snow *et al*., 2005), contributing to the formation of a hydrated, anti-adhesive matrix that facilitates cellular proliferation and migration (Kinsella *et al*., 2004). VCAN is essential for regulating early TGF-β signalling during embryonic and foetal limb morphogenesis, influencing the development of autopodial joints (Choocheep *et al*., 2010). Depletion of VCAN in murine embryonic limb buds (*Prx1*-Cre/*Vcan*$^{flox/flox}$) leads to delayed cartilage development and impaired joint formation (Choocheep *et al*., 2010). Furthermore, its absence affects postnatal joint maturation and strengthening, evidenced by reduced TGF-β accumulation and fewer *Scx*$^{+}$ cells in the joints (Higuchi *et al*., 2021). Like ACAN, VCAN is also upregulated following injury

and in tendinopathic tendons, indicating its importance in tissue repair and pathology (Berglund *et al*., 2006; Corps *et al*., 2004; Scott *et al*., 2008).

Lubricin (**PRG4**) is another significant large aggregating proteoglycan predominantly found in the loose connective tissue regions of tendons (Funakoshi *et al*., 2008; Sun *et al*., 2006, 2015). It plays a crucial role in facilitating tissue gliding and reducing shear and compression forces by providing necessary lubrication in areas exposed to significant stress (Funakoshi *et al*., 2008; Hayashi *et al*., 2013; Kohrs *et al*., 2011; Sun *et al*., 2006, 2015). Unlike other large aggregating proteoglycans, PRG4 expression tends to increase with age, suggesting its growing importance in maintaining tendon function throughout life (Thornton *et al*., 2015). In mice deficient in PRG4 (*Prg4*$^{-/-}$), there is increased friction between the tendon fascicles, leading to rougher tendon surfaces and more abrasive tissue interactions (Reuvers *et al*., 2011). This heightened friction is linked to several structural issues, including abnormal cartilage development and excessive growth of the synovial membrane and cartilage-like tissues (Reuvers *et al*., 2011). These structural changes hinder the tendon's ability to properly relax after stretching, exacerbating stress on bones and muscles under load (Reuvers *et al*., 2011). The presence of PRG4 is therefore essential not only for reducing mechanical stress within the tendon but also for preserving the structural integrity of surrounding tissues.

2.3.2.4 Glycoproteins and Elastin

Besides the proteoglycans, non-collagenous tendon ECM is composed of various **glycoproteins** with essential roles in ECM assembly, signalling regulation, and repair processes. These include **tenascins** (**TNC**, **TNXB**), which are involved in cellular adhesion and migration (Chiquet-Ehrismann and Tucker, 2011; Midwood *et al*., 2016); **periostin** (**POSTN**), which regulates collagen maturation and enhances the biomechanical and healing properties of the tendon (Ackerman *et al*., 2024; Norris *et al*., 2007; Rolnick *et al*., 2022); **tenomodulin** (**TNMD**), crucial for the growth and maintenance of tendon cells and collagen fibrils (Alberton *et al*., 2015; Dex *et al*., 2016; Docheva *et al*., 2005; Shukunami *et al*., 2018); and **thrombospondins** (**THBS1**, **THBS3**, **THBS4**, and **COMP**), which are involved in cellular communication, migration, proliferation,

inflammation, and angiogenesis regulation, as well as ECM assembly and matrix stabilisation (Bornstein *et al*., 2000; Frolova *et al*., 2014; Rosini *et al*., 2018; Subramanian *et al*., 2007; Subramanian and Schilling, 2014). Additionally, elastic fibres composed of **elastin** (**ELN**) and **fibrillins 1** and **2** (**FBN1**, **FBN2**), along with associated molecules like **fibulin 4** (**EFEMP2**), contribute significantly to the elasticity and structural integrity of tendons, helping them resist deformation under mechanical stress (Eekhoff *et al*., 2017; Godinho *et al*., 2017; Markova *et al*., 2016; Svärd *et al*., 2020). These and other previously described proteins are detailed in terms of their functions, expression patterns, and implications in mutant phenotypes in Appendix Table 2, providing a comprehensive overview of their roles in tendon physiology.

2.4 Tendon Development

Tendon development is multifaceted and can be categorised into three groups based on the mesodermal (paraxial and lateral) or ectodermal (neural crest) origins within the vertebrate embryo. These distinct developmental niches result in varied interactions with the surrounding environment and cells, introducing diversity in the processes governing tendon development. Comparative studies of tendon formation across species, with a focus on limb tendons, have been instrumental in understanding these intricacies. While modern limb development studies primarily draw from embryonic chick, mouse, fly, and zebrafish models, information on human limb development, and particularly tendon development, remains limited. Nonetheless, there are similarities in the roles of signalling networks involved in limb bud development among different vertebrates. Recent publications, such as those by B. Zhang *et al.* (2023), contribute valuable insights to these processes. Here, I provide a summary of the current knowledge, with a primary focus on findings from chick and mouse studies.

2.4.1 Vertebrate limb development

In humans, the zygote's cleavage initiates the process of embryonic development, setting the stage for cell subdivision into three germ layers: endoderm, mesoderm, and ectoderm. As development progresses, the cells within the mesoderm differentiate further into lateral plate, intermediate, and

paraxial mesoderm as well as chordamesoderm, ultimately giving rise to the musculoskeletal structures as well as nerves, blood, and endothelial cells.

At the end of the 4th week, when the body axes are established and the neural tube formation is complete, limb buds begin to appear as localised swellings on the lateral sides of the embryo. The separation of cells from the somatopleure epithelium, which overlays the lateral plate mesoderm, occurs via **epithelial-to-mesenchymal transition** and leads to the creation of limb mesenchyme during its budding phase (Gros and Tabin, 2014) (Figure 10A,D). This process occurs through complex signalling events including retinoic acid (RA) gradients that prompt the activation of TBX transcription factors, and the establishment of mesoderm with *Hox* genes and β-catenin/TCF/LEF signalling (Nishimoto *et al*., 2015). The positive feedback loop between FGF10, regulated by TBX transcription factors and released by undifferentiated mesenchymal cells (Nishimoto *et al*., 2015), and FGF8, released by ectodermal epithelial cells at the tip of the growing limb bud, leads to the initiation of the **apical ectodermal ridge (AER)** – a thickened region of ectoderm crucial for promoting limb elongation along the proximodistal axis (Crossley *et al*., 1996; Jin *et al*., 2019; Ohuchi *et al*., 1997; Vogel *et al*., 1996) (Figure 10B). During this phase, cells persist in an undifferentiated state, focusing on migration and proliferation (Gros and Tabin, 2014; Jin *et al*., 2019). Further signalling by FGFs and other factors leads to the establishment of specialised zones within the limb bud, leading to the establishment of additional morphogenetic gradients of Sonic hedgehog (SHH) controlling anterior/posterior patterning, and WNTs and BMPs controlling dorsal/ventral patterning, differentiation, and termination of the limb development (Geetha-Loganathan *et al*., 2008; Logan *et al*., 1997; Riddle *et al*., 1993; Tickle and Towers, 2017) (Figure 10C,E).

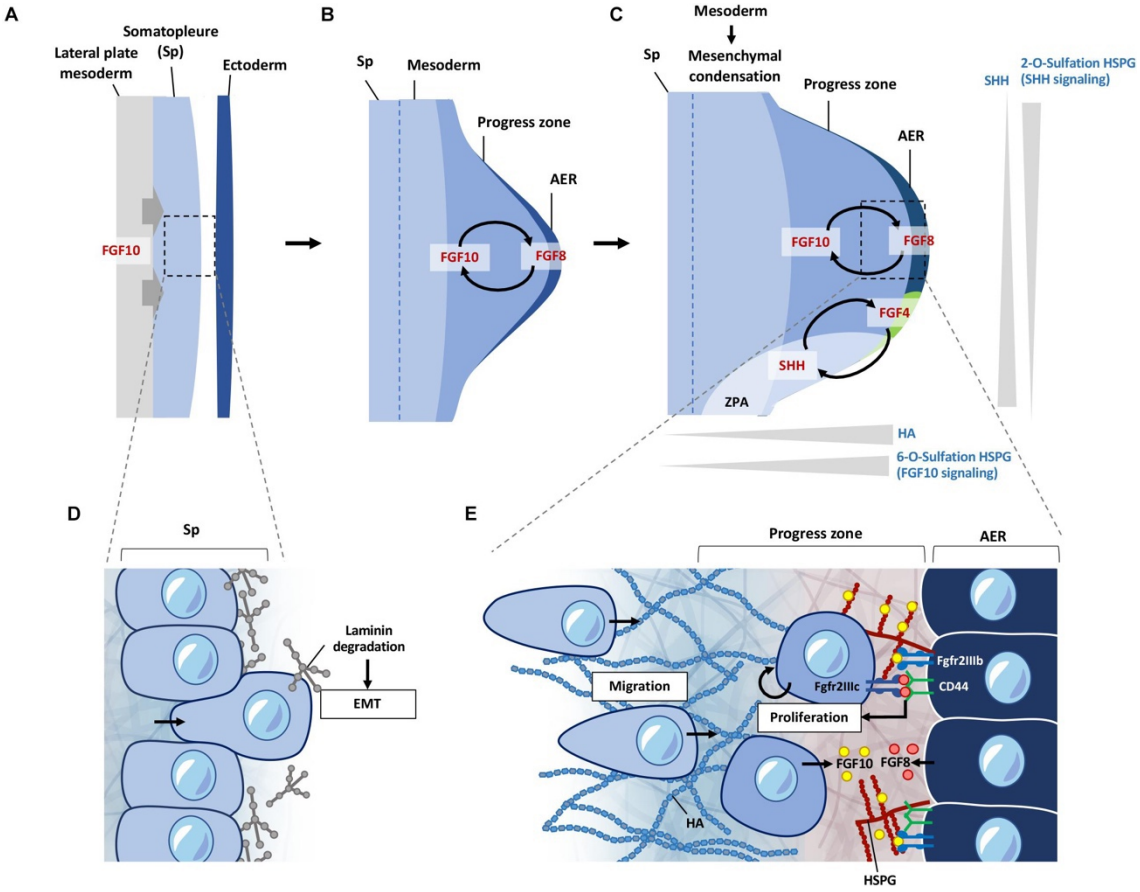


Figure 10. Schematic of early embryonic limb bud development. (A) *Signaling by FGF10 from the lateral plate mesoderm induces epithelial-mesenchymal transition (EMT) in somatopleure (Sp) epithelial cells, directing them toward the ectoderm.* ***(B)*** *The release of FGF8 from the ectoderm facilitates the formation of the apical ectodermal ridge (AER) and activates cell proliferation and migration within the progress zone through a positive feedback mechanism.* ***(C)*** *Various gradients are created that determine limb positioning and polarity, controlled by the sulfation patterns of heparan sulfate proteoglycan (HSPG) which affect the diffusion of FGF and SHH signals.* ***(D)*** *Sp cells migrate to form the limb bud mesenchyme following laminin degradation during EMT.* ***(E)*** *Detailed view of the mechanisms governing FGF feedback loop establishment and cell proliferation. Briefly, FGF10 from the limb mesenchyme attaches to 6-O sulfated HSPG and interacts with Fgfr2b receptors on AER cells, which then produce FGF8. This FGF8, bound by CD44, is presented to Fgfr2c receptors in the progress zone, stimulating cell proliferation. Additionally, FGF8 boosts FGF10 synthesis, sustaining the FGF10-FGF8 feedback loop. Hyaluronic acid (HA), prevalent in the progress zone but absent from the AER, diminishes during mesenchymal condensation. Reproduced from Ma et al. (2020) (CC BY 4.0).*

The ECM plays an important role in directing limb dub development by directly influencing presentation and activation of signalling molecules, as well as cell interactions and behaviours (reviewed in Ma *et al*., 2020). This is thought to occur through the establishment of a hydrated environment that effectively isolates cells from close contacts with each other and from structural barriers, thereby offering space for morphogenetic changes (Li *et al*., 2007; Toole, 2001). Kosher and Savage (1981) demonstrated a progressive increase in HA content

from the proximal to distal axis, with a corresponding correlation in the cellular differentiation state observed along this axis. Additionally, differential sulfation patterns of **heparan sulfate proteoglycans (HSPGs)** have been shown to control the presentation and activity of FGF and SHH signalling molecules (Figure 10C). Other ECM components such as **laminin** (e.g., **LAMA1-5, LAMB1-4, LAMC1-3**), **vimentin** (**VIM**) (Gros and Tabin, 2014), and **fibronectin** (**FN**) (Zhu *et al*., 2020), have also been shown to be compartmentalised, further supporting the necessity of ECM for correct limb bud development.

2.4.2 Limb musculoskeletal tissue development

In mice, limb buds begin to appear at embryonic day (E) 9-9.5, with forelimbs preceding hindlimbs by half a day (Huang, 2017) (Figure 11). As they outgrow in the proximodistal direction, the stylopod (arm/thigh), zeugopod (forearm/shank) and autopod (wrist/foot) segments are formed at E10, E11, and E11.5, respectively (Huang, 2017). The development of skeletal connective tissues and muscles is initiated in parallel to this segment formation. Mesenchyme cells of the lateral plate give rise to prechondrogenic (E10) and tendon (E10.5) progenitors (Akiyama *et al*., 2005; Bi *et al*., 1999; Carlson, 2018; Schweitzer *et al*., 2001), while myogenic precursors arise in the paraxial mesoderm of the somites around E8.5-9.5 and migrate into the limb bud by E10.5 (Murphy and Kardon, 2011) (Figure 11). Prechondrogenic progenitors condense, differentiate, and give rise to cartilage templates (E12.5) before forming first embryonic bones (E14.5), some of which will then be supplemented by bone eminences generated by a separate progenitor population (E14.5) (Akiyama *et al*., 2005; Blitz *et al*., 2013; Huang, 2017) (Figure 11). Concurrently, myogenic precursor cells differentiate to form all initial limb muscles by E14.5 (Edom-Vovard *et al*., 2002; Huang, 2017). Finally, tendon progenitors differentiate to form tendons that connect muscles to bones or bone eminences (E14.5-16.5). Full tendon and skeletal patterning is then complete at around E16.5 (Huang, 2017) (Figure 11).

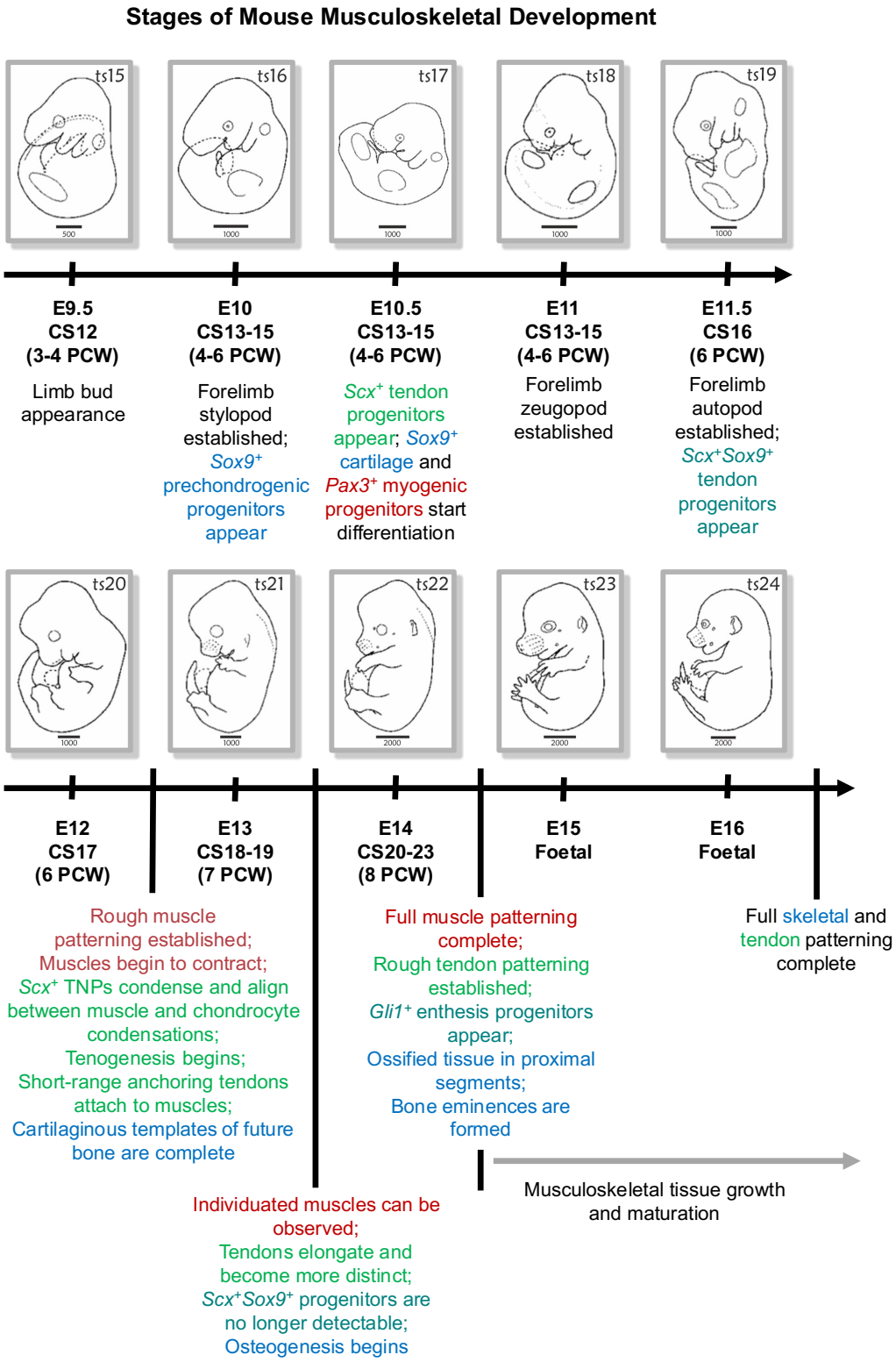


Figure 11. Timeline summary of mouse embryonic and early foetal musculoskeletal tissue development. *This figure summarises key stages for the development of tendons and their attachment structures, with each timepoint indicated by embryonic day (E), the approximated corresponding human Carnegie Stage (CS), and the equivalent human post-conception weeks (pcw). Size bars represent dimensions in microns. Images of mouse Theiler stages (ts) are adapted from the EMAP eMouse Atlas Project (http://www.emouseatlas.org), Richardson et al. (2014) (CC BY 3.0).*

Tendon morphogenesis occurs in close spatial and temporal association with muscle formation and development (Edom-Vovard *et al*., 2002; Kardon, 1998; Kieny and Chevallier, 1979). Initially, tendon and muscle progenitor cell pools overlap in the dorsoventral regions of E10-11.5 early limb buds (Schweitzer *et al*., 2001). As myogenic progenitors separate and aggregate into dorsal and ventral (extensor and flexor) muscle masses, subsequent rounds of splitting occur, forming pairs of stylopod, zeugopod, and autopod muscle groups. These groups then divide and develop into individual limb muscles by E14.5 (Carlson, 2018; Edom-Vovard *et al*., 2002; Huang, 2017). As myogenic precursors aggregate and split, tendon precursors migrate to form proximal, intermediate, and distal pairs of condensed tendon primordia in-between the different segment muscle groups (Edom-Vovard *et al*., 2002; Edom-Vovard and Duprez, 2004; Kardon, 1998; Schweitzer *et al*., 2001).

Despite the common space shared between muscle and tendon precursors in the early stages of development, limb tendon development initiation is independent of muscles (Brent *et al*., 2005; Edom-Vovard and Duprez, 2004; Kardon, 1998; Schweitzer *et al*., 2001). However, they can be required in later developmental stages (after E12.5 in mice) for full tendon differentiation and maturation, especially in proximal and intermediate tendons (Charvet *et al*., 2012; Edom-Vovard *et al*., 2002; Kardon, 1998; Kieny and Chevallier, 1979; Schweitzer *et al*., 2001). For example, avian and mouse embryo studies show that stylopod and zeugopod tendons can start to form in the absence of muscle-producing somites, however their morphogenesis is never complete as the rudimentary tendons eventually degrade (Edom-Vovard *et al*., 2002; Havis *et al*., 2014; Kardon, 1998; Schweitzer *et al*., 2001). On the other hand, distal autopod tendons complete their morphogenesis even in the absence of muscles (Edom-Vovard *et al*., 2002; Havis *et al*., 2014; Kardon, 1998), though they appear smaller than normal and will never fully mature (Huang *et al*., 2015b; Kardon, 1998; Kieny and Chevallier, 1979; Oldfield and Evans, 2003). Thus, proximal and intermediate tendons are regulated in a manner different from the distal autopod tendons. Interestingly, the former are likely initiated by the signals coming from the AER (Schweitzer *et al*., 2001), while the latter rely on signals from cartilage for their induction in the early stages of development (Huang, 2017; Hurle *et al*., 1990).

2.4.3 Stages of embryonic tendon morphogenesis

Tendon morphogenesis within developing limbs can be broadly categorised into four stages: initiation, condensation, elongation, and maturation. Tendon development begins with the commitment to the tendon lineage of the superficial proximomedial limb mesenchymal cells within the limb bud at around mouse E10.5-11 (Schweitzer *et al*., 2001). The signalling events leading to tendon fate induction are still not fully understood; nevertheless, studies have shown that (1) the ectoderm is necessary for induction of tendon cell fate (Schweitzer *et al*., 2001), (2) repression by mesenchymal BMP gradients assures that only the proximomedial cells actually assume this cell fate (Schweitzer *et al*., 2001), and (3) FGF signalling is likely to be involved (Tozer and Duprez, 2005).

Upon commitment to the tendon cell fate, cells begin to express high levels of ***scleraxis* (*SCX*)** (Schweitzer *et al*., 2001), which encodes a bHLH transcription factor that has been shown to effect tendon cell differentiation and ECM deposition through transcriptional regulation of genes important in tendon development such as ***tenomodulin*** (***TNDM***) and **type I collagens** (***COL1A1*, *COL1A2***) (Docheva *et al*., 2005; Murchison *et al*., 2007; Shukunami *et al*., 2006) (Figure 11). Besides ECM-related regulation, SCX is also essential for the condensation, differentiation, and recruitment of cells required for elongation of long force-transmitting and intermuscular tendons (Huang *et al*., 2019; Murchison *et al*., 2007). At around E11.5, a distinct population of *SCX*$^{+}$ cells expressing chondrogenic marker ***SOX9*** is observed in the region of the future tendon-bone attachment unit, acting as a population of progenitors destined to give rise to the bone eminences connecting tendons and long bones (Blitz *et al*., 2013; Soeda *et al*., 2010; Sugimoto *et al*., 2013) (Figure 11). The commitment of *SCX*$^{+}$ tendon and *SCX*$^{+}$*SOX9*$^{+}$ bone eminence progenitors is maintained through TGF-β signalling pathways, with the latter additionally effected by SCX/BMP signalling (Blitz *et al*., 2013, 2009; Pryce *et al*., 2009; Zelzer *et al*., 2014).

In parallel with limb bud elongation, at ~E12.5, proximal tendon progenitors begin to condense, aggregating into more organised, cohesive structures positioned between the differentiating myocyte and chondrocyte condensations

(Chaplin and Greenlee, 1975; Richardson *et al*., 2007). This process facilitates efficient cell communication, coordinated gene expression, and the synchronised deposition of ECM that is necessary for cell differentiation and tendon morphogenesis. Condensation is driven by signalling pathways that regulate cell-to-cell interactions (e.g., β-catenin), fostering tendon progenitor adhesions via connexin and cadherin junctions, including cadherin-11 (CDH11), N-cadherin (CDH2), connexin-32 (GJB1), and -43 (GJA1) (Richardson *et al*., 2007; Theodossiou *et al*., 2020). Concurrently, morphological transformations occur as initially round tenoblasts adopt a spindle-shaped form, connecting to each other via cell-to-cell junctions in a highly aligned, organised manner. This microenvironment provides a crucial foundation for further differentiation, with cells initiating the expression of ***mohawk* (*MKX*)** – a homeobox transcription factor regulating type I collagens required for tendon growth and maturation (Anderson *et al*., 2006; Ito *et al*., 2010; Liu *et al*., 2010). Shortly, the initial tendon-characteristic ECM composed of short, immature, and disorganised small-diameter type III and I collagen fibrils starts to be deposited (Edom-Vovard and Duprez, 2004; Kalson *et al*., 2015; Marturano *et al*., 2013; Ros *et al*., 1995). Other ECM components, such as proteoglycans (e.g., DCN, BGN, FMOD, LUM) and glycoproteins (e.g., TNMD, COMP, TNC), also begin to be synthesised and assembled (Lorda-Diez *et al*., 2014; Marturano *et al*., 2013; Chavaunne T Thorpe *et al*., 2013). Finally, differentiating tenocytes begin to express transcription factors ***early growth response 1* and *2* (*EGR1*, *EGR2*)** (Ito *et al*., 2010; Lejard *et al*., 2011; Liu *et al*., 2010; Murchison *et al*., 2007; Shukunami *et al*., 2006).

2.4.4 Embryonic tendon attachment

It is also around E12.5 that the developing muscles begin to spontaneously contract, providing novel mechanical and molecular cues to the tendon and the surrounding ECM that are necessary for further growth, elongation, and attachment to bones and muscles (Felsenthal and Zelzer, 2017; Schwartz *et al*., 2013; Subramanian *et al*., 2018). Specifically, the mechanical force generated by muscle contractions induces TGF-β-mediated signalling within *SCX*$^{+}$ tenocytes, prompting the extension of projections along the force axis towards the contracting muscle. Through close interactions and signalling between

muscle and tendon progenitors, a dynamic crosstalk ensues, instigating changes in ECM transcription within both cell populations and guiding the initial formation of the MTJ (Subramanian *et al*., 2018), including the expression of MTJ-specific collagen XXII (Lipp *et al*., 2023). Therefore, at around E12.5-13.5, short-range (i.e. single segment) tendons form first attachments to the developing muscle and begin to recruit new *SCX*$^{+}$ mesenchymal progenitors to elongate, eventually forming the long-range multi-segment tendons (Huang *et al*., 2015b; Murchison *et al*., 2007; Subramanian *et al*., 2018) (Figure 11). At this point, the MTJ is populated by both somitic ***PAX3***-lineage and lateral plate mesoderm *OSR1*-lineage cells expressing myocyte markers *PAX7* and *MYOD* (*myogenic differentiation*), as well as *SCX*$^{+}$ tenocytes (Figure 11). Later, at E14.5-15.5, subsets of *SCX*-lineage cells also contribute to the *PAX7*$^{+}$*MYOD*$^{+}$ populations, highlighting their ability to transdifferentiate from tenogenic to myogenic progenitors (Esteves de Lima *et al*., 2021).

Further, at E12.5, the cartilaginous templates of future bones consisting of differentiated *SOX9*$^{+}$ chondroprogenitors are formed. At this stage, populations of undifferentiated cells expressing *SCX, SOX9,* and *GDF5 (growth differentiation factor 5)* position next to them (Dyment *et al*., 2015). Shortly following muscle attachment, this distinct population of *SCX*$^{+}$*SOX9*$^{+}$*GDF5*$^{+}$ cells initiates the formation of the tendon-bone attachment through formation of fibrocartilaginous bone eminences (Blitz *et al*., 2013). Here, SCX drives the expression of *BMP4*, which, along with other potential yet unknown BMP ligands and pathways, is required for bone eminence initiation (Blitz *et al*., 2009; Zelzer *et al*., 2014). These cells regulate both tenogenic and chondrogenic programmes through genetic enhancers shared with tenocytes and chondrocytes (Kult *et al*., 2021). Eventually, they differentiate into separate populations of *SCX*$^{+}$*SOX9*$^{-}$ fibroblasts on the tendon side and *SCX*$^{-}$*SOX9*$^{+}$ chondrocytes on the cartilage side at the tendon-bone interface, thus forming the future fibrocartilaginous zones of the enthesis (Blitz *et al*., 2013; Dyment *et al*., 2015; Eyal *et al*., 2019; Fang *et al*., 2022a; Schwartz *et al*., 2015). This differentiation is controlled by Krüppel-like factors KLF2 and KLF4, whose inhibition impairs the process (Kult *et al*., 2021).

Further bone attachment site development is influenced by its interaction with the adjacent bone. In **stationary entheses** that remain fixed in their position

relative to the bone, *SOX9*$^{+}$ chondroprogenitors begin to express *GLI1* (Felsenthal *et al*., 2018). Conversely, in **migratory entheses** that transition along the bone during growth, a separate population of *GLI1*$^{+}$ progenitors localises alongside *SOX9*$^{+}$ chondroprogenitors, ultimately replacing them during postnatal maturation (Felsenthal *et al*., 2018). The onset of *GLI1* expression within the enthesis occurs around E14.5 and is regulated by Sonic Hedgehog (HH) signalling, subsequently transitioning to Indian HH signalling after birth (Fang *et al*., 2022a; Felsenthal *et al*., 2018) (Figure 11). *GLI1* ablation or HH signalling downregulation leads to decreased production of enthesis fibrocartilaginous matrix proteins, causing impaired postnatal mineralisation, thus highlighting *GLI1's* role in initiating pathways that form the fibrocartilaginous interface (Breidenbach *et al*., 2015; Liu *et al*., 2013; Schwartz *et al*., 2015). The MTJ maturation and completion of the transition zone are facilitated by the onset of stronger muscle loading after birth.

2.4.5 Tendon foetal and postnatal maturation

At E14.5-15.5, once an immature tendon structure is established and the initial muscle and bone attachments are formed, foetal development ensues and the tendon DNA-to-dry mass ratio declines, coinciding with the rapid doubling of tissue dimensions in the subsequent days (Marturano *et al*., 2013; Schiele *et al*., 2015; Scott and Hughes, 1986). This phase is characterised by increased synthesis and aggregation of tendon collagen fibrils, which are assembled within **fibripositors** – specialised actin-rich membranous compartments at the cell surface that are used prenatally for collagen production (Birk and Trelstad, 1986; Canty and Kadler, 2005; Humphries *et al*., 2008; Richardson *et al*., 2007). The fibrils are directed from the Golgi to the ECM through these plasma membrane channels, with intracellular actin filaments guiding their parallel alignment and deposition into uniform bundles within spaces between the tightly connected cells (Canty *et al*., 2004; Canty and Kadler, 2005) (Figure 12). This process is dependent on the local mechanobiological environment, requiring tension for proper formation (Kapacee *et al*., 2008).

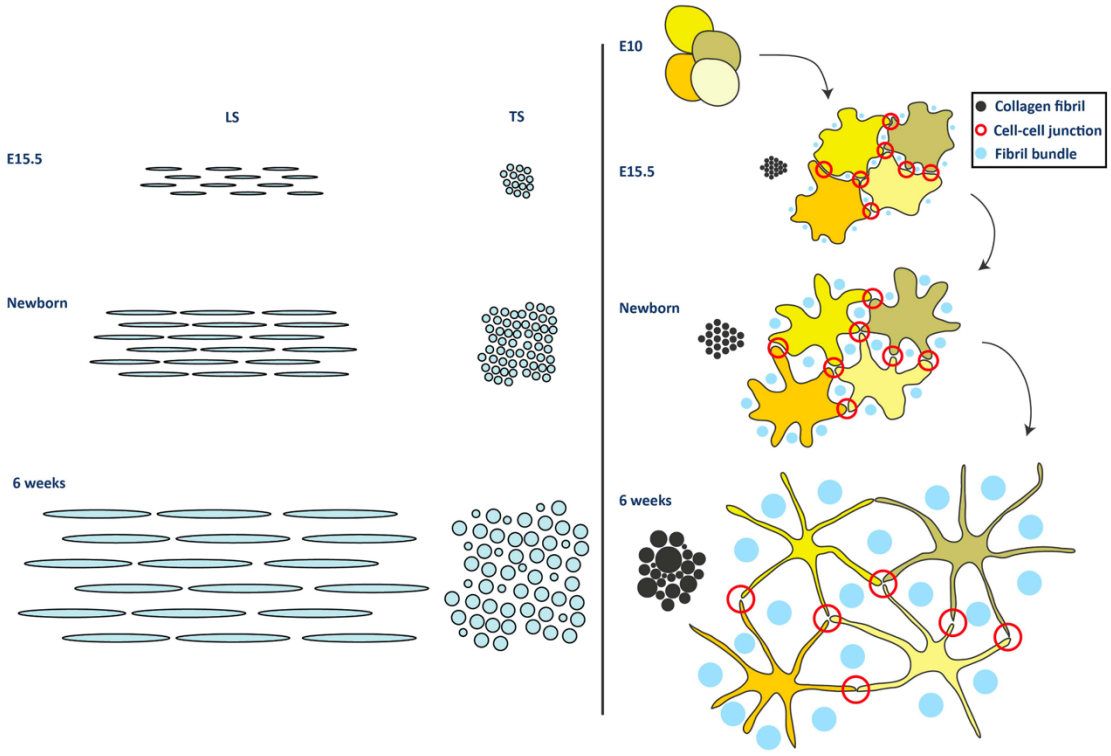


Figure 12. Schematic diagrams of tendon ECM development: collagen fibril and cellular morphology changes over time. Left panel *shows the evolution of collagen fibrils in both longitudinal and transverse section (LS and TS, respectively) views at embryonic day (E) 15.5, newborn, and 6 weeks postnatal stages. During early foetal development, ECM fibril synthesis and aggregation are accelerated, leading to increases in fibril numbers, diameters, and lengths. Following birth, fibrils expand by increasing their diameters and lengths, but not numbers. Fibril diameter heterogeneity can be observed at 6 weeks post-birth.* ***Right panel*** *shows cellular and fibril transformations at the same developmental stages, highlighting the transition from rounded progenitors at E10 to specialised, stellate interconnected tendon fibroblasts, which organise collagen fibril bundles within the spaces formed by cell-cell adhesions. Reproduced from Kalson et al. (2015) (CC BY 4.0).*

Simultaneously, the collagens adopt an undulating crimp-like pattern (Kalson *et al*., 2015; Shah *et al*., 1982). While the precise mechanisms of crimp formation remain incompletely understood, tension-induced tendon cell contraction and pulling on the IFM fibre bundles was shown to initiate and maintain this pattern *in vitro* (Herchenhan *et al*., 2012; Lavagnino *et al*., 2017). Additionally, studies have shown that actin filaments within tendon progenitors also formed a crimp pattern (Herchenhan *et al*., 2012), suggesting a possible interaction between intracellular actin and collagen crimping.

The synthesis and organisation of collagen fibrils critically depend on various collagen types, including fibrillar V, VI, XI and FACIT XII and XIV, which are integral to the regulation of fibrillogenesis and the assembly and organisation of

fibrils into suprastructures (see section 2.3.1). Once synthesised, collagen fibrils are cross-linked via LOX-catalysed reactions, which enhance their tensile strength, resilience, elastic modulus, and overall mechanical properties (Marturano *et al*., 2014, 2013). During development, an increase in LOX levels and activity corresponds with heightened foetal movement, indicating a functional adaptation (Pan *et al*., 2018). Concurrently, there is a shift in the ratio of collagen types III to I, which decreases within the fascicles but increases in the endotenon and outer sheath regions (Birk and Mayne, 1997; Bland and Ashhurst, 1997; Buckley *et al*., 2013; Kuo *et al*., 2008). These adjustments enhance the mechanical integrity of the tissue, evident by improved tensile strength and elastic modulus, which facilitate better ambulation (Edom-Vovard and Duprez, 2004; McBride *et al*., 1988, 1985; Ros *et al*., 1995; Scott and Hughes, 1986; Zhang *et al*., 2005).

At birth, collagen fibrils appear small and uniform in diameter (Strocchi *et al*., 1991), but as the tissue grows and endures increasing mechanical loads, these fibrils expand both linearly and laterally through the aggregation and fusion of intermediate fibrils (Ezura *et al*., 2000; Provenzano and Vanderby, 2006) (Figure 12). This significant maturation phase generally commences around P4-10, coinciding with the onset of crawling and walking (Steffen *et al*., 2023a). It is characterised by dynamic cellular responses to mechanical stimuli, resulting in altered gene expression and subsequent modifications in the ECM composition. For example, SLRPs such as DCN and LUM structure the early postnatal tendon ECM, ensuring proper fibril alignment and spacing. However, after about P10, FMOD replaces the role of LUM, promoting the fusion and growth of collagen fibrils into mature, large-diameter structures essential for tendon strength (section 2.3.2; Ezura *et al.*, 2000) (Figure 13). Consequently, fibril elongation accelerates, leading to a heterogeneous mix of small and larger fibrils (Ezura *et al*., 2000) (Figures Figure 12, Figure 13). By P30, tendons triple in their bodyweight (Ansorge *et al*., 2011) and contain three distinct fibril populations: small initial fibril intermediates, growing fibrils, and mature, long, large-diameter fibrils (Ezura *et al*., 2000; Zhang *et al*., 2006) (Figure 13). In the outer sheaths rich in collagen III, the fibril diameters remain comparatively small (Birk and Mayne, 1997).

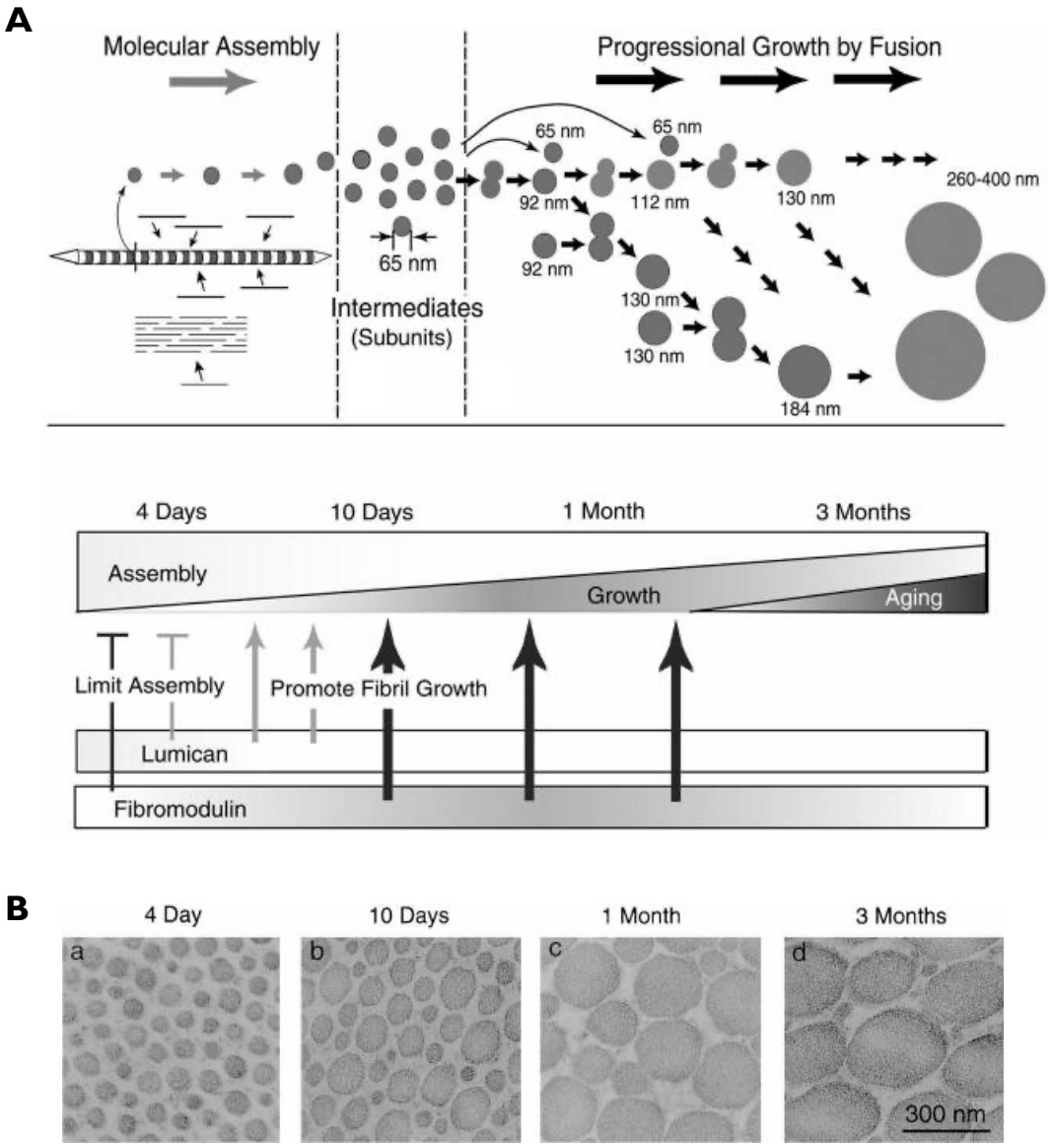


Figure 13. Schematic diagram and transmission electron micrographs of fibril expansion in murine postnatal tendon development. (A) *Schematic diagram shows the stages of collagen fibril assembly and growth at various postnatal timepoints (4 days, 10 days, 1 month, and 3 months). It also shows the expression patterns of lumican and fibromodulin genes, which regulate fibril development by either constraining or facilitating fibril growth.* ***(B)*** *Microscopy images show transverse sections of wild type mouse flexor tendons at the same timepoints. Adapted from Ezura et al., (2000) (CC BY 4.0).*

As more significant mechanical stresses and physical activity begin to be introduced, the tenocytes sense and respond by adapting their gene expression patterns and changing their cytoskeletal organisation and ECM composition (Subramanian and Schilling, 2015). Thus, during childhood, tendons expand and significantly increase their collagen fibril diameters, mechanical load capacity, and elastic modulus (Strocchi *et al*., 1991; Zhang *et al*., 2005). By late adolescence, the tendons appear mature, with undulating collagen fibrils of

large but variable diameters adapted for mechanical loads (Strocchi *et al*., 1991). With advanced age, however, the fibrils lose their undulating appearance, decrease in average diameter and density, but increase in concentration (Strocchi *et al*., 1991).

The cellular landscape within the tendon also undergoes profound alterations from developing to aged stages. Embryonic and early postnatal tendons (<P21 in mice) are significantly more cellular than adult tendons, with high cell density facilitating rapid growth and ECM expansion (Marturano *et al*., 2013; Meller *et al*., 2009). As tendons mature, tendon cell density decreases with the increasing ECM volume and mechanical demands (Grinstein *et al*., 2019; Kalson *et al*., 2015; Marturano *et al*., 2013). During this maturation, tenocytes transition from a rounded morphology to an elongated, stellate shape, aligning along developing fibres and maintaining early cellular connections (Kalson *et al*., 2015; Schiele *et al*., 2015; Theodossiou and Schiele, 2019).

While cells proliferate rapidly during development and the early postnatal stages, this activity declines sharply as tendon collagen fibrils begin to expand and mature (~P21-P28 in mice) (Grinstein *et al*., 2019; Steffen *et al*., 2023a). Subsequently, only a small percentage of cells capable of division remains, which correlates with the dwindling regenerative capacity of the tendon (Grinstein *et al*., 2019). During this period, healing responses, though still effective, become less robust and begin to resemble those seen in adult tissue; for example, a three-day delay in cell proliferation and ECM component production begins to be observed (Ansorge *et al*., 2012).

As tendons age, tendon cells exhibit reduced metabolic and synthetic activity, their nuclei enlarge, and their cytoplasmic projections shorten, diminishing their ability to communicate and coordinate ECM maintenance (Almekinders and Deol, 1999; Ippolito *et al*., 1980; Kannus *et al*., 2005; Nakagawa *et al*., 1994; Strocchi *et al*., 1991). This decline is marked by increased stiffness, diminished elasticity (Delabastita *et al*., 2019), and a significant decrease in the proliferative potential and accumulation of senescence markers in tendon cells, including TSPCs, which are crucial for maintaining tissue homeostasis (Kohler *et al*., 2013; Lui and Wong, 2020; Peffers *et al*., 2015).

2.4.6 Foetal and postnatal maturation of the enthesis and the MTJ

During foetal development, *SOX9*$^{+}$ chondrocytes mature into unmineralised fibrochondrocytes, while enthesis progenitors – marked by *SCX*, *SOX9*, and *GDF5* – proliferate and synthesise a scaffold consisting of ACAN, BGN, and collagens I and II that attaches to the underlying primary cartilage (Dyment *et al*., 2015). The presence of these progenitor cells declines after birth, and by murine P8, fibrocartilage *GLI1*-lineage cells become predominant (Dyment *et al*., 2015; Felsenthal *et al*., 2018). In stationary entheses, this transition involves *SOX9*$^{+}$ enthesis progenitors developing into *GLI1*$^{+}$ cells (Felsenthal *et al*., 2018), while in migrating entheses, a separate population of *GLI1*$^{+}$ progenitors (initially co-localised with enthesis progenitors during embryonic development) gradually replaces them as the enthesis moves along the developing bone (Felsenthal *et al*., 2018).

Postnatal maturation of the tendon enthesis involves several key cellular and molecular events. *GLI1*$^{+}$ cells initially form unmineralised fibrocartilage, which begins to mineralise approximately 1-2.5 weeks after birth in mice, depending on the tendon type (Blitz *et al*., 2009; Dyment *et al*., 2015; Schwartz *et al*., 2015). This initial mineralisation is driven by biochemical signals, with Indian Hedgehog (IHH) expressed by chondrocytes playing a critical role. (Blitz *et al*., 2009; Schwartz *et al*., 2015). IHH induces the expression of *collagen type X* and *alkaline phosphatase* (*ALP*) in cells at the base of the enthesis (Amano *et al*., 2014), leading to the replacement of the flexible primordial ECM with a more rigid, stable matrix characteristic of the enthesis.

As mineralisation advances from the cartilage toward the tendon, HH signalling prompts *GLI1*$^{+}$ cells to integrate into the developing fibrocartilage (Dyment *et al*., 2015). By late postnatal development (P56 in mice), cells within the mineralised fibrocartilage cease to express GLI1 and no longer respond to HH signals. In contrast, non-mineralised regions continue to harbour HH-responsive cells that maintain GLI1 expression, indicating a transition towards a more stable and mature fibrocartilaginous structure (Dyment *et al*., 2015; Felsenthal *et al*., 2018; Schwartz *et al*., 2015). This change is influenced significantly by muscle loading, which not only supports mineralisation, but also maintains the integrity of mineralised fibrocartilage by reducing the activity of Indian

Hedgehog (IHH) and its responsive cells from P14 onwards (Schwartz *et al*., 2015). This regulatory mechanism prevents the remodelling of tissue into bone, underscoring the importance of diminishing GLI1 expression in mineralised areas to maintain the structural stability and prevent unnecessary bone formation. Consequently, reduced muscle load during early postnatal development leads to delayed enthesis maturation, increased osteoclast activity, and consequent resorption and remodelling of the mineralised bone and fibrocartilage surfaces (Schwartz *et al*., 2015, 2013; Thomopoulos *et al*., 2007). The overall patterning of the enthesis is further regulated by other factors, including GLI3, TGF-β, BMP, and FGF (reviewed in Killian, 2022), while regulatory genes such as *Pbx1*, *Pbx2*, *Hoxa11*, and *Hoxd11* act as proximal and distal regulators in mice (Eyal *et al*., 2019).

Similarly to the enthesis, the maturation of the MTJ exhibits significant structural and functional adaptations and is influenced by muscle loading. At birth (P0), the murine MTJ is composed of a small population of previously identified embryonic bi-fated cells co-expressing fibrogenic (e.g., *PDGFRα*, *Osr1*, *Col1a1*, *Dcn*) and myogenic (e.g., *Pax7*, *Myf5*, *MyoD1*, *Cdh15*) markers, alongside more differentiated populations of *Tcf4*$^{+}$ muscle connective tissue fibroblasts, *Ly6a*$^{+}$ fibro-adipogenic precursors, and *MyoG*$^{+}$ myocytes (Yaseen *et al*., 2021). During early postnatal development, mechanical forces generated by growing muscle fibres induce reciprocal signalling with tendons, consolidating their connection. By P21, the MTJ undergoes notable morphological changes, particularly in the distribution and frequency of COL22A1 fibres, which increase and form smaller invaginations to enhance the junction's surface area and mechanical stability (Lipp *et al*., 2023). Both static growth and cyclic loading are crucial for MTJ maturation and maintenance throughout adulthood, influencing the expression of growth factors and signalling molecules necessary for the junction's strength and functionality (Lipp *et al*., 2023; Valdivia *et al*., 2017).

2.4.7 Key developmental regulators

Tendon development is controlled through the action of several interrelated molecular signalling pathways. To date, it is believed that FGF and TGF-β families are the main sources of signalling molecules that regulate the expression of factors involved in tendon development initiation, organisation,

differentiation, and maintenance. For details on those, the reader is referred to excellent reviews by Huang, Lu and Schweitzer (2015), Subramanian and Schilling (2015), Huang (2017), Nakamichi and Asahara (2021), and He *et al.* (2022).

2.5 Tendon Injury Repair

Tendon development and repair involve common signalling pathways and cellular processes. Despite these shared mechanisms, the outcomes diverge significantly. During development, the differentiation of progenitor cells is tightly regulated, resulting in a structured ECM that endows tendons with their strength, flexibility, and resilience. In contrast, adult tendon repair often culminates in the formation of adhesions and scar-like tissue that lacks the original tendon's precise organisation, leading to diminished strength and mechanical properties (Bruns *et al*., 2000). Crucially, perinatal tendons repair faster and with minimal scarring, demonstrating a regenerative capacity that is absent in adult tendons (Beredjiklian *et al*., 2003; Dyment and Galloway, 2015; Favata *et al*., 2006; He *et al*., 2022; Howell *et al*., 2021; Ribitsch *et al*., 2021). For this reason, considerable research focuses on understanding the drivers of regenerative healing during tendon development, aiming to replicate these outcomes in injured adult tendons.

2.5.1 Stages of tendon repair

Tendon repair generally adheres to the standard wound healing framework, which encompasses three overlapping phases: the initial inflammatory phase, the fibroblastic proliferative phase, and the long remodelling phase (Figure 14). The duration and specific processes within these phases vary, influenced by the unique anatomy and physiology of each tendon (Killian *et al*., 2012; Thomopoulos *et al*., 2015).

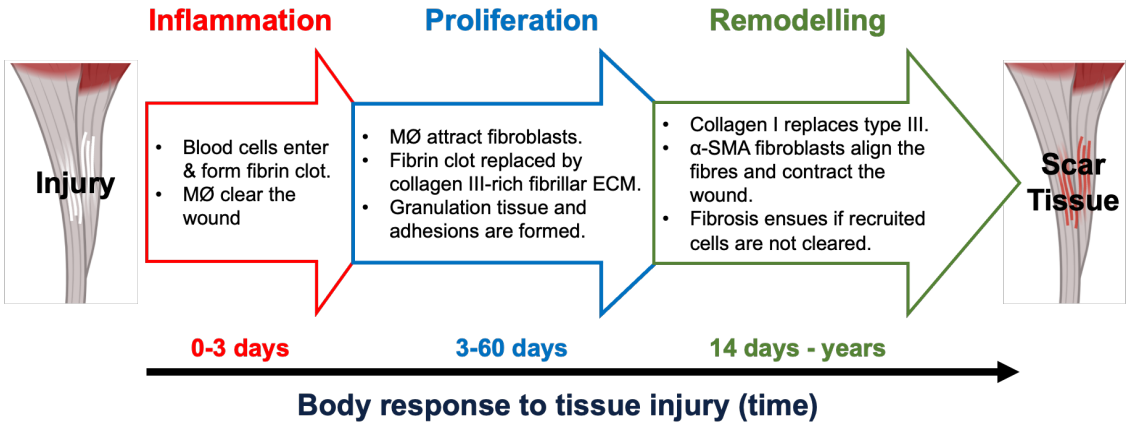


Figure 14. Stages of adult tendon repair. *Timelines for the different stages are given for mouse tendon repair. MØ denote macrophages. Tendon icons created with BioRender.com.*

Initially, injury leads to increased vascular permeability, resulting in an influx of blood cells at the wound site. Activated platelets deposit a provisional ECM scaffold which contains various proteoglycans alongside fibrinogens and fibronectins, known as a **fibrin clot** (Pakshir and Hinz, 2018; Voleti *et al*., 2012). This clot stabilises the wound and supports cell movement and immobilisation of signalling molecules essential for the subsequent healing phases (Pakshir and Hinz, 2018). Inflammatory cells, including mast cells, neutrophils, and macrophages, also converge on the site, securing it against pathogens and clearing necrotic debris. Here, macrophages play an essential role, secreting growth factors and chemokines that attract and mobilise local fibroblasts and vascular cells (Howell *et al*., 2021; Pakshir and Hinz, 2018).

During the proliferative phase, which begins several days post-injury, these cells multiply and start replacing the fibrin clot with a collagen type III-rich ECM, simultaneously forming new blood vessels. This results in the formation of a fibrovascular scar, called **granulation tissue**, that enhances the tendon's structural integrity (Alhajj and Goyal, 2024; Hope and Saxby, 2007).

Approximately 2 weeks post-injury, the remodelling phase initiates, overlapping with the proliferative phase. This stage involves the gradual replacement of collagen type III with type I, which is aligned along the axis of mechanical stress, cross-linked, and organised into bundles to restore some of the tendon's mechanical strength (Bruns *et al*., 2000). As this process unfolds, tissue cellularity decreases and the remaining tenocytes revert to their original stellate

shapes (Oshiro *et al*., 2003). Over subsequent months to years, the repaired tendon undergoes maturation, marked by decreased metabolic activity and vascularity, and increases in collagen bundle thickness and biomechanical properties (Amiel *et al*., 1983; Hope and Saxby, 2007; Sorg *et al*., 2018). During this stage, fibroblasts transition into *ACTA2*$^{+}$ alpha smooth muscle actin (α-SMA)-producing myofibroblasts that strengthen the ECM and facilitate wound contraction (Hinz *et al*., 2002; Pakshir and Hinz, 2018).

The long-term maturation phase is crucial for the tendon to regain its full functionality and mechanical resilience. However, successful resolution of the wound healing response requires the apoptosis of recruited cells. A failure in this process can lead to the prolonged presence of activated immune cells and myofibroblasts, resulting in chronic fibrosis, which perpetuates the thickening and stiffening of scar tissue and the formation of adhesions to nearby tissues (Pakshir and Hinz, 2018). Even if these cells are removed, the persistent fibrotic ECM can continue to influence molecular bioavailability and cell behaviour, necessitating remodelling to fully resolve the fibrotic response (Pakshir and Hinz, 2018; Parker *et al*., 2014). This challenge is compounded by the age-related decline in ECM remodelling capabilities, which makes fibrosis a more likely outcome (Korcari *et al*., 2023; Kwan *et al*., 2023; Lui and Wong, 2020; Stowe *et al*., 2023). Consequently, fibrosis is a common complication in chronic tendinopathies and overuse injuries (Aström and Rausing, 1995; Disser *et al*., 2023).

The healing processes of tendon injuries vary considerably, influenced by factors such as tendon anatomy, injury type, and location. For example, injuries to the fully detached supraspinatus tendon enthesis heal without angiogenesis or significant immune cell infiltration, with local cells instead producing a collagen type I and II ECM plug rather than forming a fibrin clot (Vinestock *et al*., 2022). Instead, angiogenesis and macrophage infiltration and activation occurs mostly outside the enthesis repair site (Huang *et al*., 2020). This variability extends even within the same type of tendon, as seen in murine Achilles tendons where the healing dynamics differ between partial midbody injuries, which show minimal vascular and immune response, and complete transections, which induce significant clot formation and immune activity (Howell *et al*., 2021; Sakabe *et al*., 2018). Additionally, location-specific

differences within tendons further complicate the healing landscape. For example, canine flexor tendon intrasynovial regions, which are avascular and proteoglycan-rich, exhibit minimal vascular growth and subdued inflammatory and metabolic responses, contrasting with the active healing observed in the well-vascularised, collagen-rich extrasynovial regions (Shen *et al*., 2021).

Compounding this complexity is the involvement of both intrinsic and extrinsic cellular populations during tendon repair. Intrinsic cells generally include resident tendon fibroblasts and intra- or interfascicular TSPCs, whereas extrinsic cells may consist of fibroblasts, TSPCs, or vascular-origin cells migrating from external tendon layers like the epi- and paratenon (Cadby *et al*., 2014; Killian *et al*., 2012; Mienaltowski *et al*., 2013). Notably, while both cell types contribute to foetal regenerative repair, adult tendon repair is predominantly mediated by extrinsic cells (Dyment *et al*., 2013; Howell *et al*., 2017; Moser *et al*., 2021; Sakabe *et al*., 2018) (Table 2), highlighting a shift in cellular dynamics with maturation and age.

2.5.2 Differences in repair of developing and aged tendons

In addition to the above, the healing processes of tendon injuries demonstrate differences across developmental stages, as illustrated by various studies focusing on foetal, neonatal, and adult tendon healing. In adult sheep tendons, the healing response a week after partial tenotomies of extensor tendons was characterised by disrupted collagen alignment, prominent granulation tissue, increased adhesions, and significant inflammatory cell infiltration (Beredjiklian *et al.*, 2003). In contrast, second trimester (80-85 days gestation) foetal sheep tendons showed no histological abnormalities, adhesions, or inflammatory cell activity (Beredjiklian *et al.*, 2003). Further investigation by Favata *et al.* (2006) determined that this regenerative capacity was attributable to the intrinsic properties of the developing tendon rather than the extrinsic foetal environment. By transplanting adult and foetal sheep extensor tendons into SCID mice and performing partial tenotomies 1-week post-implantation, they found that adult tendons developed disordered granulation tissue (Figure 15A) and showed elevated levels of pro-inflammatory markers TGF-β1, bFGF, and CD44 seven days post-injury (D7). In contrast, foetal tendons not only achieved complete histological and mechanical restoration (Figure 15B,C), but also showed full

vascularisation and minimal upregulation of these inflammatory markers. Additional support for the intrinsic nature of foetal healing was provided by Longaker *et al.* (1994), who conducted reverse experiments where skin grafts from adult and foetal sheep were transplanted onto 60-day gestation sheep *in utero*, left to heal for 40 days, then subjected to a full-thickness tear. The wounds from the adult grafts displayed visible scar formation at D14, whereas the 60-day foetal graft wounds were indistinguishable from normal dermal tissue, highlighting a significant disparity in healing capacities based on developmental stages.

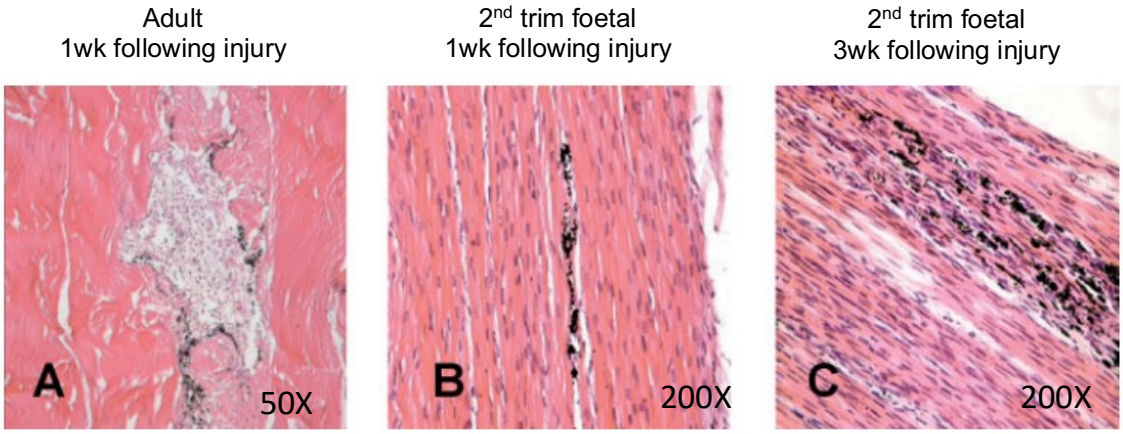


Figure 15. Comparison of adult and foetal tendon repair outcomes following injury. *Haematoxylin and eosin-stained sections show injury sites (marked with black charcoal) of adult (A) and foetal (B, C) sheep extensor tendons transplanted into adult SCID mice 1 or 3 weeks post-injury. Images are shown at X50 or X200 magnification. Adapted, with permission, from Favata et al. (2006).*

This regenerative trend extends into postnatal development, as observed in neonate models. Early P5-7 murine neonates can regenerate and return to normal function after complete tendon transection injuries within just 10-14 days (Ansorge *et al*., 2012; Howell *et al*., 2017). However, as neonates mature and experience increasing mechanical loads from movement, the healing processes start to show a decline. For instance, around P21-28, cell proliferation decreases while collagen fibrils undergo expansive growth. This process coincides with a delayed tendon healing response characterised by a three-day lag in ECM production and cell proliferation, prolonging the return to normal function (Ansorge *et al*., 2012; Grinstein *et al*., 2019).

Collectively, these studies highlight the exceptional regenerative capabilities of foetal tissues, which inherently heal without scar formation, unlike adult tissues

which often exhibit fibrotic responses. To better understand these differences in healing, it is crucial to examine the cellular populations, niches, and molecular mechanisms involved.

2.5.3 Cellular contributions to scarless and scarred repair

In P5 neonatal mice with complete Achilles transection, *Scx*$^{+}$ intrinsic tendon stub cells and *Scx*$^{-}$*Acta2*$^{+}$ epitenon cells rapidly infiltrate and proliferate at the injury site by D3 (Table 2; Howell *et al.*, 2017). By D14, the wound gap contains limited regions of α-SMA and is primarily filled with uniform collagen by *Scx*$^{+}$ cells, leading to the restoration of function by the same day and complete mechanical recovery by D56. The transient presence of α-SMA in these regions highlights a brief fibrotic response that is effectively overcome by the proliferation of tendon-specific cells. Conversely, in adult mice, *Scx*$^{-}$*Acta2*$^{+}$ epitenon cells dominate the early response without contributions from intrinsic *Scx*$^{+}$ tendon stub cells (Howell *et al*., 2017). These extrinsic cells contribute to a scarred, vascularised environment by D14, marked by abundant α-SMA and disorganised ECM, culminating in incomplete mechanical restoration and *Scx*$^{+}$ tendon stub ectopic ossification by day 56. This indicates a reliance on fibrotic pathways due to the quiescence of *Scx*$^{+}$ tenocytes, which do not contribute to the healing process post-injury.

In contrast to complete transection injuries, partial transection in adult mice showcases a distinct cellular response and healing trajectory. Specifically, partial transections also see an early proliferation and migration of extrinsic *Sca1*$^{+}$*Scx*$^{-}$ paratenon cells into the injury site by D7 (Table 2; Sakabe *et al.*, 2018). However, by D14, these cells begin producing Scx and contribute to an initial formation of collagen III-rich granulation tissue. This process is significant as it indicates an active involvement of adaptive cellular mechanisms not seen in complete transections of older mice, where intrinsic *Scx*$^{+}$ tendon stub cells remain largely quiescent and uninvolved (Table 2). As the healing progresses to D28 in partial transections, collagen III is replaced with collagen I deposited by *Scx*$^{+}$ cells that now dominate the repair site. This differs from complete transections where the repair is characterised by persistent α-SMA expression, disorganised ECM, and incomplete mechanical recovery, underlining a predominantly fibrotic healing with limited functional restoration.

The critical role of Scx in tendon repair becomes apparent when *Scx* is knocked out at the time of injury, leading to a failure of *Sca1*$^{+}$ paratenon cells to downregulate *Sca1* and activate *Scx* after migrating to the wound site (Table 2; Sakabe *et al.*, 2018). This disruption in cellular signalling hampers ECM deposition and the transition from collagen III to collagen I. Consequently, a chondrocyte-like ECM comprising collagen II and Acan forms at the wound sites by 4 and 6 weeks post-injury, followed by ectopic ossification and the presence of differentiated chondrocytes at 8 and 15 weeks (Sakabe *et al*., 2018). This sequence underlines a critical dependency on Scx for successful tendon repair and regeneration.

Table 2. Summary of select murine studies on neonatal and adult tendon repair. *Acta2 gene encodes alpha-smooth muscle actin (α-SMA), a marker of contractile myofibroblasts. P: day post-natal; D: day post-injury.*

Ref	Model	Age	Injury	Observations
Dyment *et al.*, 2013	C57BL/6-ScxGFP	Adult, 20 weeks (5 months)	Full-length central Patellar tendon injury	On D3, tendon stubs are *Scx*$^{-}$, the defect site is filled with *Scx*$^{-}$ cells, while the paratenon thickens and its cells express *Fmod* and *Tnc*. By D7, these paratenon cells express *Acta2* and migrate to the wound site. By D14, they turn on *Scx* expression and form a "bridge" layer covering the defect with collagen fibres oriented circumferentially to the tendon axis. The actual site of the defect remains *Acta2*$^{+}$*Scx*$^{-}$, with collagen aligned parallel to the tendon axis. The cells within the original tendon stubs closest to the defect also begin expressing *Acta2*.
Maeda *et al.*, 2011	C57BL/6-ScxGFP	Adult, 10-12 weeks (2.5-3 months)	Complete Achilles tendon transection	Loss of mechanical load due to complete transection leads to ECM disorganisation and tenocyte death, excessive release of active TGF-β from the ECM, and the consequent loss of *Scx* expression and decrease in mechanical properties, including stiffness, ultimate stress, and peak force.
Sakabe *et al.*, 2018	C57BL/6-ScxGFP	Adult, 10-12 weeks (2.5-3 months)	Partial Achilles tendon transection	Very little angiogenesis and fibrinogen following injury. *Scx*$^{+}$ cells are absent from the injury site by D2. *Sca1*$^{+}$*Scx*$^{-}$ paratenon cells close to the wound proliferate and migrate into it by D7. Those cells turn on *Scx* expression by D14 and produce the initial collagen III-rich granulation tissue. Resident *Scx*$^{+}$ tendon fibroblasts also migrate towards the wound, but in later stages. By D28, collagen III becomes replaced with collagen I, and the *Scx*$^{+}$ cells fill up the wound site. The collagen is aligned mostly perpendicularly to the tendon axis. Additionally, COMP is deposited at that time.

	C57BL/6-Scx$^{flox/flox}$/ScxGFP	Adult, 10-12 weeks (2.5-3 months)	Partial Achilles tendon transection	Scx deletion at time of injury lead to *Sca1*$^{+}$ paratenon cell inability to turn on *Scx* and downregulate *Sca1* following migration to the wound site (reported at D28). Consequently, ECM deposition was disrupted, COMP was not deposited, and the deposited collagen III was not replaced by collagen I, showing a requirement for Scx. Instead, chondrocyte-like ECM consisting of collagen II and Acan was observed in the wound sites at 4 and 6 weeks post-injury, with further ectopic ossification and differentiated chondrocyte presence reported at 8 and 15 weeks post-injury.
Ansorge *et al.*, 2012	C57BL/6	Neonatal, P7 and P21	0.3mm biopsy punch full thickness, half width injury of Achilles tendon	Neonatal P7 mice: smaller cross-sectional area and collagen fibril diameters, increased maximum stress and modulus at D10 compared to D3. No changes in BGN or DCN quantity. Normal mechanical function restored by D10. Neonatal P21 mice: no changes in cell proliferation or ECM deposition between injured and uninjured tendons at D3. Bigger cross-sectional area, unchanged or slightly decreased maximum stress and modulus, and higher BGN and DCN content at D10 compared to D3. Mechanical properties not restored by D10.
Grinstein *et al.*, 2022 (pre-print)	Axin2:Cre^{ERt2}; ROSA^{LSLTdTomato}	Adult, 16 weeks (4 months)	0.3mm biopsy punch full thickness, half width injury of Achilles tendon	At D10, *Axin2*- and *Scx*-lineage cells infiltrate the wound site, adopt a rounded morphology, and proliferate. *Scx* is downregulated. At D20 and D30, *Axin2*- and *Scx*-lineage cells express Scx, their morphology is changed from rounded to elongated.
Nichols *et al.*, 2023 (pre-print)	GLASTCre^{ERT}; Ai9$^{F/+}$; Scx^{GFP+}	Adult, 11-13 weeks (2.75-3.25 months)	Complete transection and repair of the flexor digitorum longus tendon	At D3-7, epitenon *GLAST*$^{+}$ cells proliferate at the periphery of the injury site. At D10, *GLAST*$^{+}$ cells are present in both the layer bridging the entry site of the wound (periphery) as well as the wound gap itself. These cells begin expressing *Scx* in the filled wound gap at D10 and in the peripheral layer at D14. Other, non-*GLAST*$^{+}$ cells of the *Scx*-lineage also contribute to the wound gap, filling about 67% of it by D28. *GLAST*+ cells do not express α-SMA or CD146, remaining distinct from those populations.

Howell *et al.*, 2017	C57BL/6-ScxGFP, ScxCre^{ERT2}, Ai14 Rosa26-TdTomato Cre	Neonatal, P5 Adult, 20-25 weeks (5-6 months)	Complete Achilles tendon transection	P5 neonatal mice: At D3, intrinsic tendon stub *Scx*$^{+}$ cells and *Scx*$^{-}$*Acta2*$^{+}$ epitenon cells infiltrate the wound site and proliferate. The latter persist until D14 when they are removed. Wound gap is filled by the intrinsic *Scx*$^{+}$ cells, and function is recovered by D14, with all mechanical properties restored by D56. Collagen organisation was uniform in the repaired tendon. Adult mice: At D3, *Scx*$^{-}$*Acta2*$^{+}$ epitenon cells infiltrate the wound site, while the original intrinsic *Scx*$^{+}$ tendon stub cells do not proliferate or get involved in repair. At D14, *Scx*$^{+}$ cells remain in the stubs, while gap is filled by *Scx*$^{-}$ *Acta2*$^{+}$ epitenon cells. Scar is formed, and function and mechanical parameters are not restored by D56. Additionally, ectopic ossification of *Scx*$^{+}$ cells is observed at D56 in tendon stubs. ECM remained disorganised and exhibited non-collagenous regions. By D56, both neonatal and adult injured tendons had smaller collagen fibril diameters than uninjured controls, suggesting incomplete collagen fibril maturation. While both expressed scar-associated markers (α-SMA, Fb1, and Col3a1) at some point, the neonatal tendon fibrosis was only transient as cells eventually underwent tendon-specific differentiation at D7-14 (Mkw, Tnmd and Col1A1); in the adults, the extrinsic *Acta2*$^{+}$ cells persisted.
Howell *et al.*, 2021	C57BL/6-ScxGFP, Macrophage-Fas-Induced Apoptosis (MaFIA), MaFIA/ScxGFP	Neonatal, P5	Complete Achilles tendon transection	By D3, robust immune response with presence of F4/80^{+} macrophages, T cells, and upregulated expression of inflammatory cytokines *Il6, Il1β, Il12β,* and *Il18*. The macrophages were closely localised to the *Scx*$^{+}$ cells at the injury site. Macrophage and monocyte depletion in P5 mice inhibited *Scx*$^{+}$ cell proliferation and formation of a *Scx*$^{+}$ "neotendon" that filled the gap site, leading to inferior repaired tendon function, including lower stiffness and maximal force.

Vinestock *et al.*, 2022	C57BL/6	Neonatal, P7	Achilles enthesis needle punch injury (32-gauge)	Unmineralised enthesis heals without inflammation or angiogenesis, illustrated by the absence of F4/80$^+$ macrophages and Cd31/Pecam1 by D7. Instead of a fibrin clot, an ECM plug was formed between D3 and D7, with the area surrounding it remaining acellular due to extensive apoptosis. The ECM of both the plug and the surrounding hypocellular area had disorganised and misaligned fibres positive for Col1a1 and Col2a1, but not Col3a1. The enthesis regained function by D56. However, while the enthesis was successfully mineralised and the mechanical properties were restored, the tidemark remained disrupted 5 months after injury, highlighting an imperfect healing response.
Moser *et al.*, 2018	ScxCre^{ERT2}, αSMACre^{ERT2}, Sox9Cre^{ERT2}, Axin2Cre^{ERT2}, Ai14 Rosa26-TdTomato Cre	Adult, 14-18 weeks (3.5-4.5 months)	Supraspinatus tendon middle portion to insertion site needle punch injury (26-gauge)	By D28, the tendon healed by formation of a disorganised, hypercellular scar of unknown origin that was NOT formed by cells from *Scx*$^+$, *Sox9*$^+$, *Axin2*$^+$, or *Acta2*$^+$ lineages. The scar was negative for *Sca1*. Gait appeared minimally affected by D14.
	Sox9Cre^{ERT2}, Axin2Cre^{ERT2}, Ai14 Rosa26-TdTomato Cre	Adult, 20-25 weeks (5-6 months)	Full supraspinatus tendon detachment at the enthesis, followed by surgical repair	By D28, the tendon healed by formation of a massive, disorganised, *Axin2*$^+$ hypercellular scar. Gait was abnormal at D28.
Moser *et al.*, 2020	C57BL/6, ScxCre^{ERT}2, αSMACre^{ERT2}, Ai14 Rosa26-TdTomato Cre	Adult, not specified	Full supraspinatus tendon detachment at the enthesis, followed by surgical repair	By D28, the tendon healed by formation of a massive, disorganised, *Acta2*$^+$ hypercellular scar with very few *Scx*-lineage cells present. Tendon structure was not preserved. Mechanical properties (stiffness, maximum force, work to yield) were not recovered by D28.

Differential healing responses between full and partial tendon transections can largely be attributed to variations in tissue integrity, cellular activities, and mechanical loading, which directly affect TGF-β signalling and the downstream *Scx* expression (Chen *et al*., 2008; Sakabe *et al*., 2018). TGF-β exists in two forms: active and soluble, or inactive and ECM-bound. Mechanical load promotes the release and activation of ECM-bound TGF-β, thereby enhancing healing through increased *Scx* expression (Maeda *et al*., 2011). Loss of tensile

load leads to rapid loss of *Scx* expression, causing decreases in collagen type I, COMP, and mechanical properties (Maeda *et al*., 2011). In scenarios where tensile load is maintained, as seen in partial transections, *Scx* continues to be expressed by tenocytes, thus contributing to the repair processes. In contrast, full transections result in a loss of mechanical load, causing ECM destabilisation that triggers an over-release of active TGF-β, which in its excess causes widespread tendon cell death and loss of *Scx* expression even in surviving tenocytes (Maeda *et al*., 2011). Moreover, the excessive and prolonged TGF-β activity promotes chondrogenic (Furumatsu *et al*., 2009; Kim *et al*., 2014; Yang *et al*., 2011) and myofibroblast differentiation (Evans *et al*., 2003; Thomas *et al*., 2007), further exacerbating tissue fibrosis as these cells contract the ECM and perpetuate the continued release of TGF-β (Wipff *et al*., 2007). While the early proliferation of intrinsic *Scx*-lineage cells and the activation of *Scx* in extrinsic α-SMA-producing cells by D14 do not entirely depend on TGF-β signalling, the proliferation of non-*Scx* lineage cells, subsequent recruitment of *Scx*$^{+}$ cells and the overall functional restoration do dependent it (Kaji *et al*., 2020). This underscores the complex interplay of TGF-β-dependent and independent mechanisms in tendon healing and regeneration.

However, recent pre-prints present conflicting findings regarding *Scx* expression following tendon injury (Table 2). A study by Grinstein *et al.* (2022) indicates that partial biopsy needle punches in the Achilles tendon result in the downregulation of *Scx* at D10, whereas a study by Nichols *et al.* (2023) shows that complete transection and repair of the flexor digitorum longus tendon lead to increased *Scx* expression 10 days post-injury. These divergent results underscore the need for careful consideration of other variables potentially influencing the processes and outcomes of the tendon injury response.

2.5.4 Tissue niche contributions to scarless and scarred tendon repair

Beyond the cellular composition and tissue architecture, it is crucial to consider how the general niche composition also plays a pivotal role in shaping tendon healing responses. Research shows that tendons healed after injury typically exhibit smaller and less mature collagen fibrils compared to uninjured tendons (Ansorge *et al*., 2011; Howell *et al*., 2017). Tendon healing is most effective before significant mechanical loading and fibril expansion occurs, underscoring

a key limitation in the regenerative processes of the ECM. Namely, regeneration tends to restore only the immature, simpler characteristics of the ECM rather than replicating the original mature, long, extensively crosslinked, and stiff collagen fibres found in adult tendons. Therefore, endogenous repair mechanisms prioritise quick initial recovery, focusing on simpler structural restoration over complete functional equivalence, and thus making it simpler for the foetal immature tendons to replicate.

Contributing to their regenerative ability, foetal tendons feature a higher proportion of cells per surface area compared to adult tendons (Kannus *et al*., 2005). Moreover, these cells have a greater capacity for proliferation and are substantially more metabolically active, priming them for rapid healing responses (Ansorge *et al*., 2012; Grinstein *et al*., 2019). Additionally, research indicates that collagen turnover within the tendon ECM is more dynamic during earlier life stages, significantly slowing down after late adolescence, about 17 years of age in humans (Heinemeier *et al*., 2018, 2013). This period aligns with the peak in collagen fibril diameter and density, but a decrease in fibril concentration and tenocyte number (Strocchi *et al*., 1991). As tendons age, they exhibit a reduction in water, proteoglycan, and glycosaminoglycan content (Ippolito *et al*., 1980; Kannus *et al*., 2005; Peffers *et al*., 2014), which also correlates with the shortening of collagen fibrils and an increase in tensile stress (Masic *et al*., 2015). These biochemical and structural changes highlight a critical aspect of tendon ageing and repair: as the ECM becomes less dynamic and more constrained in its adaptive responses, adult tendons exhibit less effective healing compared to their foetal counterparts, leading to differing outcomes in tendon regeneration and functionality.

The variations in the composition of the ECM between developing and adult tendons play an especially significant role in influencing their healing responses. For example, compared to adult tendons, developing tendon ECM is characterised by high concentrations of GAGs such as HA and CS (Bleacher *et al*., 1993; Mast *et al*., 1991; Rolfe and Grobbelaar, 2012), which create a highly hydrated, less dense matrix that not only prevents scar formation, but also diminishes the inflammatory responses while enhancing fibroblast proliferation and migration (see section 2.3.2; Longaker *et al.*, 1989, 1991; Abate, Schiavone and Salini, 2014; Honda *et al.*, 2017; Oliva *et al.*, 2021). Reflecting the benefits

of this foetal healing environment, exogenous addition of HA to adult tendon injuries has shown efficacy in reducing scar tissue formation (Abate *et al*., 2014; Costa *et al*., 2023; Frizziero *et al*., 2022, 2020).

The concept of ECM modulation of tendon repair is further illustrated by the role of CD44, the primary receptor for HA, whose expression varies significantly between developing and adult tendons. In adults, elevated levels of both CD44 and HA (Berglund *et al*., 2007) correlate with fibrotic, less efficient healing processes. Conversely, in regenerative foetal tendons, post-injury CD44 expression is downregulated, while HA levels remain elevated (Favata *et al*., 2006). CD44 facilitates fibroblast migration towards the wound site and reduces active levels of local TGF-β (Acharya *et al*., 2008), thus diminishing *Scx* expression. Moreover, CD44 expression is required for the differentiation of fibroblasts into fibrosis-driving myofibroblasts (Meran *et al*., 2011; Midgley *et al*., 2013; Simpson *et al*., 2009; Woods *et al*., 2021). Studies involving CD44 knockout mice have therefore shown improved mechanical properties during adult tendon healing (H. Ansorge *et al*., 2009), likely due to accumulation of soluble HA. These findings highlight the significance of the foetal niche in regulating regenerative healing.

2.6 High-resolution transcriptomics in the study of tendon biology

The study of tendon biology is progressing toward a new phase, where high-resolution transcriptomic technologies (see section 2.2.3, Table 1) are becoming increasingly prevalent. Methods such as single-cell RNA sequencing (scRNA-seq), single-nucleus RNA sequencing (snRNA-seq), and spatial transcriptomics provide insights into gene expression at the cellular level, enabling exploration of the cellular heterogeneity and molecular interactions that regulate tendon function and contribute to its pathophysiology.

scRNA-seq, in particular, has facilitated transcriptomic profiling at the single-cell level, revealing distinct cellular subpopulations and their potential roles in tendon biology (Table 1). By capturing the full transcriptome of thousands of individual cells, scRNA-seq enables the identification of rare cell types and transient cellular states that are often undetectable in bulk RNA sequencing. For example, it can differentiate between various fibroblast subsets or identify

inflammatory cell populations contributing to degenerative tendon disorders such as tendinopathy (Table 1).

Methodologically, scRNA-seq involves the dissociation of tissues to generate a single-cell suspension, followed by cell barcoding and mRNA capture using droplet microfluidics (e.g., 10X Genomics), combinatorial indexing, or well-based platforms. Captured RNA is reverse-transcribed into cDNA, which is then amplified, sequenced, and aligned to a reference genome for downstream analyses. Computational pipelines are then applied to cluster cells based on their transcriptomic profiles, typically visualised through dimensionality reduction techniques such as principal component analysis (PCA), uniform manifold approximation and projection (UMAP), or diffusion maps. Advanced downstream analyses can then be performed to predict cellular differentiation trajectories through pseudotime or experimental time, assess dynamic gene regulation (e.g., RNA velocity), identify enriched pathways within specific cell types, and reconstruct gene regulatory networks. In the future, machine learning approaches are anticipated to enhance causal inference from the extensive biological networks generated by high-resolution transcriptomic studies (Lagemann *et al.*, 2023), further enhancing the interpretation of complex cellular behaviours in tendon biology.

Despite its utility, scRNA-seq presents specific challenges, particularly for ECM-rich tissues such as tendons (reviewed in Ramos-Mucci *et al.*, 2022). Tissue dissociation protocols required for scRNA-seq can disrupt cell-cell interactions and alter transcriptional profiles, potentially introducing biases and resulting in the underrepresentation of hard-to-dissociate cellular compartments (Grinstein *et al.*, 2018; Mattei *et al.*, 2020). Additionally, scRNA-seq often struggles with the detection of low-abundance transcripts and long non-coding RNAs due to limited sequencing depth (Ziegenhain *et al.*, 2017). In contrast, snRNA-seq isolates nuclei and captures nuclear RNA, including pre-mRNA, bypassing the need for complete tissue dissociation and thus avoiding the use of ECM-disrupting enzymes (Mimpen *et al.*, 2021). However, snRNA-seq misses cytoplasmic RNAs, leading to an overrepresentation of unspliced transcripts and necessitating additional considerations with computational analyses designed for scRNA-seq data. Current efforts by the Tendon Seed Network are aimed at clarifying the differences between scRNA-seq and snRNA-seq in

tendon biology, with the goal of optimising the use of both techniques for understanding tendon cellularity and function.

In addition to scRNA-seq and snRNA-seq, a further dimension of information is provided by spatial transcriptomics approaches, which enable the direct mapping of transcriptional profiles onto tissue sections and facilitating the association of molecular data with histological features. This is particularly important in ECM-rich tendon tissues, where tissue organisation plays a key role in cellular function and ECM interactions.

Several spatial transcriptomics approaches exist, each with distinct advantages. Sequencing-based methods, such as 10x Genomics Visium (Ståhl *et al.*, 2016), use spatially barcoded arrays to capture RNA from tissue sections. This provides insights into gene expression gradients, ECM composition, and the spatial organisation of cell types. For example, Visium has been applied to investigate the biology of healthy rat patellar tendons (Steffen et al., 2023) and fibrotic tendon healing (Ackerman et al., 2022), revealing key regulatory pathways involved in tendon homeostasis and repair.

While Visium provides a comprehensive overview of tissue-wide gene expression, its primary limitation lies in its resolution, typically capturing the transcriptomes of multiple cells within a single barcoded spot. However, integrating data from scRNA-seq or snRNA-seq with spatial information from Visium presents a powerful strategy to partially mitigate this limitation, allowing cell type deconvolution and enhancing the depth of transcriptomic analysis. Innovative higher-resolution methodologies continue to emerge, such as 10X Genomics's Xenium, which the Tendon Seed Network is currently evaluating as an alternative to Visium. Xenium can characterise up to 5,000 genes at subcellular spatial resolution, offering opportunities for much more detailed spatial transcriptomic analyses in tendon biology.

Other higher-resolution, low-throughput methods such as probe-based techniques offer alternatives for targeted detection of specific genes with enhanced spatial resolution. For instance, *in situ* hybridization (ISH) techniques like multiplexed error-robust fluorescence ISH (MERFISH) (Chen *et al.*, 2015) and RNAscope (F. Wang *et al.*, 2012) enable localisation of gene expression. While these are limited by the total number of probes and thus do not yield

genome-wide data, they are valuable for validation of specific expression patterns identified in scRNA-seq or bulk RNA-seq studies.

Overall, high-resolution transcriptomics represent a significant advancement in tendon biology field, offering insights into the transcriptional landscapes of tendons. The rapid development of these techniques, particularly with potential integration with other -omics approaches such as metabolomics, proteomics, and epigenetics, will aid in furthering our understanding of all aspects of tendon biology, clarifying the interactions and regulatory mechanisms involved in tendon development, homeostasis, and pathology.

2.7 Conclusions

This literature review synthesises the current understanding of the structure and function of healthy tendons, tracing their development from embryonic stages through to postnatal maturation and highlighting the changes that occur as tendons age or are injured. While significant strides have been made in delineating the cellular populations and signalling processes essential for tendon development, homeostasis, and repair, achieving a fully comprehensive overview remains challenging. This is largely due to the complexities involved in comparing and synthesising studies that may use different methodologies or focus on varied aspects of tendon biology.

Nevertheless, the advent of continuously evolving high-resolution technologies such as single-cell RNA sequencing and advanced imaging modalities, offers substantial promise in bridging the remaining gaps. These tools enable a granular analysis of tendon tissues, facilitating the identification of novel cell types and states, detailed mapping of cellular interactions, and enhanced understanding of the molecular mechanisms underpinning tendon function and dysfunction. To capitalise on these advances, future research should focus on building comprehensive atlases of tendon cells and structures across various developmental and pathological stages. Such atlases would provide invaluable standardised references that could drive forward the understanding of age-, injury-, or disease-specific changes in tendon biology, aiding in development of targeted therapies for tendon dysfunctions. Additionally, there is a critical need for high-level transcriptomic comparisons across model organisms, which could

reveal fundamental principles and unique species-specific strategies in tendon disease resistance and healing responses, potentially highlighting new targets for therapeutic intervention.

Chapter 3: Methods

In this thesis, single-nucleus and spatial RNA-sequencing data were generated from human foetal tendons (Appendix Table 3) by the author for the analyses in Chapter 4. To investigate the developmental origins of these foetal tendon cells, the dataset was integrated in Chapter 5 with a previously published atlas of human embryonic whole limbs (B. Zhang *et al.*, 2023). This dataset was used because the small size of embryonic tendons precluded direct dissection and sequencing. Chapter 6 involved a comparative analysis between developing and aged tendons, using histological and transcriptional data from foetal samples (generated by the author) and unpublished adult tendon datasets from the Tendon Seed Network (Baldwin *et al.*, 2021, 2023), which were already processed and annotated. This approach allowed for a detailed examination of age-related changes in tendon biology while maximising the utility of available resources.

3.1 Declaration

All work presented in this thesis – including tissue collection, dissection, experimental processing, nuclei and RNA extraction, library preparation, data analysis, and interpretation – was conducted by the author, with or without assistance from colleagues, unless otherwise stated. Contributions from collaborators or external sources are clearly acknowledged in the relevant sections and summarised in Appendix Table 4.

3.2 Ethics

3.2.1 Human developmental tissue samples

Human foetal material was supplied by the Joint MRC/Wellcome Trust (grant #MR/R006237/1) Human Developmental Biology Resource (HDBR, www.hdbr.org) under the MTA license (R60786/CN008) with REC 18/LO/0822. Specifically, fresh foetal lower limbs aged 9-20 post-conception weeks (pcw) were provided by the HDBR London UCL Institute of Child Health. All samples used in this work were sourced from elective terminations with no abnormalities recorded. Sample metadata is summarised in Appendix Table 3.

3.2.2 Human adult tissue samples

Ethical approval for the Oxford Musculoskeletal Biobank (OMB, 19/SC/0134) was granted by the Oxford Research Ethics Committee B for all work on human Achilles and quadriceps tendons. Written informed consent according to the Declaration of Helsinki was obtained from all patients. Healthy Achilles and quadriceps tendon tissues were collected from patients undergoing above- or below-the-knee amputations (e.g., OMB0785) or suprapatellar nailing of tibial shaft fracture (e.g., OMB1266). Ruptured quadriceps tendon samples were obtained from patients with acute full quadriceps tendon ruptures, with surgeries performed 8 to 9 days post-rupture. Sample metadata is summarised in Appendix Table 3.

3.3 Human Tendon Tissue Acquisition and Processing

Fresh tissues were supplied in either DMEM-F12 (Dulbecco's Modified Eagle Medium/Nutrient Mixture F-12) media supplemented with 10% Foetal Bovine Serum and 1% Penicillin/Streptomycin (for OMB tissues) or RPMI (Roswell Park Memorial Institute) medium with no additives (for HDBR tissues). The tissues were washed in PBS (phosphate-buffered saline) and dissected to retain only the regions of interest. Adult tissues were cut into 1 cm pieces and photographed to retain topographical reference.

The tissues were then either formalin-fixed or snap-frozen in liquid nitrogen as soon as possible after collection. Following formalin-fixation (with different lengths of time depending on the size of the samples), the samples were resuspended in 70% IMS (industrial methylated spirit) and stored at room temperature. After dehydration, formalin-fixed tissues were paraffin-embedded and sectioned. Snap-frozen tissues were stored at -70°C to -80°C before being used for single-nuclei or spatial RNA-sequencing.

3.4 10X Chromium Single-Nucleus RNA-Sequencing

3.4.1 Nuclei isolation

Nuclei isolation for samples outlined in Appendix Table 1 was carried out following protocols for large (adult) and small (foetal) tissues developed and

published by the Tendon Seed Network (Mimpen *et al*., 2021). Briefly, tendons were cut into ~1 mm pieces on dry ice and dissociated in CST buffer (292 mM NaCl, 20 mM Tris-HCL 7.5 pH, 2 mM CaCl2, 42 mM MgCl2, 0.5% CHAPS, 0.01% BSA, RNase and protease inhibitors) on a rotor for 2 or 10 min at 4°C. After addition of PBS + 2% or 1% BSA (bovine serum albumin), the suspensions were strained through 20 or 40 µm strainers (Greiner Bio-one), with former numbers used for foetal and latter for adult tissues. The nuclei-containing suspensions were then centrifuged at 500 g for 5 min at 4°C. Following centrifugation, the supernatant was discarded and the nuclei within the pellet were stained with DAPI and counted manually using a haemocytometer (NanoEntek DHC-N01) and fluorescence microscopy.

3.4.2 Library preparation and sequencing

Nuclear suspensions, diluted in PBS with 1% BSA to a concentration of 200-1000 nuclei/µl, were loaded onto a Chromium Next GEM Chip G (10x Genomics) with the aim of recovering 1,000-10,000 nuclei per sample. The samples were then processed using the Chromium Controller (10x Genomics) and prepared into libraries using the Chromium Next GEM Single Cell 3' Reagent Kits v3.1 (10x Genomics, 2019) following the manufacturer's instructions. Libraries were indexed with the single-index kit T Set A (10x Genomics). Quality control assessments for cDNA and final libraries were conducted using High Sensitivity ScreenTape assays on a 4150 TapeStation System (Agilent). The final libraries were pooled together and sequenced on a NovaSeq 6000 (Illumina) by Genewiz (UK) with a minimum sequencing depth of approximately 20,000 read pairs per expected nucleus.

3.4.3 Data pre-processing, quality control, normalisation, and dimensionality reduction

The raw sequencing files were aligned with CellRanger v7.0 (Zheng *et al*., 2017) using the 10x Genomics' pre-built GRCh38-2020-A reference (compiled from ENSEMBL's 98th release of the human reference genome) with default settings. The output raw_feature_bc_matrix.h5 files were then input into the CellBender 0.2.2 (Fleming *et al*., 2023) *remove-background* function using custom values for expected-cells, total-droplets-included, epochs and low-

count-threshold parameters, which were selected based on the properties of individual samples and what was expected. The command was rerun until optimal conditions (incl. training and test loss converging, expected number of cells selected, no error or warning messages in log files etc) were achieved for each individual sample.

The data processing and analysis was carried out using Python and R packages. Briefly, the CellBender .h5 output files were converted into h5ad using an auxiliary function *anndata_from_h5()*. The resulting cell counts were compared with expected counts from cell loading into the 10X reaction. Metadata was then added to each sample anndata object. To obtain spliced and unspliced count matrices, Velocyto 0.17.17 (La Manno *et al*., 2018) package function *velocyto run10x* was used with a masking h38_repeat_mast.gtf file and refdata-gex-GRCh38-2020-A/genes/genes.gtf file. The resulting sample loom output files were loaded using a custom *load_loom_files()* function, compared with the cellbender files, then merged using *scvelo.utils.merge()* (Bergen *et al*., 2020) to retain overlapping barcodes.

The merged files were loaded and filtered to remove: 1) genes that were detected in fewer than 20 cells (*scanpy.pp.filter_genes(adata,min_cell=20)),* 2) genes with 0 umi counts *(adata = adata[:, np.asarray(adata.X.sum(axis=0)).-reshape(-1) > 0])*, and 3) cells with fewer than 200 umi counts (*adata = adata[np.asarray(adata.X.sum(axis=1)).reshape(-1) > 200]))*. While somewhat redundant, it was done to test that the functions worked as expected. Following this basic filtering, low quality reads were removed using permissive automatic thresholding based on median absolute deviations (MAD), as described in the current single-cell best practices guidelines (Fleming *et al*., 2023). Cells were marked as outliers and filtered out if they differed by 5 MADs in their logarithmical total counts, genes-by-counts, and percentage counts in top 20 genes. Additionally, cells with more than 10% mitochondrial counts and 3 MADs were also removed. Doublets were then removed individually for each sample using scDblFinder with default settings using a custom *doublet_removal*() function. Finally, QC plots were analysed to determine the necessity of additional filtering thresholds for each individual sample. The cells were then filtered by manually defined minimal genes-by-counts thresholds (from 200 to

500). Table 3 shows the output cell and gene counts for each of the QC and filtering steps.

Table 3. Foetal sample cell and gene counts following individual quality control and filtering steps.

Sample	Cells					Genes				
	Unfiltered	Basic Filtering	MAD Filtering	Doublet Removal	Manual Filtering	Unfiltered	Basic Filtering	MAD Filtering	Doublet Removal	Manual Filtering
DEV16134_Quad	8376	8375	7863	7161	7160	36601	18966	18966	18966	18966
DEV16135 + DEV16171_Quad	11486	11472	10554	9383	9099	36601	21700	21700	21700	21700
DEV15985_Quad	10326	10193	9368	8476	8377	36601	21687	21687	21687	21687
DEV16569_Quad	8555	7999	7425	6858	6075	36601	20238	20238	20238	20238
DEV16134_Ach	2507	2507	2326	2248	2217	36601	15341	15341	15341	15341
DEV15983_Ach	5905	5902	5506	5148	5128	36601	18461	18461	18461	18461
DEV15984_Ach	5859	5856	5564	5222	5214	36601	18182	18182	18182	18182
DEV15985_Ach	8384	8374	7982	7324	6547	36601	17726	17726	17726	17726
DEV16136_Quad	7241	7228	6727	6247	5843	36601	20867	20867	20867	20867
DEV16127_Ach	7413	7331	6978	6474	6240	36601	20703	20703	20703	20703
DEV16135 +DEV16171_Ach	7182	7181	6667	6169	6008	36601	17737	17737	17737	17737
DEV16127_Quad	12434	12134	11215	9873	9514	36601	21953	21953	21953	21953
DEV16569_Ach	9376	9374	9219	8310	8309	36601	18360	18360	18360	18360
DEV15984_Quad	7092	7039	6507	6028	5756	36601	19583	19583	19583	19583
DEV16136_Ach	414	414	374	372	372	36601	4828	4828	4828	4828

For normalisation, the pre-processed and filtered concatenated anndata object was split into separate adult-only and developmental-only sample objects. Each was normalised using a shifted logarithm approach based on the delta method (referred to as **log1pPF**) involving *scanpy.pp.normalize_total(target_sum= None)* followed by *scanpy.pp.log1p()*, as recommended by the recent comprehensive data transformation benchmark study (Ahlmann-Eltze and Huber, 2023; Schaar and Heumos, 2023). Top 3,500 highly variable genes were then selected for adult-only and developmental-only objects using scIB package's *preprocessing.hvg_batch()* function, with flavor and batch_key parameters set to 'cell_ranger' and 'sampletype', respectively.

Donor sexes were determined by calculating XIST gene counts and percentages of Y chromosome genes. Additional filtering was done to remove 51 genes detected in less than 5 counts and remove counts with fewer than 200 genes expressed. Cell cycle phase was then determined using *scib.preprocessing.score_cell_cycle()*. The data was then scaled using a

custom function *split_and_scale()* that split the concatenated objects by sampletype and applied *scanpy.pp.scale()* individually for each sample. Dimensionality reduction in the form of principal component analysis (PCA) was then applied to scaled highly variable gene counts, and neighbours (n_neighbors=30, npcs=15) were calculated to produce uniform manifold approximation (UMAP) plots. Further downstream analysis is described in individual chapter methods sections.

3.5 10X Visium Spatial RNA-Sequencing

Foetal Achilles (*N*=1) and quadriceps tendons (*N*=2) (Appendix Table 3) were dissected from both legs of a single 20 pcw foetus and flash frozen in liquid nitrogen. In preparation for Visium ST, the samples were cut to ≤0.65 cm^2 to fit the Visium slide regions. We were able to retain enthesis-to-MTJ as well as adjacent muscle tissue regions for both types of tendons. The cut samples were embedded in cold OCT mounting medium (VWR) on dry ice and cut longitudinally into 10 µm sections, which were then fixed and stained with H&E to verify tissue morphology and suitability. The sections were prepared for sequencing according to the 10X Genomics recommended protocols. Libraries were sequenced using Illumina NextSeq500 (paired-end) at a depth of 54,000 (Quad2 tendon), 74,000 (Ach) and 119,000 (Quad1) mean reads per spot. The data and images were processed with SpaceRanger (v.1.3.1, 10X Genomics) using default settings and mapped to the GRCh38 reference genome.

3.6 Data from Embryonic Whole Limbs

Single-cell RNA-sequencing (*N*=25 from different hind limb regions of 11 donors) and Visium spatial RNA-sequencing (*N*=8 from different hind limb regions of two 6pcw and one 8pcw donors) files were provided by the Teichmann group at the Wellcome Sanger Institute (Cambridge, UK) (Appendix Table 3). The tissues were collected, processed and sequenced by the group in accordance with the methods published in B. Zhang *et al*., 2023. For this analysis, the raw sequencing files were processed and aligned in the same way as was done for the foetal samples to minimise bias, using same versions of the CellRanger and CellBender packages for the single-cell data and the

SpaceRanger package for the spatial data. Further data processing and analysis was carried out as described previously in section 3.3.3.

3.7 Data from Adult Tendons

Processed, integrated, and annotated human adult quadriceps and Achilles tendon single-nuclei RNA-sequencing datasets (*N*=26 from 12 donors) were provided by the Tendon Seed Network (Oxford, UK) (Baldwin *et al*., 2023, 2021). Briefly, the raw sequencing files were processed using the cribbslab package pipeline *scflow quantnuclei* (Python v3.8.15; https://github.com/cribbslab/scflow). Quality control of Fastq files was performed using fastqc (v0.12.1). Fastq files were mapped to the human Ensembl GRCh38 transcriptome (release 106) using *kallisto bustools kb count* (v0.27.3, https://www.kallistobus.tools/kb_usage/-kb_count/) with kmer size = 31. Spliced and unspliced matrices were merged to create the count matrix for downstream analysis. The snRNA-seq analysis and annotation was performed by Dr Jolet Mimpen (quadriceps tendons) and Dr Carla Cohen (Achilles tendons) in R (v4.3.1) and RStudio Server (v2023.03.1, build 446) using SingleCellExperiment (v1.22.0) and Seurat (v4.3.0.1). The counts were log-normalised using Seurat's default functions. QC metrics were calculated with scuttle (v1.10.1). Filtering thresholds for number of cells (nCount), number of features (nFeature) and mitochondrial ratios (mitoRatio) were set manually for each sample to remove poor-quality cells. Doublets were detected and removed with scDblFinder (v1.12.0) using the default settings. Ambient RNA was detected using *decontX()* from the package celda (v1.14.0). Further ambient RNA detection was performed using SoupX (v1.6.2) and the soupX-adjusted count matrix was used for downstream analysis steps. Integration of samples was performed using Harmony (v0.1) implemented within the Seurat workflow, with a combined sample donor and tissue type variable specified for batch correction. Clusters were defined with Seurat's *FindClusters(),* and a cluster comprising nuclei with high decontX scores was removed. Clustering resolution was chosen using Clustree (v0.5.0). Annotation was subsequently performed by assessing cluster-specific expression of manually curated gene sets.

3.8 Data and Code Availability

Raw and processed annotated foetal tendon data is available upon request from the CZI Lattice. All code for the analysis is freely available at https://github.com/AlinaKurjan/DPhilCode.

Chapter 4: Transcriptomic Analysis of Human Foetal Achilles and Quadriceps Tendons

4.1 Introduction

The development of the human musculoskeletal system is a complex process initiated early in embryogenesis and extending through foetal development. While the embryonic stages of tendon development are relatively well understood, much less is known about the subsequent foetal period. This phase marks a critical point in development, shifting the focus from the foundational cellular differentiation and basic tissue patterning seen in early tendon morphogenesis to robust tissue growth characterised by significant expansions and changes in the ECM essential for tendon maturation. Understanding these changes is essential not only for uncovering the detailed biological processes underlying musculoskeletal development, but also for informing advancements in targeted therapies and regenerative approaches that can address a spectrum of tendon pathologies and injuries.

In this chapter, single-nucleus and spatial RNA-sequencing techniques are used to analyse the cellular heterogeneity and spatial organisation within foetal Achilles and quadriceps tendons. Using snRNA-seq, major cell types within tendons at 12, 17, and 20 post-conception weeks (pcw) are characterised, outlining their distinct transcriptomic landscapes. Subsequently, spatial RNA-seq is applied to 20 pcw tendons to map these cell types along the tendon's length, correlating their gene expression patterns with their specific anatomical positions. The focus is then placed on ECM-depositing fibroblasts, highlighting their matrisomal gene expression profiles and the evolution of their biological function pathways from 12 to 20 weeks. This research clarifies the complex molecular and cellular events that underpin the beginning of tendon maturation during critical early stages of foetal life, thereby enriching our understanding and extending the existing literature on tendon biology.

4.2 Methods

4.2.1 Challenges of analysing generated datasets

The analysis of the dataset presents several significant challenges, stemming from both technical and biological factors, which require careful consideration to ensure reliability. One of the foremost challenges pertains to the presence of nested batch effects within the dataset. Specifically, foetal Achilles or quadriceps tendon tissues were obtained from donors, either matched or unmatched, at distinct developmental stages spanning 12, 17, and 20 pcw. These developmental variations introduce complex biological variation that includes inter- and intra-donor differences as well as wide-ranging differences across and within the developmental stages. Furthermore, the data is susceptible to technical variation stemming from differences in library preparation and sequencing processes, coupled with variations in sequencing dates and batches. These technical discrepancies can significantly confound the analysis by introducing non-biological sources of variability. Consequently, it is imperative to employ not only appropriate statistical methods to disentangle batch effects from genuine biological signals, but also robust normalisation methods and quality control measures to mitigate the impact of technical variations.

In addition, there are unknown sources of biological variation from factors such as differences in maternal health, and the undisclosed health status of the foetus (besides any disclosed screened genetic abnormalities that have been avoided for the purpose of this study). These uncharacterised variables can contribute to heterogeneity within the dataset, potentially complicating the identification of biologically relevant patterns. Exploring methods for capturing and controlling latent sources of biological variation is therefore paramount to ensuring analytical integrity.

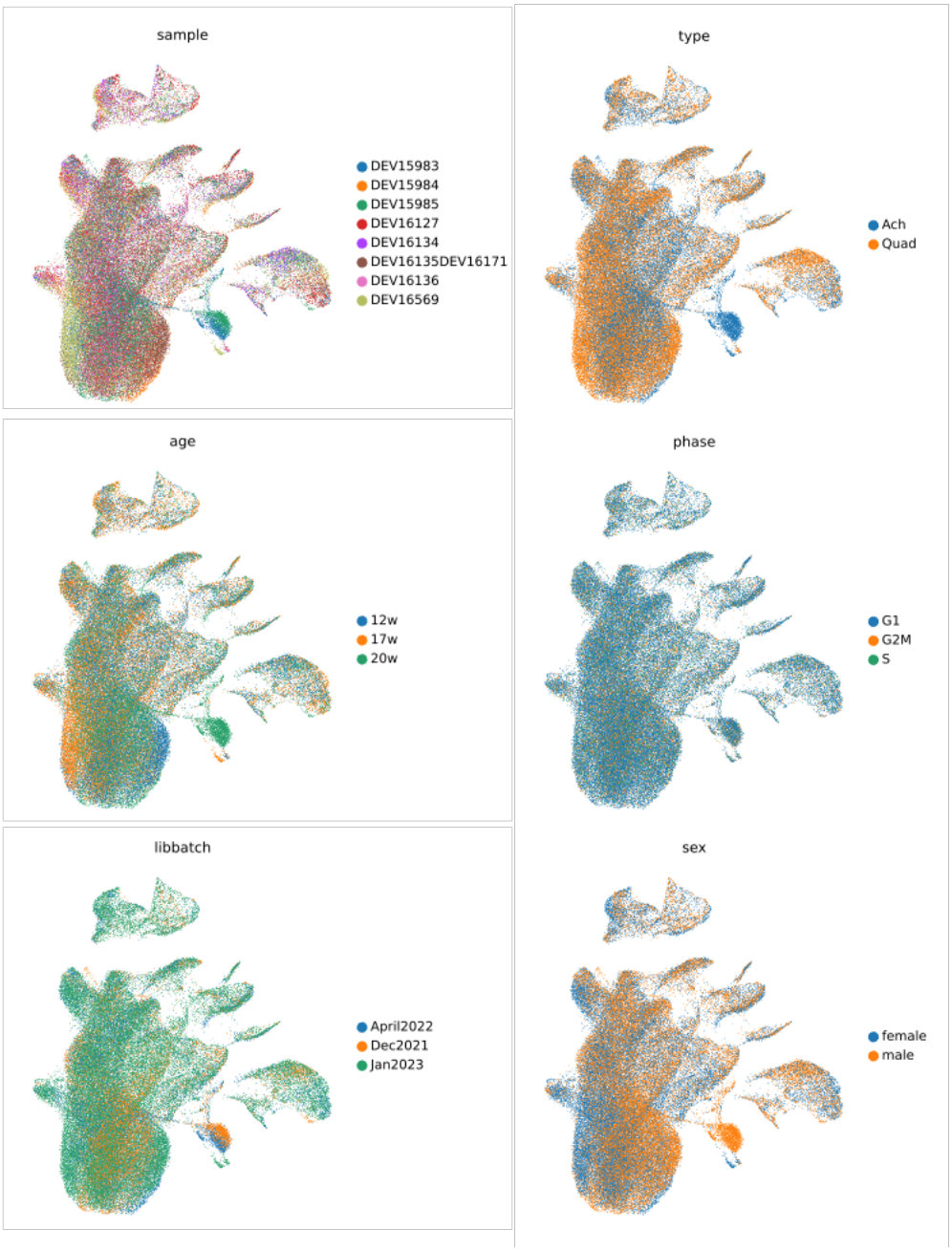
4.2.2 Single-nucleus RNA-sequencing data analysis

4.2.2.1 Data integration, batch correction, and annotation

Developmental sample data were integrated and batch-corrected using scvi-tools' (Gayoso *et al*., 2022) single-cell Variational Inference (scVI) modelling on

all unnormalised gene counts, with the main batch effects of interest specified to be ‘sampletype’ and ‘libbatch’, corresponding to different donor and tissue type (e.g., DonorID1_AchillesTendon and DonorID1_QuadTendon) and library preparation batches, respectively (see metadata in Appendix Table 3). Model hyperparameters were optimised using manual runs with different parameters as well as scVI’s autotune functionality, which determined the best fitting parameters to be 'n_latent': 30, 'n_layers': 2, ‘dropout_rate': 0.1, 'gene_likelihood': 'zinb', ‘dispersion’: ‘gene-batch’. The model was trained using 398 epochs until model training and validation sets were stably converged. The resulting latent representation embeddings used as basis for the computation of a neighbourhood graph of observations and dimensionality reduction with UMAP (Figure 16B).

A Unintegrated foetal tendon snRNA-seq data



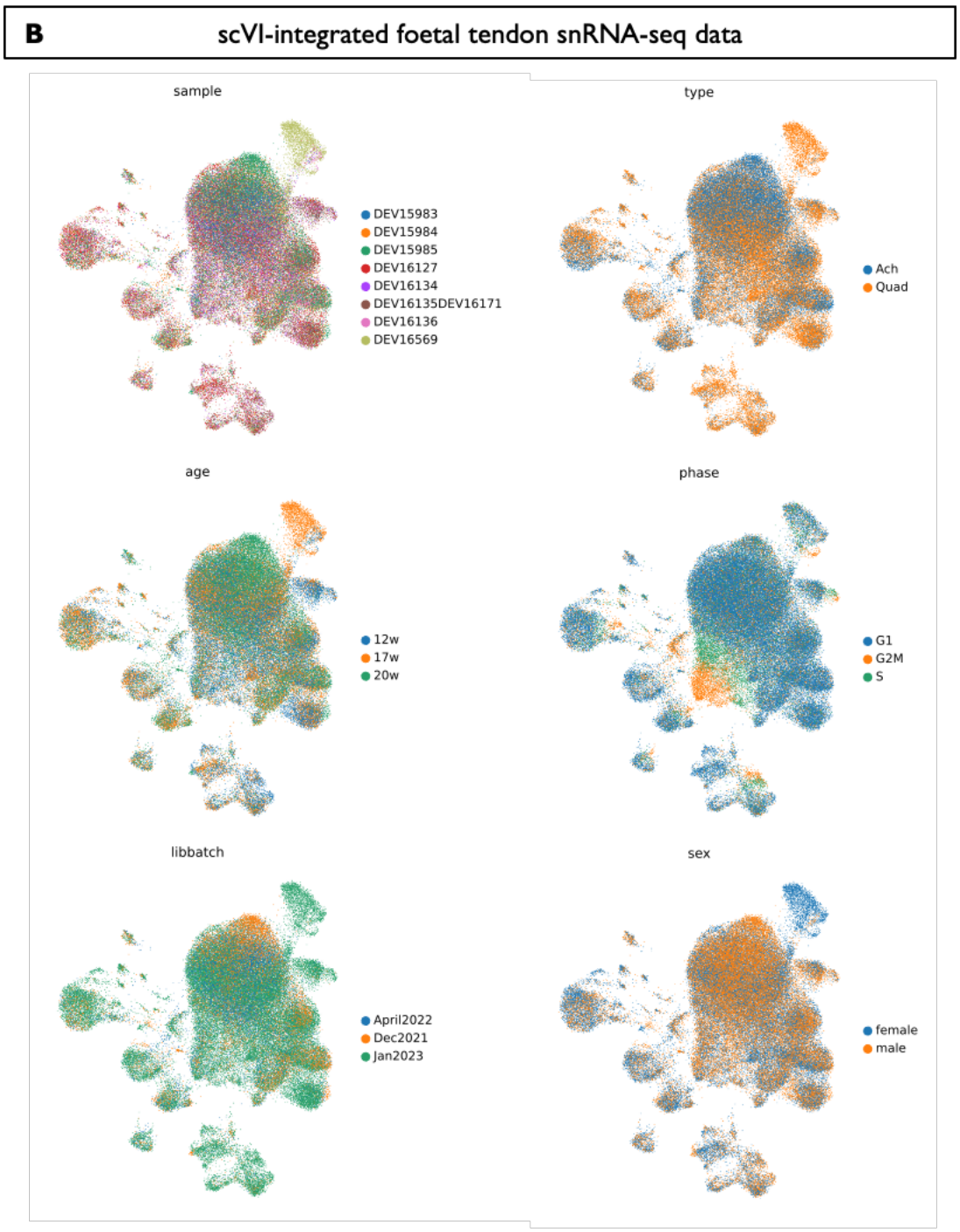
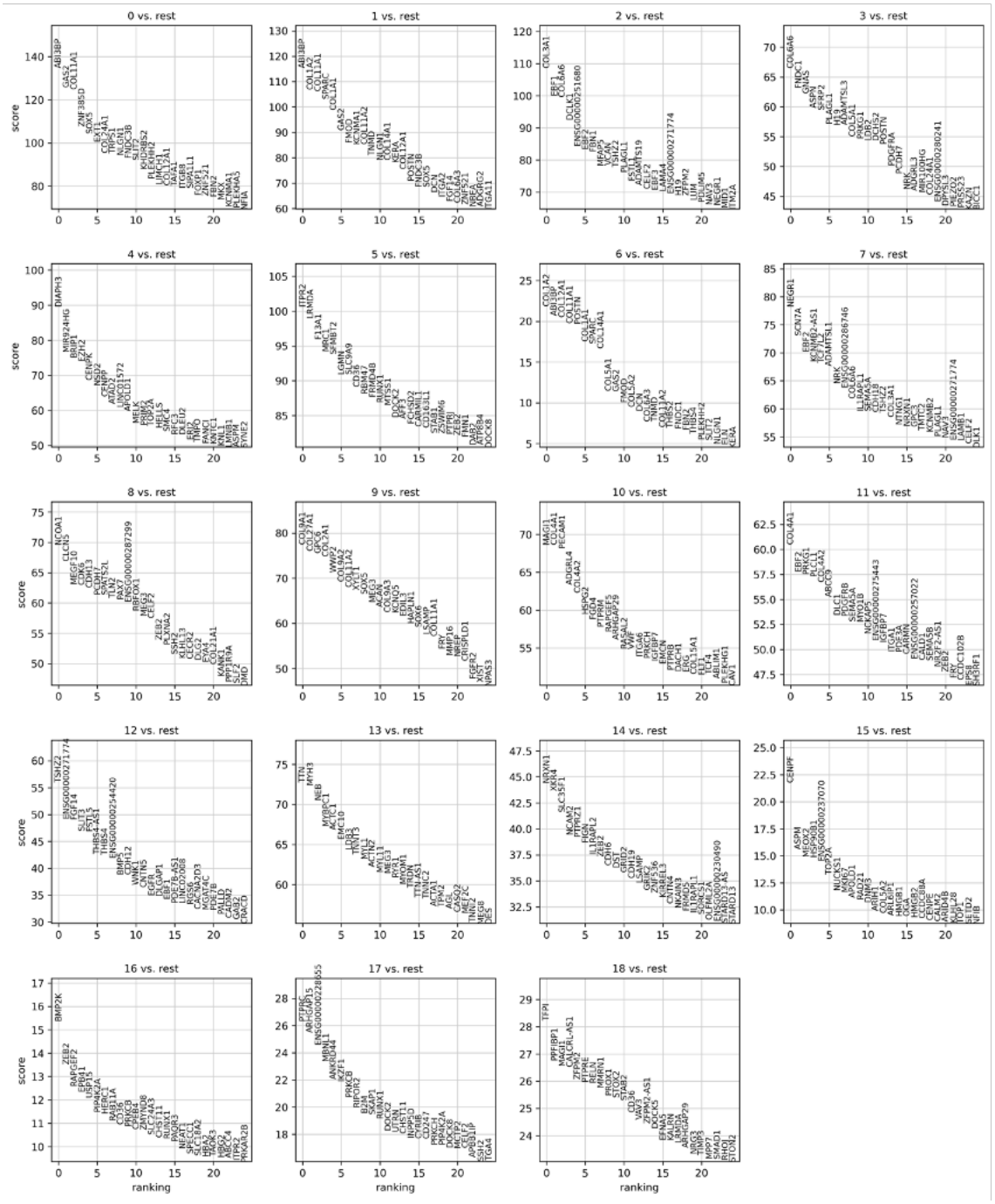


Figure 16. UMAP plots of foetal tendon samples before (A) and after integration and batch correction using scVI (B). *The UMAPs (Uniform Manifold Approximation and Projection) show the distribution of cells from foetal tendon samples, coloured according to various biological and technical factors – donor identity ("sample"), tendon type, donor age, cell cycle phase, library preparation batches ("libbatch"), and donor sex.* ***Panel A*** *shows cells prior to any batch correction or integration, while* ***panel B*** *shows the same data after corrections using scVI. Samples were corrected for both the "libbatch" and "sampletype" (combined sample ID and tendon type variable).*

Data clustering was carried out using scanpy's Leiden algorithm, identifying a total of 19 clusters (0-18) at 0.6 resolution (Figure 17B). Normalised and log-

transformed cluster gene counts were then ranked using a Wilcoxon rank-sum test using *scanpy.tl.rank_genes_groups()* (Figure 17A).

A



B

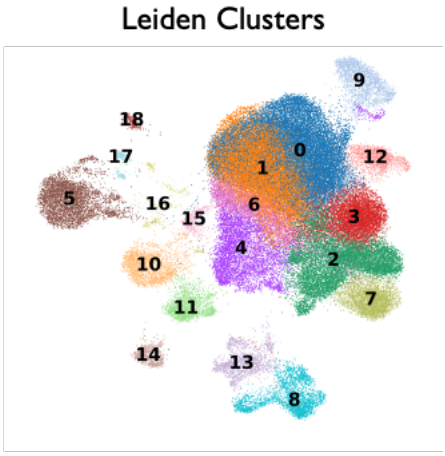


Figure 17. Leiden clustering and between-cluster differential gene expression analysis of foetal tendon cell data. *Tendon snRNA-seq data clustering using the Leiden algorithm identified 19 distinct cell clusters based on gene expression profiles. Differential gene expression analysis was performed between these clusters using the Wilcoxon rank-sum test to identify genes differentially expressed across clusters.* ***Panel A*** *shows ranked gene plots for each cluster, illustrating the top 25 differentially expressed genes when compared to all other clusters. X-axis represents the log fold changes of each gene, while the y-axis indicates the negative* log_{10} *of the p-value.* ***Panel B*** *features a UMAP plot showing the distribution of cells within the identified Leiden clusters at a resolution of 0.6.*

The clusters were manually annotated by checking known cell type markers (see Figures 19-24) and by querying top 350-550 Leiden cluster DEGs with CellMESH (Y. Zhang *et al*., 2023) and g:GOSt functional profiling (Raudvere *et al*., 2019) tools. Heatmaps and hierarchical clustering dendrograms were also consulted in the process to make the best guesses for the previously undefined cell types. Clusters of cells differentially expressing cell division markers (4, 15) as well as a small cluster containing a mix of different markers of immune cell subsets (16) were labelled as 'Unknown' to utilise the predictive capabilities of scANVI labelling.

Following scVI integration and cell type labelling, scANVI was run with the scVI model as basis for 25 epochs. The resulting latent representation embeddings were used for the computation of a neighbourhood graph of observations and dimensionality reduction with UMAP (Figure 18). scANVI cell type label predictions ('C_scANVI', Figure 25A) were considered when finalising cell type annotations.

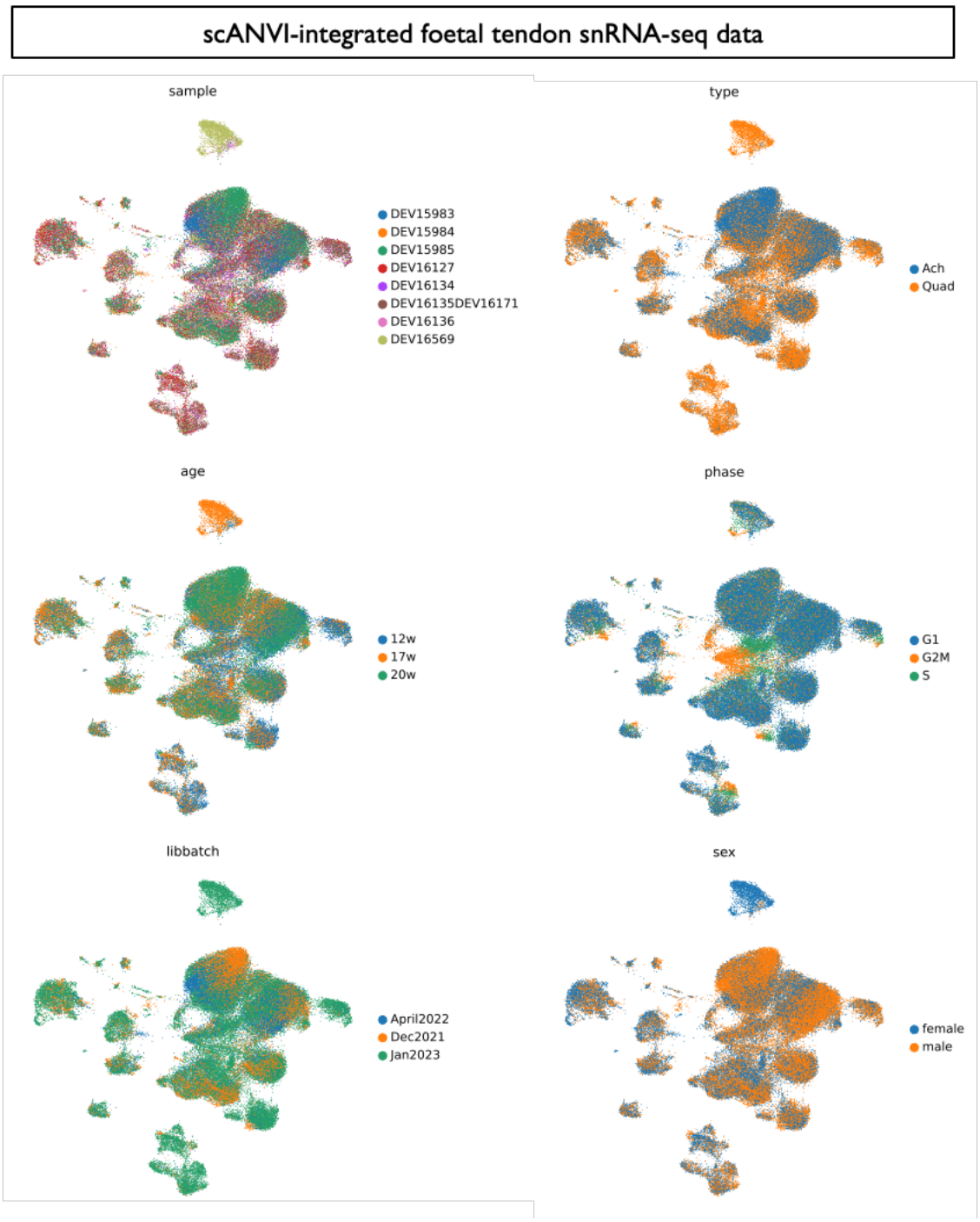


Figure 18. UMAP plots of foetal tendon samples after label refining using scANVI. *scANVI model was initialised from the original trained scVI model (see Figure 16B) to reassign cell types labelled as "unknown" into their most likely related clusters. The UMAPs show the distribution of cells from foetal tendon samples, coloured according to various biological and technical factors – donor identity ("sample"), tendon type, donor age, cell cycle phase, library preparation batches ("libbatch"), and donor sex.*

4.2.2.2 Pseudobulk differential gene expression analysis with DESeq2

For differential gene expression (DGE) analysis of cell types across different ages, the raw single-nuclei sequencing counts were converted into

"pseudobulk" expression profiles using custom functions (see code). Briefly, the data were first partitioned by distinct cell types, and a donor-filtering criterion was applied to retain only tissue donors with a minimum cell count threshold of 30. Three pseudoreplicates were then generated by randomly subsampling cells within retained donors, and these pseudoreplicates were subsequently transformed into pseudobulk samples by aggregating expression counts. Metadata associated with donors, experimental conditions, and cell identity were preserved.

DGE analysis was carried out individually for each of the cell type pseudobulked counts using DESeq2 (v1.40.2). Both LRT and Wald tests were done to assess the differences between different developmental timepoints and tissue types. Wald test results are shown in Appendix Figure 6. LRT results with *p-adjusted* values of <0.01 were clustered to investigate common patterns in gene expression changes over time. The resulting cluster gene lists were subjected to pathway analysis against all expressed genes using the gProfiler g:GOSt tool (Raudvere *et al*., 2019) with Benjamini-Hochberg FDR set to <0.05 and pathway term sizes restricted to between 20 and 500 terms. The terms in different cell types in each cluster of gene expression were compared using Venn diagrams made with ggVennDiagram (Gao *et al*., 2024) (Figure 34). Shared or cell type-specific terms for each cluster were then isolated and manually grouped into common functional categories to reduce data dimensionality and enable comparisons**.** The summary of common grouped functional categories per cluster is presented in tables shown in Appendix Figure 6.

4.2.2.3 Compositional analysis

tascCODA package functions were used to assess cell type compositional changes at different developmental timepoints (Ostner *et al*., 2021). This method not only treats the data as a multinomial distribution while addressing inter-feature dependencies, but also accommodates hierarchical cell type clusters. Additionally, tascCODA enables the modelling of covariate effects – in this case, foetal age – across all levels of the cell cluster hierarchy, ranging from a single overarching cluster to as many as 40 distinct cell subtype clusters.

Briefly, a nested stochastic block hierarchical clustering model was generated using the Schist package (Morelli *et al*., 2021). Next, a MuData object was created by generating and loading a tascCODA model, which converted the hierarchical clustering tree into an ete tree structure. The cluster of nuclei corresponding to the manually labelled Nervous System Cells was used as reference for the model as it was assumed to be the least likely to change in its composition and transcription profile during the foetal tendon 12-20 pcw developmental period.

4.2.3 Spatial RNA-sequencing data analysis

4.2.3.1 Spatial region annotation

Quadriceps and Achilles tendons along with their adjacent muscle regions (*N*=2 and *N*=1, respectively) were isolated from a single 20 pcw donor. The samples were processed, sequenced and aligned as described in section 3.4. The data were processed using Scanpy and Squidpy (Palla *et al*., 2022). Briefly, the tissue objects were manually filtered to remove: 1) cells with fewer than 500-1,000 counts or more than 10,000-20,000 counts (with exact numbers depending on individual sample properties), 2) genes that were detected in fewer than 10 cells, and 3) any ribosomal and mitochondrial reads. The counts were then normalised to log1pPF using the *scanpy.pp.normalize_total*(*target_sum=None*) and *scanpy.pp.log1p()* with default settings. Two thousand highly variable genes were selected with the "cell_ranger" flavour using *scanpy.pp.highly_variable_genes()*. After normalised count scaling with *scanpy.pp.scale()*, PCA was carried out, and neighbours and UMAPs were then calculated for the data using default Scanpy functions. Finally, all tissue objects were subjected to Leiden clustering at 1.0 resolution, identifying 7 clusters for each of the different samples (Appendix Figure 1). The identified clusters were examined by analysing the outputs of a Wilcoxon rank-sum test run using *scanpy.tl.rank_genes_groups()* (Appendix Figure 1).

To definitively annotate the different regions, the gene expression clusters and their corresponding histological properties were examined within the 10X Genomics Loupe Browser (v6.4.1). The clusters were then manually annotated to match their major histological regions (e.g., tendon, muscle, and loose

connective tissue). Annotated region neighbourhood enrichment analysis and region edge interactions analysis were carried out using Squidpy functions *sq.gr.nhood_enrichment()* and *sq.gr.interaction_matrix()*, respectively (Appendix Figure 1).

4.2.3.2 Cell type mapping with Cell2location

To infer the spatial distribution of cell types within the tissue, processed and annotated snRNA-seq data was split to retain only the unnormalised, untransformed counts belonging to the 20 pcw samples and integrated with spatial RNA-seq information using cell2location (v0.1.3) (Kleshchevnikov *et al*., 2022). First, the 20 pcw snRNA-seq samples were filtered to retain 12,731 genes that were a) present in at least 30 cells and b) had a mean expression level of at least 1.12 across all cells, as per the default setting. Donor ID ('sample') variable was provided as the 'batch_key', while refined scANVI cell type annotations were supplied as the 'labels_key'. Batch effects in the form of library preparation batches ('libbatch') and different tendon tissue types ('type') were also considered when modelling. 9,522 genes overlapping between spatial and snRNA-seq datasets were retained for the final model fitting and cell type inference.

Cell2location hyperparameters were specified based on the tissue and experiment considerations in mind as having a) expected cell abundance per Visium spot set to 17 (range of 10-32 nuclei in different regions), and b) regularisation of within-experiment variation in RNA detection sensitivity set to 20. The model was trained until convergence for a total of 15,000 iterations.

H&E images were used as basis for microanatomical tissue region identification and labelling (Appendix Figure 1). To further analyse potential tissue microenvironments in an unsupervised manner, non-negative matrix factorization (NMF) using cell2location's scikit-learn NMF wrapper function was also applied to estimated cell abundances. The model was trained using a range of factors (5-30) for decomposition of cell abundance data, with smaller factors assuming lower numbers of distinct patterns and higher likelihood of cell co-location.

4.3 Results

4.3.1 Single-nuclei resolution characterisation of foetal tendon cell types

To study the cell populations present in tendons with intrinsic regenerative capacity, Achilles and quadriceps tendons were collected and sequenced from 9 different human foetal donors aged 12 to 20 pcw. Following quality control and data preparation steps, scVI-integrated data from 91,859 nuclei were used for clustering into a total of 19 groups (see Figures 16 and 17). The complexity of this developmental data posed a challenge, as specific cell types had not been previously annotated. However, by referencing existing literature on adult human and mouse tendons (see section 2.2.3), various types of fibroblasts, immune cells, endothelial cells, smooth muscle cells, lymphatic cells, and nervous system cells were anticipated to be identified within the tendon tissue.

4.3.1.1 Fibroblasts

Initially, fibroblast populations were identified by analysing gene expression levels of established tenocyte and tendon ECM genes (Figure 19). The analysis revealed that clusters 0, 1, 2, 3, 4, 6, 7, 12, and 15 exhibited a higher proportion of cells expressing common tendon matrisomal genes, including *COL1A1*, *COL3A1*, *COL12A1*, *POSTN*, *secreted protein acidic and rich in cysteine* (*SPARC*), and *DCN*, indicating a probable fibroblast identity for these clusters. Notably, clusters 2 and 7 displayed a distinct profile characterised by increased levels of *COL6A6* and *LUM* expression, distinguishing from other fibroblast clusters.

To gain deeper insights into the functional heterogeneity of these fibroblast clusters, the expression of *SCX*, *MKX*, *TNMD*, *FMOD*, *THBS2*, and *THBS4* genes, which are known to be expressed in early tenocytes, was examined (Figure 19). Interestingly, while *SCX* was expressed in only a small fraction of cells across different clusters, clusters 0 and 1 stood out with the highest proportions of cells expressing the remaining tenocyte markers *MKX*, *TNMD*, *FMOD*, and *THBS2*, followed by clusters 6, 15, and 4. Moreover, cluster 12 showed upregulation of *THBS4* expression in the majority of its cells compared to all other clusters, suggesting a potentially distinct functional role for this

specific fibroblast population. Intriguingly, clusters 2 and 7 were distinct once again, as they either lacked or showed minimal expression of *SCX*, *MKX*, *TNMD, FMOD*, and *THBS2* genes.

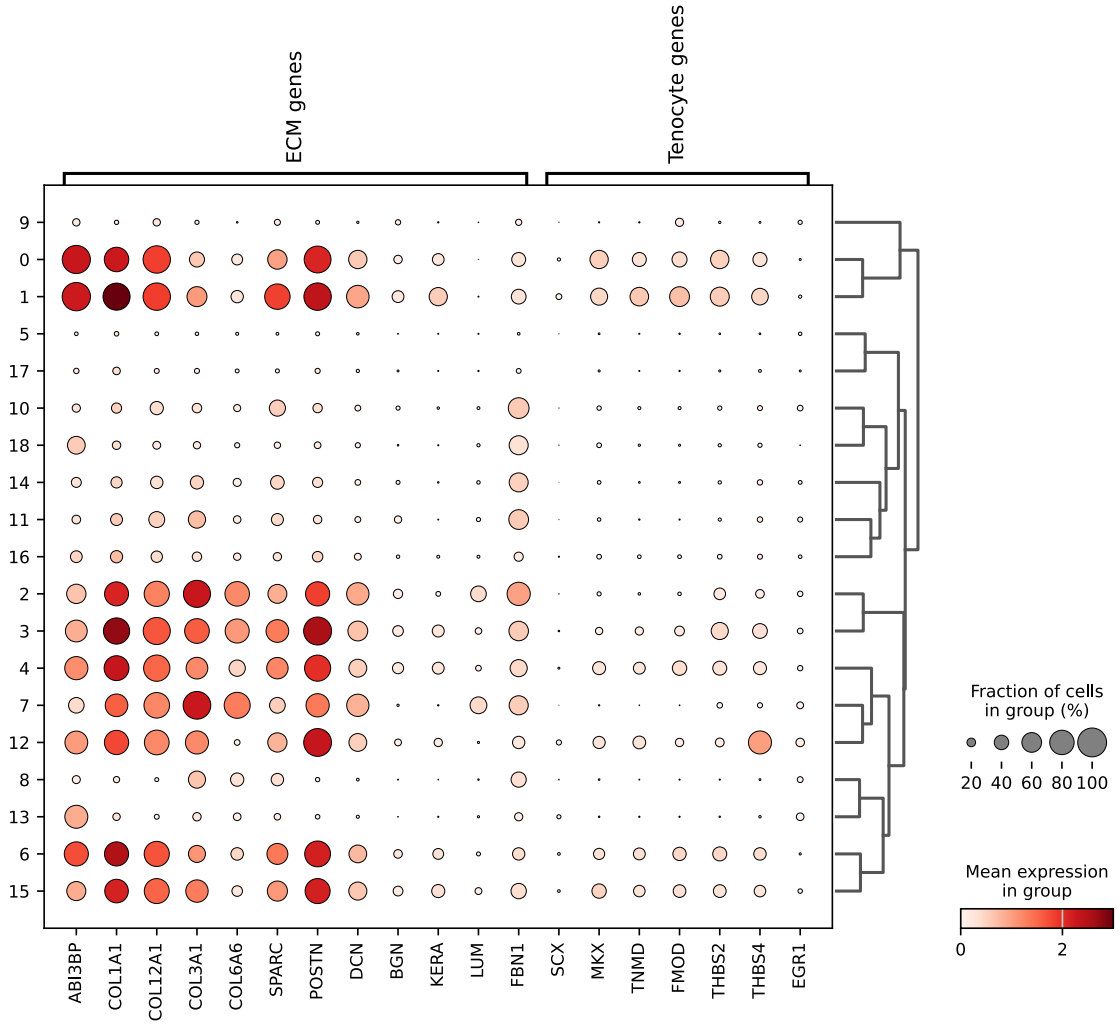


Figure 19. Expression of early developmental tendon ECM markers in foetal tendon snRNA-seq data. *Dotplot of hierarchically clustered Leiden clusters at 0.6 resolution (see Figure 17B) shows the mean log1pPF-normalised, unscaled gene expression levels alongside the proportions of expressing cells for common tenocyte (i.e., tendon fibroblast) intracellular and ECM markers.*

Differential expression analysis of tendon fibroblasts revealed distinct expression patterns of various other genes, leading to the identification of three major fibroblast subtypes (Figure 20). The first tendon fibroblast group, clustered together and referred to as “type 1”, consisted primarily of clusters 0 and 1. This group was characterised by the predominant expression of *ABI family member 3 binding protein* (*ABI3BP*), *growth arrest-specific 2* (*GAS2*), *SRY-box transcription factor 5* (*SOX5*), *COL11A1*, *COL1A1*, *MKX*, *TNMD* and

FMOD. Clusters 6, 0 and 1 were labelled as “ABI3BP GAS2 Fibroblasts” 1-3, respectively, due to their high expression of those genes. Clusters 4 and 15 were found to express markers of dividing cells, including *marker of proliferation Ki-67* (*MKI67*), *DNA topoisomerase II alpha* (*TOP2A*), *centromere protein P* (*CENPP*), and *diaphanous related formin 3* (*DIAPH3*). As a result, these clusters were categorised as a distinct group of dividing cells, later reassigned to their inferred clusters of origin using scANVI's predictive labelling capabilities (Figure 25A,B).

While initially cluster 12 could also be attributed to the first fibroblast group, it stood out as one of the more interesting and unusual clusters. It expressed genes important for early tissue growth and differentiation, including *fibroblast growth factor 14* (*FGF14*), *follistatin-like 5* (*FSTL5*), *THBS4*, *bone morphogenetic protein 5* (*BMP5*), as well as *cadherin 12* (*CDH12*), *early B-cell factor 1* (*EBF1*), *teashirt zinc finger homeobox 2* (*TSHZ2*), and *COL3A1*. Consequently, it was categorised into its own separate group, referred to as "type 3" or "FGF14 THBS4 Fibroblasts."

The second major group, “type 2”, comprised clusters 2, 3 and 7 and was characterised by patterns of elevated expression of *COL3A1*, *COL6A6*, *doublecortin-like kinase 1* (*DCLK1*), *TSHZ2*, *PLAG1-like zinc finger 1* (*PLAGL1*), *VCAN* and *FBN1*. While cluster 3 also exhibited similarities to type 1 fibroblasts (and was hence labelled as "COL6A6 FNDC1 Fibroblasts"), clusters 2 and 7 displayed distinct differences from both type 1 fibroblasts and cluster 3. They expressed genes such as *LUM*, *neuron navigator 3* (*NAV3*), *NOVA alternative splicing regulator 1* (*NOVA1*), *neuronal growth regulator 1* (*NEGR1*), *semaphorin 5A* (*SEMA5A*), and *TNXB*. Moreover, cluster 2 expressed a “universal fibroblast” marker *peptidase inhibitor 16* (*PI16*) (Muhl *et al*., 2020), while cluster 7 specifically expressed *sodium voltage-gated channel alpha subunit 7* (*SCN7A*) and *cadherin 18* (*CDH18*). These clusters were designated as "COL3A1 PI16 Fibroblasts" and "NEGR1 SCN7A Fibroblasts," respectively.

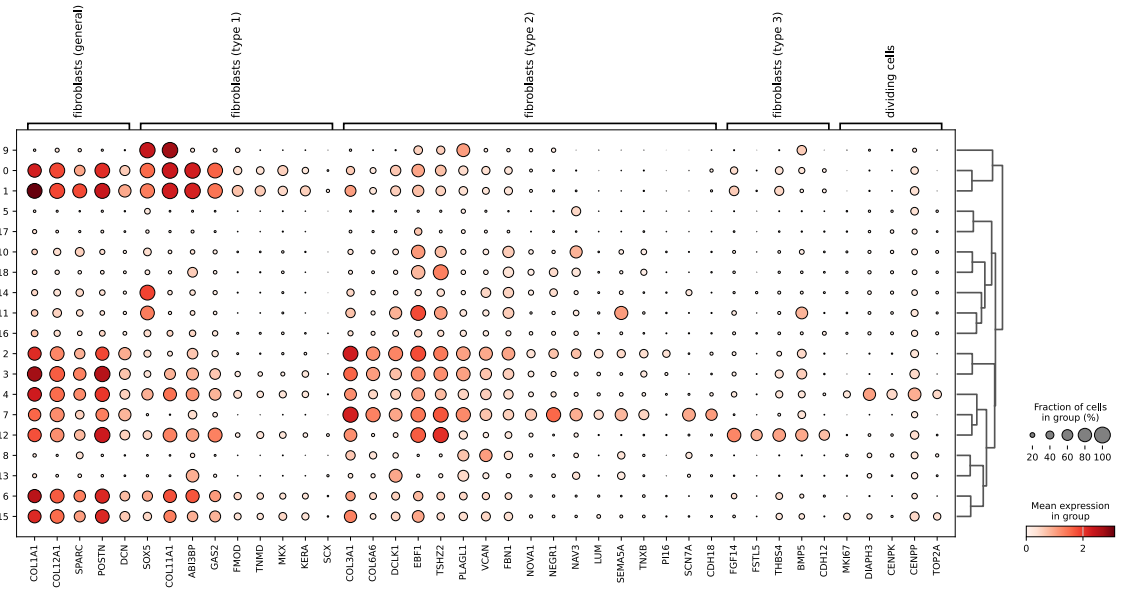


Figure 20. Expression patterns of general and type-specific fibroblast genes in foetal tendon snRNA-seq data. *Dotplot of hierarchically clustered Leiden clusters at 0.6 resolution (see Figure 17B) shows the mean log1pPF-normalised, unscaled gene expression levels alongside the proportions of expressing cells for select top differentially expressed genes relevant for fibroblasts. Fibroblast subtype groupings were determined based on distinct expression patterns of selected extracellular matrix and fibroblast-specific genes. Dividing cell markers are used to identify a separate cluster of dividing cells.*

4.3.1.2 Mural cells: endothelial cells and smooth myocytes

Following tendon fibroblast labelling, cell populations showing positive expression for genes associated with tendon loose connective tissues such as the endotenon IFM were examined. These genes encompassed type IV collagens (e.g., *COL4A1*, *COL4A2*), *perlecan* (*HSPG2*), *nidogen-1* (*NID1*), laminins (e.g., *LAMB1*, *LAMC1*), and integrin subunits (e.g., *ITGA6*, *ITGB1*) (Figure 21). Heightened gene expression patterns for these markers were observed in clusters 10, 14, and 18, while clusters 7 and 8 displayed lower expression levels of the same genes. Notably, cluster 11 exhibited heightened expression of *COL4A1* and *COL4A2*, but not the remaining genes of interest, compared to other clusters.

Further analysis using DEGs revealed the presence of markers for vascular endothelial cells (*platelet and endothelial cell adhesion molecule 1* (*PECAM1*, also known as *CD31*), *CD34*, *von Willebrand factor* (*VWF*)) and lymphatic endothelial cells (*lymphatic vessel endothelial hyaluronan receptor 1* (*LYVE1*), prospero homeobox protein 1 (*PROX1*), and *fms-related tyrosine kinase 4*

(*FLT4*)) in clusters 10 and 18, respectively. Additionally, numerous genes related to nervous system development were expressed in cluster 14, including *neurexin 1 (NRXN1*), *neural cell adhesion molecule 2* (*NCAM2*), *SOX10*, *glutamate receptor delta 2* (*GRID2*), and *protein tyrosine phosphatase receptor type Z1* (*PTPRZ1*). Lastly, cluster 11 was identified as containing smooth myocytes through the expression of markers such as *α-smooth muscle actin* (*ACTA2*), *myosin 11* (*MYH11*), *caldesmon 1* (*CALD1)*, *notch receptor 3* (*NOTCH3*), and *platelet-derived growth factor receptor beta* (*PDGFRB*).

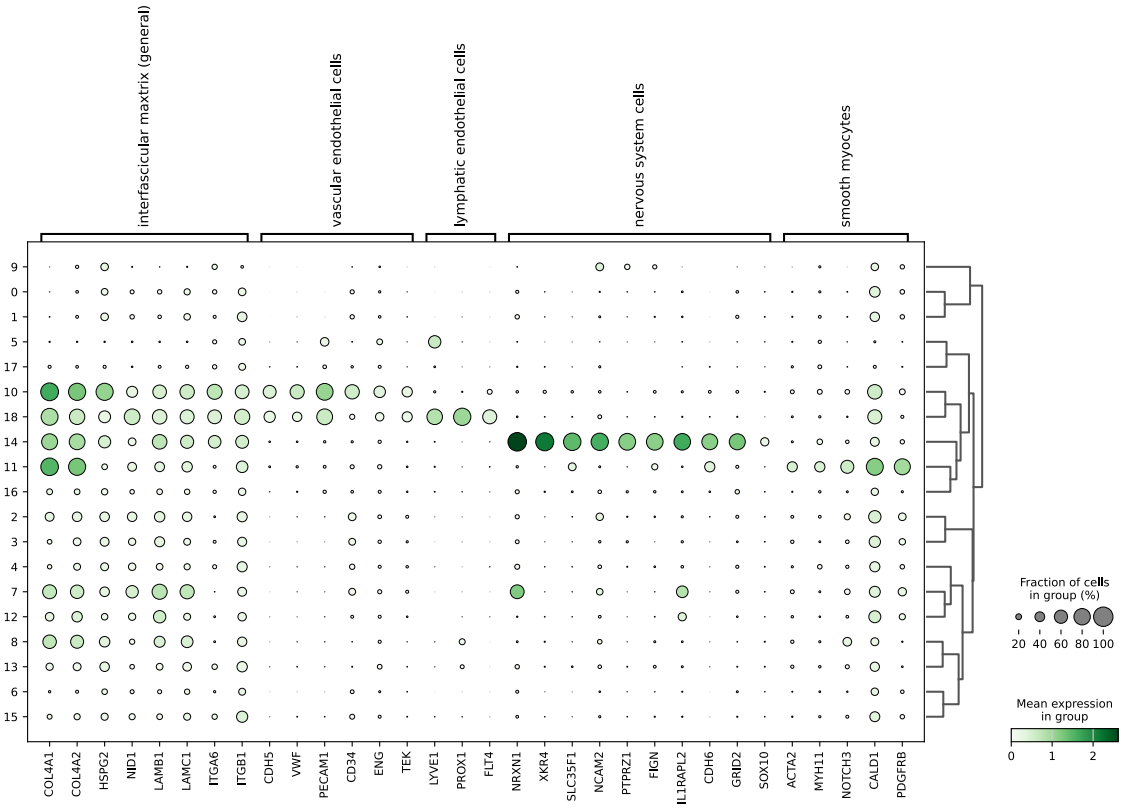


Figure 21. Expression of endotenon and interfascicular matrix-associated genes in foetal tendon snRNA-seq data. *Dotplot of hierarchically clustered Leiden clusters at 0.6 resolution (see Figure 17B) shows the mean log1pPF-normalised, unscaled gene expression levels alongside the proportions of expressing cells for select top differentially expressed genes relevant for cells found in tendon loose connective tissue regions. Genes for interfascicular matrix cells, endothelial cells, nervous system cells, and smooth myocytes were selected based on known markers gathered from relevant musculoskeletal tissue literature.*

4.3.1.3 Muscle cells: skeletal and satellite cells

Looking at cluster 8 that also expressed some of the genes associated with the IFM, we detected the presence of several genes typically upregulated in muscle progenitors such as myoblasts or satellite cells, including *paired box 7* (*PAX7*),

cadherin 15 (*CDH15*), *NCAM1* (also known as *CD56*), *delta-like 1 homolog* (*DLK1*), *myosin XVIIIb* (*MYO18B*), and *ryanodine receptor 3* (*RYR3*) (Figure 22). All those genes, except for *PAX7*, were also expressed in cluster 13, which also had high expression levels of *nestin* (*NES*), *desmin* (*DES*), *titin* (*TTN*), *myosin heavy chain 3* (*MYH3*), *troponin T type 3* (*TNNT3*), and *COL22A1*. Taken together, this gene expression pattern suggested a more advanced skeletal myocyte identity likely detected at the MTJ (see section 2.2.1.1).

4.3.1.4 Chondrocytes

After identifying potential MTJ cells, the presence of cartilage-like cells that could potentially be found in the tendon enthesis was investigated. In cluster 9, distinctive gene expression patterns that corresponded to chondrogenesis-related genes were evident (Figure 22). These genes included *COL2A1*, *COL9A1, ACAN*, *COMP*, *matrilin 1* (*MATN1*), and *hyaluronan and proteoglycan link protein 1* (*HAPLN1*). It is worth noting that cluster 9 primarily consisted of cells sourced from a single donor's quadriceps tendon sample (Figure 23). This observation raises the possibility of potential cross-contamination from the cartilage of the patella. Nevertheless, this cluster was retained for further analysis as it was still likely to offer insights relevant to the tendon enthesis.

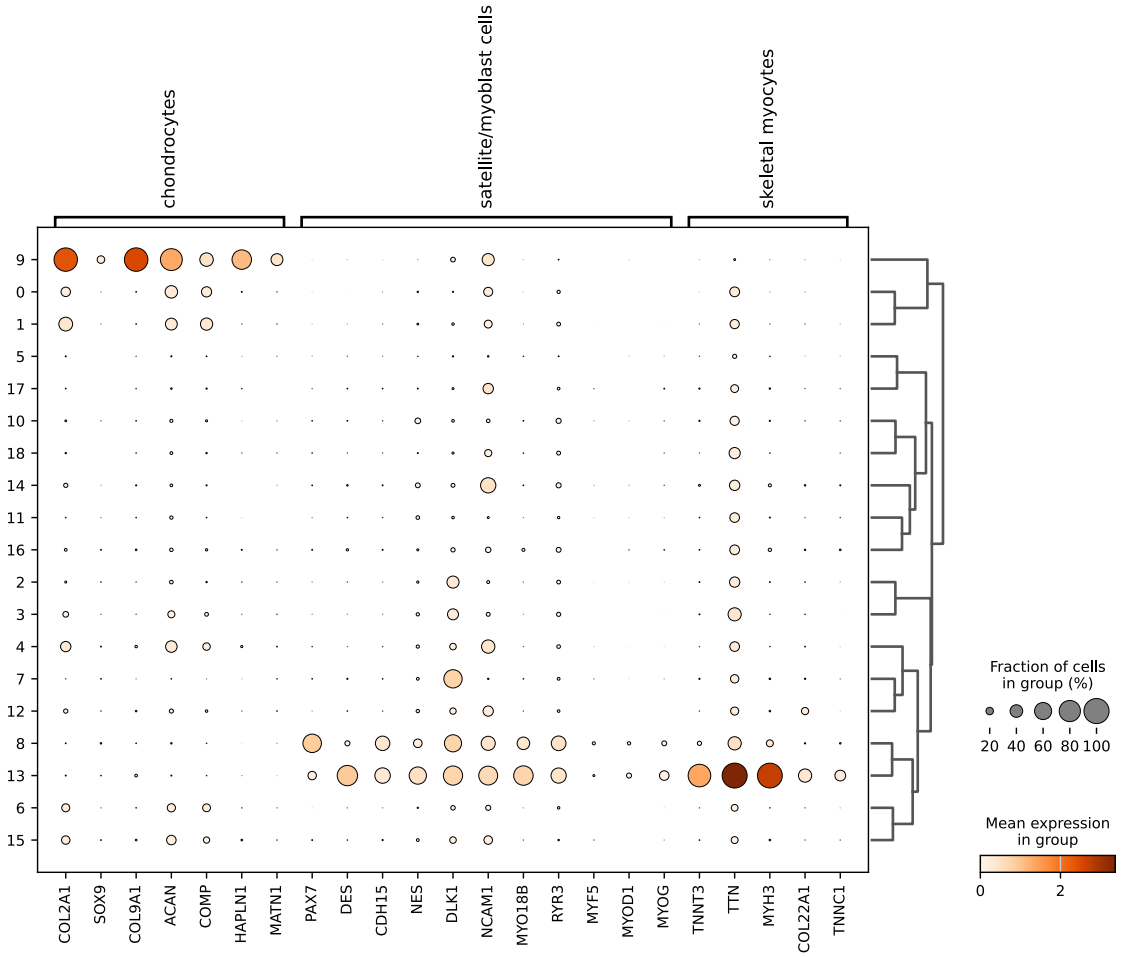


Figure 22. Expression of tendon attachment site-associated genes in foetal tendon snRNA-seq data. *Dotplot of hierarchically clustered Leiden clusters at 0.6 resolution (see Figure 17B) shows the mean log1pPF-normalised, unscaled gene expression levels alongside the proportions of expressing cells for select top differentially expressed genes relevant for cells found in tendon tissue attachment regions – the enthesis and the myotendinous junction. Genes for chondrocytes, satellite cells, and skeletal myocytes were selected based on known markers gathered from relevant musculoskeletal tissue literature.*

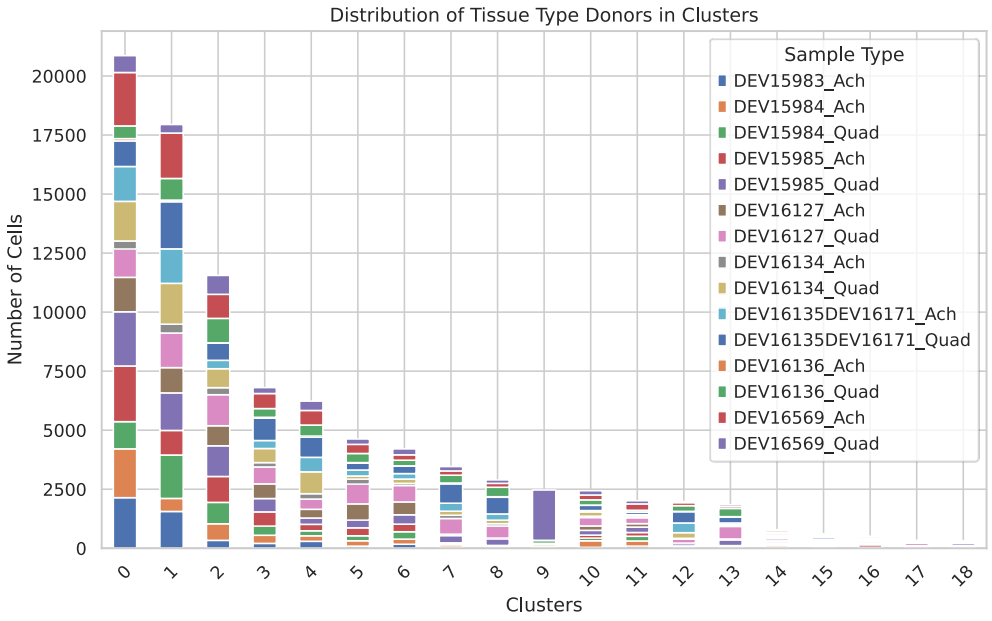


Figure 23. Distribution of foetal snRNA-seq samples across Leiden clusters. *Histogram shows the numbers of cells within each Leiden cluster (see Figure 17B), with each bar representing the number of cells assigned to a specific cluster. The cells are colour-coded according to their original human foetal tendon snRNA-seq samples, denoted by donor ID (DEV#) and tendon type (Ach: Achilles tendon, Quad: quadriceps tendon).*

4.3.1.5 Immune cells

Finally, the remaining clusters 5, 16 and 17 expressed genes associated with immune cells, including *protein tyrosine phosphatase receptor type C* (*PTPRC*, also known as *CD45*), *CD44*, *Ikaros family zinc finger 1* (*IKZF1*), *runt-related transcription factor 1* (*RUNX1*), *dedicator of cytokinesis 2* (*DOCK2*), and *inositol polyphosphate-5-phosphatase D* (*INPP5D*) (Figure 24). Notably, clusters 5 and 17 displayed more pronounced disparities in gene expression in comparison to cluster 16. Specifically, cluster 5 expressed genes characteristic of macrophages, including *coagulation factor XIII A chain* (*F13A1*), *CD163*, *mannose receptor C-type 1* (*MRC1*, also known as *CD206*), *colony stimulating factor 1 receptor* (*CSF1R*), *CD36*, *CD68*, and *legumain* (*LGMN*). In contrast, the relatively small cluster 17 (comprising 335 cells) showed markers typically associated with developing lymphocytes, such as *Src kinase associated phosphoprotein 1* (*SKAP1*), *CD247*, *CD96*, and *CD38*. However, due to the limited cell count in this cluster, definitive characterisation of cell identity proved challenging.

Lastly, cluster 16 containing 509 cells displayed a heterogeneous marker pattern indicative of a potentially hybrid cell subset encompassing immune cells and hematopoietic/progenitor stem cells. These markers included *tyrosine kinase Kit* (*KIT*), *transferrin receptor* (*TFRC*), *interleukin 18 receptor 1* (*IL18R1*), *microphthalmia-associated transcription factor* (*MITF*), *GATA binding protein 2* (*GATA2*), *BMP2 inducible kinase* (*BMP2K*), *erythrocyte membrane protein band 4.1* (*EPB41*), *phosphatidylinositol-5-phosphate 4-kinase type 2 alpha* (*PIP4K2A*), *CD36*, and *protein kinase C beta* (*PRKCB*). While the expression levels of these genes exhibited variability and were generally low, their collective presence suggested a distinctive cell subtype with attributes concurrent with both immune and hematopoietic progenitor lineages. This cluster was labelled as "Unknown" to later utilise the predictive capabilities of scANVI for label re-assignment.

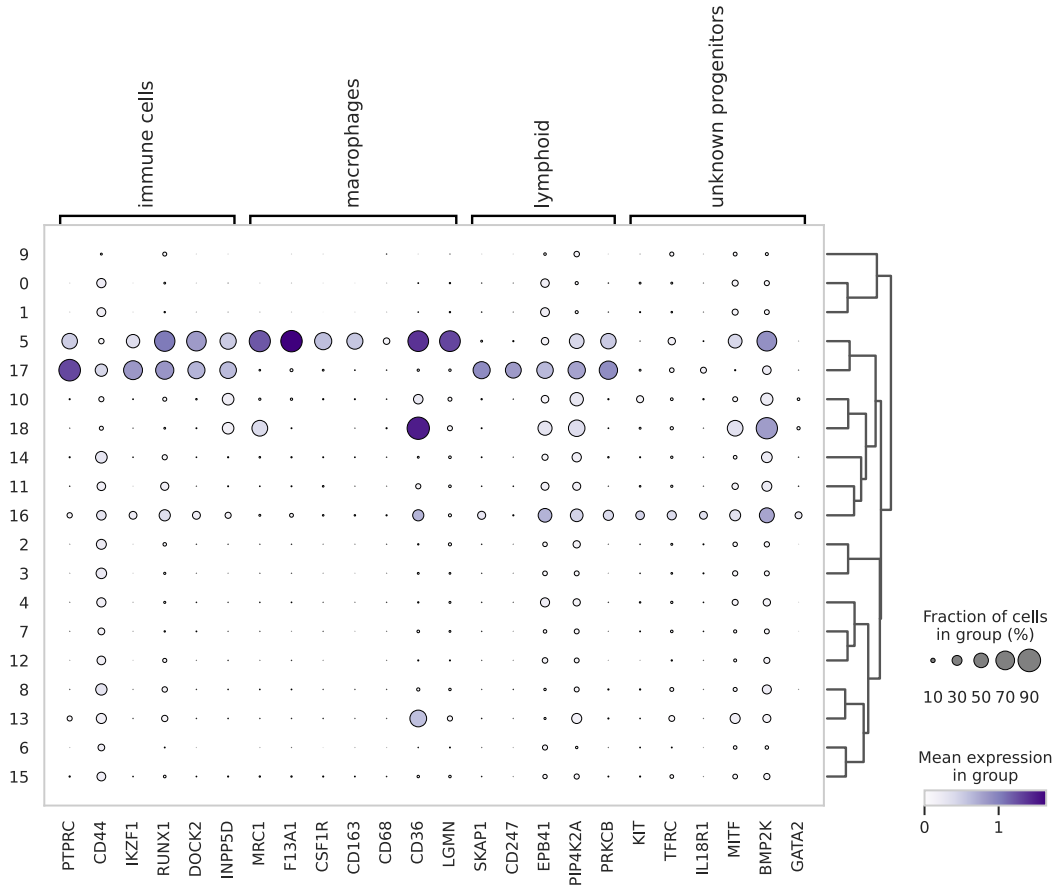


Figure 24. Expression of immune cell markers in foetal tendon snRNA-seq data. *Dotplot of hierarchically clustered Leiden clusters at 0.6 resolution (see Figure 17B) shows the mean log1pPF-normalised, unscaled gene expression levels alognside the proportions of expressing cells for select top differentially expressed genes relevant for immune cells. Genes for immune cells, including macrophages and cells of the lymphoid lineage, were selected based on known markers gathered from literature.*

4.3.1.6 Cell type label refinement with scANVI

Following putative cell type identification, data integration and label harmonisation was enhanced by initialising a scANVI model using the previously trained scVI one. The model was provided with the identified cell type labels as well as "Unknown" labels corresponding to clusters 4, 15 and 16. Both the annotated and unknown cells were mapped to latent space learned during model training and then assigned to the closest labelled cell type based on their position in that space (Figure 25A). The predicted cell types were then refined through renaming of fibroblast clusters, retaining differences between lymphatic and vascular endothelial cell type clusters, and combining all identified immune cell types into a single "Immune Cells" cluster. The final annotations are presented in Figure 25B. It is worth noting that although ABI3BP GAS2 Fibroblasts 2 and 3 likely originated from slightly different states belonging to the same cell type, we opted to analyse them further as distinct states. This approach was taken to pinpoint the variables responsible for their differentiation during the clustering process.

Overall, a total of 12 major cell types were identified in foetal 12-20 pcw Achilles and quadriceps tendons based on the Leiden clustering, manual annotation and scANVI label transfer approaches. Those types included smooth myocytes, vascular (vas) and lymphatic (lym) endothelial cells, nervous system cells, immune cells mostly consisting of macrophages, skeletal myocytes and their precursor satellite cells, chondrocytes, and 4 distinct fibroblast cell types, with one of those – expressing high *ABI3BP* and *GAS2* – subset to two differential states.

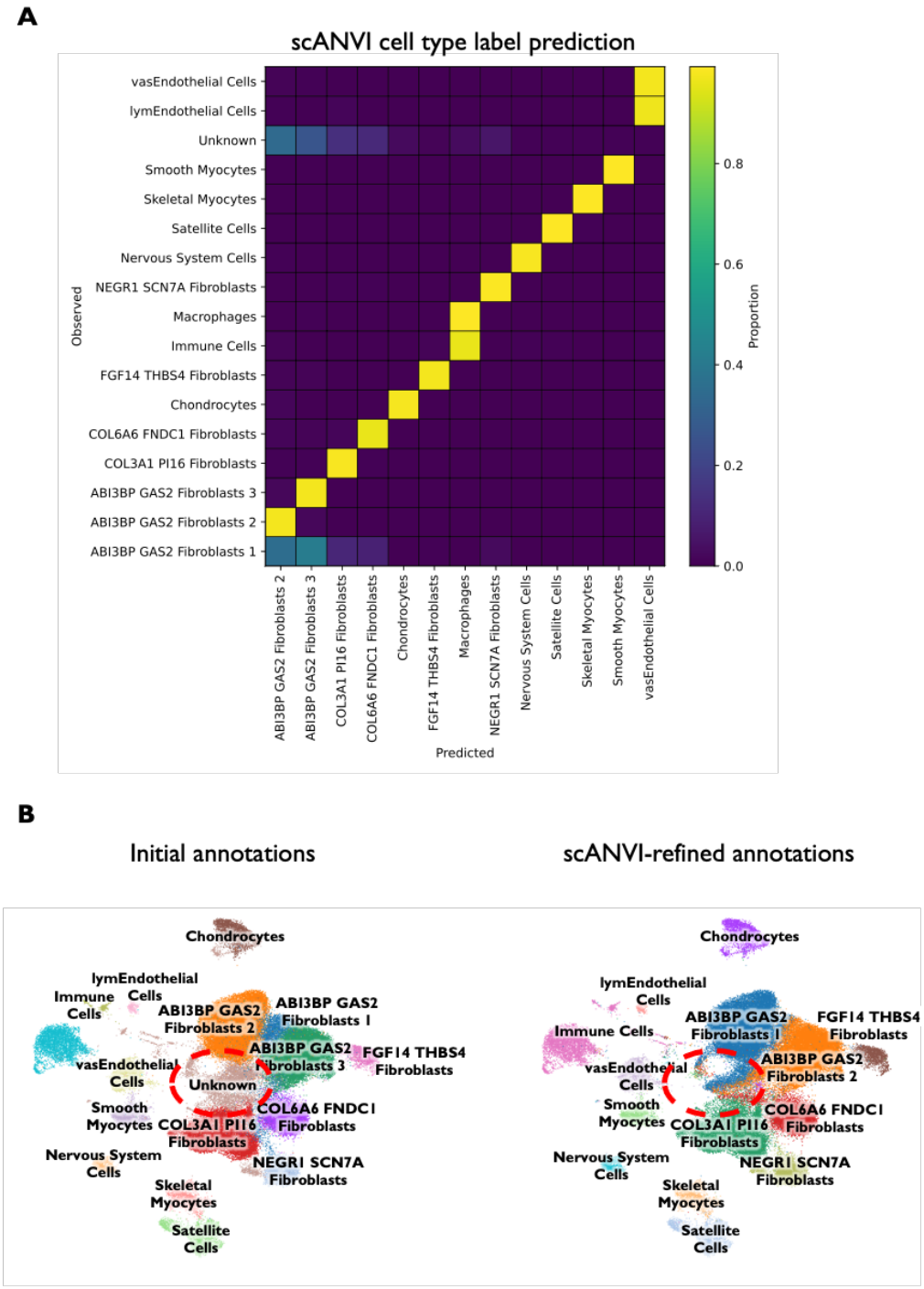


Figure 25. Foetal tendon cell type annotation before and after scANVI label prediction. *(**A**) Confusion matrix shows the performance of the scANVI model in predicting cell types from foetal tendon sample snRNA-seq data. Y-axis represents the observed cell types, while the x-axis indicates the predicted cell types from the scANVI model. Each cell in the matrix displays the proportion of cells classified into the corresponding predicted category, with colour intensity reflecting these proportions. Off-diagonal entries signify misclassifications, highlighting the cell types that were predicted incorrectly, likely due to overly fine annotation. The colour bar shows the proportion of cells within each category. (**B**) UMAP plots show the initial cell type annotations based on the analysed Leiden clusters (left) and the finalised annotations using scANVI label predictions from (A) as well as manual label refinement (right). Red circle highlights the cells expressing high levels of cell division markers that were reassigned to their most likely correct cell type clusters.*

4.3.2 Spatial transcriptomic analysis of gene expression patterns in human 20 pcw foetal Achilles and quadriceps tendons

Tendon tissues are anatomically complex (see section 2.2), making it likely that distinct cellular arrangements would be found within different microanatomical compartments. To begin understanding gene expression patterns and potential cell type distributions across different tissue regions, spatial RNA-seq profiles of one Achilles tendon and two quadriceps tendons were generated from a single 20 pcw donor (Appendix Table 3). Histopathological analysis of snap-frozen H&E-stained tissue sections, along with gene and morphology-based clustering, allowed the delineation of different topographical regions within the tendon and its neighbouring tissues.

At 20 pcw, developing tendons appeared highly cellular and displayed disparities in cell density and ECM appearance, facilitating easy demarcation of major tissue regions such as tendon fascicles, loose connective tissue (LCT) layers, and muscles (Figure 26). Namely, the regions corresponding to tendon fascicles were characterised by densely packed cells and longitudinally aligned ECM with a characteristic undulating crimp pattern. Those regions expressed the highest levels of *COL1A1, COL6A1, COL11A1, FMOD, TNMD, COMP,* and *ABI3BP*. Adjacent to these areas were sections of ECM organised in a loose, mesh-like pattern commonly associated with the IFM or other loose connective tissues such as endo-, epi-, or paratenon. In these locations, heightened expression of *COL4A1, IGFBP7, platelet endothelial aggregation receptor 1 (PEAR1), gelsolin (GSN), microfibril associated protein 5 (MFAP5), S100 calcium binding protein A10 (S100A10)*, and *FN1* was observed. Lastly, tissue regions with cylindrical cytoplasmic structures containing multiple peripheral nuclei appeared distinct from tendon regions and expressed *ACTA1, myosin light chain 1 (MYL1), DES, calsequestrin 1 (CASQ1), actin 2 (ACTN2), TTN,* and *NEB*, consistent with attached skeletal muscle tissue.

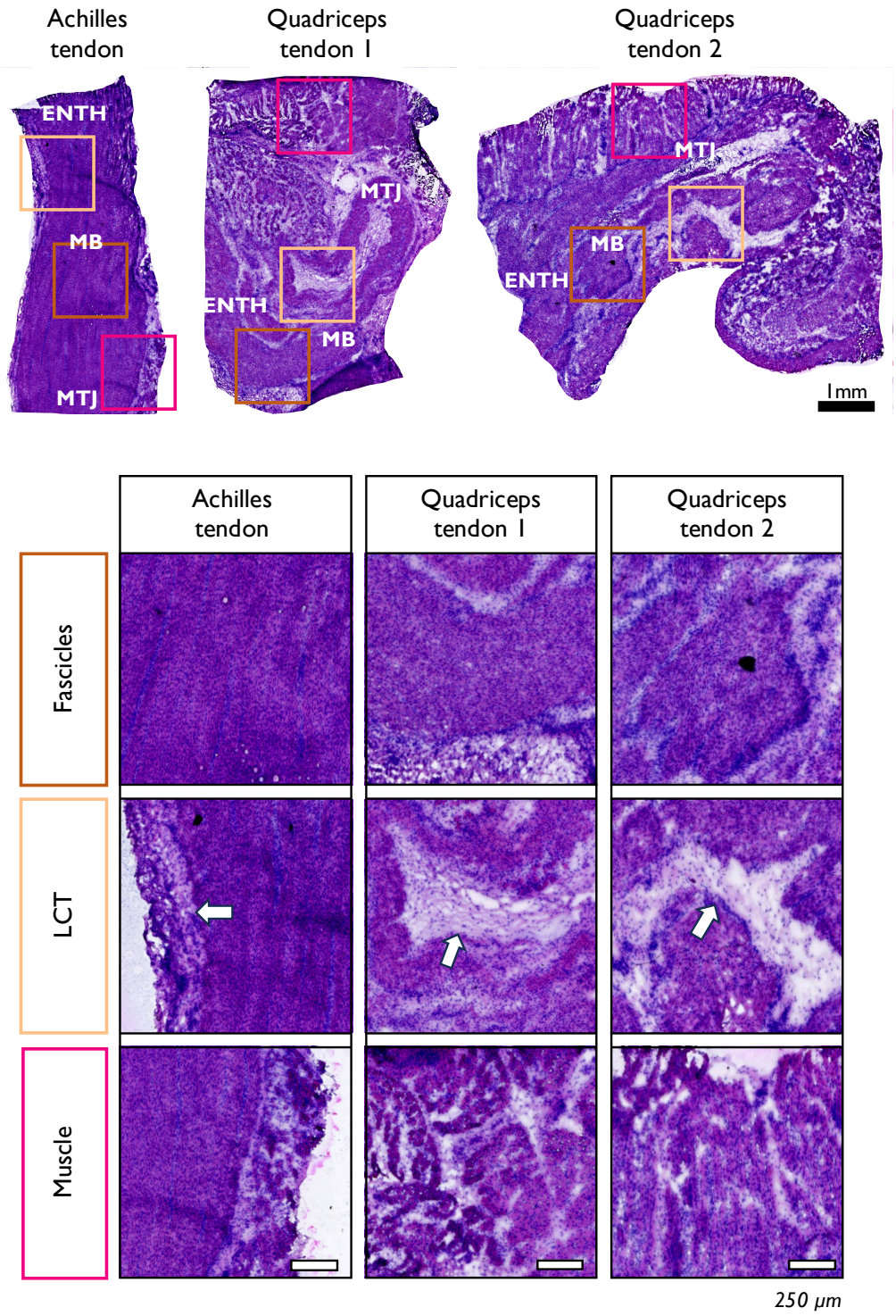


Figure 26. H&E images of snap-frozen 10μm-thick Achilles and quadriceps tendon sections used for spatial RNA-sequencing. *(Top) Whole-slide tissue sections (10X Visium) of Achilles tendon, and two sections of quadriceps tendon (labeled as quadriceps 1 and quadriceps 2). A black size bar (1 mm) applies to all sections. Boxes indicate regions that were magnified for detailed examination. Key anatomical regions are marked: ENTH for enthesis, MB for midbody, and MTJ for myotendinous junction. (Bottom) Table detailing the specific zoomed-in sections corresponding to demarcated regions in the top panel. Arrows highlight areas of loose connective tissue (LCT). White size bars on zoomed images indicate scale (250 μm).*

4.3.3 Spatial mapping of foetal single-nuclei cell types

To map the previously identified cell types to their likely spatial coordinates, cell2location was applied to the spatial RNA-seq datasets with annotated snRNA-seq data from 20 pcw donors used as the reference. In Figure 27, the Pearson correlation matrix illustrates the similarities of cell type abundances per Visium spot, revealing at least three major grouping patterns. In the biggest group, ABI3BP GAS2 Fibroblasts 1 and 2 are similarly abundant in the same sequencing regions. Interestingly, high correlations are also evident between the abundances of ABI3BP3 GAS2 Fibroblasts and FGF14 THBS4 Fibroblasts, as well as Chondrocytes. This correlation also extends to a lesser degree to COL6A6 FNDC11 Fibroblasts and vasEndothelial Cells. In the second grouping, high abundance similarities are observed between NEGR1 SCN7A Fibroblasts, Satellite Cells, and Skeletal Myocytes. Noteworthy as well is the substantial abundance similarity of lymEndothelial Cells within this grouping. Lastly, the third major cluster demonstrates significant correlations among the abundances of COL3A1 PI16 Fibroblasts and Immune Cells, as well as between Nervous System Cells and Smooth Myocytes. Remarkably, both types of endothelial cells also exhibit high abundances within this cell type grouping. Overall, the observed patterns of cell type abundances support segregation of functionally interrelated cell types into common compartments – fascicular tendon, muscle, and LCT.

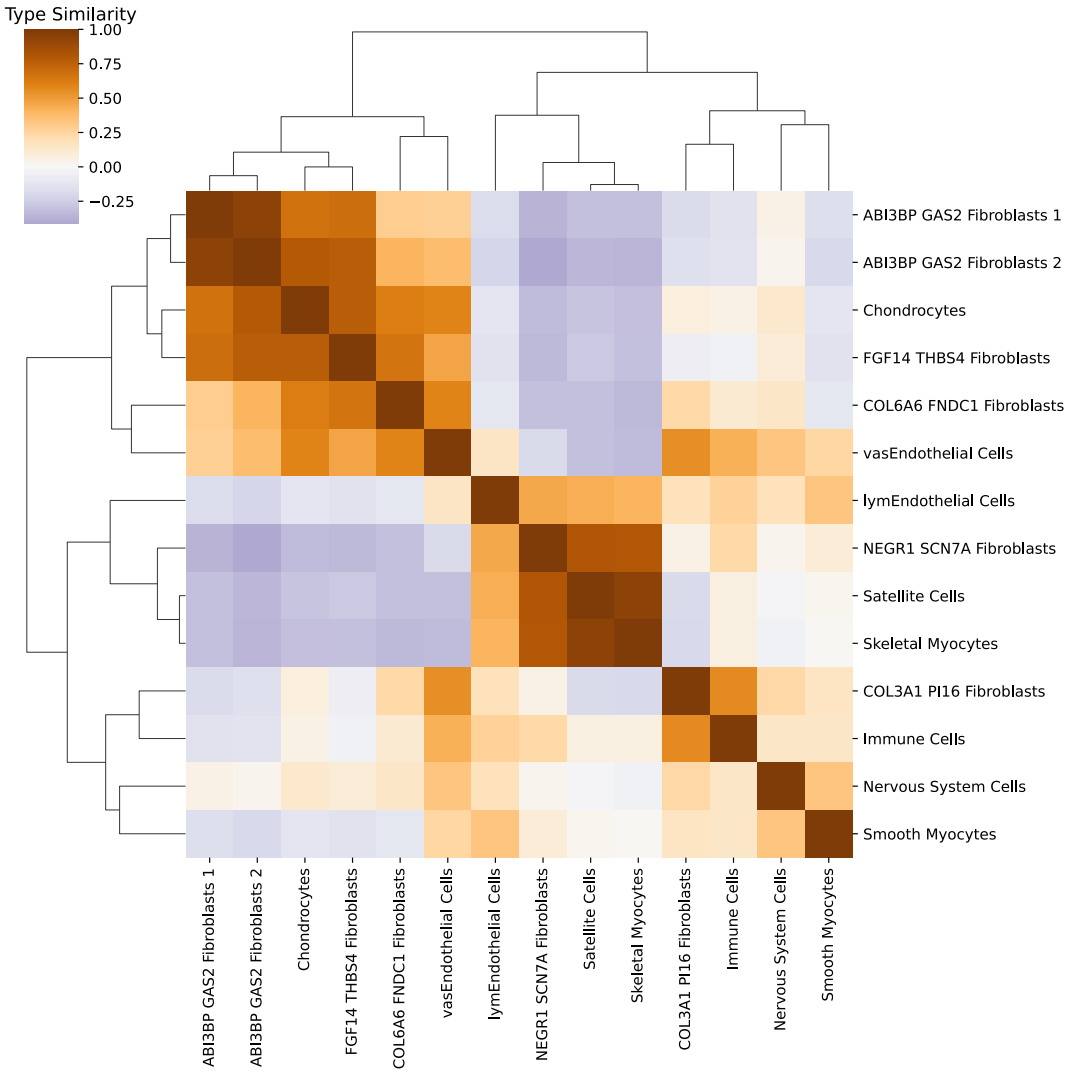


Figure 27. Pearson correlation matrix of inferred foetal tendon single-nuclei RNA-sequencing cell type abundances per single 10X Visium sequencing spot. *The more brown the colour, the more likely the cells are to be found co-located within the same spot of the 10X Visium slide.*

Relating mapped cells to the manually annotated regions, the cell type groupings were observed to be largely consistent across the different tendons (Figure 28). In both Achilles and quadriceps tendons, ABI3BP GAS2 Fibroblasts 1 and 2 were the main tenocytes found throughout the body of the developing tendon, with small proportions occasionally present in the tendon LCT regions. They were joined by FGF14 THBS4 Fibroblasts which, along with COL6A6 FNDC11 Fibroblasts, seemed to be positioned at the periphery between the tendon body and inner tendon LCT regions (Figure 29). COL3A1 PI16 Fibroblasts localised to distinct LCT regions. NEGR1 SCN7A Fibroblasts were positioned exclusively in the muscle LCT regions corresponding to the potential endo- or perimysium and were closely associated with the Skeletal Myocytes

and Satellite Cells. With regards to the vascular and lymphatic endothelial cells, smooth myocytes, nervous system cells, and immune cells, their distributions were more complex across the different tendons. Nevertheless, they could be found at different levels of abundance in every region type within quadriceps tendons (Figure 28).

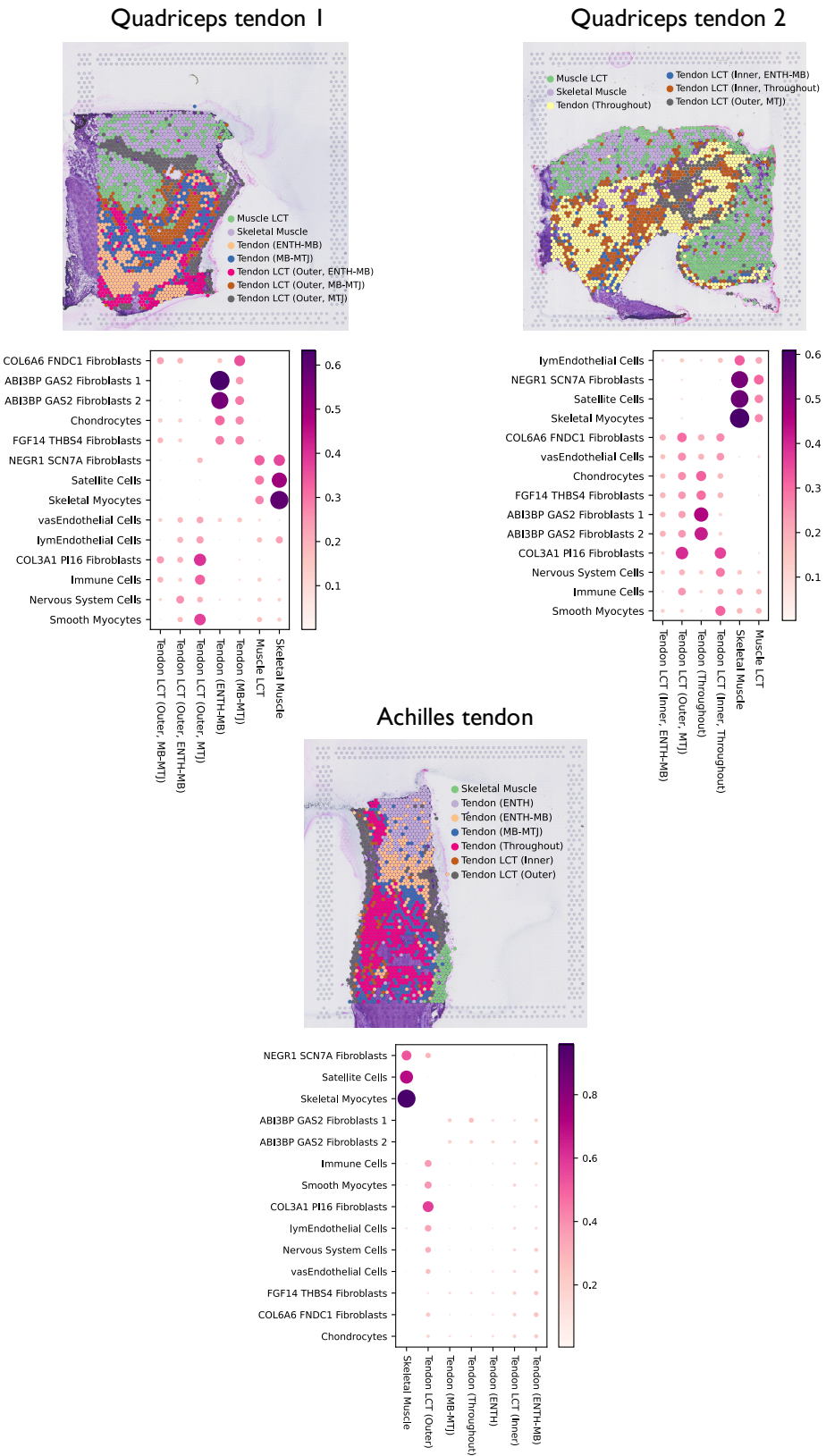
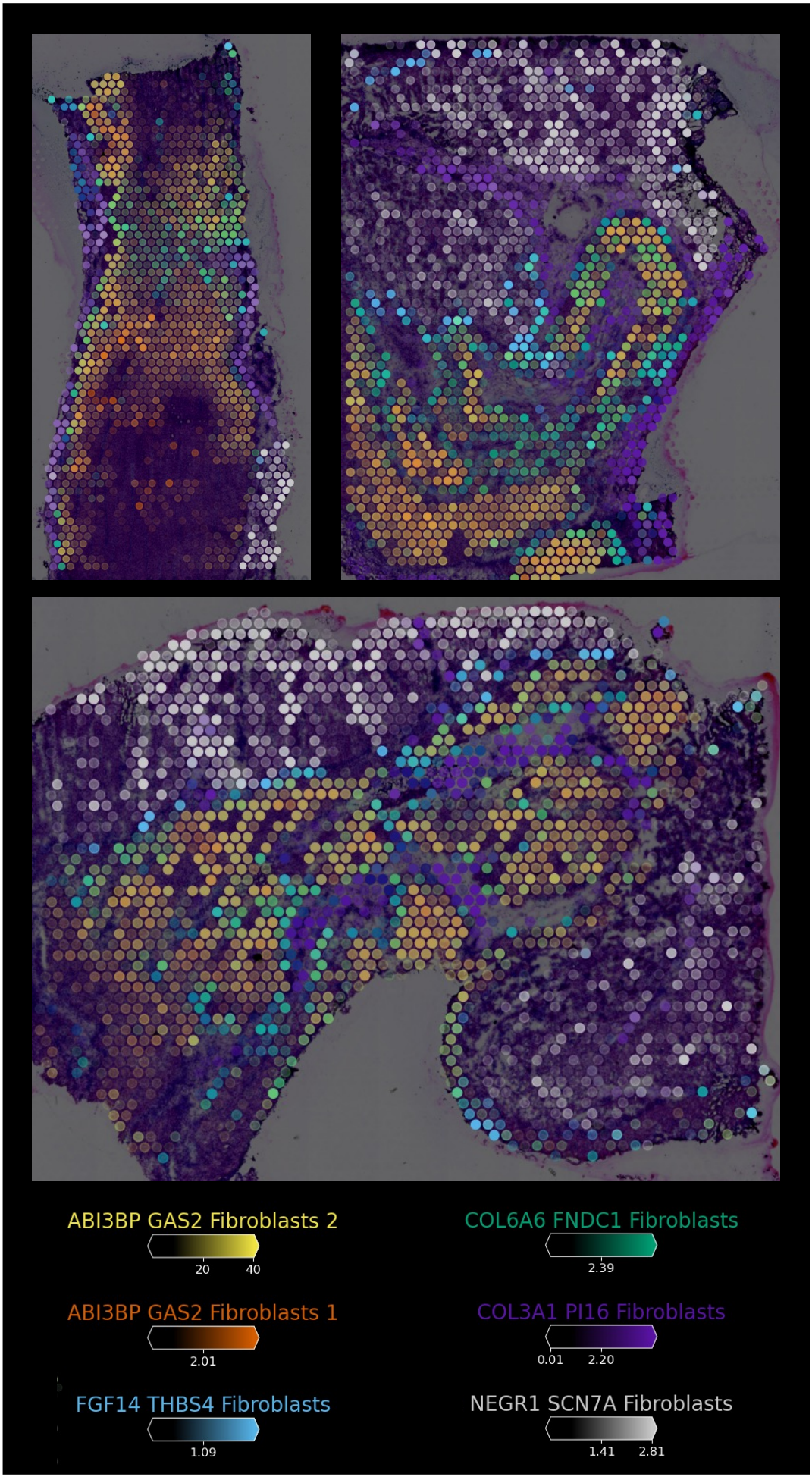


Figure 28. Abundance of cell types within each manually annotated region of spatially-resolved 20 post-conception week human foetal quadriceps and Achilles tendons. *10X Visium H&E-stained tissue sections (top) are coloured according to the manually annotated regions within each individual tendon. Dotplots (bottom) show the presence of specific cells within these manually annotated regions, with darker colours and bigger dots indicating higher prevalence.*


ABI3BP GAS2 Fibroblasts 2
20
40
COL6A6 FNDC1 Fibroblasts
2.39
ABI3BP GAS2 Fibroblasts 1
2.01
COL3A1 PI16 Fibroblasts
0.01
2.20
FGF14 THBS4 Fibroblasts
1.09
NEGR1 SCN7A Fibroblasts
1.41
2.81

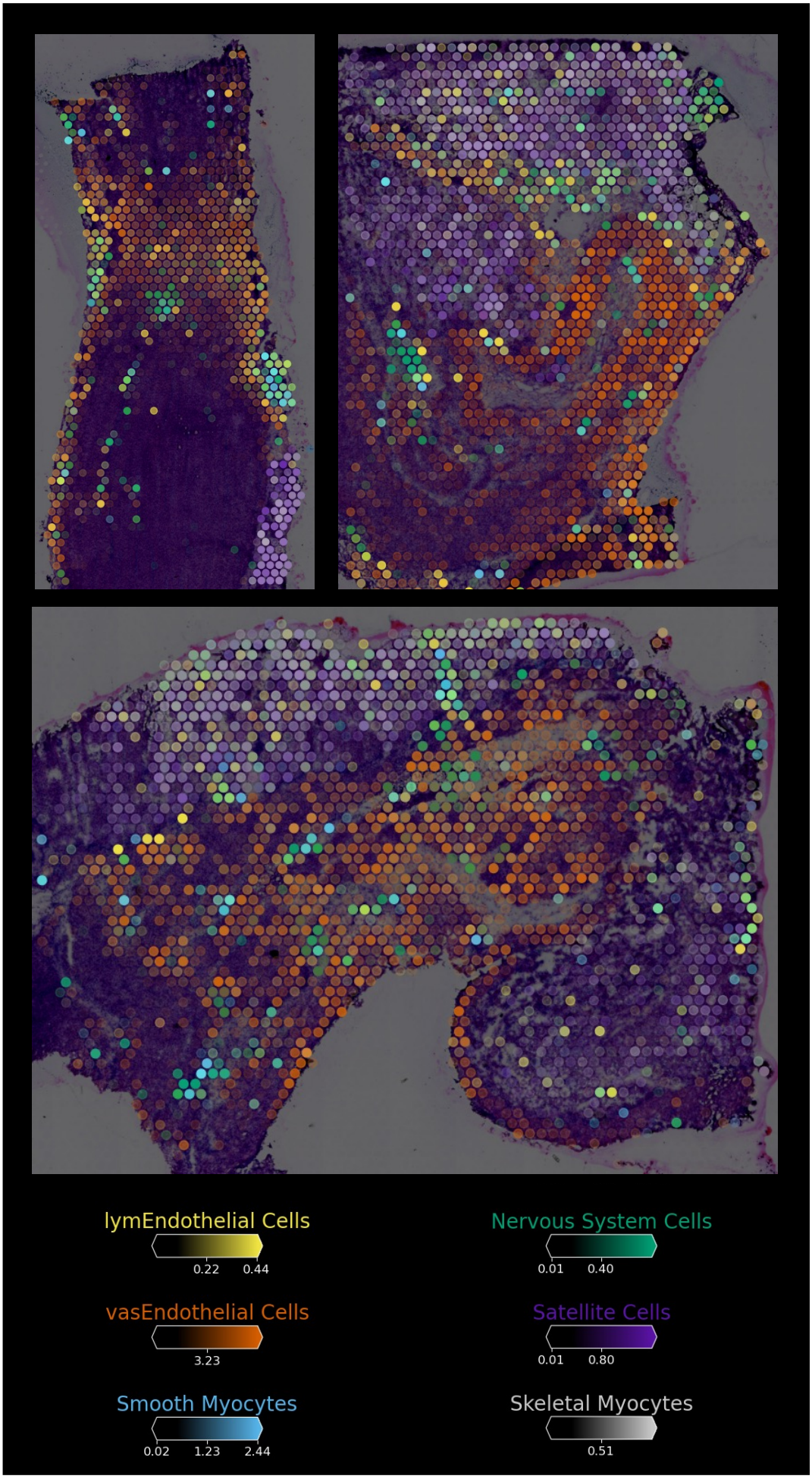

lymEndothelial Cells
0.22
0.44
Nervous System Cells
0.01
0.40
vasEndothelial Cells
3.23
Satellite Cells
0.01
0.80
Smooth Myocytes
0.02
1.23
2.44
Skeletal Myocytes
0.51

Figure 29. Cell2location mapping of Achilles and quadriceps tendon snRNA-seq cell type transcriptomic profiles from five 20 post-conception week samples. *Achilles tendon section is shown in the top left, while the quadriceps tendon sections are shown in the top right and the bottom. The intensity of the colour at each spatial location indicates the relative abundance of a given cell type, as calculated by cell2location. Discrete cell type mappings for the quadriceps tendon sample are shown in Appendix Figure 3.*

The data also revealed differences in cell type region mappings between different tendons, even within the same tissue type. Manual region annotation based on gene clustering profiles and morphological features introduces bias and limits the ability to make standardised comparisons across different developing tendons. To address this, an unbiased assessment of cell type co-location across tissues was performed using non-negative matrix factorisation (NMF) implemented within cell2location. Here, NMF served as a powerful tool for reducing the dimensionality of spatial transcriptomics data, allowing us to extract unbiased intrinsic spatial patterns and capture variations in gene expression that exist within the tissue without prior knowledge or assumptions about specific cell types or features.

Figures 30 and 31 show outcomes of combined tendon tissue spatial data decomposition into 5 and 12 components, illustrating common underlying spatial patterns across different tendons. Decomposition into 5 components showed clear patterns of spatial gene expression within the tissue regions that supported the results of cell type mappings with cell2location (Figure 30A,B). Namely, ABI3BP GAS2 Fibroblasts 1 and 2 as well as some of the FGF14 THBS4 Fibroblasts and Chondrocytes co-located together in the tissue regions corresponding to the main body of the tendon (factor 0). The other part of FGF14 THBS4 Fibroblasts and Chondrocytes co-located with COL6A6 FNDC1 Fibroblasts in regions corresponding to the peripheries of tendons and inner tendon LCTs (factor 3) (Figure 30A,B). COL3A1 PI16 Fibroblasts remained distinct and co-located with some of the Immune Cells in what appeared to be the outer LCTs of tendons, likely corresponding to tendon epi- or paratenon layers (factor 1) (Figure 30A,B). Further, as expected, large proportions of Endothelial Cells, Smooth Myocytes, Immune Cells, and Nervous System Cells co-located together predominantly in the LCT regions of tendons and muscles, including any potential interfascicular matrix regions (factor 4) (Figure 30A,B). Finally, NEGR1 SCN7A Fibroblasts co-located with Skeletal Myocytes and

Satellite Cells in the clearly demarcated muscle regions of the tissue (factor 2) (Figure 30A,B).

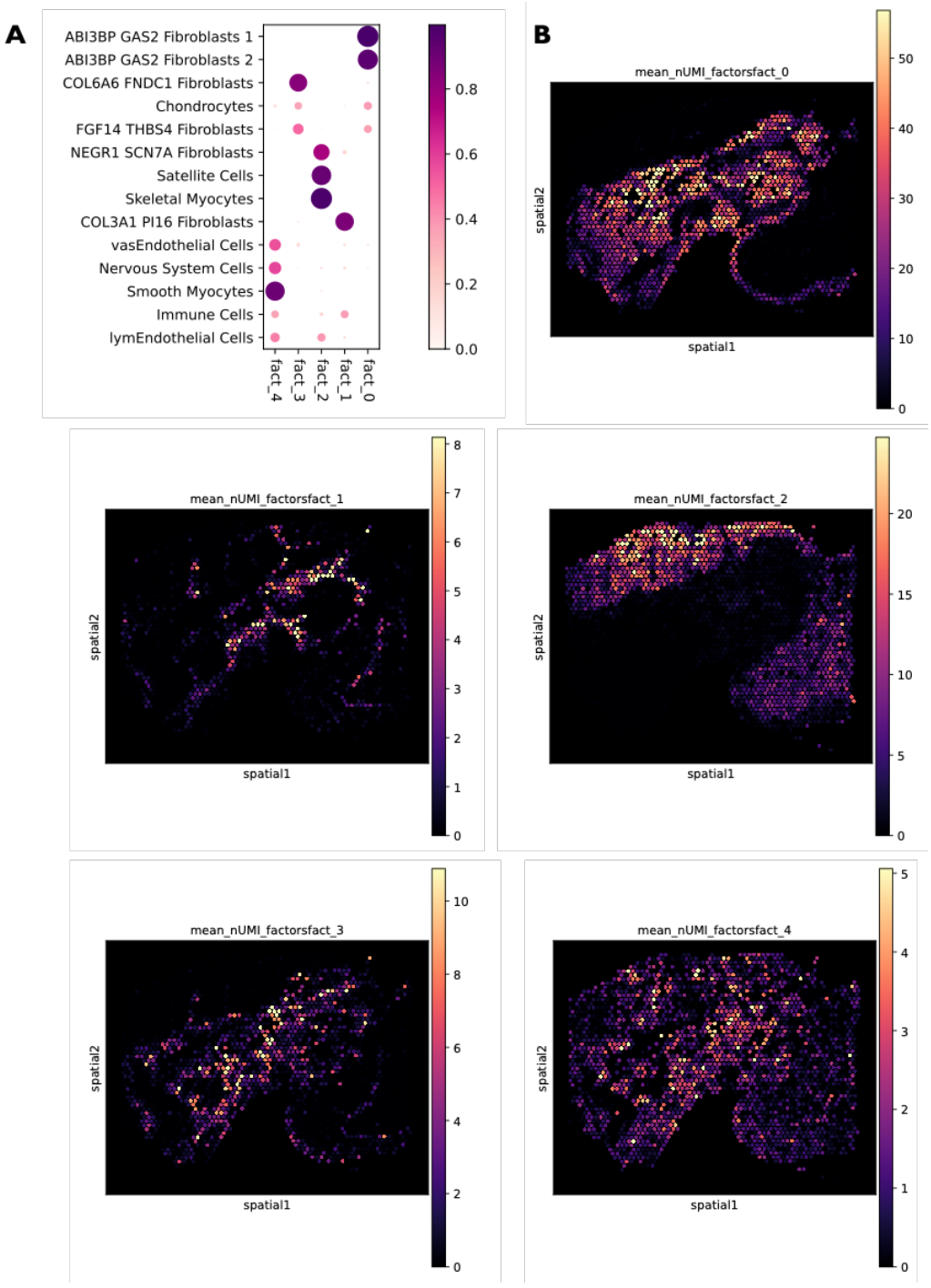


Figure 30. Unsupervised non-negative matrix factorisation (NMF) analysis of Visium ST cell2location results for 5 factors across the three 20 post-conception week tendon spatial RNA-sequencing samples. (A) *Dotplot shows NMF factors derived from mean normalised UMI counts (dot size and colour). Gene loadings represent the contribution of individual genes to each estimated cell type (factor) in the colocalisation model. These values indicate how strongly each gene is associated with each cell type.* ***(B)*** *Scatter plots show cell densities (in the form of mean normalised UMI) for a single 20 pcw quadriceps tendon sample. The results for other two samples are shown in Appendix Figure 2.*

Further data decomposition into 12 components, assuming minimal cell type co-location, allowed for more detailed exploration (Figure 31A,B). An interesting pattern emerged when comparing factor 1 data (primarily ABI3BP GAS2 Fibroblasts 1) with factor 8 data (primarily ABI3BP GAS2 Fibroblasts 2): Namely, factor 1 was characterised by very low nUMI counts of 0-2.0, yet contained the majority of type 1 fibroblasts, while factor 8 had high nUMI counts of 0-50 and contained the majority of type 2 fibroblasts (Figure 31B). This suggested that factor 1 cells were either (a) present at a lower cell density than factor 8 cells or (b) expressed, on average, fewer genes or had lower transcriptional activity. Manual H&E examination of factor 1 spots revealed comparable levels of cell density with factor 8 spots, making the latter explanation more likely.

Another interesting observation was the localisation of FGF14 THBS4 Fibroblasts between the muscle and fascicular tendon regions (factor 10) (Figure 31B), suggesting their involvement in the formation or maintenance of the MTJ. The remaining LCT fibroblasts expressing COL6A6 and FNDC1 (factor 0) or COL3A1 and PI16 (factor 5) were once again distinctly localised in different tendon LCT regions likely corresponding to the IFM and epi- or paratenon, respectively (Figure 31B). As before, NEGR1 SCN7A Fibroblasts were localised to the muscle interstitial LCT regions (factor 3) (Figure 31B).

Regarding other cell types, Chondrocytes predominated in a specific region close to the enthesis site (factor 2), with a few cells interspersed throughout the rest of the tissue (Figure 31B). Immune cells were distributed across various regions, with a noticeable concentration within the tendon and muscle LCT regions (factor 4) (Figure 31B). Endothelial and Nervous System Cells were dispersed throughout the tendon, with major vessels marked by Smooth Myocytes in factor 11 (Figure 31B). Finally, Skeletal Myocytes and Satellite Cells were appropriately located within the muscle regions (factors 6 and 9) (Figure 31B).

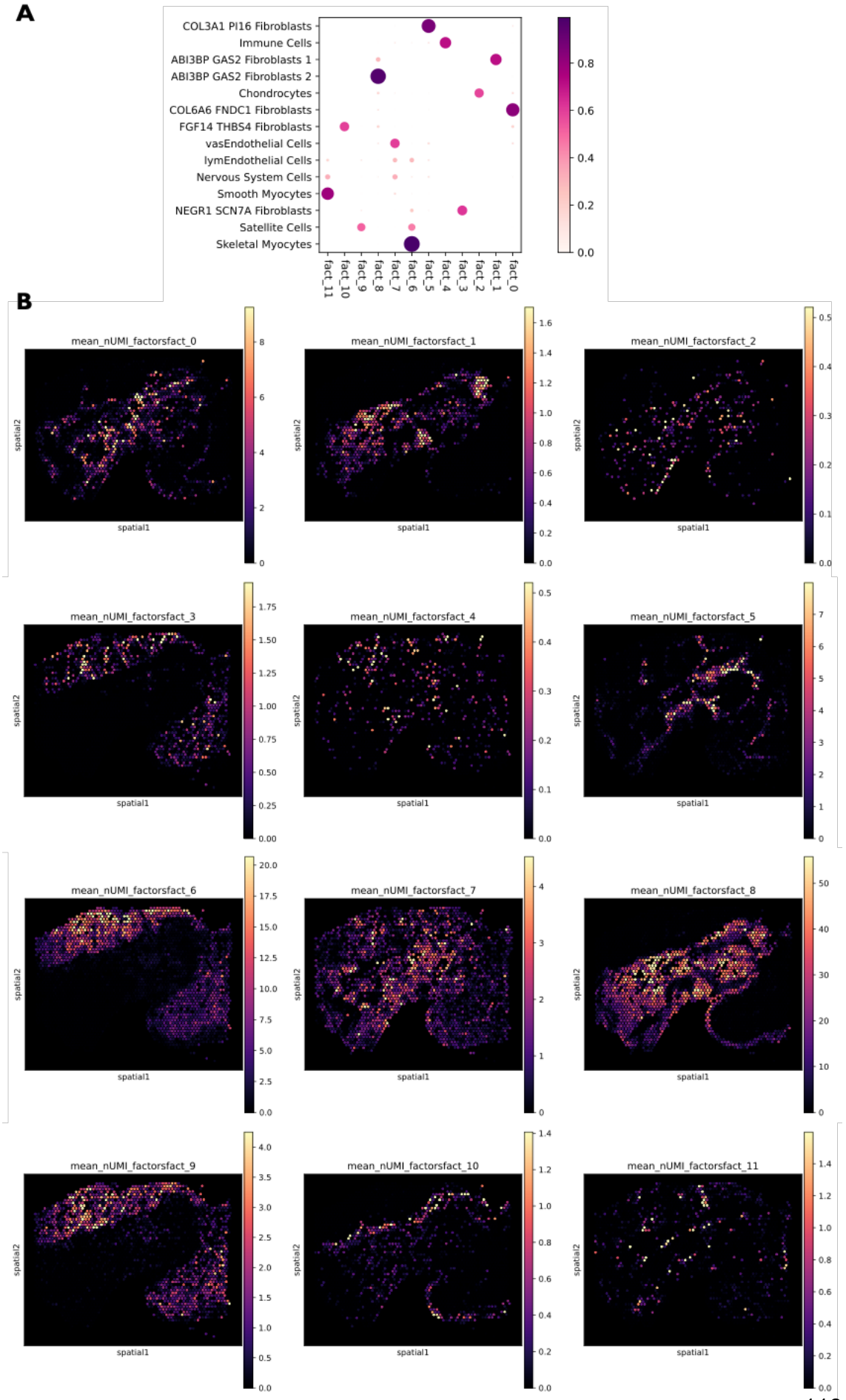

A
COL3A1 PI16 Fibroblasts
Immune Cells
ABI3BP GAS2 Fibroblasts 1
ABI3BP GAS2 Fibroblasts 2
Chondrocytes
COL6A6 FNDC1 Fibroblasts
FGF14 THBS4 Fibroblasts
vasEndothelial Cells
lymEndothelial Cells
Nervous System Cells
Smooth Myocytes
NEGR1 SCN7A Fibroblasts
Satellite Cells
Skeletal Myocytes
fact_11
fact_10
fact_9
fact_8
fact_7
fact_6
fact_5
fact_4
fact_3
fact_2
fact_1
fact_0
B
mean_nUMI_factorsfact_0
mean_nUMI_factorsfact_1
mean_nUMI_factorsfact_2
mean_nUMI_factorsfact_3
mean_nUMI_factorsfact_4
mean_nUMI_factorsfact_5
mean_nUMI_factorsfact_6
mean_nUMI_factorsfact_7
mean_nUMI_factorsfact_8
mean_nUMI_factorsfact_9
mean_nUMI_factorsfact_10
mean_nUMI_factorsfact_11
spatial1
spatial2

Figure 31. Unsupervised non-negative matrix factorisation (NMF) analysis of Visium ST cell2location results for 12 factors across the three 20 post-conception week tendon samples. (A) *Dotplot shows NMF factors derived from mean normalised UMI counts (dot size and colour). Gene loadings represent the contribution of individual genes to each estimated cell type (factor) in the colocalisation model. These values indicate how strongly each gene is associated with each cell type.* ***(B)*** *Scatter plots show cell densities (in the form of mean normalised UMI) for a single 20 pcw quadriceps tendon sample. The results for other two samples are shown in Appendix Figure 2.*

When analysing cell type-specific gene expression patterns, ABI3BP Fibroblasts 2 stood out by expressing the highest levels of *SCX, TNMD, FMOD* and *MKX* genes compared to type 1 fibroblasts, which showed minimal expression in very few cells. This observation further supported the assumed transcriptomic stability of ABI3BP Fibroblasts 2 across different tendon types (Figure 32), although it was likely influenced by their tenfold higher relative abundance within the tendons (Appendix Figure 3). Further investigation showed a similar pattern of expression for markers of cell division, including *MKI67, TOP2A, DIAPH3,* and *CENPK* (not shown), and fascicular TSPCs, including *ENG/CD105*, *THY1/CD90*, *CD44*, and *NES* (see Table 1; Yin *et al.*, 2016; Huang *et al.*, 2021; Leonardi *et al.*, 2021), although the expression of *MCAM/CD146* was sparse (Appendix Figure 4). Interestingly, COL6A6 FNDC1 and COL3A1 PI16 Fibroblasts expressed *THY1* as well as *TPPP3* and *PDGFRA* markers of sheath TSPCs defined by Harvey and colleagues (2019), but not the cell division markers, *CD34*, or the quiescent progenitor marker *AXIN2*, which was not detected in any of the fibroblasts (Appendix Figure 4). Additionally, COL6A6 FNDC1 Fibroblasts expressed intermediate levels of *FMOD* and *TNMD*, but not *SCX* or *MKX* (Figure 32).

Overall, it appeared that fascicular ABI3BP GAS2 Fibroblasts 2 were more abundant and transcriptionally active than their type 1 counterparts, expressing early tenocyte, cell division, and select canonical TSPC markers at high levels. On the other hand, inner and outer LCT fibroblasts (COL6A6 FNDC1 and COL3A1 PI16 Fibroblasts, respectively) expressed the *TPPP3* and *PDGFRA* markers of an injury-responsive type of TSPCs (Harvey *et al*., 2019). However, COL6A6 FNDC1 Fibroblasts appeared distinct due to their high expression of *FMOD* and *TNMD* markers, hinting at their role in the regulation of fibrillogenesis.

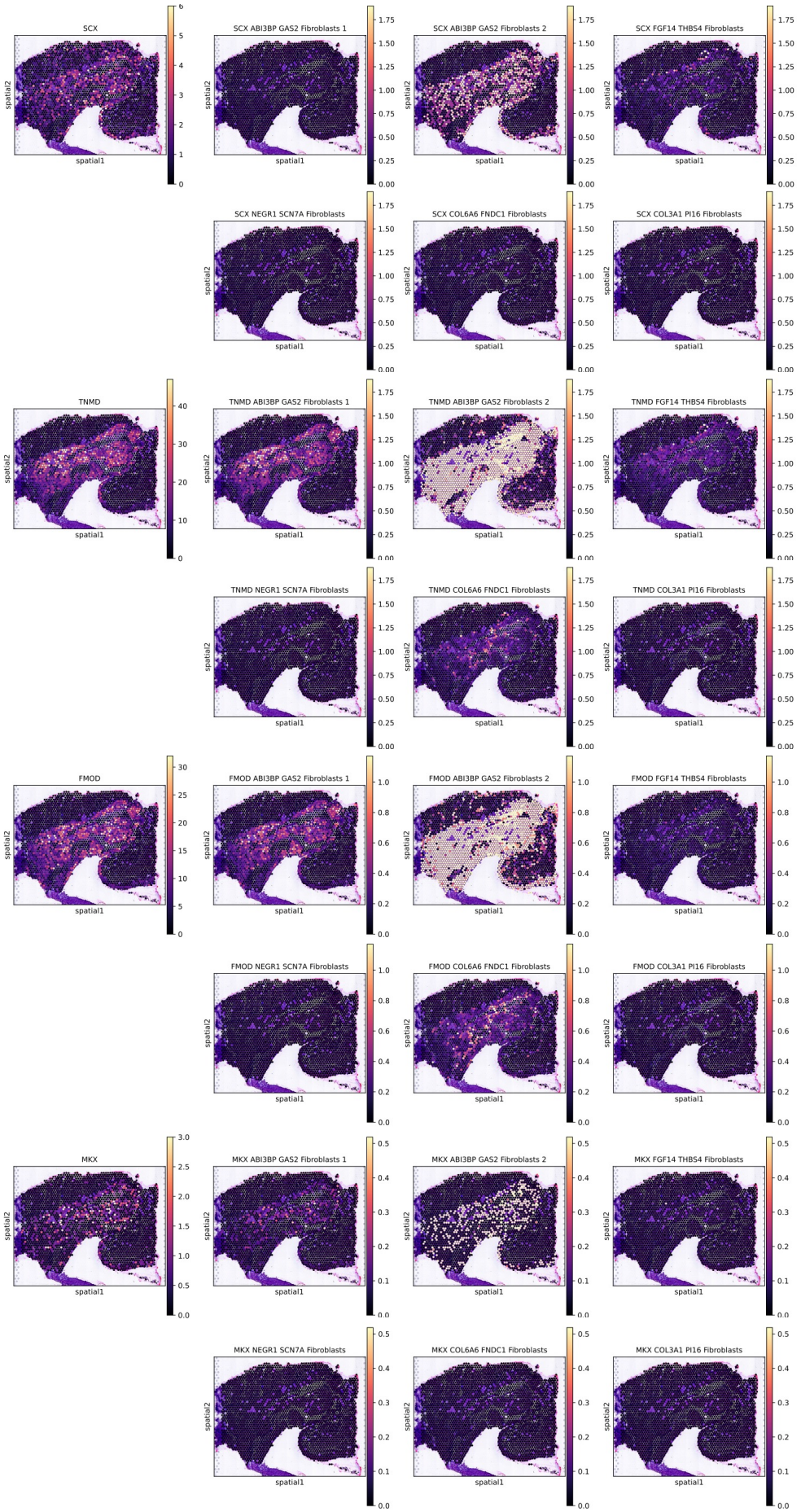

SCX
SCX ABI3BP GAS2 Fibroblasts 1
SCX ABI3BP GAS2 Fibroblasts 2
SCX FGF14 THBS4 Fibroblasts
SCX NEGR1 SCN7A Fibroblasts
SCX COL6A6 FNDC1 Fibroblasts
SCX COL3A1 PI16 Fibroblasts
TNMD
TNMD ABI3BP GAS2 Fibroblasts 1
TNMD ABI3BP GAS2 Fibroblasts 2
TNMD FGF14 THBS4 Fibroblasts
TNMD NEGR1 SCN7A Fibroblasts
TNMD COL6A6 FNDC1 Fibroblasts
TNMD COL3A1 PI16 Fibroblasts
FMOD
FMOD ABI3BP GAS2 Fibroblasts 1
FMOD ABI3BP GAS2 Fibroblasts 2
FMOD FGF14 THBS4 Fibroblasts
FMOD NEGR1 SCN7A Fibroblasts
FMOD COL6A6 FNDC1 Fibroblasts
FMOD COL3A1 PI16 Fibroblasts
MKX
MKX ABI3BP GAS2 Fibroblasts 1
MKX ABI3BP GAS2 Fibroblasts 2
MKX FGF14 THBS4 Fibroblasts
MKX NEGR1 SCN7A Fibroblasts
MKX COL6A6 FNDC1 Fibroblasts
MKX COL3A1 PI16 Fibroblasts
spatial1
spatial2

Figure 32. Fibroblast type-specific gene expression of established early tendon cell markers in Visium spatial transcriptomics data of 20 post-conception week foetal quadriceps tendon. *Scatterplots show the normalised expression levels for SCX, MKX, TMND, and FMOD genes, with color intensity indicating the relative abundance of gene expression in different spatial regions of the tissue. Each fibroblast subtype is assessed separately.*

4.3.4 Matrisomal gene expression profiling of foetal tendon fibroblasts

Next, the matrisomal gene expression profiles were characterised across identified cell types, specifically focusing on tendon fibroblasts. This analysis revealed high expression of class I SLRPs *DCN* and *ASPN*, as well as a class III SLRP *OGN*, across all examined fibroblast subsets (Figure 33). These molecules are known for their roles in collagen fibril assembly and matrix organisation (see section 2.3.2.2), highlighting their importance during the first and second trimesters of tendon development. In contrast, *BGN*, another class I SLRP, demonstrated low and inconsistent expression at the same developmental phases (Figure 33).

The expression profiles of class II SLRPs were more selective: *KERA* and *FMOD* were primarily expressed in ABI3BP GAS2 Fibroblasts 2, while *LUM* expression was restricted to COL3A1 PI16 and NEGR1 SCN7A Fibroblasts. Additionally, the expression of large aggregating proteoglycans *VCAN* and *ACAN*, which are critical for cellular adhesion and matrix hydration, was observed in specific fibroblast populations: *ACAN* was expressed by ABI3BP GAS2 Fibroblasts, while *VCAN* was most prominently expressed in COL3A1 PI16, COL6A6 FNDC1, and NEGR1 SCN7A Fibroblasts (Figure 33).

Furthermore, the examination of glycoprotein expression across all fibroblast populations revealed ubiquitous expression of key genes including *SPARC*, *LAMA2*, *ABI3BP*, *POSTN*, *FBN2*, *FBN1*, *FN1*, *LAMB1*, *FNDC1*, and *slit homolog 2 protein* (*SLIT2*) (Appendix Figure 5). Interestingly, *THBS2* was selectively expressed in ABI3BP GAS2, COL3A1 PI16, and COL6A6 FNDC1 Fibroblasts. Additionally, unique expression patterns were also observed for *COMP* in ABI3BP GAS2 Fibroblasts, and for *SLIT3* in FGF14 THBS4 Fibroblasts (Appendix Figure 5).

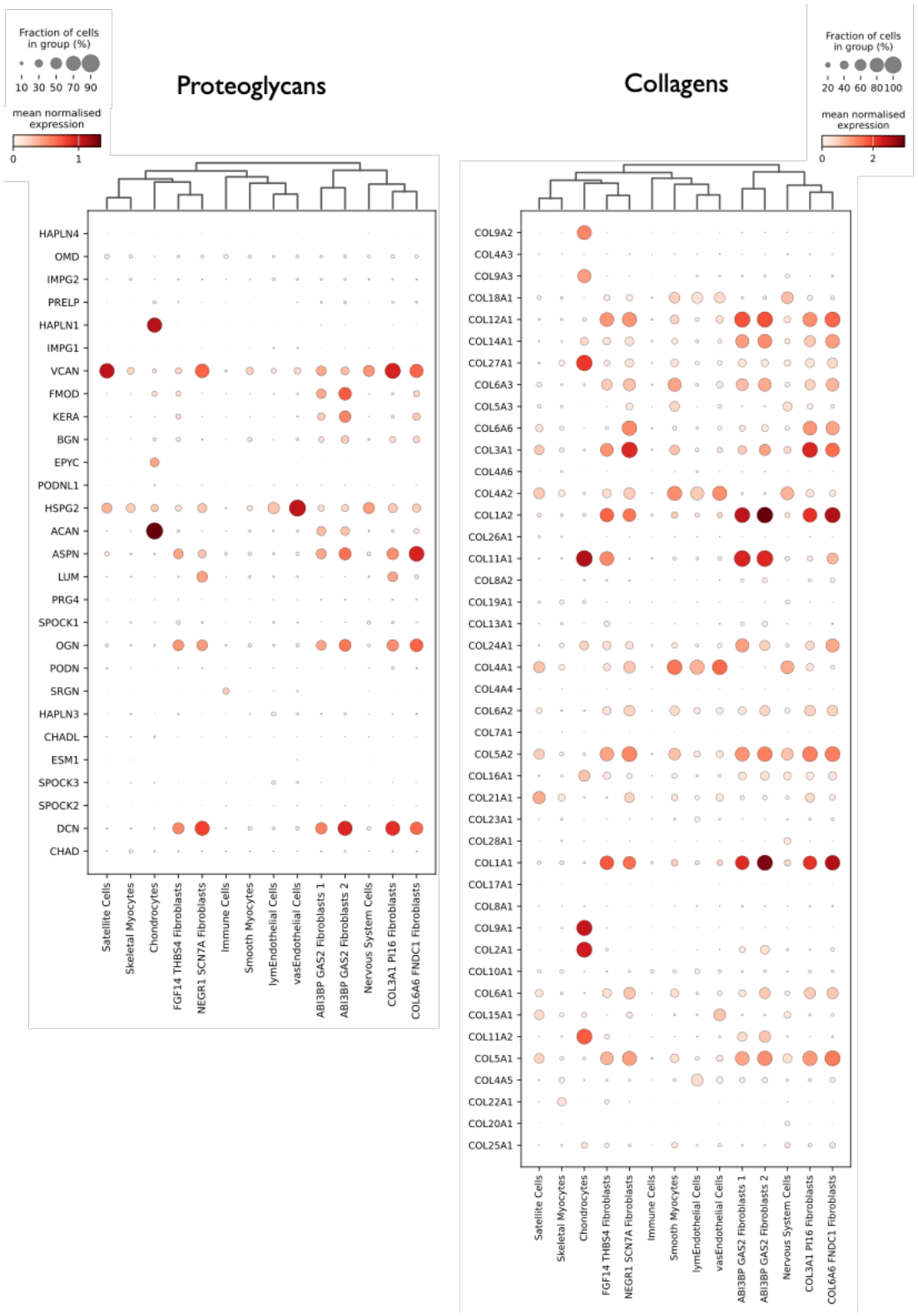


Figure 33. Foetal 12-20 post-conception week tendon proteoglycan and collagen gene expression profiles. *Dotplots of hirerchically clustered cell types show the mean normalised expression levels alognside the proportions of expressing cell types for all proteoglycan and collagen genes present in the data. The lists of matrisomal genes were obtained from the matrisomeDB database (Shao et al., 2020). The remaining matrisomal gene dotplots are shown in Appendix Figure 5.*

Ubiquitous and high expression of genes encoding collagen types I (*COL1A1*, *COL1A2*), III (*COL3A1*), V (*COL5A1*, *COL5A2*), and XII (*COL12A1*) was observed across all fibroblasts (Figure 33). A less prevalent, yet substantial medium-level expression of type VI collagen (*COL6A1*, *COL6A2*, *COL6A3*) was also noted, with *COL6A6* expression being exclusive to COL3A1 PI16, COL6A6 FNDC1, and NEGR1 SCN7A Fibroblasts (Figure 33), potentially indicating a niche-specific function for this collagen gene in tendon biology.

Interestingly, the expression pattern of collagen XI was more specific. *COL11A1* was present in all fibroblasts except COL3A1 PI16 and NEGR1 SCN7A, while *COL11A2* was uniquely expressed in ABI3BP GAS2 Fibroblasts. This suggests that the regulation of collagen XI is finely tuned, which may have implications for the microstructural organisation of the tendon matrix. In addition, *COL4A1* and *COL4A2* were specifically noted in FGF14 THBS4 and NEGR1 SCN7A Fibroblasts, possibly reflecting their role in basement membrane structure and tissue compartmentalisation. A particularly intriguing finding was the low expression of *COL22A1* in a small subset of FGF14 THBS4 Fibroblasts (Figure 33). Given the established role of COL22A1 in MTJ formation (Charvet *et al*., 2013; Koch *et al*., 2004), coupled with their spatial localisation at the interface between muscle and tendon proper regions (factor 10 in Figure 31), these results suggest their identity as MTJ-forming cells.

Finally, NEGR1 SCN7A Fibroblasts expressed high levels of the ECM-affiliated proteins *glypican 3* (*GPC3*), *GPC6*, and *semaphorin 5A* (*SEMA5A*) (Appendix Figure 5), signifying their involvement in complex signalling pathways and matrix interactions. COL3A1 PI16 and COL6A6 FNDC1 Fibroblasts also expressed *GPC3* and *GPC6*, along with *collectin-12* (*COLEC12*) (Appendix Figure 5), revealing a shared molecular signature that could denote a common functional framework among these fibroblasts. The ubiquitous expression of *SEMA3C* across all fibroblasts pointed to their generalised role in regulating fibroblast behaviour and ECM assembly.

4.3.5 Temporal dynamics of tendon cell type gene expression across foetal development

Following the detailed identification and description of cell types, the focus shifted towards investigating the subtle changes occurring over developmental time in individual fibroblasts. To enhance the robustness of the DGE analysis, single-nuclei data were aggregated ("pseudobulked") (Squair *et al*., 2021). Likelihood ratio tests (LRTs) were conducted, pinpointing genes exhibiting significant differential expression with developmental time. The subsequent clustering analysis of LRT results unveiled four predominant gene expression patterns consistently observed across the majority of cell types. The two primary patterns involved thousands of genes showing either gradual upregulation or downregulation across the time points. Meanwhile, the less common patterns included hundreds to thousands of genes that were initially upregulated at 17 weeks and subsequently downregulated at 20 weeks compared to 12 weeks, or initially upregulated at 17 weeks and then showed intermediate expression levels at 20 weeks (Figure 34).

To provide functional context to these gene clusters, gene ontology (GO) pathway analyses were performed, focusing specifically on biological processes (BP). The identified pathways were broadly categorised by common functions within individual fibroblast types (Appendix Figure 6)**.** Interestingly, the results revealed a substantial overlap in the identified pathways across the different fibroblasts, prompting a comparative analysis of shared and unique pathways within the gene expression clusters (Figure 34).

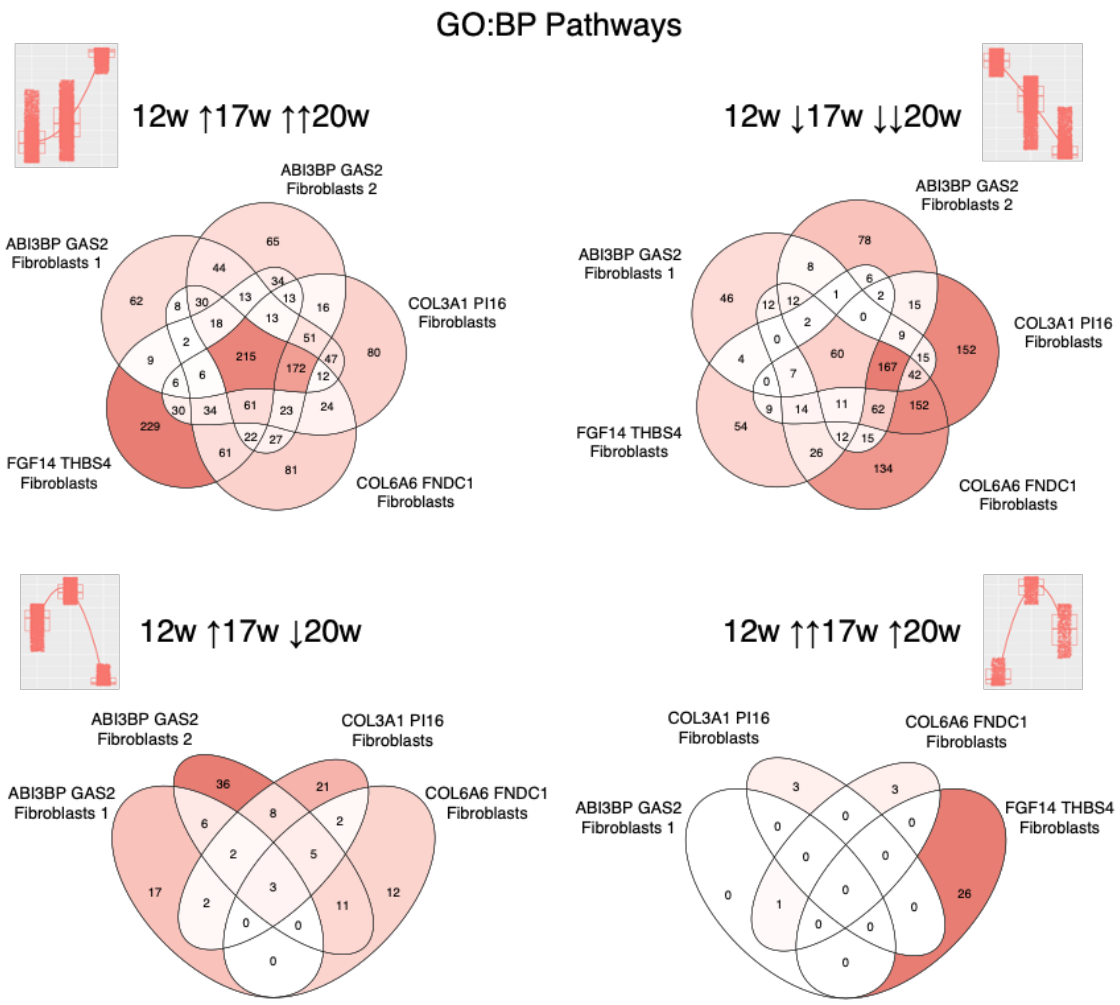


Figure 34. Venn diagrams of intersecting gene ontology biological process (GO:BP) terms in tendon fibroblasts for each of the four clustered gene expression change patterns in 12 to 20 post-conception weeks of human foetal development. *Only significant (<0.05 BH-FDR) pathways sized 20-500 terms were used. Manually summarised pathway categories for each cell type and each cluster are shown in Appendix Figure 6, while summaries of comparisons and findings are presented in Table 4.*

Among the pathways gradually upregulated during 12-20 post-conception weeks of foetal development, 215 terms were shared between different tendon fibroblasts. Those pathways were broadly summarised into 36 functional categories, which collectively indicated a high level of cellular activity and adaptability as cells appeared to be actively engaged in processes crucial for growth, differentiation, and morphogenesis of the tendon. Notably, as fibroblasts progressed through development, they underwent processes involving cell signalling (including canonical Wnt, TGF-β, and TOR), vesicle transport, autophagy, and protein modification and degradation, indicating that they were actively communicating with their surroundings and undergoing substantial

remodelling and regulation of cellular components. Furthermore, these cells also exhibited signs of significant energy utilisation and stress responses, as indicated by the activation of stress-activated protein kinase cascades (including JNK, TOR and MAPK) and the responses to various stimuli, such as hypoxia and growth factors. As expected, upregulation of pathways related specifically to limb and connective tissue morphogenesis and development, including ECM, collagen fibril, and basement membrane (BM) organisation, was also observed.

There were fewer downregulated pathways in common between the five different fibroblasts. Nevertheless, among the 60 shared terms, nearly all were related to the cell cycle and division processes, with further subcategorization into the chromosome segregation, organelle fission, DNA replication and repair, and intracellular organisation and signalling processes (e.g., Ras, Serine/Threonine kinases). Additionally, negative regulation of cell migration and neural development pointed towards a temporary halt in these processes during the transition from 12 to 20 weeks of development, possibly to allow for precise patterning and differentiation.

Finally, we saw three processes – tRNA metabolic process, tRNA processing, and small GTPase-mediated signal transduction – shared between the four tendon fibroblasts that were first upregulated at 17 weeks then downregulated below the 12w level of expression at 20 weeks. Clearly, those reflected dynamic and adaptable cellular responses, suggesting initially upregulated protein synthesis at 17 weeks of development that was then diminished by 20 weeks. This might be due to more mature cells requiring less tRNA processing with an already-established, stable tRNA pool and with suppressed cell division.

Overall, during the 12-20pcw developmental period, all tendon fibroblasts displayed high cellular activity related to growth and differentiation, while downregulated pathways suggested a shift from rapid growth to more specialised functions, with specific processes reflecting dynamic responses and changing protein synthesis needs. However, it is within the uniquely upregulated pathways that the distinctive characteristics of different fibroblast types can be discerned, providing clues to their specific functional roles (summarised in Table 4).

4.3.5.1 Biological pathways in tendon main body fibroblasts

As previously established, the ABI3BP GAS2 Fibroblasts 1 and 2 were the predominant cell types in the main body of the tendon fascicles and were likely responsible for tendon ECM deposition and maintenance. In ABI3BP GAS2 Fibroblasts 1, the uniquely upregulated processes included those related to metabolism, cell growth and homeostasis as well as cell structure, suggesting that these fibroblasts were actively engaged in tissue growth and maintenance over developmental time. Additionally, the upregulation of gene regulatory pathways involved in histone methylation (including “histone H3-K4 methylation” and “positive regulation of histone methylation”) pointed towards promotion of epigenetic mechanisms for cell specialisation. Several pathways associated with immune responses (e.g., “immune system development” and “somatic diversification of immune receptors”) were also upregulated, indicating potential immune-related roles for these fibroblasts. However, the pathways that were uniquely downregulated in this cell population also included several relating specifically to the activities of the adaptive immune system (including “B cell activation”, “positive regulation of B cell proliferation”, and “lymphocyte homeostasis”), further supporting the importance of those fibroblasts in modulation of immune cell activity. Finally, the unique downregulation of “positive regulation of ECM organisation” and “extracellular structure organisation” pathways suggested that this fibroblast type was likely becoming dedicated to maintaining existing tissue rather than participating in active growth or remodelling.

In contrast, the uniquely upregulated pathways in ABI3BP GAS2 Fibroblasts 2 highlighted enhanced activity in a multitude of processes, including p53-mediated DNA damage response and apoptosis, cell adhesion, lipid metabolism, and protein degradation. Furthermore, the promotion of mitochondrial regulation, calcium homeostasis, and energy production-related pathways underscored their contribution to cellular homeostasis. The presence of pathways associated with axon development and synapse localisation also hinted at their potential contribution to neural processes, while promotion of pattern formation, Wnt signalling regulation, and stem cell differentiation pathways indicated a role in tissue patterning and cellular differentiation. On the

other hand, ABI3BP GAS2 Fibroblasts 2 downregulated unique pathways involving cell cycle regulation, cell division, DNA repair, and chromatin remodelling. Notably, we observed downregulation of “calcineurin-NFAT signalling cascade” and “calcineurin-mediated signalling” pathways as well as the associated regulatory processes, known for their role in wound healing and fibroblast homeostasis and activation (Lieberman *et al*., 2019). Additionally, the downregulation of pathways related to muscle-related processes (including "positive regulation of muscle contraction" and "myofibril assembly") suggested a specialisation towards a non-contractile connective tissue.

In summary, while closely related, the two main tendon fascicular fibroblast populations appeared to differ in their levels of specialisation and functionality, with both being responsible for tendon tissue maintenance. With previous findings in mind, ABI3BP GAS2 Fibroblasts 1 were likely more differentiated and specialised for tissue growth and maintenance, with potential immune-modulatory and gene-regulatory functions, while ABI3BP GAS2 Fibroblasts 2 appeared to have a broader range of functions, encompassing roles in cellular homeostasis, neural processes, tissue patterning, and differentiation.

4.3.5.2 Biological pathways in tendon loose connective tissue fibroblasts

Within the inner tendon LCT (corresponding to the endotenon IFM), FGF14 THBS4 and COL6A6 FNDC1 Fibroblasts were the predominant populations likely involved in interfacing with vascular, neural, and lymphatic connections as well as maintaining tendon structure. In FGF14 THBS4 Fibroblasts, observed 229 unique upregulated pathways were identified that collectively suggested a multifaceted role in tissue remodelling, vascularisation, immune regulation, and the development of bone, muscle, and neuronal systems. Common themes included apoptotic signalling, stress responses, protein modification regulation, and increased synthesis of nucleotides as well as tendon ECM components (e.g., "glycoprotein biosynthetic process", "positive regulation of collagen metabolic process"). Additionally, heightened activity in pathways related to endothelial cell proliferation, angiogenesis, platelet function, and vascular permeability was observed, suggesting a significant role in promoting blood vessel growth within tendon tissue. Further, pathways related to immune

processes (e.g., "positive regulation involved in cytokine production", "positive regulation of lymphocyte activation", "regulation of leukocyte cell-cell adhesion") suggested a role in immune cell interactions and regulation within the tissue. Finally, the upregulation of pathways related to neurogenesis (e.g., "neuron maturation", "negative regulation of neuron differentiation", "positive regulation of neurogenesis"), “bone morphogenesis”, and “skeletal muscle organ development” pointed towards a role in regulation of the development of those systems. Conversely, pathways downregulated in these fibroblasts included those related to BMP signalling, ossification, skeletal muscle cell proliferation, regulation of neuron and dendrite development, and cell migration and adhesion.

Another population of inner tendon LCT fibroblasts, COL6A6 FNDC1 Fibroblasts, upregulated 81 unique pathways over the course of tendon development. Among those, "regulation of response to wounding" and "regulation of wound healing" (involving genes such as *plasminogen activator inhibitor 1* (*SERPINE1), thrombomodulin (THBD), caveolin 1 (CAV1), phosphatase and tensin homolog (PTEN), fibroblast activation protein (FAP), annexins 1 and 2 (ANXA1, ANXA2)*, *TGFBR1, PDGFRA, CD36, FGF2, ITGB1/CD29, CD109* etc.) as well as "positive regulation of response to cytokine stimulus" and "cellular response to glucocorticoid stimulus" emphasised participation in tissue healing, repair processes, and immune regulation, highlighting a pivotal role in preserving tendon health. Furthermore, the upregulation of "ECM assembly" and various cell adhesion pathways signified their involvement in shaping the ECM and facilitating cell-to-cell and cell-to-matrix interactions, underscoring their role in maintaining the structural integrity and function of the tendon rather than participating in tendon growth. In addition, the upregulation of "histone deacetylation" and "epigenetic regulation" pathways suggested involvement in gene expression regulation and cellular differentiation, which could contribute to the fine-tuned regulation of cell behaviour within the tendon. On the other hand, the uniquely downregulated pathways within this cell population encompassed those related to cell adhesion and migration, miRNA transcription and processing, synaptic functions and neuronal plasticity, metabolic and stress responses, as well as vascular compartment development and differentiation.

Overall, the inner tendon LCT fibroblast populations appeared distinct in their roles. The FGF14 THBS4 Fibroblasts were actively involved in the different regulatory and maintenance aspects of the inner LCT niche, including vascularisation, immune activity modulation, and the development of adjacent bone, muscle, and neuronal systems. In contrast, COL6A6 FNDC1 Fibroblasts exhibited a stable, potentially quiescent non-migratory phenotype with lower metabolic activity that was primarily dedicated to preserving the structural and functional integrity of tendon tissue, including through repair and immune modulation.

Finally, the up- and downregulated pathways in tendon outer LCT (epi- or paratenon) COL3A1 PI16 Fibroblasts suggested their involvement in tissue remodelling and adaptations to changing mechanical and structural requirements over the course of foetal development. Specifically, unique upregulation of the Hippo signalling pathway was observed, which was likely to be involved in maintenance of tendon size and structure. Additionally, upregulation of “chondrocyte development”, “epithelial cell development”, and “negative regulation of vascular associated smooth muscle cell proliferation" pathways hinted at the regulatory role of COL3A1 PI16 Fibroblasts in supporting the formation of structures with characteristics of epithelial cells within the developing tendon as well as suppressing smooth muscle cell proliferation around the vasculature, potentially preventing blood vessel infiltration into the tendon proper. Further, upregulation of pathways related to cell junction disassembly hinted at a crucial role of those cells in tissue remodelling, while upregulation of multiple pathways involving protein post-translational modifications (neddylation, peptidyl-proline modification, deglycosylation etc.) suggested that these cells were actively involved in influencing the activity and stability of proteins, including those involved in ECM maintenance and signalling. Interestingly, among the 152 uniquely downregulated pathways, several were related to muscle tissue development, stress responses, and metabolic and apoptotic processes. This analysis also revealed a significant downregulation of pathways associated with cell signalling, including positive regulation of ERK1/ERK2 and MAPK cascades as well as protein autophosphorylation, and negative regulation of protein dephosphorylation as well as JNK and TGF-β signalling pathways. Additional downregulation of

"protein methylation", "protein alkylation", "histone H3-K4 methylation" and "histone H4 acetylation" pointed at minimisation of epigenetic and protein modifications over developmental time.

Table 4. Summary of significant shared and unique gene ontology biological process (GO:BP) functions for each tendon fibroblast type. *Pcw: post-conception weeks; LCT: loose connective tissue; IFM: interfascicular matrix.*

	Predicted *in situ* location	**Summary of GO:BP functions (from 12 to 20 pcw)**	**Inferred function**
All Tendon Fibroblasts	- Promote processes crucial for growth, differentiation, and morphogenesis of the tendon. - Communicate with their surroundings and undergo substantial remodelling and regulation of cellular components. - Exhibit signs of significant energy utilisation and stress response. - Shift from rapid growth and proliferation to more specialised functions. - Suppress processes related to cell migration and neural development.		
ABI3BP GAS2 Fibroblasts 1	Fascicular Tendon	- Promote processes related to metabolism, cell growth, and homeostasis, indicating involvement in tissue growth and maintenance. - Upregulate gene regulatory pathways for histone methylation, suggesting active epigenetic mechanisms for cell differentiation. - Modulate immune cell activity. - Suppress ECM organisation processes, indicating a focus on tissue maintenance rather than active growth or remodelling.	Maintenance of tendon fascicles; gene regulation through epigenetic mechanisms; immune cell activity modulation
ABI3BP GAS2 Fibroblasts 2	Fascicular Tendon	- Promote processes related to energy production, apoptosis, cell adhesion, lipid metabolism, and protein degradation. - Influence patterning and cellular differentiation via promotion of processes related to pattern formation, Wnt signalling regulation, and stem cell differentiation. - Suppress the calcineurin-NFAT signalling cascade, with implications for wound healing and fibroblast activation. - Downregulate muscle-related processes, indicating potential involvement in the formation or maintenance of muscle tissues within or near tendons.	Maintenance of tendon fascicles; promotion of tendon tissue patterning; suppression of muscle-related processes
FGF14 THBS4 Fibroblasts	Myotendinous Junction, IFM/ Endotenon (inner LCT)	- Promote tissue remodelling and development, synthesis, and maintenance of tendon ECM components, as well as blood vessel growth and permeability. - Exhibit heightened energy production and DNA/RNA synthesis. - Regulate immune cell interactions as well as development of bone, muscle, and neuronal systems.	Tissue remodelling, vascularisation; immune modulation; regulation of bone, muscle, and neuronal systems

COL6A6 FNDC1 Fibroblasts	IFM/ Endotenon (inner LCT)	- Promote tissue healing and repair processes as well as ECM assembly. - Upregulate epigenetic mechanisms for regulation of gene expression and cell differentiation. - Downregulation of pathways related to cell adhesion, migration, synaptic functions, neuronal plasticity, metabolism, stress responses, and vascular compartment development. - Potentially quiescent (exhibit lower metabolic, protein synthesis, and migratory activity).	Tendon healing and repair; gene regulation through epigenetic mechanisms.
COL3A1 PI16 Fibroblasts	Para- or Epitenon (outer LCT)	- Promote the Hippo signalling and cell junction disassembly-related pathways, suggesting a role in modulation of tendon size and structure. - Actively influence protein activity and stability through post-translational modifications (e.g., neddylation, peptidyl-proline modification, deglycosylation). - Regulate vascularisation and chondrogenesis. Suppress vascular smooth muscle cell proliferation. - Suppress muscle tissue development, stress responses, metabolic and apoptotic processes, rapid cell signalling cascades (e.g., MAPK), and epigenetic modifications.	Tissue remodelling and maintenance; inhibition of vascular growth and muscle development.

Finally, this study aimed to quantify compositional changes in cell type proportions over time. The random sampling method used in sequencing – loading only up to 10,000 nuclei per sample from hundreds of thousands – can introduce biases and limit the accuracy of quantifying these compositional changes across conditions. To address this limitation, the tree-aggregated amplicon and single-cell compositional data analysis (tascCODA) Bayesian modelling approach, published by Ostner and colleagues (2021), was used.

After designating the Nervous System Cells as the reference group due to their assumed likely proportional stability over the 12-to-20-week developmental period, inferred cell type compositional changes in 20-week-old samples were compared against the 12-week-old ones (Figure 35). At 20 weeks, substantial proportional population decreases were noted in the muscle-specific NEGR1 SCN7A and tendon MTJ FGF14 THBS4 Fibroblasts, along with more moderate decreases in myocyte and immune cell populations. Notably, only the predominant immune cell subset corresponding to macrophages seemed to decrease in proportion (Figure 35), while the other small immune cell subtypes remained unchanged (not shown). Additionally, we observed proportional increases in subpopulations of both types of ABI3BP GAS2 Fibroblasts as well as in a major subset of tendon outer LCT COL3A1 PI16 Fibroblasts (Figure 35).

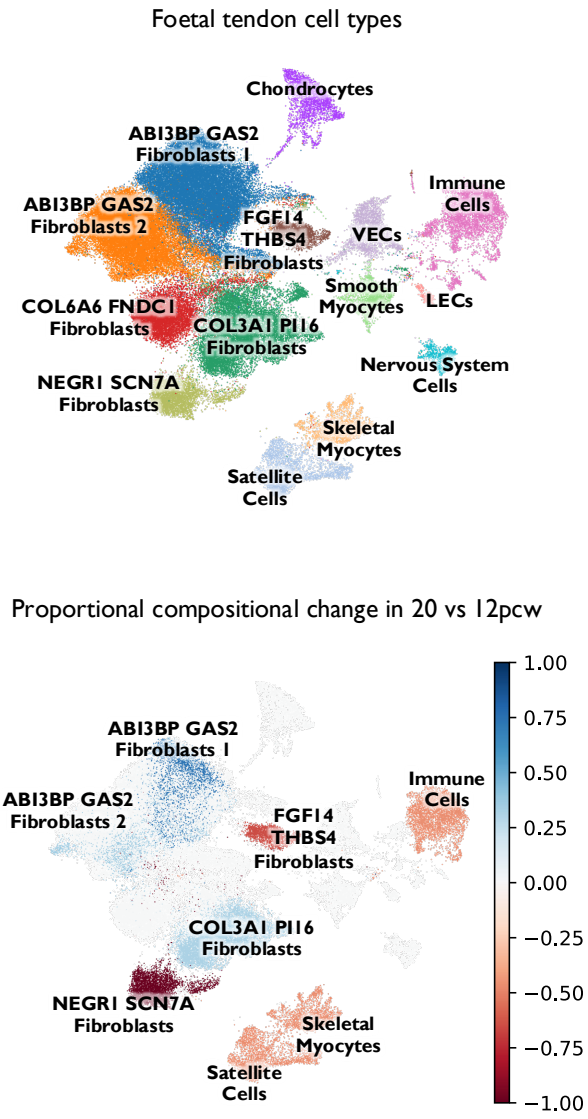


Figure 35. tascCODA-estimated compositional changes in developing tendons from 12 to 20 post-conception weeks (pcw). *UMAPs show combined 12, 17, and 20 pcw annotated foetal tendon cell types (**top**) and the tascCODA-estimated proportional changes in the composition of those cells (**bottom**). Cells in red reflect the statistically significant decreases in cell populations from 12 to 20 pcw, while changes in blue reflect the increases. The remaining cells in white-grey are unchanged in proportions.*

4.4 Discussion

This chapter provides a comprehensive overview of the transcriptional landscapes of human 12, 17, and 20 pcw foetal Achilles and quadriceps tendons, offering insights into the cellular dynamics occurring in development during early tendon maturation. Through the application of single-nucleus and spatial RNA-sequencing techniques, the study characterised 14 distinct clusters of cells expressing a range of markers indicative of various tendon-associated cell types, including fibroblasts, immune cells, endothelial cells, and nervous

system cells. Moreover, spatial RNA sequencing mapped these cells to specific anatomical locations, emphasising the importance of spatial organisation in understanding functional tissue architecture during tendon development.

4.4.1 Foetal tendon fibroblasts

A key finding of this work was the definition and localisation of 5 types of fibroblasts belonging to the three different main compartments of the tendons. The predominant foetal tendon fibroblast population characterised by high expression levels of *ABI3BP* and *GAS2* was identified within the fibrillar regions of the tendon. This population was originally subclustered into two subsets differentiated by transcriptional activity and abundance, with the second subset characterised by higher levels of both. ABI3BP GAS2 Fibroblasts expressed canonical fascicular TSPC markers *ENG*, *THY1*, *CD44*, and *NES* (Appendix Figure 4) alongside transcription factors such as *SCX*, *MKX*, and *SOX5*. Additionally, these cells demonstrated high expression of matrisomal genes, including *COL1A1*, *THBS2*, *TNMD*, *KERA*, *FMOD*, *ACAN*, and *COMP*, while showing lower expression of *COL3A1* compared to other fibroblasts. Importantly, ABI3BP GAS2 Fibroblasts highly expressed genes encoding fibrillar collagens V and XI responsible for fibril assembly initiation (Sun *et al*., 2020; Wenstrup *et al*., 2011), beaded filament-forming collagen VI responsible for fibril organisation and alignment (Di Martino *et al*., 2023; Ryan J. Leiphart *et al*., 2022), and FACIT collagens XII and XIV regulating fibril synthesis (H. L. Ansorge *et al*., 2009; Fung *et al*., 2022; Izu *et al*., 2021; Young *et al*., 2000). Considering the roles of collagens, proteoglycans, and glycoproteins identified (see section 2.3, Appendix Tables 1 and 2), this transcriptomic profile suggests that ABI3BP GAS2 Fibroblasts are the primary producers of collagen I, regulating its fibril assembly, organisation, and reinforcement. Additionally, these cells modulate cell proliferation and cell-ECM interactions within the fascicular tendon. Temporal DGE analysis further reveals that from 12 to 20 pcw, the first, less active fibroblast subset shifts focus towards tissue maintenance, while the more active second subset upregulates processes related to the ECM, pattern formation, and cell differentiation. Finally, both subsets are likely to increase in proportion from 12 to 20 pcw, underscoring

their significance for tendon growth and maturation. Overall, these fibroblasts play a crucial role in maintaining tendon structure during rapid foetal growth.

Surrounding the fibrillar ABI3BP GAS2 Fibroblasts were populations positioned within the interfascicular matrix. Among these, one group prominently expressed *COL6A6* and *FNDC1,* alongside transcription factors *TSHZ2* and *PLAGL1*, the kinase *DCLK1*, and matrisomal genes including *COL3A1*, *COL1A1*, *COL6A6*, *VCAN*, *FBN1*, and *THBS2*. Similarly to ABI3BP GAS2 Fibroblasts, these cells expressed many of the same collagen type V, VI, XI, XII, XIV genes associated with fibril synthesis, organisation, and size regulation. Importantly, they also expressed *TPPP3* and *PDGFRA* markers of injury-responsive TSPCs (Harvey *et al*., 2019), suggesting a potential role as such cells. This hypothesis was further supported by DGE analysis from 12 to 20 pcw, which revealed that COL6A6 FNDC1 Fibroblasts specifically upregulated pathways associated with tissue healing and repair while concurrently downregulating those associated with metabolism, migration, and adhesion. Overall, this expression profile implicates these fibroblasts in maintaining the structural and functional integrity of tendon tissue, potentially by laying down the initial matrix which is consequently remodelled by ABI3BP GAS2 Fibroblasts and by contributing to the formation of microfibrillar networks imparting structural elasticity and flexibility to the tendon.

Another fibroblast population found within foetal tendon IFM was characterised by high expression of *FGF14* and *THBS4.* These fibroblasts did not express any of the TSPCs markers, but instead had high levels of genes encoding various collagens (I, III, IV, V, VI, XI, XII), transcription factors (*EBF1*, *TSHZ2*), growth factors (*FGF14*, *BMP5*), signalling proteins (*DLK1*, *SLIT3*, *FSTL5*), and the cell adhesion molecule *CDH12*. DGE analysis between 12 to 20 pcw suggested a multifaceted role for these fibroblasts as they upregulated processes involved in ECM synthesis, remodelling and maintenance, blood vessel growth and permeability, regulation of immune cell interactions, and development of bone, muscle and neuronal systems. Importantly, this population was also uniquely localised at the periphery between muscle and tendon regions (Figure 31) and expressed *COL22A1* (Figure 33)*,* an MTJ-associated FACIT (Charvet *et al*., 2013; Koch *et al*., 2004), as well as *THBS4* (Appendix Figure 5), a pro-

angiogenic glycoprotein regulating MTJ repair (Frolova *et al*., 2014; Subramanian and Schilling, 2014). Hierarchical clustering linked these fibroblasts with NEGR1 SCN7A Fibroblasts identified among skeletal myocytes within the muscle regions, hinting at related functions. This expression profile, coupled with the strategic anatomical positioning, strongly suggests involvement of these cells in the formation and maintenance of the MTJ. Overall, FGF14 THBS4 Fibroblasts are implicated as key mediators of muscle-tendon crosstalk, contributing to MTJ integrity and coordinating various developmental processes crucial for tissue structure and function.

The abovementioned NEGR1 SCN7A Fibroblasts also had a distinct transcriptomic profile, which included high expression of genes for collagens I, IV, and XXI, and matrisomal proteins *TNXB*, *LUM*, and *VCAN*. This profile signifies their potential role in the regulation of ECM organisation and modulation of cellular interactions. Specifically, VCAN and TNXB have been implicated in the formation of anti-adhesive matrices that influence cell behaviour and tissue architecture (Chiquet-Ehrismann and Tucker, 2011; Higuchi *et al*., 2021; Scott *et al*., 2008), with TNXB being particularly critical to the structural and functional integrity of the MTJ (Brisset *et al*., 2020; Huijing *et al*., 2010). Moreover, COL4A1 is crucial for the formation of the basement membrane surrounding muscle fibres (Labelle-Dumais *et al*., 2019). The robust expression of *NEGR1*, *NAV3*, *NOVA1*, and *SEMA5A* – genes associated with neuronal development, axonal guidance, and cell adhesion (Hilario *et al*., 2009; Powers *et al*., 2023; Ruggiu *et al*., 2009; Singh *et al*., 2018) –suggests these fibroblasts may also support neuronal innervation, thus contributing to muscle function. The ontogenetic origin of these fibroblasts, whether tendon or muscle-derived, remains to be determined. Interestingly, the prevalence of this cell population appears to decrease from 12 to 20 pcw, providing a temporal context to their involvement in tissue development and suggesting a dynamic role in the maturing foetal musculoskeletal system.

Finally, a distinct population of fibroblasts highly expressing COL3A1 and PI16 has been identified in the LCT regions corresponding to the epi- or paratenon. These cells are transcriptionally analogous to COL6A6 FNDC1 Fibroblasts, sharing high expression levels of tendon sheath TSPC markers *TPPP3* and

PDGFRA alongside an array of other genes including *TSHZ2*, *PLAGL1*, *DCLK1*, *COL3A1*, *COL1A1*, *COL6A6*, *VCAN*, *FBN1*, and *THBS2*. They also exhibit partial transcriptional similarity with NEGR1 SCN7A Fibroblasts, particularly through the high expression of *LUM* and the absence of *COL11A1*. Between 12 and 20 pcw, these fibroblasts are involved in modulating tendon size and structure through pathways including Hippo signalling and cell junction disassembly. They also regulate protein stability and activity through post-translational modifications and play vital roles in vascularisation and chondrogenesis. Additionally, these cells suppress various physiological processes, including smooth myocyte proliferation, muscle tissue development, and stress responses, as well as metabolic, apoptotic, and epigenetic activities. Overall, COL3A1 PI16 Fibroblasts are multifaceted cells contributing to tendon morphogenesis and promoting integration with surrounding tissues to maintain and restore tendon integrity.

Comparing these fibroblasts with those characterised in prior animal and human single-cell and single-nucleus studies (see Table 1) is challenging. Although there may be similarities, definitive conclusions are hindered by the limited markers reported in existing studies, necessitating the initiation of analysis from the ground up. Moreover, the high-resolution datasets that are available predominantly focus on adult tendons, which may exhibit different transcriptomic profiles from developing or aged tendons. Chapter 6 will focus specifically on examining the differences between developing and aged tendons, using adult tendon data provided and annotated by the Tendon Seed Network (Baldwin *et al*., 2023, 2021). Nonetheless, while the comparison was complex for fibroblast populations, it was comparatively straightforward for non-fibroblast cell types with well-established markers, enabling parallels to be drawn between this dataset and the various reported cell types.

4.4.2 Foetal tendon non-fibroblast cell populations

Among the foetal tendon non-fibroblast populations, *PECAM1*$^{+}$ vascular and lymphatic endothelial cells were distinguished by their high expression of *CD34*, *VWF* and *LYVE1*, *PROX1*, *FLT4*, respectively. Smooth myocytes expressed *ACTA2*, *MYH11*, *CALD1*, *NOTCH3*, and *PDGFRB* genes involved in

contributing to vascular tone and providing structural support to blood vessels. Associated closely with these were Nervous System Cells likely involved in tendon innervation, expressing *NRXN1*, *NCAM2*, *SOX10*, *GRID2*, and *PTPRZ1* genes with roles in neural cell adhesion, signalling, and developmental regulation. Additionally, most foetal tendon samples contained Skeletal Muscle cells and their precursor *PAX7*-expressing Satellite Cells, which likely originated from the MTJ and adjacent muscle regions of sequenced tissues (see Appendix Table 3). While both populations expressed *CHD15*, *DLK1*, *NCAM1*, *MYO18B,* and *RYR3*, Skeletal Myocytes were distinguished by low levels of *PAX7* and high expression of *NES*, *DES*, *TTN*, *MYH3*, *TNNT3*, *COL22A1*, and *TNNC1*. Those populations were likely to decrease in proportion from 12 to 20 pcw. Chondrocytes expressing canonical markers such as *COL2A1*, *COL9A1*, *ACAN*, *COMP*, and *MATN1* were also identified, primarily within a single sample that had a larger section of enthesis dissected and sequenced. Finally, we identified clusters of Immune Cells expressing *PTPRC* (*CD45*), *CD44*, *IKZF1*, *RUNX1*, *DOCK2*, and *INPP5D* comprising diverse immune cell types. Due to the limited number of immune cells and the constraints of snRNA-seq in identifying surface markers typically used for their annotation, determining their precise identity was challenging. Nonetheless, the majority of immune cells within the biggest subcluster appeared to be of myeloid origin, as evidenced by high expression of macrophage markers such as *F13A1*, *CD163*, *MRC1*, *CSF1R*, *CD68*, and *LGMN*. Notably, this macrophage population decreased in proportion from 12 to 20 pcw.

The presence of *PECAM1*$^{+}$ endothelial cells in tendon has been previously described in multiple adult animal and human scRNA-seq studies (Akbar *et al*., 2021; De Micheli *et al*., 2020; Fu *et al*., 2023; Harvey *et al*., 2019; Kendal *et al*., 2020; Steffen *et al*., 2023b), however only Mimpen *et al.* (2022) described a further subset of *PROX1*$^{+}$ lymphatic endothelial cells in human adult hamstring tendons similar to the ones identified in the foetal tendon. Furthermore, foetal Smooth Myocytes expressed many of the genes that were used as markers for mouse mural cells described by Akbar *et al.* (2021) and human smooth muscle cells and mural cells referenced by Fu *et al.* (2023) and Mimpen *et al.* (2022), respectively. The foetal tendon Nervous System Cells associated with innervation shared some markers with glial nerve cells detailed by De Micheli *et*

al. (2020) and nervous system cells identified by Mimpen *et al*. (2022), while the Skeletal Myocytes mirrored those reported by Mimpen *et al.* (2022) and Akbar *et al.* (2021). Finally, the Immune Cells, particularly macrophages identified in this study, paralleled those reported in previous studies, which have also described different kinds of T cells and dendritic cells within tendons (see Table 1). Overall, these findings integrate with and expand upon the cell types and markers identified in prior studies of adult animal and human tendons (summarised in Table 1), confirming the early establishment of these cellular components and their roles in vascular support, innervation, and structural interface at the muscle-tendon junction.

4.4.3 Limitations and significance

Naturally, there are several limitations and knowledge gaps which warrant further inquiry to corroborate and expand upon the findings. Firstly, the 3′ end bias inherent in our transcriptomic assays introduces a potential skew in the data, predominantly capturing gene expression signals proximal to the polyadenylation site. This bias can result in an underrepresentation of full transcript diversity, limiting the detection of isoforms and alternative splicing events that may play significant roles in cellular differentiation and function. Thus, the scope of this transcriptomic analysis might not entirely reflect the complexity of the regulatory elements and the nuanced expression patterns operative within these cells. Secondly, Visium spatial RNA-sequencing used in this study is limited by its resolution, sequencing on average 17 cells per spot in this data. Unfortunately, this means that the technique cannot provide detailed delineation of the cellular microenvironments and the subtle gradients of signalling molecules within the developing tendon, limiting our ability to accurately map the cells to their native anatomical locations and model the microscale interactions between them and their ECM. Therefore, high-resolution spatial multiomics could significantly enhance these findings.

While the transcriptional profiles suggest the presence of distinct fibroblast populations within the developing tendon, postulating specific roles and contributions to homeostasis and repair, it is crucial to empirically confirm both the existence and function of those populations. Advanced RNA *in situ*

hybridization techniques such as RNAscope and MERFISH would allow the mapping of RNA molecules within individuals cells in their native tissue context. Additionally, immunofluorescence targeting the identified unique markers could validate the presence of these distinct cell types. Such work is already on the way, utilising an advanced multiplexed immunofluorescence imaging technique (CellDIVE) to validate the presence of the identified cell types.

Furthermore, the hypothesised involvement of specific fibroblast populations in tendon healing and other processes should be examined through *in vitro* and *in vivo* models, employing methods such as functional assays, gene knockdowns or overexpression to assess their contribution to tendon repair. For example, populations expressing different TSPC markers – ABI3BP GAS2, COL3A1 PI16, and COL6A6 FNDC1 Fibroblasts – may be isolated based on the transcriptional profiles described herein. These fibroblasts can then be studied *in vitro* to investigate properties such as stemness, responsiveness to biological stimuli, and behaviour in various functional assays, including wound closure to evaluate cell migration, collagen gel contraction to assess matrix remodelling, and biomechanical tests to measure changes in tissue strength and elasticity. Building from that, gene knockdown or overexpression experiments may help clarify the roles of pivotal genes highlighted by transcriptomic data and *in vitro* experiments, shedding light on fibroblast functionality and their impact on tendon healing. Finally, findings from *in vitro* experiments may then be translated into relevant *in vivo* models of tendon injury or disease, providing a comprehensive understanding of how these fibroblast populations contribute to tendon repair processes and potentially identifying new therapeutic targets.

In summary, this work offers insights into the cellular and molecular landscape of foetal tendon development, a critical period when the basic architecture and functional properties of tendons are established, and the tissue enters the growth and maturation stage. The identification of distinct fibroblast populations, each characterised by unique transcriptional profiles, is a substantial advance in understanding the heterogeneity and specialisation of cells within the developing tendon. The study also reveals the rapidly changing, dynamic nature of tendon development, with temporal changes in the gene expression profiles of fibroblasts occasionally suggesting shifts in their functional roles. These

findings provide a framework for future research to exploit these insights in bioengineering and clinical applications, offering new avenues for treatment strategies in tissue repair and regenerative medicine.

A fundamental unresolved question pertains to the ontogenetic origins of various identified fibroblast populations, as their precise developmental lineages have not yet been clearly delineated. Future research employing genetic lineage tracing could offer valuable insights into the provenance and developmental pathways of these fibroblast subsets. Meanwhile, the next chapter of this thesis aims to extend the investigation of foetal development back to the embryonic stages by leveraging existing transcriptomic scRNA-seq and spatial RNA-seq datasets from human embryonic whole limbs.

Chapter 5: Expansion of Tendon Development Study Using Single-Cell and Spatial RNA-Sequencing Data from Embryonic Whole Limbs

5.1 Introduction

The initiation of cell lineage decisions during early embryogenesis is pivotal for establishing the cellular diversity that underpins the development of mature tendon structures. These initial stages not only shape the architectural and functional blueprint of tendons, but also lay the groundwork for subsequent cellular behaviours critical to tendon formation. Despite the advances in understanding embryonic tendon development, significant knowledge gaps persist, particularly concerning the precise cellular compositions of embryonic tendons and the processes guiding their evolution into the foetal cell types. Thus, this chapter explores the embryonic origins of foetal tendon cells as well as the transitions in tendon development from embryogenesis through to the foetal stage.

The lack of tendon-specific molecular markers as well as small volume tissue samples pose a significant challenge to the application of high-resolution molecular analyses to the study of embryonic tendons. To overcome these obstacles, this research utilises an integrated approach, extracting embryonic tendon transcriptomic signatures from spatial and single-cell RNA-sequencing datasets obtained from whole embryonic limbs at 6-9 pcw (B. Zhang *et al*., 2023). The objectives of this study are twofold: firstly, to identify and characterise the progenitor populations active in embryonic tendon development; and secondly, to integrate this data with foetal stages, thereby delineating developmental lineage trajectories and uncovering the key genetic determinants of these developmental pathways. The methodological framework adopted here not only deepens our understanding of the mechanisms underpinning embryonic tendon development, but also provides insights into the molecular architecture that shapes the structural and functional maturation of tendons throughout early development.

5.2 Methods

5.2.1 Embryonic Visium spatial RNA-seq data analysis and reference dataset preparation

Human embryonic spatial RNA-seq data (*N*=8 from a total of two 6 pcw and one 8 pcw full embryonic leg) provided by the Teichmann group (B. Zhang *et al*., 2023) were analysed using 10X's Loupe Browser (v6.4.1) and Squidpy (Palla *et al*., 2022). Gene expression profiles of early tenocyte genes (e.g., *SCX*, *MKX*, *FMOD*, *TNMD*, *EGR1*) as well as H&E-stained sections were assessed to attempt early tendon demarcation. While it was not possible to confidently demarcate tendon regions in 6 pcw samples, a combined file of 3 regions from a single 8 pcw whole hind limb allowed demarcation of the developing tendon tissue (Figure 36). The sample was annotated in the Loupe Browser, with annotations subsequently uploaded into the spatial AnnData object. Overall, out of 2,439 Visium spots, 18 corresponded to the patellar tendon and 10 to the quadriceps tendon regions (Figure 36).

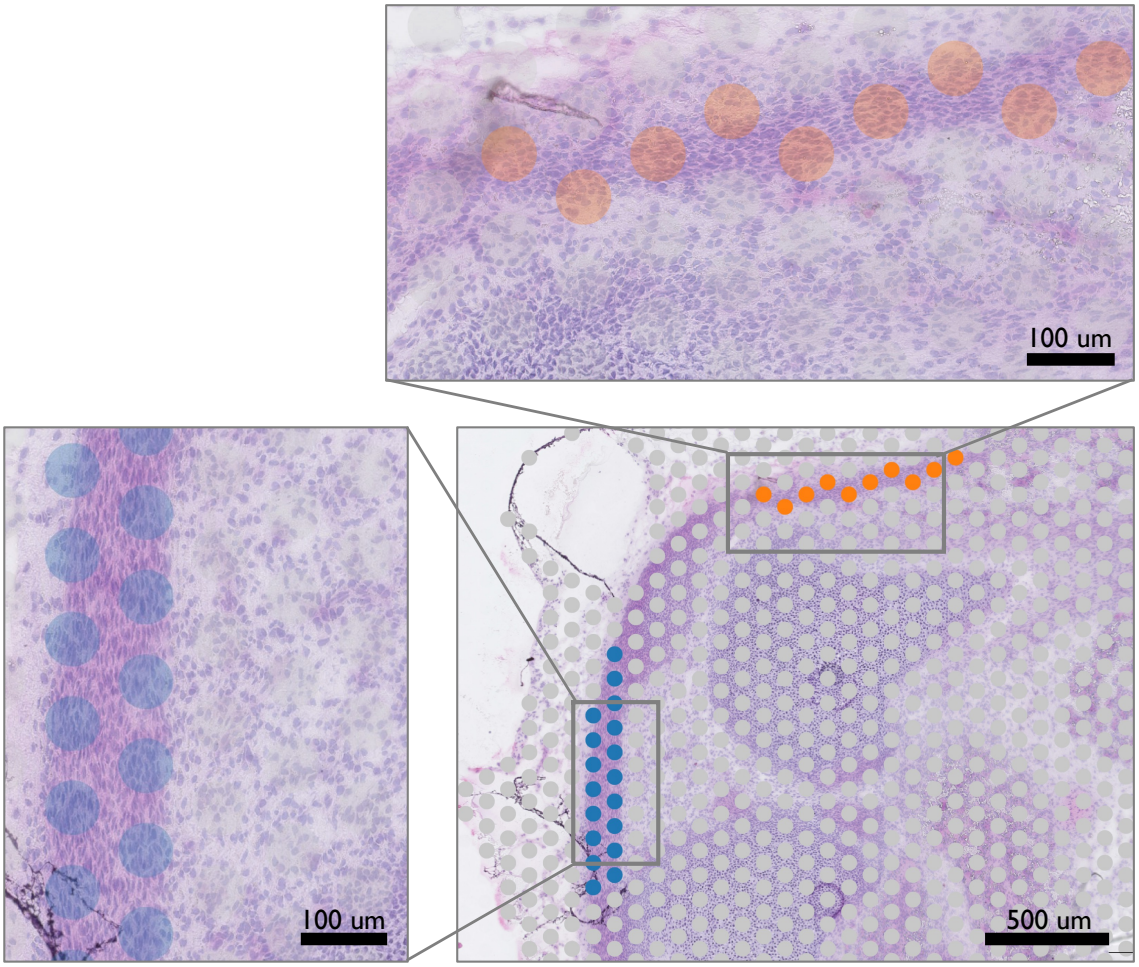


Figure 36. Tendon tissue demarcation in spatial RNA-seq data from a whole 8 post-conception week human embryonic hindlimb. *Section shows the knee region of the embryonic limb. Tissues were annotated based on the distinct H&E appearance as well as expression patterns of common early tendon markers such as SCX, MKX, TNMD, and FMOD. Orange spots correspond to the quadriceps tendon, while blue spots demarcate the patellar tendon.*

5.2.2 Embryonic scRNA-seq data integration and batch correction

Single-cell embryonic data samples from 6 to 9 pcw (*N*=25, total of 108,617 cells) were processed as described in section 3.5, then integrated and batch-corrected using scvi-tools' (Gayoso *et al.*, 2022) scVI modelling on all unnormalised gene counts, with the main batch effects of interest specified to be 'samplename' (consisting of Sample ID) , 'kit', 'seq_protocol', and 'sex' (Appendix Table 3).

As before, model hyperparameters were optimised with scVI autotune and manual runs to 'n_hidden': 256, 'n_latent': 14, 'n_layers': 3, 'dropout_rate': 0.1, 'gene_likelihood': 'nb', and 'dispersion': 'gene-batch'. The model was trained using 394 epochs until training and validation sets were stably converged. The

resulting latent representation embeddings were then used as basis for the computation of a neighbourhood graph of observations and dimensionality reduction with UMAP (Appendix Figure 7).

5.2.3 Visium spatial RNA-seq data-based random forest classifier training and tendon cell prediction in embryonic whole limb scRNA-seq data

To identify tendon cell subsets within embryonic whole limb scRNA-seq data, I applied a random forest classifier, utilising spatial RNA sequencing data as a reference. Briefly, the spatial AnnData object for the annotated slide was split into non-tendon (2,411 spots) and tendon (28 spots) datasets. To get around the issues with low sample numbers, I created “pseudodonors” by assigning the 28 tendon and 28 random non-tendon Visium spots with a distinct numeric identifier, while the remaining non-tendon spots were assigned a shared number to ensure they were treated as a single 29th pseudodonor. The "test" and "train" subsets were then concatenated into a unified AnnData object containing a total of 57 pseudodonors corresponding to 56 individual and 1 mixed expression spots. Next, I modified the *aggregate_and_filter()* function from section 16 in Heumos *et al*. (2023) to iterate through the patellar tendon, quadriceps tendon, and non-tendon data, subsetting it and creating 25 pseudoreplicates for each donor by shuffling and splitting the cell indices. The number of pseudoreplicates was chosen based on the average number of nuclei counts per single Visium spot (range of 10-31). These pseudoreplicates were then aggregated into a new AnnData object of 1,425 observations and 14,208 genes to be used as the reference dataset.

Both the spatial training and scRNAseq test data were normalised the same way to log1pPF (see section 4.2.2). Next, both objects were concatenated to harmonise their features, and the top 5,000 highly variable genes were selected using Scanpy’s built-in function with flavor=“cell_ranger” and batch_key=”modality” (corresponding to “spatial” vs “single-cell” datasets). The individual training and test datasets were then subset to those highly variable genes.

Next, scikit-learn functions (Pedregosa *et al*., 2011) were used to train the random forest classifier on the test data. Briefly, class imbalances of tendon vs non-tendon data were addressed using the Synthetic Minority Over-sampling

Technique (SMOTE) from the imblearn package (Lemaître *et al*., 2017). The spatial data were then randomly split into train and test datasets at a ratio of 80:20. The *GridSearchCV()* function was applied to select the best model hyperparameters for classifier training, and the *RandomForestClassifier()* was subsequently trained with 2,000 decision trees, using parameters such as bootstrap sampling and square root feature selection at each split, achieving high (>0.96) out-of-bag, accuracy, precision, recall, and F1 scores.

The trained classifier was then applied to the log1pPF-normalised scRNAseq data to generate predictions. Additionally, probabilities for each class (tendon vs non-tendon) were estimated. Classifier prediction performance was evaluated using Receiver Operating Characteristic (ROC) and Precision-Recall (PR) curves along with their corresponding Area Under the Curve (AUC) calculations, indicating good predictive capability with AUC-ROC of 0.96 and AUC-PR of 0.74. Furthermore, F1 scores were calculated to optimise tendon vs non-tendon classification threshold selection. The classifier's predictions were then adjusted to the optimal threshold of 0.4955, yielding refined predictions of 4,318 tendon cells among the 108,617 embryonic whole limb cells.

The Random Forest classifier predictions (“Predictions”, Figure 37) were additionally compared against the cells identified by thresholding of the top 20 spatial DEG scores above the 95th percentile of the demarcated tendon regions (Figure 37). These scores (“Score distribution”, Figure 37) were calculated using *sc.tl.score_genes(adata, gene_list = ['POSTN', 'ABI3BP', 'SCX', 'MKX', 'TNMD', 'KERA', 'FMOD', 'GAS2', 'COL11A1', 'HTRA3', 'HTRA1', 'PRSS35', 'COL1A1', 'COL1A2', 'COL3A1', 'FGF14', 'SOX9', 'SFRP2', 'CTHRC1', 'ZNF185'])* on normalised counts.

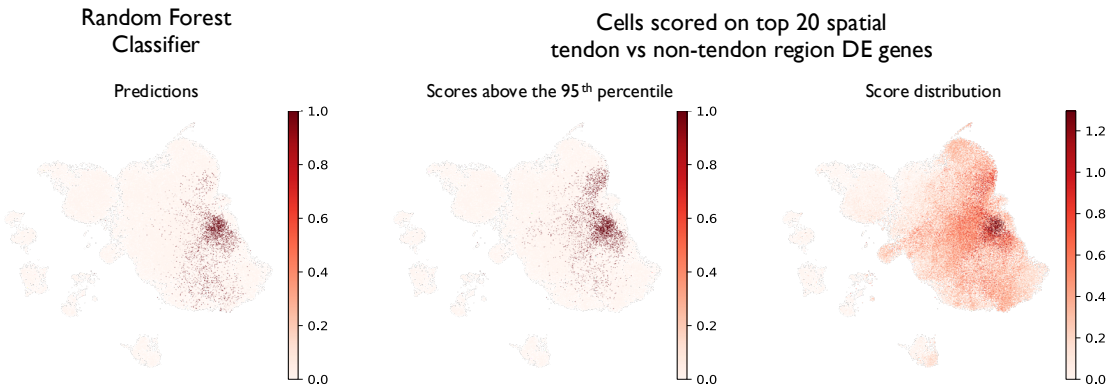


Figure 37. Comparison of random forest classifier and gene scoring methods for tendon cell identification within whole limb embryonic scRNA-seq data. *Random forest classifier was trained on the spatial gene expression profiles of tendon and non-tendon regions. The Predictions UMAP plot highlights all cells identified as tendons by this classifier. Middle and right UMAP plots show tendon cell identifiaction by cell scoring on the top 20 differentially expressed genes between spatial tendon and non-tendon regions. Right plot shows the scores. Middle plot shows the cells with scores above the 95th percentile.*

5.2.4 Embryonic tendon cell annotation

The single-cell data were subset to the random forest classifier predictions. Only samples with at least 20 cells in each of the batch effect categories (‘samplename’, ‘kit’, ‘seq_protocol’, ’sex’) were retained. Samples sequenced with 5’ v1 kit as well as those sequenced using NovaSeq 6000 were removed due to significant batch effect confounding (Appendix Table 3).

Finally, genes detected in fewer than 5 cells were removed, leaving a total of 3,092 cells and 18,119 genes from 6 donors aged 6.5-9.3pcw.

The data were re-normalised to log1pPF, and 4,000 highly variable genes were selected with flavor="cell_ranger". The effects of the cell cycle scores were regressed out to remove those significant sources of uninteresting variation (*sc.pp.regress_out(adata, [‘S_score’, ‘G2M_score’])*). The regressed counts were scaled, and the PCA was carried out with previously identified highly variable genes. The data were then clustered using Scanpy’s Leiden algorithm at 0.3 resolution, identifying 7 gene expression clusters (Figure 38A). Those were manually annotated through marker gene exploration using the results from the between-cluster Wilcoxon rank-sum test (Figure 38C). Marker sets from CZ CellxGene’s Cell Guide library for mesenchymal stem cells (CL:0000134) and chondrocytes (CL:0000138) (CZI Single-Cell Biology

Program *et al.*, 2023) were used for gene scoring to aid annotation (shown in Appendix Figure 8).

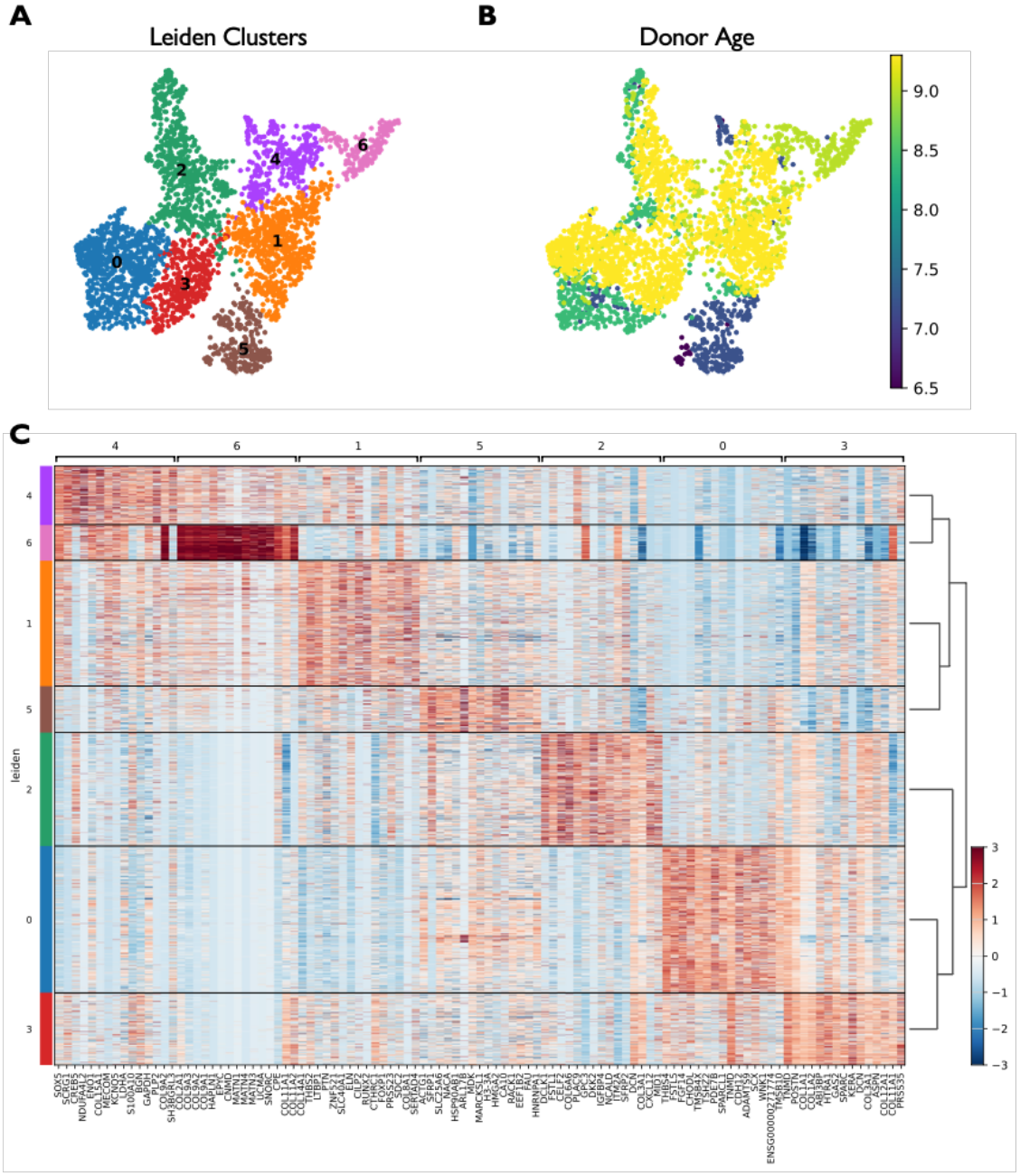


Figure 38. Embryonic tendon scRNA-seq Leiden clustering and marker gene analysis. *Embryonic tendon single-cell RNA-sequencing data clustering using the Leiden algorithm identified 7 distinct cell clusters based on gene expression profiles. Differential gene expression analysis was performed between these clusters using the Wilcoxon rank-sum test to identify genes differentially expressed across clusters. UMAP plots show* ***(A)*** *the distribution of cells within the identified Leiden clusters at a resolution of 0.3 and* ***(B)*** *donor ages presented as a continuous variable.* ***(C)*** *Clustered heatmap shows normalised and z-score scaled expression of top 15 differentially expressed genes for each Leiden cluster. Red indicates overexpression, while blue represents underexpression relative to other clusters.*

5.2.5 RNA Velocity

scVelo (v0.2.5) preprocessing functions were applied to the combined, spliced, and unspliced counts matrices to re-normalise and filter them using the default settings. The neighbours and moments were calculated using regressed PCA embeddings. RNA Velocity analysis was carried out using a dynamical gene expression model by recovering dynamics, calculating velocities, and constructing a velocity graph with default settings (*scvelo.tl.recover_dynamics()*, *scvelo.tl.velocity(mode='dynamical')*, *scvelo.tl.velocity_graph()*). Differential kinetics test was then run using the top 100 dynamical genes, and the velocity was recalculated with those in mind. The results are presented in Figure 46.

5.2.6 Embryonic data trajectory and fate analysis with Harmony, Palantir, and CellRank

To prepare for trajectory analysis, sample counts matrices were reorganised by sample age in ascending order. Harmony package's (v0.1.4, Nowotschin *et al*., 2019) *harmony.core.augmented_affinity_matrix()* function was used with top 40 PC loadings (containing over 90% of total variation) and 20 *k*-nearest neighbours (knn) to construct an augmented affinity matrix that incorporated the developmental age information into the similarity measures between cells. Force-directed layouts based on this matrix are shown in Figure 45. This matrix was then used to construct diffusion maps with 20 knn using Palantir (v1.3.1, Setty *et al.*, 2019). The diffusion map embeddings were then used to identify neighbours (knn=20) for the cell type partition-based graph abstraction (PAGA), which was subsequently used as basis for the generation of UMAPs shown in Figure 44. Furthermore, these embeddings were used to determine the multi-scale space of the data through 9 eigenvectors identified at the first eigengap. These multiscale space embeddings served as basis for tSNE dimensionality reduction, recalculation of the nearest neighbours (knn=15), and creation of the force-directed graphs shown in e.g., Figure 47.

For Palantir pseudotime trajectory analysis, differentiation initiation and termination cells were selected based on the most extreme values in multiscale diffusion components, believed to correspond to stable states (Appendix Figure 10). Palantir was run using multiscale space embeddings (with knn=20 and

num_waypoints=2000), and the results were visualised in Figure 47. To account for the possible gene dropouts affecting the analysis, Palantir's built-in MAGIC imputation for gene expression was run on the diffusion components using default settings. MAGIC-imputed counts were used for analysis of gene expression changes across pseudotime (Figure 49, Appendix Figure 11).

To analyse cell differentiation lineages further, a CellRank (v1.5.1) Palantir pseudotime kernel was initiated, and the transition matrices were computed using a Generalized Perron Cluster Cluster Analysis (GPCCA) estimator with default settings. By analysing real eigenvalue plots, 3 distinct, stable macrostates representing terminal states were identified. Absorption probabilities were then computed using default settings, calculating lineage drivers for each terminal state. A single initial state was determined using a backward kernel based on the same process. The results are summarised in Figure 50. Log1pPF-normalised, non-imputed counts were used to calculate correlations between lineage drivers shown in Figure 51.

To bridge the gap between initial and terminal states, scVelo's functions were used to recover latent time (*scvelo.tl.recover_latent_time()*) and calculate a directed PAGA incorporating Palantir pseudotime as prior (*scvelo.tl.paga(adata, groups="cell_type", root_key="initial_states_probabilities", end_key="terminal_states_probabilities", use_time_prior="palantir_pseudotime")*). This was used as basis for plotting cell fate probabilities shown in Figure 52.

5.2.7 Embryonic scRNA-seq and foetal snRNA-seq data integration with scGen and trajectory inference with Moscot and CellRank

The embryonic scRNA-seq and foetal snRNA-seq datasets were integrated using scGen, which output both corrected counts and shared corrected latent space embeddings (unlike scVI, which outputs the latter but not the former). The model was initiated by specifying different sequencing runs (libbatch) as batches and previously annotated cell types as labels. It was trained until convergence using default settings for a total of 28 epochs.

Corrected latent space embeddings were used for the generation of a Harmony augmented affinity matrix. This was followed by Palantir multiscale diffusion map calculation and force-directed graph plotting (Figure 53) as described in

section 5.2.6. Following the generation of PAGA graphs, the Immune Cells were removed from further trajectory analysis due to them being disconnected from the rest of the cells even at low thresholds.

To reconstruct developmental trajectories, moscot (multi-omics single-cell optimal transport, v0.3.3, Klein *et al.*, (2023)) was applied. The genes were re-filtered to retain only those with more than 20 counts. Next, a TemporalProblem object was initiated with scGen-corrected latent embeddings, and the proliferation and apoptosis scores were obtained. The temporal problem was solved using manually optimised parameters (epsilon=1e-3, tau_a=0.99, tau_b=0.999, scale_cost="mean", batch_size=1200). Cell transition scores were then calculated to determine putative cell ancestors and descendants (Figure 54).

CellRank (v2.0.2) RealTimeKernel was initiated from the TemporalProblem object, and the transition matrices were computed with self_transitions="all", conn_weight=0.2, and threshold="auto_local" optimised parameters. As before, GPCCA estimator was used. Overall, 7 macrostates were identified at the largest eigengap, out of which 4 corresponded to the major foetal tendon fibroblast cell types and were manually set to be terminal (Figure 55). The initial states were set manually to the putative tendon fibroblast precursor populations identified at 7.2 and 8.4pcw (Figure 55). Fate probabilities were aggregated as in section 5.2.6 using diffusion map-based PAGA with knn=20 (Figure 56).

5.2.8 Single-cell regulatory network inference and clustering analysis

Single-cell regulatory network inference and clustering (SCENIC) analysis was performed on Achilles and quadriceps tendons from 20pcw samples using pyscenic (v0.12.1; Aibar *et al.* (2017)). Gene regulatory networks (GRNs) were inferred using the GRNBoost2 algorithm with default settings. The input data were raw, unnormalised counts stored in a loom file. Human transcription factors were predefined using the 'allTFs_hg38.txt' list from the Aertslab GitHub repository. The resulting TF-gene interactions were utilised to infer co-expression modules, identify enriched motifs, and predict regulons with the "pyscenic ctx" command. Genome rankings (.feather) and motif annotation (.tbl) v10 files were obtained from the Aertslab cistarget resources webpage. A total

of 286 regulons were identified. To quantify regulon activity in individual cells, the "pyscenic aucell" command was executed with default settings. Binarization of cellular regulon activity (as either “on” or “off”) was performed using a Gaussian mixture model. Regulon-cell type specificity was assessed by calculating z-scores of regulon expression.

5.3 Results

5.3.1 A needle in a haystack: identifying tendon cells in embryonic limbs using multicell-resolution spatial transcriptomics

To begin the exploration of tendon signatures in embryonic limbs, the expression of early tendon development markers within single-cell and spatial RNA sequencing data of 6-9 pcw embryonic whole limbs sourced from the Teichmann group (B. Zhang *et al*., 2023) was assessed. It was found that markers traditionally associated with tenocyte identity – including *SCX*, *MKX*, *TNMD*, *FMOD*, and *THBS2* – were not exclusive to tendon cells, showing varying levels of expression across many different cell type clusters (Figure 39) and tissue structures, such as ligaments and fascia (Figure 40). This observation raised concerns about the reliability of conventional marker genes for identifying tenocytes in this data, prompting the investigation of alternative methods to isolate tendon-specific cells.

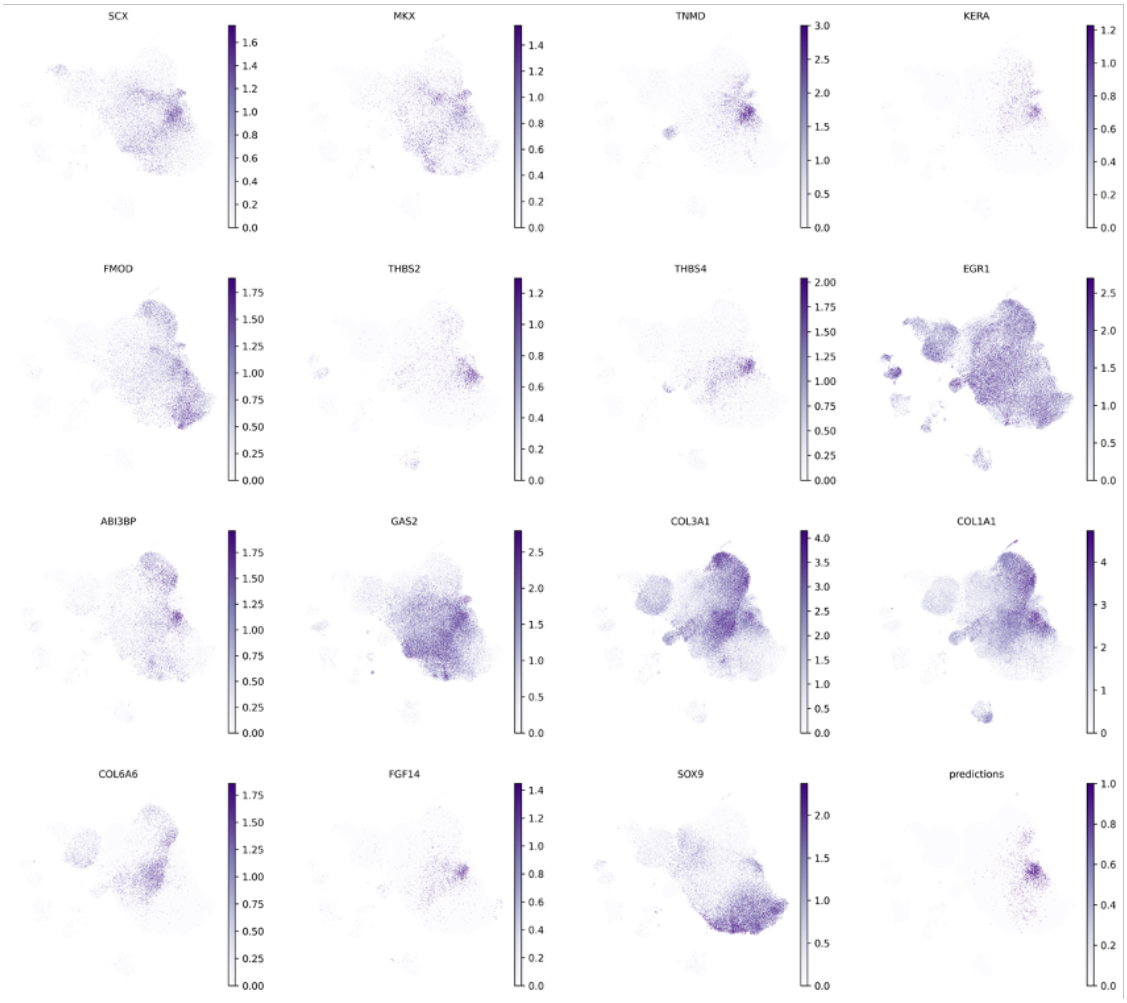


Figure 39. Expression of early tendon markers in human embryonic single-cell RNA-sequencing data from fore- and hindlimbs of 11 human embryonic donors. *The UMAPs show normalised gene expression values for early tendon markers, which were selected based on the findings from the previous chapter. These markers highlight the transcriptional profiles relevant to early tendon development. The 'predictions' panel shows the likely tendon cell types identified using a random forest classifier, which was trained on spatial RNA-sequencing data from 8 post-conception week embryonic hindlimbs (as shown in Figure 40), predicting the probable identity of tendon cell types within the fore- and hindlimb dataset.*

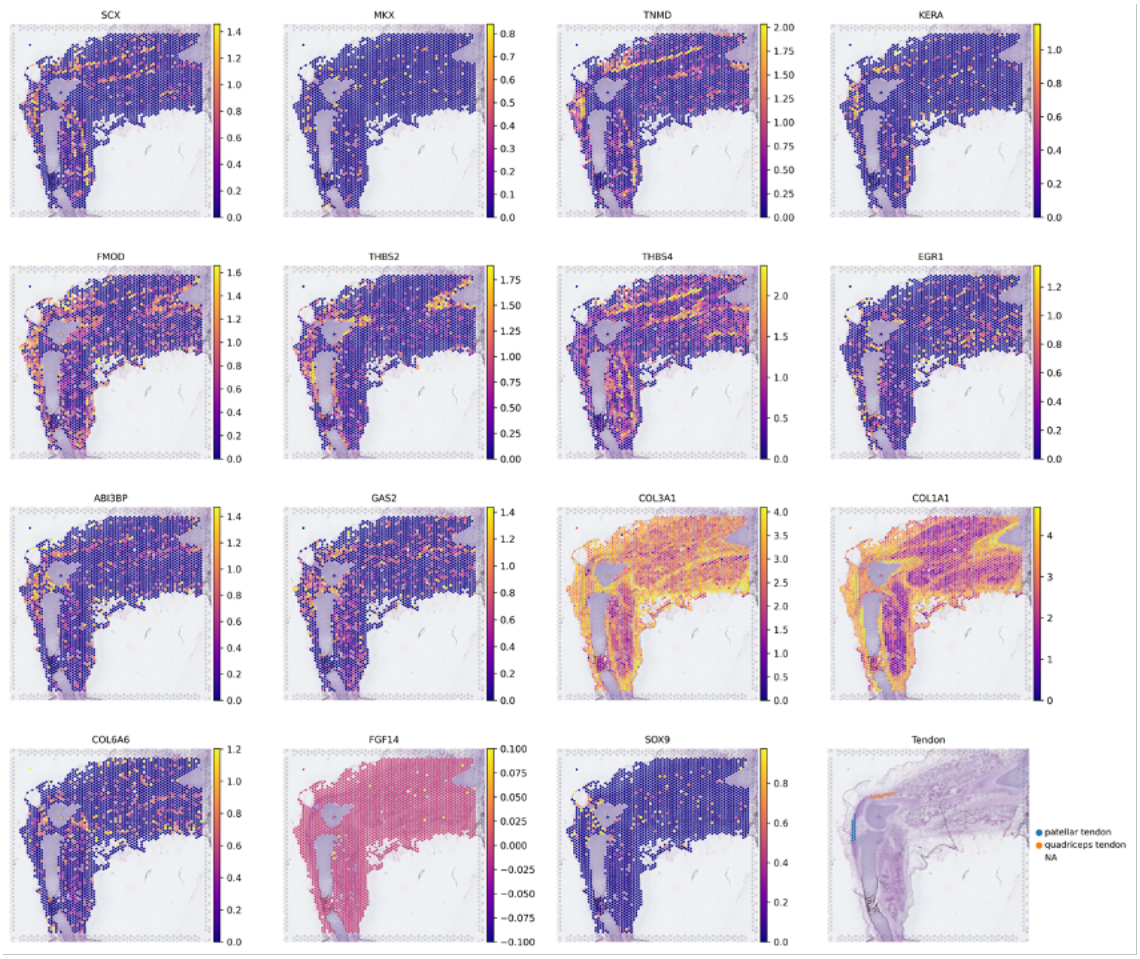


Figure 40. Tendon cell marker expression in a whole 8 post-conception week embryonic human leg. *Visium scatterplots show the normalised gene expression values for key tendon cell markers, revealing their spatial distribution within the developing leg. The 'Tendon' panel illustrates the manually annotated tendon regions identified from H&E-stained tissue sections (see Figure 36). These annotated regions were used to train the random forest classifier, enabling the identification of tendon cell types in embryonic whole limb single-cell data based on this spatial RNA-sequencing data (see Figure 39).*

To address this challenge, tendon regions within a single 8 pcw H&E-stained spatial RNAseq whole leg sample ("Tendon" in Figure 40) were manually delineated and their gene expression profiles extracted. Those profiles were then used as a reference for identifying tendon cells in the embryonic limb scRNA-seq data. A random forest classifier trained on this reference identified a subset of 4,318 cells with tendon-like profiles out of the 108,617 cells present in the entire embryonic limb scRNA-seq dataset ("predicted" in Figure 39). After refining the data to remove batches with confounding effects, 7 cell state clusters comprised of 3,092 cells from six donors aged between 6.5 to 9.3 pcw were annotated (Figure 41A,B).

5.3.2 Characterisation of embryonic tendon cell types

The youngest cell cluster observed at 6.5 and 7.2 pcw (Appendix Figure 8) was characterised by the expression of transcription factors such as *SOX4*, *FOXP2*, *RUNX1T1, HMGA2*, and *SIX1*, alongside a diverse range of genes with roles in cell structure and adhesion (e.g., *TUBB*, *ACTG1, MARCKSL1, CDH11*), stress response (e.g., *HSP90AB1*, *HSPD1*), as well as metabolism, growth, and signalling (e.g., SLC25A6, *MDK, NPM1*, *ARL17B*, *FTH1*, *EEF1A1, SFRP1*) (Figure 44). Additionally, these cells expressed *TNMD*, *TSHZ2*, *GAS2,* and *VCAN* at lower levels (Figure 44). Considering that tendon cells are believed to originate from mesenchymal stem cells (MSCs), the identity of these cells as potential MSCs was investigated.

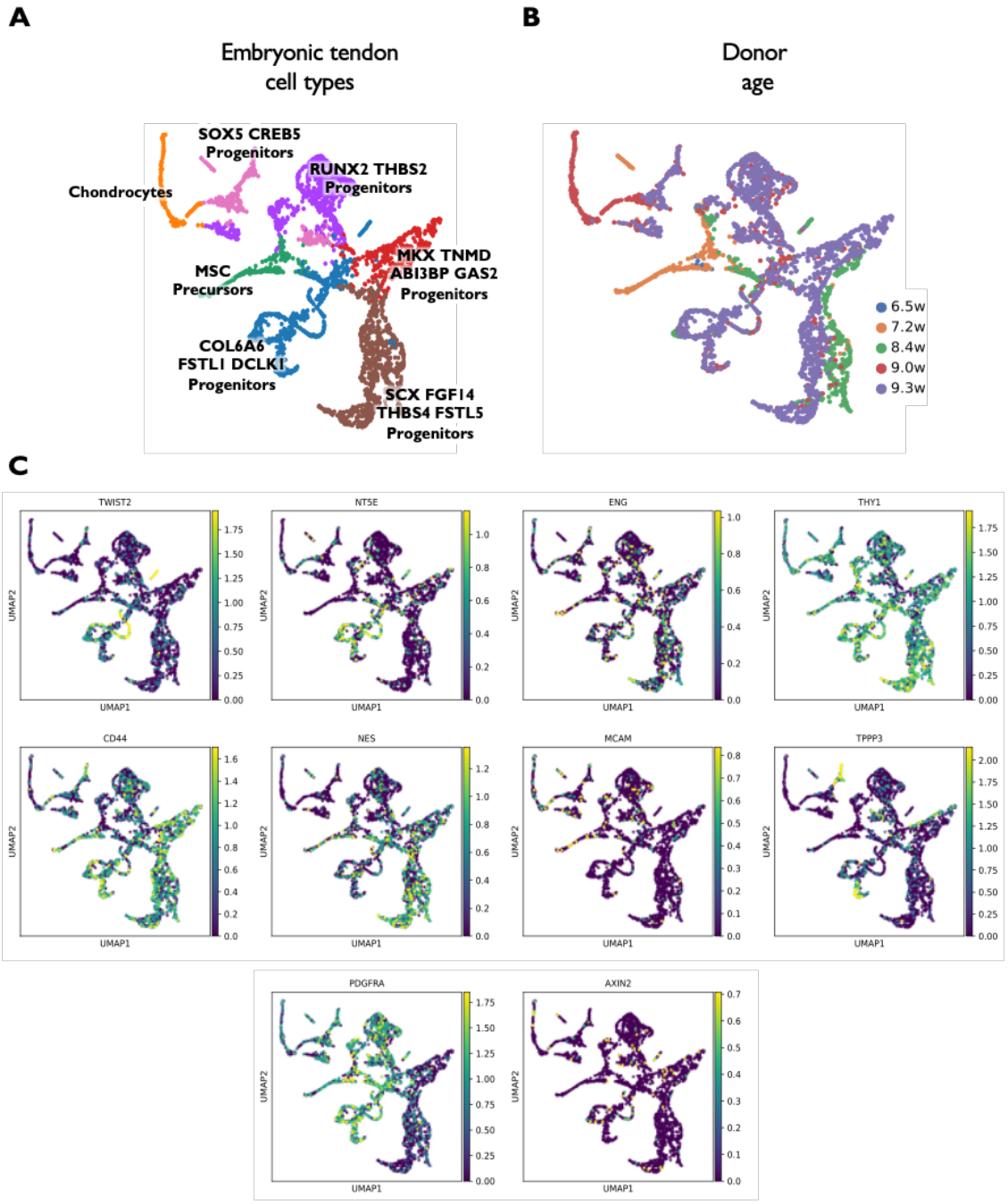


Figure 41. Expression of mesenchymal and tendon stem/progenitor cell markers in embryonic tendon cells. *UMAPs show (**A**) annotated embryonic tendon cell types, (**B**) donor ages in weeks post-conception, and (**C**) log1pPF-normalised expression of mesenchymal stem cell and tendon stem/progenitor cell markers, with greener colours corresponding to higher expression levels. The UMAPs were initiated from the cell state partition-based graph abstraction, which was calculated using a diffusion map derived from the Harmony-augmented k-nearest neighbour graph.*

Intriguingly, a cell cluster first identified at a slightly later stage of 8.4 pcw demonstrated a more definitive MSC phenotype. This cluster expressed 59 MSC markers listed in the CellXGene cell database ("MesStemCell" in Appendix Figure 8) alongside established MSC markers *CD73* (*NT5E*), *CD90*

(*THY1*), *CD44*, and *TWIST2* (Figure 41C). Further characterised by high expression levels of *COL6A6*, *FSTL1*, and *DCLK1*, this cluster expressed various collagens (I, III, IV, V, VI, XII, XIV), matrisomal genes (*ELN*, *DCN, ASPN, OGN, FNDC1, LUM, VCAN, EMILIN2, MFAP5, IGFBP6, DPT, TNXB, POSTN*), as well as loose connective tissue transcription factors *odd skipped-related-1* and *-2* (*OSR1, OSR2*) (Nassari *et al*., 2017; Stricker *et al*., 2012). Additionally, these cells expressed signalling genes associated with cell migration, adhesion, communication, and differentiation (*e.g., CREB5, CXCL12, GPC3*, *CELF2, PRKG1, AKAP12, NAV3, COLEC12, CD34*) (Figure 42C, Appendix Figure 9). These findings led to the classification of the younger cell cluster as probable MSC Precursors, while the 8.4 pcw cluster appeared to represent MSCs transitioning towards the tendon LCT fibroblast phenotypes identified in foetal samples (Figures 42 and 44). Specifically, this cluster, named COL6A6 FSTL1 DCLK1 Progenitors (or COL6A6 Progenitors, in short), shared 34, 20, and 14 of its highly expressed genes with the top 50 DEGs of foetal COL3A1 PI16 Fibroblasts, COL6A6 FNDC1 Fibroblasts, and NEGR1 SCN7A Fibroblasts, respectively (Figure 44B).

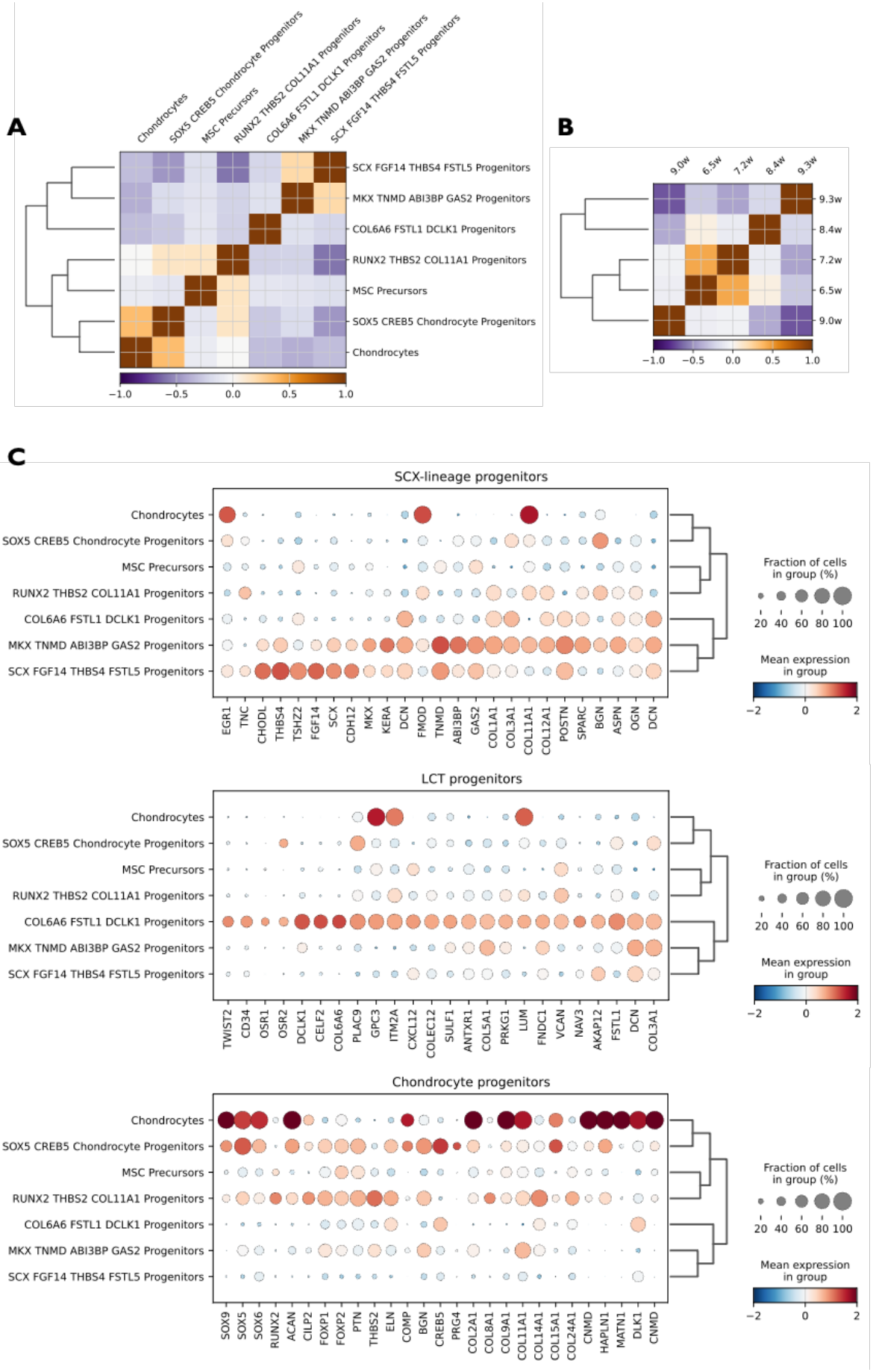

A
Chondrocytes
SOX5 CREB5 Chondrocyte Progenitors
MSC Precursors
RUNX2 THBS2 COL11A1 Progenitors
COL6A6 FSTL1 DCLK1 Progenitors
MKX TNMD ABI3BP GAS2 Progenitors
SCX FGF14 THBS4 FSTL5 Progenitors
−1.0 −0.5 0.0 0.5 1.0
B
9.0w 6.5w 7.2w 8.4w 9.3w
−1.0 −0.5 0.0 0.5 1.0
C
SCX-lineage progenitors
EGR1 TNC CHODL THBS4 TSHZ2 FGF14 SCX CDH12 MKX KERA DCN FMOD TNMD ABI3BP GAS2 COL1A1 COL3A1 COL11A1 COL12A1 POSTN SPARC BGN ASPN OGN DCN
LCT progenitors
TWIST2 CD34 OSR1 OSR2 DCLK1 CELF2 COL6A6 PLAC9 GPC3 ITM2A CXCL12 COLEC12 SULF1 ANTXR1 COL5A1 PRKG1 LUM FNDC1 VCAN NAV3 AKAP12 FSTL1 DCN COL3A1
Chondrocyte progenitors
SOX9 SOX5 SOX6 RUNX2 ACAN CILP2 FOXP1 FOXP2 PTN THBS2 ELN COMP BGN CREB5 PRG4 COL2A1 COL8A1 COL9A1 COL11A1 COL14A1 COL15A1 COL24A1 CNMD HAPLN1 MATN1 DLK1 CNMD
Fraction of cells in group (%)
20 40 60 80 100
Mean expression in group
−2 0 2

Figure 42. Characterisation of gene expression profiles in human embryonic tendon cells from 6.5 to 9.3 post-conception weeks. *Clustered matrix heatmaps show the pairwise Pearson correlation coefficients between different* ***(A)*** *donor cell types and* ***(B)*** *ages, calculated based on their transcriptional profiles. Higher correlation values (indicated by orange colour intensity) suggest similar gene expression patterns.* ***(C)*** *Dotplots show hierarchically clustered cell type log1pPF-normalised and scaled gene expression levels, alongside the proportional abundance of highly differentially expressed genes that define specific lineages, including the putative SCX-expressing (scleraxis-positive), loose connective tissue (LCT), and chondrocyte lineages. The size of each dot represents the proportion of cells expressing the gene, while the color intensity indicates the level of gene expression. Markers were selected based on the findings from the previous chapter.*

In addition to the MSC-like cells, three clusters in different stages of differentiation expressing chondrogenic markers were identified. The first cluster characterised by high expression of *RUNX2* – a master regulator of osteoblast differentiation (Yoshida *et al*., 2004) – had a transcriptomic profile indicative of multipotency with potential for differentiation into both osteogenic and chondrogenic lineages. It shared genes with MSC Precursors (Figure 42A) and expressed a variety of collagens associated with tendon and cartilage (*COL1A1*, *COL3A1* and *COL9A1-COL9A3, COL2A1*, respectively), endothelial basement membranes (*COL8A1*), and fibrillogenesis and matrix organisation (*COL11A1*, *COL12A1*, *COL14A1*, *COL24A1*) (Figure 43). Furthermore, it highly expressed a mix of matrisomal proteins, including elastin, SLRPs (*OGN*, *ASPN*, *BGN, FMOD, LUM*, and *PRELP*), and hyaline cartilage matrix proteins (*THBS2*, *VCAN, HAPLN1, ACAN, MATN4 and CILP2*), as well as various signalling molecules associated with ossification or chondrogenesis (e.g., *FGFR2, PTN, FOXP1, FOXP2*) (Figures 42C and 43, Appendix Figure 9, Appendix Table 2). This cluster was named RUNX2 THBS2 COL11A1 Progenitors (RUNX2 Progenitors, in short).

Concurrently, the other two clusters were characterised by high expression of cartilage-associated genes, including *SOX5, SOX6, SOX9, ACAN*, *CILP2*, *HAPLN1*, *COMP*, *COL2A1*, and *COL9A1-COL9A3* (Figures 42C and 43, Appendix Figure 9). These clusters displayed differential expression levels, suggesting varying stages of chondrocyte lineage differentiation. The less differentiated cluster, named SOX5 CREB5 Chondrocyte Progenitors (referred to as SOX5 Progenitors), expressed genes associated with early cartilage formation such as *CREB5* and *PRG4*. In contrast, the more differentiated Chondrocyte cluster exhibited high expression levels of all chondrocyte genes,

along with *MATN1*, *MATN3*, and *MATN4* cartilage glycoproteins across the majority of its cells (Figure 42C, Appendix Figure 9).

In summary, RUNX2 Progenitors, SOX5 Progenitors, and embryonic Chondrocytes share a closely related expression profile (Figure 42A), indicating a common pathway in early chondrogenic lineage commitment. RUNX2 Progenitors demonstrated a gene expression profile typical of an early, undifferentiated state with the potential for both osteogenic and chondrogenic differentiation. Interestingly, this cluster had 14 highly expressed genes that appeared among the top 50 DEGs of both foetal ABI3BP GAS2 Fibroblasts and foetal Chondrocytes (Figure 44B). SOX5 Progenitors, representing an intermediary stage of differentiation, shared 40% of the top 50 foetal Chondrocyte DEGs (Figure 44B). Finally, embryonic Chondrocytes, expressing the highest levels of cartilage-specific ECM components, represented the most advanced differentiation state within this developmental pathway, overlapping by 50% with the top 50 foetal Chondrocyte DEGs (Figure 44B).

Finally, the remaining two embryonic cell clusters belonged to the *SCX*-expressing tendon fibroblast lineage. The first of those showed high expression levels of *FGF14*, *THBS4*, and *FSTL5,* resembling the gene profile seen in MTJ-forming foetal FGF14 THBS4 Fibroblasts (Figure 42C). Indeed, there was an overlap of 33 out of the top 50 DEGs between this progenitor type and the fibroblast type (Figure 44B). This SCX FGF14 THBS4 FSTL5 Progenitor population (referred to as SCX Progenitors) was characterised by high levels of chondrolectin (*CHODL*), *TSHZ2*, *CDH12*, and proteoglycans *KERA*, *POSTN*, *DCN,* and *OGN* (Figure 42C). Additionally, it expressed a variety of collagens, including the typical fibrillar and FACIT types (I, III, V, VI, XII, XIV), those associated with basement membranes (*COL18A1*, *COL4A1*, *COL4A2*), the MTJ (*COL22A1*), and those involved in cell adhesion and communication (*COL13A1*) (Figure 43).

The second *SCX*-expressing cluster displayed a gene expression profile akin to foetal fascicular fibroblasts, marked by elevated levels of *MKX*, *TNMD*, *ABI3BP*, and *GAS2* (Figure 44). A comparison with foetal cell types revealed an overlap of 30 out of the top 50 DEGs with ABI3BP GAS2 Fibroblasts (Figure 44B). Appearing transcriptionally similar to FGF14 Progenitors, this cluster exhibited

even higher expression of *KERA*, *POSTN*, *SPARC*, *BGN*, *ASPN*, *OGN*, *DCN*, and collagens I, II, III, V, VI, XI, XIII, XIV, along with the highest levels of the LOX crosslinking enzyme (Figures 42C and 43, Appendix Figure 9). This population was consequently named MKX TNMD ABI3BP GAS2 Progenitors, or MKX Progenitors, in short.

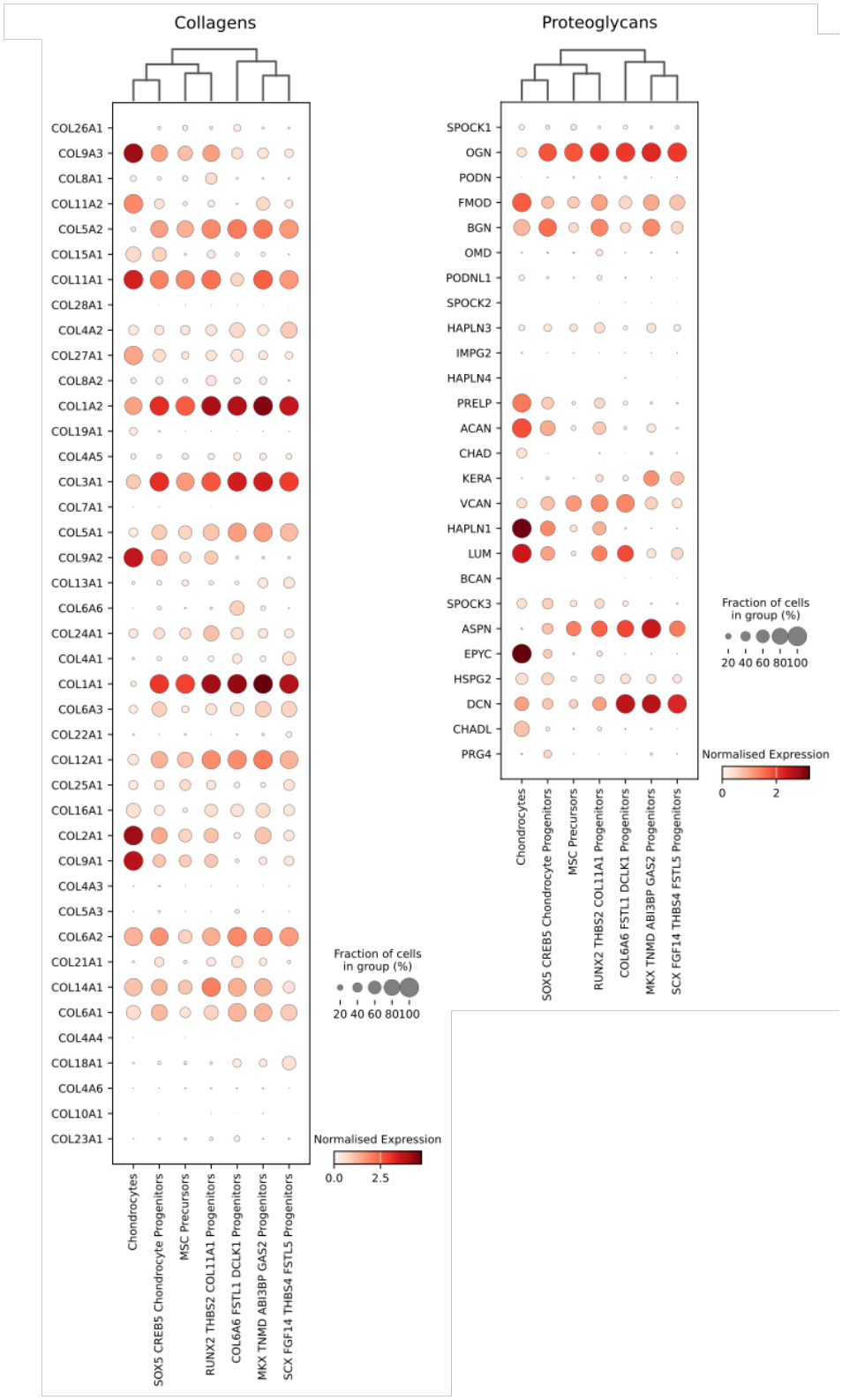


Figure 43. Human embryonic 6.5 to 9.3 post-conception week tendon collagen and proteoglycan gene expression profiles. *Dotplots show cell type clustered mean log1pPF-normalised expression levels alongside the proportions of expressing cell types for all proteoglycan and collagen genes present in the data. The lists of matrisomal genes were obtained from the matrisomeDB database (Shao et al., 2020). The remaining matrisomal gene dotplots are shown in Appendix Figure 9.*

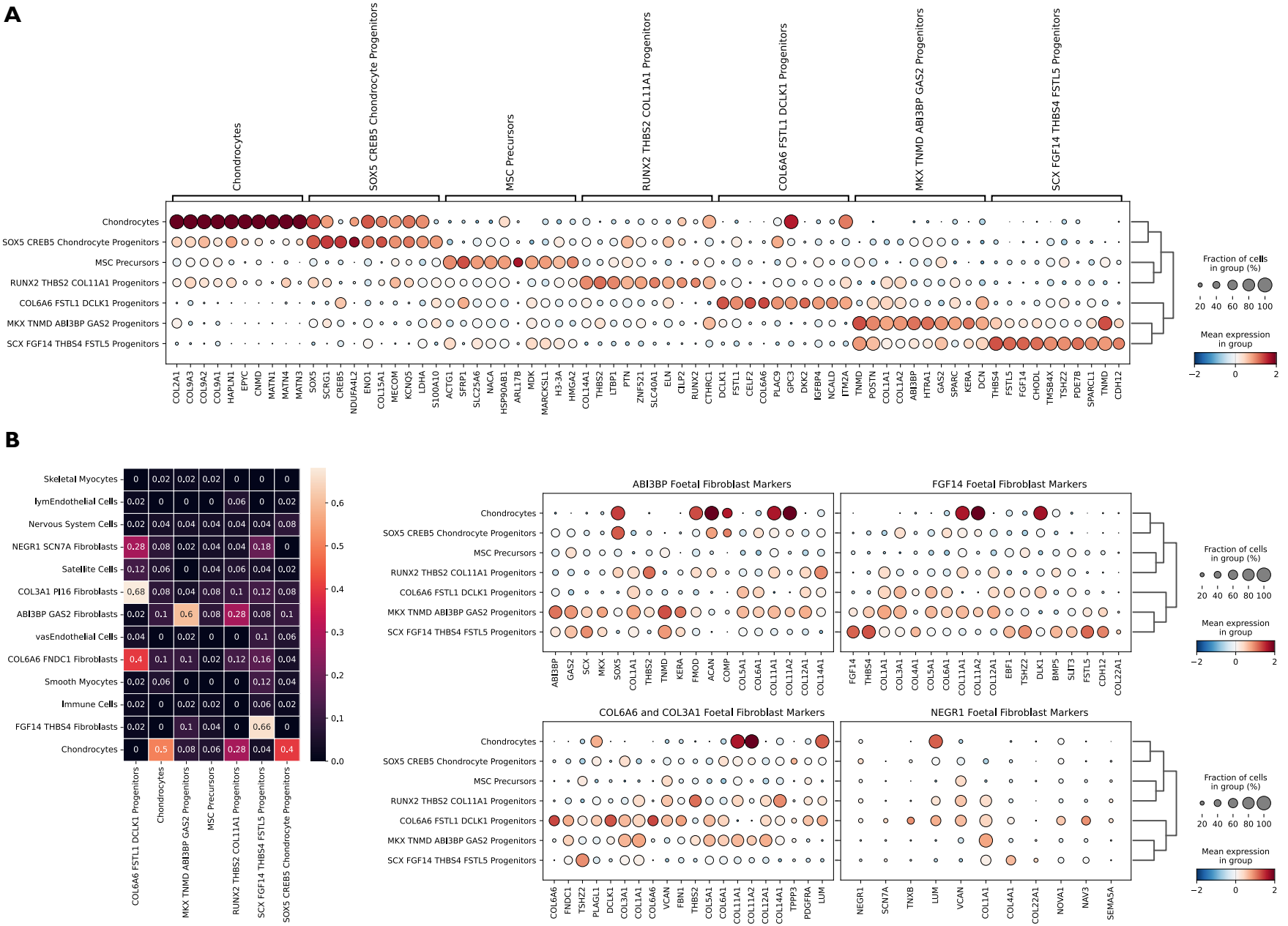

A
Chondrocytes
SOX5 CREB5 Chondrocyte Progenitors
MSC Precursors
RUNX2 THBS2 COL11A1 Progenitors
COL6A6 FSTL1 DCLK1 Progenitors
MKX TNMD ABI3BP GAS2 Progenitors
SCX FGF14 THBS4 FSTL5 Progenitors
Fraction of cells in group (%)
Mean expression in group
B
Skeletal Myocytes
lymEndothelial Cells
Nervous System Cells
NEGR1 SCN7A Fibroblasts
Satellite Cells
COL3A1 PI16 Fibroblasts
ABI3BP GAS2 Fibroblasts
vasEndothelial Cells
COL6A6 FNDC1 Fibroblasts
Smooth Myocytes
Immune Cells
FGF14 THBS4 Fibroblasts
ABI3BP Foetal Fibroblast Markers
FGF14 Foetal Fibroblast Markers
COL6A6 and COL3A1 Foetal Fibroblast Markers
NEGR1 Foetal Fibroblast Markers

Figure 44. Differentially expressed genes in human 6.5-9.3 post-conception week (pcw) embryonic tendon cell types and comparison with foetal tendon cell signatures. (A) *Dotplot showing clustered log1pPF-normalised and scaled expression of top 10 differentially expressed genes for each embryonic tendon cell type.* ***(B)*** *(Left) Matrixplot shows the proportional overlap of the top 50 differentially expressed genes identified in cell types from 12 pcw foetal tendons against an array of embryonic cell types. Each cell in the matrix represents the percentage of overlapping DEGs, calculated as the number of shared genes divided by the total number of genes in the embryonic reference set, multiplied by 100 to express the value as a percentage. (Right) Dotplots showing clustered log1pPF-normalised and scaled expression of foetal tendon fibroblast markers in embryonic cell types.*

5.3.3 Delineation of tendon cell differentiation trajectories and lineage-specific drivers in embryonic development

To check the assumptions and prepare for trajectory analysis, Harmony augmentation of the *k*-nearest neighbours graph was applied to connect cells across consecutive developmental stages, as proposed by Nowotschin *et al*. (2019). Figure 45 presents the Harmony-enhanced force-directed layouts that elucidate the lineage relationships among cell types, accompanied by diffusion maps that quantitatively trace the progression of cellular differentiation. From the diffusion distance relative to the earliest MSC Precursors, we observed that the MSC-like COL6A6 Progenitors and Chondrocytes were positioned notably further in differentiation space than the *SCX*-expressing tendon lineage cells (Figure 45B). This suggested an earlier commitment to chondrogenic and LCT fates or a more rapid differentiation pace compared to the *SCX*-expressing tendon lineage, which remained phenotypically closer to MSC Precursors during the analysed stages of embryogenesis. The differentiation of MSC Precursors towards tendon and osteo- or chondrogenic lineages was first evidenced between 6.5 and 7.2 pcw, marked by the emergence of SCX and RUNX2 Progenitor populations (Figure 45C). Subsequently, a higher proportion of more differentiated MKX Progenitors became apparent from 8.4pcw, indicating progression within the differentiation trajectory (Figure 45C).

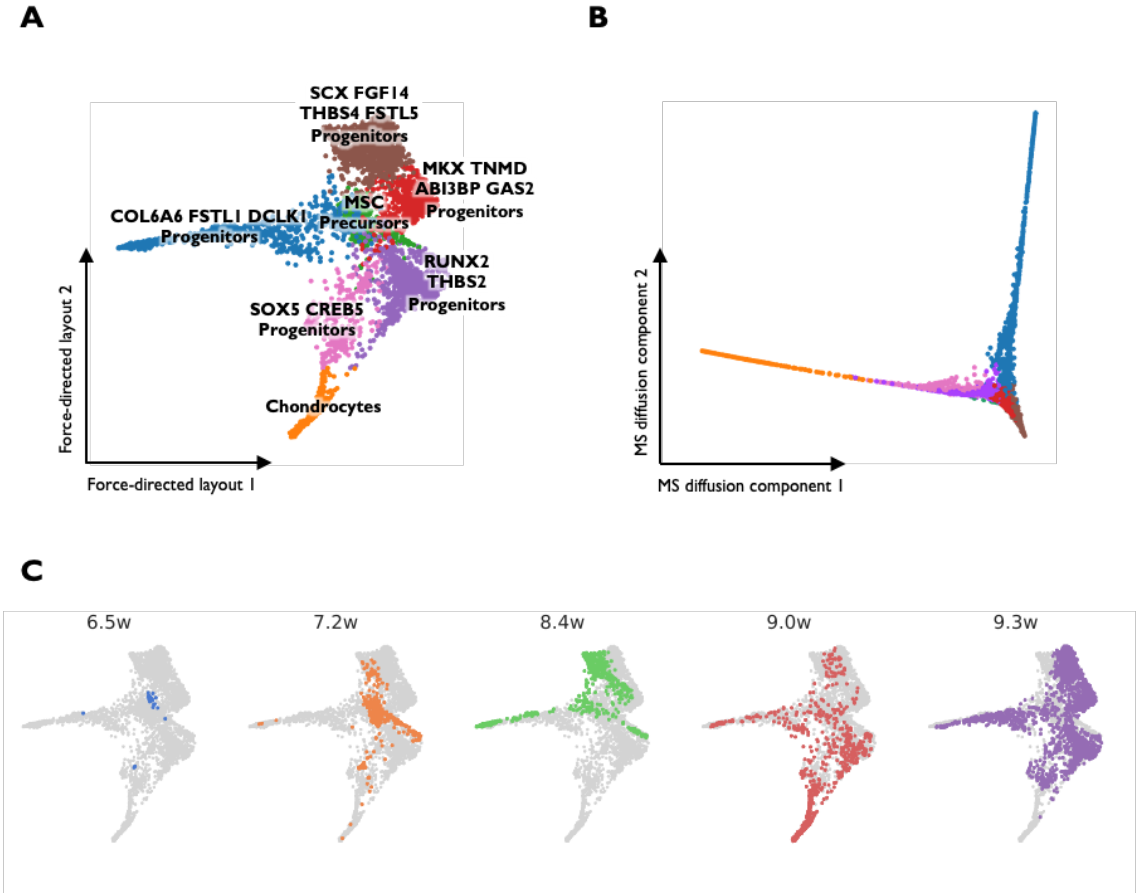


Figure 45. Visualisation of cell differentiation during embryonic tendon development using Harmony-enhanced force-directed layouts and multiscale diffusion maps. *(**A**) The Harmony-augmented force-directed layout displays the distribution of cells, annotated by their respective types. This layout simulates physical forces where similar cells attract each other while dissimilar cells repel one another, highlighting potential lineage relationships among cell populations. The subfigures in (**C**) further break down this layout by developmental timepoints, represented in post-conception weeks, showing the temporal dynamics of differentiation. (**B**) The Palantir multiscale diffusion map shows the progression of cell differentiation, with axes reflecting the primary diffusion components that capture variation in the differentiation states of the cells. These diffusion components indicate the principal directions of variation within the cell populations, enabling the identification of key differentiation trajectories. Cells positioned further along the extreme ends of the multiscale components are indicative of a more differentiated state.*

To investigate the direction and speed of gene expression changes, RNA velocity – a method that predicts future cell states by analysing the ratios of unspliced to spliced mRNA (La Manno *et al*., 2018) – was applied. The analysis revealed that MSC Precursors branched out towards four different cell fate clusters – mature tenocyte MKX Progenitors, early chondrocyte lineage RUNX2 and SOX5 Progenitors, and MSC-like COL6A6 Progenitors (Figure 46A) – a finding that was consistent with their likely multipotent nature. Additionally, SCX Progenitors also showed a tendency to differentiate towards MKX Progenitors,

aligning with their profile of higher *SCX* expression indicative of early tendon development, but lower expression of later development markers *MKX* and *TNMD* (Figure 46A). It is possible that MSC Precursors could also be giving rise to SCX Progenitors, although this possibility may be obscured by the low numbers of MSC Precursors captured in the dataset. As expected, the velocity lengths indicated substantial transcriptional changes at the MSC Precursor and SCX Progenitor lineage divergence points, marking them as crucial junctures for lineage determination (Figure 46B). On the other hand, the transitions appeared slower for more differentiated cells, such as the tendon MKX Progenitors and Chondrocytes (Figure 46B).

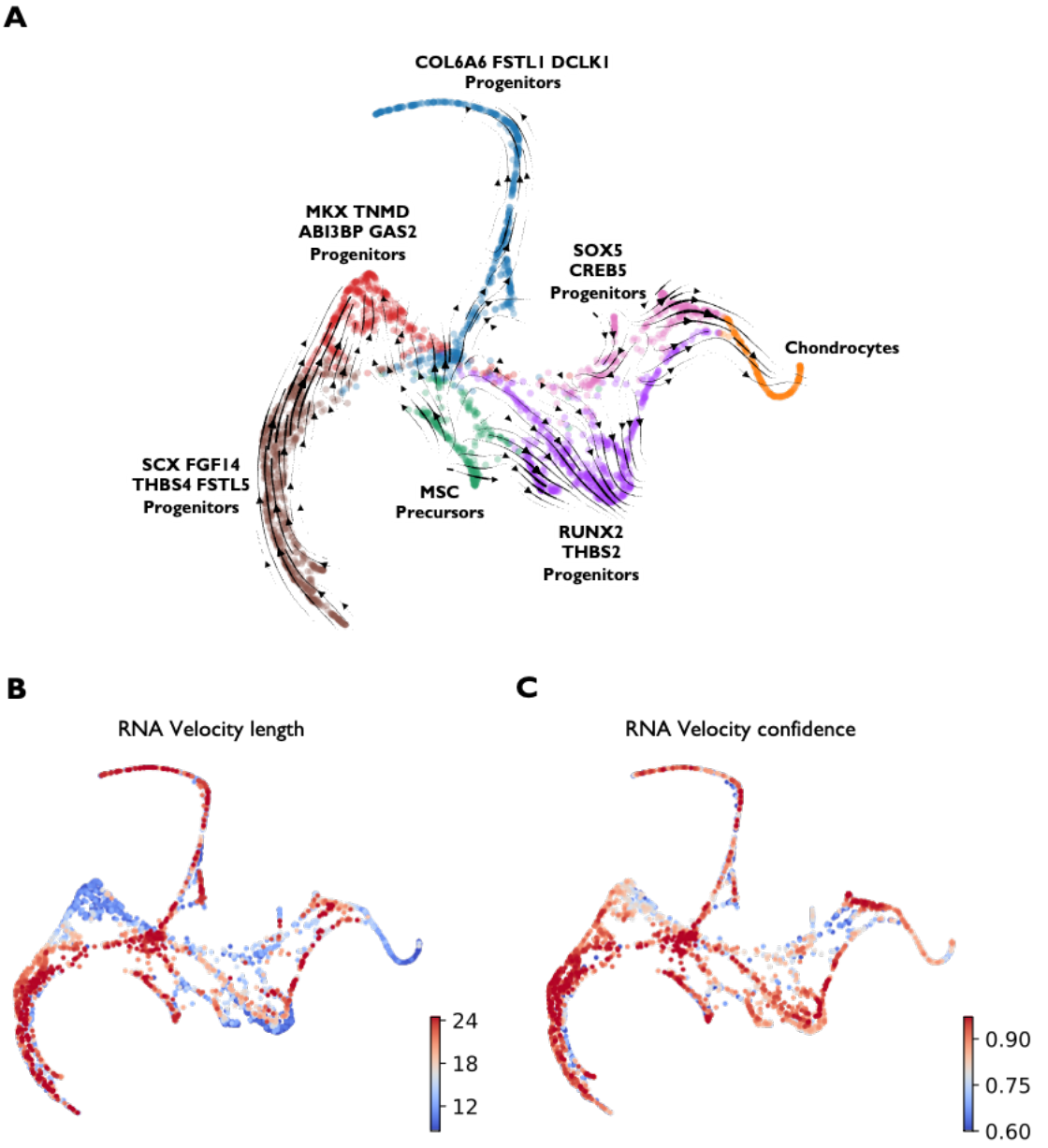


Figure 46. RNA Velocity analysis of embryonic limb tendon cells. *Force-directed layouts derived from t-SNE embeddings calculated with multiscale diffusion component embedding show the lineage relationships among various cell types.* ***(A)*** *Plot of RNA Velocity vectors. The direction and magnitude of the arrows depict the predicted future state of the cells based on the ratio of unspliced to spliced mRNA. The length and curvature of the arrows represent the speed and trajectory of transcriptional changes, respectively.* ***(B)*** *Cells coloured by the speed of transcriptional change; this is inferred from arrow lengths, where longer arrows (red) suggest rapid changes in the cell state.* ***(C)*** *Confidence levels of the velocity vectors, with warmer colours (red to yellow) denoting higher confidence.*

To further investigate the differentiation pathways of embryonic tendon cells, Palantir pseudotime trajectory analysis (Setty *et al*., 2019) was applied. Extreme values of multiscale diffusion components were used to select differentiation initiation and termination cell states, with cells from MSC Precursors chosen as

the former and cells from the Chondrocytes, COL6A6 Progenitors and MKX Progenitors as the latter (Appendix Figure 10). With this, each cell within the dataset was assigned a pseudotime, reflecting its position in the developmental sequence, as well as a branch probability, denoting its likelihood of differentiating into the respective Chondrocyte, LCT, or *SCX*-expressing Tenocyte lineages (Figure 47D).

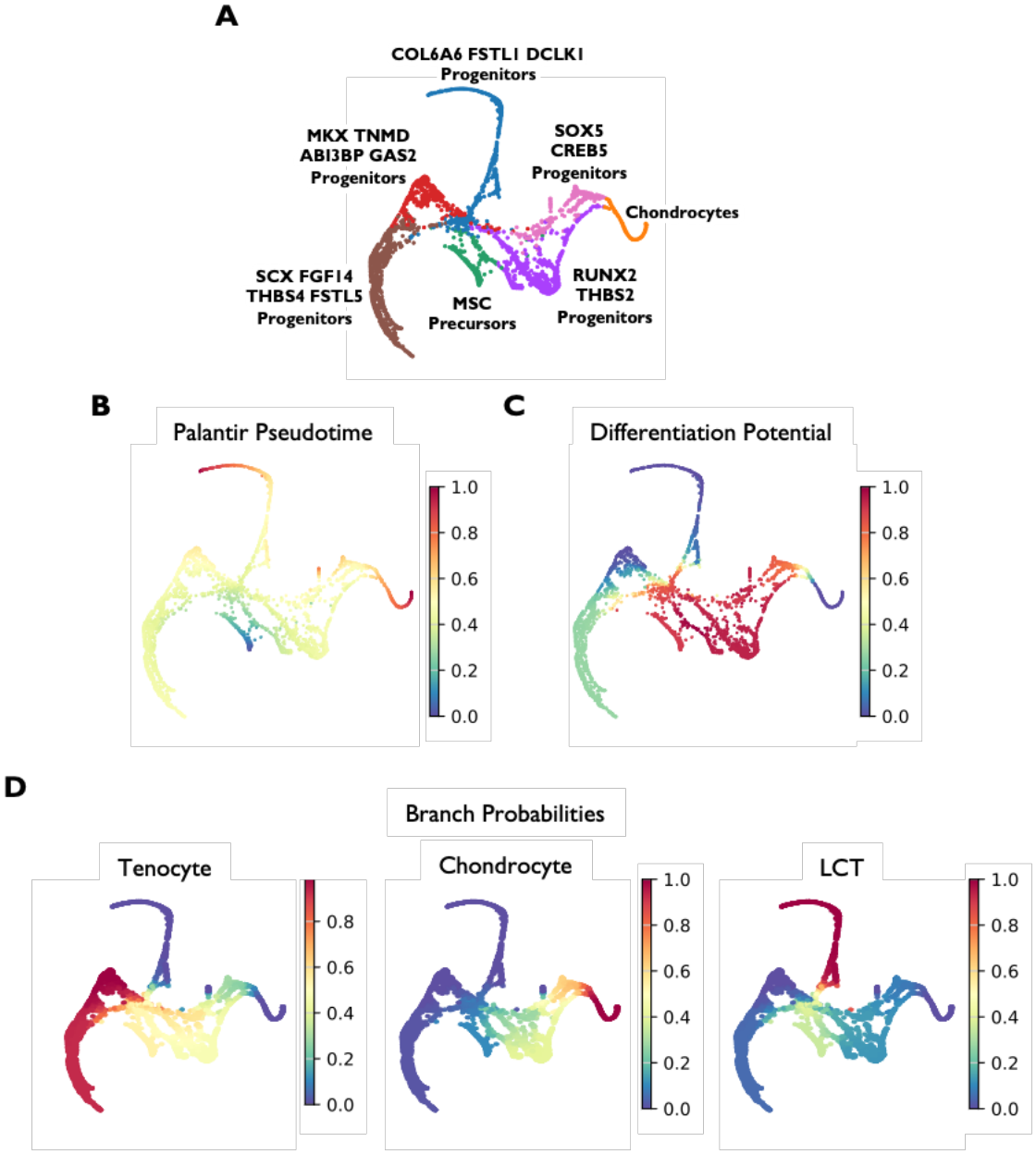


Figure 47. Palantir pseudotime trajectory analysis of human 6.5-9.3 post-conception week embryonic tendon cells. (A) *Force-directed layout derived from t-SNE embeddings with neighbours calculated using multiscale diffusion embeddings, coloured by cell type.* ***(B)*** *Palantir pseudotime analysis showing the progression from the earliest stages of differentiation (blue) to later stages (red).* ***(C)*** *Cells coloured by their differentiation potential, also referred to as entropy; this measure quantifies the degree of uncertainty in the fate decisions of cells as they differentiate. A higher*

entropy value indicates a higher uncertainty or more potential outcomes for a particular cell's fate, while a lower value suggests that cells are more committed to a particular fate with less uncertainty. ***(D)*** *Branch probabilities for three major tendon cell lineages: SCX-expressing tenocytes (left), chondrocytes (middle), and loose connective tissue (LCT, right). Warmer colours indicate higher differentiation probabilities towards a specific state.*

Inspection of branch probabilities in relation to pseudotime revealed distinct differentiation trends for the different lineages (Figure 48). The initiation of commitment to the Chondrocyte lineage occurred relatively early in development, as evidenced by a small rise in branch probabilities at early pseudotime. However, cells destined to become Chondrocytes did not reach a high probability of full commitment to the lineage until later in the differentiation timeline, pointing towards a more protracted and potentially complex differentiation process. In contrast, the *SCX*-expressing Tenocyte lineage demonstrated an earlier and more consistent commitment, with branch probabilities increasing steadily and reaching a plateau relatively quickly. Similarly, cells of the LCT lineage exhibited high branch probabilities from the onset, signifying an immediate and robust commitment to this fate, which was maintained throughout the 6.5-9.3 pcw developmental spectrum (Figure 48).

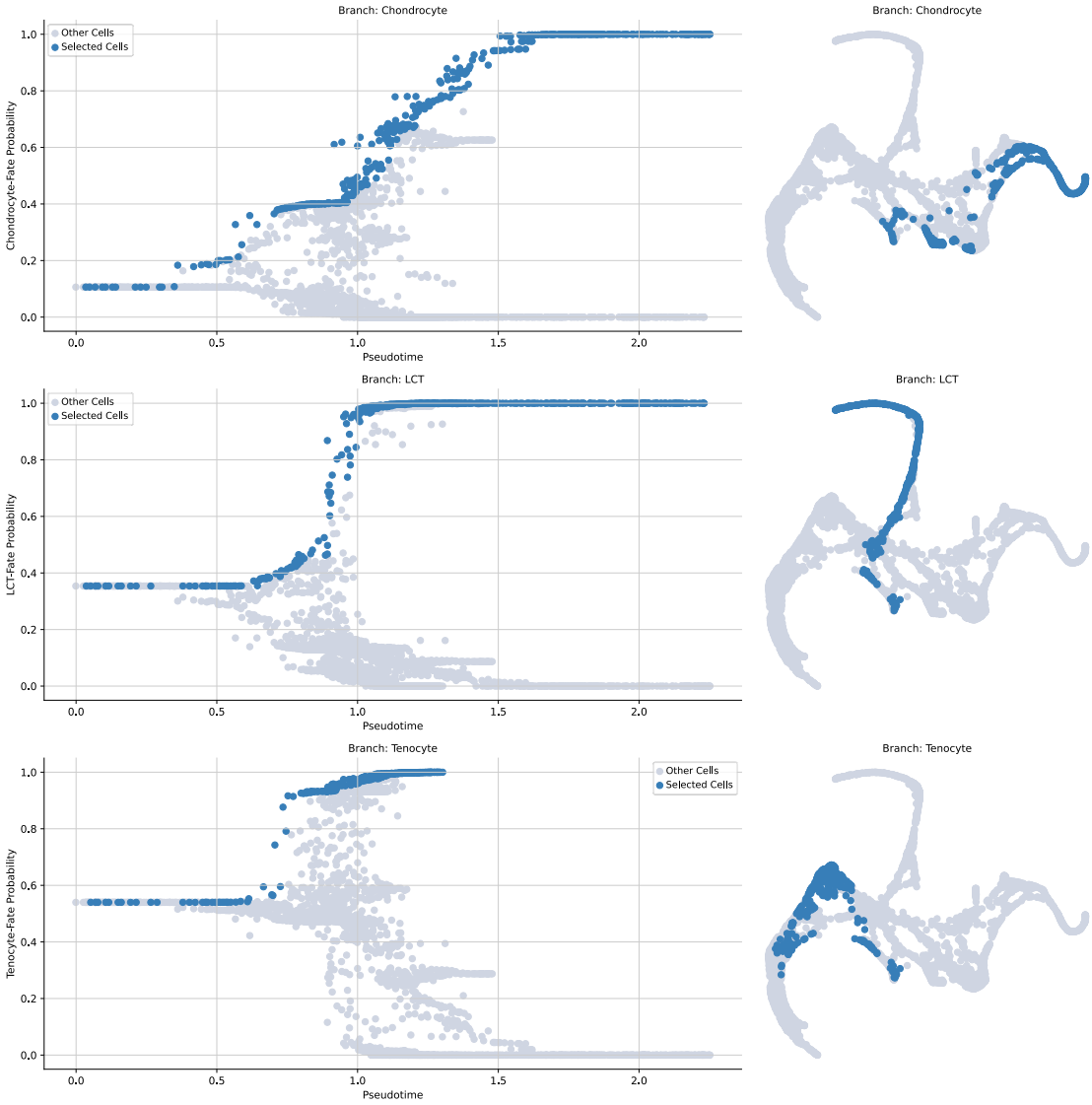


Figure 48. Analysis of differentiation branch probabilities across Palantir pseudotime. *Scatter plots show branch probabilities for Chondrocyte, loose connective tissue (LCT), and scleraxis-expressing Tenocyte lineages across Palantir pseudotime. Dark blue points represent selected cells with a higher likelihood of differentiating into the respective lineage, while light grey points depict other cells in the population. Corresponding force-directed layouts on the right reveal the positioning of cells with high probability for a given lineage.*

Following branch probability analysis, the MAGIC-imputed trends in highly variable gene expression were evaluated across pseudotime. For the Tenocyte lineage, there was a gradual increase in the expression of *SCX* over embryonic development. This was closely followed by *MKX* and *TNMD*, supportive of their roles in tendon development (Figure 49). This pattern was also observed in genes encoding collagen types I, V, VI, X, XI, XII, XIII, XIV, XXI, and various proteoglycans such as *BGN*, *DCN*, *KERA*, *PRG4*, *FMOD, OGN, HSPG2,* and *ASPN* (Figure 49, Appendix Figure 11), highlighting their increasing importance

in early tendon growth and morphogenesis. Additionally, genes involved in cellular adhesion (e.g., *CD44*, *CDH10*), signalling (e.g., *TGFB2, RARB*), and ECM remodelling (e.g., *TLL1*, *FAP*) exhibited consistent rises over pseudotime (Appendix Figure 11). Notably, expression of genes encoding many of the lesser-known collagen types VIII, IX, XV, XXIII, XXIV, XXVI, XXVII, and XXVIII, along with transcription factors *ETV1* and *RUNX3*, the glycoprotein *TNC*, and proteoglycans such as *VCAN, PRELP, HAPLN1, OMD,* and *CHADL,* peaked early and then decreased, suggesting an initial, temporal role in the differentiation of MSC Precursors towards MKX Progenitors (Appendix Figure 11). Furthermore, expressions of *EGR1* and *EGR2*, alongside transcription factors *RUNX1T1* and *PITX1*, collagens *COL22A1*, *COL4A1*, *COL4A2*, and genes impacting cell dynamics like *FGF10*, *SNAI2*, and *CLDN11*, were highest midway through pseudotime, denoting their transient early regulatory roles in cell differentiation and development processes (Appendix Figure 11).

Conversely, the LCT lineage highlighted the progressive upregulation of genes encoding collagens III, IV, V, VI, XII, XXIII, XXVI, XXVII, proteoglycans *LUM*, *HAPLN4*, *DCN*, and *HSPG2*, and cell signalling genes such as *FSTL1, PLAC9,* and *FNDC1* (Figure 49, Appendix Figure 11), pointing towards their requirement for the formation of loose connective tissue. Growth factors *GPC3* and *FGF10* also increased (Figure 49), indicating their participation in LCT cell communication and differentiation. Notably, *FMOD*, *PRELP*, and *CHADL* proteoglycans as well as *HOXA11* and *TNFRSF12A* (known as the TWEAK receptor) genes exhibited dual peaks of expression at early and late differentiation timepoints (Figure 49, Appendix Figure 11). On the other hand, early growth and transcription factors (e.g., *FGF14, FGF9, RUNX3, ETV1, FOXC1, KLF5*), collagens (e.g., types VIII, IX, XI, XIII), cartilage-associated proteoglycans (e.g., *PRG4, ACAN, CHAD, HAPLN1, CHADL*), and other specific ECM remodelling and organisation genes (e.g., *MMP15, MMP9, TNMD, ADAMTS6, TNC*) had high initial expression that diminished as cells progressed towards the LCT fate (Appendix Figure 11). Finally, specific genes involved in transcription regulation (e.g., *THSZ2*), ECM organisation (e.g., *ASPN, OGN, KERA, VCAN*, *ELN*, *COL5A3, COL10A1, COL14A1*), tissue remodelling (e.g., *FHL1*, *FAP*, *SNAI2*), and cell adhesion (e.g., *CD44, CDH2, CDH10*) reached expression peaks mid-pseudotime (Appendix Figure 11).

Comparison of the LCT and Tenocyte lineages revealed both parallels and divergences in the cell differentiation processes. In both lineages, there was clear upregulation of ECM genes, including collagens and proteoglycans, reflecting a shared requirement for those components. Growth factor gene *FGF10* also increased, suggesting a conserved role in cell communication and tissue differentiation of early limb tendon cells. Similarly, transcription factors *RUNX3*, *RUNX2*, *ETV1*, *SOX9*, *FOXC1*, and *KLF5*, along with ECM genes *MMP9* and *TNC*, initially showed high expression that later diminished, suggesting their involvement in early differentiation stages for both lineages. However, Tenocyte lineage cells uniquely displayed increasing expression of tendon markers *SCX*, *MKX*, *TNMD*, *BGN*, and *COMP,* ECM modulator *MMP15*, and growth factor genes *FGF14*, *FGF9*, all of which decreased in LCT lineage cells. In contrast, LCT lineage cells uniquely upregulated *OSR1*, *COL23A1*, *GPC3*, *RUNX1T1*, *MMP11*, and *VCAN*, which were downregulated over pseudotime in Tenocyte lineage cells (Figure 49, Appendix Figure 11).

In the Chondrocyte lineage, a distinct upregulation of transcription factors and ECM markers critical for cartilage development over pseudotime was observed. Key chondrogenic transcription factors, including *EGR1*, *EGR2*, *SOX5*, *SOX6*, *SOX9*, and *RUNX3*, showed increased expression, consistent with their roles in regulating chondrocyte differentiation and cartilage formation (Figure 49, Appendix Figure 11). ECM structural components such as *COL2A1* and *ACAN* were similarly upregulated, aligning with their function in establishing the cartilaginous matrix. Mid-pseudotime upregulation was noted for cell adhesion genes such as *PLAC9*, transcription factors *KLF5* and *FOXC1*, and ECM genes *FHL1*, *BGN*, *KERA*, *COMP*, *TNC*, and *MMP1*, along with the TWEAK receptor *TNFRSF12A*. Finally, transcription factors *RUNX2* and *ETV1* as well as ECM-related genes *FNDC1*, *DCLK1*, *PI16*, *CELF2*, *FSTL1*, *COL1A1*, *COL3A1*, *COL5A1*, *MMP9*, *TNMD*, and *VCAN* were all downregulated over pseudotime (Figure 49, Appendix Figure 11).

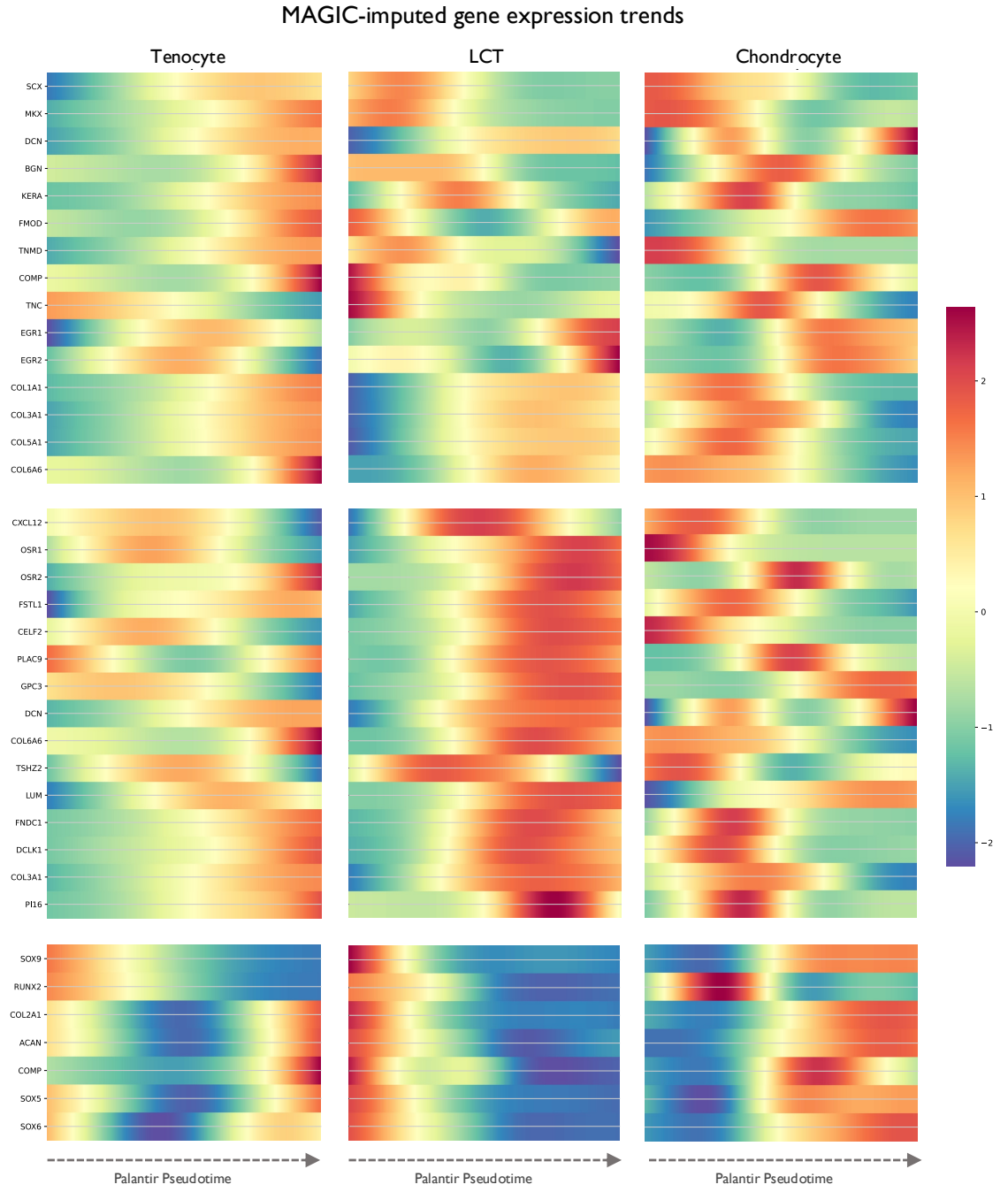


Figure 49. MAGIC-imputed gene expression trends across Palantir pseudotime for the three major embryonic tendon cell lineages. *Heatmaps show the normalised and z-score standardised gene expression levels for key markers of scleraxis-expressing Tenocyte (upper rows), loose connective tissue (LCT) (middle rows), and Chondrocyte (bottom rows) cell lineages across Palantir pseudotime. The expression data has been smoothed using MAGIC (Markov Affinity-based Graph Imputation of Cells) to highlight the dynamic changes in gene expression associated with cell differentiation. The pseudotime axis extends from the 6.5 post-conception week MSC precursor state (left) to the more differentiated states for each given lineage (right).*

To investigate the putative lineages and their drivers more closely, a Palantir pseudotime kernel was initialised using CellRank, with GPCCA (Generalized Perron Cluster Cluster Analysis) applied to estimate transition probabilities

towards the predicted initial and terminal states. The analysis delineated a trajectory from MSC Precursors to MKX Progenitors via an intermediate SCX Progenitor stage, consistent with the recognised stages of early tenocyte differentiation (Figure 50B). A similar progression was observed for Chondrocyte lineage development, with cells transitioning through RUNX2 Progenitors and subsequently SOX5 Progenitors before culminating in the terminal embryonic Chondrocyte state. Visualisation of fate probabilities across donor ages corroborated these trajectories, depicting a shift from younger, less differentiated cells to older, more defined states.

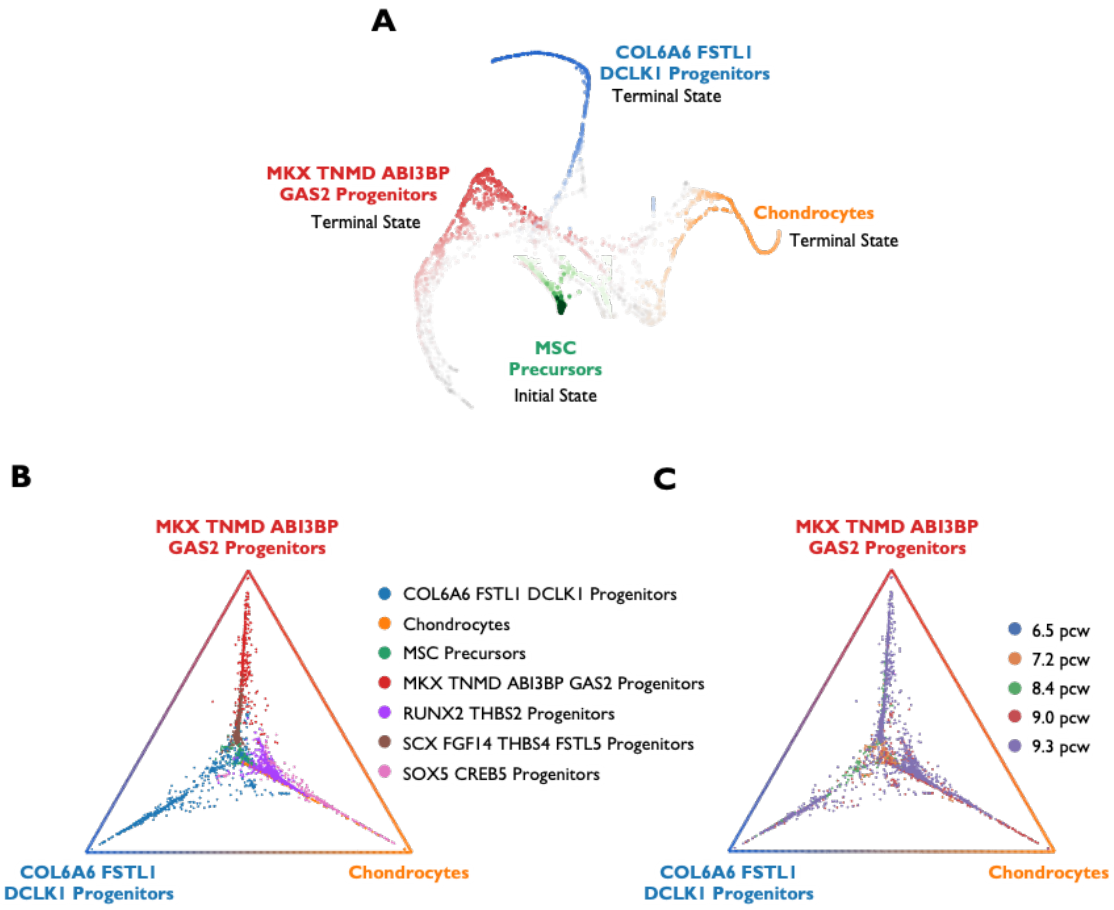


Figure 50. CellRank fate mapping of embryonic tendon cell differentiation. (A) *Force-directed graph showing the location of manually selected cells corresponding to the initial and terminal states.* ***(B,C)*** *Circular projections of fate probabilities coloured by* ***(B)*** *cell states or* ***(C)*** *donor ages in weeks post-conception (pcw) showing the trajectory and density of cells transitioning from initial MSC Precursors in the middle towards the specified terminal fates.*

The analysis of lineage-specific gene drivers revealed that many genes were significantly anti-correlated with the differentiation of alternative lineages (Figure 51), implying a role in preserving the distinct identity of their respective terminal

lineages. For instance, in the Tenocyte lineage, genes such as *SCX*, *MKX*, *TNMD*, *ABI3BP*, and *GAS2* were strongly negatively correlated with markers indicative of the LCT and chondrogenic lineages. Conversely, genes like *TWIST2*, *DCLK1*, and *CELF2* showed robust anti-correlations with tenogenic markers, implying their part in maintaining LCT identity by potentially inhibiting tenocyte differentiation pathways. The anti-correlation between LCT and Chondrogenic lineages was less pronounced, highlighting a likely closer relationship between these lineages. Notably, the anti-correlated genes for the LCT lineage displayed specificity, with genes like *LUM* and *GPC3* being anti-correlated with the Tenocyte lineage but not with the Chondrocyte one.

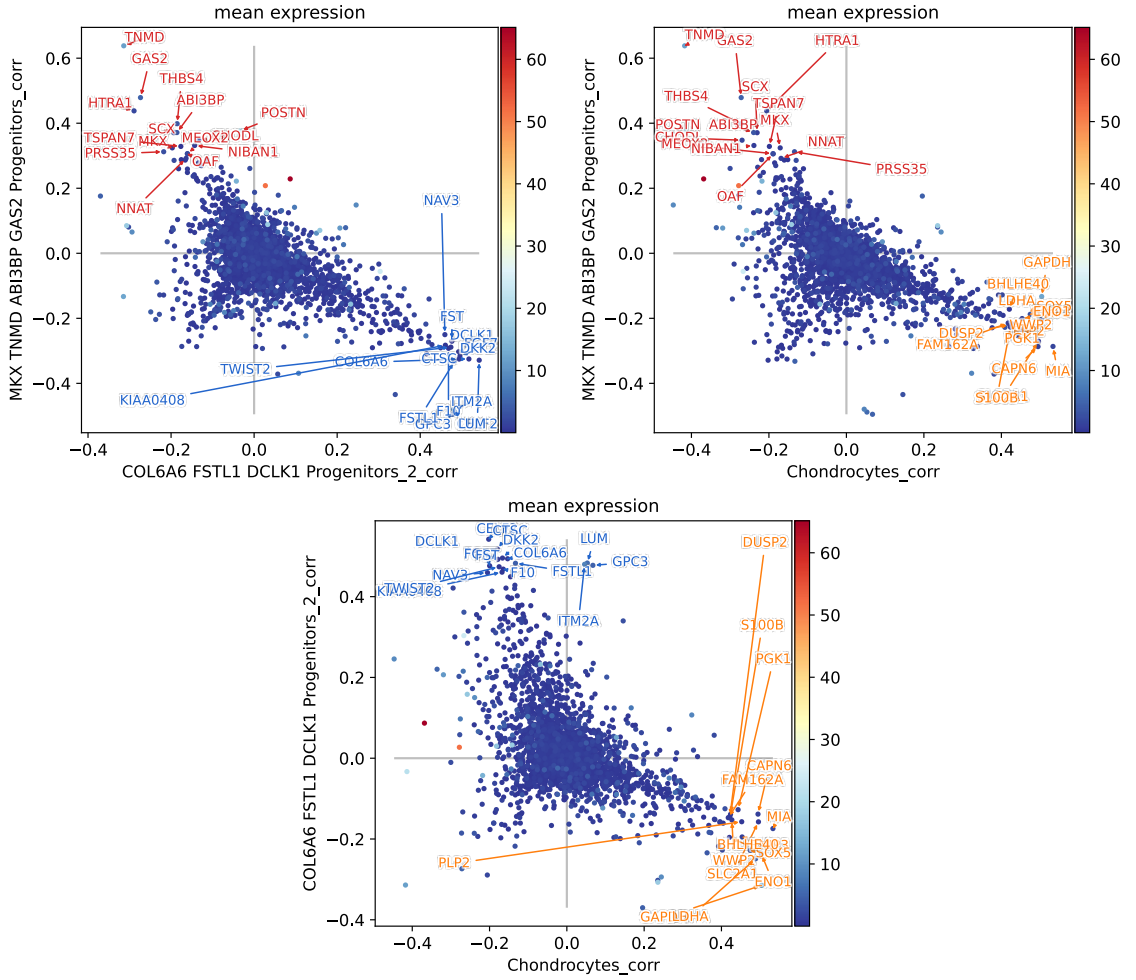


Figure 51. Gene expression correlation of CellRank lineage drivers. *X and y axes represent terminal tendon cell lineages derived from human 6.5-9.3 post-conception week embryonic limb MSC Precursor cell differentiation. The expression levels of putative lineage driver genes identified by CellRank are plotted against their correlation to the terminal state of differentiation for each lineage. Genes positioned further from the origin on the x and y axes are more strongly correlated with the terminal state. Top 15 lineage driver genes are annotated for each terminal state.*

The analysis of lineage fate probabilities revealed that most cell states preserved a degree of multipotency, retaining the potential to transition towards other cell fates even at later stages of differentiation (Figure 52). Notably, the *SCX*-expressing Tenocyte lineage cells, particularly the more differentiated MKX Progenitors, showed a higher degree of lineage commitment probabilities, with approximately 80% of these cells remaining unlikely to transition to other states. Similarly, the more immature SCX Progenitors showed a 58% probability of commitment to their lineage. In comparison, the more differentiated COL6A6 Progenitors and Chondrocytes displayed lower commitment levels of about 60% and 40%, respectively. Overall, these findings suggested an earlier and more definitive commitment within the tenocyte lineage compared to other lineages, which retained greater potential for fate transitions.

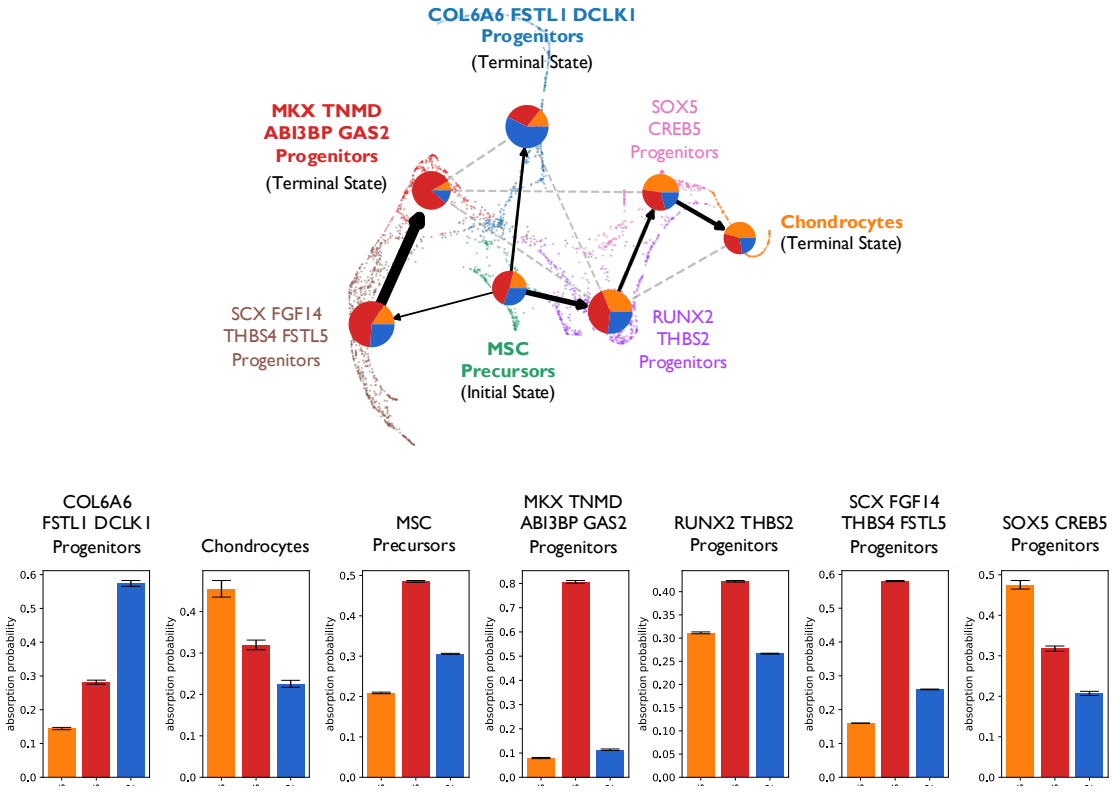


Figure 52. CellRank directed partition-based graph abstraction (PAGA) map of embryonic tendon cell fate probabilities. *Force-directed graph overlaid by directed PAGA shows probabilistic transitions from the initial state of MSC Precursors at 6.5 post-conception weeks towards the three set terminal states. Arrows represent directed transitions from one cell type to another, with thicker arrows indicating a higher probability of cells transitioning. Dashed lines indicate weaker, less probable transitions. Pie charts at each cell type node represent the proportions of cells of that type likely to transition towards chondrocyte (orange), tenocyte (red), or loose connective tissue (blue) fates. Accompanying bar graphs quantify those transition (i.e., absorption) probabilities.*

5.3.4 Probabilistic modelling of tendon cell fates in embryonic and foetal development

The integration of embryonic scRNA-seq and foetal snRNA-seq data presents a unique set of challenges, particularly when conducting trajectory analysis. One primary limitation arises from the technical differences between these methodologies. scRNA-seq, which analyses the transcriptome of whole cells, and snRNA-seq, which focuses on nuclei, often yield data with differing levels of sensitivity and transcript coverage. This discrepancy can lead to variations in the detection of gene expression levels and the identification of transcriptionally distinct cell states. Given that trajectory analysis methods assume a continuous and comprehensive sampling of cell states, these variations are likely to distort the outcomes.

This challenge was recently tackled by Qiu and collagues (2022, 2024) who reconstructed developmental trajectories of mouse embryogenesis using embryonic scRNA-seq and foetal snRNA-seq datasets. They encountered integration difficulties at the E8.5 (scRNA-seq) and E9.5 (snRNA-seq) connecting timepoints, which they overcame by generating additional E8.5 timepoint snRNA-seq data, thus enabling a more seamless integration. Unfortunately, this study could not be extended to carry out additional snRNA-seq of late embryonic tendons. Consequently, as anticipated, there were challenges in integration of data from the disparate developmental stages (9.3 pcw scRNA-seq and 12 pcw snRNA-seq). This was evidenced by 1) the persistent segregation of datasets when using Harmony, BBKNN, or scGen integration approaches, or 2) a loss of biological signal with methods such as Seurat's CCA and rPCA (not shown). The developmental gap between those stages of rapid development was sufficient to obscure intermediate cellular states, complicating the reconstruction of potential trajectories (Figure 53).

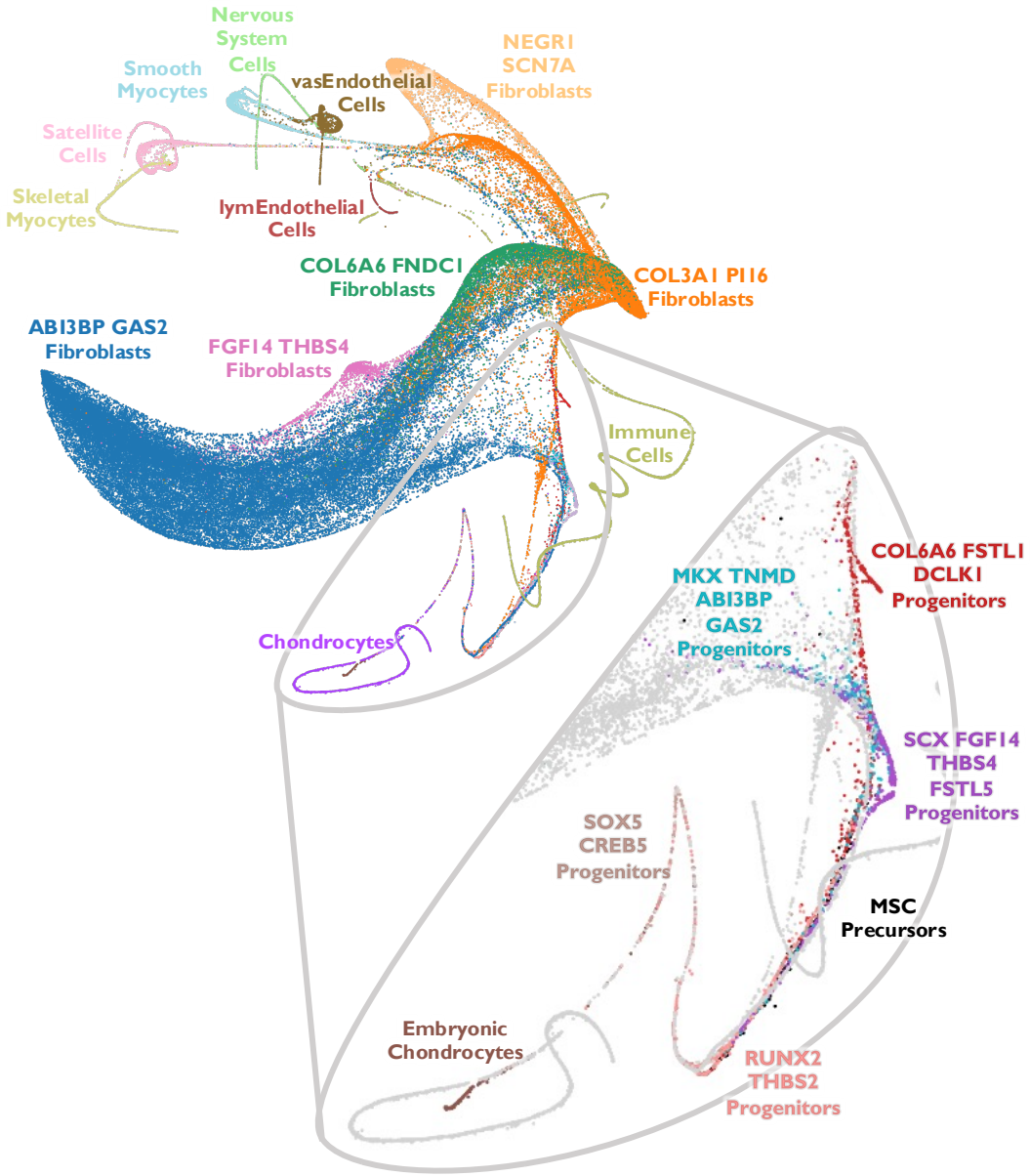


Figure 53. Force-directed layout of scGen-integrated embryonic single-cell RNA-seq and foetal single-nucleus RNA-seq datasets. *The inset shows embryonic tendon data, which remains largely segregated from the broader data, reflecting substantial transcriptional disparities that could potentially be attributed to the significant age gap (6-9 post-conception weeks (pcw) vs 12-20 pcw) as well as the inherent differences between the sequencing technologies.*

In search for solutions, I came across the Klein *et al*. (2023) preprint that cleverly applied optimal transport theory to accurately reconstruct developmental trajectories within the aforementioned mouse embryonic dataset. Their probabilistic and scalable method, named multi-omics single-cell optimal transport (moscot), was designed to deal with multi-modal unpaired data and could be applied directly to batch-corrected latent space embeddings, making it particularly suitable for this analysis.

Following data integration with scGen and correction for different experimental batches, the data were subset to exclude immune cells as they appeared disconnected from the rest of the data. Supporting Palantir's previous findings, moscot revealed early MSC Precursor differentiation into the SCX and COL6A6 Progenitors (6.5-8.4 pcw), with later differentiation into the RUNX2 and SOX5 Progenitors (8.4-9.0 pcw) (Figure 54A). As suspected, SCX Progenitors were seen to contribute to the FGF14 THBS4 and ABI3BP GAS2 Fibroblasts from 9.3 to 12 pcw, while more differentiated MKX Progenitors contributed only to the foetal ABI3BP GAS2 Fibroblast populations (Figure 54B; Appendix Figure 12). Finally, COL6A6 Progenitors contributed to the foetal COL3A1 PI16, COL6A6 FNDC1, and NEGR1 SCN7A Fibroblasts (Figure 54B; Appendix Figure 12).

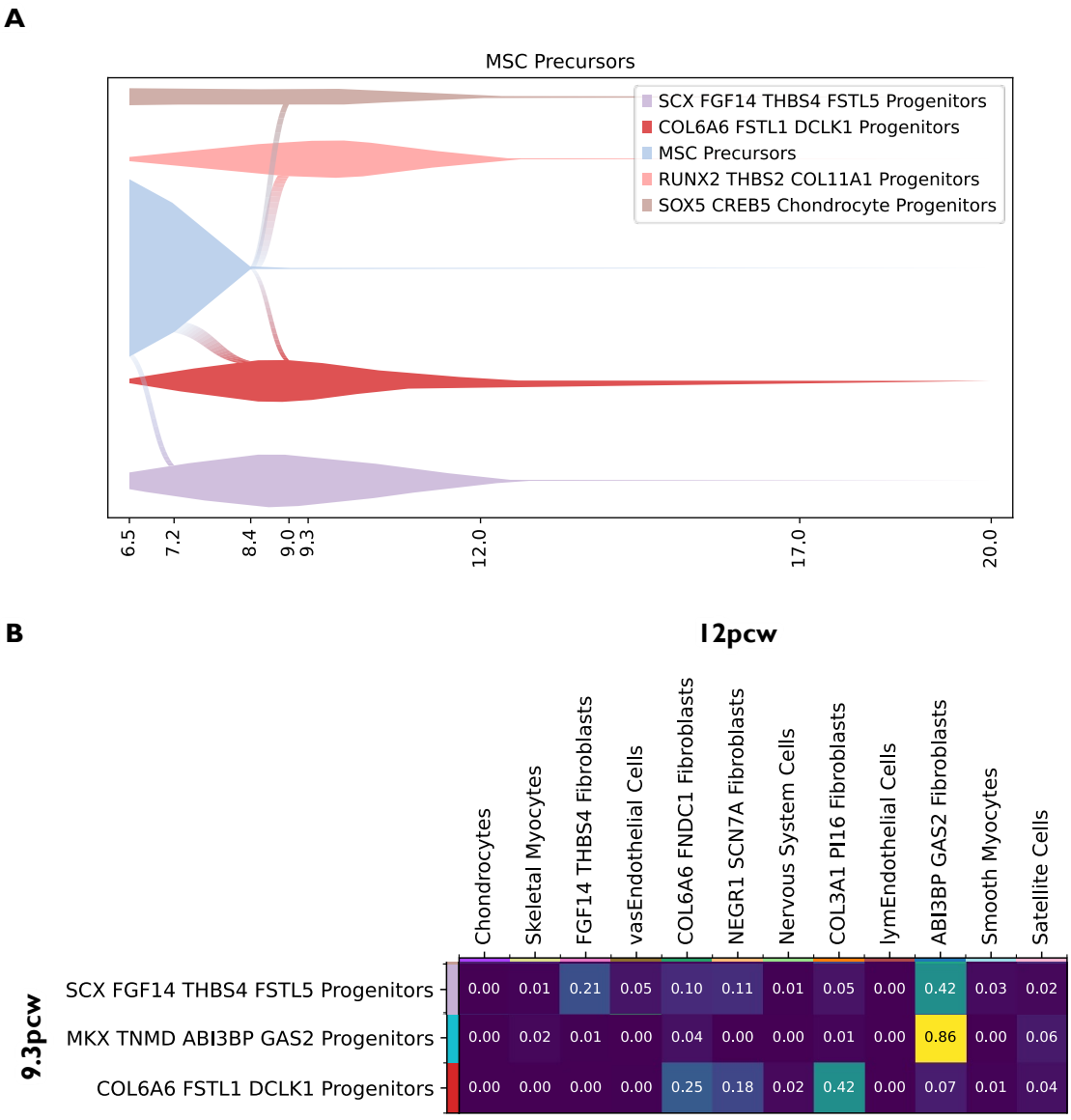


Figure 54. Moscot-CellRank analysis of human embryonic and foetal tendon cell transitions. ***(A)*** *CellRank plot shows the probability mass flow originating from the mesenchymal stem cell (MSC) precursor population into other cell types across different developmental ages.* ***(B)*** *Moscot transition matrix plot shows the descendants of the 9.2 post-conception week (pcw) fibroblast-lineage progenitor populations within 12 pcw foetal samples analysed in the previous chapter. The values represent the proportion of cells transitioning from the progenitor population to various differentiated cell types.*

The data were subset to fibroblast-lineage cells, and CellRank moscot-based experimental time kernel was initiated to estimate the average fate probabilities for cells transitioning from embryonic to foetal states. The SCX, MKX, and COL6A6 Precursors at 7.2 and 8.4 pcw were manually set as the initial states. The 7 most stable predicted macrostates were analysed, and 4 of those

corresponding to the major foetal cell types were selected as the likely terminal states (Figure 55).

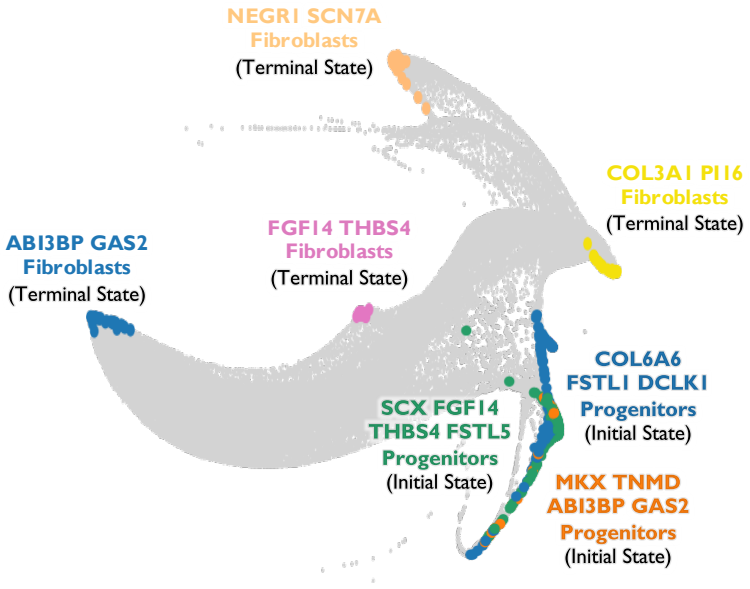


Figure 55. Force-directed layout illustrating selected developmental tendon initial and terminal state cells used in CellRank-Moscot analysis. *The layout positions cells based on their transcriptional similarities, where closer proximity indicates greater similarity in gene expression profiles. Manually selected cells from the embryonic initial states are annotated to highlight their role as precursors in the differentiation trajectory, while those representing foetal terminal states were predicted by the CellRank algorithm and indicate more mature cell types within the tendon.*

Cell fate clustering revealed similarities between the FGF14 and ABI3BP as well as NEGR1 and COL3A1 differentiation lineages (Figure 56A). However, the ABI3BP lineage stood out as the average calculated fate probabilities indicated high potential for any of the selected cell types in transitioning towards its terminal states, with about 57% of the MKX Progenitors, 52% of SCX Progenitors, and 49% of COL6A6 Progenitors being likely to commit to this lineage (Figure 56A). Conversely, other lineages showed a wider distribution of fate probabilities, indicating less definitive differentiation preferences (Figure 56A,B). Among these, COL6A6 Progenitors were predominantly inclined to differentiate into COL3A1 PI16 Fibroblasts, whereas SCX Progenitors showed a higher propensity for transitioning into FGF14 THBS4 Fibroblasts (Figure 56A,B).

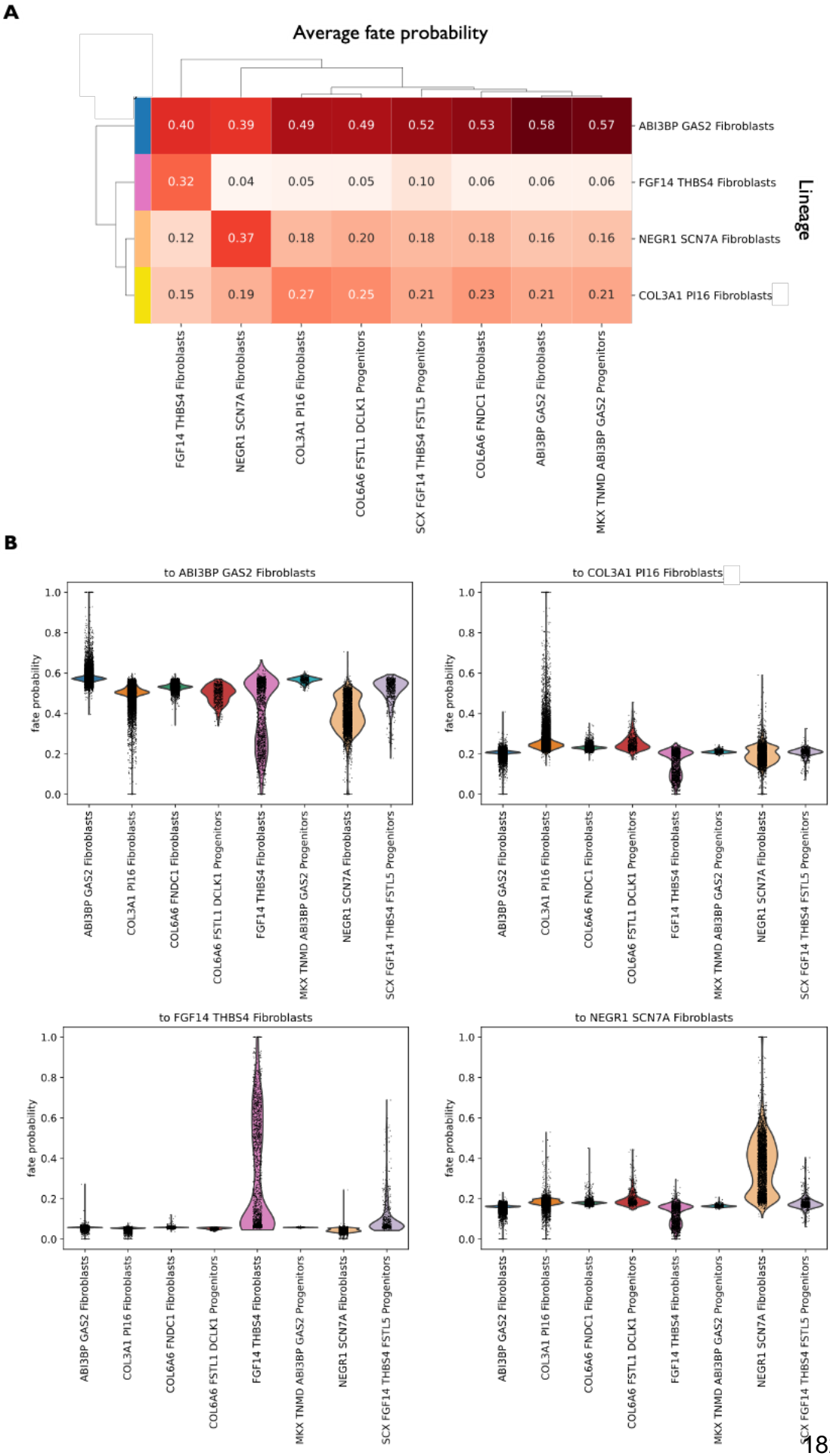
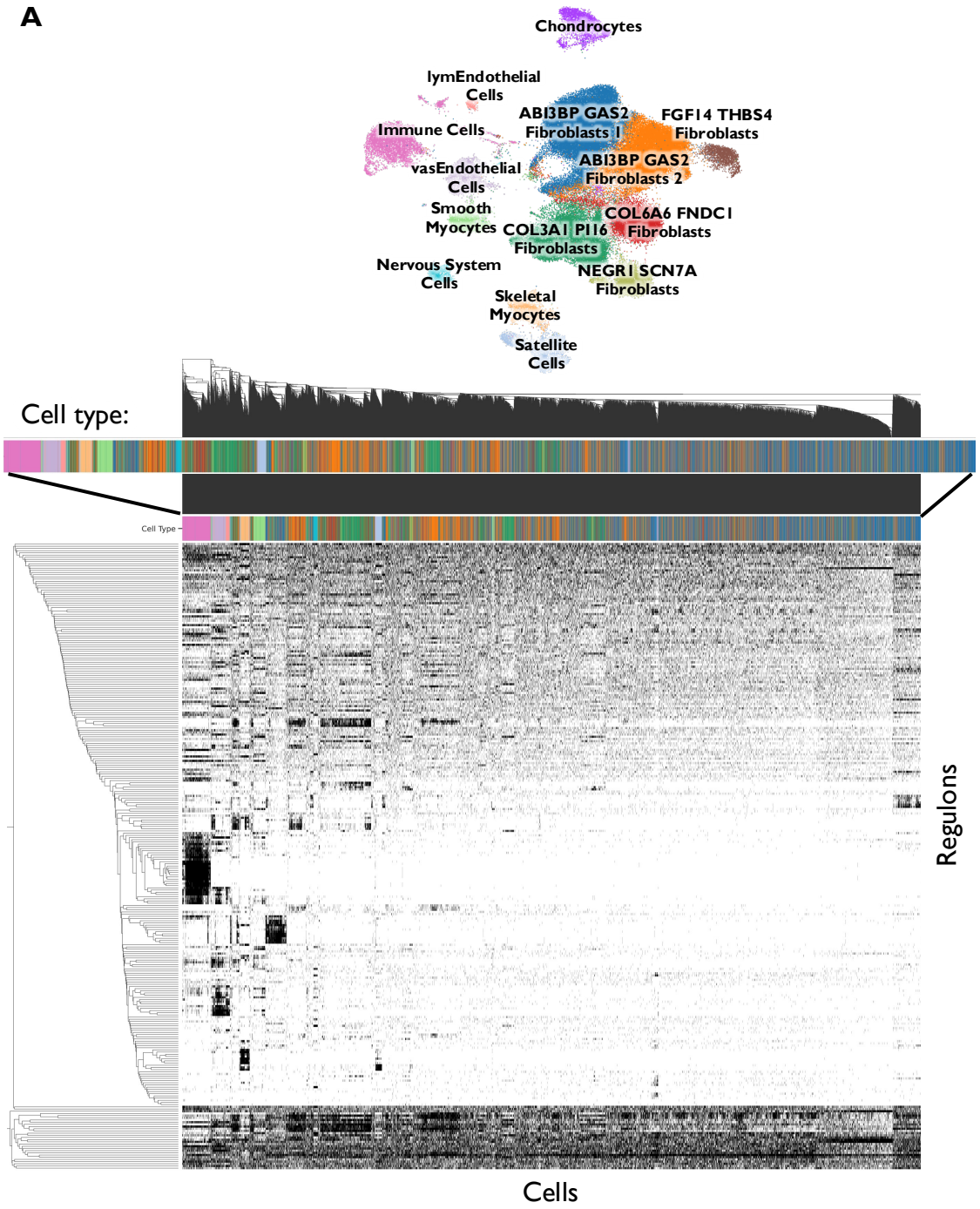

A
Average fate probability
0.40 0.39 0.49 0.49 0.52 0.53 0.58 0.57
0.32 0.04 0.05 0.05 0.10 0.06 0.06 0.06
0.12 0.37 0.18 0.20 0.18 0.18 0.16 0.16
0.15 0.19 0.27 0.25 0.21 0.23 0.21 0.21
ABI3BP GAS2 Fibroblasts
FGF14 THBS4 Fibroblasts
NEGR1 SCN7A Fibroblasts
COL3A1 PI16 Fibroblasts
Lineage
FGF14 THBS4 Fibroblasts
NEGR1 SCN7A Fibroblasts
COL3A1 PI16 Fibroblasts
COL6A6 FSTL1 DCLK1 Progenitors
SCX FGF14 THBS4 FSTL5 Progenitors
COL6A6 FNDC1 Fibroblasts
ABI3BP GAS2 Fibroblasts
MKX TNMD ABI3BP GAS2 Progenitors
B
to ABI3BP GAS2 Fibroblasts
to COL3A1 PI16 Fibroblasts
to FGF14 THBS4 Fibroblasts
to NEGR1 SCN7A Fibroblasts
fate probability
0.0
0.2
0.4
0.6
0.8
1.0
ABI3BP GAS2 Fibroblasts
COL3A1 PI16 Fibroblasts
COL6A6 FNDC1 Fibroblasts
COL6A6 FSTL1 DCLK1 Progenitors
FGF14 THBS4 Fibroblasts
MKX TNMD ABI3BP GAS2 Progenitors
NEGR1 SCN7A Fibroblasts
SCX FGF14 THBS4 FSTL5 Progenitors

Figure 56. CellRank cell fate probability distributions for embryonic and foetal tendon fibroblast lineages. (A) *Clustered heatmap showing the average fate probabilities of various embryonic progenitor and foetal fibroblast cells (x-axis) transitioning towards four major fibroblast lineages (y-axis). The lineages are clustered based on the similarity of fate probabilities.* ***(B)*** *Violin plots showing the distribution of individual cell fate probabilities for each lineage.*

The overall variability in differentiation probabilities of the fibroblast-lineage progenitor cells and more differentiated fibroblasts prompted an investigation of the gene regulatory networks underlying these and other tendon cells using SCENIC (Single-Cell Regulatory Network Inference and Clustering). Indeed, the regulon-based clustering of 20 pcw foetal cell types revealed a lack of definitive fibroblast-specific regulators (Figure 57A), suggesting a high degree of transcriptional heterogeneity within those populations. This could indicate that fibroblasts at this developmental stage are more transcriptionally plastic, exhibiting a broad range of regulatory states. This plasticity might reflect the fibroblasts' diverse origins and their ability to differentiate into multiple lineages, aligning with the earlier observed varied differentiation potentials. The lack of distinct regulon-based clustering could also imply that multiple overlapping regulatory networks govern their identity and function, rather than a few dominant pathways. In contrast, regulon-based clustering was pronounced for all non-fibroblast cells, including myocytes, endothelial cells, and immune cells (Figure 57A,B), suggesting more stable and defined regulatory states at this stage of development. Taken together, the results suggest that while 20 pcw foetal fibroblasts exhibit a complex and varied regulatory landscape, non-fibroblast cells maintain a more conserved and stable gene regulatory architecture, highlighting the distinct biological roles and developmental stages of these cell types within the foetal environment.


A
Chondrocytes
lymEndothelial Cells
ABI3BP GAS2 Fibroblasts 1
FGF14 THBS4 Fibroblasts
Immune Cells
ABI3BP GAS2 Fibroblasts 2
vasEndothelial Cells
Smooth Myocytes
COL6A6 FNDC1 Fibroblasts
COL3A1 PI16 Fibroblasts
Nervous System Cells
NEGR1 SCN7A Fibroblasts
Skeletal Myocytes
Satellite Cells
Cell type:
Cell Type
Regulons
Cells

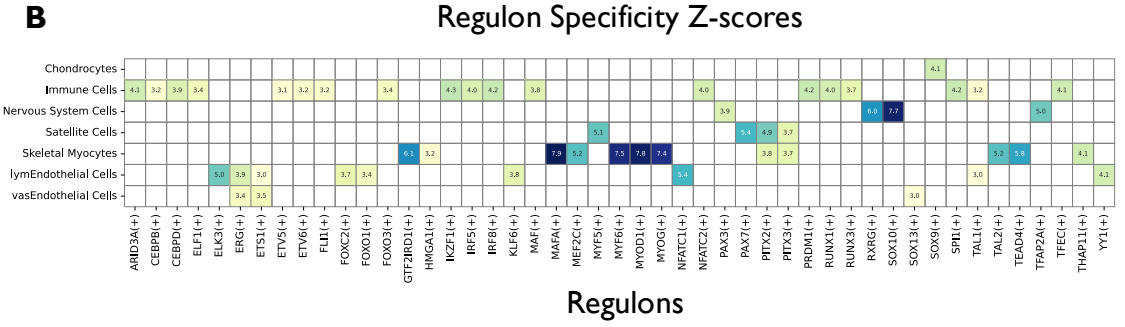

B
Regulon Specificity Z-scores
Chondrocytes
Immune Cells
Nervous System Cells
Satellite Cells
Skeletal Myocytes
lymEndothelial Cells
vasEndothelial Cells
ARID3A(+)
CEBPB(+)
CEBPD(+)
ELF1(+)
ELK3(+)
ERG(+)
ETS1(+)
ETV5(+)
ETV6(+)
FLI1(+)
FOXC2(+)
FOXO1(+)
FOXO3(+)
GTF2IRD1(+)
HMGA1(+)
IKZF1(+)
IRF5(+)
IRF8(+)
KLF6(+)
MAF(+)
MAFA(+)
MEF2C(+)
MYF5(+)
MYF6(+)
MYOD1(+)
MYOG(+)
NFATC1(+)
NFATC2(+)
PAX3(+)
PAX7(+)
PITX2(+)
PITX3(+)
PRDM1(+)
RUNX1(+)
RUNX3(+)
RXRG(+)
SOX10(+)
SOX13(+)
SOX9(+)
SPI1(+)
TAL1(+)
TAL2(+)
TEAD4(+)
TFAP2A(+)
TFEC(+)
THAP11(+)
YY1(+)
Regulons

Figure 57. SCENIC analysis of cell type-specific regulon activity. (A) *Clustermap showing regulon-based clustering in 20 post-conception week (pcw) foetal Achilles and quadriceps tendon cell types. Each row represents a regulon, and each column corresponds to an individual cell. Cell types are indicated by colours in the top bar, synchronised with the UMAP visualisation.* ***(B)*** *Z-score plot illustrating highly activated (>3.0 score) regulons for all 20 pcw foetal Achilles and quadriceps tendon cell types. Z-scores were calculated by standardising the activity of each regulon across cells and quantifying how many standard deviations a particular cell's regulon activity deviated from the mean across all cells. Colour intensity reflects the magnitude of Z-scores, with darker colours indicating higher scores.*

5.4 Discussion

This chapter examines tendon development from embryonic to foetal stages using human 6-9 pcw embryonic limb single-cell and spatial RNA-sequencing data obtained by the Teichmann group (B. Zhang *et al*., 2023). Using an unconventional approach, a random forest classifier was applied to transfer label information from spatially resolved transcriptomic profiles of 8 pcw patellar and quadriceps tendons back to the whole embryonic limb scRNA-seq data, effectively distinguishing tendon from non-tendon cell populations based on their matched spatial gene expression profiles. This led to the identification of seven distinct 6-9 pcw embryonic tendon cell types, ranging from early multipotent progenitors to more lineage-committed states. Subsequent trajectory analysis revealed the lineage pathways and transcriptional regulators guiding these cell types toward distinct lineages, while advanced probabilistic modelling on integrated embryonic single-cell and foetal single-nucleus RNA-seq data mapped the progression of these cell lineages into the foetal stages. Finally, SCENIC analysis of the regulatory networks underlying these transitions in 20 pcw tendon cell types clarified the resulting fate probabilities, demonstrating significant transcriptional plasticity within 3rd trimester foetal fibroblast populations.

5.4.1 Embryonic tendon cell types and developmental trajectories

The earliest identified cells at 6.5 and 7.2 pcw, termed MSC Precursors, displayed a diverse gene expression profile indicative of a variety of embryonic tissues. These cells featured high levels of early developmental transcription factors such as *SOX4, FOXP2, RUNX1T1, HMGA2, SIX1*, along with genes involved in cell structure, adhesion, stress response, and metabolic processes.

Notably, HMGA2, a chromatin architectural protein known for its role in maintaining cell stemness and directing mesenchymal differentiation (reviewed in Parisi *et al.*, 2020), is highly expressed in human embryonic stem cells (Li *et al*., 2006) and has been recognised as a key driver of non-myogenic connective tissue fates in mice, along with FOXP2 and RUNX1T1 (Grimaldi *et al*., 2022). Indeed, *RUNX1T1* is expressed in mouse limb mesenchyme and subsequent cartilaginous condensations at E10.5-12.5 (Yamamoto *et al*., 2019). Conversely, SIX1 has been implicated in muscle development (Wu *et al*., 2014) as a key driver of myogenic fates (Grimaldi *et al*., 2022), with its expression localised to cartilaginous and myocyte regions adjacent to or slightly overlapping with *Scx*$^{+}$ primordial tendons in embryonic mouse and chick limbs (Bonnin *et al*., 2005). This expression profile, coupled with the absence of *SCX* and definitive MSC markers, suggests a multipotent cellular identity primed for various differentiation pathways. Therefore, these precursors, perhaps better termed Connective Tissue Stem Cells, may serve foundational roles not only in tendon development, but also in broader limb morphogenesis. RNA velocity and pseudotime trajectory analyses further corroborate this, revealing the propensity of these precursors to transition towards cartilage, tendon, and tendon connective tissue fates.

In fact, the transition to the cartilage lineage cells begins early in pseudotime, initially through the intermediary RUNX2 THBS2 Progenitors first observed at 7.2 pcw (Appendix Figure 8). These progenitors bridge the gap between MSC Precursors and more differentiated states, exhibiting similarities with MSC Precursors while possessing a transcriptomic profile indicative of dual differentiation potential towards osteogenic and chondrogenic fates. As development progresses, the pathway narrows with a shift towards SOX5 CREB5 Progenitors at the same developmental stage, which focus more explicitly on chondrogenesis. In these progenitors, the concerted action of SOX5, SOX6, and SOX9 regulates key chondrocyte-specific genes (e.g., *ACAN*, *COL2A1*) essential for early differentiation during embryonic connective tissue chondrogenesis (Dy *et al*., 2010; Lefebvre *et al*., 2001; Ng *et al*., 1997; Zhao *et al*., 1997). Additionally, CREB5 enhances chondrogenic specialisation by modulating TGF-β and EGFR pathways critical for PRG4 expression, which in turn provides essential lubrication and structural support at tendon entheses

(Rees *et al*., 2002; C.-H. Zhang *et al*., 2021; Zhang *et al*., 2022). As these progenitors differentiate into embryonic Chondrocytes observed from 9.0 pcw, their expression of cartilage-specific genes intensifies and begins to include specific genes such as matrilins 1, 3, and 4. The trajectory then continues into the foetal period, where these cells mature into foetal Chondrocytes.

During this transition from MSC Precursors to embryonic Chondrocytes, key transcription factors such as *EGR1, EGR2, SOX5, SOX6, SOX9*, and *RUNX3* increase in expression, aligning with their vital roles in chondrocyte differentiation and cartilage formation (Akiyama *et al*., 2005; Dy *et al*., 2010; Lefebvre *et al*., 2001; Yoshida *et al*., 2004). In particular, EGR1 and EGR2, known for their involvement in embryonic chick and mouse tendon development, regulate the expression of SCX and collagens I, III, V, XII and XIV (Lejard *et al*., 2011), suggesting their potential role in forming the tendon-to-bone attachment unit. Meanwhile, early chondrogenic driver *RUNX2* and ECM-related genes characteristic of tendon and its loose connective tissue lineages (e.g., *FNDC1*, *DCLK1*, *PI16, FSTL5, TNMD, VCAN*, *COL1A1, COL3A1, COL5A1*) show decreased expression. Indeed, analysis of lineage drivers reveals significant anti-correlations between Chondrocyte-specific genes and those of other MSC Precursor lineages, supporting the tightly regulated nature of chondrocyte developmental pathways that promote essential chondrogenic genes while inhibiting those that could divert cells to non-chondrogenic lineages.

Compared to the chondrogenic lineage, the differentiation of MSC Precursors towards *SCX*-expressing MKX TNMD ABI3BP GAS2 Progenitors or putative *SCX*-negative loose connective tissue COL6A6 FSTL1 DCLK1 Progenitors occurs relatively quickly. This differentiation likely progresses through an intermediate SCX FGF14 THBS4 FSTL5 Progenitor state emerging around 7.2 pcw (Appendix Figure 8). These progenitors are marked by high expression of *SCX*, a key regulator of tenogenic development, and exhibit relatively lower levels of downstream genes such as *MKX* and *TNMD*, indicating a nascent differentiation state (Anderson *et al*., 2006; Ito *et al*., 2010; Liu *et al*., 2010; Schweitzer *et al*., 2001; Shukunami *et al*., 2018, 2006). They also express substantial levels of ECM components (e.g., *KERA*, *POSTN*, *DCN, OGN*, and collagens I, III, V, VI, XII, XIV) essential for initial tendon matrix assembly and

stabilisation, alongside basement membrane- and MTJ-specific collagens (*COL18A1, COL4A1, COL4A2* and *COL22A1*, respectively), suggesting their role in structural interface establishment within the developing musculoskeletal system (Charvet *et al*., 2013; Kague *et al*., 2010; Koch *et al*., 2004; Pöschl *et al*., 2004). While basement membrane collagens contribute to cellular filtration and structural scaffolding required for compartmentalisation and stability (Kague *et al*., 2010; Pöschl *et al*., 2004), COL22A1 is vital for anchoring muscle fibres to tendons (Charvet *et al*., 2013; Koch *et al*., 2004), illustrating the functional integration of these progenitors with adjacent tissues during early development.

As these cells advance to more differentiated tendon cells around 8.4 pcw, marked by the emergence of MKX Progenitors, there is a notable shift in gene expression. This includes an increased expression of the abovementioned tendon matrix genes (and other important components including *FMOD*, *BGN* and *ASPN)* as well as a reduction in basement membrane and MTJ collagens, alongside early development transcription factors such as *EGR1*, *EGR2*, *RUNX1T1*, *PITX1*, and *TSHZ2*. Concurrently, there is an upregulation of the LOX enzyme, indicative of enhanced collagen crosslinking and ECM organisation, reflecting their progression towards specialised tendon functions. Therefore, the two SCX-expressing progenitor states represent distinct stages of tendon lineage commitment, with SCX Progenitors contributing to both the basic tendon structure and its functional integration with adjacent tissues, while MKX Progenitors become more focused on specialised tendon structure and function. In support of this, the probabilistic descendant analysis predicts that 9.2 pcw SCX Progenitors transition towards 5 distinct fascicular, LCT, and muscle compartment 12 pcw foetal fibroblast types, while MKX Progenitors transition exclusively towards foetal fascicular ABI3BP GAS2 Fibroblasts.

Finally, MSC Precursors also differentiate towards the COL6A6 FSTL1 DCLK1 Progenitors around 8.4 pcw. These cells express established MSC markers such as *TWIST2*, *CD73*, *CD90*, and *CD44*, along with *CD34*, which is indicative of their role as MSCs (Lin *et al*., 2012). Notably, they also express *CXCL12*, a stromal cell-derived factor 1 (SDF1) chemokine that not only guides the migration and adhesion of $CD34^+$ cells (Lataillade *et al*., 2000), but also positively regulates *COL3A1* and *OSR1* essential for loose connective tissue development (Nassari *et al*., 2017; Stricker *et al*., 2012). This migratory and

adhesive capability is supported by their expression of genes like *GPC3*, *CELF2*, *PRKG1*, *AKAP12*, *NAV3*, *COLEC12*, and *DCLK1*, with the latter involved in epithelial-mesenchymal transition and cell migration (Mohammadi *et al*., 2018). In addition to the migratory MSC-like nature, these progenitors are distinguished by their high expression of various collagens (I, III, IV, V, VI, XII, XIV), and matrisomal genes including *DCN, ASPN, OGN, FNDC1, LUM, VCAN, IGFBP6, DPT, TNXB,* and *POSTN*. Crucial to their functional role in promoting elasticity and resilience in developing tendon LCT, they highly express ELN, which contributes to the formation of elastic fibres (Eekhoff *et al*., 2017; Godinho *et al*., 2017); EMILIN2, which regulates blood vessel assembly and elastic fibre organisation (Andreuzzi *et al*., 2020; Colombatti *et al*., 2012); and MFAP5, which enhances the deposition of elastin onto microfibrillar templates in connective tissues (Thomson *et al*., 2019; Uitto *et al*., 2013). Additionally, these progenitors express FSTL1, a secreted glycoprotein downstream of TGF-β signalling that is found in the embryonic limb tendon epi- and paratenon and is necessary for tendon development independent of SCX (Sylva, 2014). In fact, FSTL1 knockout in mice leads to an almost complete absence of tendons at E18.5 (Sylva, 2014), highlighting the critical role of these progenitors in tendon and connective tissue development. Overall, COL6A6 Progenitors represent MSCs transitioning towards the tendon LCT fibroblast phenotypes seen in foetal stages, with descendants of this cluster likely to transition to 12 pcw foetal LCT COL3A1 PI16 Fibroblasts, COL6A6 FNDC1 Fibroblasts, or muscle NEGR1 SCN7A Fibroblasts.

In the embryonic development of tendon and LCT lineages, initial similarities in gene expression and cellular functions are evident, particularly in the shared use of ECM components and growth factors critical for early cell communication and tissue differentiation. However, as differentiation advances, these pathways increasingly diverge, leading to a clear anti-correlation in gene expression as cells commit to their specific lineage pathways – a pattern also observed in the chondrocyte lineage. Overall, this divergence illustrates that commitment to fascicular, LCT, and tendon attachment site cells occurs late in embryonic development (~8 pcw), underscoring the importance of distinct regulatory pathways in shaping specialised foetal tissue structures.

Intriguingly, probabilistic fate modelling of transitions between 7.2 and 8.4 pcw embryonic and 20 pcw most differentiated fibroblast cells revealed significant distinctions in cell lineage commitments. The ABI3BP GAS2 Fibroblast lineage displayed higher commitment probabilities compared to the other lineages, which showed a broader spread, indicating less definitive differentiation pathways. Further exploration using SCENIC uncovered extensive transcriptional heterogeneity and a lack of definitive fibroblast-specific regulators, suggesting that fibroblast differentiation at this stage is controlled by a complex array of overlapping regulatory networks. This transcriptional plasticity highlights the cells' diverse origins and their capacity for multiple lineage commitments, contrasting sharply with the more stable and defined regulatory states of non-fibroblast cells such as myocytes and endothelial cells. That said, there are several limitations that could have biased these findings and should be taken into consideration.

5.4.2 Limitations and significance

This study faces significant methodological and data-driven limitations, primarily stemming from the complex sample metadata with strong batch effects (e.g., multiple different experimental batches and sequencing protocols) as well as the unconventional approach of inferring scRNA-seq tendon gene expression profiles from lower-resolution spatial transcriptomic data. Given the small size of tendons at embryonic stages, direct dissection and isolation of sufficient nuclei for sequencing were impractical. Consequently, reliance was placed on a single 8 pcw spatial RNA-seq sample to derive tendon signatures. This transfer of data from lower to higher sequencing resolution might have caused inaccuracies, such as the omission or erroneous integration of cell types that do not accurately represent those in developing tendons. This could explain the absence of canonical, undifferentiated MSCs or typical *SOX9*$^{+}$*SCX*$^{+}$ cells known for contributing to bone-to-tendon attachment units (Blitz *et al*., 2013; Sugimoto *et al*., 2013). Despite these challenges, the results align with expectations, such as the expression of *CXCL12* and its downstream *OSR1* LCT driver in cells resembling foetal LCT cells. However, to strengthen the reliability of these findings, it is crucial to experimentally validate the results and replicate the

methodology with a larger sample set to confirm the observed patterns and enhance the study's overall validity.

Another limitation arises from integrating single-cell and single-nucleus RNA sequencing data from non-overlapping developmental stages, specifically between embryonic 9 pcw and foetal 12 pcw timepoints. This wide age gap poses challenges in capturing intermediate states of differentiation and accurately reconstructing lineage trajectories due to differing sequencing coverages and limited temporal resolution of the data. These issues were partially mitigated by employing the moscot optimal transport-based approach (Klein *et al.*, 2023). However, the study would benefit from incorporation of additional snRNA-seq data from the 9 pcw timepoint that would overlap with the existing single-cell data. This would lead to better alignment of the datasets and offer a more seamless view of developmental transitions. Overall, these findings need to be validated through direct experimental approaches, including protein- and RNA-level investigations, as described in the previous chapter.

In conclusion, the findings from this chapter offer significant insights into the complex processes of tendon and limb connective tissue development, revealing both the dynamic transitions between embryonic and foetal stages and the detailed gene regulatory networks that guide these processes. The ability to identify distinct lineage commitments and the differential expression patterns among fascicular, LCT, and tendon attachment site cells provides a foundational understanding that is critical for both basic developmental biology and clinical applications. I hope that the discovery and transcription profiling of early regenerative embryonic tendon progenitors will aid in progressing regenerative medicine and tissue engineering approaches, informing the design of targeted interventions promoting tendon healing or engineered biocompatible tendon grafts.

Despite the advancements made in understanding tendon development, unresolved research questions and gaps remain, particularly concerning the properties of identified cell types and their potential roles in tendon regeneration. While exploring these aspects falls beyond the scope of current work, the subsequent chapter addresses another critical gap: the transcriptional

differences between regenerative foetal cell populations and non-regenerative adult tendon cells.

Chapter 6: Comparative Analysis of Developing and Aged Human Tendons

6.1 Introduction

Studies of tendon injury and healing have highlighted significant differences in regenerative capacities between developing and adult tendons (see section 2.5). Namely, injured foetal, neonatal, and young tendons can regenerate in a scarless manner, effectively restoring the native ECM structure. In contrast, adult tendons typically repair with persistent scarring or ectopic bone formation, characterised by disorganised ECM and inferior mechanical properties (Ansorge *et al*., 2011; Beredjiklian *et al*., 2003; Chan *et al*., 1998; Favata *et al*., 2006; Howell *et al*., 2017; Lui *et al*., 2012). Crucially, the regenerative healing capabilities of foetal tendons appear to be influenced by the intrinsic properties of the tendon rather than the extrinsic environment (Favata *et al*., 2006). Since tendon healing is predominantly driven by the cell populations found within the main body and the loose connective tissue layers of tendon (Garner *et al*., 1989; Grinstein *et al*., 2022; Harvey *et al*., 2019; Pakshir and Hinz, 2018; Snedeker and Foolen, 2017; Voleti *et al*., 2012; Walia *et al*., 2022), variations in these populations between development and adulthood may account for the observed differences in regenerative and fibrotic healing outcomes. Therefore, exploring the transcriptional differences between developing and aged tendons at the level of individual cells is crucial to understanding the underlying mechanisms of tendon regeneration and scarring.

Building on the identification and characterisation of embryonic and foetal tendon progenitors, this chapter extends the comparison to aged healthy and ruptured tendon cells. Initial investigations involve histological examinations of foetal and adult tissues to delineate the structural changes that tendons undergo from development through to maturity. Key aspects such as cellular density and morphology, proteoglycan content, and collagen alignment are discussed using Bonar scoring and image analysis. Following this, annotated adult Achilles and quadriceps tendon data provided by the Tendon Seed Network (see Methods section 3.6) is used to establish cellular relationships between developing and aged tendons. Matrisomal gene expression profiling, as well as full or matrisome-specific pseudobulk differential gene expression

analyses, are carried out to facilitate gene expression comparisons between development and adulthood. This analysis is then complemented by the examination of developing and aged fibroblast gene regulatory network profiles. By integrating histological data with deep transcriptional profiling, this research endeavours to provide a detailed depiction of the molecular continuum from tendon development to ageing, offering insights into potential therapeutic targets for enhancing tendon repair in adults.

6.2 Methods

6.2.1 Histology, Bonar scoring, image data quantification, and statistical analysis

Histochemical staining of foetal and adult sectioned formalin-fixed tissues was performed by the Histology Team at the Kennedy Institute of Rheumatology. The slides were stained with haematoxylin and eosin (H&E), alcian blue, masson's trichrome, and picrosirius red. Slides were scanned with Motic EasyScan One. PSR-stained slides were additionally imaged under polarized light using an Olympus BX40.

The tissues were evaluated using the Bonar scoring system, which evaluates key histopathological features including cellularity, vascularity, collagen organisation, morphology, and ground substance staining. The scoring was performed once by the author. Each feature was scored on a scale from 0 to 3 following the criteria detailed in Table 1 of the publication by Fearon *et al.* (2014).

QuPath (v0.4.3) classification functions were used to manually delineate tendon regions within H&E-stained tissue samples. From these regions, 3-6 random 250x250 μm tiles were extracted and processed using ImageJ. First, haematoxylin and eosin channels were separated using colour deconvolution. Subsequently, the haematoxylin channel was used for nuclei segmentation using the StarDist ImageJ plugin (v0.3.0) (see Figure 61). Following this segmentation, quantitative analyses were performed to determine the number of nuclei, the mean area of the nuclei, and the maximum distance to the centroid of each nucleus. These metrics were aggregated at the sample level, associating each set of measurements with corresponding metadata.

Statistical analysis was performed using *scipy* (v1.11.1), *statsmodels* (v0.14.0), and *scikit_posthocs* (v0.9.0). The normality of the data distributions for the number of nuclei, their areas, and maximum distances to their centres was assessed using the Shapiro-Wilk test as well as visual inspections of histograms and Q-Q plots. For data that approximated normal distributions – the nucleus area and maximum distance to nucleus centroid variables – analysis of variance (ANOVA) was performed to test for significant differences across different age groups. For the number of nuclei, which exhibited an almost bimodal distribution, the Kruskal-Wallis H-test was used to assess significant differences across age groups. Post-hoc analysis was conducted to identify specific group differences. Tukey's Honest Significant Difference test was used following the ANOVA, and Dunn's test with Bonferroni correction was employed after the Kruskal-Wallis H-test.

6.2.2 Data integration with scVI-scANVI

Processed, filtered, and annotated adult Achilles tendon (*N*=6, split by microanatomical regions; Appendix Table 3) and quadriceps tendon (*N*=7, healthy or torn midbodies; Appendix Table 3) datasets provided by the TSN (Baldwin *et al*., 2023, 2021) were concatenated with embryonic and foetal tendon data. Cells with fewer than 200 genes and genes in fewer than 30 counts were filtered out, yielding 176,691 cells and 32,869 genes. Top 7,000 highly variable genes were selected in a batch-aware manner using *scanpy.pp.highly_variable-_genes(batch_key="sampletype")*. Data integration was performed using scVI modelling (Gayoso *et al*., 2022) on unnormalised, highly variable counts, with the library preparation batches ("libbatch"), "sampletype", and the cell cycle phase scores ("G2M_score" and "S_score") specified as the main batch effects (Appendix Figure 13). The model's hyperparameters were optimised with scVI's autotune to 'n_hidden': 256, 'n_latent': 50, 'n_layers': 1, 'dropout_rate': 0.1, 'gene_likelihood': 'zinb', and 'dispersion': 'gene-batch'. The model was trained for 80 epochs until training and validation set convergence. Next, the cell type labels were harmonised using the scANVI model. The resulting embeddings were used for the computation of neighbourhood graphs and dimensionality reduction with UMAP (Appendix Figure 13).

6.2.3 Scanpy-based differential gene expression analysis

The log1pPF-normalised data were subjected to Wilcoxon rank-sum test differential gene expression analysis (*scanpy.tl.rank_genes_groups()*), which was performed separately for foetal and adult cell populations. For each specified cell type within foetal tendons, the top 50 differentially expressed genes were extracted. Marker gene overlap analysis using *scanpy.tl.marker_gene_overlap()* was then conducted to quantify and visualise transcriptional similarities between the foetal top 50 DEGs and the marker genes derived from the adult differential expression analysis. Normalisation of overlap scores was performed relative to the foetal DEGs, providing a proportion of foetal marker genes detected in each adult cell type. The results of this analysis were visualised in Figure 63A using a clustermap generated with seaborn (v0.12.2; Waskom, 2021). Gene expression scores were calculated with *scanpy.tl.score_genes()* for each cell based on the average expression of the top 50 foetal DEGs. These scores were then scaled to the 99th percentile of their distribution and visualised using UMAPs in Figure 63B. Matrisomal gene expression profile plots in Figure 65 and Appendix Figure 14 were generated using log1p-normalised data.

6.2.4 Cell type harmonisation with CellHint

To achieve more robust cell type label harmonisation, CellHint (v1.0.0; Xu *et al.*, 2023) was applied to the different tendon types across the embryonic, foetal, and adult age groups (specified as ‘grouptype’ in Figure 63B). Specifically, the *cellhint.harmonize()* function was used to calculate euclidean distances between cells within batch-corrected scVI embeddings, constructing a harmonisation graph of cell type annotations. The datasets were specified to be harmonised sequentially, from embryonic to adult stages, capturing both developmental and condition-specific variations in cell types.

6.2.5 DESeq2-based pseudobulk differential gene expression analysis

For differential gene expression analysis across different cell types, the raw single-nuclei sequencing counts were converted into grouped “donor + tissue type + cell type” pseudobulk expression profiles using custom functions as

described previously in section 4.2.2.2. Differential gene expression analysis was carried out separately for the specified groups containing specific CellHint-paired foetal and adult cell types using DESeq2 (v1.40.2). Wald tests were used to identify all genes that were significantly up- or downregulated in adult cell types compared to the foetal cell types (with *p-adjusted* < 0.01, log_2FC > +/-1). These genes were used for pathway analysis against all expressed genes using the gProfiler g:GOSt tool (Raudvere *et al*., 2019) with Benjamini-Hochberg FDR set to <0.01 and term sizes restricted to between 20 and 500 terms. The identified up- or downregulated GO:BP terms for each CellHint-aligned pair of foetal and adult fibroblasts were compared against each other using Venn diagrams made with Venny (Oliveros, 2015) (Figure 66). The pair-specific pathways were then manually summarised by common functions into broad categories to reduce enable comparisons (Figures 67-70). Additionally, matrisomal genes were specifically isolated from the significant genes list and presented separately (Figures 67-70).

6.2.6 SCENIC analysis

SCENIC analysis was conducted on embryonic and adult quadriceps tendon datasets, along with remaining datasets from foetal stages at 12 and 17 pcw, using pyscenic v0.12.1 (Aibar *et al*., 2017), following the approach described in section 5.2.8. A total of 335 embryonic regulons, 285 regulons from 12 pcw foetal samples, 237 regulons from 17 pcw foetal samples, and 193 adult regulons were identified. Additionally, 286 regulons specific to 20 pcw foetal samples were previously identified and included in the analysis.

Regulon activity within individual cells was quantified using the *pyscenic aucell* command, with an AUC threshold of 0.1 applied to the embryonic dataset and the default threshold of 0.05 applied to the adult and remaining foetal datasets. Binarization of regulon activity was achieved using a Gaussian mixture model, resulting in matrices indicating active and inactive regulons per cell.

The binarized regulon matrices underwent several transformations to extract and normalise regulon activation patterns across different cell populations. Initially, cells were grouped according to their cell type annotations, allowing the aggregation of active regulons by calculating the sum of active cells per regulon

within each group. Subsequently, these summaries were normalised based on the total cell count per group to account for variations in cell numbers. Next, normalised regulon activation frequencies within each group were further z-score normalised, facilitating comparative analysis across developmental stages and conditions. The z-scored regulon activity patterns were visualised using custom *seaborn* clustermaps (Figure 71). Individual regulons were explored and summarised using The STRING database (*stringdb,* v.12.0) (Szklarczyk *et al*., 2023). Large regulons were subjected to pathway analysis with gProfiler g:OST as previously described.

6.3 Results

6.3.1 Histological examination of foetal and aged tendons

In the study of tendon pathology, the Bonar and Movin scales are established histological scoring systems that evaluate the severity and progression of tissue degeneration in adult tendons. These frameworks allow for the quantitative assessment of histopathological features, including cellularity, collagen organisation, vascularity, and ground substance accumulation. Typically, Bonar scores range from 0-4 for healthy tendons to 6-12 for pathological ones (Fearon *et al*., 2014; Maffulli *et al*., 2008). It is not well understood whether the histological characteristics of prenatal tendons align more closely with those of healthy adult tendons or those exhibiting pathological changes. To address this knowledge gap, the Bonar scoring system, as detailed by Fearon *et al.* (2014), was applied to foetal tendons from 11 to 20 pcw (Table 5).

Table 5. Bonar scores of individual foetal and adult healthy control tendon tissues. *Scoring was performed once by a single individual (author). The scoring criteria applied are detailed in Table 1 of Fearon et al. (2014). Pcw: post-conception weeks; Yr: years of age.*

Tissue	Age	Cell morpho-logy	Collagen arrange-ment	Cellu-larity	Vascu-larity	Ground substance	Total
Achilles tendon	11 pcw	1	2	1	3	3	**10**
Quadriceps tendon	11 pcw	2	2	1	3	3	**11**
Achilles tendon	12 pcw	2	2	1	3	3	**11**
Quadriceps tendon	12 pcw	3	2	1	3	3	**12**
Quadriceps tendon	13 pcw	2	2	1	3	3	**11**
Achilles tendon	13 pcw	1	2	1	3	3	**10**

Achilles tendon	14 pcw	2	2	1	2	3	**10**
Achilles tendon	14 pcw	2	2	1	3	3	**11**
Achilles tendon	15 pcw	2	1	1	3	2	**9**
Achilles tendon	15 pcw	2	2	1	3	2	**10**
Achilles tendon	16 pcw	1	1	1	3	3	**9**
Achilles tendon	17 pcw	2	1	1	3	3	**10**
Achilles tendon	17 pcw	2	1	1	2	3	**9**
Achilles tendon	17 pcw	2	1	1	3	3	**10**
Achilles tendon	19 pcw	2	1	1	3	3	**10**
Quadriceps tendon	19 pcw	2	1	1	2	3	**8**
Patellar tendon	20 pcw	1	1	1	3	3	**9**
Quadriceps tendon	20 pcw	1	1	1	3	3	**9**
Achilles tendon	20 pcw	1	1	1	3	3	**9**
Patellar tendon	20 pcw	1	1	1	3	3	**9**
Achilles tendon	45 yr	0	1	0	0	0	**1**
Quadriceps tendon	45 yr	1	2	0	0	0	**3**

According to the scoring criteria, foetal tendons exhibited hypercellularity at all developmental stages (Figure 58), scoring as grade 1 for cellularity (Table 5). Nuclei generally appeared oblate or rounded, with minimal discernible cytoplasm (Figure 58), resulting in scores ranging between grades 1 and 2 for cell morphology. In terms of vascularity, the frequent presence of blood vessels was observed within the examined regions, leading to scores of 2 or 3. Additionally, the alcian-blue stained acidic polysaccharides, such as GAGs found in proteoglycans, were uniformly high across all tendons regardless of type or developmental stage, aligning with a grade 3 classification on the scoring scale for ground substance (Figure 59). Finally, collagen arrangement varied across individual tendons and developmental stages; while generally highly organised with distinct parallel bundles (Figure 59), the non-homogeneous polarization led to scores of grades 1 to 2. Collectively, these findings resulted in overall scores ranging from 8 to 12 for foetal tendons, with higher scores observed in earlier developmental stages. This scoring pattern places foetal tendons in the range typically classified as pathological in adult tissues, highlighting that the Bonar score criteria include tissue characteristics that are common to both developmental processes and degenerative changes.

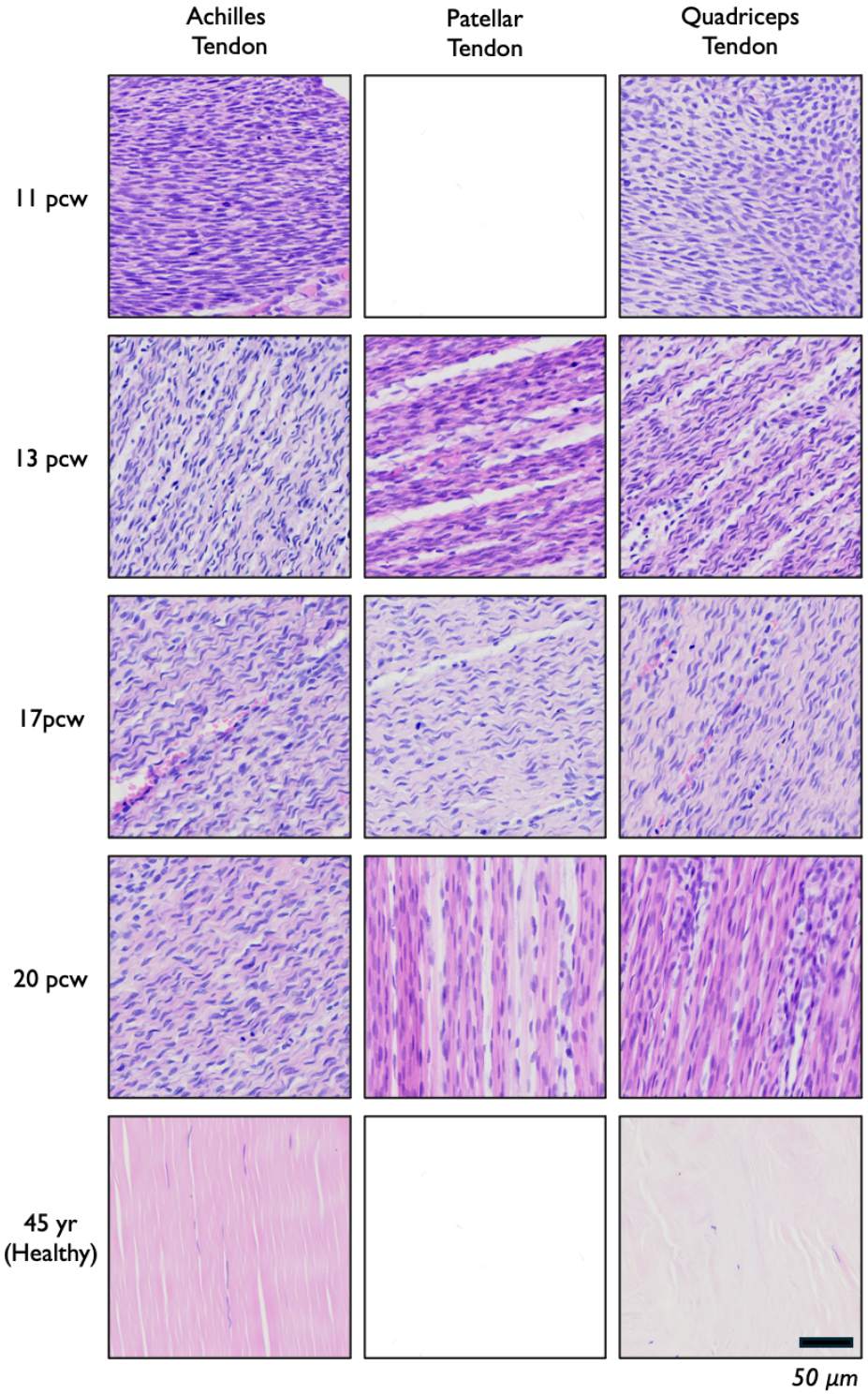


Figure 58. Photomicrographs of foetal and adult Achilles, patellar, and quadriceps tendon tissues stained with haematoxylin and eosin. *Size bar corresponds to 50 µm. Foetal tissues are denoted by post-conception weeks (pcw) and adult tissues by years (yr). White squares indicate placeholders for results that are still being generated.*

In examining the collagen alignment of picrosirius red-stained foetal tendons under polarized light, developmental changes in birefringence were observed, reflecting the maturation of collagen fibres. At 11 pcw, early foetal collagen

fibres had low birefringence, appearing predominantly blue-green (Figure 59). This colouration is characteristic of thin, loosely organised fibres, likely indicative of type III collagen. As development progressed, an increase in the organisation of collagen was noted at 12 pcw with the emergence of yellow fibres (Figure 59), suggesting the presence of more densely organised type I collagen. By 16 pcw, a shift to red-coloured birefringence was observed, marking a further thickening and maturation of collagen fibres. Additionally, the initial crimp patterns of collagen, which were frequent and angular at 12 pcw, evolved to become more elongated by 20 pcw, resembling more closely the crimp structure seen in adult tendons (Figure 59).

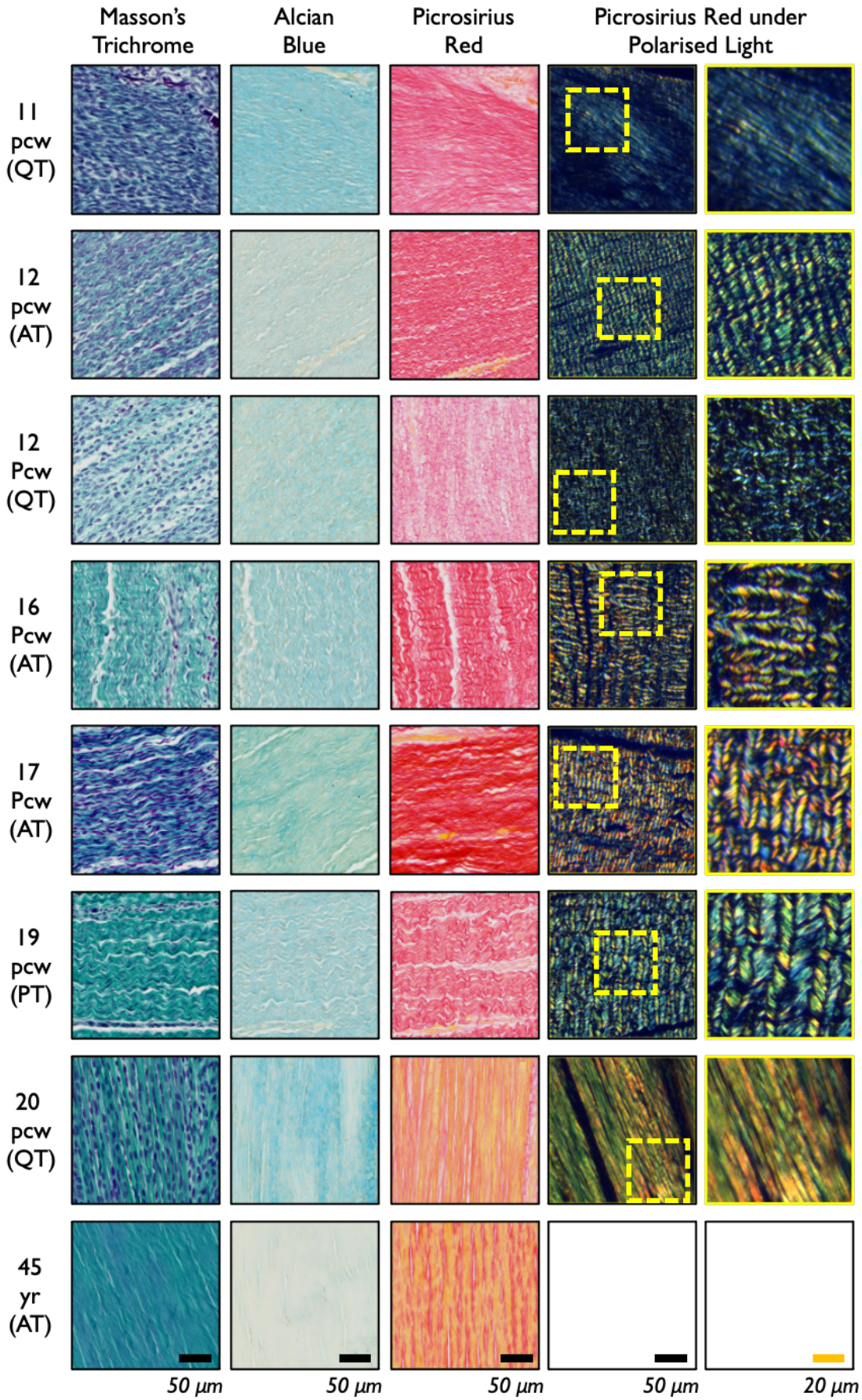

Masson's Trichrome
Alcian Blue
Picrosirius Red
Picrosirius Red under Polarised Light
11 pcw (QT)
12 pcw (AT)
12 Pcw (QT)
16 Pcw (AT)
17 Pcw (AT)
19 pcw (PT)
20 pcw (QT)
45 yr (AT)
50 μm
50 μm
50 μm
50 μm
20 μm

Figure 59. Photomicrographs of foetal and adult tendon tissues stained with masson's trichrome, alcian blue, and picrosirius red. *Brightfield microscopy was used for visualisation, with polarizing light filters additionally applied to the picrosirius red-stained tissues. Masson's trichrome stains for collagen fibres (blue), muscle fibres (red), and cell nuclei (dark purple). Alcian blue specifically stains for acidic mucopolysaccharides and glycosaminoglycans, which are components of proteoglycans and glycoproteins forming the ground substance (blue). Picrosirius red stains for collagen fibres, which appear red under brightfield microscopy and show varying colours (red, orange, yellow, and green) under polarized light, depending on the thickness and type of collagen. The size bars correspond to 50 µm (black) or 20 µm (orange). Examined tissues include Achilles tendon (AT), quadriceps tendon (QT), and patellar tendon (PT). Foetal tissues are denoted by post-conception weeks (pcw) and adult tissues by years (yr). White squares indicate placeholders for results that are still being generated.*

To quantitatively assess the differences between foetal and adult tendons across developmental stages, image analysis measuring the numbers, areas, and maximum distances to centroids of nuclei was performed using StarDist. (Figure 60A). The mean number of nuclei per 250 µm² area decreased from 919.83 (± 2.92 SD) at 11 pcw to 501.98 (± 114.37 SD, $p<0.03$) at 19 pcw. This number reduced drastically to 23.08 (± 13.82 SD, $p<0.01$) by 45 years of age, with a slight increase to 84.5 (± 50.24 SD, $p<0.03$) at 84 years (Figure 60A). Therefore, these results confirm a significant decrease in nuclear density per surface area as development progresses, eventually reaching a plateau in adulthood.

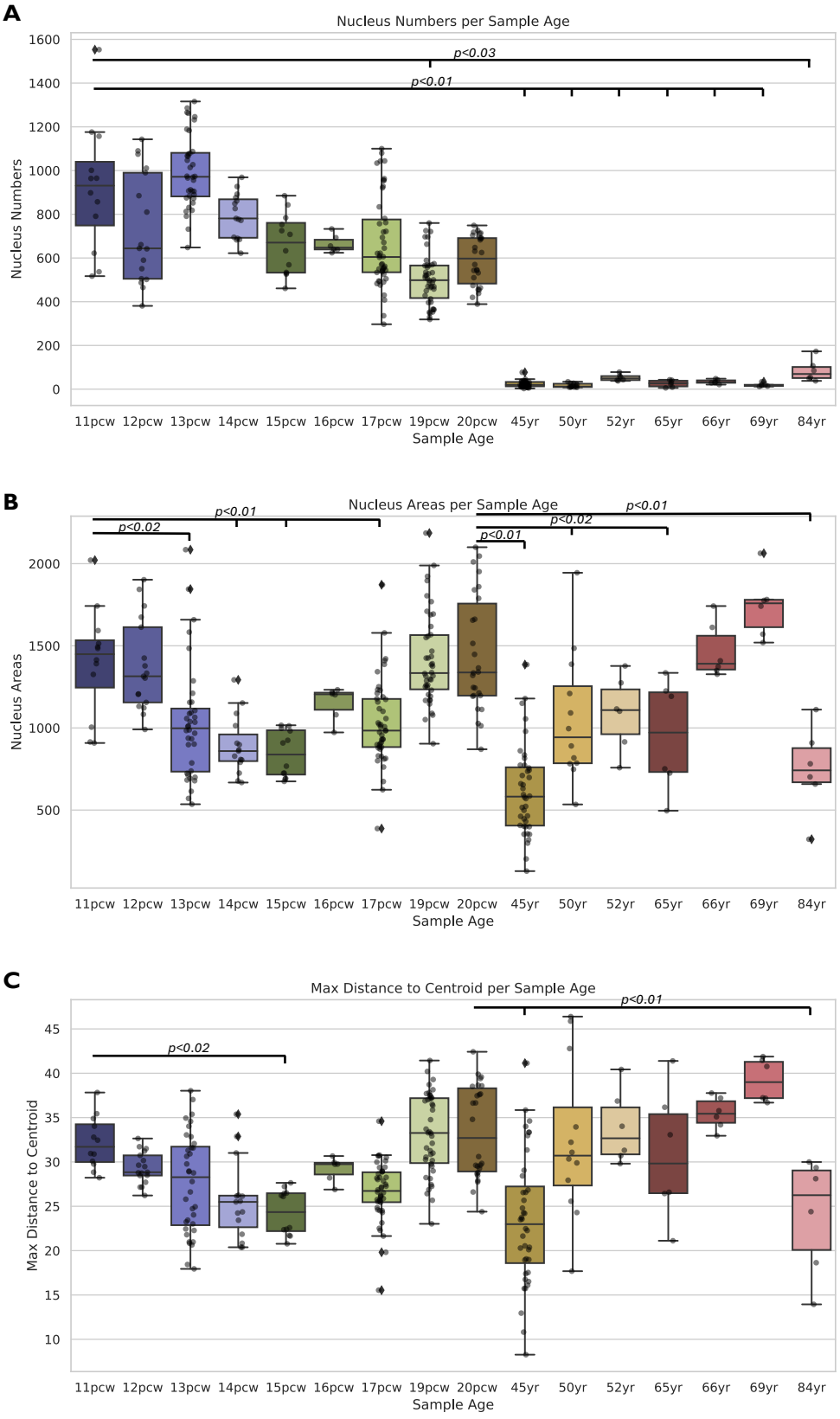


Figure 60. Results of StarDist quantification of nuclear properties in haematoxylin-stained tissues. *Boxplots display (A) nuclei numbers, (B) nuclei areas, and (C) maximum distances to nuclei centroids for each sample age. Foetal tissues are denoted by post-conception weeks (pcw) and adult tissues by years (yr). Adult ages correspond to single donors. Statistical analysis was performed using a Kruskal-Wallis*

test followed by Dunn's post-hoc test for nuclei numbers (A), and ANOVA with Tukey HSD for nuclei areas and distances (B, C), measured in pixels within 250 µm² tiles. Significant comparisons against a single timepoint are shown: all foetal and adult comparisons against 11 pcw in (A), and foetal comparisons against 11 pcw and adult comparisons against 20 pcw in (B) and (C).

In terms of nuclear morphology, mean nuclear area reduced from 1400.48 pixels (± 331.45 SD) at 11 pcw to 842.95 pixels (± 141.81 SD, $p<0.01$) at 15 pcw, followed by a gradual return to 1448.66 pixels (± 357.00 SD) by 20 pcw (Figure 60B). Among adult samples, certain age groups exhibited smaller nuclear areas compared to 20 pcw: specifically, the 45-year-old (617.00 pixels, ± 273.66 SD, $p<0.01$), 65-year-old (954.19 pixels, ± 340.24 SD, $p<0.02$), and 84-year-old (747.51 pixels, ± 264.75 SD, $p<0.01$) individuals. Interestingly, no significant differences were observed in samples from individuals aged 52 (1090.36 pixels, ± 227.18 SD), 66 (1468.57 pixels, ± 168.70 SD), or 69 (1742.07 pixels, ± 192.20 SD) years compared to 20 pcw (Figure 60B). Additionally, the analysis of maximal centroid distances revealed a decrease from 32.18 pixels (± 2.92 SD) at 11 pcw to 24.40 pixels (± 2.57 SD) at 15 pcw ($p<0.02$), followed by an increase to 33.42 pixels (± 5.26 SD) by 20 pcw (Figure 60C), supporting a transition from elongated to more rounded and back to elongated nuclear shapes during the 2nd to 3rd trimester of foetal development (Figure 61). In adult tissues, maximal centroid distances were significantly reduced in the youngest (45 years, 23.41 pixels ± 7.32 SD) and oldest (84 years, 24.07 pixels ± 6.50 SD) samples compared to the 20 pcw samples ($p<0.01$), while distances in other adult samples were similar to those at 20 pcw, averaging at least 30.79 pixels (Figure 60C). Overall, these results indicate complex and dynamic changes in nuclear size and morphology throughout development and ageing.

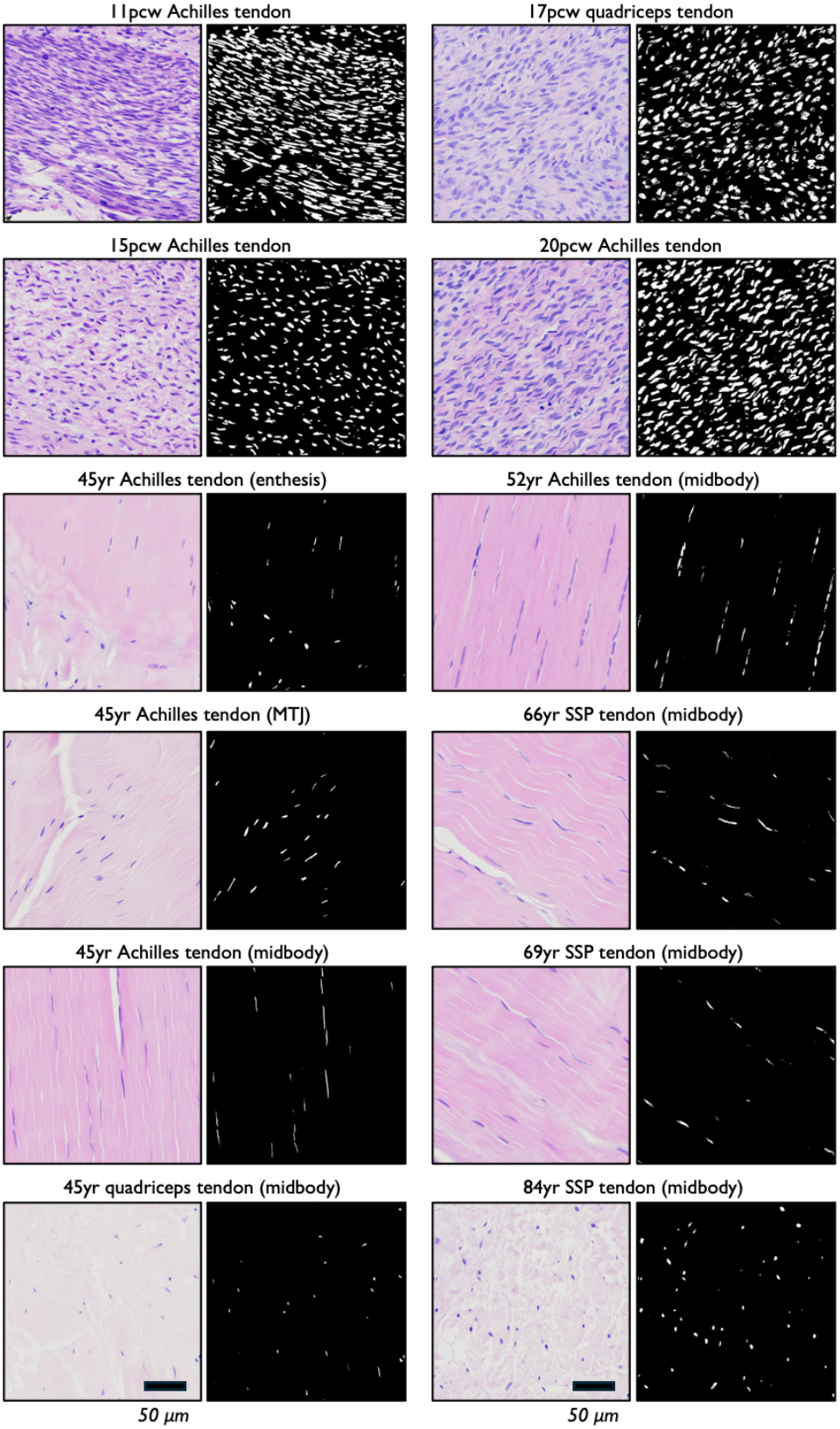


Figure 61. Examples of foetal and adult tendon sample tiles used for StarDist nuclei segmentation. *Left panels show the original H&E-stained images, while right panels display the corresponding isolated haematoxylin channels used for nuclei segmentation and measurements with StarDist. Size bars correspond to 50 µm. Foetal tissues are denoted by post-conception weeks (pcw) and adult tissues by years (yr). SSP: supraspinatus tendon of the shoulder; MTJ: myotendinous junction.*

The observed differences in quantification results for adult tissue nuclei density and morphology can be partly explained by significant inter- and intra-donor tissue variability. For example, the 45-year-old Achilles and quadriceps tendon tissues exhibited both elongated and round nuclei depending on their anatomical location (e.g., midbody vs enthesis) (Figure 61). Additionally, some samples were not completely pathology-free; the 52-year-old Achilles tendon came from an insensate tissue sample and appeared more cellular, while the 84-year-old supraspinatus tendon sample had only round nuclei with disorganised ECM tissue lacking distinct bundles (Figure 61), hinting at a degree of degeneration. Therefore, the results need to be interpreted with caution.

6.3.2 Comparison of developing and aged tendon cell types

To elucidate the cellular dynamics throughout tendon development and ageing, datasets comprising scRNA-seq and snRNA-seq data from embryonic (5-9 pcw), foetal (12-20 pcw), and adult (25-76 yr) tendons were analysed (Appendix Table 3). These datasets were integrated using scVI, followed by the application of the scANVI model to refine embeddings based on the original dataset-specific cell type annotations (Figure 62).

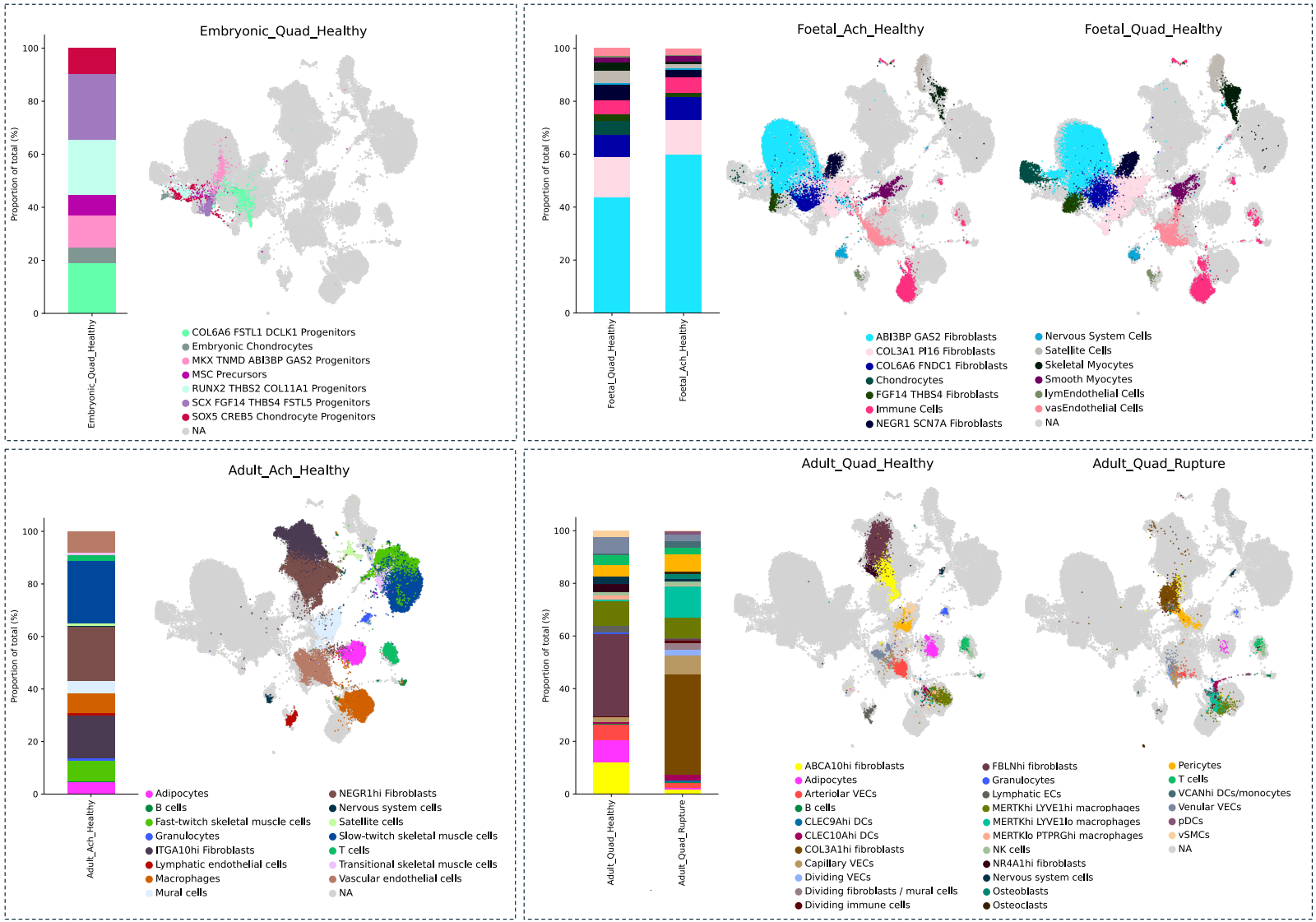
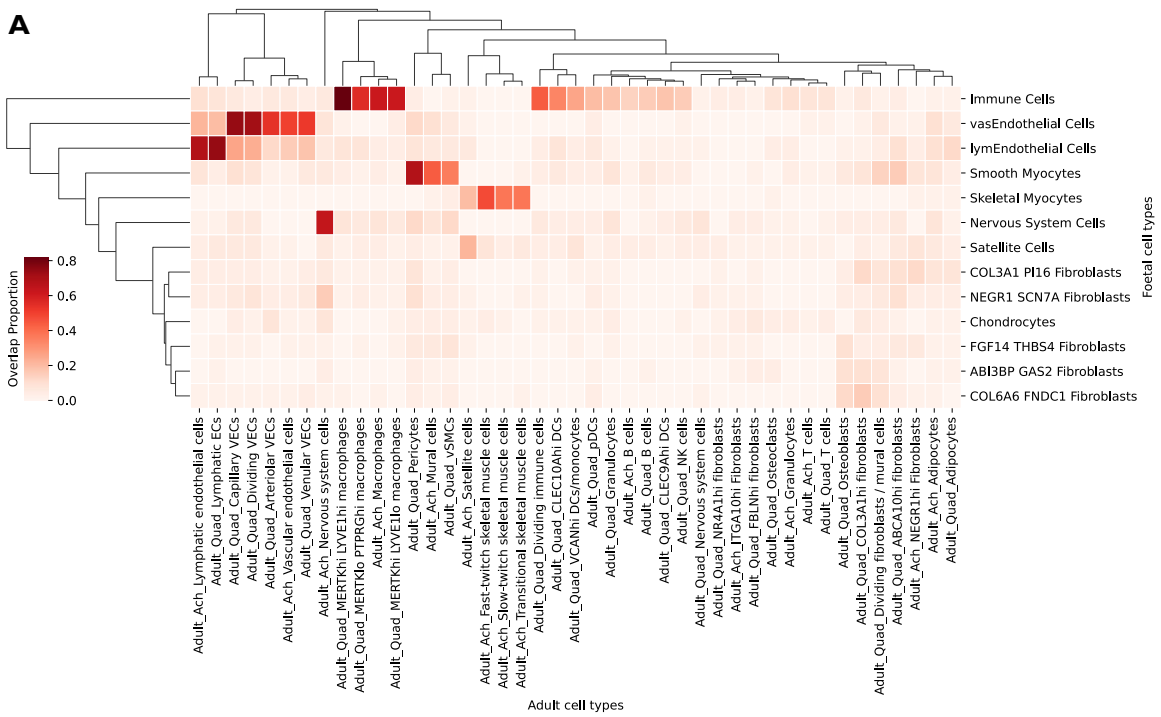


Figure 62. Original cell type annotations of scANVI-integrated embryonic, foetal, and adult tendon data. *Bar charts show cell type proportions for each dataset. Annotated adult tendon datasets were provided by Dr Carla Cohen (Achilles tendon) and Dr Jolet Mimpen (quadriceps tendon).*

It became evident that comprehensive data integration was challenging, even when employing other robust methods like scGen and Harmony, as the developing and adult fibroblast populations remained mostly distinct from each other. A comparative analysis of DEGs between foetal and adult tendon cell types was therefore performed to identify initial commonalities and differences. This analysis revealed a significant overlap of the top 50 foetal DEGs in adult non-fibroblast populations, including immune, endothelial, muscle, and nervous system cells (Figure 63A), suggesting conservation of biological functions essential for tendon maintenance across different life stages. Conversely, foetal and adult fibroblast populations showed largely distinct gene expression profiles (Figure 63A), reflecting their role in the dynamic and context-dependent processes of tendon development, maintenance, and repair. Notably, fibroblasts from ruptured adult quadriceps tendons showed higher expression levels of top 50 DEGs for foetal ABI3BP GAS2 Fibroblasts and COL6A6 FNDC1 Fibroblasts compared to those from healthy adult tendons (Figure 63B), suggesting potential developmental regressions or shifts to a more “developmental” state in these cells, possibly as a mechanism to initiate repair processes.


A
Overlap Proportion
0.8
0.6
0.4
0.2
0.0
Immune Cells
vasEndothelial Cells
lymEndothelial Cells
Smooth Myocytes
Skeletal Myocytes
Nervous System Cells
Satellite Cells
COL3A1 PI16 Fibroblasts
NEGR1 SCN7A Fibroblasts
Chondrocytes
FGF14 THBS4 Fibroblasts
ABI3BP GAS2 Fibroblasts
COL6A6 FNDC1 Fibroblasts
Foetal cell types
Adult_Ach_Lymphatic endothelial cells
Adult_Quad_Lymphatic ECs
Adult_Quad_Capillary VECs
Adult_Quad_Dividing VECs
Adult_Quad_Arteriolar VECs
Adult_Ach_Vascular endothelial cells
Adult_Quad_Venular VECs
Adult_Ach_Nervous system cells
Adult_Quad_MERTKhi LYVE1hi macrophages
Adult_Quad_MERTKlo PTPRGhi macrophages
Adult_Ach_Macrophages
Adult_Quad_MERTKhi LYVE1lo macrophages
Adult_Quad_Pericytes
Adult_Ach_Mural cells
Adult_Quad_vSMCs
Adult_Ach_Satellite cells
Adult_Ach_Fast-twitch skeletal muscle cells
Adult_Ach_Slow-twitch skeletal muscle cells
Adult_Ach_Transitional skeletal muscle cells
Adult_Quad_Dividing immune cells
Adult_Quad_CLEC10Ahi DCs
Adult_Quad_VCANhi DCs/monocytes
Adult_Quad_pDCs
Adult_Quad_Granulocytes
Adult_Ach_B cells
Adult_Quad_B cells
Adult_Quad_CLEC9Ahi DCs
Adult_Quad_NK cells
Adult_Quad_Nervous system cells
Adult_Quad_NR4A1hi fibroblasts
Adult_Ach_ITGA10hi Fibroblasts
Adult_Quad_FBLNhi fibroblasts
Adult_Quad_Osteoclasts
Adult_Ach_Granulocytes
Adult_Ach_T cells
Adult_Quad_T cells
Adult_Quad_Osteoblasts
Adult_Quad_COL3A1hi fibroblasts
Adult_Quad_Dividing fibroblasts / mural cells
Adult_Quad_ABCA10hi fibroblasts
Adult_Ach_NEGR1hi Fibroblasts
Adult_Ach_Adipocytes
Adult_Quad_Adipocytes
Adult cell types

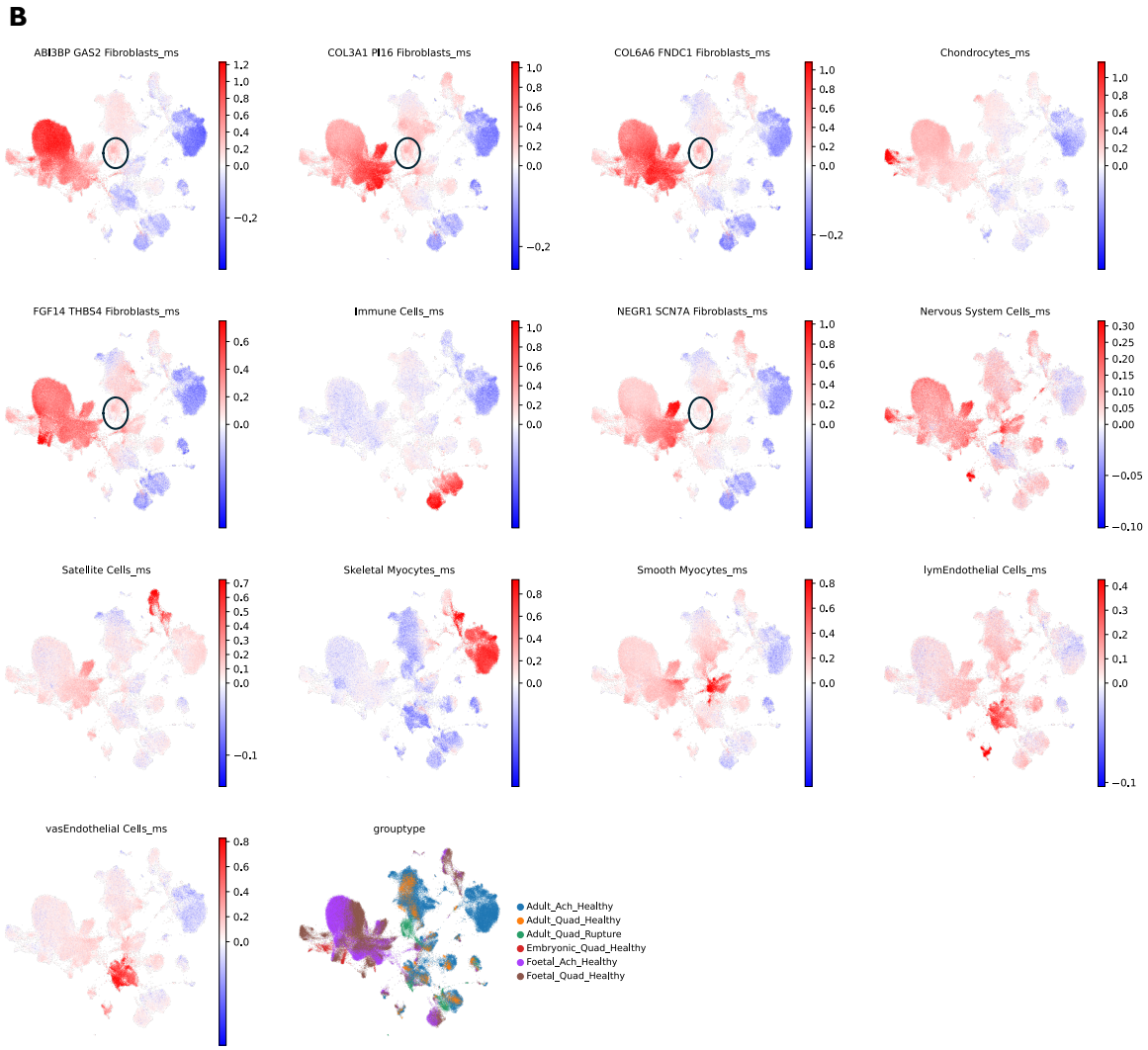
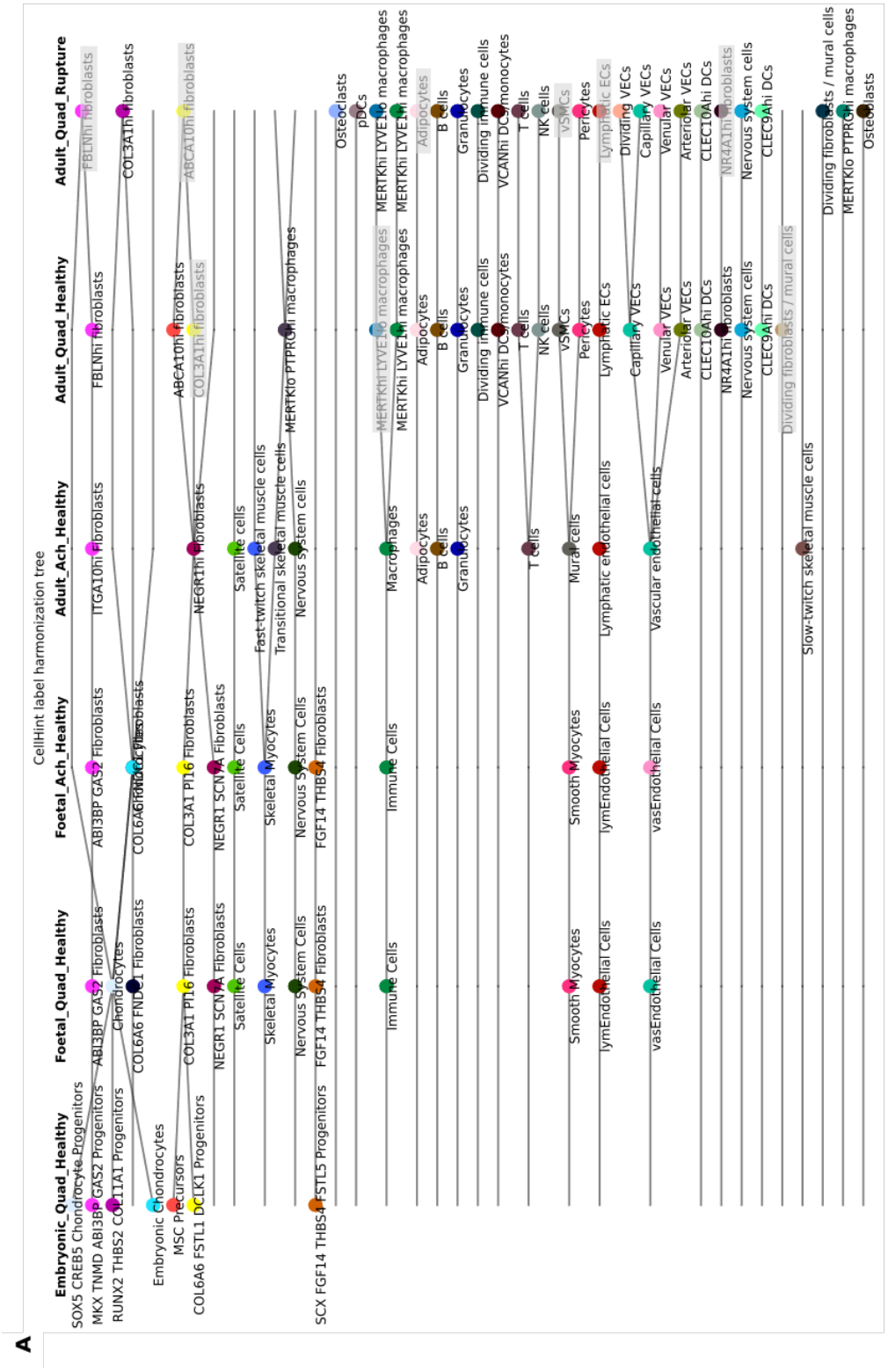

B
ABI3BP GAS2 Fibroblasts_ms
COL3A1 PI16 Fibroblasts_ms
COL6A6 FNDC1 Fibroblasts_ms
Chondrocytes_ms
FGF14 THBS4 Fibroblasts_ms
Immune Cells_ms
NEGR1 SCN7A Fibroblasts_ms
Nervous System Cells_ms
Satellite Cells_ms
Skeletal Myocytes_ms
Smooth Myocytes_ms
lymEndothelial Cells_ms
vasEndothelial Cells_ms
grouptype
Adult_Ach_Healthy
Adult_Quad_Healthy
Adult_Quad_Rupture
Embryonic_Quad_Healthy
Foetal_Ach_Healthy
Foetal_Quad_Healthy

Figure 63. Marker gene overlap between foetal and adult tendon cell types. (A) *Clustermap shows normalised overlap of the top 50 differentially expressed genes (DEGs) in foetal cell types (rows) with those identified in adult cell types (columns), computed using the Wilcoxon rank-sum test. Overlap is expressed as a proportion of the foetal marker gene set, with darker shades indicating higher marker overlap.* ***(B)*** *UMAPs showing the spatial distribution of gene expression scores for the same top 50 DEGs specific to individual foetal tendon cell types. Colour intensity is scaled to the 99th percentile of the score distribution and indicates the relative expression level of the markers within the cells, with red corresponding to high expression of the top 50 foetal DEGs. Black ovals highlight the rupture-specific fibroblast population.*

To understand the relationships between largely distinct developing and adult cell types, initial evaluations using scANVI's consolidated cell type label predictions were performed; however, these provided limited insights due to their low resolution. Consequently, a more robust cell type label harmonisation method, CellHint (Xu *et al*., 2023), was utilised. The harmonisation graph generated by CellHint illustrated the relationships and transitions among different tendon cell types across developmental stages and healthy or ruptured conditions (Figure 64). Reassuringly, this analysis confirmed the consistency of cell type labels across different datasets, showing a high degree of nomenclature agreement (e.g., foetal “lymEndothelial Cells” linked to adult “Lymphatic endothelial cells” and “Lymphatic ECs”) (Figure 64A). Furthermore, CellHint effectively refined the classification of foetal cell types, linking foetal Immune Cells to adult Macrophages expressing MERTK, and aligning Skeletal Myocytes with Transitional and Fast-twitch Skeletal Muscle Cells in the muscle and MTJ regions of adult Achilles tendons (Figure 64A).

In addition to improving classification, CellHint highlighted differences in cell type composition between developing and mature tendons. Firstly, the adult tendon immune cell repertoire appeared more diverse, featuring both lymphoid (T, B, NK cells) and myeloid (granulocytes, macrophages, monocytes, dendritic cells) lineages, in contrast to foetal tendons, where macrophages predominated (Figure 64A). Secondly, Adipocytes and NR4A1hi fibroblasts, which were absent during development, were identified in adult tendons (Figure 64A). Lastly, while there was a correspondence between foetal and adult Achilles Nervous System Cells, adult quadriceps Nervous System Cells remained distinct, potentially representing a unique population of cells expressing nervous system markers with no developmental counterparts (Figure 64A).


A
CellHint label harmonization tree
Embryonic_Quad_Healthy
Foetal_Quad_Healthy
Foetal_Ach_Healthy
Adult_Ach_Healthy
Adult_Quad_Healthy
Adult_Quad_Rupture
SOX5 CREB5 Chondrocyte Progenitors
MKX TNMD ABI3BP GAS2 Progenitors
RUNX2 THBS2 COL11A1 Progenitors
Embryonic Chondrocytes
MSC Precursors
COL6A6 FSTL1 DCLK1 Progenitors
SCX FGF14 THBS4 FSTL5 Progenitors
ABI3BP GAS2 Fibroblasts
Chondrocytes
COL6A6 FNDC1 Fibroblasts
COL3A1 P16 Fibroblasts
NEGR1 SCN7A Fibroblasts
Satellite Cells
Skeletal Myocytes
Nervous System Cells
FGF14 THBS4 Fibroblasts
Immune Cells
Smooth Myocytes
lymEndothelial Cells
vasEndothelial Cells
ABI3BP GAS2 Fibroblasts
Chondrocytes
COL6A6 FNDC1 Fibroblasts
COL3A1 P16 Fibroblasts
NEGR1 SCN7A Fibroblasts
Satellite Cells
Skeletal Myocytes
Nervous System Cells
FGF14 THBS4 Fibroblasts
Immune Cells
Smooth Myocytes
lymEndothelial Cells
vasEndothelial Cells
ITGA10hi Fibroblasts
COL6A6 Chondrocytes/Fibroblasts
NEGR1hi fibroblasts
Satellite cells
Fast-twitch skeletal muscle cells
Transitional skeletal muscle cells
Nervous system cells
Macrophages
Adipocytes
B cells
Granulocytes
T cells
Mural cells
Lymphatic endothelial cells
Vascular endothelial cells
FBLNhi fibroblasts
ABCA10hi fibroblasts
COL3A1hi fibroblasts
MERTKio PTPRChi macrophages
MERTKhi LYVE1hi macrophages
Dividing immune cells
VCANhi DC/monocytes
T cells
NK cells
vSMCs
Pericytes
Lymphatic ECs
Capillary VECs
Venular VECs
Arterial VECs
CLEC10Ahi DCs
NR4A1hi fibroblasts
Nervous system cells
CLEC9Ahi DCs
Dividing fibroblasts / mural cells
Slow-twitch skeletal muscle cells
Osteoclasts
pDCs
MERTKhi LYVE1lo macrophages
MERTKhi LYVE1hi macrophages
Adipocytes
B cells
Granulocytes
Dividing immune cells
VCANhi DC/monocytes
T cells
NK cells
vSMCs
Pericytes
Lymphatic ECs
Dividing VECs
Capillary VECs
Venular VECs
Arterial VECs
CLEC10Ahi DCs
NR4A1hi fibroblasts
Nervous system cells
CLEC9Ahi DCs
Dividing fibroblasts / mural cells
Dividing fibroblasts / mural cells
MERTKlo PTPRChi macrophages
Osteoblasts

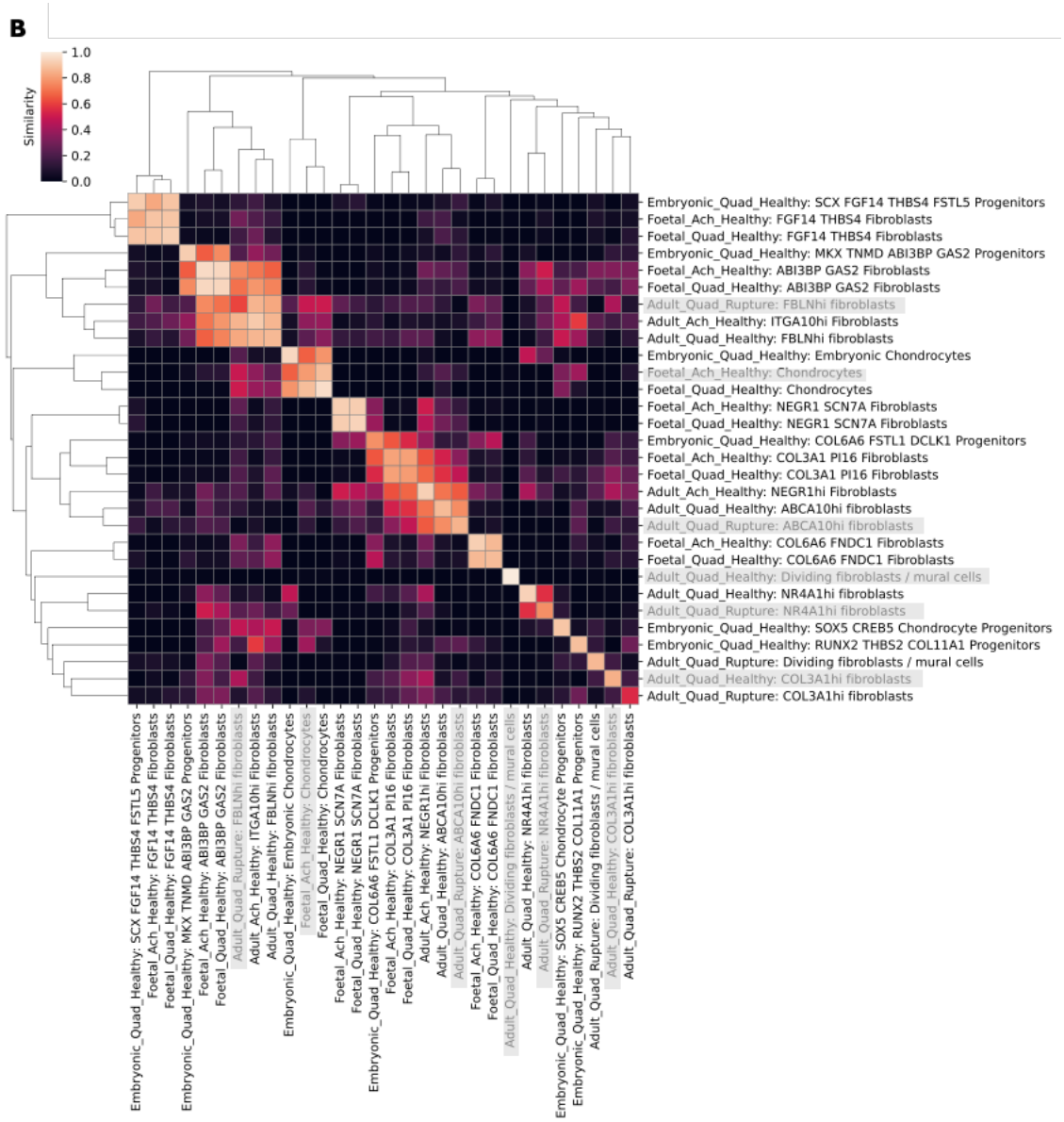


Figure 64. CellHint harmonisation of annotated cell types across different tendon datasets. (A) *Harmonisation tree plot showing relationships between annotated cell types across different studies and conditions. Transcriptional distances were calculated from the batch-corrected scVI embeddings.* ***(B)*** *Cell type cluster heatmap showing membership probabilities of cells across different clusters after harmonisation. Greyed out cell types represent unusually low cell populations within a given dataset (see Appendix Table 5).*

Importantly, tracing fibroblast populations from development to adulthood supported initial hypotheses regarding the lineage pathways of embryonic tendon progenitors. Specifically, MKX TNMD ABI3BP GAS2 Progenitors were linked to foetal ABI3BP GAS2 Fibroblasts, SCX FGF14 THBS4 FSTL5 Progenitors to foetal FGF14 THBS4 Fibroblasts, and COL6A6 FSTL1 DCLK1 Progenitors to foetal COL3A1 PI16 Fibroblasts (Figure 64A,B). Additionally, SOX5 CREB5 Progenitors, RUNX2 THBS2 COL11A1 Progenitors, and

Embryonic Chondrocytes were connected to foetal Chondrocytes (Figure 64A,B). Further comparison of the developing and adult fibroblast populations revealed significant relationships: foetal ABI3BP GAS2 Fibroblasts, forming the main body of the tendon, were linked to adult Achilles tendon ITGA10hi Fibroblasts and healthy quadriceps tendon FBLN1hi Fibroblasts (Figure 64A,B). Additionally, foetal outer LCT COL3A1 PI16 Fibroblasts and muscle LCT NEGR1 SCN7A Fibroblasts were associated with various adult fibroblast populations, including NEGR1hi Fibroblasts in the Achilles and ABCA10hi Fibroblasts in healthy quadriceps tendons (Figure 64A,B). Moreover, embryonic RUNX2 THBS2 COL11A1 Progenitors, along with foetal Chondrocytes and tendon inner LCT COL6A6 FNDC1 Fibroblasts – expressing TSPC markers and pathways involved in injury response and wound repair – were linked to ruptured adult quadriceps tendon COL3A1hi Fibroblasts (Figure 64A,B). Interestingly, foetal FGF14 THBS4 Fibroblasts found at the MTJ did not align with any adult cell populations, suggesting a unique or transient role during development.

To further assess the potential functional differences between fibroblast populations, matrisomal gene expression profiles were analysed. Adult fibroblasts exhibited reduced expression of matrisomal genes, both in terms of the number of genes and the proportion of cells expressing them, compared to developmental fibroblasts (Figure 65). Expression of collagen XI and XIV genes, both involved in early tendon formation, was low in adult populations. This trend extended to fibrillogenesis-regulating proteoglycans such as *ASPN*, *FMOD*, *ACAN*, *LUM*, *BGN*, and *OGN*, which showed diminished expression in adult fibroblast populations compared to their developmental counterparts (Figure 65).

Interestingly, the predominant population of ruptured tendon fibroblasts, COL3A1hi Fibroblasts, expressed the highest levels of collagens I, III, V, and VI (chains 1 and 3) relative to other healthy adult fibroblast populations, suggesting the involvement of these collagens in the injury response or early repair process. Concurrently, this population had the lowest level of *DCN*, which was instead highly expressed in more than half of all healthy ABCA10hi and FBLNhi Fibroblasts. Notably, an unusual group of quadriceps tendon NR4A1hi Fibroblasts, were characterised by high expression of *VCAN*, *DCN*, and *PRG4*,

potentially implicating them in roles where friction reduction is important (Figure 65).

Regarding glycoproteins, all adult fibroblasts showed minimal expression of FBN2 and ELN, which are important for elastic fibre formation and ECM elasticity (Appendix Figure 14). COL3A1hi Fibroblasts were the only adult population expressing *POSTN* and *SPARC*, both of which are associated with ECM organisation and repair. Additionally, these fibroblasts highly expressed *TNC*, *FN1*, and *EDIL3*, which are involved in cell adhesion, migration, and repair. Meanwhile, other adult fibroblast populations highly expressed *LAMA2* and *SNED1*, which regulate cell-ECM interactions (Appendix Figure 14).

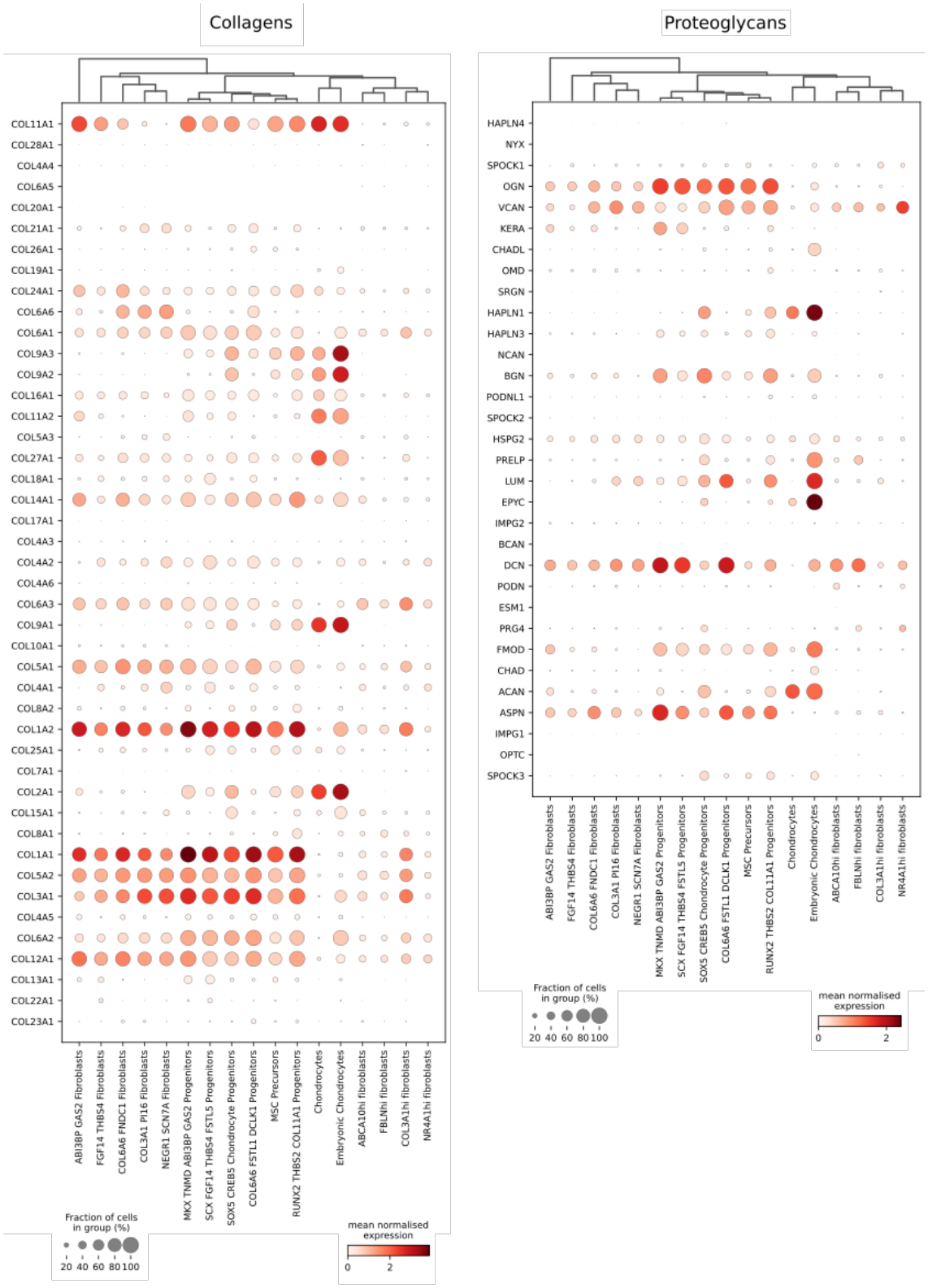


Figure 65. Embryonic, foetal, and adult tendon fibroblast proteoglycan and collagen gene expression profiles. *Dotplots of hirerchically clustered cell types show the mean normalised expression levels alognside the proportions of expressing cell types for all collagen and proteoglycan genes present in the data. The lists of matrisomal genes were obtained from the matrisomeDB database (Shao et al., 2020). The remaining matrisomal gene dotplots are shown in Appendix Figure 14.*

6.3.3 Comparison of foetal and adult fibroblast transcriptomic profiles

To gain potential functional insights to the differences between CellHint-aligned foetal and adult quadriceps tendon fibroblasts, differential gene expression analysis was performed using DESeq2 on “pseudobulked” counts. This analysis identified 262 pathways that were downregulated across both healthy and ruptured adult fibroblast types compared to developmental tendons (Figure 66). A significant number of these pathways were associated with energy metabolism, such as "oxidative phosphorylation" and "mitochondrial ATP synthesis coupled electron transport," pointing at a reduced need for high metabolic activity necessary for energy production. Additionally, pathways involved in nucleotide biosynthesis (e.g., "purine ribonucleoside triphosphate biosynthetic process", "nucleotide biosynthetic process"), protein folding and quality control (e.g., "chaperone-mediated protein folding", "proteasomal protein catabolic process"), and other transcription and translation-related regulatory pathways (e.g., "translational initiation", "regulation of RNA splicing", "RNA localization") were also downregulated, reflecting a lower requirement for nucleotide and protein synthesis and maintenance post-development. Naturally, this was accompanied by downregulation of several apoptotic and cell cycle regulatory pathways (e.g., "regulation of apoptotic signaling pathway", "mitotic nuclear division", “regulation of mitotic cell cycle”) as well as telomere maintenance pathways (e.g., "telomere maintenance via telomerase"), underscoring a reduced need for frequent cycles of division and programmed cell death used to shape and form tissues. Finally, several stress response pathways, including "response to oxidative stress" and "response to unfolded protein", showed reduced activity. Collectively, these findings imply a transition from the high metabolic and biosynthetic demands of development to a more maintenance-oriented, potentially quiescent state in all selected adult tendon fibroblasts.

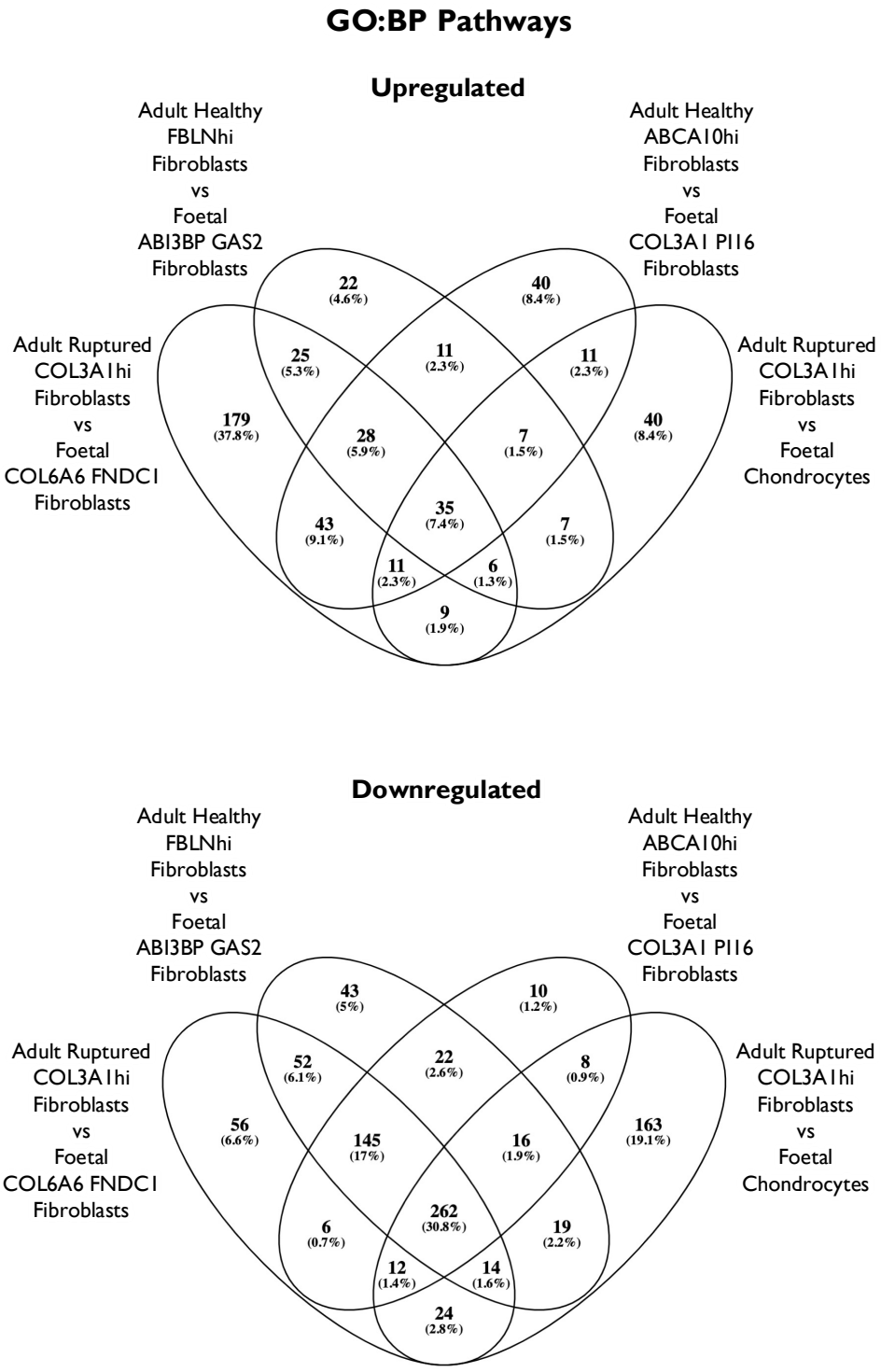


Figure 66. Venn diagrams of intersecting upregulated or downregulated gene ontology biological process (GO:BP) pathways in CellHint-paired foetal and adult cell types. *Only significant (<0.01 BH-FDR) pathways with term sizes of 20-500 were used.*

In contrast, only 35 pathways were commonly upregulated in the paired fibroblasts (Figure 66), encompassing categories such as cellular signalling, structural organisation, cell migration, and nervous system development. Enhanced pathways included "regulation of small GTPase mediated signal

transduction" and "Wnt signaling pathway", suggesting an increased emphasis on cellular functions such as growth, differentiation, and motility. This was supported by the upregulation of migration-related pathways like "epithelial cell migration" and "smooth muscle cell migration", vital for tissue remodelling and wound healing. Structural and adhesion-related pathways such as "positive regulation of cell projection organization", "cell junction assembly", "cell-substrate adhesion", "actomyosin structure organization", and "focal adhesion assembly" were also more active, indicating a focus on reinforcing cellular interactions and stability. Additionally, key nervous system pathways like "axonogenesis", "axon guidance", and "regulation of neuron projection development" were elevated, emphasizing the ongoing need for neural integration and support within the tissue matrix. Overall, these results underscore the adaptive capacity of adult fibroblasts to maintain tissue integrity, support dynamic tissue remodelling, and enhance cellular communication that is critical for functional stability and responsiveness in mature tendon tissue.

The analysis of significantly up- or downregulated matrisomal genes provided deeper insights into the functional profiles of adult fibroblasts. Relative to their linked foetal counterparts, all adult fibroblasts upregulated *extracellular matrix protein 2* (*ECM2*) and downregulated genes associated with various key functions. Specifically, they showed significantly decreased expression of genes linked to cartilage (*COL2A1*, *COL9A1*, *COL9A3*), early developmental fibrillogenesis (*LUM*), and growth factor signalling (*insulin-like growth factor binding proteins 2, 4, and 5* (*IGFBP2*, *IGFBP4*, *IGFBP5*)). Additionally, genes involved in elastic fibre formation (*EFEMP1, EFEMP2*, *EMILIN1, FBLN1, microfibril-associated glycoproteins 2* and *4* (*MFAP2*, *MFAP4*)), cell adhesion (*transforming growth factor-beta-induced protein* (*TGFBI*), *von Willebrand factor A domain-containing 1* (*VWA1*)), collagen deposition and processing (*collagen triple helix repeat containing 1* (*CTHRC1*), *procollagen c-endopeptidase enhancer* (*PCOLCE*)), and calcification inhibition (*matrix gla protein* (*MGP*)) were also downregulated. This gene expression profile indicates that adult fibroblasts are less engaged in tissue growth, additionally showing a reduction in cartilage and elastic fibre formation as well as an increased susceptibility to tissue mineralisation.

In the following section, the analysis is focused on the specific differences in gene expression within individual CellHint-aligned adult and foetal fibroblast groups, aiming to elucidate the transcriptomic transitions from highly proliferative states characteristic of foetal development to the more transcriptionally quiescent states observed in adult fibroblasts. These differences may reveal potential cellular and molecular pathways that govern fibroblast function and adaptability.

In comparing foetal inner tendon loose connective tissue COL6A6 FNDC1 Fibroblasts and adult ruptured tendon COL3A1hi Fibroblasts (Figure 67), the latter upregulated genes involved in 325 GO:BP pathways, 179 of which were unique to this comparison (Figure 66). Among those, neural and synaptic pathways such as "gliogenesis", “nerve development”, "modulation of chemical synaptic transmission", and "regulation of synapse structure or activity" were prevalent (Figure 67A). Additionally, the expression of pathways supporting muscle and vascular functions, including "positive regulation of angiogenesis", "regulation of vasculogenesis", and "cardiac muscle contraction", was also elevated. These changes coincided with an enhanced expression of immune and inflammatory response pathways, such as "myeloid leukocyte differentiation" and "regulation of macrophage differentiation". Furthermore, upregulation was also noted in pathways involved in molecular transport, calcium signalling, metabolic processes, mechanotransduction, stress responses, as well as general tissue or organ morphogenesis (e.g., “embryonic organ development”) and remodelling (e.g., “tissue remodeling”, “regulation of extracellular matrix assembly”) (Figure 67A).

Conversely, the 56 uniquely downregulated pathways (out of a total of 571) were related to cell cycle and division regulation, RNA and protein synthesis, vesicle and organelle transport, response to stimuli and stress, autophagy, apoptosis, and certain metabolic processes (Figure 67A). Notably, specific pathways related to matrisomal protein metabolism and TGF-β signalling, such as "collagen (or) proteoglycan metabolic process" and "regulation of transforming growth factor beta receptor signaling pathway," were also diminished (Figure 67A). Overall, it is evident that COL3A1hi Fibroblasts in ruptured adult tendons are engaged in a reparative program involving neural regeneration, vascular and muscle support, immune modulation, ECM

remodelling, and adaptation to mechanical stress, aimed at restoring tendon structure and function. However, unlike developing fibroblasts, they do not appear to fully exit the quiescent state and adopt proliferative capacities, potentially limiting the efficacy of adult tendon repair.

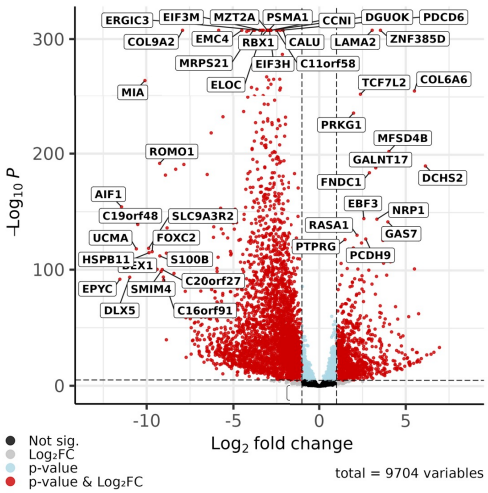
Compared to foetal COL6A6 FNDC1 Fibroblasts, adult ruptured tendon COL3A1hi Fibroblasts upregulated collagens involved in fibril assembly and regulation (*COL5A1*, *COL5A3*, *COL6A3*, *COL6A6*), mineralisation (*COL10A1*), and angiogenesis suppression (*COL18A1*) (Birk and Brückner, 2011; Ricard-Blum, 2011) (Figure 67B). In contrast, downregulated collagens included developmental fibril assembly initiators (*COL11A1-2*), basement membrane collagens (*COL8A1-2*, *COL15A1*), transmembrane collagen *COL13A1*, and *COL26A1*, known for its unusual emilin-containing domain (Ricard-Blum, 2011). Interestingly, no proteoglycans were upregulated; instead, those important for tissue development, such as *FMOD*, *BGN*, *ACAN*, *OGN*, and *podocan-like 1* (*PODNL1*), were downregulated (Figure 67B). Among the glycoproteins, those associated with scaffolding and structural support (e.g., *TNXB, LAMA2, LAMB1, FBN1, dermatopontin* (*DPT*)), cell adhesion and signalling (e.g., *neogenin 1* (*NTN1*), *netrin G1* (*NTNG1*), *intercellular adhesion molecule 10* (*IGSF10*), *spondin 2* (*SPON2*)), and tissue repair (e.g., *tumour necrosis factor alpha-induced protein 6* (*TNFAIP6*), *POSTN*) showed upregulation (Figure 67B). Conversely, proteins regulating collagen and elastic fibre formation and stabilisation (e.g., *MATN1*, *MATN3*, *MATN4*, *COMP*, *FBN3*, *ELN, EMI domain-containing protein 1* (*EMID1*)), along with specific mediators of cell adhesion and signalling (e.g., *TNC*, *THBS2*, *SPARC-related modular calcium-binding protein 1* (*SMOC1*), *EDIL3* (*EGF-like repeat and discoidin I-like domain-containing protein 3*)), as well as tissue remodelling proteins (e.g., *SPP1*, *cysteine-rich with EGF-like domains 2* (*CRELD2*), *milk fat globule-EGF factor 8* (*MFGE8*), *cartilage intermediate layer protein 2* (*CILP2*), *r-spondin 3* (*RSPO3*)) were downregulated.

This matrisomal profile further reflects an adaptation from developmental to reparative functions, characterised by the upregulation of collagens involved in fibril assembly, regulation, mineralisation, and angiogenesis suppression, paired with a decrease in collagens associated with developmental processes and tissue formation. The consistent downregulation of proteoglycans associated

with development and ECM remodelling further indicates a reduction in activities associated with early tissue formation.

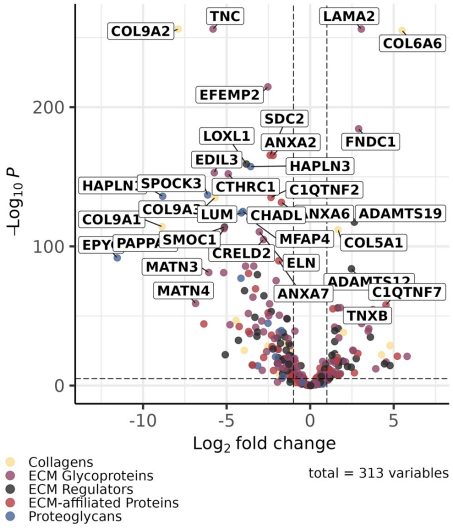
Adult Ruptured COL3A1hi Fibroblasts vs Foetal COL6A6 FNDC1 Fibroblasts (inner LCT)

A



Downregulated BH FDR <0.01 (571):	Upregulated BH FDR <0.01 (325):
- Energy Metabolism and Mitochondrial Function - Nucleotide and Ribose Phosphate Mechanism - Protein Metabolism and Folding - RNA Metabolism - Protein Translation - Cell Cycle and Division - Response to Stress and Apoptosis - Autophagy and Senescence - Responses to TGF-b Signalling	- Cell Adhesion and Extracellular Matrix Organisation - Muscle Development and Contraction - Calcium Ion Transport and Homeostasis - Neuron and Synapse Development and Organisation - Cell Signalling and Transduction (Wnt signalling, GTPase, Rac, Rho, and GPCR transduction pathways) - Organ/Tissue Developmental Processes and Cell Growth - Vascular Development and Blood Circulation - Cell Migration and Morphogenesis - Immune and Inflammatory Responses

B



Downregulated padj <0.01, log2FC < -1 (127):	Upregulated padj <0.01, log2FC > 1 (66):
Collagens: COL9A1, COL9A2, COL9A3, COL8A1, COL2A1, COL26A1, COL11A2, COL11A1, COL15A1, COL8A2, COL13A1 **Proteoglycans:** EPYC, HAPLN1, SPOCK3, PODNL1, LUM, CHADL, PRELP, FMOD, ACAN, OGN, SPOCK1, OMD **Glycoproteins:** MATN4, MATN3, TNC, EDIL3, EFEMP1, SMOC1, CTHRC1, MATN1, MFAP2, PCOLCE2, CILP2, MFAP4, NPNT, NELL2, LTBP1, IGFBP2, ELN, TSKU, FBN3, CRELD2, VWA1, CRISPLD2, EFEMP2, MFGE8, IGFBP5, MFAP1, IGFBP3, GAS6, RSPO3, FBLN2, IGFBP4, COMP, MGP, TGFBI, CRISPLD1, FBLN1, SMOC2, THBS2, EMID1, AEBP1, EMILIN1, SRPX, SPARC **ECM-affiliated Proteins:** LGALS1, SDC4, GPC1, CLEC11A, SEMA3E, SDC1, SDC2, C1QTNF3, GPC5, SEMA5B, C1QTNF2, C1QTNF4, ANXA2, PLXNA4, ANXA5, ANXA7, ANXA6, LGALS3, GREM1, C1QTNF1, C1QTNF6 **ECM Regulators:** PAPPA2, CSTB, CST3, TIMP1, LOXL1, HYAL2, SERPINF1, MMP11, CTSD, CTSH, CTSK, SERPINH1, MMP28, EGLN2, CTSA, CTSB, PLOD3, PLOD1, SERPING1, P4HTM, TIMP3, SERPINI1, ADAMTS6, ADAMTS17, MMP2, SERPINE1, CTSC, MMP14, KAZALD1, ADAMTSL1, ADAM15	**Collagens:** COL6A6, COL5A3, COL10A1, COL6A3, COL5A1, COL18A1 **Glycoproteins:** HMCN2, EYS, FGL2, TNXB, NTN1, MFAP5, EMILIN2, LAMA2, FNDC1, ECM2, IGSF10, POSTN, NTNG1, DPT, LAMB1, FBN1, LAMA1, TNFAIP6, MATN2, HMCN1, RSPO2, SLIT2, ABI3BP, SPON2, POMZP3 **ECM-affiliated Proteins:** FREM3, C1QTNF7, PLXNC1, EMCN, FREM1, SEMA6C, SEMA3C, ELFN1, SEMA6D, SEMA3D, PLXNA3 **ECM Regulators:** MMP19, MMP21, ITIH5, ADAM33, ADAMTS19, ADAMTS12, PCSK6, PAPPA, ADAM32, ADAM19, ADAM12, ADAMTS2, ADAMTSL3, ADAM22, SULF2, ADAMTS9, CD109, ADAMTS15, ADAMTS5, SULF1, FAM20A, FAM20C, MMP24, SERPINB1

Figure 67. Analysis of significantly up- and downregulated genes and pathways in adult ruptured COL3A1hi Fibroblasts vs foetal COL6A6 FNDC1 fibroblasts. (A) *Volcano plot illustrating significantly up- and downregulated genes determined by the DESeq2 Wald test (p-adjusted < 0.01, log2FC ±1). The table to the right summarises the results of gene ontology (GO) biological processes (BP) analyses conducted using the gProfiler g:GOSt tool (Raudvere et al., 2019). GO:BP pathways sized 20-500 terms with Benjamini-Hochberg (BH) FDR values <0.01 were analysed and categorised by common functions (e.g. different pathways related to apoptosis were grouped together*

into an "Apoptosis" category). The numbers in brackets show the total number of different GO:BP pathways meeting the BH FDR criteria. ***(B)*** *Volcano plot and accompanying table showing significantly up- and downregulated matrisomal genes, identified using the DESeq2 Wald test (p-adjusted < 0.01, log2FC ±1).*

When compared to 17 pcw Chondrocytes, ruptured COL3A1hi Fibroblasts uniquely upregulated 40 pathways (out of 126 total) involved in cell cycle regulation, nucleotide and protein metabolism, intracellular transport, morphogenesis, and signalling (e.g., "regulation of smoothened signaling pathway", "TOR signaling", "cellular response to transforming growth factor beta") (Figure 68A). Concurrently, they uniquely downregulated 163 pathways (out of 519) related to signal transduction (e.g., "Wnt signaling", "intracellular receptor signaling"), metabolic processes, stress responses, and cellular differentiation (e.g., "regulation of stem cell differentiation", "cartilage development"). Despite the unique pathway patterns, the overall analysis was consistent with previous comparisons of COL3A1hi Fibroblasts against COL6A6 FNDC1 Fibroblasts, supporting the narrative of a shift from actively dividing cells with high metabolic demands towards a more maintenance-oriented state (Figure 68A).

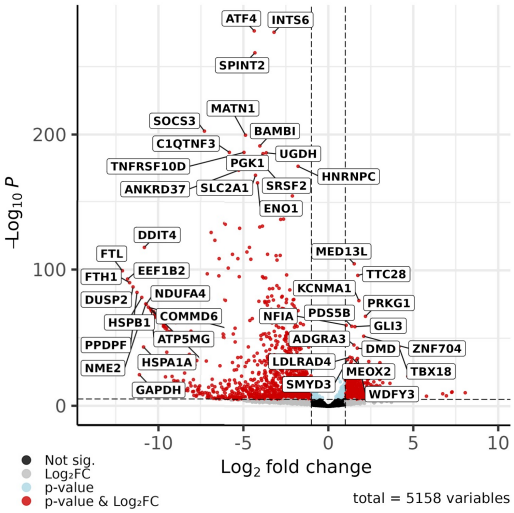
Interesting differences were observed in matrisomal gene expression (Figure 68B). Compared to foetal Chondrocytes, COL3A1hi Fibroblasts upregulated structural *COL1A1*, fibril assembly-related *COL5A2*, transmembrane *COL25A1*, cell communication and stability-supporting *COL12A1,* and mineralisation-associated *COL24A1* (W. Wang *et al*., 2012). In contrast to their upregulation in the previous comparison, basement membrane collagens *COL8A1* and *COL15A1* were downregulated in COL3A1hi Fibroblasts compared to foetal Chondrocytes (Figure 68B). Furthermore, chondrogenesis-regulating *ASPN* was upregulated, while proteoglycans involved in regulating fibrillogenesis (e.g., *FMOD*, *DCN*, *OGN*, *epiphycan* (*EPYC*), *proline/arginine-rich end leucine-rich repeat protein* (*PRELP*), *chondroadherin* (*CHAD*)), cell-matrix interactions (e.g., *sparc/osteonectin, cwcv and kazal-like domains proteoglycan 1 and 3* (*SPOCK1*, *SPOCK3*)), and tissue hydration and elasticity (e.g., *PRG4*, *HAPLN1*) were significantly downregulated. Among glycoproteins, those associated with scaffolding (e.g., *LAMA2*), cell adhesion and signalling (e.g., *TNC*, *SMOC1*, *SPON1*, *cysteine-rich secretory protein LCCL domain-containing 1* (*CRISPLD1*), *sushi, von Willebrand factor type A, EGF, and pentraxin*

domain-containing 1 (SVEP1)), and ECM remodelling (e.g., *FNDC1*, *thrombospondin type 1 domain-containing 4* (*THSD4*), slit guidance ligand 3 (*SLIT3*), *latent transforming growth factor beta binding protein 2* (*LTBP2*)) were upregulated. Conversely, the downregulated glycoproteins largely overlapped with those in the previous comparison against COL6A6 FNDC1 Fibroblasts (Figure 68B).

Overall, the matrisomal profiles of COL3A1hi Fibroblasts show significant differences when compared to foetal COL6A6 FNDC1 fibroblasts and foetal Chondrocytes, supporting distinct functional roles or these cells. Compared to foetal Chondrocytes, COL3A1hi Fibroblasts exhibit a profile that is less involved in developmental processes and more focused on structural and signalling functions necessary for maintaining and repairing adult tendon tissue. This is evidenced by the upregulation of collagens and proteins associated with cell communication and stability, suggesting an enhanced capacity for structural support. Furthermore, the increased expression of *COL1A1* and genes linked to mineralisation indicates an adaptation geared towards reinforcing the mechanical strength and durability of the tendon. Conversely, the downregulation of basement membrane collagens, along with proteoglycans involved in fibrillogenesis and proteins crucial for tissue elasticity, signifies a departure from the properties typical of developing tendon ECM, shifting towards a more fibrous and repair-oriented matrix profile.

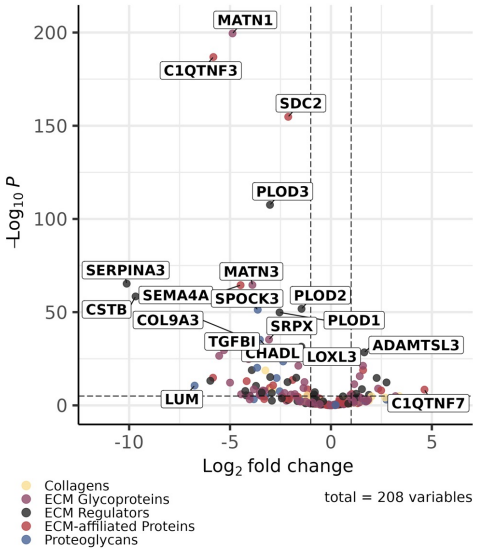
Adult Ruptured COL3A1hi Fibroblasts vs Foetal Chondrocytes

A



Downregulated BH FDR <0.01 (519):	Upregulated BH FDR <0.01 (126):
- Energy Metabolism and Mitochondrial Function - Nucleotide and Ribose Phosphate Mechanism - Protein Metabolism and Folding - RNA Metabolism - Protein Translation - Cell Cycle and Division - Response to Stress and Apoptosis - Autophagy	- Cell Migration and Adhesion - Cell Morphogenesis - Muscle Cell Development and Differentiation - Neuron and Axon Development - Limb Development and Morphogenesis - Cell Signalling (GTPase, Wnt, TGF-b, Smoothened, TOR and insulin) - Cell Cycle and Division - Metabolism and Energy Production - Protein Modification and Degradation

B



Downregulated padj <0.01, log2FC < -1 (78):	Upregulated padj <0.01, log2FC > 1 (28):
Collagens: COL9A3, COL9A2, COL6A2, COL9A1, COL2A1, COL15A1, COL8A1 **Proteoglycans:** LUM, EPYC, PRELP, SPOCK3, CHADL, DCN, HAPLN1, CHAD, SPOCK1, FMOD **Glycoproteins:** MATN4, TGFBI, MGP, MATN1, IGFBP4, CTHRC1, EFEMP1, MFAP4, MATN3, VWA1, IGFBP7, PCOLCE, IGFBP2, IGFBP5, EFEMP2, SRPX, FBLN1, MFAP2, COMP, PCOLCE2, GAS6, LAMB2, NID2, AEBP1 **ECM-affiliated Proteins:** GPC3, C1QTNF3, SEMA4A, LGALS3, LGALS1, ANXA5, ANXA2, GPC1, PLXNA2, SDC2, SDC1, GPC5, LMAN1, ANXA6, ANXA7 **ECM Regulators:** SERPINA3, CSTB, TIMP1, SERPINH1, CTSL, CTSD, LOXL1, EGLN3, SERPINE1, PLOD3, P4HA2, SERPINE2, CST3, PLOD1, TIMP3, LOXL2, MMP2, P4HA1, CTSB, LOXL3, PLOD2	**Collagens:** COL1A1, COL5A2, COL24A1, COL12A1, COL25A1 **Proteoglycans:** ASPN **Glycoproteins:** ECM2, FNDC1, LAMA2, SPON1, LTBP2, THSD4, SLIT3, SMOC1, CRISPLD1, SVEP1, TNC **ECM-affiliated Proteins:** C1QTNF7, SEMA6D, PLXDC2, COLEC12 **ECM Regulators:** CD109, ADAM12, ADAM22, ADAMTSL3, ADAMTS19, FAM20C, MMP16

Figure 68. Analysis of significantly up- and downregulated genes and pathways in adult ruptured COL3A1hi Fibroblasts vs foetal Chondrocytes. (A) *Volcano plot illustrating significantly up- and downregulated genes determined by the DESeq2 Wald test (p-adjusted < 0.01, log2FC ±1). The table to the right summarises the results of gene ontology (GO) biological processes (BP) analyses conducted using the gProfiler g:GOSt tool (Raudvere et al., 2019). GO:BP pathways sized 20-500 terms with Benjamini-Hochberg (BH) FDR values <0.01 were analysed and categorised by common functions (e.g. different pathways related to apoptosis were grouped together into an "Apoptosis" category). The numbers in brackets show the total number of different GO:BP pathways meeting the BH FDR criteria.* ***(B)*** *Volcano plot and accompanying table showing significantly up- and downregulated matrisomal genes, identified using the DESeq2 Wald test (p-adjusted < 0.01, log2FC ±1).*

Following the examination of the characteristics of tendon fibroblasts from ruptured tendons relative to developmental stages, attention is now directed

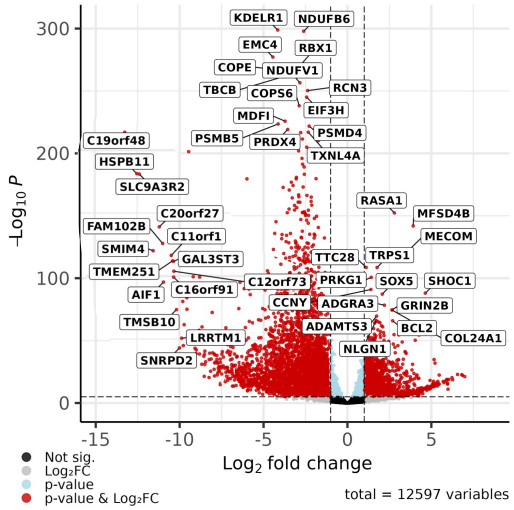
towards the properties of adult healthy tendon fibroblasts and their differences from foetal counterparts. FBLNhi Fibroblasts were compared against foetal main body ABI3BP GAS2 Fibroblasts, with a total of 141 upregulated and 573 downregulated pathways identified (Figure 69A). The former were largely in line with the previously reported maintenance-focused phenotype common to all adult fibroblasts. Among the 22 uniquely upregulated pathways were those related specifically to ion transport and regulation (e.g., "regulation of sodium ion transmembrane transporter activity", "ligand-gated ion channel signaling pathway"), cellular and molecular transport (e.g., "microtubule-based movement", "cilium movement"), and signal transduction and synaptic transmission (e.g., "synaptic transmission, glutamatergic", "Fc receptor signaling pathway"). Metabolic and catabolic processes, including "positive regulation of hydrolase activity" and "lipid modification", were also elevated. Furthermore, pathways involved in developmental processes like "positive regulation of chondrocyte differentiation" were upregulated (Figure 69A). In general, the downregulated pathways were consistent with the other comparisons, and the 43 unique identified pathways were all associated with the previously reported quiescent, less metabolically active phenotype.

Among the matrisomal genes, upregulated collagens were associated with mineralisation (*COL10A1*, *COL24A1*), basement membrane organisation (*COL4A3*, *COL8A1*), and fibrillogenesis regulation (e.g., *COL5A3*, *COL6A3*, *COL6A6*) (Figure 69B). Additionally, *COL27A1*, typically found in the enthesis (Alcaide-Ruggiero *et al*., 2021), was upregulated. Conversely, downregulated collagens included structural *COL3A1*, basement membrane *COL4A1-2*, MTJ-specific *COL22A1*, neuromuscular development-associated *COL25A1* (Munezane *et al*., 2019), and the unusual *COL26A1* (Figure 69B). The upregulated proteoglycans included cartilage-associated *OMD* and *ACAN*, as well as *interphotoreceptor matrix proteoglycan 2* (*IMPG2*), while the downregulated proteoglycans were primarily involved in fibrillogenesis and ECM modulation (*KERA*, *OGN*, *ASPN*, *DCN*, *BGN*, and *CHADL*), cell-matrix interactions (*SPOCK1*), and tissue hydration and elasticity (*HAPLN3*). Upregulated glycoproteins were primarily associated with structural support and ECM organisation of collagen fibres, cartilage matrix, and basement membrane components (e.g., *MMRN2*, *HMCN1*, *SMOC1*, *MATN2*, *COMP*, *LAMA1-3*,

CILP2), cell adhesion, migration, and signalling (e.g., *SNED1*, *TSPEAR*, *RSPO2*, *SLIT2*, *SPON1*, *ABI3BP*, *SVEP1*), and immune response modulation (e.g., *FGL2*, *CRISPLD2*) (Himes *et al*., 2014; Liu *et al*., 2008). In contrast, downregulated glycoproteins included those associated primarily with organisation and structural integrity of elastic fibres and microfibrils (e.g., *FBLN2*, *FBLN5*, *MFAP1*), mineralisation (e.g., *SPP1*, *BGLAP*), cell adhesion, migration, and signalling (e.g., *SPARC*, *SPARCL1*, *SPON2*, *THBS4*, *TNC*, *LTBP4*, *RSPO3*), and immune modulation via *TNFAIP6* and *MFGE8* (Figure 69B).

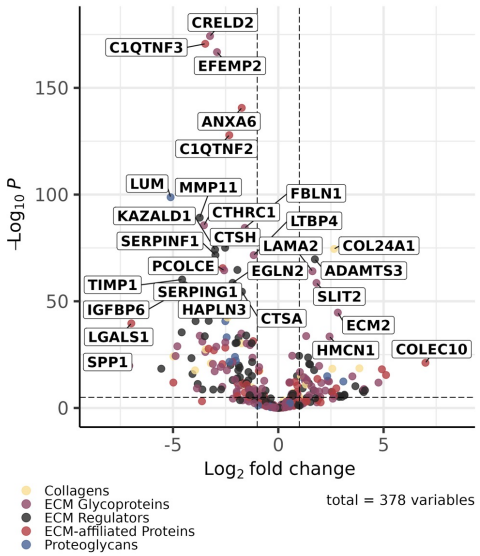
These results suggest that, compared to foetal ABI3BP GAS2 Fibroblasts, adult healthy FBLNhi Fibroblasts are oriented towards maintaining and reinforcing established structures and functions, with diminished capacity for extensive tissue remodelling and growth factor-mediated adaptability. The presence of enthesis-associated collagens like *COL27A1* as well as the upregulation of proteoglycans and glycoproteins associated with cartilaginous matrix and ECM organisation further supports a robust structural framework, essential for resilience to mechanical stress. Additionally, the downregulation of *COL3A1* points at a reduced need for this typically temporary protein structure common during tissue formation and early repair.

A



Downregulated BH FDR <0.01 (573):	Upregulated BH FDR <0.01 (141):
- Energy Metabolism and Mitochondrial Function - Nucleotide and Ribose Phosphate Mechanism - Protein Metabolism and Folding - RNA Metabolism - Protein Translation - Proteolysis, Protein Catabolism - Cell Cycle and Division - Response to Stress and Apoptosis	- Cell Migration and Adhesion - ECM Organisation - Cell Morphogenesis - Neuron and Axon Development - Limb Development and Morphogenesis - Cell Signalling (GTPase, Wnt, TGF-b, Smoothened, P3PKB) - Ion Transport - Protein and Lipid Metabolism

B



Downregulated padj <0.01, log2FC < -1 (124):	Upregulated padj <0.01, log2FC > 1 (74):
Collagens: COL9A1, COL22A1, COL9A3, COL4A1, COL3A1, COL26A1, COL6A2, COL4A2, COL2A1, COL25A1 **Proteoglycans:** LUM, HAPLN3, ASPN, DCN, SPOCK1, BGN, OGN, KERA, CHADL **Glycoproteins:** SPP1, IGFBP2, IGFBP4, IGFBP6, EFEMP1, MFAP4, MFAP2, CTHRC1, BGLAP, CRELD2, MGP, TSKU, VWA1, EFEMP2, RSPO3, FBN3, PCOLCE, TNFAIP6, IGFBP5, SPARCL1, LAMC3, VWCE, NTNG2, IGFBP3, NTNG1, FBLN2, MFAP1, SPON2, NTN4, FBLN1, EMILIN1, IGFBP7, THBS4, LGI4, MFGE8, NELL2, FBLN5, LTBP4, SPARC, TNC, TGFBI **ECM-affiliated Proteins:** LGALS1, CLEC14A, ANXA8, C1QTNF3, GPC5, GPC3, ANXA2, ANXA1, C1QTNF2, SDC4, GPC1, CLEC11A, SEMA4A, SEMA3A, SEMA7A, ANXA5, ANXA6, ANXA7, C1QL1 **ECM Regulators:** CSTB, CST3, TIMP1, SERPING1, AGT, C17orf58, HYAL2, A2M, MMP11, CTSC, TLL1, SERPINE2, F13A1, KAZALD1, SERPINF1, PLAT, CTSH, CTSK, CTSL, CTSZ, LOXL1, ADAM15, CTSF, HTRA3, MMP2, SERPINE1, CTSA, CTSD, P4HTM, P4HA2, MMP14, MMP23B, EGLN2, EGLN3, TIMP3, SERPINB6, PLOD1, PLOD3, MMP15, OGFOD2	**Collagens:** COL10A1, COL24A1, COL6A6, COL4A3, COL6A3, COL5A3, COL8A1, COL27A1 **Proteoglycans:** IMPG2, OMD, ACAN **Glycoproteins:** EYS, MMRN2, SNED1, ECM2, TSPEAR, HMCN1, NDNF, GLDN, SMOC1, NTN1, LGI2, RSPO2, MATN2, FGL2, SLIT2, COMP, LAMA2, SPON1, POMZP3, LAMA1, CRIM1, CILP2, ABI3BP, LAMA3, CRISPLD2, SVEP1 **ECM-affiliated Proteins:** COLEC10, FREM3, C1QTNF7, PLXNC1, MUC20, SEMA4G, EMCN, MUC4, MUC1, SEMA3D, PLXNB1, SFTPD, CLEC4A **ECM Regulators:** SERPIND1, MASP2, MMP19, MMP21, CELA2B, ADAM21, ADAMTS18, A2ML1, MEP1B, ADAMTS13, HPSE2, PAPPA, ADAMTS3, CD109, ADAM32, HYAL1, ADAMTS19, ADAMTS17, ADAMTS14, ADAM22, ADAMTS6, LOXL3, ADAM12, ADAMTSL2

Figure 69. Analysis of significantly up- and downregulated genes and pathways in adult healthy FBLNhi Fibroblasts vs foetal ABI3BP GAS2 fibroblasts. (A) *Volcano plot illustrating significantly up- and downregulated genes determined by the DESeq2 Wald test (p-adjusted < 0.01, log2FC ±1). The table to the right summarises the results of gene ontology (GO) biological processes (BP) analyses conducted using the gProfiler g:GOSt tool (Raudvere et al., 2019). GO:BP pathways sized 20-500 terms with Benjamini-Hochberg (BH) FDR values <0.01 were analysed and categorised by common functions (e.g. different pathways related to apoptosis were grouped together into an "Apoptosis" category). The numbers in brackets show the total number of different GO:BP pathways meeting the BH FDR criteria.* ***(B)*** *Volcano plot and accompanying table showing significantly up- and downregulated matrisomal genes, identified using the DESeq2 Wald test (p-adjusted < 0.01, log2FC ±1).*

Finally, in the comparison of adult healthy ABCA10hi Fibroblasts versus outer LCT foetal COL3A1 PI16 Fibroblasts, 186 upregulated and 482 downregulated pathways were identified (Figure 70A). Among the 40 unique upregulated pathways were those associated with cellular morphogenesis (e.g., "regulation of cell shape", "cellular component assembly involved in morphogenesis"), cell adhesion and polarity (e.g., "regulation of cell-cell adhesion", "establishment or maintenance of epithelial cell apical/basal polarity"), apoptosis and autophagy (e.g., "extrinsic apoptotic signaling pathway", "regulation of autophagy"), and signal transduction (e.g., "regulation of p38MAPK cascade", "positive regulation of NF-kappaB transcription factor activity", "epidermal growth factor receptor signaling pathway"). Additionally, pathways related to vascular and haemostasis functions (e.g., "kidney vasculature development", "blood vessel remodeling", “regulation of vascular permeability”, "platelet activation", "regulation of platelet aggregation") and muscle adaptation (e.g., “myoblast fusion”, “muscle adaptation”) showed increased activity. Interestingly, "regulation of epithelial to mesenchymal transition" was also upregulated (Figure 70A). Conversely, the 10 unique downregulated pathways were associated with metabolism (e.g., “glutathione metabolic process”, “fatty acid oxidation”), stress (“response to arsenic-containing substance”), and regulation of cell growth signal transduction (e.g., “positive regulation of TOR signaling”, “negative regulation of signal transduction by p53 class mediator”) (Figure 70A).

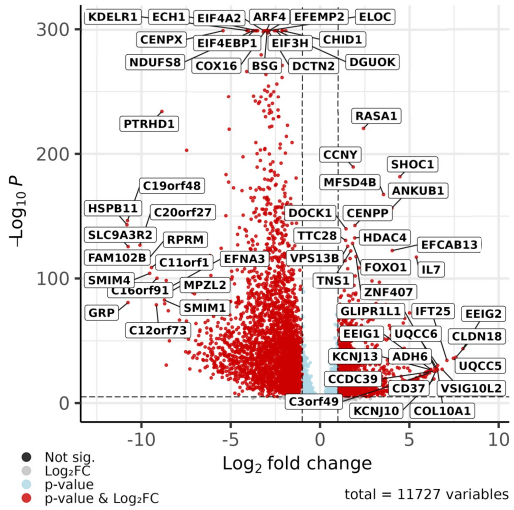
Together with the remaining common up- and downregulated pathways, these findings indicate that adult healthy ABCA10hi Fibroblasts are functionally oriented towards maintaining cellular structure and integrity, with potential enhancements in cell adhesion and autophagy. The upregulation of pathways involved in vascular development and haemostasis hints at a role in supporting vascular health and blood flow regulation, while the increased activity in muscle adaptation pathways points to their capacity to aid in muscle function. The elevated regulation of epithelial to mesenchymal transition pathway also highlights their potential for tissue remodelling and repair.

Similarly to the previous healthy comparison of FBLNhi Fibroblasts, upregulated collagens in ABCA10hi Fibroblasts were associated with mineralisation (e.g., *COL10A1*), basement membrane organisation (e.g., *COL4A1*, *COL4A3*), and fibrillogenesis regulation (e.g., *COL5A3*, *COL6A3, COL6A6*) (Figure 70B).

Additionally, *COL28A1*, which contains a cell adhesion-mediating VWF domain and is associated with nervous system structures (Veit *et al*., 2006), was uniquely upregulated. In contrast, downregulated collagens included main structural *COL1A1*, filament-forming *COL6A2*, transmembrane *COL13A1*, and the emilin-containing *COL26A1*. Upregulated proteoglycans included those linked to lubrication (*PRG4*), cell-matrix interactions and mineralisation (*CHAD*, *OMD*) as well as ECM organisation (*IMPG2*, *PODN*) (Figure 70B). In contrast, downregulated proteoglycans were associated with ECM organisation (*DCN*, *FMOD*, *ASPN*, *OGN*), cell-matrix interactions (*SPOCK3*), and tissue hydration and elasticity (*HAPLN3*). The glycoproteins analysed largely overlapped with those from the previous comparison. For instance, common upregulated glycoproteins included *MMRN2*, *HMCN2*, and *LAMA1* involved in ECM organisation, as well as *SNED1*, *RSPO2*, and *SPON1* involved in cell adhesion, migration, and signalling. Unique to ABCA10hi Fibroblasts, *vitrin* (*VIT*), *tenascin-W* (*TNN*), and the neuronal-associated *cysteine-rich motor neuron 1* (*CRIM1*) were also upregulated. Conversely, downregulated glycoproteins were predominantly involved in mineralisation (e.g., *BGLAP*), microfibril and elastic fibre assembly (e.g., *FBLN2*, *FBLN5*, *FBN3*, *MATN4*), and neural system-associated activities (e.g., neural EGFL-like 2 (*NELL2*), reelin (*RELN*), neuron-derived neurotrophic factor (*NDNF*)), cell migration and signalling (e.g., *SPARC*, *SPON2*, CRELD2), and immune modulation (e.g, *TNFAIP6* and *MFGE8)* (Figure 70B).

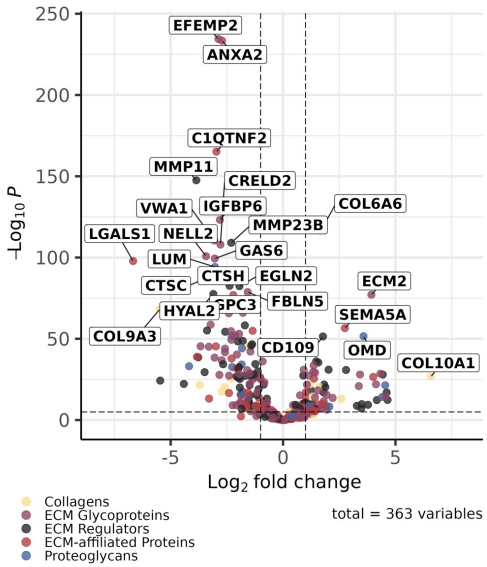
Overall, similarly to the FBLNhi Fibroblasts, ABCA10hi Fibroblasts show a profile indicative of robust ECM maintenance and structural support, with upregulation of collagens, proteoglycans, and glycoproteins involved in mineralisation, ECM organisation, and cell adhesion when compared to outer tendon LCT COL3A1 PI16 Fibroblasts. The distinctive up- and downregulation of neural-associated collagens and glycoproteins in ABCA10hi Fibroblasts suggests a specialised role in cell adhesion and signalling within the ECM, possibly reflecting a requirement for interactions with neural tissues. Additionally, the downregulation of COL1A1 and proteins involved in microfibril and elastic fibre assembly suggests a transition away from active remodelling towards sustaining the mature tendon structure and function.

A



Downregulated BH FDR <0.01 (482):	Upregulated BH FDR <0.01 (186):
- Energy Metabolism and Mitochondrial Function - Nucleotide and Ribose Phosphate Mechanism - Protein Metabolism and Folding - RNA Metabolism - Protein Translation - Proteolysis, Protein Catabolism - Cell Cycle and Division - Response to Stress and Apoptosis - "Epithelial-to-mesenchymal transition" - "Stem cell population maintenance"	- Cell Migration and Adhesion - ECM Organisation - Cell Morphogenesis - Neuron and Axon Development - Limb Development and Morphogenesis - Cell Signalling (GTPase, Wnt, TGF-b, Smoothened, P3PKB) - Ion Transport - Protein and Lipid Metabolism

B



Downregulated padj <0.01, log2FC < -1 (124):	Upregulated padj <0.01, log2FC > 1 (74):
Collagens: COL9A3, COL9A1, COL9A2, COL26A1, COL13A1, COL6A2, COL2A1, COL1A1 **Proteoglycans:** SPOCK3, LUM, ASPN, FMOD, HAPLN3, DCN, OGN **Glycoproteins:** BGLAP, NELL2, MFAP2, MFAP4, VWA1, CTHRC1, GAS6, EFEMP2, MGP, IGFBP6, CRELD2, RELN, VWCE, PCOLCE, TGFBI, IGFBP3, TSKU, FBN3, MATN4, FBLN1, SPARC, SRPX, IGFBP2, FRAS1, EFEMP1, AEBP1, COCH, FBLN5, VWA5A, TNFAIP6, EMILIN1, MFAP1, EDIL3, IGFBP5, FBLN2, NDNF, MFGE8, PXDNL, LGI4, SPON2, NID2 **ECM-affiliated Proteins:** LGALS1, ANXA3, ANXA2, ANXA5, GPC3, ANXA1, CLEC2B, CLEC14A, SDC1, SDC4, SEMA3A, SEMA4A, PARM1, C1QTNF2, C1QTNF3, C1QTNF4, C1QTNF6, ANXA6, ANXA8, LMAN1, GPC1, SDC3, SEMA4F, SEMA3D, SEMA6D, PLXNA3 **ECM Regulators:** MASP1, CSTB, MMP11, AGT, CST3, CTSC, TIMP1, CTSD, CTSH, SERPINF1, CTSD, CTSF, LOXL1, SERPINE1, P4HTM, HPSE2, EGLN2, PAPPA2, MMP23B, MMP17, MMP2, ADAMTS1, ADAMTSL2, ADAM15, ADAMTSL3, PLOD1, PLOD3, P4HTM, SERPINB6, SERPING1, LOX, F10, C17orf58	**Collagens:** COL10A1, COL4A3, COL6A6, COL5A3, COL28A1, COL4A1, COL6A3 **Proteoglycans:** PRG4, CHAD, OMD, IMPG2, PODN **Glycoproteins:** MMRN2, EYS, NTN4, ECM2, SNED1, VIT, TNN, POMZP3, HMCN2, GLDN, PCOLCE2, EGFLAM, SPON1, LAMA1, MATN2, HMCN1, FBN1, RSPO2, LAMA4, IGFBP7, CRIM1, NTNG1 **ECM-affiliated Proteins:** FREM3, SEMA5A, EMCN, PLXDC1, PLXNA2, GPC6, MUC20, CLEC3B, PLXND1, CLEC2L, SEMA5B, SEMA3C, CLEC2D, C1QTNF7 **ECM Regulators:** MASP2, MMP21, ADAMTS16, ADAM21, ADAMTS18, A2M, SERPINE3, MEP1B, ADAMTS14, ADAM32, ADAM19, CD109, TLL1, ADAMTS3, ADAMTSL3, ADAMTS19, MMP19, ADAMTS15, ADAM12, MMP24, EGLN3, MMP16, LOXL3

Figure 70. Analysis of significantly up- and downregulated genes and pathways in adult healthy ABCA10 fibroblasts vs foetal COL3A1 PI16 fibroblasts. (A) *Volcano plot illustrating significantly up- and downregulated genes determined by the DESeq2 Wald test (p-adjusted < 0.01, log2FC ±1). The table to the right summarises the results of gene ontology (GO) biological processes (BP) analyses conducted using the gProfiler g:GOSt tool (Raudvere et al., 2019). GO:BP pathways sized 20-500 terms with Benjamini-Hochberg (BH) FDR values <0.01 were analysed and categorised by common functions (e.g. different pathways related to apoptosis were grouped together into an "Apoptosis" category). The numbers in brackets show the total number of different GO:BP pathways meeting the BH FDR criteria.* ***(B)*** *Volcano plot and accompanying table showing significantly up- and downregulated matrisomal genes, identified using the DESeq2 Wald test (p-adjusted < 0.01, log2FC ±1).*

To gain a deeper understanding of these observed relationships and further elucidate the molecular underpinnings that link developing and adult fibroblast populations, gene regulatory network analysis was conducted using SCENIC. This analysis aimed to assess similarities in transcriptional regulation across different developmental stages and conditions. By identifying and quantifying the activity of specific regulons – clusters of genes regulated by a common transcription factor – SCENIC allow the comparison of the regulatory networks potentially driving the phenotypic similarities and differences between foetal and adult fibroblast populations.

Unexpectedly, there was a large number of dataset-specific regulons identified (Appendix Figure 15), with only very few regulons actively maintained across the studied stages of development and adulthood (Figure 71). One such example was the RARG (retinoic acid receptor gamma) regulon, which was active in embryonic RUNX2 Progenitors, foetal 17 pcw Chondrocytes, and adult ruptured tendon COL3A1hi Fibroblasts (Figure 71). In this data, RARG was associated with the regulation of 19 genes broadly involved in various cellular processes, including small GTPase-mediated signal transduction (*ARHGEF10L*), regulation of the PI3K/AKT signalling pathway (*PIK3R1*), and cell adhesion and migration (*BOC, PCDH9, ZFHX3*). Of particular interest were the *platelet-derived growth factor D* (*PDGFD*) and *DCLK1* genes, both of which are involved in epithelial-to-mesenchymal transition (EMT) and play important roles in wound healing (Broner *et al*., 2021; Folestad *et al*., 2018; Kong *et al*., 2008; Vijai *et al*., 2021). Interestingly, well-known EMT regulators that are regulated by SCX, *TWIST1* and *SNAI1* (Al-Hattab *et al*., 2018), were specifically highly activated in ruptured COL3A1hi Fibroblasts compared to the healthy ones (Figure 71). In this data, TWIST1 and SNAI1 regulons were associated with the regulation of 7 (*BCL7A, BICC1, CACNB2, COL1A2, HMCN1, HTRA1, PLEKHA5*) and 6 (*COL4A1, EFNB2, KDR, MIR31HG, PALLD, SLC45A4*) genes, respectively. Overall, it appears that the COL3A1hi Fibroblasts may be undergoing EMT to enable wound healing responses, making the cells more migratory and thus likely enabling them to migrate towards the site of injury.

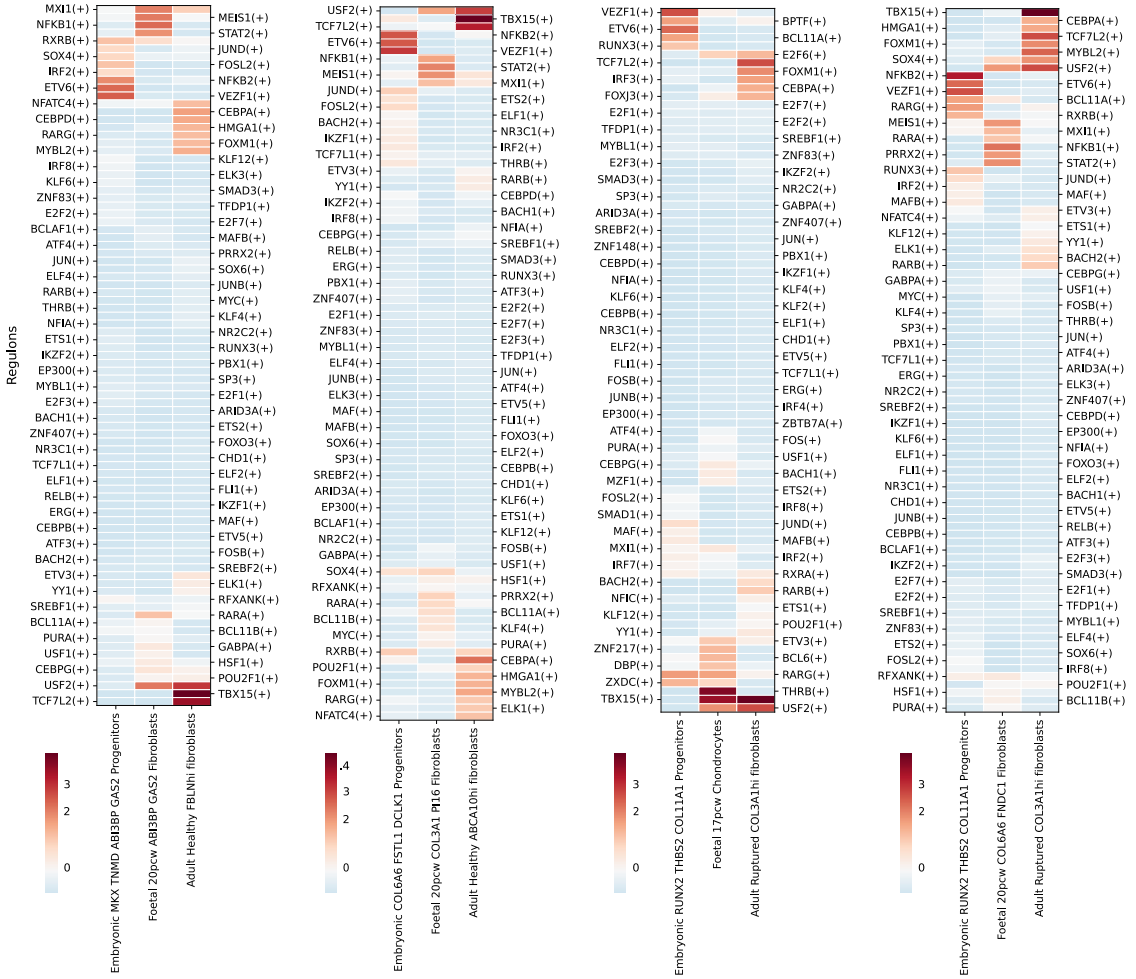


Figure 71. Comparative analysis of shared SCENIC regulon activation patterns in specific fibroblast cell types across developing and adult datasets. *Hierarchical clustermaps show summarised and z-score normalised regulon activity patterns in selected fibroblast cell types. SCENIC regulons are clustered using average linkage and Euclidean distance, while cell types remain unclustered. The colour bar quantifies the regulon activation z-score values, with blue corresponding to the below-mean activation, white representing mean activation, and red denoting above-mean activation. Regulon names are alternately labeled on the left and right axes to enhance readability. These plots show only the regulons that were shared across the different datasets. The full regulon plots including dataset-specific regulons are shown in Appendix Figure 15.*

Both ruptured and healthy adult fibroblasts as well as 17 pcw Chondrocytes showed high activation of the TBX15 regulon, which consisted of 615 associated genes. GO pathway analysis indicated a strong association of these genes with pathways involved in cellular growth and differentiation (e.g., "positive regulation of cell growth", "epithelial cell proliferation“, “positive regulation of chondrocyte differentiation”), tissue organisation (e.g., "extracellular matrix organization", "cell-matrix adhesion", “basement membrane organisation”), signal transduction and pathway regulation (e.g., "Wnt signaling pathway", "Notch signaling pathway", "response to transforming growth factor

beta", “platelet-derived growth factor receptor signalling pathway”, "phosphatidylinositol 3-kinase/protein kinase B signal transduction"), vascular, muscle, and nervous system functions (e.g., “regulation of vascular permeability”, "muscle cell development”, “axonogenesis”, "synapse organization"), and general developmental processes (e.g., "organ morphogenesis", “regulation of bone development”). TBX15 transcription factor is involved in early skeletal muscle system development in the limb, with first expression reported in the limb mesenchyme (Singh *et al*., 2005). This regulon’s activity in adulthood signifies its continued importance in maintaining and regulating tendon-specific biological processes beyond development.

Overall, these findings suggest that the regulatory networks in developing and adult tendon fibroblasts are largely distinct. The few shared regulons indicate that only a limited set of regulatory pathways – those essential for fundamental cellular functions – are preserved across both stages. Consequently, the transcriptional landscapes of tendon fibroblasts undergo substantial reprogramming from development to adulthood, reflecting distinct roles for different transcription factors and their associated gene networks in driving phenotypic and functional characteristics at each stage of maturation.

6.4 Discussion

The results of this chapter highlight the complex transcriptional landscapes and cellular dynamics that distinguish human foetal and adult tendon tissues, providing insights into the mechanisms underlying tendon development, ageing, and the adaptations to tendon rupture. Through histological examinations and matrisomal gene expression profiling, significant structural and molecular differences between developmental stages and adulthood have been uncovered. Specifically, foetal tendons manifest distinct cellular densities, morphologies, and collagen alignments compared to their adult counterparts. Furthermore, elucidation of cellular relationships across different developmental stages and ageing conditions has shed light on the uniqueness of gene regulatory networks governing tendon fibroblast-mediated homeostasis and repair mechanisms, emphasising the dynamic changes in gene expression that accompany tendon maturation.

6.4.1 Developing and aged tendon tissue comparisons

During the initial phases of foetal tendon development, a reduction in tendon cell density accompanies the increase in ECM volume and escalating mechanical demands (Grinstein *et al*., 2019; Kalson *et al*., 2015; Marturano *et al*., 2013; Schiele *et al*., 2015; Scott and Hughes, 1986). This increase in ECM is particularly marked by enhanced synthesis and aggregation of tendon collagens (Birk and Trelstad, 1986; Canty and Kadler, 2005; Humphries *et al*., 2008; Richardson *et al*., 2007), which begin to form an undulating, crimp-like structure crucial for the biomechanical functionality of the tendon (Kalson *et al*., 2015; Shah *et al*., 1982). Concurrently, cells proliferate vigorously during these developmental stages, rendering the tissue significantly more cellular compared to adult tendons (Grinstein *et al*., 2019; Marturano *et al*., 2013; Meller *et al*., 2009; Steffen *et al*., 2023a). The present study substantiates these observations, revealing a marked hypercellularity in developmental tissues, a decline in the average number of nuclei per surface area from 11 pcw onward, and the onset of collagen crimping around 12 pcw. Notably, the reduction in cellular density, which plateaus in late adulthood, correlates with a transition from a proliferative to a more homeostatic state, wherein cellular activities shift from growth to maintenance.

A novel observation in this thesis is the alteration in nuclear morphology within the 11-20 pcw foetal tendons, which likely reflects adaptive cellular responses to mechanical and biochemical cues within the developing tissue. Initially, elongated nuclei are observed, indicative of cellular migration and alignment necessary for establishing the ECM framework during early foetal development. By 15 pcw, nuclei become more rounded, likely correlating with increased ECM synthesis activity. This aligns with the previous findings showing that as the pluripotent stem cells undergo differentiation, their nuclei become progressively smoother and rounder due to the onset of differentiation and the acquisition of a perinuclear actin cap (Khatau *et al*., 2012). Finally, the re-elongation of nuclei towards the later stages of foetal development and in adulthood likely represents a return to a state optimised for tensile loading and force transmission (Kalson *et al*., 2015; Schiele *et al*., 2015; Theodossiou and Schiele, 2019). The observation that adult tendon nuclei, particularly within the

midbody, mirror the nuclear morphology seen in the later stages of foetal development (17-20 pcw) is particularly significant. This suggests that the structural adaptations occurring during late foetal development are preserved into adulthood, providing a foundation for lifelong tendon functionality. It also highlights the critical role of the late foetal period in establishing the baseline morphological characteristics of adult tendons.

In addition to insights into nuclear morphology and cellularity, this study has also uncovered significant changes in the ECM across tendon development and adulthood. Firstly, there is a comparative abundance of ground substance during development compared to adulthood, as observed in alcian-stained tissues and matrisomal gene expression analyses. This finding aligns with previous research indicating that aged tendons have reduced proteoglycan content, contributing to a stiffer, less elastic tendon with diminished regenerative capacity (Delabastita *et al*., 2019; Korcari *et al*., 2023; Peffers *et al*., 2014). This contrast highlights the pivotal role of proteoglycans in the developing tendon environment, where a proteoglycan-rich ECM fosters conditions essential for viscoelasticity, collagen fibrillogenesis, cellular migration, differentiation, and morphogenesis (see sections 2.3.2.2 and 2.3.2.3).

Secondly, the initial low birefringence observed in foetal tendon collagens increases progressively with development, indicating an ongoing process of collagen alignment and crosslinking. Birefringence, a measure of the orderly arrangement of collagen fibres, rises as these fibres become more organised and tightly aligned, suggesting enhanced structural maturation (Wolman and Kasten, 1986). This process is supported by previous research demonstrating a decrease in the ratio of collagen types III to I within tendon fascicles during development (Birk and Mayne, 1997; Bland and Ashhurst, 1997; Buckley *et al*., 2013; Kuo *et al*., 2008). Importantly, this developmental pattern mirrors the processes observed in tissue repair and regeneration, where the initial deposition of collagen III-rich ECM with low birefringence is followed by remodelling into highly birefringent collagen type I (Bruns *et al*., 2000). Overall, this parallel emphasises that the processes observed in tendon maturation closely resemble those in tissue repair and regeneration.

6.4.2 Developing and aged tendon cellular compositions and fibroblast transcriptomic profiles

In the analysis of developing and aged tendon cellular compositions and fibroblast transcriptomic profiles, key distinctions and similarities between embryonic, foetal, and adult tendon cells were revealed through the use of combined scRNA-seq and snRNA-seq datasets. The results highlighted a clear contrast in the preservation and differentiation of non-fibroblast and fibroblast populations throughout tendon development. Non-fibroblast cells, such as immune and endothelial cells, consistently clustered together and shared key differentially expressed genes across developmental stages. This suggests a stable, fundamental role in tendon biology, indicating these cells may maintain basic physiological functions across the lifespan. In contrast, fibroblast populations showed significant age- and health-specific heterogeneity, characterised by distinct differentially expressed genes and clear separation in dimensionally reduced embeddings between developmental and adult stages. This heterogeneity implies that fibroblast populations are more responsive to the demands of the tendon niche, adapting dynamically to changes in tissue state and mechanical requirements, unlike the more conserved non-fibroblast populations.

The findings concerning the immune cells are of particular importance due to their implications for tendon injury responses. The immune cell repertoire in adult tendons, comprising diverse lymphoid and myeloid cell lineages, contrasts markedly with foetal tendons where macrophages are predominant. This diversity creates a complex immunological environment where achieving a balance between pro- and anti-inflammatory responses becomes challenging. Research has shown that prolonged inflammation, especially involving lymphoid cells, persists at tendon injury sites in biopsies from patients with chronic tendinopathy (Millar *et al*., 2017) and in those with torn and repaired Achilles tendons (Noah *et al*., 2020). This ongoing inflammation leads to tissue degeneration and fibrosis, ultimately hindering effective repair processes (Chisari *et al*., 2020; Garcia-Melchor *et al*., 2021; Hou *et al*., 2021; Millar *et al*., 2017; Noah *et al*., 2020; Russo *et al*., 2022). Conversely, the simpler immune environment in foetal tendons, dominated by macrophages, supports their role in tissue development and repair, promoting an anti-inflammatory environment

conducive to growth and healing (Chisari *et al*., 2020; Epelman *et al*., 2014; Howell *et al*., 2021; Muscat *et al*., 2022; Wynn *et al*., 2013). These distinctions in immune cell composition between foetal and adult tendons underscore different strategies for managing tendon injuries, suggesting that adult tendons require a nuanced immune response to support complex repair processes, whereas foetal tendons achieve rapid tissue growth and efficient repair through a streamlined, macrophage-driven response.

In addition to the differences in immune cell repertoires, this work identified several unique or transient cellular populations in developing and adult tendons. Foetal FGF14 THBS4 Fibroblasts, localised at the MTJ, were found exclusively during development, suggesting a specific and transient role most likely related to MTJ formation and strengthening. In contrast, Adipocytes, NR4A1hi Fibroblasts, and a population of quadriceps tendon Nervous System Cells, absent during development, were observed in adult tendon tissues, indicating potential adaptations to ageing or pathological changes (Sim *et al*., 2022). Furthermore, the detection of a rupture-specific COL3A1hi Fibroblast population in adult tendons, which expresses several genes typically active during foetal development, suggests that tendon injuries may initiate a partial reactivation of developmental pathways. This phenomenon is not unique to tendons; similar processes have been observed in other injured tissues such as skin and kidneys, where specific developmental mechanisms are reactivated under certain conditions to promote early stages of repair (Bielefeld *et al*., 2013; Little and Kairath, 2017; Matsubayashi and Millard, 2013). The reactivation of these foetal genes in adult tendon fibroblasts following injury implies that these cells may revert to a more 'primitive' state, potentially enhancing their capacity for tissue regeneration and repair. However, despite this reactivation, repair processes often result in scar formation and adhesions, indicating that other factors and changes in the adult fibroblasts' overall transcriptomic profiles influence the repair outcome.

As tendons age, there is a documented decline in the metabolic and synthetic activity of tendon cells, correlating with increased stiffness and reduced elasticity in the tissue (Almekinders and Deol, 1999; Delabastita *et al*., 2019; Ippolito *et al*., 1980; Kannus *et al*., 2005; Nakagawa *et al*., 1994; Strocchi *et al*., 1991). This physiological shift is reflected in the results of the pseudobulk DGE

analysis, which revealed a significant transition in all adult fibroblasts from the heightened metabolic and biosynthetic activities typical of foetal development to a more subdued, maintenance-oriented state. Importantly, this shift is accompanied by the upregulation of pathways involved in cellular growth, differentiation, signalling, structural organisation, cell migration, and nervous system development, coupled with the downregulation of pathways related to the formation of cartilage and elastic fibres. Additionally, the observed reduction in the expression of matrisomal genes, particularly proteoglycans and collagens involved in early fibrillogenesis, in adult fibroblasts compared to their developmental counterparts reflects the reduced demand for new ECM synthesis once tendon maturation is complete, aligning with the biological need for greater tissue stability and durability in the adulthood (Birk and Trelstad, 1986; Humphries *et al*., 2008). Together, these adaptations suggest that adult fibroblasts are geared towards maintaining tissue homeostasis rather than promoting growth. However, the decreased focus on cartilage and elastic fibre formation along with the increased susceptibility to tissue mineralisation may contribute to the reduced elasticity and increased stiffness observed in aged tendons, potentially exacerbating the decline in tendon function and increasing the risk of injury.

Further insights are derived from the comparative analysis of linked foetal and adult fibroblast populations. Specifically, the comparison between foetal tendon main body ABI3BP GAS2 Fibroblasts and loose connective tissue COL3A1 PI16 Fibroblasts with adult healthy FBLN1hi and ABCA10hi Fibroblasts, respectively, demonstrates a significant shift in adult fibroblasts towards maintaining and reinforcing established structures and functions. Both adult fibroblast populations upregulate matrisomal genes critical for collagen type V and VI-mediated fibril assembly and regulation, mineralisation, ECM structural support, and cell migration, all of which are essential for creating a robust structural framework that is resilient to mechanical stress (Al Makhzoomi *et al*., 2021; Kalson *et al*., 2015). Concurrently, they downregulate matrisomal genes involved in developmental fibrillogenesis and elasticity, as well as specific genes linked to cell migration and immune modulation.

Distinct differences emerge when examining the specific functional adaptations of these adult fibroblast populations. FBLN1hi Fibroblasts, associated with the

main tendon body, exhibit upregulation in pathways linked to a variety of maintenance-related activities, including ion transport and regulation, cellular and molecular transport, metabolic regulation, and signal transduction and synaptic transmission. Additionally, they uniquely upregulate genes supporting enthesis function while downregulating genes linked to the MTJ and neuromuscular development. This suggests a focus on processes that contribute to the stability and resilience, aligning with their role in maintaining the integrity of the main fibrillar tendon body without fostering development of adjacent structures (McNeilly *et al*., 1996; Kannus, 2000; Franchi *et al*., 2007; Kalson *et al*., 2015, Steffen *et al*., 2023b).

In contrast, loose connective tissue-associated ABCA10hi Fibroblasts upregulate pathways critical for cellular adhesion, morphogenesis, vascular development, and muscle adaptation, indicating a comprehensive role in supporting tendon resilience and integration with surrounding tissues. The unique upregulation of genes such as *VIT*, *TNN*, and *CRIM1* further supports their involvement in interfacing with vascular, neural, and smooth muscle populations, typical of tendon loose connective tissue functions. However, these cells show a downregulation in pathways associated with neural system activities, which may reflect a specialised adaptation to their local microenvironment.

Importantly, the comparison between foetal COL6A6 FNDC1 Fibroblasts or Chondrocytes and adult rupture-specific tendon COL3A1hi Fibroblasts shows that the latter not only upregulate pathways essential for tendon homeostasis, but also tendon repair, including neural, vascular, and muscle support, immune modulation, ECM remodelling, and adaptations to mechanical stress. Similar to the healthy adult fibroblasts, their matrisomal profile also reveals upregulation of collagens involved in type V and VI-mediated fibril assembly and regulation, mineralisation, as well as angiogenesis suppression, with an accompanying increase in specific glycoproteins involved in laminin-based ECM scaffolding, cell adhesion, and tissue repair and remodelling. Concurrently, there is a decrease in collagens and proteoglycans associated with developmental fibrillogenesis and tissue formation, alongside a reduction in proteoglycans that contribute to cartilaginous and elastic ECM structures and specific genes that regulate cell adhesion.

Finally, the distinct regulatory networks observed between developing and adult tendon fibroblasts underscore significant transcriptional reprogramming from development through to maturity. The minimal overlap of regulons shared between these stages highlights the specialised roles of different transcription factors in dictating the phenotypic and functional characteristics of fibroblasts at each stage of maturation. For instance, the presence of pathways and regulons related to the epithelial-to-mesenchymal transition in adult ruptured fibroblasts suggests a role for this process in tendon healing. Typically associated with wound healing and cancer, it is a complex process involving a transformation of cells into a more migratory and invasive phenotype (Kalluri and Weinberg, 2009). This adaptation could therefore be crucial for the repair processes following tendon injuries, facilitating cell movement and tissue remodelling, and would require further investigation.

Overall, the shift from the active developmental expansion of tendons to a lower metabolic maintenance state in adulthood likely represents an evolutionary adaptation where adult tendons trade some regenerative potential for increased resilience against mechanical stresses, thus mitigating further injury risk. Understanding these changes could be useful for developing therapeutic strategies that not only enhance tendon repair, but also ensure the maintenance of tissue strength and functionality. By specifically targeting these pathways and potentially recreating aspects of the native developmental tendon niche, therapeutic approaches could foster more effective regeneration.

6.4.3 Limitations and significance

Despite the promising findings, this study faces several limitations that need to be addressed to strengthen the conclusions and facilitate future research. In addition to the previously discussed challenges of integrating single-cell and single-nucleus RNA-seq data with strong batch effects (see section 5.4.2), a further complication arises from using different alignment and mapping tools for adult and developmental datasets – kallisto and CellRanger, respectively. This discrepancy could potentially lead to the misidentification of the same biological transcripts as different ones, complicating data integration and analysis. However, it this issue should not significantly impact the study's findings, as no major problems were identified at any stage of the analysis.

Another limitation is related to the tissue accessibility for the histology study. The inability to achieve balanced groups with fully representative samples of healthy or diseased adult tissues containing all microanatomical regions resulted in considerable inter- and intra-donor variations. Efforts are underway to rectify this limitation by collecting and staining more samples to ensure a more comprehensive and representative dataset in future studies.

A further limitation stems from the absence of paediatric samples from the analysis. This gap hinders the ability to bridge the vast transcriptomic differences between developing and aged tendons, leading to reliance on CellHint-based predictions regarding the relationships between fibroblast populations. Additionally, the lack of imaging and spatial data validation is another notable limitation, restricting the ability to generalise the likely functions of identified adult fibroblasts. Therefore, future work will focus on including younger samples as well as carrying out cell identity-focussed imaging and spatial visualisation to provide a more continuous view of the transcriptomic landscape across different life stages, enhancing the understanding of tendon development and aging.

Of course, transcriptional profiling alone is limited, with any potential identified cell types, regulatory pathways, and gene expression changes requiring functional validation through *in vitro* and, ideally, *in vivo* experiments. Collaborative efforts with the Galloway group are currently addressing this limitation by mapping the human tendon data to established tendon repair models in zebrafish and mice. Early results from this collaboration are promising, paving the way into the future functional validation studies of developing tendon cellular and ECM niches in tendon repair.

In conclusion, despite the limitations, the findings of this work significantly advance our understanding of human tendon development and maturation by elucidating the dynamic transitions in tissue properties, cellular populations, and transcriptomic profiles from development through to adulthood. This research highlights the critical roles of cellular and ECM changes in shaping tendon properties and underscores the continuity between foetal development and adult tendon morphology, emphasising the importance of late developmental stages in determining adult tendon characteristics. Moreover, it reveals the

adaptive capacity of adult fibroblasts to maintain tissue integrity and support dynamic remodelling while also pointing to their limited proliferative capacity and ability to reactivate developmental programs in response to injury as potential targets for therapeutic intervention. By detailing these processes, the study sets a robust foundation for future research aimed at validating the molecular mechanisms driving these transformations. It is hoped that these findings will pave the way for developing targeted therapies to improve tendon repair and maintain tendon health throughout an individual's life.

Chapter 7: Discussion and Conclusions

7.1 Introduction

The study of tendinopathies and tendon injuries requires a deeper understanding of the cellular and molecular mechanisms underlying tendon development, aging, and repair. Current therapeutic strategies often focus on symptom management rather than addressing root causes or promoting comprehensive tissue regeneration. This deficiency largely results from research gaps, particularly in understanding human tendon development. Therefore, the primary aim of this research was to begin elucidating these fundamental aspects by examining the transcriptional landscapes of human tendons across various developmental stages, from embryonic to aged healthy and ruptured tissues.

This thesis provides a detailed investigation into the anatomy and physiology of human tendons, emphasising the transitions that occur during development and ageing. Utilising single-nucleus, and spatial RNA-sequencing techniques, the research characterises the key cell types and their spatial distributions within maturing foetal tendons. The origins of these cells are traced back to embryonic stages, offering insights into the lineage pathways and transcriptional regulators that guide early, intrinsically regenerative tendon formation. Additionally, a comparative analysis between the histological and transcriptional profiles of aged and developing tendons highlights critical disparities, shedding light on the dynamic changes that occur over time.

The findings from this thesis aim to fill the existing gaps in tendon biology, providing a foundation for the discovery of novel therapeutic targets and the development of strategies to enhance tendon repair. This discussion synthesises the results from each chapter, contextualising them within the broader field and exploring their implications. The strengths and limitations of the study are critically evaluated, and future research directions are proposed to further advance the understanding of tendon biology and translate these insights into effective clinical interventions.

7.2 Summary of Findings

7.2.1 Cellular heterogeneity and functional specialisation in foetal tendon development

This work has revealed the complex cellular heterogeneity in 12, 17, and 20 post-conception week foetal Achilles and quadriceps tendons. Using single-nucleus and spatial RNA-sequencing, 14 distinct cell types were identified and mapped back to the tissue of origin. Those cells encompassed various fibroblasts and myocytes, as well as immune, endothelial, and nervous system cells. Among these, five major types of fibroblasts were localised within different compartments of the foetal tendon, each uniquely contributing to tendon structure and function.

The largest fibroblast population, ABI3BP GAS2 Fibroblasts, was predominantly located throughout the main fibrillar body of the tendon. Characterised by high expression of matrisomal genes and transcription factors like *SCX*, *MKX*, and *SOX5*, these cells expressed markers associated with fascicular TSPCs (see Table 1) and appeared to be the main drivers of fibrillar tendon-specific ECM production, including collagen I fibril assembly, organisation, and reinforcement. Additionally, these cells actively contributed to modulation of immune cell activity and suppression of features specific to contractile tissues. Temporal DGE analysis indicated a functional shift in these fibroblasts towards enhanced ECM processes and pattern formation between 12 and 20 pcw, emphasising their importance in tendon growth and maturation.

COL6A6 FNDC1 Fibroblasts, found throughout tendon interfascicular matrix (i.e., endotenon), appeared as regulators of early tendon fibrillogenesis. These fibroblasts expressed injury-responsive sheath TSPC markers *TPPP3* and *PDGFRA* and upregulated genes involved in fibril synthesis, wound healing, and injury responses. Temporal DGE analysis suggested their involvement in tissue healing and repair, highlighting their significance in maintaining structural and functional tendon integrity through initial matrix deposition and microfibrillar network formation. Conversely, COL3A1 PI16 Fibroblasts, localised within the outer loose connective tissue layers (i.e., epi- and/or paratenon), shared transcriptional similarities, including TSPC markers, with COL6A6 FNDC1 Fibroblasts. However, these cells appeared more focused on cell

morphogenesis, remodelling, and cell interactions. Moreover, they appeared to have a role in modulating cellular activities such as differentiation and vascularisation, suggesting an involvement in maintaining tendon integrity, facilitating integration with adjacent structures, and managing tendon adaptation to mechanical and biological demands.

Residing primarily at the tendon-muscle tissue boundaries, FGF14 THBS4 Fibroblasts expressed MTJ-associated genes such as *COL22A1* and *THBS4*. Their transcriptomic profile indicated versatile roles in ECM synthesis, vascularisation, immune interactions, and various developmental processes, implicating them as key mediators of muscle-tendon crosstalk and MTJ integrity. Additionally, NEGR1 SCN7A Fibroblasts, located in the muscle endo- or perimysium near the MTJ, likely contributed to the structural and functional integration of tendon and muscle tissues. These fibroblasts appeared involved in muscle-like ECM organisation and neuronal support. The decreasing prevalence of both these muscle-connected populations from 12 to 20 pcw suggested a transient role in early musculoskeletal development, contributing to overall tendon tissue architecture and neural innervation.

Among non-fibroblast populations, *PECAM1*$^{+}$ vascular and *PROX1*$^{+}$ lymphatic endothelial cells, alongside *ACTA2*$^{+}$ smooth myocytes, contributed to vascular support and structural integrity within tendons. Innervating cells expressing neural markers such as *NRXN1*, *NCAM2*, and *SOX10,* with transcriptomic similarities to glial cells, suggested a supportive role in neural development and tendon innervation. Additionally, *PAX7*-expressing satellite cells and myocytes, likely originating from MTJ regions, exhibited gene expression patterns indicative of involvement in muscle differentiation and function, supporting the interconnectedness of muscle and tendon development. Finally, immune cells – primarily foetal macrophages expressing *F13A1*, *MRC1*, and *CD163* – contributed to tendon tissue development, although their proportion decreased over time, suggesting a temporal role in immune regulation during tendon maturation. Many of these cell populations are also observed across existing studies on adult tendons (see Table 1), reinforcing the notion that these cell types are established early and play diverse roles in the development and maintenance of tendon tissues.

7.2.2 Differentiation pathways and lineage commitments in embryonic and foetal tendon development

To provide a comprehensive view of the cellular and molecular mechanisms driving early tendon development, the transition from embryonic to foetal stages was examined using single-cell and spatial RNA-sequencing data from human 6-9 pcw embryonic limbs provided by the Teichmann group (B. Zhang *et al*., 2023). A random forest classifier was trained on tendon-specific regions isolated from 8 pcw spatial RNA-seq data and then applied to the scRNA-seq data, identifying seven embryonic tendon cell types, ranging from early multipotent progenitors to more lineage-committed states. Trajectory analysis revealed the lineage pathways and transcriptional regulators guiding these cells toward distinct lineages, mapping their progression into foetal stages.

Among the identified cell populations, the earliest progenitors were classified as MSC Precursors or Connective Tissue Stem Cells. Detected at 6.5 and 7.2 pcw, these cells appeared multipotent, expressing mesenchymal differentiation regulator *HMGA2* alongside both non-myogenic (*FOXP2* and *RUNX1T1*) and myogenic (*SIX1*) fate markers. Notably, these cells did not express canonical mesenchymal stem cell markers. Nevertheless, subsequent RNA velocity and pseudotime trajectory analyses supported their multipotent potential, indicating a clear propensity of these progenitors to differentiate towards cartilage, fibrillar tendon, and MSC-like tendon connective tissue lineages.

The transition of MSC precursors to the cartilage lineage began early in pseudotime at 7.2 pcw with the emergence of RUNX2 THBS2 Progenitors. These cells were transcriptionally similar to MSC precursors but additionally expressed tendon matrisomal genes and genes that regulate both chondrogenic and osteogenic fates. This lineage pathway narrowed with the shift towards SOX5 CREB5 Progenitors from 7.2 pcw onward, which focused explicitly on chondrogenesis. These progenitors regulated key chondrocyte-specific genes essential for early differentiation, such as *SOX5*, *SOX6*, *SOX9*, *ACAN*, and *COL2A1*. As these cells differentiated into embryonic Chondrocytes observed from 9.0 pcw onward, their expression of cartilage-specific genes intensified and became more defined, including genes like matrilins 1, 3, and 4. This

differentiation process led to their eventual maturation into foetal Chondrocytes by 17 pcw.

MSC Precursors were also observed to differentiate along two distinct pathways: towards SCX-expressing MKX TNMD ABI3BP GAS2 Progenitors of the fibrillar tendon lineage, and towards SCX-negative COL6A6 FSTL1 DCLK1 Progenitors of the loose connective tissue lineage. This differentiation process likely proceeded through an intermediate state of SCX FGF14 THBS4 FSTL5 Progenitors, which were observed from 7.2 pcw onward and expressed genes involved in establishing the tendon foundational structure, tissue compartmentalisation, and integration with adjacent tissues.

As these cells committed to the fibrillar tenocyte lineage, they further differentiated into MKX TNMD ABI3BP GAS2 Progenitors, observed from 8.4 pcw onward. These progenitors focused on specialised tendon structure and function, evidenced by increased expression of tendon-specific ECM genes and the crosslinking enzyme *LOX*, as well as a reduction in basement membrane and MTJ collagens. Probabilistic descendant analysis showed that 9 pcw MKX Progenitors transitioned exclusively towards 12 pcw foetal fascicular ABI3BP GAS2 Fibroblasts.

Concurrently, commitment to the loose connective tissue lineage became evident as SCX Progenitors ceased *SCX* expression and transitioned towards *SCX*-negative COL6A6 FSTL1 DCLK1 Progenitors. These progenitors, observed around 8.4 pcw, expressed the FSTL1 marker of the epi- and peritenon cells alongside canonical MSC markers such as *TWIST2*, *CD73*, *CD90*, *CD44*, and *CXCL12*. Moreover, they expressed genes essential for the development and function of tendon loose connective tissue, including *COL3A1*, *OSR1, LUM,* and *ELN*. Descendants of these cells were predicted to transition towards 12 pcw foetal LCT COL3A1 PI16 Fibroblasts, and COL6A6 FNDC1 Fibroblasts, or muscle NEGR1 SCN7A Fibroblasts.

Probabilistic fate modelling of transitions between 7.2 and 8.4 pcw embryonic cells and the most differentiated fibroblast cells at 20 pcw revealed significant distinctions in cell lineage commitments. Commitment to fascicular, loose connective tissue, and chondrocyte fates occurred late in embryonic development, around 8 pcw, with increased cell type-specific specialisation and

significant anti-correlation observed in lineage drivers. The ABI3BP GAS2 Fibroblast fascicular tenocyte lineage exhibited higher commitment probabilities, indicating more definitive differentiation pathways compared to the broader spread of other lineages. SCENIC analysis further uncovered extensive transcriptional heterogeneity and a lack of definitive fibroblast-specific regulators even at 20 pcw, highlighting the transcriptional plasticity and diverse origins of these cells. This contrasts sharply with the more stable and defined regulatory states of non-fibroblast cells such as myocytes and endothelial cells, emphasising the unique adaptability and multifaceted roles of fibroblasts in tendon development and maturation.

Overall, the differentiation pathways of MSC Precursors into various fibroblast lineages reveal the complexity of tendon development, offering deeper insights into the cellular populations that drive late embryonic and foetal tendon tissue formation and specialisation.

7.2.3 Comparative analysis of structural and molecular changes in developing and aged tendons

To understand how cellular populations and lineages established during development evolve to meet the functional demands of mature tissue, histological and snRNA-seq data from adult (25-84 years) human Achilles and quadriceps tendons were compared with those from developing tendons.

Histological examinations uncovered significant structural and molecular disparities between foetal and adult tendons. Specifically, foetal tendons displayed higher cellular densities, vascularity, and a greater abundance of ground substance compared to their adult counterparts, which translated into higher Bonar scores typically associated with pathological features. Quantification of nuclei-associated features revealed changes in nuclear morphology in foetal tendons throughout development. Initially elongated nuclei at 11 pcw, indicative of cellular migration and alignment during early development, transitioned to rounded nuclei at 15 pcw, correlating with increased ECM synthesis. By 19 pcw, the nuclei re-elongated, optimising the cells for higher tensile loads associated with the active phases of foetal movement. In adult tendons, nuclear morphologies varied widely depending on

the tendon type and microanatomical region but averaged roughly the same nuclear lengths and areas as those observed in late foetal development.

The analysis of developing and aged tendon cellular compositions and fibroblast transcriptomic profiles also revealed significant age- and health-specific heterogeneity. Non-fibroblast cells, including immune and endothelial cells, exhibited stable expression profiles throughout tendon development and maturation, suggesting a conserved fundamental role in maintaining basic physiological functions from an early stage. However, adult tendons displayed a more complex immune cell repertoire, featuring diverse lymphoid and myeloid lineages, compared to the predominantly macrophage-driven immune environment in foetal tendons. This diversity in adult tendons may contribute to the distinct repair outcomes of tendon injuries. Furthermore, adult tendons hosted several unique cell populations not present during development, such as adipocytes and specific types of nervous system cells.

In contrast, fibroblast populations showed distinct differentially expressed genes and clear separation between developmental and adult stages, reflecting dynamic adaptations to the tendon niche. Predicted relationships included links between foetal main body-forming ABI3BP GAS2 Fibroblasts and healthy adult ITGA10hi or FBLN1hi Fibroblasts, and between foetal outer LCT COL3A1 PI16 Fibroblasts or muscle LCT NEGR1 SCN7A Fibroblasts and adult healthy NEGR1hi or ABCA10hi Fibroblasts, respectively. Additionally, connections between foetal Chondrocytes or tendon inner LCT COL6A6 FNDC1 Fibroblasts with adult rupture-specific COL3A1hi Fibroblasts suggested a potential reactivation of developmental pathways in response to injury.

While those fibroblast populations could be linked between developmental and adult stages, a few exhibited no direct counterparts in either phase. For example, FGF14 THBS4 Fibroblasts, localised at the foetal tendon MTJ, were found exclusively during development, supporting the observed compositional decrease from 12 to 20 pcw and suggesting a specific, temporal role in early MTJ formation and strengthening. In adult tendons, NR4A1hi Fibroblasts, which express both neural and fibroblast markers, emerged as a unique population with no developmental equivalent.

The thesis revealed a significant transition in adult fibroblasts from the heightened metabolic and biosynthetic activities typical of foetal development to a maintenance-oriented state. This shift involved the upregulation of pathways related to cellular growth, differentiation, signalling, and structural organisation, alongside the downregulation of pathways associated with cartilage and elastic fibre formation. The reduction in matrisomal gene expression, particularly proteoglycans and collagens involved in early fibrillogenesis, in adult fibroblasts reflected the decreased demand for new ECM synthesis once tendon maturation was complete. These adaptations suggested that adult fibroblasts were geared towards maintaining tissue homeostasis, with the decreased focus on developmental fibrillogenesis and elasticity contributing to the reduced regenerative capacity and increased stiffness observed in aged tendons. Moreover, there was minimal overlap in regulons between developing and adult tendon fibroblasts, signifying that different regulatory mechanisms are at play during the different stages of tendon development and maintenance.

Comparative analysis of linked foetal and adult fibroblast populations demonstrated significant functional adaptations. Adult FBLN1hi Fibroblasts, associated with the main tendon body, focused on maintenance-related activities such as ion transport, metabolic regulation, and synaptic transmission, while uniquely upregulating genes supporting enthesis function. In contrast, ABCA10hi Fibroblasts, associated with loose connective tissue, supported cellular adhesion, morphogenesis, vascular development, and muscle adaptation. The rupture-specific COL3A1hi Fibroblasts demonstrated a shift from developmental to reparative functions, characterised by the upregulation of collagens for fibril assembly, regulation, mineralisation, and angiogenesis suppression, paired with a decrease in collagens tied to developmental processes. These fibroblasts engaged in a reparative program supporting neural regeneration, vascular and muscle adaptation, immune modulation, and ECM remodelling. Moreover, the presence of epithelial-to-mesenchymal transition pathways suggested that this process might have played a role in tendon healing by facilitating cell movement and tissue remodelling. However, unlike their developing counterparts, these adult fibroblasts were less proliferative and metabolically active, potentially limiting the efficacy of adult tendon repair.

In conclusion, the comparative analysis of developing and adult tendons provides insights into the broader context of tendon development and aging. The changes in cellular compositions and transcriptional profiles underscore the complexity of tendon biology, revealing how developmental processes lay the foundation for tissue function and resilience in adulthood. The persistence of stable expression profiles in non-fibroblast cells throughout life stages emphasises their role in maintaining tendon integrity, while the diversity in fibroblast activities showcases their adaptability to meet specific functional demands at various stages. The findings particularly illustrate how adult tendons adapt to prioritise structural integrity and mechanical resilience over the regenerative capabilities evident in foetal tendons. This adaptation likely represents an evolutionary strategy to optimise tendon function and durability in response to increased mechanical demands and the cumulative risk of injury over a lifetime.

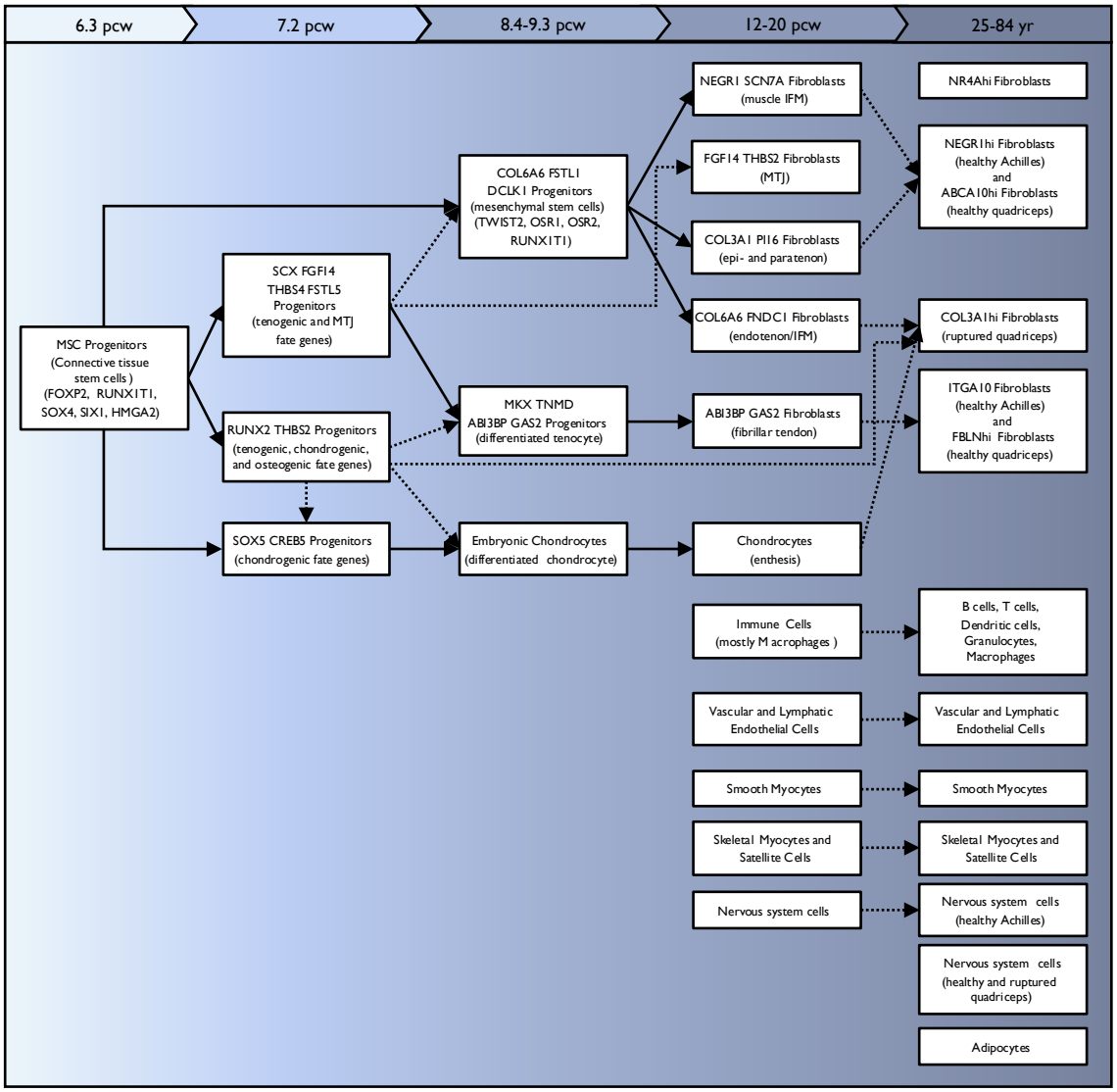


Figure 72. Timeline summary of identified embryonic, foetal, and adult tendon cell lineages. *The chart illustrates the progression from the earliest identified embryonic tendon progenitors to adult fibroblasts. Solid arrows denote connections confirmed in this thesis through RNA velocity and/or pseudotime analyses, whereas dotted arrows indicate connections inferred from transcriptional similarity.*

7.3 Implications of the Findings and Directions for Future Research

7.3.1 Tendon development

The study's findings align with existing research on tendon development, confirming the presence of *SCX*-expressing tendon progenitors in both embryonic and foetal stages. These progenitors adhere to the expected gene expression sequence during early embryonic tendon cell differentiation, where *SCX* precedes *MKX* and *TNMD* (see section 2.4.3). Importantly, this work extends the investigation of *SCX*-positive progenitors into the foetal stages,

revealing *ABI3BP* and *GAS2*-expressing fibroblasts as predominant fascicular tendon populations (Figure 72).

A significant novel discovery was the identification of a *SCX*-negative embryonic progenitor population expressing COL6A6 and FSTL1, which differentiated from a common Connective Tissue Stem Cell progenitor into several distinct loose connective tissue foetal tendon and adjacent muscle fibroblast types (Figure 72). The lineage drivers for these cells – including *TWIST2*, *OSR1*, *OSR2*, *RUNX1T1*, *DCLK1*, *CELF2*, and others – were notably anti-correlated with those of the primary, well-studied *SCX*-expressing lineage (*SCX*, *MKX*, *TNMD*, *ABI3BP*, *GAS2* etc.). This finding suggests a complex regulatory network controlling tendon cell differentiation that diverges late in embryonic development, highlighting an entirely new trajectory for embryonic tendon cells. Moreover, the descendants of these *SCX*-negative progenitors express markers characteristic of injury-responsive sheath tendon stem/progenitor cells (*TPPP3*, *PDGFRA;* see section 2.2.3), highlighting their potential relevance in tendon repair and regeneration.

A key question that remains unresolved is whether this 8.4 pcw *SCX*-negative progenitor population is preceded by the 7.2 pcw *SCX, FGF14, THBS4 and FSTL5*-expressing progenitor type that gives rise to the main foetal tendon fascicular *ABI3BP* and *GAS2*-expressing fibroblasts (Figure 72). Previous studies of tendon development have predominantly focused on the main *SCX*-expressing tendon lineage, with insufficient attention given to the origins of tendon loose connective tissue, likely due to a lack of definitive markers. Studies utilising Scx-GFP labelling in mice suggest uniform *Scx* expression across tendons up to foetal E19 (Pryce *et al*., 2007; Schweitzer *et al*., 2001). However, the small size of the embryonic mouse tendons may obscure smaller, *SCX*-negative regions of tendon loose connective tissue due to the limited resolution of imaging techniques used and the constraints associated with the use of large and bright GFP proteins.

Future research should therefore concentrate on confirming the presence of 8.4 pcw *SCX*-negative COL6A6 FSTL1 DCLK1 Progenitors in embryonic tendon tissues and determining whether they descend from the 7.2 pcw population of *SCX*-expressing progenitors (Figure 72). Employing lineage tracing of the

identified 6.5 pcw Connective Tissue Stem Cells would enable a comprehensive understanding of their developmental trajectory. It would also help clarify any connections between the identified 7.2 pcw SCX FGF14 THBS4 FSTL5 Progenitors and MTJ-specific foetal FGF14 THBS4 Fibroblasts, as well as between 7.2 pcw RUNX2 THBS2 Progenitors and other transcriptionally similar embryonic and foetal tendon cells (Figure 72). High-resolution imaging of these populations, employing gene expression-focused techniques such as MERFISH or RNAscope, would further validate these findings. Given the significance of tendon loose connective tissue layer cells in tendon repair (see sections 2.5.2 - 2.5.3), addressing these gaps could provide deeper insights into tendon biology and facilitate the development of more effective strategies for promoting regenerative tendon tissue repair.

7.3.2 Potential influence of non-fibroblast populations on repair outcomes in injured aged and developing tendons

Comparisons between developing and aged tendon populations revealed a significant diversity of immune cells, a conservation of original non-fibroblast populations established during development, and a complete diversification of fibroblast populations (Figure 72). Additionally, comparisons between developing and healthy or ruptured tendon populations highlighted further complexities.

While foetal tendons were primarily found to contain myeloid cell populations (predominantly *F13A1, CD163,* and *MRC1*-expressing macrophages), adult tendons featured a more diverse immune cell repertoire, including both innate and adaptive myeloid and lymphoid cells – a finding corroborated by other studies in mice and humans (see section 2.2.3 and Table 1). Foetal macrophages are critical not only for immune surveillance and inflammatory responses, but also for proper tissue development, homeostasis, and remodelling (reviewed in Mezu-Ndubuisi and Maheshwari (2021)). The transition from a primarily myeloid population in foetal tendons to a more varied immune cell repertoire in adulthood facilitates a more complex immune response. While myeloid cells are essential for initiating inflammation and tissue remodelling (Chisari *et al.*, 2020; Sunwoo *et al.*, 2020), lymphoid cells get involved in later stages of repair, playing a role in long-term immune regulation

(Yang *et al*., 2021). Interestingly, macrophage depletion in postnatal mice leads to regenerative failure in tendon repair, resulting in tendons with inferior structural and mechanical properties (Howell *et al*., 2021); conversely, reduction of lymphoid *CD8*-expressing T cells improves repaired tendon properties post-injury (Blomgran *et al*., 2017). Instead, if lymphoid cell activation is prolonged, it can lead to formation of tissue adhesions (Wojciak and Crossan, 1993).

Although this work did not delve into detailed investigations of the transcriptomic differences between developing and adult immune cells, understanding these aspects – including their origins and functional profiles – would be crucial for elucidating the homeostatic and remodelling niches of both developing and adult tendons. Similarly, investigating the transcriptional changes within non-fibroblast populations such as endothelial, nervous system, and muscle cells across development could lead to new insights into the differences in structural and functional tendon repair outcomes. Therefore, future research should focus on these areas to provide a more comprehensive understanding of tendon biology and improve strategies for effective tendon repair and regeneration.

To achieve this, transcriptome-level changes can be investigated using this study's data and correlated with functional changes through *in vitro* experiments. For example, immune cell populations from developing and aged tendons can be isolated using well-known cell type markers and techniques such as magnetic bead isolation or fluorescence-activated cell sorting. These isolated cells can then be subjected to various assays to assess their inflammatory responses and phagocytic activity. Additionally, co-culture systems with tendon fibroblasts can be used to study the effects of these immune cells on fibroblast behaviour, collagen production, and matrix remodelling. Studying the effects of immune cell transplantation between young and adult mice could then further inform the roles of these immune cells in the repair processes following tendon injury.

7.3.3 Potential influence of fibroblast populations on repair outcomes in injured aged and developing tendons

Based on the results, it was not possible to conclusively determine the presence of tendon stem cells in adult tendons or to identify cell types exhibiting stem-like characteristics, as noted in previous adult tendon studies (see section 2.2.3 and

Table 1). Firstly, adult tendons did not express markers typically associated with tendon stem/progenitor cells (see Table 1). Secondly, in the ruptured tendon samples – where tendon stem cells may be expected to play a role – a distinct rupture-specific fibroblast cluster emerged, characterised by high expression of *COL3A1* and some developmental fibroblast markers but not TSPC markers. This cluster was largely transcriptionally distinct from developing tendon cells, demonstrating limited reactivation of developmental programs and a unique regulon network profile.

This discrepancy suggests that the adult COL3A1hi Fibroblasts associated with tendon injury might be fundamentally different from regenerative foetal tendon fibroblasts, or that they might partially mirror developmental aspects but are modified by their niche and interactions affecting repair outcomes. The origins of these cells complicate this understanding further, as it is unclear whether they were reprogrammed from existing fascicular fibroblasts or derived from loose connective tissue populations. Harmonisation of cell types across studies indicated that these cells most closely resembled embryonic RUNX2 THBS2 Progenitors, foetal inner loose connective tissue *COL6A6*-expressing Fibroblasts, and foetal Chondrocytes (Figure 72), highlighting a likely complex and multifaceted origin.

Furthermore, this study's findings contrast with existing mouse tendon repair research. The fully ruptured quadriceps tendon samples analysed in this thesis were collected from patients 8-9 days post-rupture, a period typically associated with the fibroblastic proliferative stage during which collagen type III-rich granulation tissue forms but remodelling with collagen type I has not yet begun (see section 2.5.1). At this same stage, mouse studies reveal active migration and infiltration of cells expressing markers such as *Acta2*, *Sca1*, *Axin2*, or *Glast* from the inner or outer layers of tendon loose connective tissues toward the injury site (Dyment *et al.*, 2013; Howell *et al.*, 2017; Moser *et al.*, 2018, 2021; Sakabe *et al.*, 2018; Grinstein *et al.*, 2022; Nichols *et al.*, 2023; see Table 2). However, such gene expression was not observed in COL3A1hi or other adult fibroblasts in this study.

A significant factor contributing to this discrepancy is the age difference between the subjects in mouse studies and human patients. Mouse studies

typically involve younger mice, aged 2.5 to 6 months (see Table 2), which, given a typical mouse lifespan of 1.5-2 years, are analogous to human young adults. In contrast, the tendon samples in this study came from elderly patients aged 67, 69, and 75 years. To enhance the relevance of these studies to human conditions, particularly since the elderly represent a substantial portion of the population requiring tendon injury treatments (Meng *et al*., 2023; Minagawa *et al*., 2013), future research should consider using older mice, aged 18-24 months, to better model elderly human conditions, which may have different tissue repair processes compared to younger populations.

Additionally, to fully understand the origins and roles of these cells and their comparison to developmental stages, it is essential to examine different stages of tendon healing, not just at days 8-9 post-rupture. This comprehensive approach can realistically be achieved only using model organisms. Therefore, future work should involve mapping human developing and adult tendon populations to those in the commonly used mouse and zebrafish models. This would enable studies to draw parallels in human tendon repair using both developing and older models, examining various post-injury timepoints. A collaboration between the Snelling and Galloway lab groups is currently underway to achieve this crucial step in advancing the field of tendon repair.

Finally, current research underscores that tendon healing is most effective before significant mechanical loading and fibril expansion occur, with regenerated tendons typically displaying smaller, more immature collagen fibrils compared to uninjured tendons (Ansorge *et al*., 2011; Howell *et al*., 2017). Additionally, developing tendons regenerate with highly aligned collagen fibres, whereas adult tendons often heal through the formation of persistent disorganised granulation tissue (see section 2.5.2). Interestingly, ruptured adult tendon COL3A1hi Fibroblasts downregulate genes involved in development-associated collagen fibril initiation (e.g., *COL11A1-2*), collagen deposition and processing (e.g., *CTHRC1*, *PCOLCE*, *MGP*), and elastic fibre production (e.g., *EMILIN1*, *FBLN1*, *MFAP2* etc.), which may contribute to the inefficient repair of collagen and elastic fibres. Moreover, these and other adult tendon fibroblasts also significantly reduce their metabolic and protein synthesis pathways, aligning with previous findings that foetal tendon cells are more metabolically active and have higher proliferative capabilities (Ansorge *et al*., 2012; Grinstein

et al., 2019). Coupled with the evidence showing a sharp decline in tendon ECM turnover after late adolescence (Heinemeier *et al*., 2018, 2013), the adult tendon fibroblasts appear almost "exhausted" or "quiescent".

To improve repair outcomes, it is crucial to reprogram these less metabolically and synthetically active adult fibroblasts into active, developmental-like cells. Ideally, this reprogramming should involve intrinsic (fascicular and interfascicular matrix) fibroblasts (see section 2.5.3), making them capable of expressing lineage-specific genes necessary for the reconstruction of affected structures – such as *SCX* for fascicular injuries, *SOX5*, *-6*, and *-9* for enthesis regions, and *COL22A1* and *THBS4* for MTJ regions. Future work should therefore focus on investigating stimuli capable of achieving this reprogramming. This could, for instance, involve the use of small molecule drugs that stimulate early *SCX*-lineage activation, or the development of biomaterials designed to appropriately mimic the specific regenerative tendon niches. The latter would necessitate comprehensive investigations into the regenerative tendon proteomes, focusing particularly on the pericellular ECM. By reprogramming "exhausted" adult fibroblasts to resemble their developmental counterparts and creating a supportive regenerative niche, it may be possible to significantly improve tendon healing and regeneration in aged populations.

7.4 Strengths and Limitations of the Study

The research detailed in this thesis represents a substantial advancement in tendon biology, leveraging single-nucleus and spatial RNA-sequencing techniques to obtain high-resolution insights into human tendon transcriptomics using tissues that are very challenging to acquire. Moreover, the study utilises both published and unpublished internal datasets to navigate the experimental challenges associated with limited sizes of embryonic tendon tissues and the scarcity of adult tendon samples. Specifically, a novel analytical framework was developed to extract and analyse tendon-specific signatures from embryonic whole limb data, and the adult tendon populations defined by other researchers were mapped to developmental tendon cells. The employment of recent, state-of-the-art methods for data analysis across these tasks underlined the high quality and ambitious scope of this work.

However, the research faced several challenges that impacted its execution. The COVID-19 pandemic significantly hindered tissue collection during the first year of my DPhil, prompting a shift in focus towards mastering experimental and computational analysis techniques. Additionally, certain experimental approaches, such as CellDIVE staining, did not yield the expected results despite substantial efforts and time investment. The ECM-rich, highly autofluorescent nature of tendon tissues posed considerable difficulties for staining, and coupled with limited access to essential microscopy equipment, these experiments were eventually discontinued. Consequently, the focus shifted towards an in-depth analysis of increasingly complex and technically demanding transcriptomic datasets. This included tackling integration challenges due to batch effects and variations in sequence alignment algorithms across different sequencing technologies and developmental stages. The limited availability of tissues, particularly paediatric samples, further restricted the study's ability to elucidate transcriptomic differences between developmental and aged tendons. While the thesis provides a comprehensive transcriptional profile, additional validation through imaging and functional assays is essential to confirm the roles and relationships of the identified cell types. Further specific experimental limitations are discussed in detail in the individual results chapters of the thesis.

Despite these challenges, the thesis has successfully provided new insights that push the boundaries of current knowledge in tendon biology. The integration of embryonic, foetal, and adult tendon data offers a comprehensive view of the lifecycle of human tendons, marking a significant contribution to the field. Ultimately, I am pleased with the output and overall quality of this work, which not only advances our understanding but also lays the groundwork for future research directions in tendon biology.

7.5 Conclusion

In conclusion, this thesis significantly advances our understanding of tendon biology, elucidating the complex transcriptional landscapes that characterise human tendon development and aging. By leveraging single-nucleus and spatial RNA-sequencing techniques, this research has identified 14 distinct cell types within foetal Achilles and quadriceps tendons and has outlined the

developmental trajectories of seven embryonic progenitors contributing to various functional elements of the tendon, including the main body fibroblasts, loose connective tissue fibroblasts, and chondrocytes. Moreover, comparative analyses between developing and adult tendons revealed significant structural and molecular differences, particularly in cellular densities, compositions, and ECM organisation. Adult tendons demonstrated a complex immune cell repertoire, conserved non-fibroblast populations, and distinct “exhausted” fibroblast populations focused on maintaining homeostasis. The limited reactivation of developmental repair programs in ruptured aged tendons further emphasised the challenges in tendon repair in older populations. These findings lay the groundwork for future research, which should focus on validating these findings and translating them into clinical applications to enhance tendon repair and improve patient outcomes, ultimately addressing the significant global health challenge posed by tendon diseases.

Appendix: Tables and Figures

Appendix Table 1. Overview of tendon collagens.

Classification and Supramolecular Structure	Protein	Encoded by	Role in Tendons or Attachment Sites	Expression and Protein Localisation Patterns in Tendon or Attachment Sites	Associated Diseases	Relevant Phenotype in Mutant Organisms	References
Fibril-forming: striated fibrils with periodicity of 64-67nm	Collagen I	COL1A1 COL1A2	Main structural component that confers tensile strength.	Highly expressed and deposited throughout the tendon during both development and postnatal growth phases. Foetal tissues have only minimal levels of prolyl 3-hydroxylation in type I collagen sites compared to adult tissues. Cross-links are reversible in foetal but irreversible in adult tendons.	Osteogenesis Imperfecta (Brittle Bone Disease), Ehlers-Danlos Syndrome (EDS) types I and II.	Reduced tendon thickness, abnormal cell maturation, perturbed collagen fibril growth. In osteogenesis imperfecta: brittle bones, susceptibility to fractures at or near tendon attachments, leading to joint instability and abnormal joint mechanics. Phenotypes range from mild to lethal after birth.	Park *et al*., 2020 Buckley *et al*., 2013 Marini *et al*., 2007 Hudson *et al*., 2021

Fibril-forming: striated fibrils with periodicity of 64-67nm	Collagen II	COL2A1	Plays a supportive role in shock absorption and force distribution at the tendon-bone interface.	Localised in the unmineralised and mineralised fibrocartilage zones of the enthesis.	Achondrogenesis, Kniest Dysplasia, Spondyloepiphyseal Dysplasia Congenita, Stickler Syndrome, and other chondrodysplasias.	Mutations lead to abnormal cartilage development and function. Homozygous knockouts are postnatal lethal as cartilage fibrils are not formed.	Buckley *et al*., 2013 Nourissat *et al*., 2010 Fukuta *et al*., 1998
Fibril-forming: striated fibrils with periodicity of 64-67nm	Collagen III	COL3A1	Regulates collagen I fibril diameter (when co-occurring), contributes to tendon flexibility. Presence is associated with smaller fibril diameters, reduced modulus, and decreased fibre alignment. Interacts with integrins, likely affecting cell adhesion, migration, proliferation and differentiation.	Highly expressed and co-localised with collagen type I throughout the tendon during early embryonic development. Expression diminishes with maturation and becomes mainly restricted to the endo- and epitenon by birth. Temporarily surges during early healing response.	Ehlers-Danlos Syndrome type IV (Vascular EDS), characterised by fragile blood vessels and organs.	Mutations lead to altered fibril diameter distributions. Homozygous knockouts are early postnathal lethal due to brain defects and vascular vessel ruptures.	Birk & Mayne, 1997 Liu *et al*., 1997 Kuo *et al*., 2008 Kim *et al*., 2005 Maffulli *et al*., 2000 Dahlgren *et al*., 2005 Buckley *et al*., 2013

Network-forming: basement membrane chicken-wire network with lateral association	Collagen IV	COL4A1 COL4A2 COL4A3 COL4A4 COL4A5 COL4A6	Integral component of basement membranes. Contributes to the formation of a protective basement membrane epithelium (peritenon) on the surface of tendons that prevents adhesions to surrounding tissues and enables gliding.	Found in the basement membrane of the tendon blood vessels as well as on the surface of tendons (peritenon). Therefore, expressed in endo, epi- and paratenon.	Porencephaly, Cerebrovascular Disease, HANAC (Hereditary Angiopathy with Nephropathy Aneurysm and Cramps)	Deficiency is embryonic lethal. Mutations in COL4A1 cause vascular dysfunction, including reduced endothelial attachment and altered blood pressure regulation. 3-month-old Col4a1+/Svc mice: tendons had developed, but the basement membrane was patchy and spontaneous adhesions formed.	Taylor *et al*., 2011 Van Agtmael *et al*., 2010 Zhang *et al*., 2021
Regulatory fibril-forming: striated fibrils, retain regulatory, noncollagenous N-terminal domains	Collagen V	COL5A1 COL5A2 COL5A3	Essential for the initiation of fibril assembly. Intercalates into type I, II, and III fibrils, regulating fibril diameter and overall fibre organisation.	Expressed at low levels during development. Predominantly found in the pericellular matrix and enriched in the MTJ. Preferentially localised on the tenocyte surface as distinct foci in tendons and in cell culture.	Ehlers-Danlos Syndrome types I and II, characterised by joint hypermobility, skin hyperextensibility, and tissue fragility (impaired healing).	Embryonic lethality in homozygous mutants due to cardiovascular defects. Heterozygous mice show EDS phenotype, with smaller tendons comprising larger yet fewer fibrils that are disorganised. Reduction in maximum mechanical load and stiffness. Col5a1+/− tendons have overall diminished recovery post-injury. However, controlled and mild heterozygous knockdown at the time of injury leads to improved healing outcomes compared to WT.	Wenstrup *et al*., 2004 & 2011 Sun *et al*., 2011 & 2020 Connizzo., *et al*. 2015 Malfait *et al*., 2005 Watanabe *et al*., 2007 Leiphart *et al*., 2022 Smith, Zhang and Birk, 2014 Johnston *et al*., 2017

Beaded filament-forming: broad-banded fibril networks	Collagen VI	COL6A1 COL6A2 COL6A3 COL6A4 (inactive) COL6A5 COL6A6	Integral to matrix assembly processes. Modulates fibril sise. Associates with biglycan to regulate fibre alignment and distribution.	Expression higher and more widespread during development. Localised throughout the tendon initially, with subsequent enrichment in the pericellular regions, especially in the enthesis. Co-localised with biglycan.	Bethlem Myopathy and Ullrich Congenital Muscular Dystrophy, both presenting with muscle weakness and joint stiffness.	Disorganised extracellular micro-domains, altered collagen fibre organisation, smaller diameter fibrils, decreased mechanical properties.	Izu *et al*., 2011 Thakkar *et al*., 2014 Liu *et al*., 2015 Leiphart *et al*., 2022 Antoniel *et al*., 2020 di Martino *et al*., 2023
FACIT: associated with fibrils, other interactions	Collagen IX	COL9A1, COL9A2, COL9A3	Collagen IX molecules are located on the surface of type II collagen fibrils, acting as bridging scaffolds between fibrils and other matrix components in cartilage. Provide structural integrity and contribute to the tissue's resistance to compressive forces.	Localised throughout the enthesis.	Multiple Epiphyseal Dysplasia, Osteochondrosis dissecans, Stickler syndrome.	Mutations in the genes encoding Collagen IX have been linked to multiple epiphyseal dysplasia, characterised by abnormalities in cartilage and bone development. COL9A1-/- mutant mice develop severe degenerative joint disease characterised by loss of cartilage, changes in the organisation of the collagen fibril network, and other degenerative alterations postnatally.	Fukuta *et al*., 1998 Fässler *et al*., 1994 Czarny-Ratajczak *et al*., 2001 Posey *et al*., 2008
Network-forming: hexagonal lattices	Collagen X	COL10A1	Although primarily involved in bone growth, Collagen X's role in endochondral ossification could imply a structural or regulatory role at the ossifying enthesis, contributing to the attachment of tendon to bone.	Localised in mineralised fibrocartilage zone of the enthesis. Expressed by hypertrophic chondrocytes during endochondral ossification.	Schmid Metaphyseal Chondrodysplasia.	Not directly reported in the context of tendons/enthesis. However, mutations causing diseases like Schmid Metaphyseal Chondrodysplasia could indirectly affect enthesis function or development through altered bone	Fukuta *et al*., 1998 Apostolakos *et al*., 2014

						formation processes.	
Regulatory fibril-forming: striated fibrils, retain regulatory, noncollagenous N-terminal domains	Collagen XI	COL11A1 COL11A2	Essential for the initiation of fibril assembly. Intercalates into type I, II, and III fibrils, regulating fibril diameter and overall fibre organisation.	High expression in early postnatal development, decreasing significantly as tendons mature; almost absent in adult tendons.	Stickler Syndrome (various types), Marshall Syndrome, Fibrochondrogenesis, Otospondylomegaepiphyseal Dysplasia.	Abnormally structured fibrils with smaller diameter, evidence of deregulated lateral fibril junctions, leading to compromised biomechanical characteristics like maximum load, stiffness, and modulus.	Sun *et al*., 2020 Wenstrup *et al*., 2011
FACIT: associated with fibrils, other interactions	Collagen XII	COL12A1	Regulates intercellular communication, affects collagen type I synthesis. Essential for the integration of developing tendon matrix and fascicle structure. Involved in fibril alignment, assembly, and tenocyte structuring, contributing to the stabilization of fibrils before crosslinking events.	Expressed throughout the tendon during initial embryonic stages but becomes localised to fascicular and interfascicular extracellular matrix as well as the tenocyte surfaces, connecting neighbouring tenocytes by birth.	Bethlem Myopathy, Ullrich Congenital Muscular Dystrophy (overlap with Collagen VI-related conditions). Myopathic Ehlers-Danlos Syndrome with tendon and ligament laxity, joint hypermobility, and muscle weakness.	Tenocytes exhibit altered morphology and disrupted cellular activities, leading to impaired cellular communication. Reduced tissue resilience, decrease in type I collagen.	Izu *et al*., 2021 Zhang *et al*., 2003 Fung *et al*., 2022 Tzortzaki *et al*., 2003 Wälchli *et al*., 1994

FACIT: associated with fibrils, other interactions	Collagen XIV	COL14A1	Regulates early stages of collagen type I fibrillogenesis.	High expression in early embryonic development, decreasing significantly as tendons develop and mature; almost absent in adult tendons.	Not directly linked; potential association with Punctate Palmoplantar Keratoderma.	Premature fibril growth, altered mechanical properties in early postnatal tendons. Return to normal phenotype and functionality upon maturation.	Ansorge *et al*., 2009 Young *et al*., 2000 Wälchli *et al*., 1994
FACIT-like: interfacial regions, basement membrane zones	Collagen XXII	COL22A1	Serves as a fibroblast adhesion molecule at the myotendinous junction (MTJ), reinforcing skeletal muscle insertions.	Expression begins during embryonic development after the onset of muscle contractions (~E13.5) and intensifies with age. Localised specifically to the MTJ and associates with microfibrillar elements, diverging from other FACITs.	Not directly linked; potential association with Muscular Dystrophy and Pulmonary Systemic Sclerosis.	Loss-of-function results in muscular dystrophy due to MTJ disruption, characterised by reduced force transmission capacity with fibre detachment.	Koch *et al*., 2004 Jakobsen *et al*., 2017 Charvet *et al*., 2013 Lipp *et al*., 2023
Regulatory fibril-forming: thin, non-striated fibrils (10nm in diameter)	Collagen XXVII	COL27A1	Provides structural support and tensile strength.	Expressed primarily in cartilaginous tissues (enthesis). Might be activated by SOX9.	Steel syndrome; potential association with Fibrochondrogenesis type 1. Some alleles are associated with increased Achilles tendinopathy and injury risk.	Mutations lead to abnormal skeletal development; specific tendon phenotypes have not been characterised	Pace *et al*., 2003 Jenkins *et al*., 2005 Kotabagi *et al*., 2017 Kim *et al*., 2021

Appendix Table 2. Overview of tendon non-collagenous ECM proteins.

Type	Protein	Encoded by	Role in Tendons or Attachment Sites	Expression and Protein Localisation Patterns in Tendon or Attachment Sites	Associated Diseases	Relevant Phenotype in Mutant Organisms	References
Small leucine-rich proteoglycan (Class I); CS/DS-containing	Decorin	DCN	Binds to fibrillar collagens, regulating fibrillogenesis, diameter and spacing of fibrils. Similar stucturally and functionally to BGN (binds to the same sites) and can be compensated by it. Regulates TGF-β activity (e.g. cell growth suppression) and immune signaling. Essential during early postnatal development for structuring the tendon ECM and regulating growth by limiting lateral growth of collagen fibrils. Has minor roles in adult tendon maintenance.	Predominantly at the surface of fibrocartilaginous regions of tendon. Decorin mRNA expression high at P1, peaks at P4–10, then decreases dramatically, becoming sustained at ~50% of peak expression. Actual detectable protein increases throughout, rising gradually from P4 to P30. Protein initially found throughout the ECM, but is then localised to the pericellular ECM by P30. Expression decreases post-injury.	Congenital Stromal Corneal Dystrophy.	***Dcn*-/- mice:** abberant collagen fibril structure and bigger, more irregular (i.e. not circular) diameters observed postnatally after initiation of linear and lateral fusions and growth (P10 onwards). Decreased mechanical strength and stiffness at maturity (P150), but not at end of fibril growth phase (P60). Phenotype worse in positional (e.g., tail) vs load-bearing flexor tendons. Increase in BGN in load-bearing tendons to compensate. Decreased mechanical properties post-injury in P120 adult tendons. **Inducible (I-) *Dcn*-/- (P150 adults):** Minimal effect on tendon mechanics and injury healing responses. **I-*Dcn*-/-*Bgn*-/- (P7 neonates):** decreased cross-sectional areas, fibril diameter, and tendon stiffness. **I-*Dcn*-/-*Bgn*-/- (P150 adults):** Mimics the Dcn-/- phenotype with larger fibril diameters and mechanical vulnerabilities such as decreased stiffness and increased tissue viscosity.	Hildebrand *et al*., 1994 Zhang *et al*., 2005, 2006 Robinson *et al*., 2005, 2017 Abbah *et al*., 2016 Anders and Schaefer, 2014 Moreth, Iozzo, and Schaefer, 2012 Beach *et al*., 2024 Leahy *et al*., 2023 Iozzo and Schaefer, 2015 Dunkman *et al*., 2014

Small leucine-rich proteoglycan (Class I); CS/DS-containing	Biglycan	BGN	Very similar both structurally and functionally to DCN, binds to the same sites on collagen. Can be compensated by it. Also regulates TGF-β activity and immune signalling (generally pro-inflammatory). Plays a more substantial role in tendon healing by negatively impacting late-stage tendon mechanical properties and healing-related gene expression. Has a more dominant role in maintaining adult tendon integrity and homeostasis compared to DCN.	Throughout the tendon, varying by age. BGN mRNA expression is highest at P1 and decreases rapidly to a barely detectable level at P30. BGN protein decreases by 50% from P4 to P30. Protein initially found throughout the ECM, but then localised to the pericellular ECM by P30. Usually co-expressed and co-localised with collagen VI during healing and development.	Spondyloepimetaphyseal Dysplasia, Meester-Loeys Syndrome, Osteoporosis.	***Bgn*-/- mice:** Comparable phenotypes to Dcn-/- but with normal fibril diameters in flexor tendons and slightly decreased diameters in positional tendons. Decreased mechanical properties post-injury in P120 adult tendons **I-*Bgn*-/- (P150 adults):** Significant changes in tendon mechanics and healing responses, including improved healing outcomes, increased linear modulus, and expression of ECM-related and growth factor genes relative to WT tendons. **I-*Dcn*-/-*Bgn*-/- (P7 neonates), I-Dcn-/-Bgn-/- (P150 adult):** see above ***Fmod*-/-*Bgn*-/- mice:** smaller, abnormal collagen fibrils, decreased stiffness, ectopic tendon fibrocartilage ossification, severe osteoarthritis.	Corsi *et al*., 2002 Dourte *et al*., 2013 Schaefer *et al*., 2005 Robinson *et al*., 2005, 2017 Zhang *et al*., 2005 Beach *et al*., 2024 Robinson *et al*., 2017 Leiphart *et al*., 2022 Leahy *et al*., 2023 Ameye *et al*., 2002 Dunkman *et al*., 2014
Small leucine-rich proteoglycan (Class I); no GAG chains; carries an aspartic acid sequence that binds calcium	Asporin	ASPN	Competes for collagen binding sites with DCN (but not BGN). Able to bind and limit TGF-β activity. Has a role in chondrogenesis regulation and collagen mineralisation. Specific role in tendon unknown.	Expression and protein levels (human and equine, respectively) are significantly lower in old vs young tendons. Highly expressed in developing skeleton, particularly in cartilage/bone, but also throughout the tendon (at E15.5).	Osteoarthritis, Intervertebral Disc Degeneration, Periodontal Ligament Mineralization, Pulmonary Fibrosis, Keloids	***Aspn*-/- mice:** increased skin mechanical toughness without significant changes in collagen fibril structure, but with upregulation of collagens I and III, lysyl oxidases, LUM, and profound alterations in GAG composition, with double the amounts of more sulfated CS/DS and the DCN and BGN core proteins. Tendon-specific phenotypes unknown.	Kalamajski *et al*., 2009 Peffers *et al*., 2014, 2015 Maccarana *et al*., 2017 Fan *et al*., 2022 Henry *et al*., 2001 Lorenzo *et al*., 2001

Small leucine-rich proteoglycan (Class II); KS-containing (type II, poorly sulfated)	Fibromodulin	FMOD	Competes for the same binding sites as LUM. Regulates fibrillogenesis throughout postnatal development. Especially important for the correct formation of mature, large-diameter fibrils in later postnatal development. Contributes to tissue stiffness.	Expressed at P10. Expression peaks at P14, with subsequent slight decrease to P30, then rapid decrease observed at P56 onwards. Expression significantly lower in old vs young equine tendons. Protein levels similar at P4 and P10, with increase by 30% at P30. Protein is localised throughout the tendon early in postnatal development (P10), but then becomes concentrated in the fascicular tendon.	Myopia, Ehler-Danlos Syndrome, Pseudoachon droplasia.	***Fmod-/-* mice:** reduced number and abnormal, disorganised fibre bundles, likely due to lateral fusion defects. Irregular fibril diameters. Populations of both thinner and thicker fibrils, but the proportion of thinner diameter fibrils is higher than in WT. Fibrils larger than WT at P4 (~72nm). More smaller-sized fibrils (~64nm) at P30 than WT. Cells distribution is disorganised, with them appearing further apart. Reduced stiffness. Reduced endotenon tissue. Increased LUM protein as compensation. ***Fmod-/-Lum-/-* mice:** premature fibril diameter heterogeneity and larger fibrils (~87nm) at P4, increased number of small-diameter, irregular fibrils (P30-84). ***Fmod-/-Bgn-/-* mice:** smaller, abnormal collagen fibrils, decreased stiffness, ectopic tendon fibrocartilage ossification, severe osteoarthritis.	Svensson *et al*., 1999 Ameye *et al*., 2002 Ezura *et al*., 2000 Jepsen *et al*., 2002
Small leucine-rich proteoglycan (Class II); KS-containing (type II, poorly sulfated)	Lumican	LUM	Competes for the same binding sites as FMOD. Regulates fibrillogenesis during early postnatal development.	Peak expression at P8-10 with subsequent decrease to adulthood. Protein levels decrease from P4 to P30 by about 60%. Protein is localised throughout the tendon early in postnatal development, but then becomes concentrated in the loose connective tissue matrices.	Myopia, Corneal Diseases.	***Lum-/-* mice:** thicker collagen fibrils (in skin and cornea). Irregular fibrils (i.e. not circular), not as pronounced as Fmod-/- or Fmod-/-Lum-/- in later development (P30+). ***Fmod-/-Lum-/-* mice:** premature fibril diameter heterogeneity and larger fibrils (~87nm) at P4, increased number of small-diameter, irregular fibrils (P30-84).	Chakravarti *et al*., 1998 Svensson *et al*., 1999 Ezura *et al*., 2000

Small leucine-rich proteoglycan (Class II); KS-containing (type II, poorly sulfated)	Keratocan	KERA	Stucturally similar to LUM, also regulated by it. Function unknown in tendon, likely collagen fibrillogenesis regulation similar to LUM.	Widely expressed in various embryonic mesenchymal tissues. Abundant in cornea and sclera, less in skin, ligament, cartilage, artery, muscle. Shows high tendon-specific expression in early embryogenesis. Protein is co-localised with fibrillar collagens in fascicles and in the endotenon.	Corneal Diseases.	***Kera*-/- mice (cornea):** increased collagen fibril diameter, cornea is flattened and overall corneal thickness is reduced. ***Chst5*-/- mice (reduced corneal sulfation, akin to lower sulfation seen in tendon):** lower diameter fibrils that are abnormally tightly packged. Not enough known about effects in tendon.	Chakravarti, 2006 Liu *et al*., 2003 Rees *et al*., 2009 Zhang *et al*., 2023 Hayashida *et al*., 2006 Carlson *et al*., 2005
Small leucine-rich proteoglycan (Class III); KS-containing	Osteoglycin / Mimecan	OGN	Contributes to tendon strength. Influences collagen fibrillogenesis, ECM organisation, and cellular behaviours. Regulates pathological processes such as fibrosis, neovascularisation, and tumourigenesis.	Protein levels are significantly lower in old vs young equine tendons.	No direct associations.	***Ogn*-/- mice** have mild phenotypes. In skin: thicker collagen fibril diameters and reduced tensile strength. In tendons: reduced biomechanical properties with a more compliant, weaker mouse tail tendon with compromised ability to yield after elastic deformation.	Tasheva *et al*., 2002 Peffers *et al*., 2014 Nulali *et al*., 2022 Boote, Ma, Goh, 2023
Large aggregating proteoglycan (lectican); CS/KS-containing HA-binding hyalectan	Aggrecan	ACAN	Provides resistance to compressive and tensile forces. Impairs TGF-β signalling via the ALK5/SMAD3 pathway. Binds to hyaluronan, which itself binds to CD44. Lysed by ADAMTS5.	Localised to the fibrocartilage regions of the enthesis. Upregulated following injury and in tendinopathy.	Spondyloepimetaphyseal Dysplasia, Osteochondritis Dissecans, Osteoarthritis.	***Adamts5*-/- mice (Acan accumulation):** increased ACAN pericellular deposition, including in the tendon main body, more heterogeneic collagen fibril diameters, weakened enthesis prone to rupture. Positional tendons have larger cross-sectional area and a decreased tensile modulus. Load-bearing tendons have a higher modulus. ***CD44*-/- mice (limited Acan binding to HA):** improved tendon healing in the form of increased tensile strength, elastic modulus, collagen fibril organisation, increased expression of several collagens	Wang *et al*., 2012 Waggett *et al*., 1998 Corps *et al*., 2006 Ansorge, Beredjiklian and Soslowsky, 2009 Velasco *et al*., 2011 Berglund *et al*., 2006

						and ELN.	
Large aggregating proteoglycan (lectican); CS/DS-containing HA-binding hyalectan	Versican	VCAN	Provides tensile force resistance. Regulates cell–matrix interactions through HA-, TGF- and BMP-signalling, cytokine and growth factor binding, and other interactions with the ECM and cell surface molecules. Role in creating a hydrated, anti-adhesive matrix that promotes cellular proliferation and migration.	Highly expressed in cartilage and tendon midsection. Expression highest during developmental and perinatal period. Protein is localised around the vessels in the endotenon and in the pericellular ECM around tenocytes. Enriched in regions of fibrocartilage metaplasia. Upregulated following injury and compression as well as in tendinopathy.	Wagner Syndrome (type 1), Vitreoretinopathy, Gastic and Pancreatic Cancers.	***Vcan*-/- mice:** embryonic lethal due to cardiac complications. **Perinatal 4-6mo mice with no Vcan expression in mesenchymal condensation areas of cartilage primordium (*Prx1*-Cre/*Vcan* flox/flox):** decreased TGFβ accumulation, delayed chondrocyte differentiation, decreased numbers of *Scx*+ cells in the joint.	Yoon and Halper, 2005 Kinsella, Bressler and Wight, 2004 Bode-Lesniewska *et al*., 1996 Corps *et al*., 2004 Scott *et al*., 2008 Higuchi *et al*., 2021 Berglund *et al*., 2006 Choocheep *et al*., 2010

Large aggregating proteoglycan	Lubricin	PRG4	Lubrication of fascicles, allowing gliding.	Localised mostly to endo-, epi-, and peritenon, with regions subjected to more stress, shear force and compression showing higher protein levels. Low protein levels also noted within fascicles. Tension increases expression (at least in chondrocytes). Expression also increases with ageing.	Camptodactyly-Arthropathy-Coxa Vara-Pericarditis Syndrome, Arthritis, Synovitis.	***Prg4*-/- mice:** increased interfascicular friction, abnormal cartilage, synovial and chondroid hyperplasia, rougher tendon surface, lower relaxation ratio and higher stress from load on bones and muscles.	Sun *et al*., 2006, 2015 Funakoshi *et al*., 2008 Kohrs *et al*., 2011 Reuvers *et al*., 2011 Thornton *et al*., 2015 Hayashi *et al*., 2013
Glycoprotein	Tenascin C	TNC	Binds to and interacts with fibronectins and integrins, collagens, periostin, fibrillins etc. Influences cell migration and growth by limiting adhesion. Can lead to cell migration, cancer cell invasion/metastasis. Responses are cell type-specific and can be contradicting.	Expression is high in early embryogenesis, but is downregulated after birth (still detectable). Protein is concentrated in regions undergoing tissue remodeling and/or high force (e.g. mineralised fibrocartilage in the enthesis, MTJ), but is also detected around fibroblasts and collagen fibres. Increased expression is associated with tumourigenesis, infections, inflammation, and chronic tendinopaty.	Deafness, Breast Cancer, Glioblastoma, Vascular Disease. Some alleles are associated with increased Achilles and rotator cuff tendinopathy and/or injury risk.	***Tnc*-/- mice:** (general) mild phenotype, differences arise mostly during injury with reduced inflammation and healing response. Reduced tumour angiogenesis and lung metastasis.	Geffrotin *et al*., 2000 Edom-Vovard *et al*., 2002 Järvinen *et al*., 2003 Chiquet-Ehrismann and Tucker, 2011 Kluger *et al*., 2017 Midwood *et al*., 2016 de Palma *et al*., 2004 Saupe *et al*., 2013 Mackie and Tucker, 1999 Karlsen *et al*., 2022

Glycoprotein	Tenascin XB	TNXB	Unknown. TNXB is a short isoform of TNX, which associates with collagen type I, interacts with decorin, and is involved in collagen deposition and maturation. Binds to and interacts with integrins. Modulates cell adhesion (mostly anti-adhesive), may play roles in tissue remodeling and response to injury by affecting cell morphology, growth, and migration.	Widespread and steady expression throughout development and in the adult. Protein is twice as abundant as TNC in adult tendon. Expression is dramatically reduced in tumourigenesis.	Myopathy, Classical-like Ehlers-Danlos Syndrome.	**clEDS due to TNXB mutations in human:** skin and joint hyperextensibility, vascular fragility, poor wound healing, slowly progressing muscular weakness. ***Tnxb*-/- mice:** (Skin) hyperextensible skin, normal size and shape but increased interfibrillar distance (i.e. decreased density) of collagen fibres. Likely due to fibroblasts being prevented from depositing collagen type I. (Muscle-Tendon unit) lower active force, lower maximal rate of relaxation, and longer time delay between first stimulation pulse and initial force rise. Increased compliance and decreased stiffness of tissues surrounding the individual muscles. Decreased load and directionality of myofascial force transmission.	Geffrotin *et al*., 1995; 2000 Brisset *et al*., 2020 Juneja and Veillette, 2013 Chiquet-Ehrismann and Tucker, 2011 Mao *et al*., 2002 Huijing *et al*., 2010
Glycoprotein	Periostin	POSTN	Regulates collagen fibril maturation and crosslinking, contributes to the growth of fibrocartilage, activates tenocytes following injury and supports αSMA+ myofibroblast proliferation and differentiation. Required for scar formation and effective tendon healing.	Co-localises with and binds to collagen type I. Upregulated following injury.	Colorectal, Lung, and Breast Cancer, Myocardial Infarction, Osteoporosis.	***Postn*-/- mice:** (Enthesis) lower chondrocyte proliferation, less collagen type II and GAGs, shorter enthesis tidemark in postnatal mice; (Skin) reduced collagen fibril diameter and crosslinking, increase in compliance (less stiff), impaired wound closure following injury; (Tendon) impaired healing following injury characterised by delays in wound closure, increased collagen type III production, decreased cell proliferation, reduced tensile strength and stiffness, fewer but larger-sized collagen fibrils.	Nishiyama *et al*., 2011 Mutsuzaki, Yoshida, and Nakajima, 2022 Norris *et al*., 2007 Rolnick *et al*., 2022 Ackerman *et al*., 2024

Glycoprotein	Tenomodulin	TNMD	Regulates tenocyte proliferation, collagen fibril maturation, and homeostasis. Has anti-angiogenic effects.	Expression is transactivated by SCX. Expressed mostly in tenocytes and localised preferentially in the avascular regions of tendons and fibrocartilage.	Epicondylitis, Trichothiodystrophy 6 (nonphotosensitive), Tendinopathy.	***Tnmd*-/- mice:** (Tendon): Reduced tenocyte proliferation at birth with subsequent decrease in cell density at P14 onwards, higher collagen fibre heterogeneity with increased maximum diameter. Reduction in self-renewal and earlier onset of tendon stem/progenitor cell senescence. Phenotype akin to aged tendon.	Docheva *et al*., 2005 Shukunami *et al*., 2018 Alberton *et al*., 2015 Dex *et al*., 2016
Glycoprotein	Thrombospondin 1	THBS1	Regulates cell-ECM and ECM-ECM interactions, negatively affects cell migration and proliferation. Activator of TGF-β, positively regulates inflammation. Important for mechanotransduction. Modulator of elastic fibre organisation. Anti-angiogenic.	Expressed in all regions of the tendon. More studies needed.	Different Cancers (e.g., colorectal, lung, ovarian, gastic etc.).	***Thbs1*-/- mice:** share some similarities in phenotype to TGF-β-null mice, though not perinatal lethal. More studies needed to elucidate specific effects on connective tissues, including tendon.	Kannus *et al*., 1998 Crawford *et al*., 1998 Yamashiro *et al*., 2018
Glycoprotein	Thrombospondin 2	THBS2	Regulates cell-ECM and ECM-ECM interactions, inflammation, angiogenesis, migration and proliferation. Regulates collagen fibrillogenesis. Anti-angiogenic. Has a role in cartilage regeneration and protection from inflammation.	Expression is higher during development and reduces/is absent in mature tendons.	Intervertebral Disk Disease, Colorectal and Gastric Cancers, Myocardial Infarction.	***Thbs2*-/- mice:** increased and irregularly-shaped collagen fibril diameters, disorganised fascicles and loose, flexible tendons. Increased angiogenesis.	Simantov, Fibbraio, Silverstein, 2005 Kyriakides *et al*., 1998 Bornstein *et al*., 2000 Juneja and Veillette, 2013 Sadoun and Reed, 2003 Niu *et al*., 2023

Glycoprotein	Thrombospondin 4	THBS4	Regulates cell-ECM and ECM-ECM interactions, inflammation, angiogenesis, migration and proliferation. Regulates collagen fibrillogenesis. Pro-angiogenic. May be involved in MTJ formation.	Expressed in all regions of the tendon. Protein product - TSP4 - is localised predominantly in tenocyte PCM, with fewer proteins detected among collagen fibrils.	Prostate Cancer, Myocardial Infarction, Nephroma.	***Thbs4*-/- mice:** more varied and larger-sized collagen fibril diameters, reduced vascular inflammation response. Impairment of muscle function with age. Not compensated by other TSP members (THBS1-3, COMP). ***Tsp4b*-/- in zebrafish:** muscle detachment due to defects in laminin localisation and reduced integrin-mediated binding at MTJ.	Frolova *et al*., 2014 Subramanian and Schilling 2014
Glycoprotein	Cartilage oligomeric matrix protein / Thrombospondin 5	COMP	Binds collagen types I, II, and IX. Influences organisation of collagen fibrils, including assembly, degeneration, and repair. Reinforces fibrils. May be involved in MTJ formation by regulating tenocyte adhesion to muscle integrins.	Expressed in all regions of the tendon, with higher expression observed in load-bearing tendons. Levels and synthesis increase with age, as response to load, or in disease. Co-localises with TSP4.	Multiple Epiphyseal Displasia, Pseudoachondroplasia, Carpal Tunnel Syndrome, Arthritis.	***Comp*-/- mice:** normal tendon and skeletal development, likely compensated by other thrombospondins. ***Tsp* disruption in *Drosophila* (most similar to COMP)** leads to reduction in integrin-mediated adherens junctions at the MTJ. COMP mutations lead to disease, altered skeletal development, and smaller, more lax tendons. With the null mutant phenotype in mind, this could potentially be due to alteration of COMP protein properties rather than the absence of COMP function.	Södersten *et al*., 2005 Smith *et al*., 1997 Hecht *et al*., 1998 Svensson *et al*., 2002 Piróg *et al*., 2010 Subramanian *et al*., 2007

Elastin	Elastin	ELN	Provides elasticity to tissues, resists deformation in response to fibre direction loading. Important for quasi-static and viscoelastic shear and transverse tensile behavior. Provides support for maintenance of collagen crimp morphology.	Higher protein concentration in load-bearing vs positional tendons, decreases with ageing without fragmentation. Interspersed within collagen fibers and associated with fibrillins 1 and/or 2. Localised mostly around tenocytes in the IFM (~90%), with much lower levels detected in the fascicles. Poor turnover rate and remodelling capability, low turnover in adulthood.	Supravalvular Aortic Stenosis, Cutis Laxa, Williams-Beuren Syndrome, Ehlers-Danlos Syndrome.	**Enzymatic digestion of Eln with elastase:** decreased failure load, decreased stiffness, and increased fascicle sliding in fascicle–IFM–fascicle units subject to shearing of the IFM. Decreased resistance to off-axis loading and low-strain tensile loading, with a slightly decreased or unchanged linear modulus. BUT: elastase can digest GAGs and some collagens. ***Eln*-/- mice** die early after birth due to stenotic arteries. ***Eln*+/- mice:** increased linear stiffness, more uniformly oriented collagen fibres. Reduced collagen area fraction, fewer small (<50 nm) fibrils, and more large (>170 nm) fibrils in load-bearing tendon. Mechanical properties not changed compared to WT.	Lee *et al*., 2023 Godinho *et al*., 2017 Henninger *et al*., 2015 Eekhoff *et al*., 2017 Svärd *et al*., 2020
Glycoprotein	Fibulin 4	EFEMP2	Essential for elastic fibre formation. Regulates collagen and elastin crosslinking LOX enzyme activity.	Expressed predominantly in tenocyte PCM, with lower expression in fascicles. Co-localises with fibrillins 1 and 2. Not present in tendon sheaths.	Cutis Laxa, Aortic Aneurysm, Doyne Honeycomb Retinal Dystrophy.	***Fbln4*-/- mice:** early perinatal lethal due to cardiopulmonary failure. No intact elastic fibres. Tendons have disorganised tenocytes and disrupted ECM compartments, collagen fibrils packed irregularly and fewer in number. ***Lox*-/- mice:** similar phenotype to the above.	Markova *et al*., 2016 Mäki *et al*., 2005

Appendix Table 3. Sample metadata for single-cell (sc), single-nucleus (sn), and spatial RNA sequencing experiments. *"Full tendon" refers to regions containing the enthesis, the midbody, and the myotendinous junction with a small amount of connecting muscle. Kit refers to the relevant 10X Chemistry. W: weeks post-conception; Yr: age in years.*

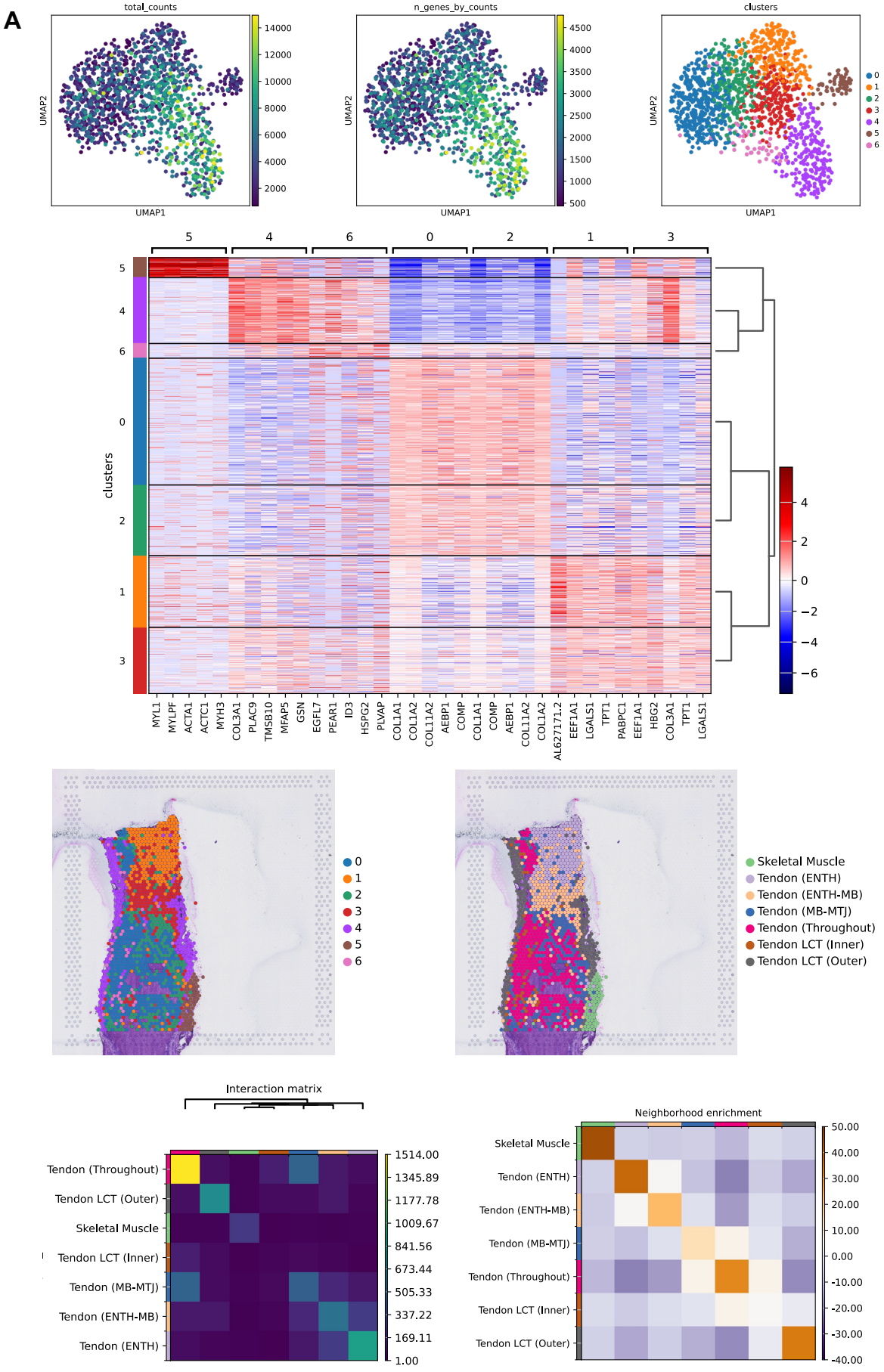
	Patient ID	Age	Sex	Tissue Type	Microanatomy	Library Seq Batch	Kit	Seq Protocol	Seq Type
Embryonic (HDBR) – data provided by Teichmann group (B. Zhang *et al.*, 2023)	BRC2078	5.1w	female	Hindlimb	Whole	Unknown	3' v2	Illumina-C HiSeq 4000 Paired end	scRNA-seq
	BRC2114	6.5w	male	Hindlimb	Thigh	Unknown			
	BRC2131	7.1w	male	Hindlimb	Thigh	Unknown			
					Thigh	Unknown			
	BRC2092	7.2w	male	Hindlimb	Thigh	Unknown			
					Thigh	Unknown			
	BRC2091	8.0w	female	Hindlimb	Thigh	Unknown			
	BRC2083	8.4w	female	Hindlimb	Thigh	Unknown			
					Thigh	Unknown			
	BRC2181	9.0w	male	Hindlimb	Thigh	Unknown			
					Thigh	Unknown			
	BRC2172	9.3w	female	Hindlimb	Thigh	Unknown			
	BRC2173	9.3w	male	Hindlimb	Thigh	Unknown			
	BRC2254	5.6w	male	Forelimb	Distal	Unknown	5' v1	Illumina-HTP NovaSeq 6000 Paired end	
					Middle	Unknown			
					Proximal	Unknown			
				Hindlimb	Distal	Unknown			
					Middle	Unknown			
					Proximal	Unknown			
	BRC2243	6.1w	male	Forelimb	Proximal	Unknown	3' v2		
					Middle	Unknown			
					Distal	Unknown			
				Hindlimb	Proximal	Unknown			
					Middle	Unknown			
					Distal	Unknown			
	BRC2245	6.1w	female	Hindlimb	Whole	Unknown	3' v1		spatial RNA-seq
					Whole	Unknown			
	BRC2218	6.2w	female	Hindlimb	Whole	Unknown			
	BRC2218+ BRC2217	6.2w	female + male	Hindlimb	Whole	Unknown			
	BRC2196	8w	male	Hindlimb	Distal	Unknown			
					Middle	Unknown			
					Proximal	Unknown			
					Foot	Unknown			

Foetal (HDBR) – data collected by the author	DEV15983	20w	male	Achilles tendon	Midbody	Apr-22	3' v3.1	Illumina-HTP NovaSeq 6000 Paired end	snRNA-seq
	DEV15984	20w	female	Achilles tendon	Midbody	Apr-22			
				Quadriceps tendon	Midbody	Apr-22			
	DEV15985	20w	male	Achilles tendon	Midbody	Dec-21			
				Quadriceps tendon	Midbody	Dec-21			
	DEV16127	17w	female	Achilles tendon	Full tendon	Jan-23			
				Quadriceps tendon	Full tendon	Jan-23			
	DEV16134	12w	male	Achilles tendon	Full tendon	Jan-23			
				Quadriceps tendon	Full tendon	Jan-23			
	DEV16135 + DEV16171	12w	male+ male	Achilles tendon	Full tendon	Jan-23			
				Quadriceps tendon	Full tendon	Jan-23			
	DEV16136	12w	female	Achilles tendon	Full tendon	Jan-23			
				Quadriceps tendon	Full tendon	Jan-23			
	DEV16569	17w	female	Achilles tendon	Full tendon	Jan-23			
				Quadriceps tendon	Full tendon	Jan-23			
	DEV16126	20w		Achilles tendon	Full tendon + muscle	Oct-22	3' v1	Illumina NextSeq500 Paired end	spatial RNA-seq
				Quadriceps tendon	Full tendon + muscle	Oct-22			
				Quadriceps tendon	Full tendon + muscle	Oct-22			
Adult (OMB) – data provided by the Tendon Seed Network (Baldwin *et al.*, 2023, 2021)	OMB0785	74yr	male	Achilles tendon	Enthesis	Oct-21	3' v3.1	Illumina-HP NovaSeq 6000 Paired end	snRNA-seq
					Midbody	Oct-21			
					MTJ	Oct-21			
					Muscle	Oct-21			
	OMB1556	51yr	male	Achilles tendon	Enthesis	Aug-22			
					Midbody	Aug-22			
					MTJ	Aug-22			
					Muscle	Aug-23			
	OMB1250	45yr	male	Achilles tendon	Enthesis	Oct-21			
					Midbody	Oct-21			
					MTJ	Oct-21			
					muscle	Aug-23			
	OMB1691	58yr	male	Achilles tendon	Enthesis	Aug-23			
					Midbody	Aug-23			
					MTJ	Aug-23			
	OMB1687	76yr	female	Achilles tendon	Enthesis	Aug-23			
					Midbody	Aug-23			
					MTJ	Aug-23			
	OMB1284	50yr	Male	Achilles tendon	Enthesis	Oct-21			
	OMB0792	29yr	Male	Quadriceps tendon	Midbody (Healthy)	Oct-21			
	OMB0778	67yr	Male	Quadriceps tendon	Midbody (Tear)	Oct-21			
	OMB1266	25yr	male	Quadriceps tendon	Midbody (Healthy)	Oct-21			
	OMB0793	69yr	Male	Quadriceps tendon	Midbody (Tear)	Oct-21			

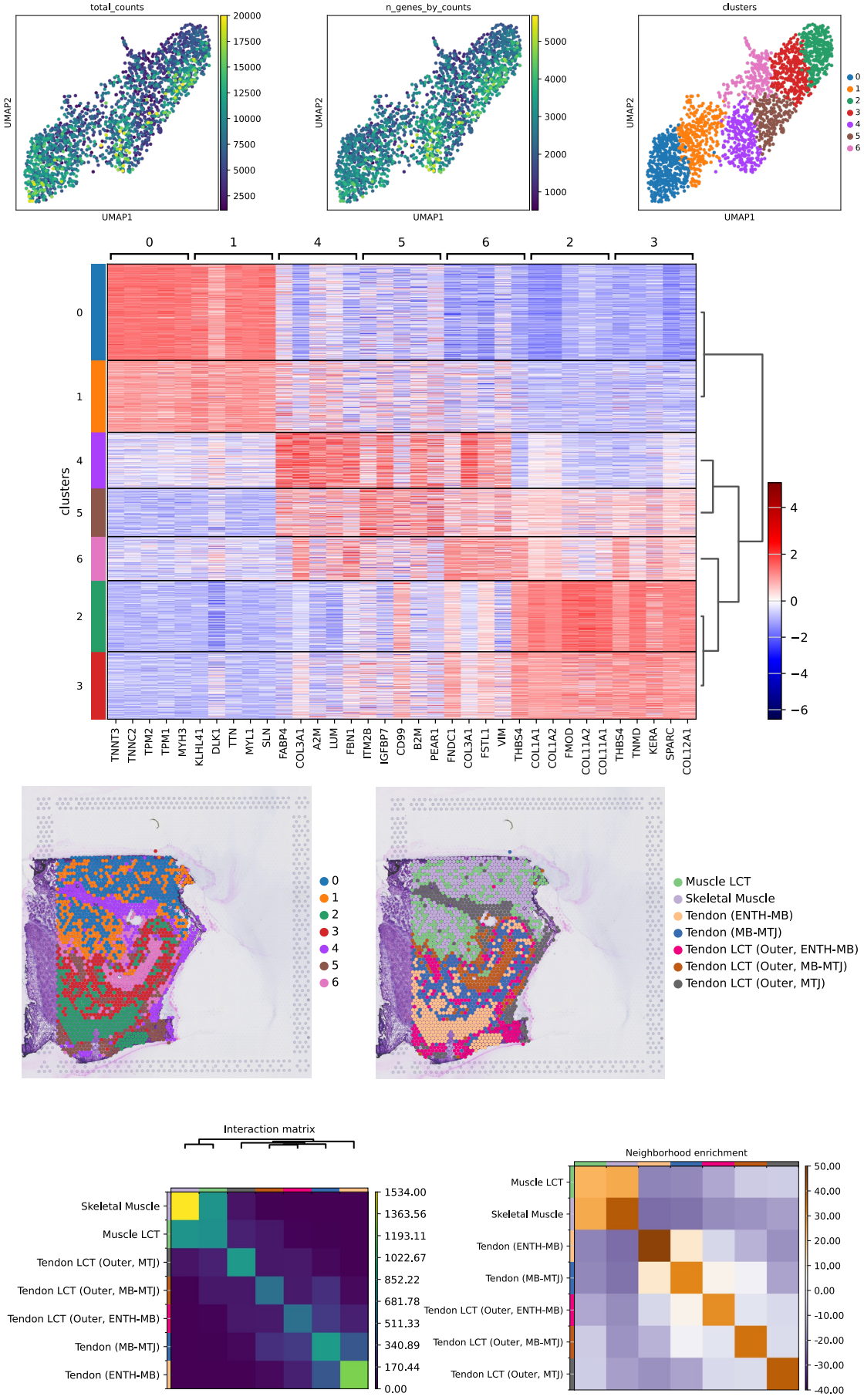
	OMB1248	44yr	Male	Quadriceps tendon	Midbody (Healthy)	Oct-21			
	OMB0779	75yr	Male	Quadriceps tendon x2	Midbody (Tear) x2	Oct-21, Dec-21			

Appendix Table 4. Summary of data collection, processing, and analysis contributions for Chapters 4–6.

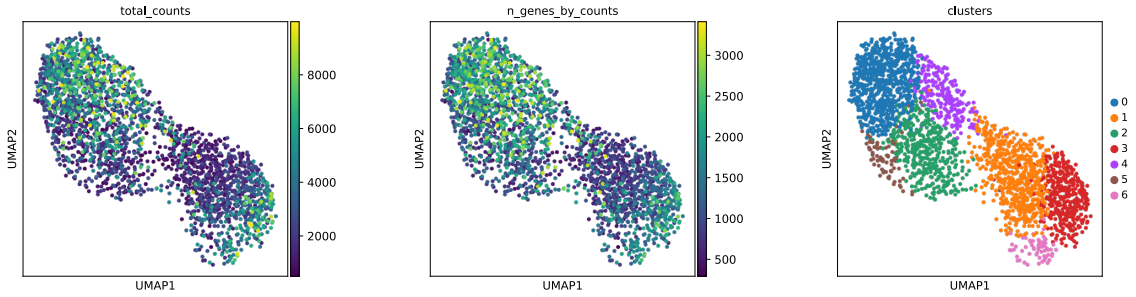
Chapter 4	The single-nucleus RNA-sequencing data (*N*=15 from 9 donors) and spatial RNA-sequencing data (*N*=3 from 1 donor) were fully collected, processed, and analysed by the author. The snRNA-seq libraries were sequenced by Genewiz (UK), while the spatial RNA libraries were sequenced in-house by the author.
Chapter 5	The single-cell RNA-sequencing data (*N*=25 from 11 donors) and spatial RNA-sequencing data (*N*=8 from 2 donors) were originally collected and processed by B. Zhang *et al.*, 2023, from the Teichmann group at the Sanger Institute, Cambridge, UK. The author re-analysed this data starting from CellRanger-aligned files.
Chapter 6	Single-nucleus RNA-sequencing data (*N*=26 from 12 donors) were collected, processed, and analysed by Dr. Jolet Mimpen (quadriceps tendons) and Dr. Carla Cohen (Achilles tendons) of the Tendon Seed Network (Baldwin *et al.*, 2021, 2023). The snRNA-seq libraries were sequenced by Genewiz (UK). The author used the annotated and integrated dataset for comparative analysis with developmental data. Tissue preparation and sectioning for developmental tendons were performed by the author, while Dr. Mimpen prepared and sectioned the adult tendon samples. Immunohistochemical staining of all slides was performed by the Histology Team at the Kennedy Institute, NDORMS, Oxford, UK.

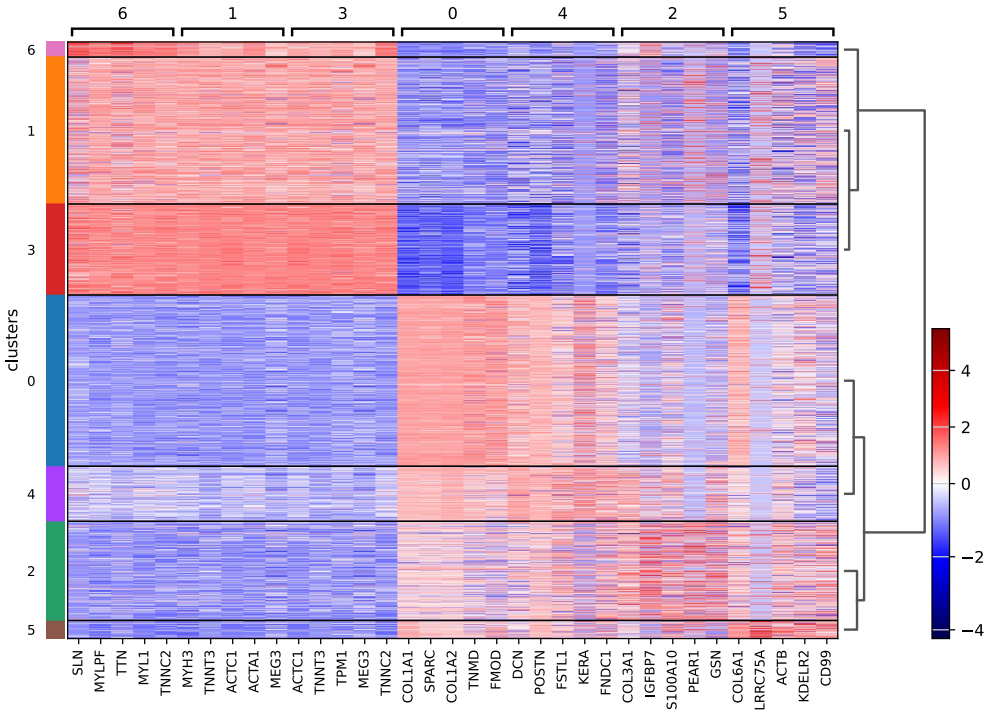

A
total_counts
n_genes_by_counts
clusters
UMAP1
UMAP2
clusters
MYL1
MYLPF
ACTA1
ACTC1
MYH3
COL3A1
PLAC9
TMSB10
MFAP5
GSN
EGFL7
PEAR1
ID3
HSPG2
PLVAP
COL1A1
COL1A2
COL11A2
AEBP1
COMP
AL627171.2
EEF1A1
LGALS1
TPT1
PABPC1
HBG2
Skeletal Muscle
Tendon (ENTH)
Tendon (ENTH-MB)
Tendon (MB-MTJ)
Tendon (Throughout)
Tendon LCT (Inner)
Tendon LCT (Outer)
Interaction matrix
Neighborhood enrichment

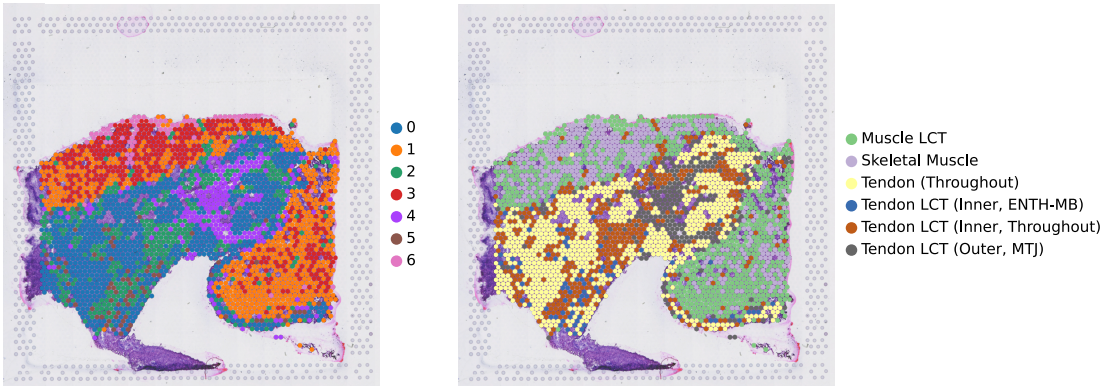
B

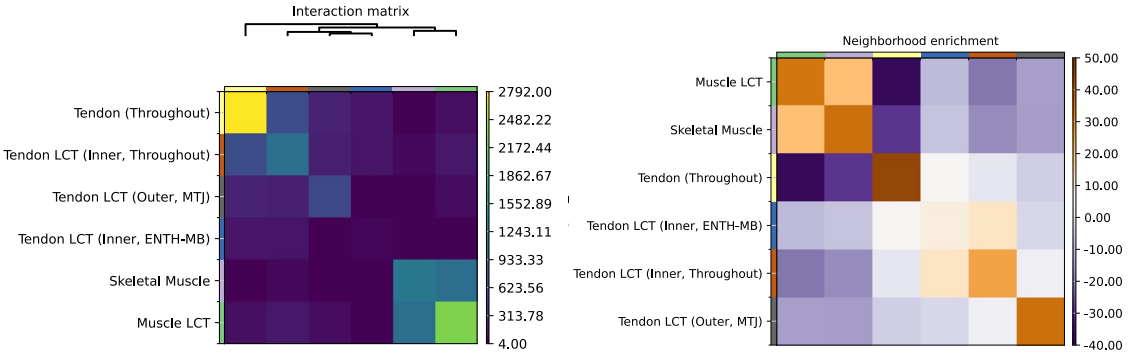

total_counts
n_genes_by_counts
clusters
UMAP1
UMAP2
clusters
TNNT3 TNNC2 TPM2 TPM1 MYH3 KLHL41 DLK1 TTN MYL1 SLN FABP4 COL3A1 A2M LUM FBN1 ITM2B IGFBP7 CD99 B2M PEAR1 FNDC1 COL3A1 FSTL1 VIM THBS4 COL1A1 COL1A2 FMOD COL11A2 COL11A1 THBS4 TNMD KERA SPARC COL12A1
Muscle LCT
Skeletal Muscle
Tendon (ENTH-MB)
Tendon (MB-MTJ)
Tendon LCT (Outer, ENTH-MB)
Tendon LCT (Outer, MB-MTJ)
Tendon LCT (Outer, MTJ)
Interaction matrix
Neighborhood enrichment

C

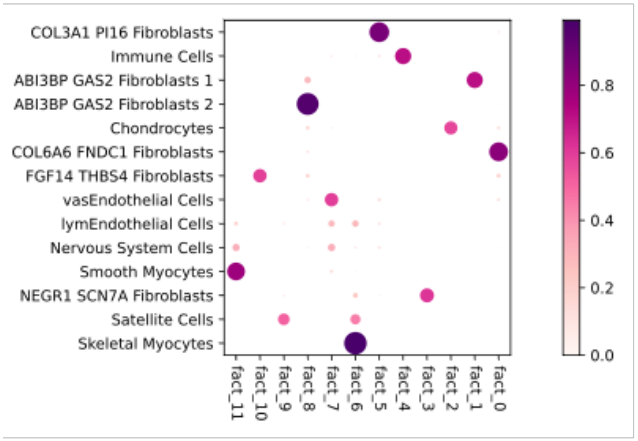

total_counts
n_genes_by_counts
clusters
UMAP1
UMAP2

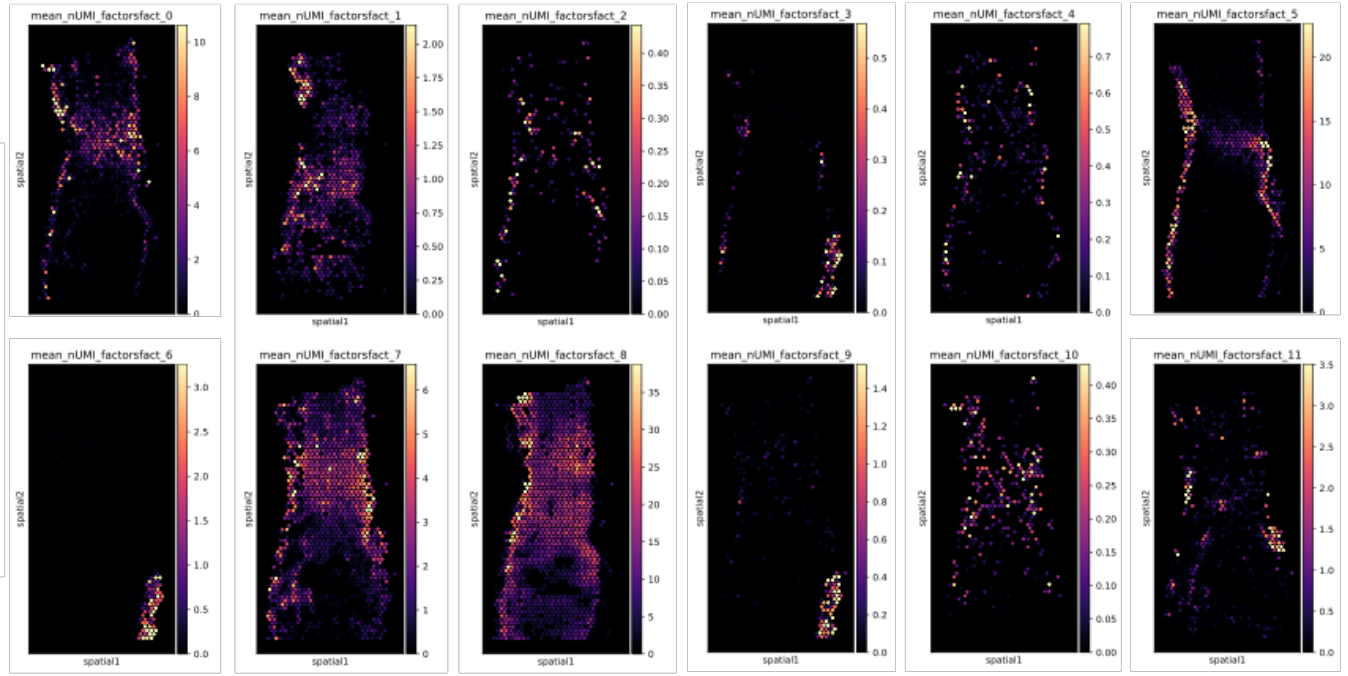

clusters
SLN
MYLPF
TTN
MYL1
TNNC2
MYH3
TNNT3
ACTC1
ACTA1
MEG3
ACTC1
TNNT3
TPM1
MEG3
TNNC2
COL1A1
SPARC
COL1A2
TNMD
FMOD
DCN
POSTN
FSTL1
KERA
FNDC1
COL3A1
IGFBP7
S100A10
PEAR1
GSN
COL6A1
LRRC75A
ACTB
KDELR2
CD99

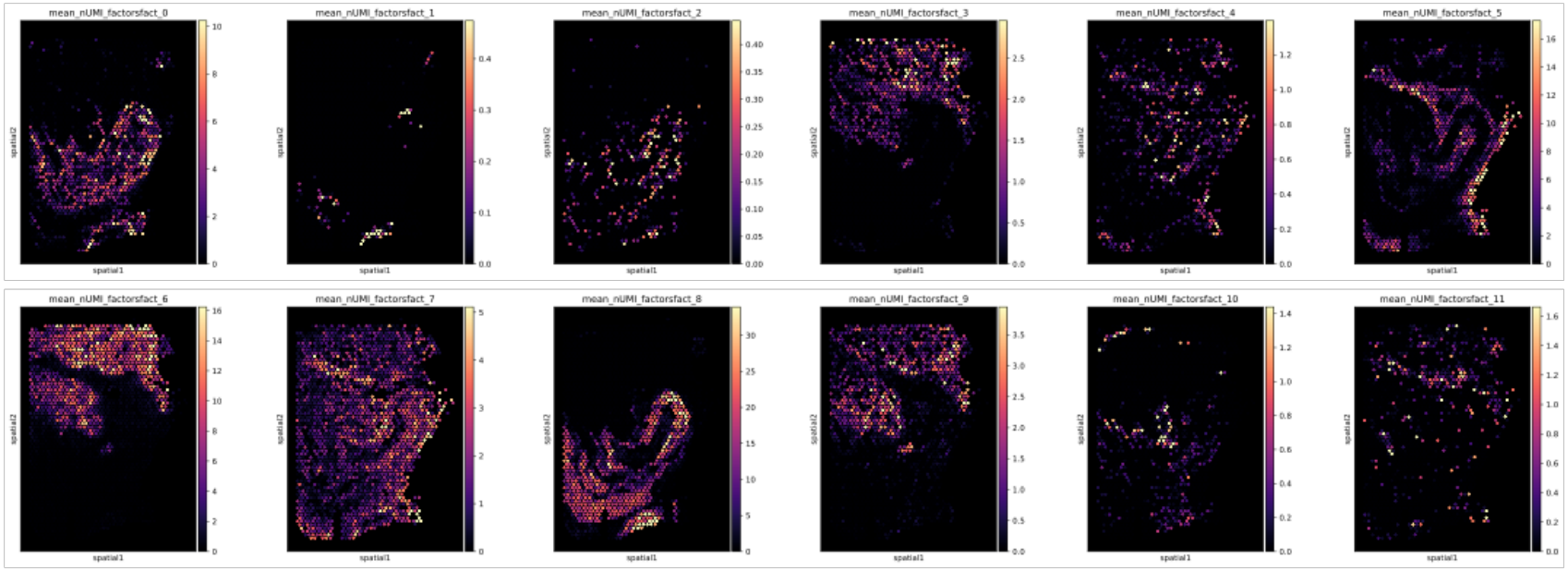

Muscle LCT
Skeletal Muscle
Tendon (Throughout)
Tendon LCT (Inner, ENTH-MB)
Tendon LCT (Inner, Throughout)
Tendon LCT (Outer, MTJ)

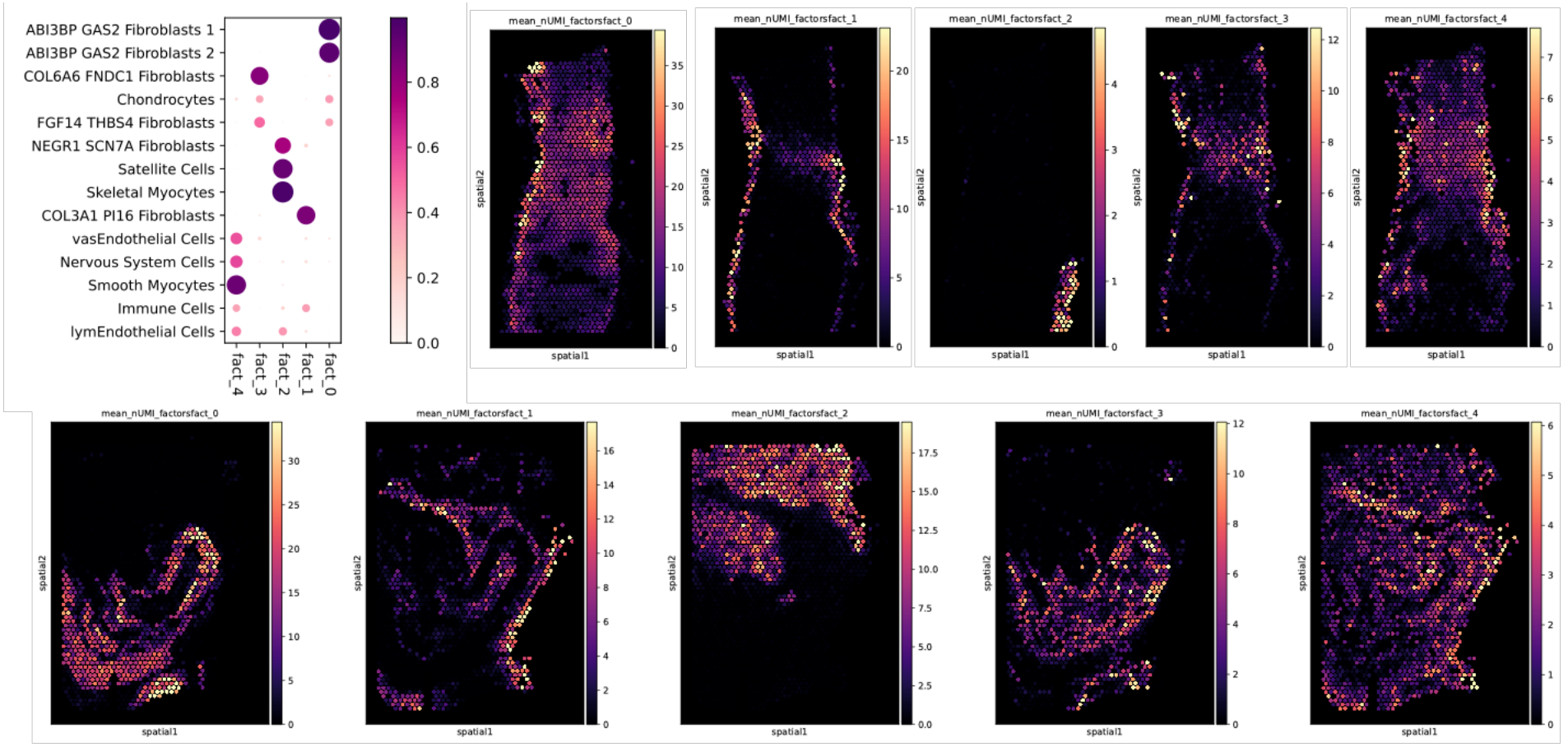

Interaction matrix
Neighborhood enrichment
Tendon (Throughout)
Tendon LCT (Inner, Throughout)
Tendon LCT (Outer, MTJ)
Tendon LCT (Inner, ENTH-MB)
Skeletal Muscle
Muscle LCT

Appendix Figure 1. Analysis of spatial RNA-seq data of human foetal 20 pcw Achilles and quadriceps tendons tendons. *Subfigure A corresponds to the Achilles tendon data, while subfigures B and C show two different quadriceps tendons. (From top to bottom) UMAPs show total counts, genes-by-counts and Leiden clusters of the spatial RNA-seq data (calculated at resolution of 1.0). Heatmaps show scaled gene expression of top 5 differentially expressed genes for each of the clusters, identified using between-cluster Wilcoxon rank-sum tests. Spatial expression plots show tissue distributions of Leiden clusters (left) and manually annotated regions (right). Matrix plots showing annotated tissue region edge interaction and neighbourhood enrichment scores.*

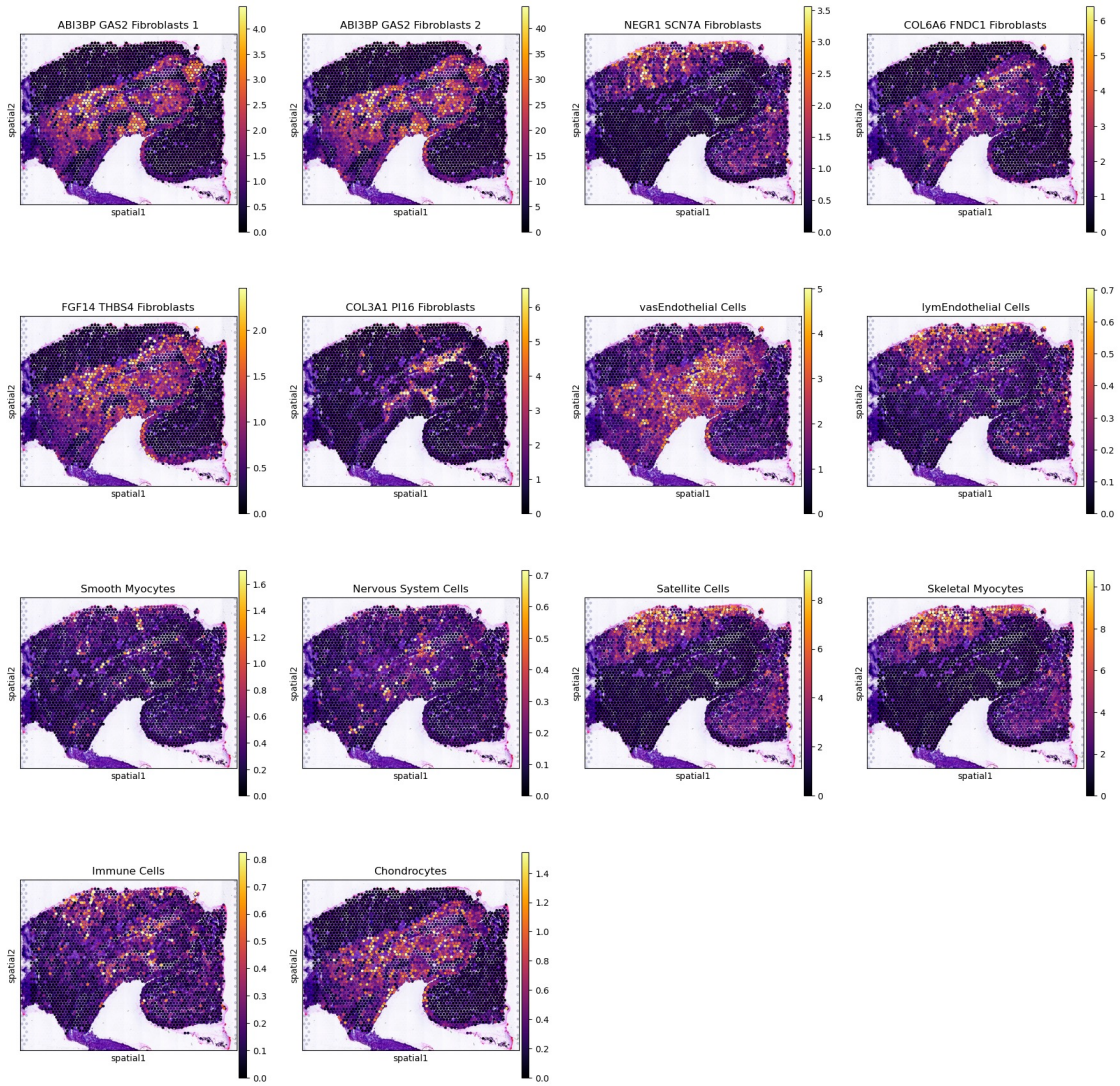

COL3A1 PI16 Fibroblasts
Immune Cells
ABI3BP GAS2 Fibroblasts 1
ABI3BP GAS2 Fibroblasts 2
Chondrocytes
COL6A6 FNDC1 Fibroblasts
FGF14 THBS4 Fibroblasts
vasEndothelial Cells
lymEndothelial Cells
Nervous System Cells
Smooth Myocytes
NEGR1 SCN7A Fibroblasts
Satellite Cells
Skeletal Myocytes
fact_11
fact_10
fact_9
fact_8
fact_7
fact_6
fact_5
fact_4
fact_3
fact_2
fact_1
fact_0
0.8
0.6
0.4
0.2
0.0


mean_nUMI_factorsfact_0
mean_nUMI_factorsfact_1
mean_nUMI_factorsfact_2
mean_nUMI_factorsfact_3
mean_nUMI_factorsfact_4
mean_nUMI_factorsfact_5
mean_nUMI_factorsfact_6
mean_nUMI_factorsfact_7
mean_nUMI_factorsfact_8
mean_nUMI_factorsfact_9
mean_nUMI_factorsfact_10
mean_nUMI_factorsfact_11
spatial1
spatial2


mean_nUMI_factorsfact_0
mean_nUMI_factorsfact_1
mean_nUMI_factorsfact_2
mean_nUMI_factorsfact_3
mean_nUMI_factorsfact_4
mean_nUMI_factorsfact_5
mean_nUMI_factorsfact_6
mean_nUMI_factorsfact_7
mean_nUMI_factorsfact_8
mean_nUMI_factorsfact_9
mean_nUMI_factorsfact_10
mean_nUMI_factorsfact_11
spatial1
spatial2



Appendix Figure 2. Unsupervised* non-negative matrix factorisation (NMF) *analysis of Visium ST cell2location results for 12 and 5 factors across the three tendon samples. *Dotplot shows NMF factors derived from mean normalised UMI counts (dot size and colour). Gene loadings represent the contribution of individual genes to each estimated cell type (factor) in the colocalization model. These values indicate how strongly each gene is associated with each cell type. Scatter plots show cell densities (in the form of mean normalised UMI) for the remaining 20pcw Achilles (top) and quadriceps (bottom) tendons not shown in Figures 30 or 31.*

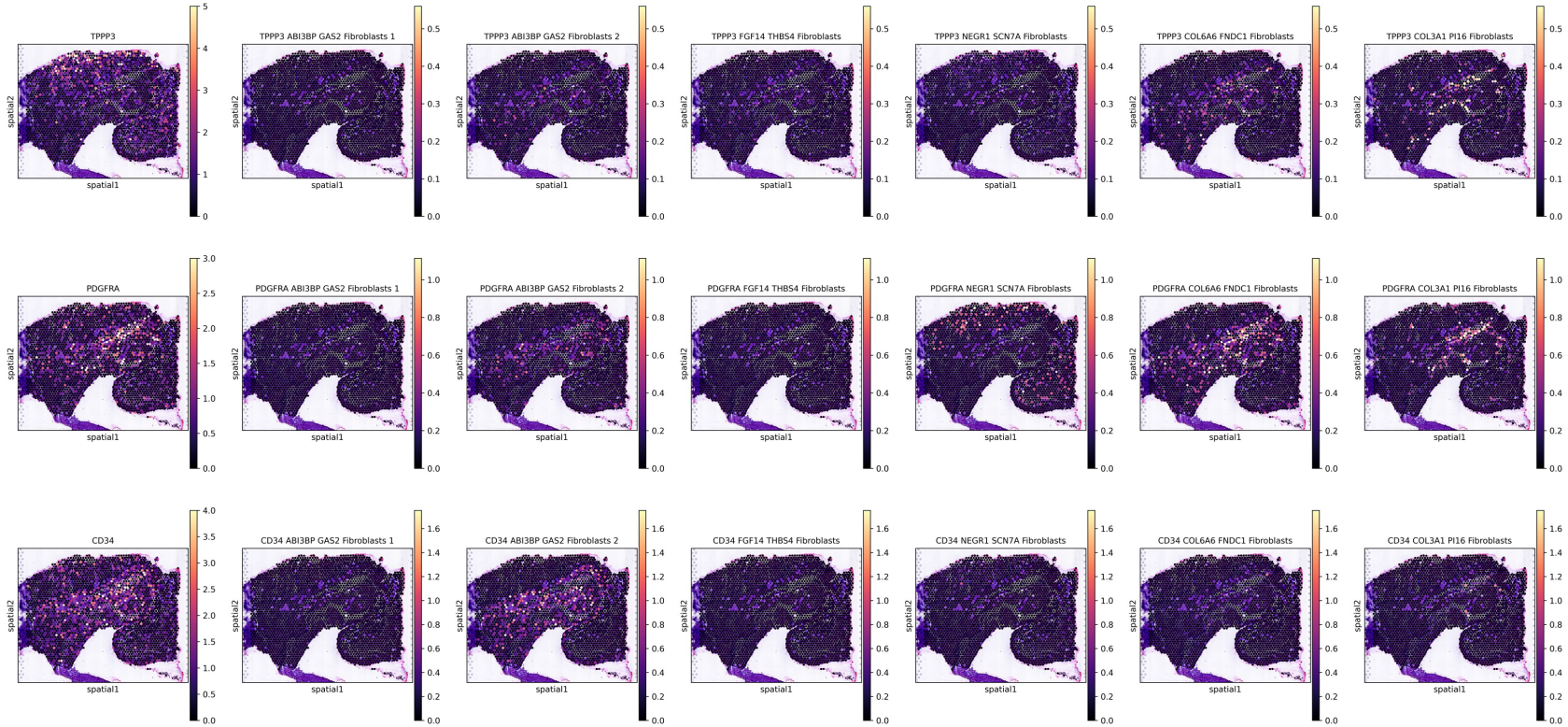


Appendix Figure 3. Cell2location discrete mapping of quadriceps tendon scRNA-seq cell type transcriptomic profiles from five 20 pcw single-nuclei RNA-sequencing samples. *The intensity of the colour at each spatial location indicates the relative abundance of a given cell type.*

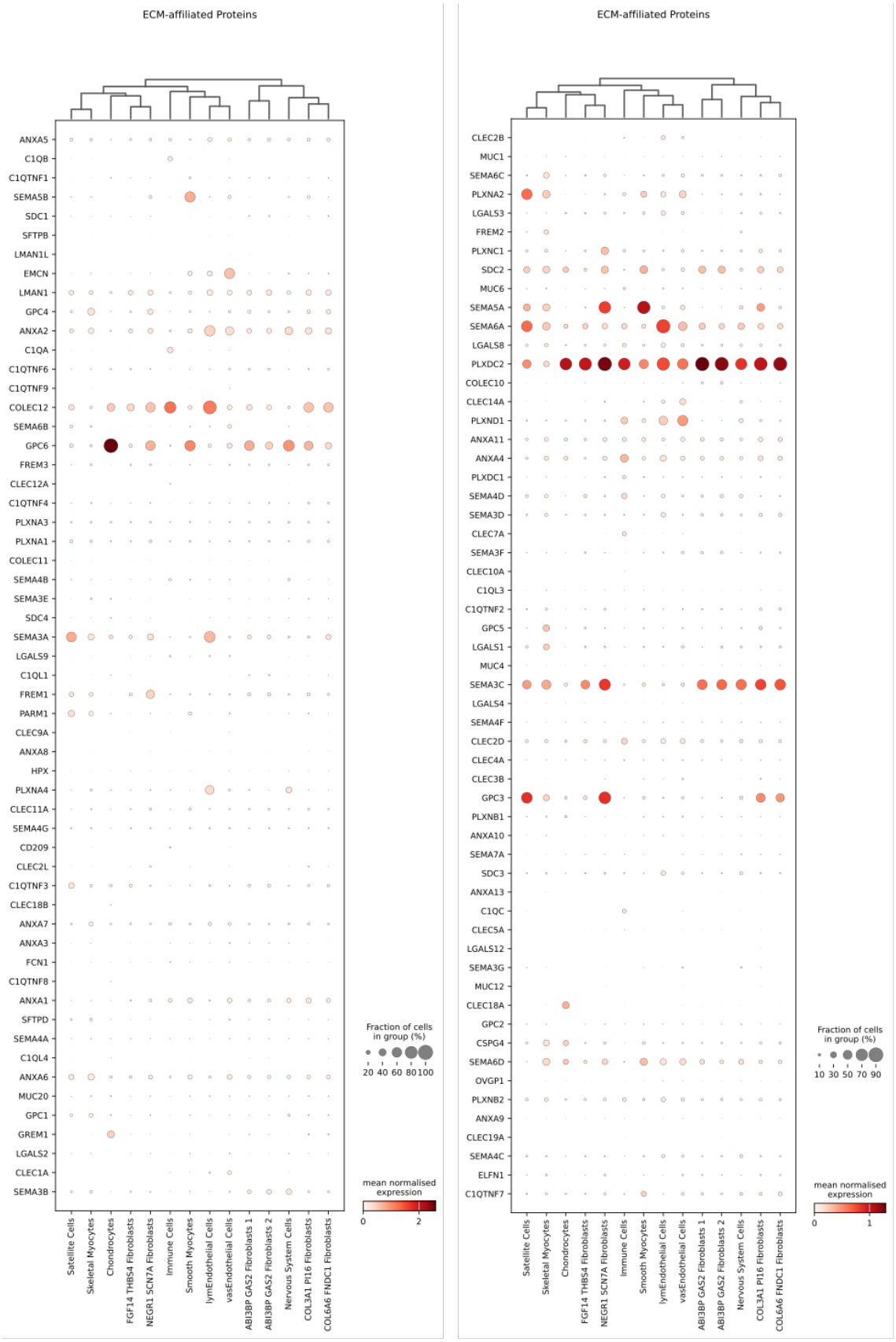
Fascicular TSPC Markers:

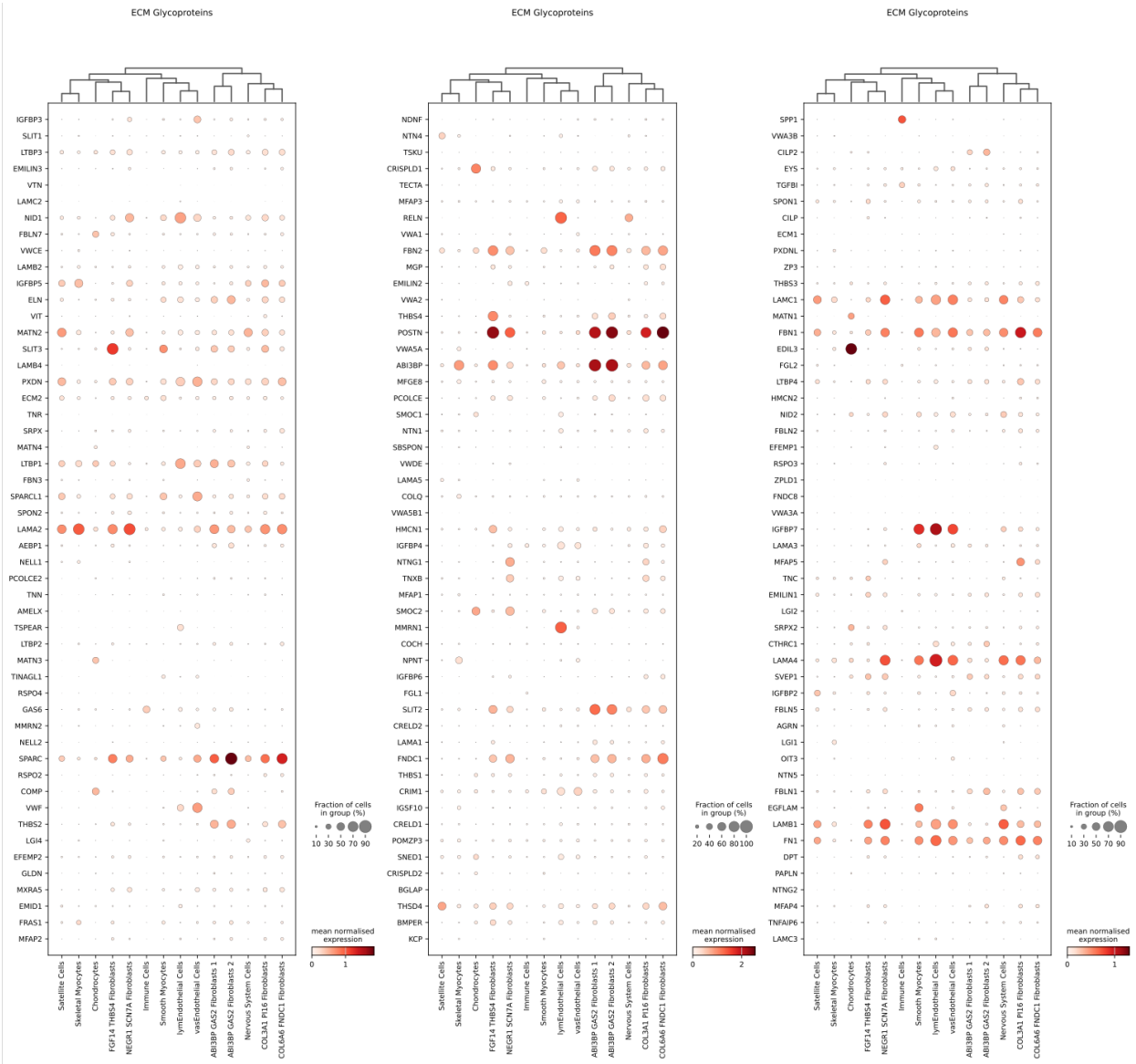


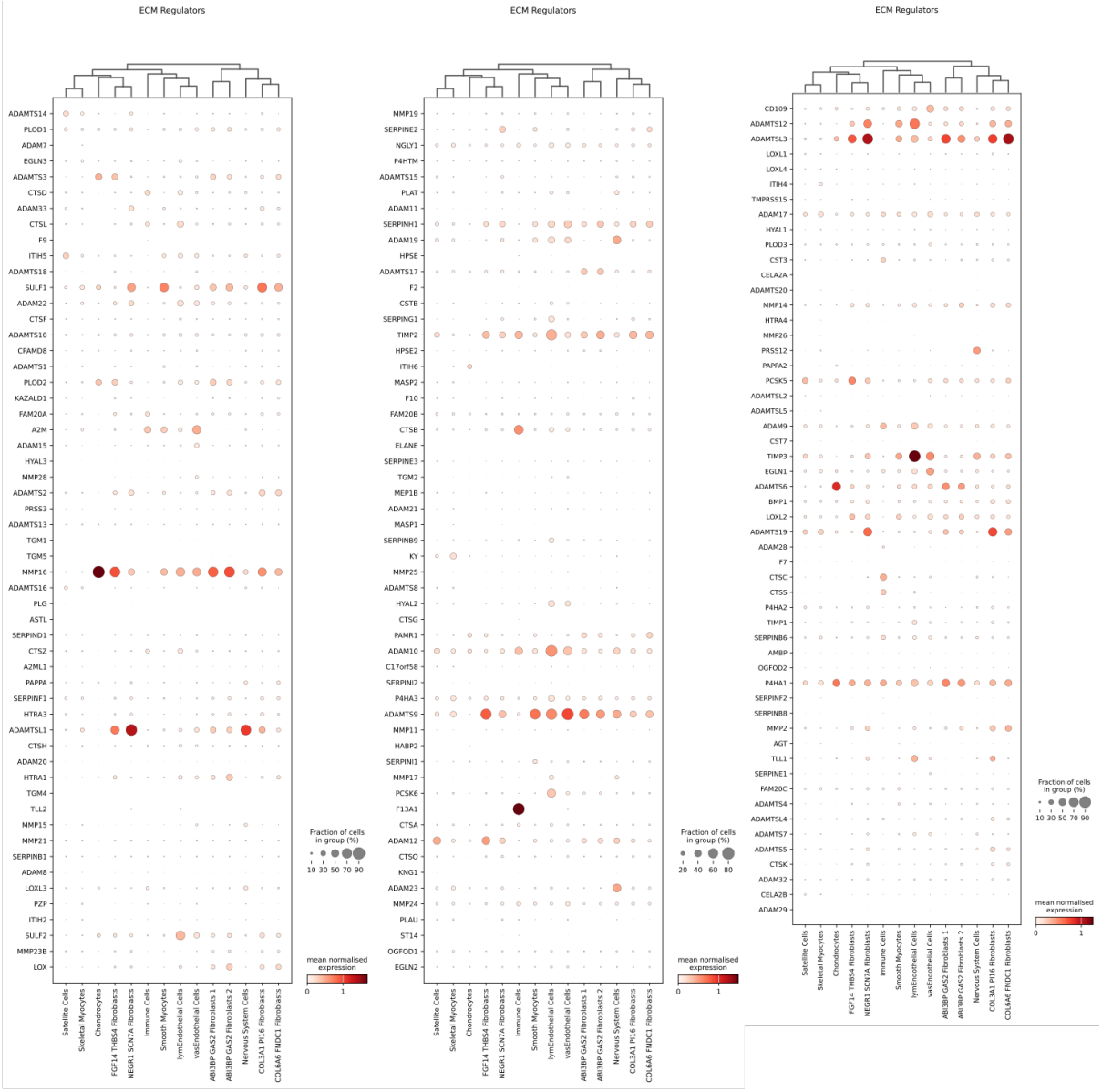
Sheath TSPC Markers:



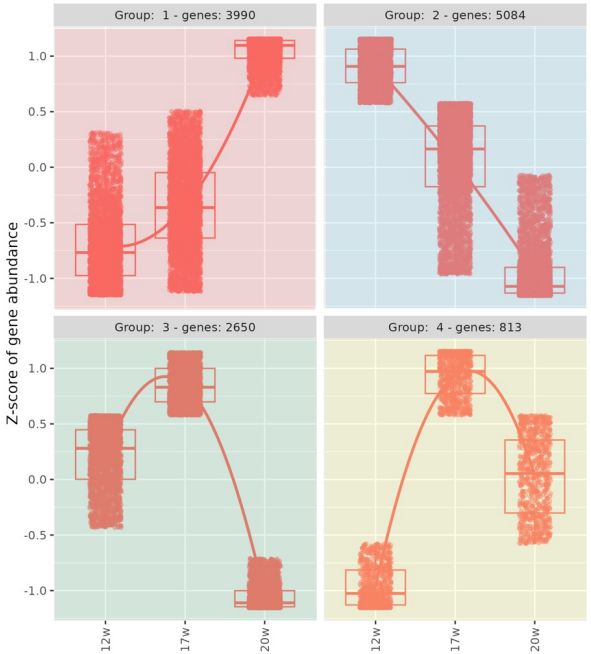
Appendix Figure 4. Fibroblast type-specific expression of fascicular and sheath TSPC markers. *All markers outlined at the top of Table 1 were used if they were present in the data. Scores represent normalised gene expression values.*


ECM-affiliated Proteins
ANXA5
C1QB
C1QTNF1
SEMA5B
SDC1
SFTPB
LMAN1L
EMCN
LMAN1
GPC4
ANXA2
C1QA
C1QTNF6
C1QTNF9
COLEC12
SEMA6B
GPC6
FREM3
CLEC12A
C1QTNF4
PLXNA3
PLXNA1
COLEC11
SEMA4B
SEMA3E
SDC4
SEMA3A
LGALS9
C1QL1
FREM1
PARM1
CLEC9A
ANXA8
HPX
PLXNA4
CLEC11A
SEMA4G
CD209
CLEC2L
C1QTNF3
CLEC18B
ANXA7
ANXA3
FCN1
C1QTNF8
ANXA1
SFTPD
SEMA4A
C1QL4
ANXA6
MUC20
GPC1
GREM1
LGALS2
CLEC1A
SEMA3B
Satellite Cells
Skeletal Myocytes
Chondrocytes
FGF14 THBS4 Fibroblasts
NEGR1 SCN7A Fibroblasts
Immune Cells
Smooth Myocytes
lymEndothelial Cells
vasEndothelial Cells
ABI3BP GAS2 Fibroblasts 1
ABI3BP GAS2 Fibroblasts 2
Nervous System Cells
COL3A1 PI16 Fibroblasts
COL6A6 FNDC1 Fibroblasts
Fraction of cells in group (%)
20 40 60 80 100
mean normalised expression
0
2
ECM-affiliated Proteins
CLEC2B
MUC1
SEMA6C
PLXNA2
LGALS3
FREM2
PLXNC1
SDC2
MUC6
SEMA5A
SEMA6A
LGALS8
PLXDC2
COLEC10
CLEC14A
PLXND1
ANXA11
ANXA4
PLXDC1
SEMA4D
SEMA3D
CLEC7A
SEMA3F
CLEC10A
C1QL3
C1QTNF2
GPC5
LGALS1
MUC4
SEMA3C
LGALS4
SEMA4F
CLEC2D
CLEC4A
CLEC3B
GPC3
PLXNB1
ANXA10
SEMA7A
SDC3
ANXA13
C1QC
CLEC5A
LGALS12
SEMA3G
MUC12
CLEC18A
GPC2
CSPG4
SEMA6D
OVGP1
PLXNB2
ANXA9
CLEC19A
SEMA4C
ELFN1
C1QTNF7
Satellite Cells
Skeletal Myocytes
Chondrocytes
FGF14 THBS4 Fibroblasts
NEGR1 SCN7A Fibroblasts
Immune Cells
Smooth Myocytes
lymEndothelial Cells
vasEndothelial Cells
ABI3BP GAS2 Fibroblasts 1
ABI3BP GAS2 Fibroblasts 2
Nervous System Cells
COL3A1 PI16 Fibroblasts
COL6A6 FNDC1 Fibroblasts
Fraction of cells in group (%)
10 30 50 70 90
mean normalised expression
0
1

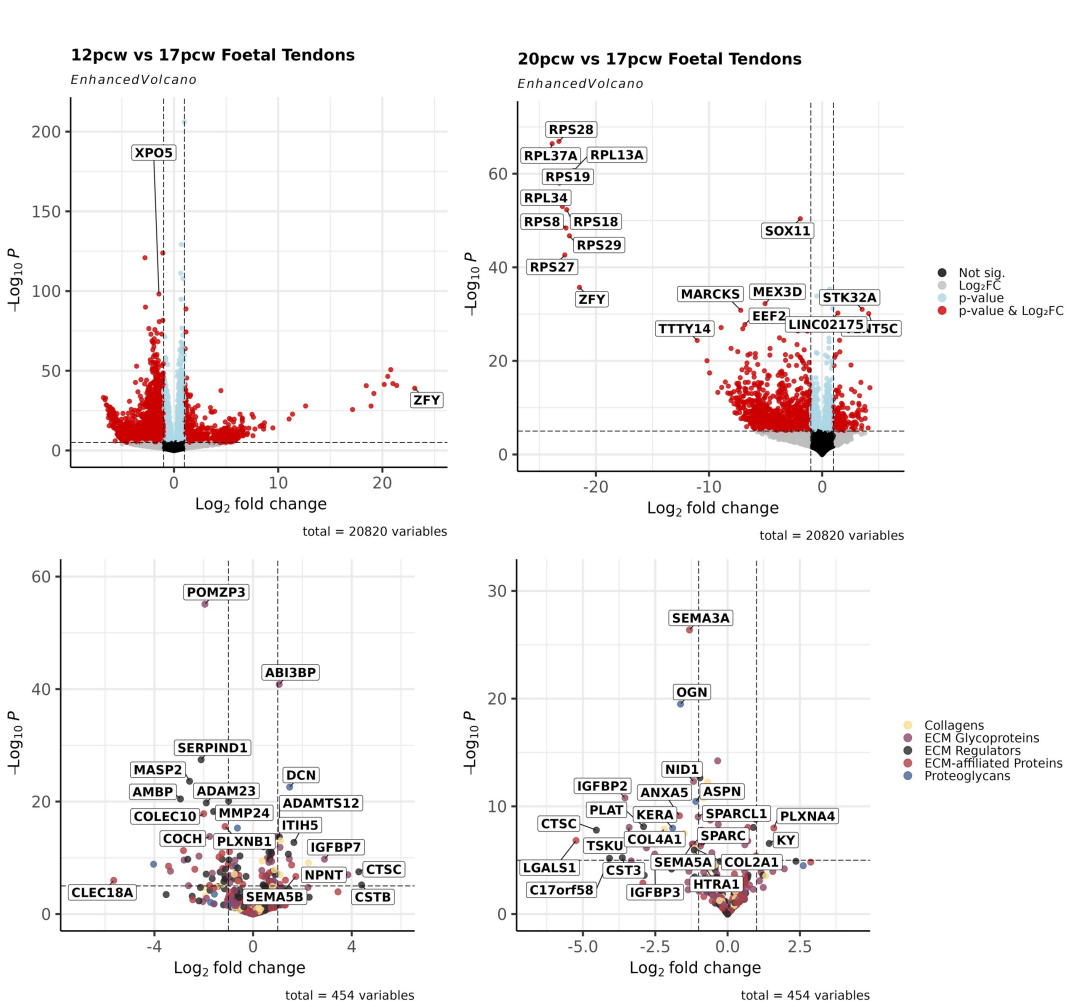

ECM Glycoproteins
IGFBP3
SLIT1
LTBP3
EMILIN3
VTN
LAMC2
NID1
FBLN7
VWCE
LAMB2
IGFBP5
ELN
VIT
MATN2
SLIT3
LAMB4
PXDN
ECM2
TNR
SRPX
MATN4
LTBP1
FBN3
SPARCL1
SPON2
LAMA2
AEBP1
NELL1
PCOLCE2
TNN
AMELX
TSPEAR
LTBP2
MATN3
TINAGL1
RSPO4
GAS6
MMRN2
NELL2
SPARC
RSPO2
COMP
VWF
THBS2
LGI4
EFEMP2
GLDN
MXRA5
EMID1
FRAS1
MFAP2
Fraction of cells in group (%)
10 30 50 70 90
mean normalised expression
0 1
Satellite Cells
Skeletal Myocytes
Chondrocytes
FGF14 THBS4 Fibroblasts
NEGR1 SCN7A Fibroblasts
Immune Cells
Smooth Myocytes
lymEndothelial Cells
vasEndothelial Cells
ABI3BP GAS2 Fibroblasts 1
ABI3BP GAS2 Fibroblasts 2
Nervous System Cells
COL3A1 P16 Fibroblasts
COL6A6 FNDC1 Fibroblasts
ECM Glycoproteins
NDNF
NTN4
TSKU
CRISPLD1
TECTA
MFAP3
RELN
VWA1
FBN2
MGP
EMILIN2
VWA2
THBS4
POSTN
VWA5A
ABI3BP
MFGE8
PCOLCE
SMOC1
NTN1
SBSPON
VWDE
LAMA5
COLQ
VWA5B1
HMCN1
IGFBP4
NTNG1
TNXB
MFAP1
SMOC2
MMRN1
COCH
NPNT
IGFBP6
FGL1
SLIT2
CRELD2
LAMA1
FNDC1
THBS1
CRIM1
IGSF10
CRELD1
POMZP3
SNED1
CRISPLD2
BGLAP
THSD4
BMPER
KCP
Fraction of cells in group (%)
20 40 60 80 100
mean normalised expression
0 2
Satellite Cells
Skeletal Myocytes
Chondrocytes
FGF14 THBS4 Fibroblasts
NEGR1 SCN7A Fibroblasts
Immune Cells
Smooth Myocytes
lymEndothelial Cells
vasEndothelial Cells
ABI3BP GAS2 Fibroblasts 1
ABI3BP GAS2 Fibroblasts 2
Nervous System Cells
COL3A1 P16 Fibroblasts
COL6A6 FNDC1 Fibroblasts
ECM Glycoproteins
SPP1
VWA3B
CILP2
EYS
TGFBI
SPON1
CILP
ECM1
PXDNL
ZP3
THBS3
LAMC1
MATN1
FBN1
EDIL3
FGL2
LTBP4
HMCN2
NID2
FBLN2
EFEMP1
RSPO3
ZPLD1
FNDC8
VWA3A
IGFBP7
LAMA3
MFAP5
TNC
EMILIN1
LGI2
SRPX2
CTHRC1
LAMA4
SVEP1
IGFBP2
FBLN5
AGRN
LGI1
OIT3
NTN5
FBLN1
EGFLAM
LAMB1
FN1
DPT
PAPLN
NTNG2
MFAP4
TNFAIP6
LAMC3
Fraction of cells in group (%)
10 30 50 70 90
mean normalised expression
0 1
Satellite Cells
Skeletal Myocytes
Chondrocytes
FGF14 THBS4 Fibroblasts
NEGR1 SCN7A Fibroblasts
Immune Cells
Smooth Myocytes
lymEndothelial Cells
vasEndothelial Cells
ABI3BP GAS2 Fibroblasts 1
ABI3BP GAS2 Fibroblasts 2
Nervous System Cells
COL3A1 P16 Fibroblasts
COL6A6 FNDC1 Fibroblasts

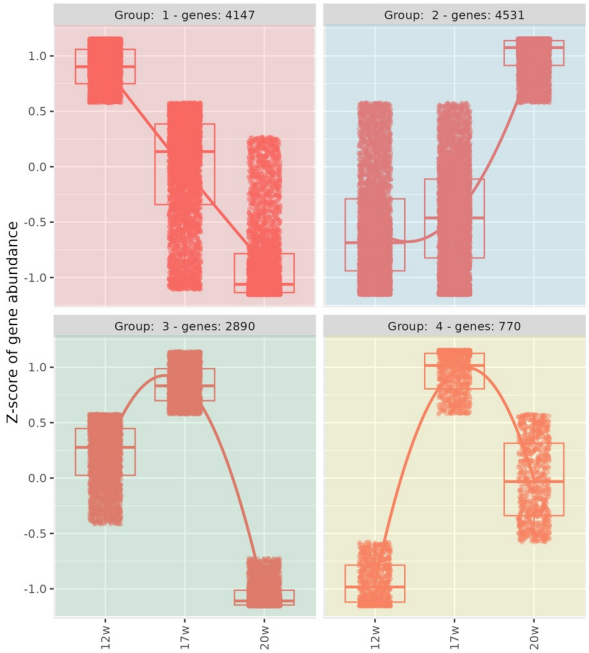


Appendix Figure 5. Foetal 12-20 pcw tendon matrisomal gene expression profiles. *Dotplots show the mean normalised expression levels alongside the proportions of expressing cell types for matrisomal genes categorised as ECM-affiliated proteins, ECM glycoproteins, and ECM regulators. The lists of matrisomal genes were obtained from the matrisomeDB database (Shao et al., 2020). The plots for collagens and proteoglycans are shown in Figure 33.*

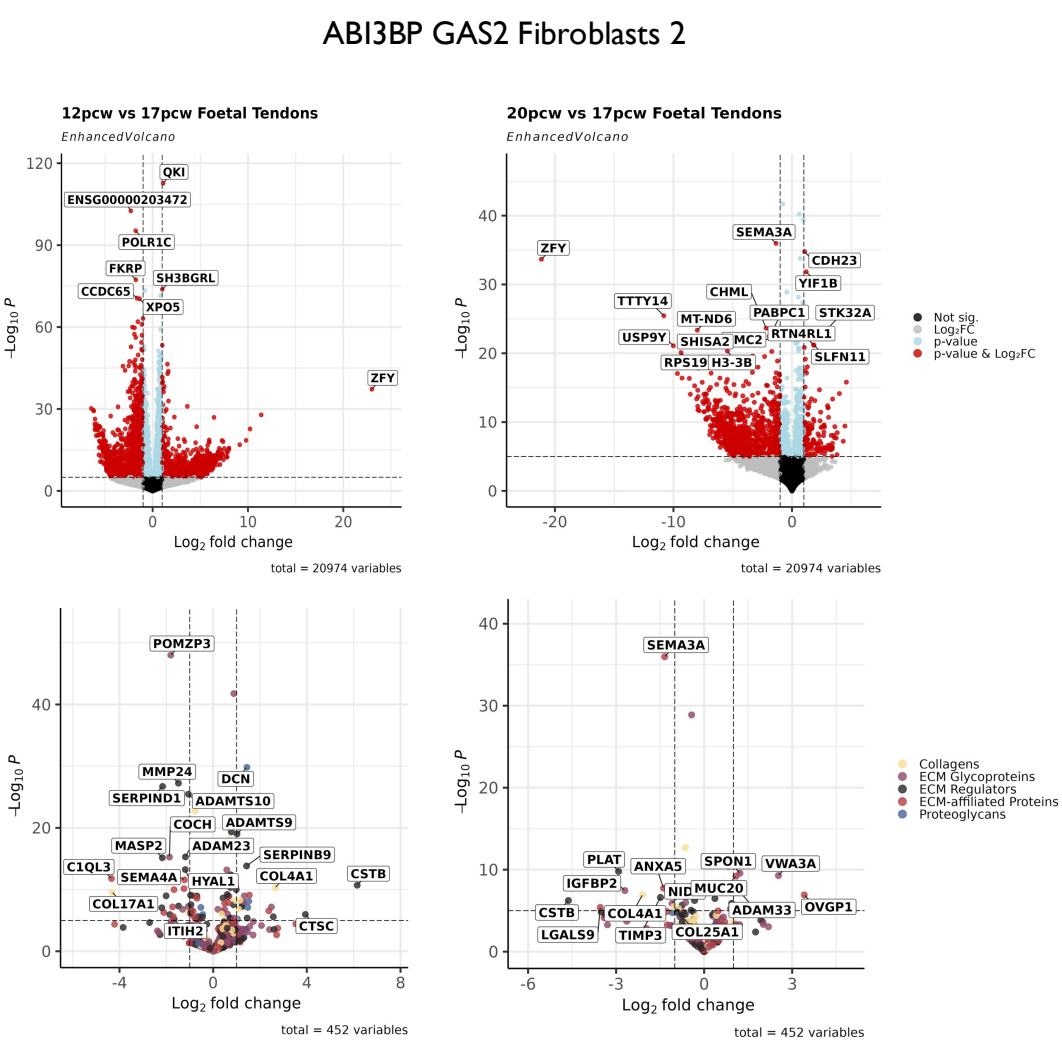


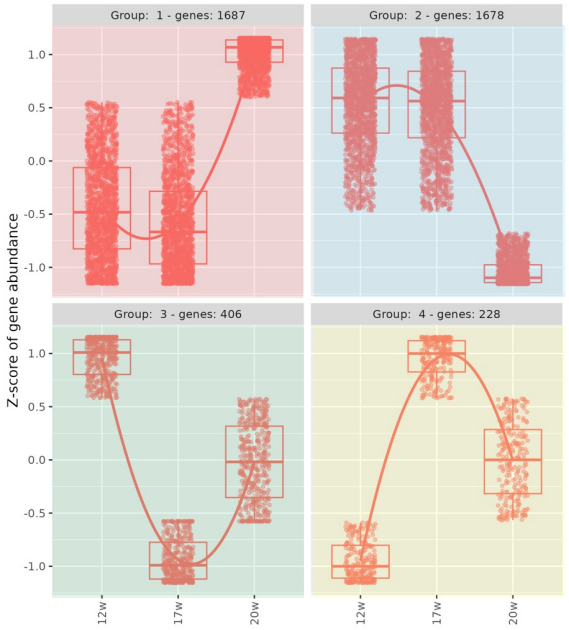
BH FDR <0.01 (389):	BH FDR <0.01 (233):
Cell Signalling and Communication (Wnt, TGFb) Development and Morphogenesis Cytoskeleton and Cell Structure Metabolism and Energy Derivation Autophagy and Cellular Stress Response Protein Degradation and Modification Cellular Transport Cytoskeleton and Cell Structure Gene Expression and Transcription Cell Proliferation, Growth and Differentiation	Cell Cycle Regulation, DNA Replication and Repair Ribosome and Protein Synthesis Protein Modification and Localisation Cell Division Metabolic Processes Cell Signalling and Regulation RNA Processing and Transport Differentiation and Development
BH FDR <0.05 (30):	**BH FDR <0.05 (1):**
RNA and Chromatin Modification Cytoskeletal Organisation and Movement Protein Modification and Transport Transcription and Chromatin Remodelling Cell Signalling and Response	Cellular Transport





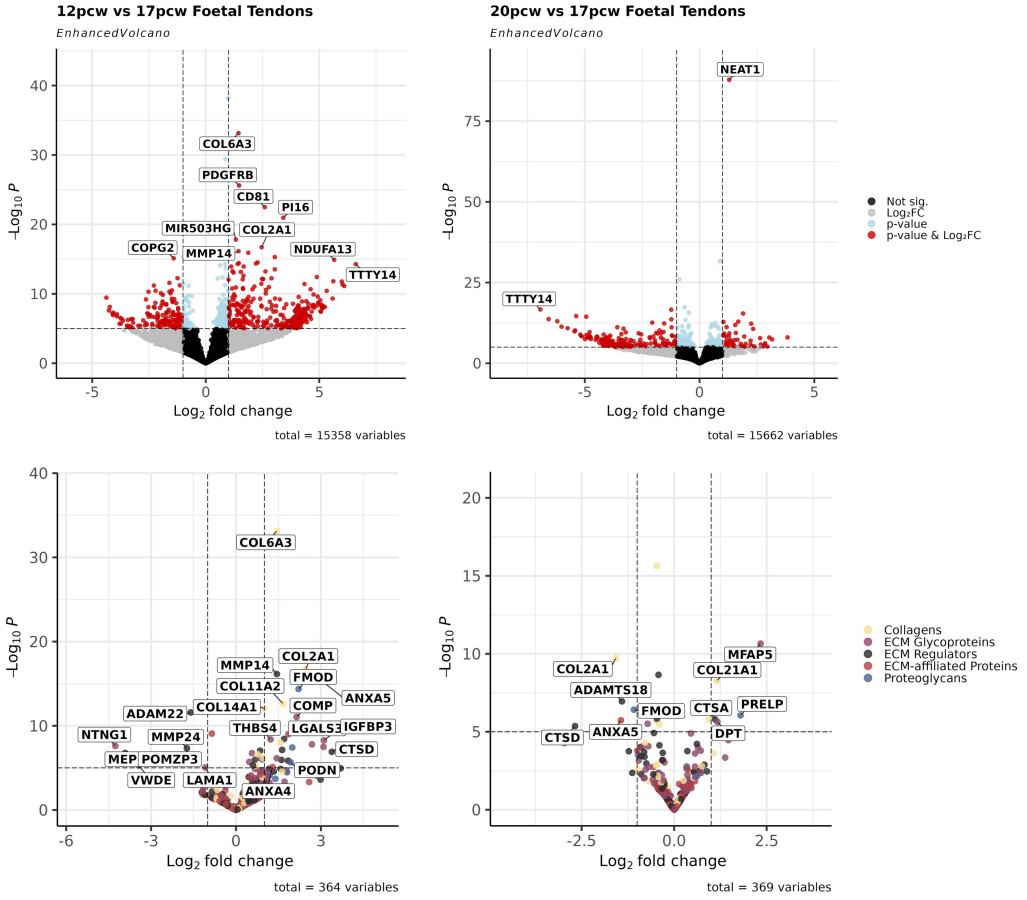
BH FDR-adjusted p-value <0.05 (460):	BH FDR <0.01 (481):
Cell Cycle and DNA Processes Chromosome and Nuclear Dynamics Microtubule and Spindle Dynamics RNA Processing and Metabolism Cellular Organization and Structure Ribosome Biogenesis Other Cellular Processes Metabolic Processes	Protein Degradation and Modification Cellular Transport Cell Signalling and Communication (Wnt, TGFb) Development and Morphogenesis Autophagy and Cellular Stress Response Cytoskeleton and Cell Structure Gene Expression and Transcription Metabolism and Energy Derivation Immune Response
BH FDR-adjusted p-value <0.05 (71):	**BH FDR <0.05 (0):**
Metabolic Processes Transport Post-transcriptional Processing and Modification Cell Signalling	NA

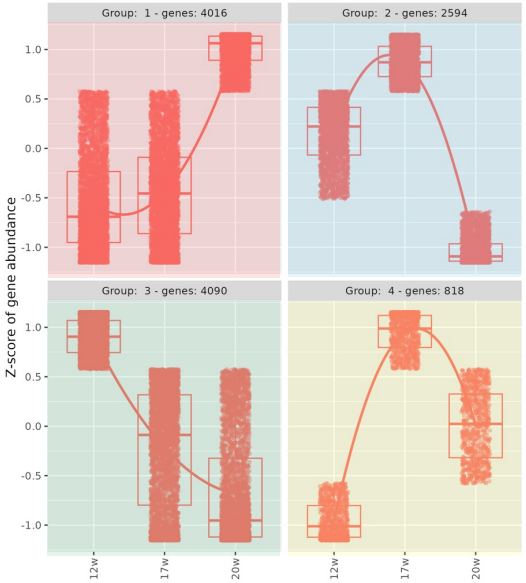




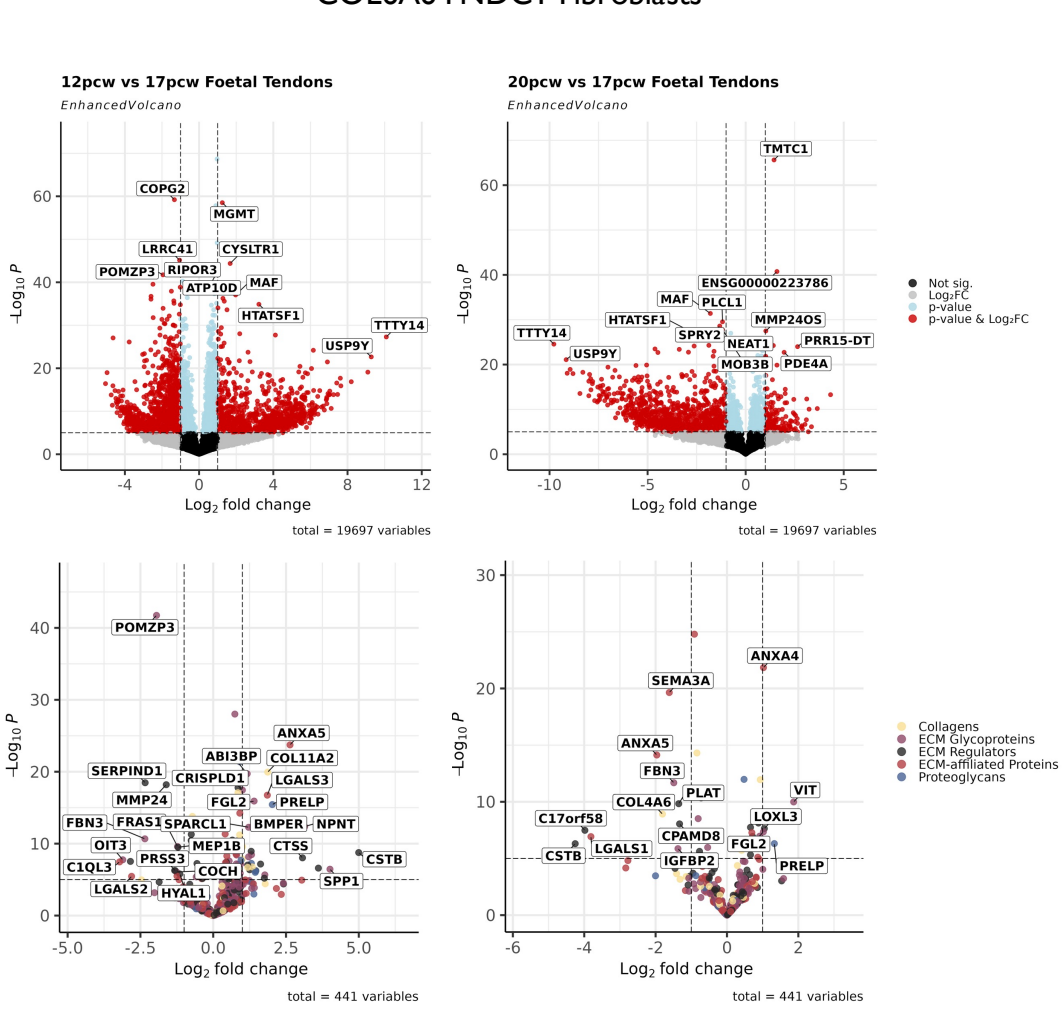
BH FDR <0.01 (409):	BH FDR <0.05 (208):
Cellular Metabolism and Energy Production Extracellular Structure and Tissue Development (incl. ECM and BM organisation, ETM transition) Immune Responses (innate, TNF) Cell Signalling and Response Cellular Dynamics and Mobility Protein and Enzyme Regulation Intracellular Transport and Localization Cellular and Tissue Maintenance	Cell Cycle Regulation DNA Replication and Repair Neural and Synaptic Development Cytoskeletal and Structural Organization Developmental and Morphogenic Processes Regulation of Cellular Structure and Organization Regulation of Signalling Pathways (Ras, Rho) Cellular Responses and Sensing
BH FDR <0.05 (15):	**BH FDR <0.05 (26):**
Ribosome Biogenesis and Function Positive Regulation of Translation Negative Regulation of kinase activity	Cellular Stress Response Regulation of Metabolic Processes Response to IL-4 vEGF receptor, Hippo signalling Regulation of Autophagy Protein Modification and Localization

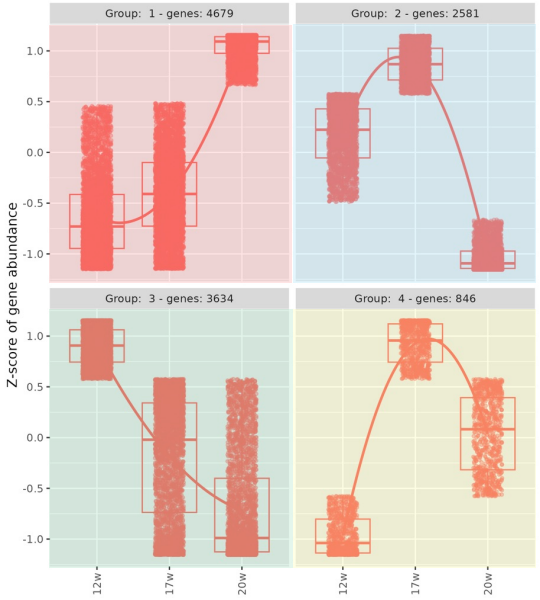
FGF14 THBS4 Fibroblasts



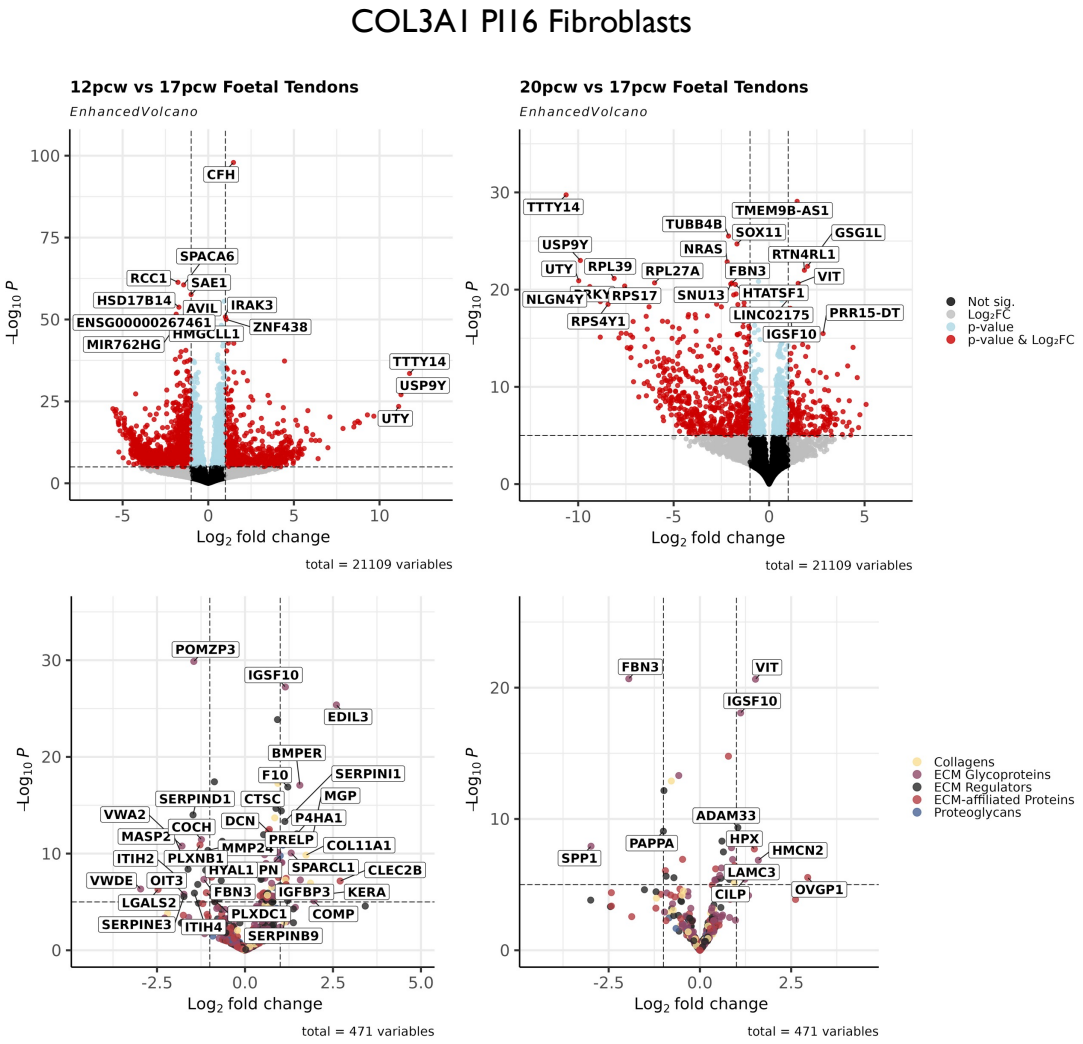


BH FDR <0.01 (400):	BH FDR <0.05 (33):
Cellular Stress Response Extracellular Matrix Organisation and Remodelling Cell Signalling and Receptor Pathways (Wnt, TGFb, Sr/Thr) Autophagy and Cellular Homeostasis Cell-Matrix and Cell-Cell Adhesion Tissue Morphogenesis and Development Metabolic Regulation	RNA Processing and Transport Cell Signalling and Response Amino Acid Metabolism Nucleic Acid Transport Metabolic Processes Haematopoiesis
BH FDR <0.01 (447):	**BH FDR <0.05 (4):**
Cell Cycle Regulation, DNA Replication and Repair Ribosome and Protein Synthesis Cell Division Metabolic Processes Cell Signalling and Regulation RNA Processing and Transport Differentiation and Development Cellular Respiration Synaptic and Neuronal Processes	Cellular Transport Lipid Modification

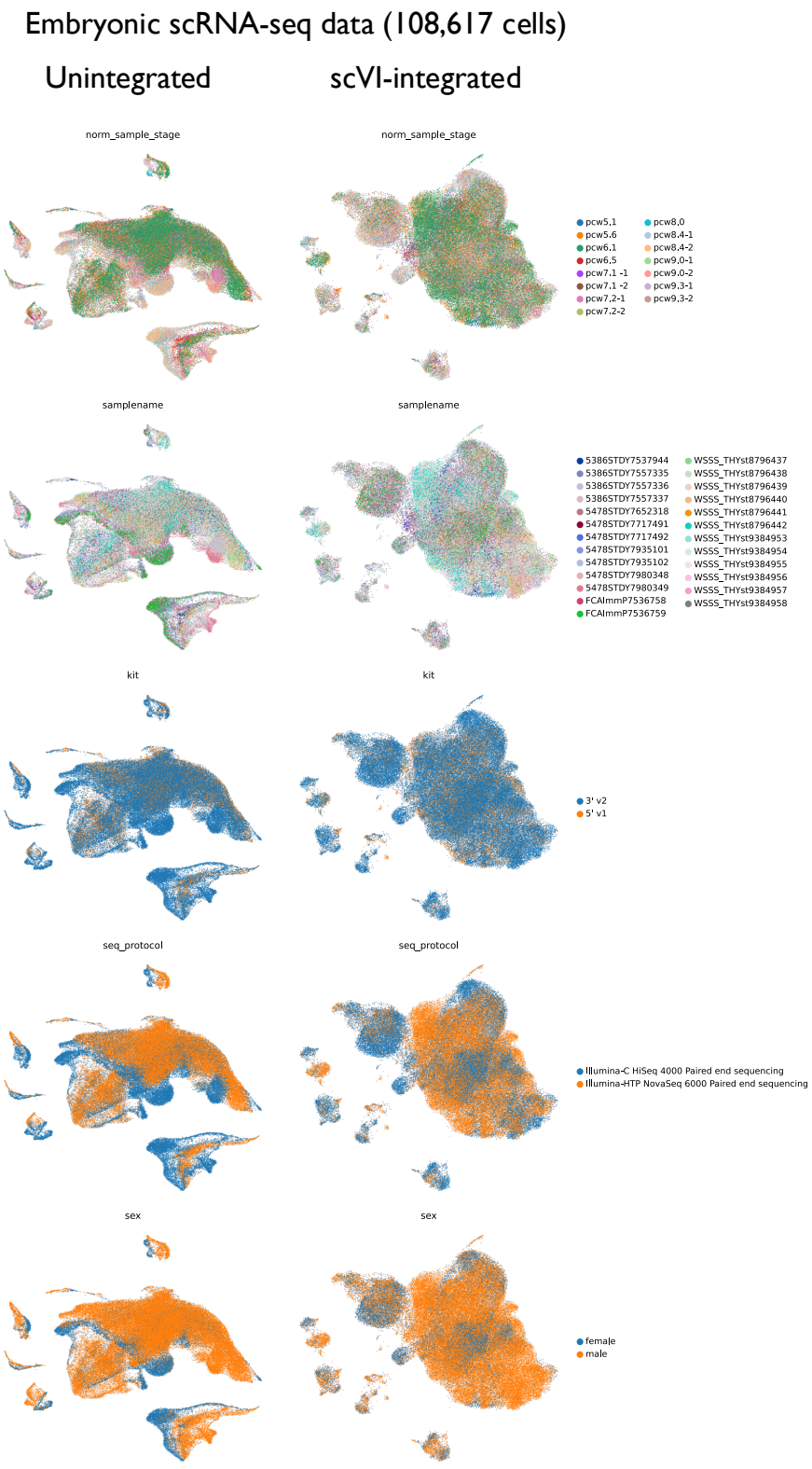




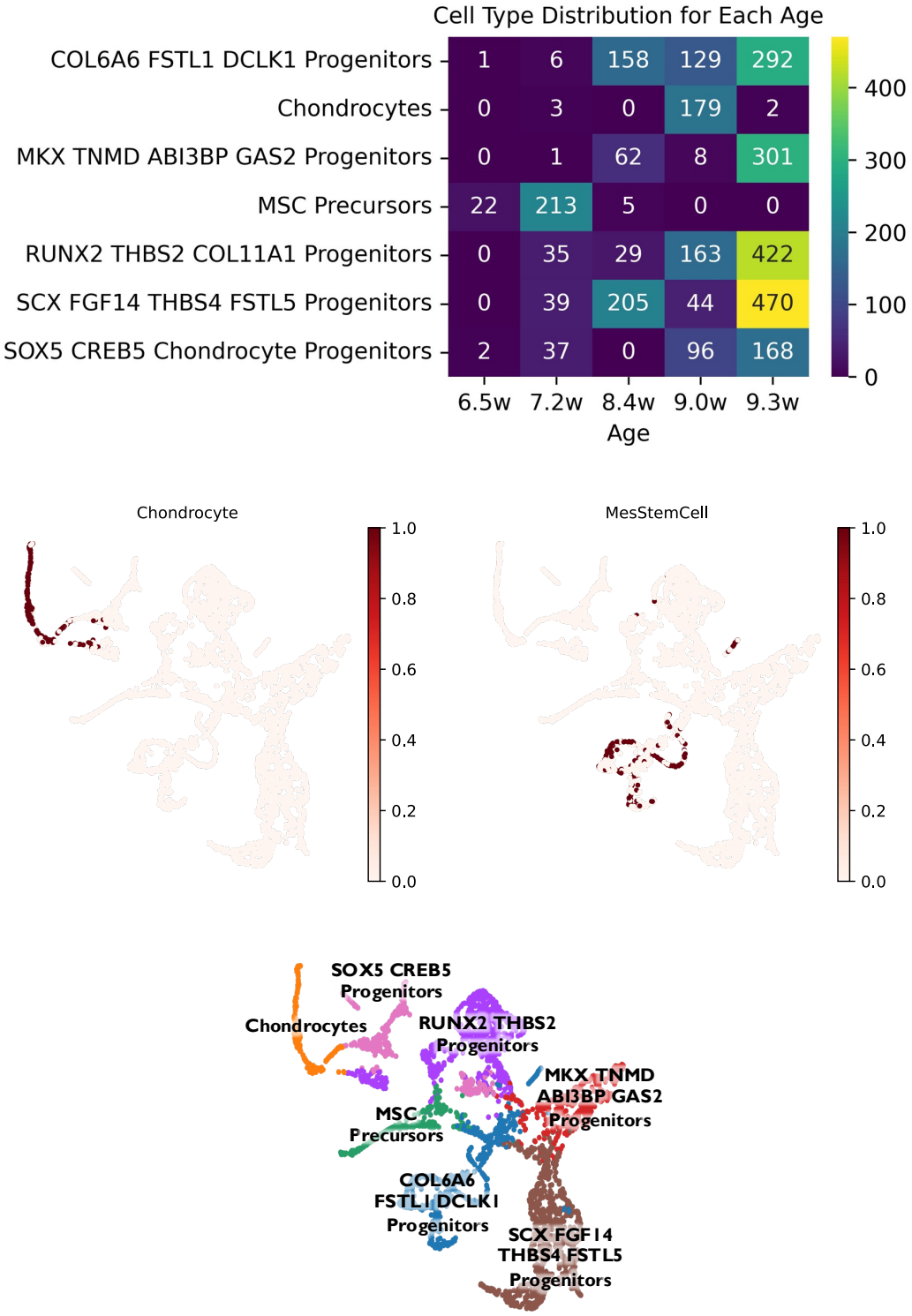
BH FDR <0.01 (440):	BH FDR <0.05 (43):
Cellular and Vesicle Transport Cytoskeleton and Cell Structure Cell Signalling and Communication (Wnt, TGFb) Protein Degradation and Modification Autophagy and Cellular Stress Response Development and Morphogenesis Gene Expression and Transcription Metabolism and Energy Derivation Immune Response Cell Proliferation, Growth and Differentiation	RNA Processing and Transport Cell Signalling and Response Amino Acid Metabolism Nucleic Acid Transport Lipid Biosynthesis Metabolic Processes Cytoskeletal Organisation and Movement
BH FDR <0.01 (450):	**BH FDR <0.05 (3):**
Cell Cycle Regulation, DNA Replication and Repair Ribosome and Protein Synthesis Cell Division Metabolic Processes Cell Signalling and Regulation RNA Processing and Transport Differentiation and Development	Mast Cell Activation



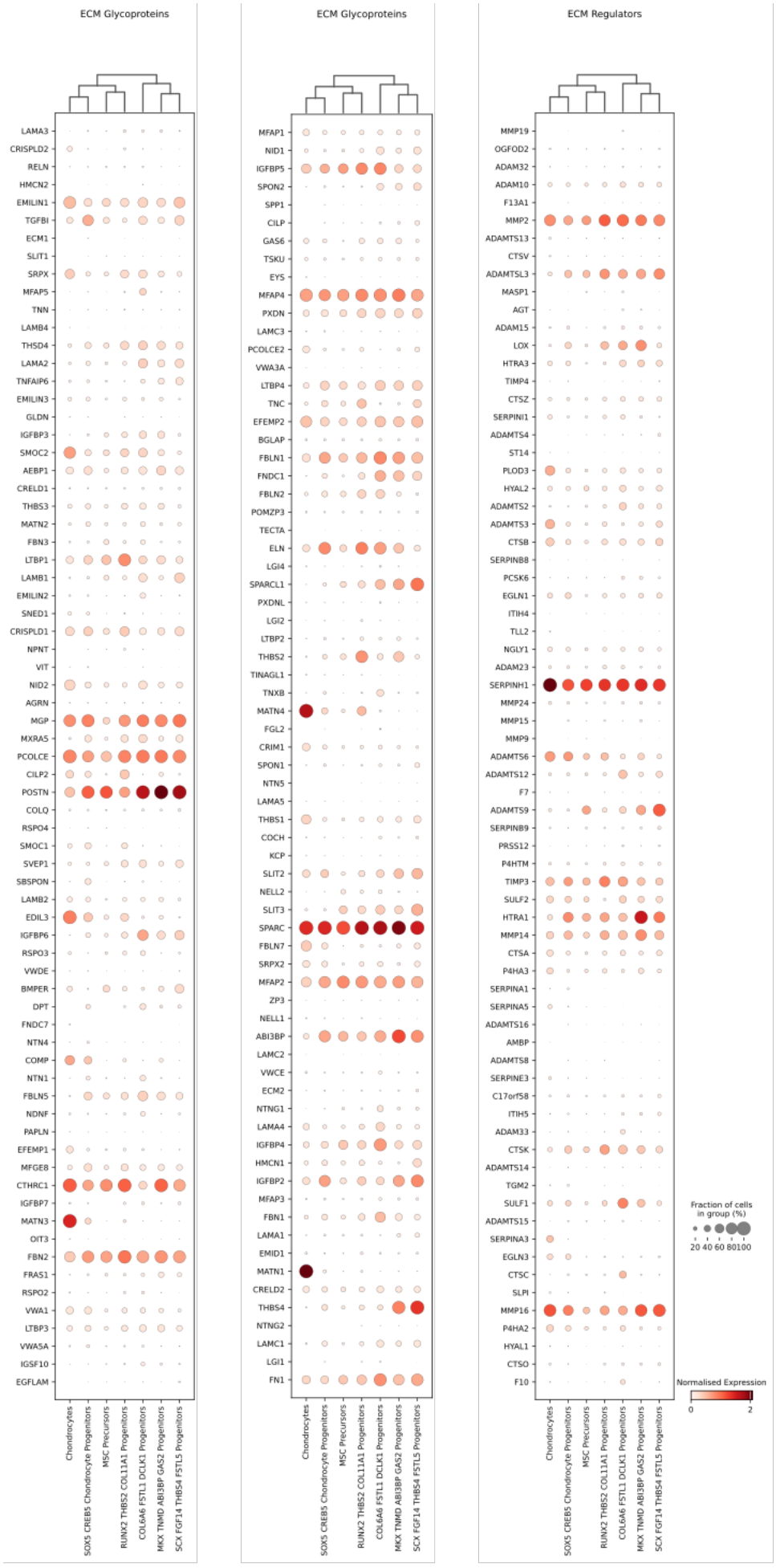
Appendix Figure 6. DESeq2 LRT and Wald differential gene expression analysis of transcriptomic changes in 12, 17, and 20 pcw human foetal Achilles and quadriceps tendon fibrillar and loose connective tissue fibroblasts. *(Left) Boxplot of DESeq2 LRT (p-adjusted <0.01) z-score gene abundance results showing common gene expression pattern clusters (groups) occurring from 12, to 17, to 20pcw. The table below shows the manually summarised results of gene ontology (GO) biological processes (BP) analyses carried out with the gProfiler g:GOSt tool (Raudvere et al., 2019). Briefly, each cluster was subjected to GO:BP analysis, and select numbers of terms with Benjamini-Hochberg (BH) FDR values <0.05 or <0.01 were analysed and categorised by common function (e.g. different pathways related to cell division were grouped together into a "Cell Division" category). BH FDR of <0.01 was chosen when there were too many significant terms at <0.05 to categorise manually. In table headings, the numbers in brackets correspond to the total number of the different GO:BP pathways meeting the BH FDR criteria. (Right) plots showing the results of DESeq2 Wald tests comparing gene expression per cell type at 12 vs 17pcw and 20 vs 17pcw. Top row shows overall gene expression profiles, while the bottom row highlights the different ECM proteins and their categories.*

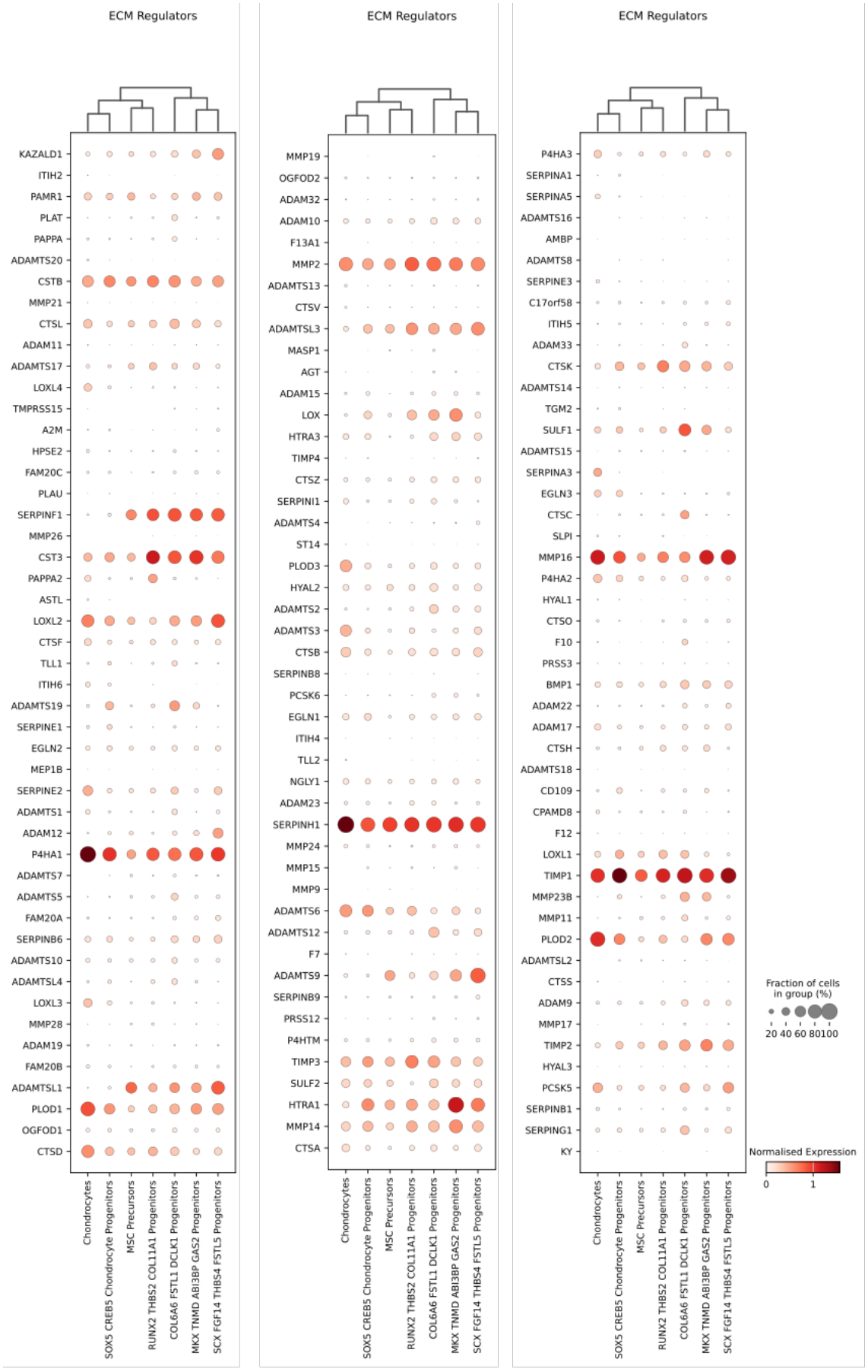


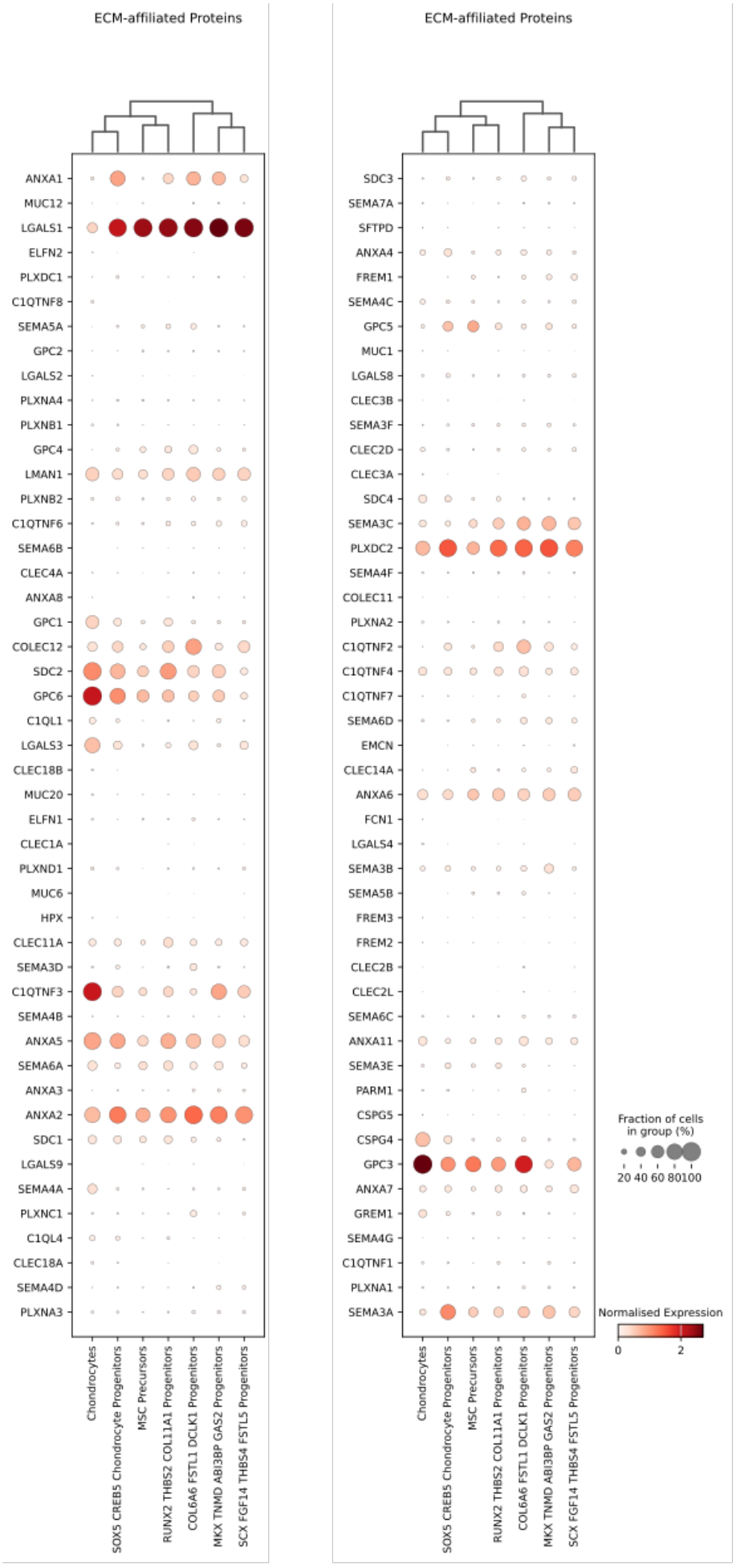
Appendix Figure 7. Embryonic sample UMAPs before (left) and after (right) integration and batch correction with scVI. *Sc-RNA-seq data containing 108,617 cells from 25 hindlimb and forelimb region samples from 11 donors were integrated to minimise the influence of technical ('seq_protocol', 'kit') and biological (samplename', 'sex') batch effects.*



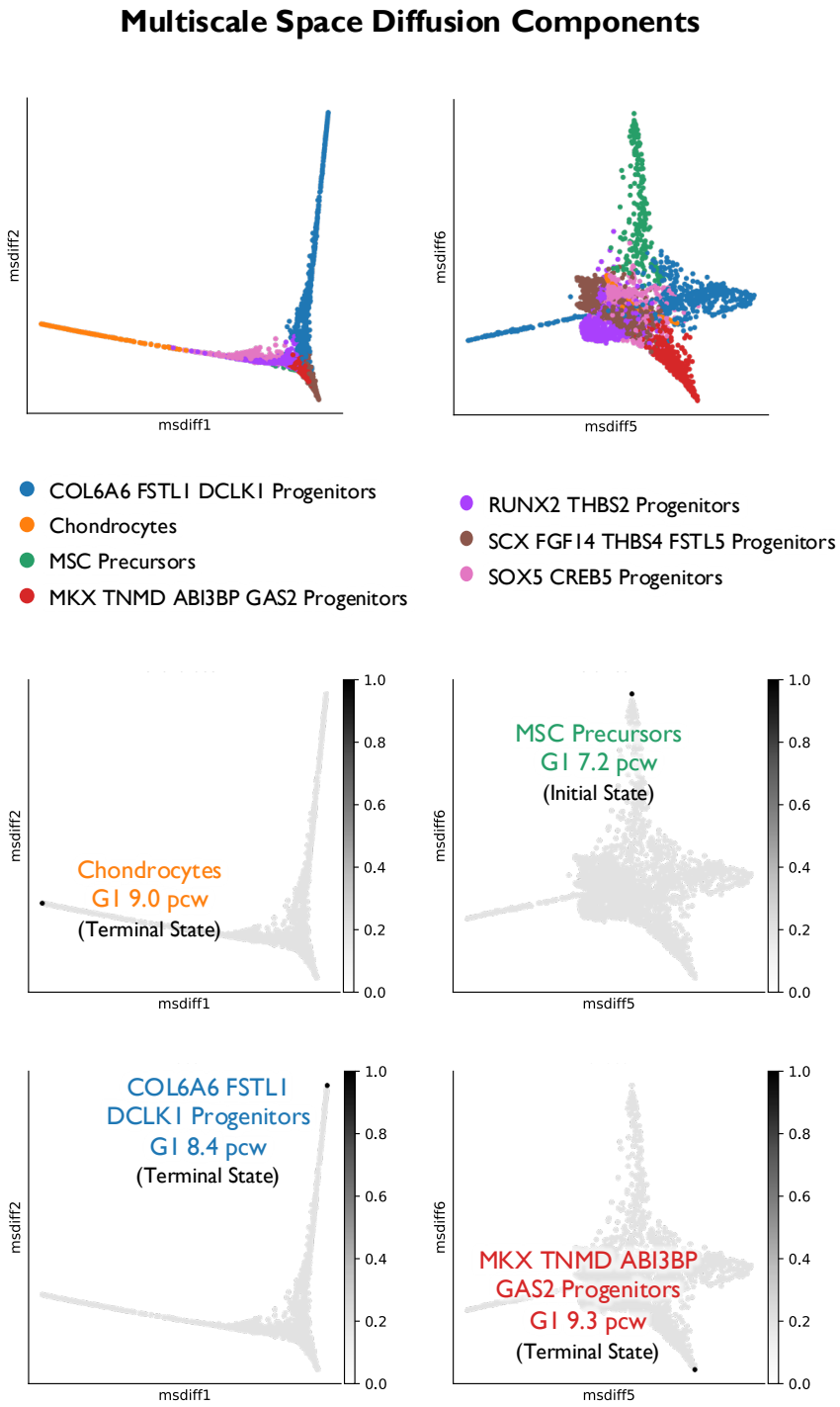
Appendix Figure 8. Embryonic tendon cell type annotation. *(Top) Matrixplot shows numbers of cells of each identified cell type across sample ages. (Middle) Partition-graph abstraction (PAGA)-based UMAPs showing cells scoring above the 95th percentile for the expression of chondrocyte (CL:0000138; top 25 genes) and mesenchymal stem cell (CL:0000134; top 59 genes) markers taken from the CZ CellxGene's Cell Guide library (CZI Single-Cell Biology Program et al., 2023). (Bottom) UMAP showing final cell type annotations of embryonic tendon cells.*


ECM Glycoproteins
LAMA3
CRISPLD2
RELN
HMCN2
EMILIN1
TGFBI
ECM1
SLIT1
SRPX
MFAP5
TNN
LAMB4
THSD4
LAMA2
TNFAIP6
EMILIN3
GLDN
IGFBP3
SMOC2
AEBP1
CRELD1
THBS3
MATN2
FBN3
LTBP1
LAMB1
EMILIN2
SNED1
CRISPLD1
NPNT
VIT
NID2
AGRN
MGP
MXRA5
PCOLCE
CILP2
POSTN
COLQ
RSPO4
SMOC1
SVEP1
SBSPON
LAMB2
EDIL3
IGFBP6
RSPO3
VWDE
BMPER
DPT
FNDC7
NTN4
COMP
NTN1
FBLN5
NDNF
PAPLN
EFEMP1
MFGE8
CTHRC1
IGFBP7
MATN3
OIT3
FBN2
FRAS1
RSPO2
VWA1
LTBP3
VWA5A
IGSF10
EGFLAM
Chondrocytes
SOX5 CREB5 Chondrocyte Progenitors
MSC Precursors
RUNX2 THBS2 COL11A1 Progenitors
COL6A6 FSTL1 DCLK1 Progenitors
MKX TNMD ABI3BP GAS2 Progenitors
SCX FGF14 THBS4 FSTL5 Progenitors
ECM Glycoproteins
MFAP1
NID1
IGFBP5
SPON2
SPP1
CILP
GAS6
TSKU
EYS
MFAP4
PXDN
LAMC3
PCOLCE2
VWA3A
LTBP4
TNC
EFEMP2
BGLAP
FBLN1
FNDC1
FBLN2
POMZP3
TECTA
ELN
LGI4
SPARCL1
PXDNL
LGI2
LTBP2
THBS2
TINAGL1
TNXB
MATN4
FGL2
CRIM1
SPON1
NTN5
LAMA5
THBS1
COCH
KCP
SLIT2
NELL2
SLIT3
SPARC
FBLN7
SRPX2
MFAP2
ZP3
NELL1
ABI3BP
LAMC2
VWCE
ECM2
NTNG1
LAMA4
IGFBP4
HMCN1
IGFBP2
MFAP3
FBN1
LAMA1
EMID1
MATN1
CRELD2
THBS4
NTNG2
LAMC1
LGI1
FN1
Chondrocytes
SOX5 CREB5 Chondrocyte Progenitors
MSC Precursors
RUNX2 THBS2 COL11A1 Progenitors
COL6A6 FSTL1 DCLK1 Progenitors
MKX TNMD ABI3BP GAS2 Progenitors
SCX FGF14 THBS4 FSTL5 Progenitors
ECM Regulators
MMP19
OGFOD2
ADAM32
ADAM10
F13A1
MMP2
ADAMTS13
CTSV
ADAMTSL3
MASP1
AGT
ADAM15
LOX
HTRA3
TIMP4
CTSZ
SERPINI1
ADAMTS4
ST14
PLOD3
HYAL2
ADAMTS2
ADAMTS3
CTSB
SERPINB8
PCSK6
EGLN1
ITIH4
TLL2
NGLY1
ADAM23
SERPINH1
MMP24
MMP15
MMP9
ADAMTS6
ADAMTS12
F7
ADAMTS9
SERPINB9
PRSS12
P4HTM
TIMP3
SULF2
HTRA1
MMP14
CTSA
P4HA3
SERPINA1
SERPINA5
ADAMTS16
AMBP
ADAMTS8
SERPINE3
C17orf58
ITIH5
ADAM33
CTSK
ADAMTS14
TGM2
SULF1
ADAMTS15
SERPINA3
EGLN3
CTSC
SLPI
MMP16
P4HA2
HYAL1
CTSO
F10
Chondrocytes
SOX5 CREB5 Chondrocyte Progenitors
MSC Precursors
RUNX2 THBS2 COL11A1 Progenitors
COL6A6 FSTL1 DCLK1 Progenitors
MKX TNMD ABI3BP GAS2 Progenitors
SCX FGF14 THBS4 FSTL5 Progenitors
Fraction of cells in group (%)
20 40 60 80100
Normalised Expression
0
2

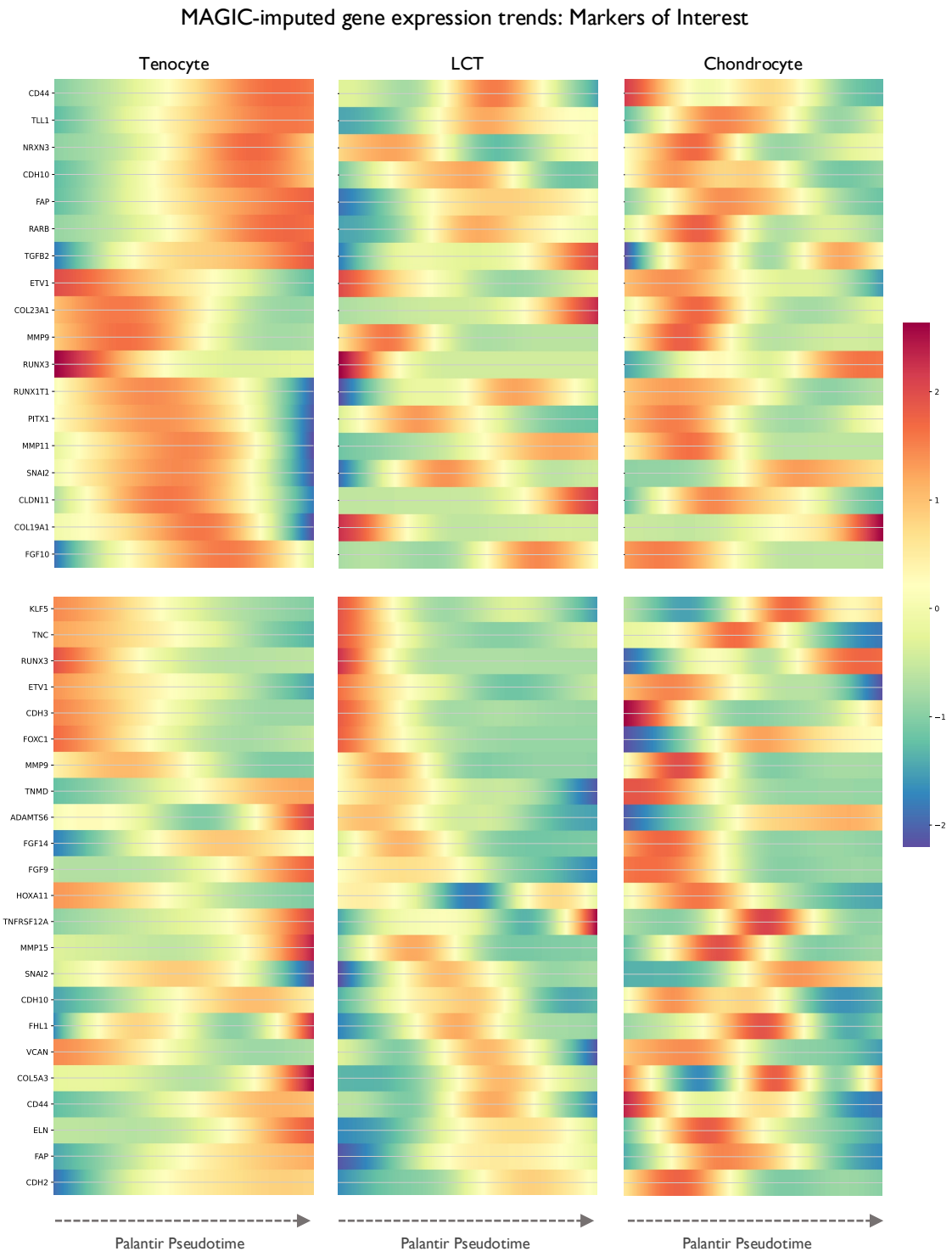

ECM Regulators
KAZALD1
ITIH2
PAMR1
PLAT
PAPPA
ADAMTS20
CSTB
MMP21
CTSL
ADAM11
ADAMTS17
LOXL4
TMPRSS15
A2M
HPSE2
FAM20C
PLAU
SERPINF1
MMP26
CST3
PAPPA2
ASTL
LOXL2
CTSF
TLL1
ITIH6
ADAMTS19
SERPINE1
EGLN2
MEP1B
SERPINE2
ADAMTS1
ADAM12
P4HA1
ADAMTS7
ADAMTS5
FAM20A
SERPINB6
ADAMTS10
ADAMTSL4
LOXL3
MMP28
ADAM19
FAM20B
ADAMTSL1
PLOD1
OGFOD1
CTSD
Chondrocytes
SOX5 CREB5 Chondrocyte Progenitors
MSC Precursors
RUNX2 THBS2 COL11A1 Progenitors
COL6A6 FSTL1 DCLK1 Progenitors
MKX TNMD ABI3BP GAS2 Progenitors
SCX FGF14 THBS4 FSTL5 Progenitors
ECM Regulators
MMP19
OGFOD2
ADAM32
ADAM10
F13A1
MMP2
ADAMTS13
CTSV
ADAMTSL3
MASP1
AGT
ADAM15
LOX
HTRA3
TIMP4
CTSZ
SERPINI1
ADAMTS4
ST14
PLOD3
HYAL2
ADAMTS2
ADAMTS3
CTSB
SERPINB8
PCSK6
EGLN1
ITIH4
TLL2
NGLY1
ADAM23
SERPINH1
MMP24
MMP15
MMP9
ADAMTS6
ADAMTS12
F7
ADAMTS9
SERPINB9
PRSS12
P4HTM
TIMP3
SULF2
HTRA1
MMP14
CTSA
Chondrocytes
SOX5 CREB5 Chondrocyte Progenitors
MSC Precursors
RUNX2 THBS2 COL11A1 Progenitors
COL6A6 FSTL1 DCLK1 Progenitors
MKX TNMD ABI3BP GAS2 Progenitors
SCX FGF14 THBS4 FSTL5 Progenitors
ECM Regulators
P4HA3
SERPINA1
SERPINA5
ADAMTS16
AMBP
ADAMTS8
SERPINE3
C17orf58
ITIH5
ADAM33
CTSK
ADAMTS14
TGM2
SULF1
ADAMTS15
SERPINA3
EGLN3
CTSC
SLPI
MMP16
P4HA2
HYAL1
CTSO
F10
PRSS3
BMP1
ADAM22
ADAM17
CTSH
ADAMTS18
CD109
CPAMD8
F12
LOXL1
TIMP1
MMP23B
MMP11
PLOD2
ADAMTSL2
CTSS
ADAM9
MMP17
TIMP2
HYAL3
PCSK5
SERPINB1
SERPING1
KY
Chondrocytes
SOX5 CREB5 Chondrocyte Progenitors
MSC Precursors
RUNX2 THBS2 COL11A1 Progenitors
COL6A6 FSTL1 DCLK1 Progenitors
MKX TNMD ABI3BP GAS2 Progenitors
SCX FGF14 THBS4 FSTL5 Progenitors
Fraction of cells in group (%)
20 40 60 80100
Normalised Expression
0
1

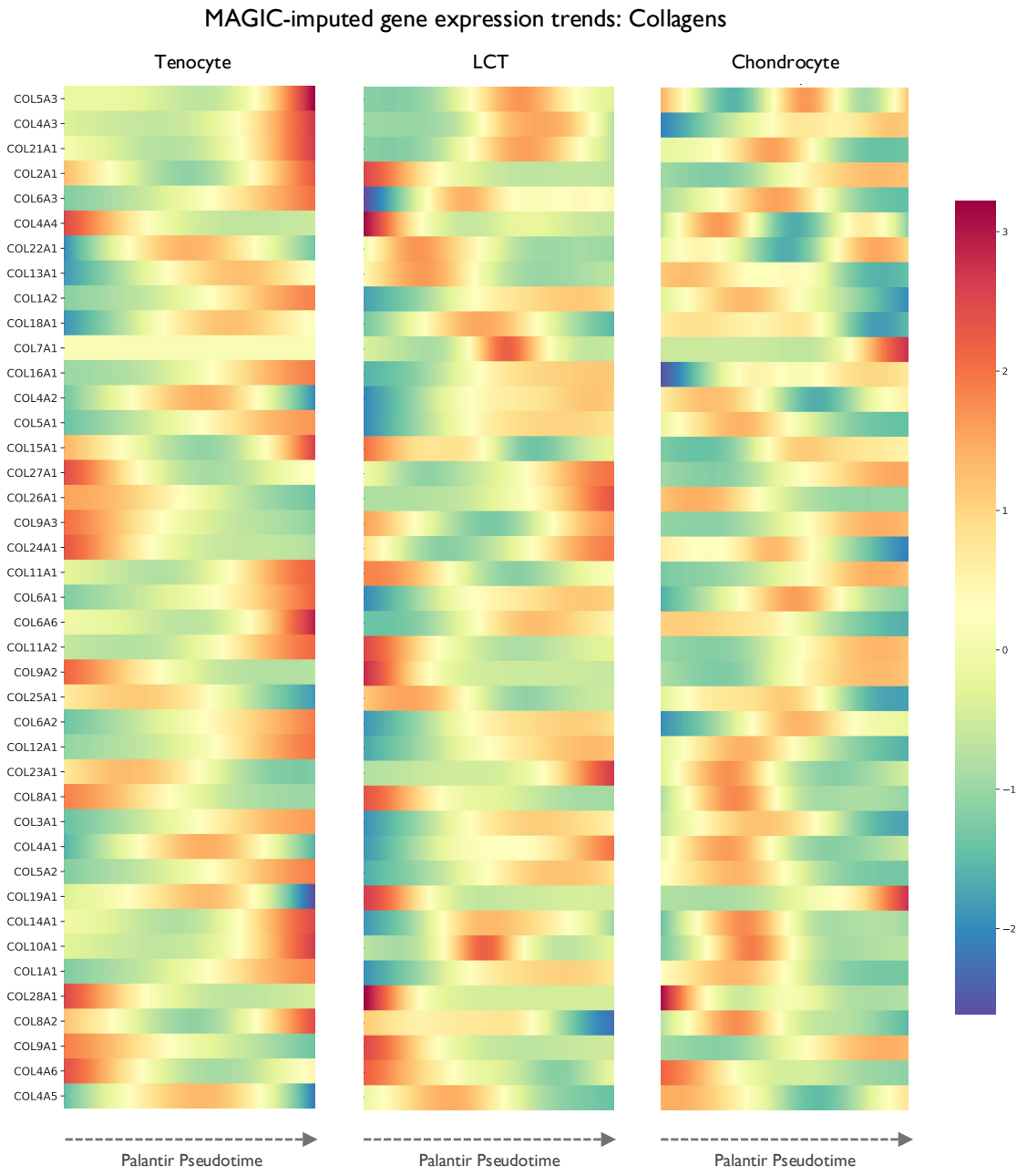

ECM-affiliated Proteins
ANXA1
MUC12
LGALS1
ELFN2
PLXDC1
C1QTNF8
SEMA5A
GPC2
LGALS2
PLXNA4
PLXNB1
GPC4
LMAN1
PLXNB2
C1QTNF6
SEMA6B
CLEC4A
ANXA8
GPC1
COLEC12
SDC2
GPC6
C1QL1
LGALS3
CLEC18B
MUC20
ELFN1
CLEC1A
PLXND1
MUC6
HPX
CLEC11A
SEMA3D
C1QTNF3
SEMA4B
ANXA5
SEMA6A
ANXA3
ANXA2
SDC1
LGALS9
SEMA4A
PLXNC1
C1QL4
CLEC18A
SEMA4D
PLXNA3
Chondrocytes
SOX5 CREB5 Chondrocyte Progenitors
MSC Precursors
RUNX2 THBS2 COL11A1 Progenitors
COL6A6 FSTL1 DCLK1 Progenitors
MKX TNMD ABI3BP GAS2 Progenitors
SCX FGF14 THBS4 FSTL5 Progenitors
ECM-affiliated Proteins
SDC3
SEMA7A
SFTPD
ANXA4
FREM1
SEMA4C
GPC5
MUC1
LGALS8
CLEC3B
SEMA3F
CLEC2D
CLEC3A
SDC4
SEMA3C
PLXDC2
SEMA4F
COLEC11
PLXNA2
C1QTNF2
C1QTNF4
C1QTNF7
SEMA6D
EMCN
CLEC14A
ANXA6
FCN1
LGALS4
SEMA3B
SEMA5B
FREM3
FREM2
CLEC2B
CLEC2L
SEMA6C
ANXA11
SEMA3E
PARM1
CSPG5
CSPG4
GPC3
ANXA7
GREM1
SEMA4G
C1QTNF1
PLXNA1
SEMA3A
Fraction of cells in group (%)
20 40 60 80100
Normalised Expression
0
2
Chondrocytes
SOX5 CREB5 Chondrocyte Progenitors
MSC Precursors
RUNX2 THBS2 COL11A1 Progenitors
COL6A6 FSTL1 DCLK1 Progenitors
MKX TNMD ABI3BP GAS2 Progenitors
SCX FGF14 THBS4 FSTL5 Progenitors

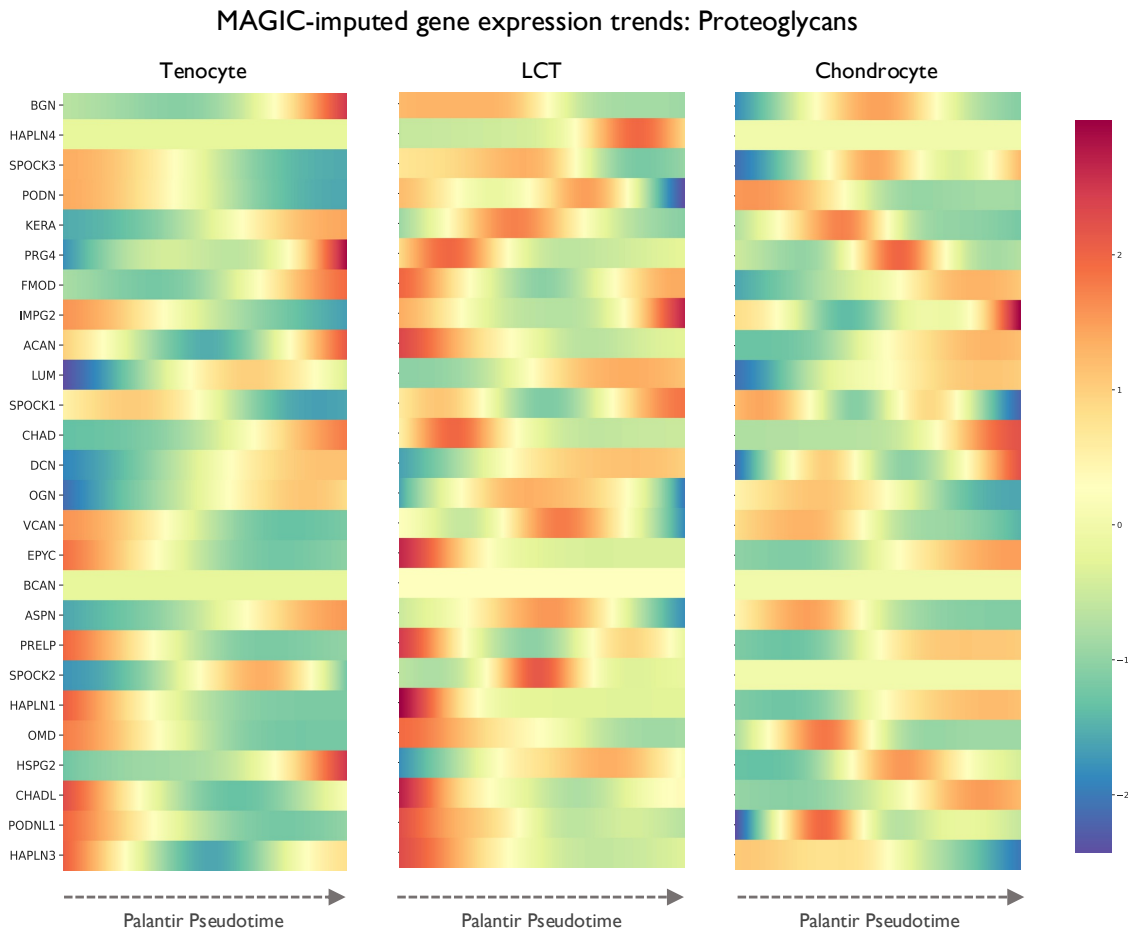
Appendix Figure 9. Embryonic 6-9pcw tendon matrisomal gene expression profiles. *Dotplots show the mean normalised expression levels alongside the proportions of expressing cell types for matrisomal genes categorised as ECM-affiliated proteins, ECM glycoproteins, and ECM regulators. The lists of matrisomal genes were obtained from the matrisomeDB database (Shao et al., 2020). The plots for collagens and proteoglycans are shown in Figure 43.*



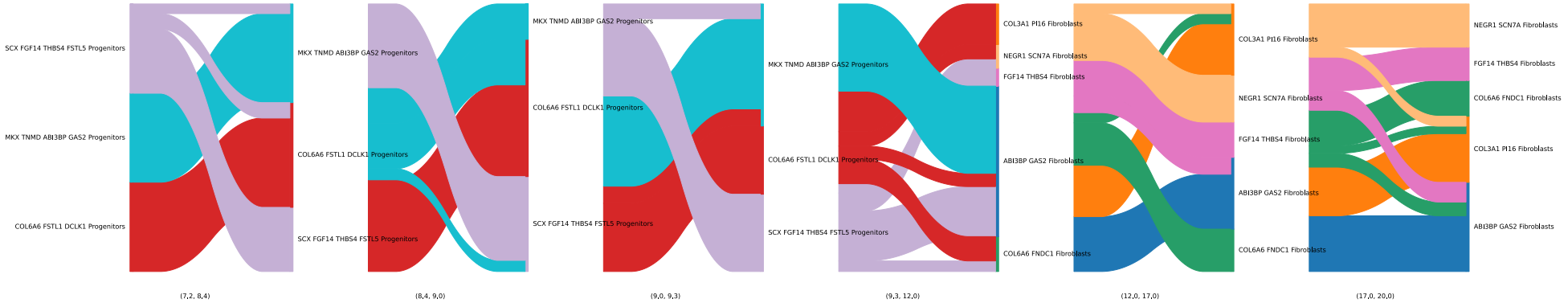
Appendix Figure 10. Selection of initial and terminal states using multiscale space embedding components for Palantir pseudotime calculation. *Multiscale space was calculated based on the Palantir diffusion map embeddings.*


MAGIC-imputed gene expression trends: Markers of Interest
Tenocyte
LCT
Chondrocyte
CD44
TLL1
NRXN3
CDH10
FAP
RARB
TGFB2
ETV1
COL23A1
MMP9
RUNX3
RUNX1T1
PITX1
MMP11
SNAI2
CLDN11
COL19A1
FGF10
KLF5
TNC
RUNX3
ETV1
CDH3
FOXC1
MMP9
TNMD
ADAMTS6
FGF14
FGF9
HOXA11
TNFRSF12A
MMP15
SNAI2
CDH10
FHL1
VCAN
COL5A3
CD44
ELN
FAP
CDH2
2
1
0
−1
−2
Palantir Pseudotime
Palantir Pseudotime
Palantir Pseudotime

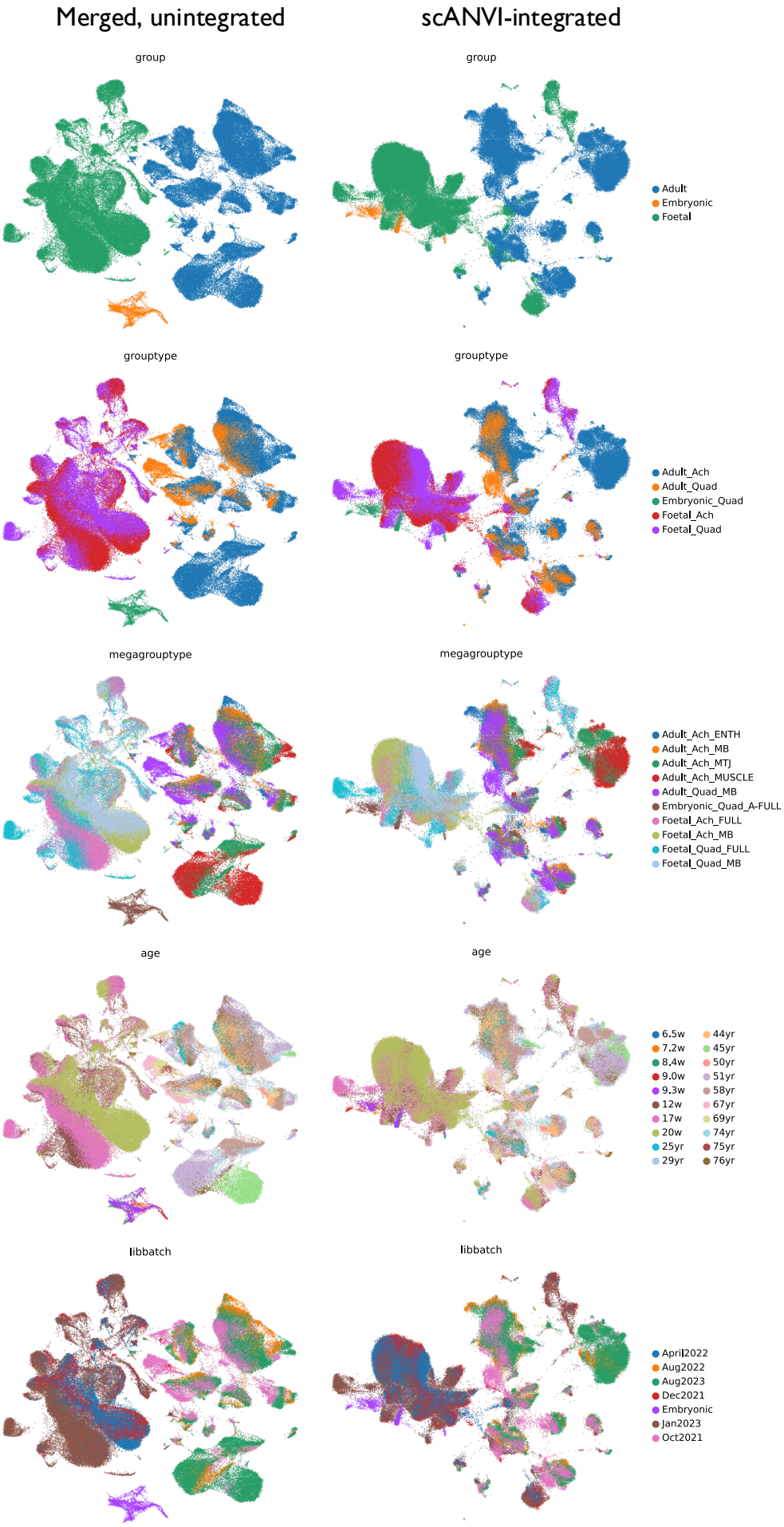

MAGIC-imputed gene expression trends: Collagens
Tenocyte
LCT
Chondrocyte
COL5A3
COL4A3
COL21A1
COL2A1
COL6A3
COL4A4
COL22A1
COL13A1
COL1A2
COL18A1
COL7A1
COL16A1
COL4A2
COL5A1
COL15A1
COL27A1
COL26A1
COL9A3
COL24A1
COL11A1
COL6A1
COL6A6
COL11A2
COL9A2
COL25A1
COL6A2
COL12A1
COL23A1
COL8A1
COL3A1
COL4A1
COL5A2
COL19A1
COL14A1
COL10A1
COL1A1
COL28A1
COL8A2
COL9A1
COL4A6
COL4A5
Palantir Pseudotime
Palantir Pseudotime
Palantir Pseudotime
3
2
1
0
−1
−2

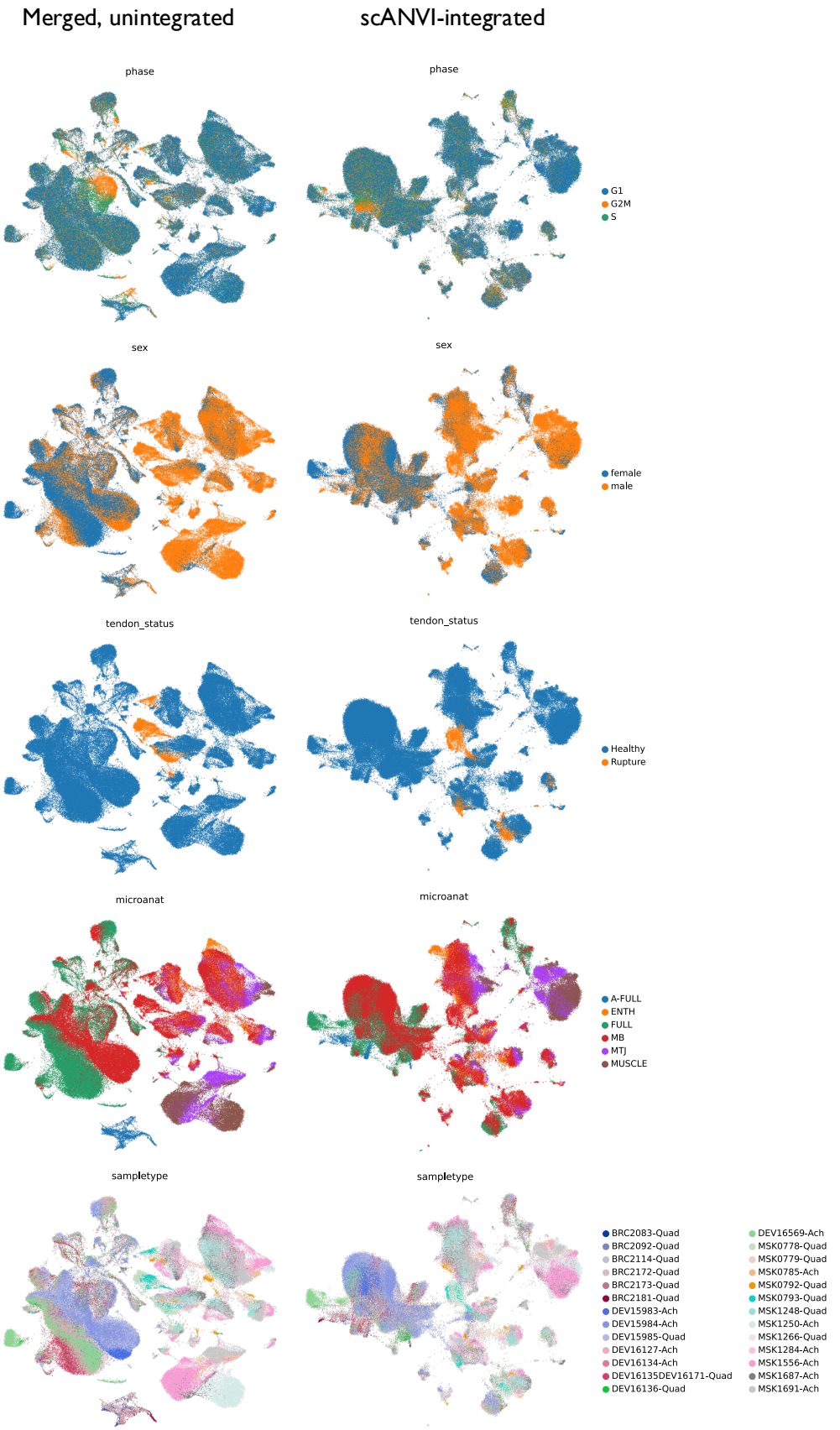


Appendix Figure 11. MAGIC-imputed gene expression trends across Palantir pseudotime for the three lineages identified in 6.5-9.3 pcw embryonic tendon cells. *Heatmaps show the z-score standardised gene expression levels for (1st plot) markers of interest for Tenocyte (upper row) and loose connective tissue (LCT) (bottom row) cell lineages, (2nd plot) collagens, and (3rd plot) proteoglycans across Palantir pseudotime. The expression data has been smoothed using MAGIC (Markov Affinity-based Graph Imputation of Cells) to highlight the dynamic changes in gene expression associated with cell differentiation. The pseudotime axis extends from the 6.5 pcw MSC precursor state (left) to the more differentiated 9.3 pcw states for each given lineage (right).*



Appendix Figure 12. Moscot sankey diagram plot showing developing tendon fibroblast lineage cell type transitions from 7.2 pcw to 20 pcw.


Merged, unintegrated
scANVI-integrated
group
Adult
Embryonic
Foetal
grouptype
Adult_Ach
Adult_Quad
Embryonic_Quad
Foetal_Ach
Foetal_Quad
megagrouptype
Adult_Ach_ENTH
Adult_Ach_MB
Adult_Ach_MTJ
Adult_Ach_MUSCLE
Adult_Quad_MB
Embryonic_Quad_A-FULL
Foetal_Ach_FULL
Foetal_Ach_MB
Foetal_Quad_FULL
Foetal_Quad_MB
age
6.5w
7.2w
8.4w
9.0w
9.3w
12w
17w
20w
25yr
29yr
44yr
45yr
50yr
51yr
58yr
67yr
69yr
74yr
75yr
76yr
libbatch
April2022
Aug2022
Aug2023
Dec2021
Embryonic
Jan2023
Oct2021



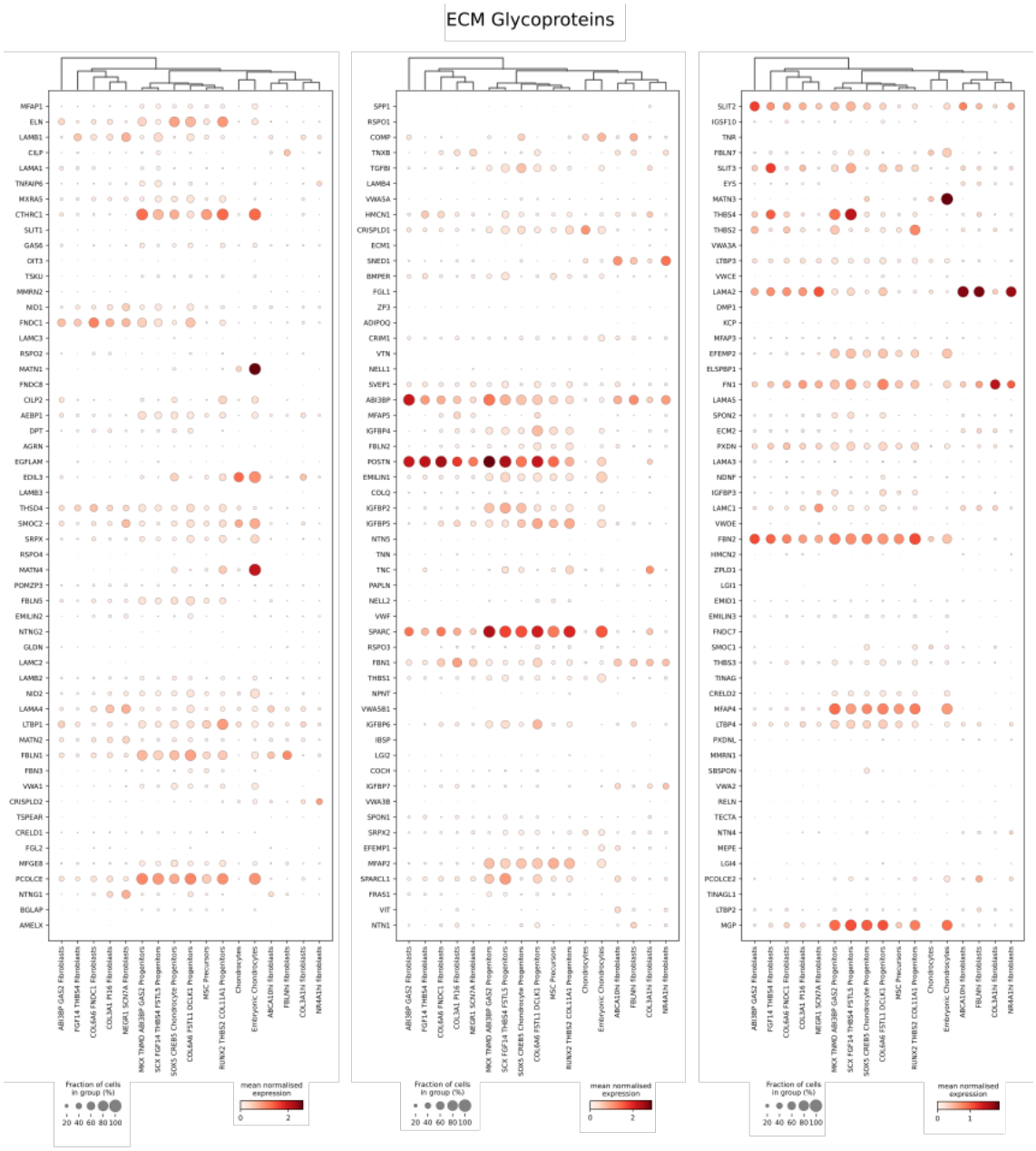
Appendix Figure 13. UMAPs showing embryonic, foetal and adult Achilles and quadriceps tendon data before (left) and after (right) integration with scANVI. *Sn-RNA-seq data containing 176,691 cells were integrated to minimise the influence of technical ('libbatch') and biological ('sampletype', 'G2M score', 'S score') batch effects.*

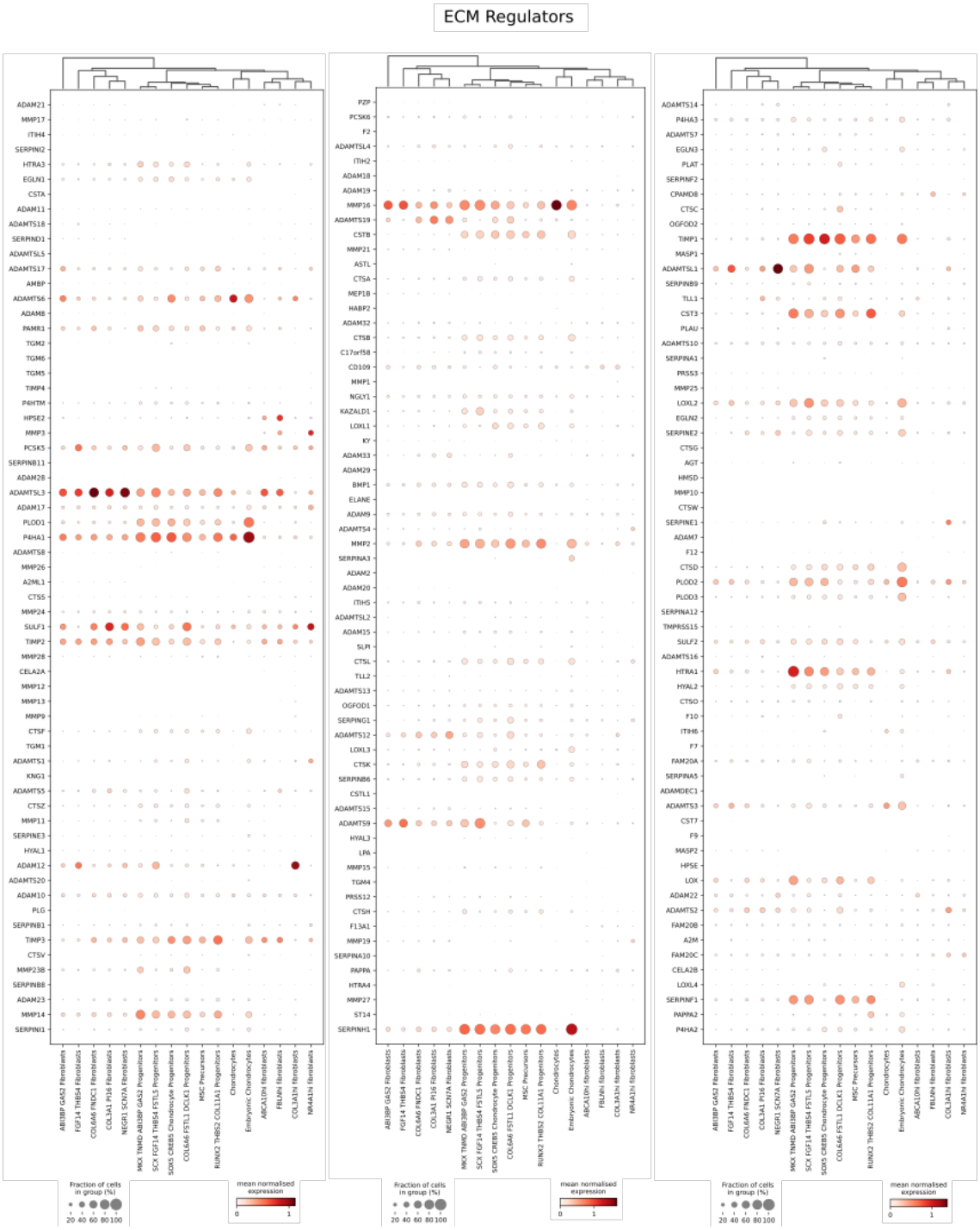
Appendix Table 5. Data cell type counts by study.

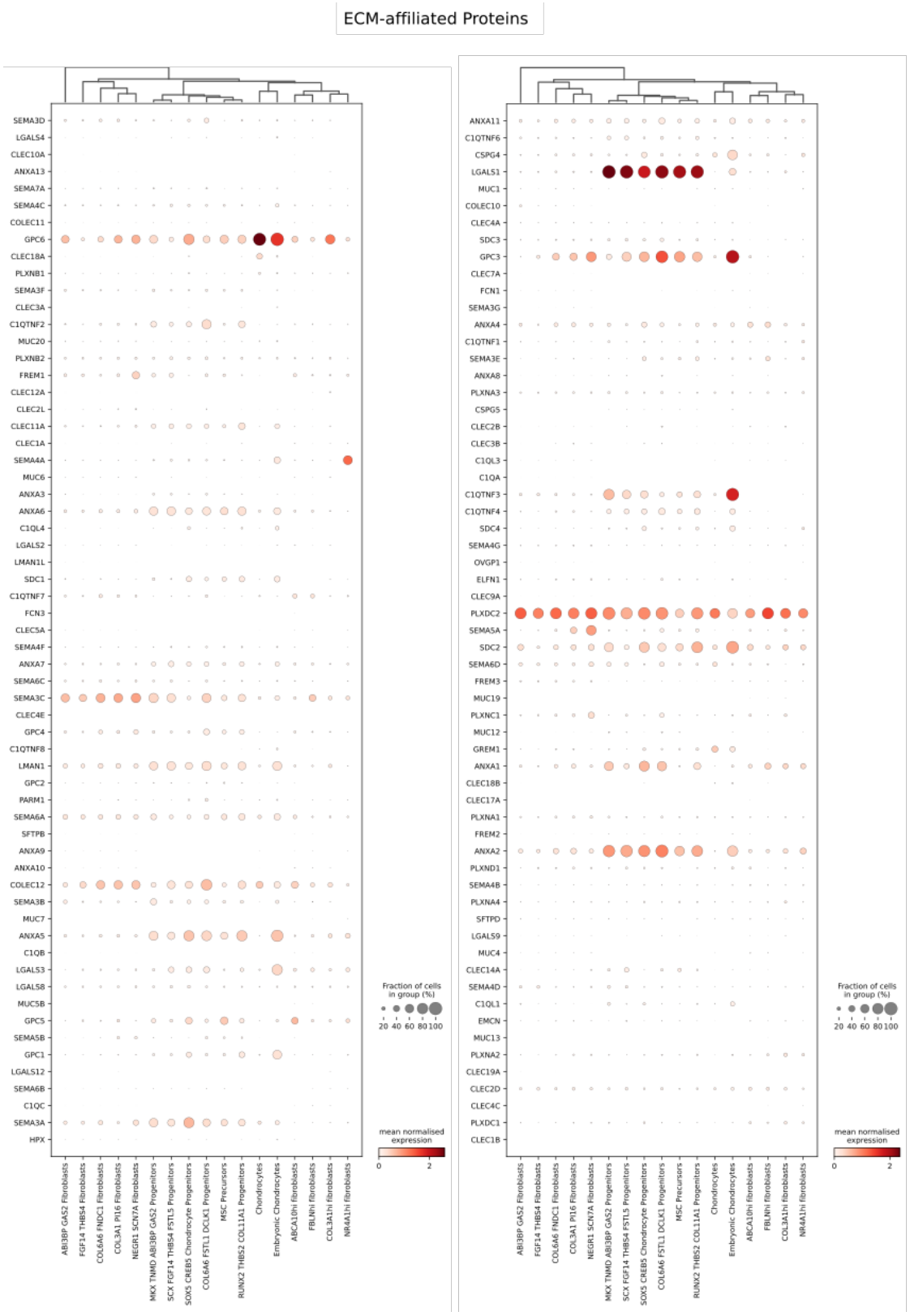
Yellow highlights show unusually low cell type populations that are likely resulting from coarse annotation.

Cell Type	Embryonic Quad T Healthy	Foetal Quad T Healthy	Foetal Achilles T Healthy	Adult Achilles T Healthy	Adult Quad T Healthy	Adult Quad T Ruptured
ABCA10hi Fibroblasts	0	0	0	0	867	102
ABI3BP GAS2 Fibroblasts	0	22639	23977	0	0	0
Adipocytes	0	0	0	3195	622	31
Arteriolar VECs	0	0	0	0	435	102
B cells	0	0	0	241	12	21
CLEC9Ahi DCs	0	0	0	0	4	20
CLEC10Ahi DCs	0	0	0	0	45	121
COL3A1 PI16 Fibroblasts	0	7887	5280	0	0	0
COL3A1hi Fibroblasts	0	0	0	0	13	2127
COL6A6 FNDC1 Fibroblasts	0	4488	3397	0	0	0
COL6A6 FSTL1 DCLK1 Progenitors	586	0	0	0	0	0
Capillary VECs	0	0	0	0	126	399
Chondrocytes	0	2582	39	0	0	0
Dividing VECs	0	0	0	0	0	112
Dividing fibroblasts / mural cells	0	0	0	0	4	137
Dividing immune cells	0	0	0	0	22	51
Embryonic Chondrocytes	184	0	0	0	0	0
FBLNhi Fibroblasts	0	0	0	0	2262	31
FGF14 THBS4 Fibroblasts	0	1358	647	0	0	0
Fast-twitch skeletal muscle cells	0	0	0	5468	0	0
Granulocytes	0	0	0	499	54	12
ITGA10hi Fibroblasts	0	0	0	11138	0	0
Lymphatic endothelial cells	0	209	85	832	177	10
MERTKhi LYVE1hi macrophages	0	0	0	0	676	443
MERTKhi LYVE1lo macrophages	0	0	0	0	46	647
MERTKlo PTPRGhi macrophages	0	0	0	0	132	32
MKX TNMD ABI3BP GAS2 Progenitors	372	0	0	0	0	0
MSC Precursors	240	0	0	0	0	0
Macrophages	0	2820	2369	5062	0	0
Mural cells	0	0	0	3396	0	0
NEGR1 SCN7A Fibroblasts	0	2926	1023	0	0	0
NEGR1hi Fibroblasts	0	0	0	14136	0	0
NK cells	0	0	0	0	69	71
NR4A1hi fibroblasts	0	0	0	0	234	13
Nervous System Cells	0	465	351	158	197	53
Osteoblasts	0	0	0	0	0	92
Osteoclasts	0	0	0	0	0	53

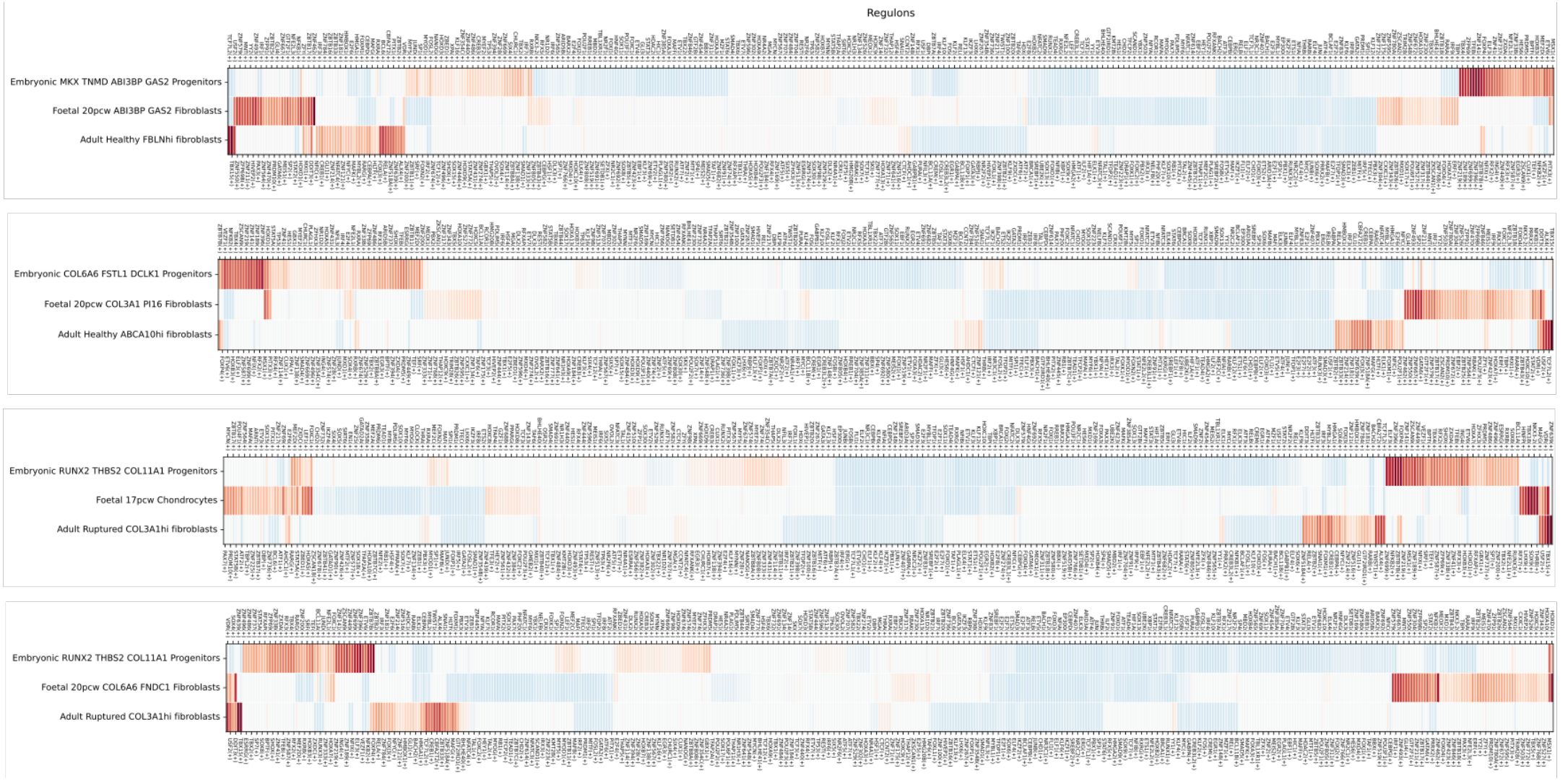
Pericytes	0	0	0	0	333	370
RUNX2 THBS2 COL11A1 Progenitors	649	0	0	0	0	0
SCX FGF14 THBS4 FSTL5 Progenitors	758	0	0	0	0	0
SOX5 CREB5 Chondrocyte Progenitors	303	0	0	0	0	0
Satellite Cells	0	2278	647	637	0	0
Skeletal Myocytes	0	1570	272	0	0	0
Slow-twitch skeletal muscle cells	0	0	0	16435	0	0
Smooth Myocytes	0	1078	960	0	0	0
T cells	0	0	0	1499	262	133
Transitional skeletal muscle cells	0	0	0	758	0	0
VCANhi DCs/monocytes	0	0	0	0	43	137
Vascular endothelial cells	0	1524	988	5475	0	0
Venular VECs	0	0	0	0	466	136
pDCs	0	0	0	0	0	72
vSMCs	0	0	0	0	166	10


ECM Glycoproteins
Fraction of cells in group (%)
mean normalised expression


ECM Regulators
Fraction of cells in group (%)
mean normalised expression



Appendix Figure 14. Embryonic, foetal, and adult tendon fibroblast matrisomal gene expression profiles. *Dotplots show the mean normalised expression levels alongside the proportions of expressing cell types for matrisomal genes categorised as ECM-affiliated proteins, ECM glycoproteins, and ECM regulators. The lists of matrisomal genes were obtained from the matrisomeDB database (Shao et al., 2020). The plots for collagens and proteoglycans are shown in Figure 65.*



Appendix Figure 15. Comparative analysis of shared SCENIC regulon activation patterns in specific fibroblast cell types across developing and adult datasets. *Hierarchical clustermaps show summarised and z-score normalised regulon activity patterns in selected fibroblast cell types. SCENIC regulons are clustered using average linkage and Euclidean distance, while cell types remain unclustered. The colour bar quantifies the regulon activation z-score values, with blue corresponding to the below-mean activation, white representing the absence of the regulon from the datasert, and red denoting above-mean activation. These plots show all regulons identified across the different datasets. Figure 71 shows the shared regulon plots.*

References

10X Genomics, 2019. Chromium Single Cell 3' Reagent Kits User Guide (v3.1 Chemistry) – CG000204 Rev D. 10x Genomics. https://www.10xgenomics.com/support/single-cell-gene-expression/documentation/steps/library-prep/chromium-single-cell-3-reagent-kits-user-guide-v-3-1-chemistry

Aaron, J.E., 2012. Periosteal Sharpey's fibers: a novel bone matrix regulatory system? Front. Endocrinol. 3. https://doi.org/10.3389/fendo.2012.00098

Abate, M., Schiavone, C., Salini, V., 2014. The Use of Hyaluronic Acid after Tendon Surgery and in Tendinopathies. BioMed Res. Int. 2014, e783632. https://doi.org/10.1155/2014/783632

Abbah, S.A., Thomas, D., Browne, S., O'Brien, T., Pandit, A., Zeugolis, D.I., 2016. Co-transfection of decorin and interleukin-10 modulates pro-fibrotic extracellular matrix gene expression in human tenocyte culture. Sci. Rep. 6, 20922. https://doi.org/10.1038/srep20922

Acharya, P.S., Majumdar, S., Jacob, M., Hayden, J., Mrass, P., Weninger, W., Assoian, R.K., Puré, E., 2008. Fibroblast migration is mediated by CD44-dependent TGFβ activation. J. Cell Sci. 121, 1393–1402. https://doi.org/10.1242/jcs.021683

Ackerman, J.E., Best, K.T., Muscat, S.N., Pritchett, E.M., Nichols, A.E.C., Wu, C.-L., Loiselle, A.E., 2022. Defining the spatial-molecular map of fibrotic tendon healing and the drivers of Scleraxis-lineage cell fate and function. Cell Rep. 41, 111706. https://doi.org/10.1016/j.celrep.2022.111706

Ackerman, J.E., Muscat, S.N., Adjei-Sowah, E., Korcari, A., Nichols, A.E.C., Buckley, M.R., Loiselle, A.E., 2024. Identification of Periostin as a critical niche for myofibroblast dynamics and fibrosis during tendon healing. Matrix Biol. 125, 59–72. https://doi.org/10.1016/j.matbio.2023.12.004

Ackermann, P.W., 2015. Tendinopathies in Sports: From Basic Research to the Field, in: Doral, M.N., Karlsson, J. (Eds.), Sports Injuries: Prevention, Diagnosis, Treatment and Rehabilitation. Springer, Berlin, Heidelberg, pp. 1–15. https://doi.org/10.1007/978-3-642-36801-1_180-1

Ackermann, P.W., Salo, P., Hart, D.A., 2016. Tendon Innervation, in: Ackermann, P.W., Hart, D.A. (Eds.), Metabolic Influences on Risk for Tendon Disorders. Springer International Publishing, Cham, pp. 35–51. https://doi.org/10.1007/978-3-319-33943-6_4

Ahlmann-Eltze, C., Huber, W., 2023. Comparison of transformations for single-cell RNA-seq data. Nat. Methods 20, 665–672. https://doi.org/10.1038/s41592-023-01814-1

Ahmed, I.M., Lagopoulos, M., McConnell, P., Soames, R.W., Sefton, G.K., 1998. Blood supply of the achilles tendon. J. Orthop. Res. 16, 591–596. https://doi.org/10.1002/jor.1100160511

Aibar, S., González-Blas, C.B., Moerman, T., Huynh-Thu, V.A., Imrichova, H., Hulselmans, G., Rambow, F., Marine, J.-C., Geurts, P., Aerts, J., van den Oord, J., Atak, Z.K., Wouters, J., Aerts, S., 2017. SCENIC: single-cell regulatory network inference and clustering. Nat. Methods 14, 1083–1086. https://doi.org/10.1038/nmeth.4463

Akbar, M., MacDonald, L., Crowe, L.A.N., Carlberg, K., Kurowska-Stolarska, M., Ståhl, P.L., Snelling, S.J.B., McInnes, I.B., Millar, N.L., 2021. Single cell and spatial transcriptomics in human tendon disease indicate dysregulated immune homeostasis. Ann. Rheum. Dis. 80, 1494–1497. https://doi.org/10.1136/annrheumdis-2021-220256

Akiyama, H., Kim, J.E., Nakashima, K., Balmes, G., Iwai, N., Deng, J.M., Zhang, Z., Martin, J.F., Behringer, R.R., Nakamura, T., De Crombrugghe, B., 2005. Osteo-chondroprogenitor cells are derived from Sox9 expressing precursors. Proc. Natl. Acad. Sci. U. S. A. 102, 14665–14670. https://doi.org/10.1073/pnas.0504750102

Al Makhzoomi, A.K., Kirk, T.B., Dye, D.E., Allison, G.T., 2021. Contribution of glycosaminoglycans to the structural and mechanical properties of tendons – A multiscale study. J. Biomech. 128, 110796. https://doi.org/10.1016/j.jbiomech.2021.110796

Albers, I.S., Zwerver, J., Diercks, R.L., Dekker, J.H., Van den Akker-Scheek, I., 2016. Incidence and prevalence of lower extremity tendinopathy in a Dutch general practice population: a cross sectional study. BMC Musculoskelet. Disord. 17, 16. https://doi.org/10.1186/s12891-016-0885-2

Alberton, P., Dex, S., Popov, C., Shukunami, C., Schieker, M., Docheva, D., 2015. Loss of Tenomodulin Results in Reduced Self-Renewal and Augmented Senescence of Tendon Stem/Progenitor Cells. Stem Cells Dev. 24, 597–609. https://doi.org/10.1089/scd.2014.0314

Alcaide-Ruggiero, L., Molina-Hernández, V., Granados, M.M., Domínguez, J.M., 2021. Main and Minor Types of Collagens in the Articular Cartilage: The Role of Collagens in Repair Tissue Evaluation in Chondral Defects. Int. J. Mol. Sci. 22, 13329. https://doi.org/10.3390/ijms222413329

Alfredson, H., 2005. The chronic painful Achilles and patellar tendon: research on basic biology and treatment. Scand. J. Med. Sci. Sports 15, 252–259. https://doi.org/10.1111/j.1600-0838.2005.00466.x

Alhajj, M., Goyal, A., 2024. Physiology, Granulation Tissue, in: StatPearls. StatPearls Publishing, Treasure Island (FL).

Al-Hattab, D.S., Safi, H.A., Nagalingam, R.S., Bagchi, R.A., Stecy, M.T., Czubryt, M.P., 2018. Scleraxis regulates Twist1 and Snai1 expression in the epithelial-to-mesenchymal transition. Am. J. Physiol.-Heart Circ. Physiol. 315, H658–H668. https://doi.org/10.1152/ajpheart.00092.2018

Almekinders, L.C., Deol, G., 1999. The effects of aging, antiinflammatory drugs, and ultrasound on the in vitro response of tendon tissue. Am. J. Sports Med. 27, 417–421. https://doi.org/10.1177/03635465990270040301

Amano, K., Densmore, M., Nishimura, R., Lanske, B., 2014. Indian Hedgehog Signaling Regulates Transcription and Expression of Collagen Type X via Runx2/Smads Interactions. J. Biol. Chem. 289, 24898–24910. https://doi.org/10.1074/jbc.M114.570507

Amiel, D., Akeson, W.H., Harwood, F.L., Frank, C.B., 1983. Stress deprivation effect on metabolic turnover of the medial collateral ligament collagen. A comparison between nine- and 12-week immobilization. Clin. Orthop. 265–270.

Anders, H.-J., Schaefer, L., 2014. Beyond Tissue Injury—Damage-Associated Molecular Patterns, Toll-Like Receptors, and Inflammasomes Also Drive Regeneration and Fibrosis. J. Am. Soc. Nephrol. JASN 25, 1387–1400. https://doi.org/10.1681/ASN.2014010117

Anderson, D.M., Arredondo, J., Hahn, K., Valente, G., Martin, J.F., Wilson-Rawls, J., Rawls, A., 2006. Mohawk is a novel homeobox gene expressed in the developing mouse embryo. Dev. Dyn. 235, 792–801. https://doi.org/10.1002/dvdy.20671

Andreuzzi, E., Fejza, A., Capuano, A., Poletto, E., Pivetta, E., Doliana, R., Pellicani, R., Favero, A., Maiero, S., Fornasarig, M., Cannizzaro, R., Iozzo, R.V., Spessotto, P., Mongiat, M., 2020. Deregulated expression of Elastin Microfibril Interfacer 2 (EMILIN2) in gastric cancer affects tumor growth and angiogenesis. Matrix Biol. Plus 6–7, 100029. https://doi.org/10.1016/j.mbplus.2020.100029

Ansorge, H., Beredjiklian, P., Soslowsky, L., 2009. CD44 deficiency improves healing tendon mechanics and increases matrix and cytokine expression in a mouse patellar tendon injury model. J. Orthop. Res. Off. Publ. Orthop. Res. Soc. 27, 1386–1391. https://doi.org/10.1002/jor.20891

Ansorge, H.L., Adams, S., Birk, D.E., Soslowsky, L.J., 2011. Mechanical, Compositional, and Structural Properties of the Post-natal Mouse Achilles Tendon. Ann. Biomed. Eng. 39, 1904–1913. https://doi.org/10.1007/s10439-011-0299-0

Ansorge, H.L., Hsu, J.E., Edelstein, L., Adams, S., Birk, D.E., Soslowsky, L.J., 2012. Recapitulation of the Achilles tendon mechanical properties during neonatal development: a study of differential healing during two stages of

development in a mouse model. J. Orthop. Res. 30, 448–456. https://doi.org/10.1002/jor.21542

Ansorge, H.L., Meng, X., Zhang, G., Veit, G., Sun, M., Klement, J.F., Beason, D.P., Soslowsky, L.J., Koch, M., Birk, D.E., 2009. Type XIV Collagen Regulates Fibrillogenesis *. J. Biol. Chem. 284, 8427–8438. https://doi.org/10.1074/jbc.M805582200

Apostolakos, J., Durant, T.J., Dwyer, C.R., Russell, R.P., Weinreb, J.H., Alaee, F., Beitzel, K., McCarthy, M.B., Cote, M.P., Mazzocca, A.D., 2014. The enthesis: a review of the tendon-to-bone insertion. Muscles Ligaments Tendons J. 4, 333–342.

Åström, M., Rausing, A., 1995. Chronic Achilles Tendinopathy: A Survey of Surgical and Histopathologic Findings Mats. Clin. Orthop. Relat. Res. 151.

Aström, M., Rausing, A., 1995. Chronic Achilles tendinopathy. A survey of surgical and histopathologic findings. Clin. Orthop. 151–164.

Avery, N.C., Bailey, A.J., 2005. Enzymic and non-enzymic cross-linking mechanisms in relation to turnover of collagen: relevance to aging and exercise. Scand. J. Med. Sci. Sports 15, 231–240. https://doi.org/10.1111/j.1600-0838.2005.00464.x

Bailey, A.J., 2001. Molecular mechanisms of ageing in connective tissues. Mech. Ageing Dev. 122, 735–755. https://doi.org/10.1016/S0047-6374(01)00225-1

Baldwin, M., Buckley, C.D., Guilak, F., Hulley, P., Cribbs, A.P., Snelling, S., 2023. A roadmap for delivering a human musculoskeletal cell atlas. Nat. Rev. Rheumatol. 19, 738–752. https://doi.org/10.1038/s41584-023-01031-2

Baldwin, M.J., Cribbs, A.P., Guilak, F., Snelling, S.J.B., 2021. Mapping the musculoskeletal system one cell at a time. Nat. Rev. Rheumatol. 17, 247–248. https://doi.org/10.1038/s41584-021-00600-7

Bank, R.A., TeKoppele, J.M., Oostingh, G., Hazleman, B.L., Riley, G.P., 1999. Lysylhydroxylation and non-reducible crosslinking of human supraspinatus tendon collagen: changes with age and in chronic rotator cuff tendinitis. Ann. Rheum. Dis. 58, 35–41. https://doi.org/10.1136/ard.58.1.35

Beach, Z.M., Bonilla, K.A., Dekhne, M.S., Sun, M., Adams, T.H., Adams, S.M., Weiss, S.N., Rodriguez, A.B., Shetye, S.S., Birk, D.E., Soslowsky, L.J., 2022. Biglycan Has a Major Role in Maintenance of Mature Tendon Mechanics. J. Orthop. Res. Off. Publ. Orthop. Res. Soc. 40, 2546–2556. https://doi.org/10.1002/jor.25299

Beach, Z.M., Nuss, C.A., Weiss, S.N., Soslowsky, L.J., 2024. Neonatal Achilles Tendon Microstructure is Negatively Impacted by Decorin and Biglycan

Knockdown After Injury and During Development. Ann. Biomed. Eng. 52, 657–670. https://doi.org/10.1007/s10439-023-03414-8

Benjamin, M., Kaiser, E., Milz, S., 2008. Structure-function relationships in tendons: a review. J. Anat. 212, 211–228. https://doi.org/10.1111/j.1469-7580.2008.00864.x

Beredjiklian, P.K., Favata, M., Cartmell, J.S., Flanagan, C.L., Crombleholme, T.M., Soslowsky, L.J., 2003. Regenerative versus reparative healing in tendon: A study of biomechanical and histological properties in fetal sheep. Ann. Biomed. Eng. 31, 1143–1152. https://doi.org/10.1114/1.1616931

Bergen, V., Lange, M., Peidli, S., Wolf, F.A., Theis, F.J., 2020. Generalizing RNA velocity to transient cell states through dynamical modeling. Nat. Biotechnol. 38, 1408–1414. https://doi.org/10.1038/s41587-020-0591-3

Berglund, M., Hart, D.A., Wiig, M., 2007. The inflammatory response and hyaluronan synthases in the rabbit flexor tendon and tendon sheath following injury. J. Hand Surg. Eur. Vol. 32, 581–587. https://doi.org/10.1016/J.JHSE.2007.05.017

Berglund, M., Reno, C., Hart, D.A., Wiig, M., 2006. Patterns of mRNA Expression for Matrix Molecules and Growth Factors in Flexor Tendon Injury: Differences in the Regulation Between Tendon and Tendon Sheath. J. Hand Surg. 31, 1279–1287. https://doi.org/10.1016/j.jhsa.2006.06.011

Bestwick, C.S., Maffulli, N., 2000. Reactive Oxygen Species and Tendon Problems: Review and Hypothesis. Sports Med. Arthrosc. Rev. 8, 6.

Bi, W., Deng, J.M., Zhang, Z., Behringer, R.R., De Crombrugghe, B., 1999. Sox9 is required for cartilage formation. Nat. Genet. 22, 85–89. https://doi.org/10.1038/8792

Bi, Y., Ehirchiou, D., Kilts, T.M., Inkson, C.A., Embree, M.C., Sonoyama, W., Li, L., Leet, A.I., Seo, B.M., Zhang, L., Shi, S., Young, M.F., 2007. Identification of tendon stem/progenitor cells and the role of the extracellular matrix in their niche. Nat. Med. 13, 1219–1227. https://doi.org/10.1038/nm1630

Bielefeld, K.A., Amini-Nik, S., Alman, B.A., 2013. Cutaneous wound healing: recruiting developmental pathways for regeneration. Cell. Mol. Life Sci. 70, 2059–2081. https://doi.org/10.1007/s00018-012-1152-9

Birch, H.L., 2007. Tendon matrix composition and turnover in relation to functional requirements. Int. J. Exp. Pathol. 88, 241–248. https://doi.org/10.1111/j.1365-2613.2007.00552.x

Birk, D.E., Brückner, P., 2011. Collagens, Suprastructures, and Collagen Fibril Assembly, in: Mecham, R.P. (Ed.), The Extracellular Matrix: An

Overview. Springer, Berlin, Heidelberg, pp. 77–115. https://doi.org/10.1007/978-3-642-16555-9_3

Birk, D.E., Mayne, R., 1997. Localization of collagen types I, III and V during tendon development. Changes in collagen types I and III are correlated with changes in fibril diameter. Eur. J. Cell Biol. 72, 352–361.

Birk, D.E., Trelstad, R.L., 1986. Extracellular compartments in tendon morphogenesis: collagen fibril, bundle, and macroaggregate formation. J. Cell Biol. 103, 231–240. https://doi.org/10.1083/jcb.103.1.231

Bland, Y.S., Ashhurst, D.E., 1997. Fetal and postnatal development of the patella, patellar tendon and suprapatella in the rabbit; changes in the distribution of the fibrillar collagens. J. Anat. 190 (Pt 3), 327–342. https://doi.org/10.1046/j.1469-7580.1997.19030327.x

Bleacher, J.C., Adolph, V.R., Dillon, P.W., Krummel, T.M., 1993. Fetal tissue repair and wound healing. Dermatol. Clin. 11, 677–683. https://doi.org/10.1016/s0733-8635(18)30220-1

Blitz, E., Sharir, A., Akiyama, H., Zelzer, E., 2013. Tendon-bone attachment unit is formed modularly by a distinct pool of Scx-and Sox9-positive progenitors. Dev. Camb. 140, 2680–2690. https://doi.org/10.1242/dev.093906

Blitz, E., Viukov, S., Sharir, A., Shwartz, Y., Galloway, J.L., Pryce, B.A., Johnson, R.L., Tabin, C.J., Schweitzer, R., Zelzer, E., 2009. Bone Ridge Patterning during Musculoskeletal Assembly Is Mediated through SCX Regulation of Bmp4 at the Tendon-Skeleton Junction. Dev. Cell 17, 861–873. https://doi.org/10.1016/j.devcel.2009.10.010

Blomgran, P., Hammerman, M., Aspenberg, P., 2017. Systemic corticosteroids improve tendon healing when given after the early inflammatory phase. Sci. Rep. 7, 12468. https://doi.org/10.1038/s41598-017-12657-0

Bode-Lesniewska, B., Dours-Zimmermann, M.T., Odermatt, B.F., Briner, J., Heitz, P.U., Zimmermann, D.R., 1996. Distribution of the large aggregating proteoglycan versican in adult human tissues. J. Histochem. Cytochem. Off. J. Histochem. Soc. 44, 303–312. https://doi.org/10.1177/44.4.8601689

Bonnin, M.-A., Laclef, C., Blaise, R., Eloy-Trinquet, S., Relaix, F., Maire, P., Duprez, D., 2005. Six1 is not involved in limb tendon development, but is expressed in limb connective tissue under Shh regulation. Mech. Dev. 122, 573–585. https://doi.org/10.1016/j.mod.2004.11.005

Boote, C., Ma, Q., Goh, K.L., 2023. Age-dependent mechanical properties of tail tendons in wild-type and mimecan gene-knockout mice – A preliminary study. J. Mech. Behav. Biomed. Mater. 139, 105672. https://doi.org/10.1016/j.jmbbm.2023.105672

Bornstein, P., Kyriakides, T.R., Yang, Z., Armstrong, L.C., Birk, D.E., 2000. Thrombospondin 2 modulates collagen fibrillogenesis and angiogenesis. J. Investig. Dermatol. Symp. Proc. 5, 61–66. https://doi.org/10.1046/j.1087-0024.2000.00005.x

Breidenbach, A.P., Aschbacher-Smith, L., Lu, Y., Dyment, N.A., Liu, C., Liu, H., Wylie, C., Rao, M., Shearn, J.T., Rowe, D.W., Kadler, K.E., Jiang, R., Butler, D.L., 2015. Ablating hedgehog signaling in tenocytes during development impairs biomechanics and matrix organization of the adult murine patellar tendon enthesis. J. Orthop. Res. 33, 1142–1151. https://doi.org/10.1002/jor.22899

Brent, A.E., Braun, T., Tabin, C.J., 2005. Genetic analysis of interactions between the somitic muscle, cartilage and tendon cell lineages during mouse development. Development 132, 515–528. https://doi.org/10.1242/dev.01605

Brisset, M., Metay, C., Carlier, R.-Y., Badosa, C., Marques, C., Schalkwijk, J., vanVlijmen-Willems, I., Jimenez-Mallebrera, C., Keren, B., Jobic, V., Laforêt, P., Malfatti, E., 2020. Biallelic mutations in *Tenascin-X* cause classical-like Ehlers-Danlos syndrome with slowly progressive muscular weakness. Neuromuscul. Disord. 30, 833–838. https://doi.org/10.1016/j.nmd.2020.09.002

Broner, E.C., Trujillo, J.A., Korzinkin, M., Subbannayya, T., Agrawal, N., Ozerov, I.V., Zhavoronkov, A., Rooper, L., Kotlov, N., Shen, L., Pearson, A.T., Rosenberg, A.J., Savage, P.A., Mishra, V., Chatterjee, A., Sidransky, D., Izumchenko, E., 2021. Doublecortin-Like Kinase 1 (DCLK1) Is a Novel NOTCH Pathway Signaling Regulator in Head and Neck Squamous Cell Carcinoma. Front. Oncol. 11, 677051. https://doi.org/10.3389/fonc.2021.677051

Bruns, J., Kampen, J., Kahrs, J., Plitz, W., 2000. Achilles tendon rupture: Experimental results on spontaneous repair in a sheep-model. Knee Surg. Sports Traumatol. Arthrosc. 8, 364–369. https://doi.org/10.1007/s001670000149

Buckley, M.R., Evans, E., Satchel, L.N., Matuszewski, P.E., Chen, Y.-L., Elliott, D.M., Soslowsky, L.J., Dodge, G.R., 2013. Distributions of Types I, II and III Collagen by Region in the Human Supraspinatus Tendon. Connect. Tissue Res. 54, 374. https://doi.org/10.3109/03008207.2013.847096

Cadby, J.A., Buehler, E., Godbout, C., Weeren, P.R. van, Snedeker, J.G., 2014. Differences between the Cell Populations from the Peritenon and the Tendon Core with Regard to Their Potential Implication in Tendon Repair. PLOS ONE 9, e92474. https://doi.org/10.1371/journal.pone.0092474

Can, T., Faas, L., Ashford, D.A., Dowle, A., Thomas, J., O'Toole, P., Blanco, G., 2014. Proteomic analysis of laser capture microscopy purified

myotendinous junction regions from muscle sections. Proteome Sci. 12, 25. https://doi.org/10.1186/1477-5956-12-25

Canty, E.G., Kadler, K.E., 2005. Procollagen trafficking, processing and fibrillogenesis. J. Cell Sci. 118, 1341–1353. https://doi.org/10.1242/jcs.01731

Canty, E.G., Lu, Y., Meadows, R.S., Shaw, M.K., Holmes, D.F., Kadler, K.E., 2004. Coalignment of plasma membrane channels and protrusions (fibripositors) specifies the parallelism of tendon. J. Cell Biol. 165, 553–563. https://doi.org/10.1083/jcb.200312071

Canty-Laird, E.G., Lu, Y., Kadler, K.E., 2012. Stepwise proteolytic activation of type I procollagen to collagen within the secretory pathway of tendon fibroblasts in situ. Biochem. J. 441, 707–717. https://doi.org/10.1042/BJ20111379

Carlson, B.M., 2018. Limb Development, in: Human Embryology and Developmental Biology. Elsevier, St. Louis, pp. 183–198.

Carlson, E.C., Liu, C.-Y., Chikama, T., Hayashi, Y., Kao, C.W.-C., Birk, D.E., Funderburgh, J.L., Jester, J.V., Kao, W.W.-Y., 2005. Keratocan, a Cornea-specific Keratan Sulfate Proteoglycan, Is Regulated by Lumican. J. Biol. Chem. 280, 25541–25547. https://doi.org/10.1074/jbc.M500249200

Carlsson, L., Li, Z., Paulin, D., Thornell, L.-E., 1999. Nestin Is Expressed during Development and in Myotendinous and Neuromuscular Junctions in Wild Type and Desmin Knock-Out Mice. Exp. Cell Res. 251, 213–223. https://doi.org/10.1006/excr.1999.4569

Chan, B.P., Fu, S.C., Qin, L., Rolf, C., Chan, K.M., 1998. Pyridinoline in relation to ultimate stress of the patellar tendon during healing: An animal study. J. Orthop. Res. 16, 597–603. https://doi.org/10.1002/jor.1100160512

Chaplin, D.M., Greenlee, T.K., 1975. The development of human digital tendons. J. Anat. 120, 253–274.

Charvet, B., Guiraud, A., Malbouyres, M., Zwolanek, D., Guillon, E., Bretaud, S., Monnot, C., Schulze, J., Bader, H.L., Allard, B., Koch, M., Ruggiero, F., 2013. Knockdown of col22a1 gene in zebrafish induces a muscular dystrophy by disruption of the myotendinous junction. Development 140, 4602–4613. https://doi.org/10.1242/dev.096024

Charvet, B., Ruggiero, F., Le Guellec, D., 2012. The development of the myotendinous junction. A review. Muscles Ligaments Tendons J. 2, 53–63.

Chaudhuri, J., Bains, Y., Guha, S., Kahn, A., Hall, D., Bose, N., Gugliucci, A., Kapahi, P., 2018. The role of advanced glycation end products in aging and metabolic diseases: bridging association and causality. Cell Metab. 28, 337–352. https://doi.org/10.1016/j.cmet.2018.08.014

Chen, C.H., Cao, Y., Wu, Y.F., Bais, A.J., Gao, J.S., Tang, J.B., 2008. Tendon Healing In Vivo: Gene Expression and Production of Multiple Growth Factors in Early Tendon Healing Period. J. Hand Surg. 33, 1834–1842. https://doi.org/10.1016/j.jhsa.2008.07.003

Chen, K.H., Boettiger, A.N., Moffitt, J.R., Wang, S., Zhuang, X., 2015. Spatially resolved, highly multiplexed RNA profiling in single cells. Science 348, aaa6090. https://doi.org/10.1126/science.aaa6090

Chen, Z., Li, M., Chen, P., Tai, A., Li, J., Bassonga, E.L., Gao, J., Liu, D., Wood, D., Kennedy, B.F., Zheng, Q., Zheng, M.H., 2024. Mechanical overload-induced release of extracellular mitochondrial particles from tendon cells leads to inflammation in tendinopathy. Exp. Mol. Med. 1–17. https://doi.org/10.1038/s12276-024-01183-5

Chiquet-Ehrismann, R., Tucker, R.P., 2011. Tenascins and the Importance of Adhesion Modulation. Cold Spring Harb. Perspect. Biol. 3, a004960. https://doi.org/10.1101/cshperspect.a004960

Chisari, E., Rehak, L., Khan, W.S., Maffulli, N., 2020. The role of the immune system in tendon healing: a systematic review. Br. Med. Bull. 133, 49–64. https://doi.org/10.1093/bmb/ldz040

Choi, R., Smith, M., Clarke, E., Little, C., 2018. Cellular, matrix, and mechano-biological differences in load-bearing versus positional tendons throughout development and aging: a narrative review. Connect. Tissue Res. 59, 483–494. https://doi.org/10.1080/03008207.2018.1504929

Choocheep, K., Hatano, S., Takagi, H., Watanabe, Hiroki, Kimata, K., Kongtawelert, P., Watanabe, Hideto, 2010. Versican Facilitates Chondrocyte Differentiation and Regulates Joint Morphogenesis*. J. Biol. Chem. 285, 21114–21125. https://doi.org/10.1074/jbc.M109.096479

Cognetti, D.J., Sheean, A.J., Arner, J.W., Wilkerson, D., Bradley, J.P., 2023. Surgical Management of Patellar Tendinopathy Results in Improved Outcomes and High Rates of Return to Sport: A Systematic Review. J. Knee Surg. 36, 1171–1190. https://doi.org/10.1055/s-0042-1757701

Colombatti, A., Spessotto, P., Doliana, R., Mongiat, M., Bressan, G.M., Esposito, G., 2012. The EMILIN/Multimerin Family. Front. Immunol. 2. https://doi.org/10.3389/fimmu.2011.00093

Connizzo, B.K., Freedman, B.R., Fried, J.H., Sun, M., Birk, D.E., Soslowsky, L.J., 2015. Regulatory role of collagen V in establishing mechanical properties of tendons and ligaments is tissue dependent. J. Orthop. Res. 33, 882–888. https://doi.org/10.1002/jor.22893

Cook, J.L., Feller, J.A., Bonar, S.F., Khan, K.M., 2004. Abnormal tenocyte morphology is more prevalent than collagen disruption in asymptomatic athletes' patellar tendons. J. Orthop. Res. 22, 334–338. https://doi.org/10.1016/j.orthres.2003.08.005

Cook, J.L., Purdam, C.R., 2009. Is tendon pathology a continuum? A pathology model to explain the clinical presentation of load-induced tendinopathy. Br. J. Sports Med. 43, 409–416. https://doi.org/10.1136/bjsm.2008.051193

Corps, A.N., Robinson, A.H.N., Movin, T., Costa, M.L., Hazleman, B.L., Riley, G.P., 2006. Increased expression of aggrecan and biglycan mRNA in Achilles tendinopathy. Rheumatol. Oxf. Engl. 45, 291–294. https://doi.org/10.1093/rheumatology/kei152

Corps, A.N., Robinson, A.H.N., Movin, T., Costa, M.L., Ireland, D.C., Hazleman, B.L., Riley, G.P., 2004. Versican splice variant messenger RNA expression in normal human Achilles tendon and tendinopathies. Rheumatology 43, 969–972. https://doi.org/10.1093/rheumatology/keh222

Corsi, A., Xu, T., Chen, X.-D., Boyde, A., Liang, J., Mankani, M., Sommer, B., Iozzo, R.V., Eichstetter, I., Robey, P.G., Bianco, P., Young, M.F., 2002. Phenotypic Effects of Biglycan Deficiency Are Linked to Collagen Fibril Abnormalities, Are Synergized by Decorin Deficiency, and Mimic Ehlers-Danlos-Like Changes in Bone and Other Connective Tissues. J. Bone Miner. Res. 17, 1180–1189. https://doi.org/10.1359/jbmr.2002.17.7.1180

Costa, F.R., Costa Marques, M.R., Costa, V.C., Santos, G.S., Martins, R.A., Santos, M.D.S., Santana, M.H.A., Nallakumarasamy, A., Jeyaraman, M., Lana, J.V.B., Lana, J.F.S.D., 2023. Intra-Articular Hyaluronic Acid in Osteoarthritis and Tendinopathies: Molecular and Clinical Approaches. Biomedicines 11. https://doi.org/10.3390/biomedicines11041061

Couppé, C., Hansen, P., Kongsgaard, M., Kovanen, V., Suetta, C., Aagaard, P., Kjær, M., Magnusson, S.P., 2009. Mechanical properties and collagen cross-linking of the patellar tendon in old and young men. J. Appl. Physiol. 107, 880–886. https://doi.org/10.1152/japplphysiol.00291.2009

Crossley, P.H., Minowada, G., MacArthur, C.A., Martin, G.R., 1996. Roles for FGF8 in the induction, initiation, and maintenance of chick limb development. Cell 84, 127–136. https://doi.org/10.1016/S0092-8674(00)80999-X

Cuthbert, R.J., Watad, A., Fragkakis, E.M., Dunsmuir, R., Loughenbury, P., Khan, A., Millner, P.A., Davison, A., Marzo-Ortega, H., Newton, D., Bridgewood, C., McGonagle, D.G., 2019. Evidence that tissue resident human enthesis γδT-cells can produce IL-17A independently of IL-23R transcript expression. Ann. Rheum. Dis. 78, 1559–1565. https://doi.org/10.1136/annrheumdis-2019-215210

Czarny-Ratajczak, M., Lohiniva, J., Rogala, P., Kozlowski, K., Perälä, M., Carter, L., Spector, T.D., Kolodziej, L., Seppänen, U., Glazar, R., Królewski, J., Latos-Bielenska, A., Ala-Kokko, L., 2001. A Mutation in *COL9A1* Causes Multiple Epiphyseal Dysplasia: Further Evidence for

Locus Heterogeneity. Am. J. Hum. Genet. 69, 969–980. https://doi.org/10.1086/324023

CZI Single-Cell Biology Program, Abdulla, S., Aevermann, B., Assis, P., Badajoz, S., Bell, S.M., Bezzi, E., Cakir, B., Chaffer, J., Chambers, S., Cherry, J.M., Chi, T., Chien, J., Dorman, L., Garcia-Nieto, P., Gloria, N., Hastie, M., Hegeman, D., Hilton, J., Huang, T., Infeld, A., Istrate, A.-M., Jelic, I., Katsuya, K., Kim, Y.J., Liang, K., Lin, M., Lombardo, M., Marshall, B., Martin, B., McDade, F., Megill, C., Patel, N., Predeus, A., Raymor, B., Robatmili, B., Rogers, D., Rutherford, E., Sadgat, D., Shin, A., Small, C., Smith, T., Sridharan, P., Tarashansky, A., Tavares, N., Thomas, H., Tolopko, A., Urisko, M., Yan, J., Yeretssian, G., Zamanian, J., Mani, A., Cool, J., Carr, A., 2023. CZ CELL×GENE Discover: A single-cell data platform for scalable exploration, analysis and modeling of aggregated data. https://doi.org/10.1101/2023.10.30.563174

Dahlgren, L.A., Brower-Toland, B.D., Nixon, A.J., 2005. Cloning and expression of type III collagen in normal and injured tendons of horses. Am. J. Vet. Res. 66, 266–270. https://doi.org/10.2460/ajvr.2005.66.266

Dakin, S.G., Martinez, F.O., Yapp, C., Wells, G., Oppermann, U., Dean, B.J.F., Smith, R.D.J., Wheway, K., Watkins, B., Roche, L., Carr, A.J., 2015. Inflammation activation and resolution in human tendon disease. Sci. Transl. Med. 7. https://doi.org/10.1126/scitranslmed.aac4269

De Micheli, A.J., Swanson, J.B., Disser, N.P., Martinez, L.M., Walker, N.R., Oliver, D.J., Cosgrove, B.D., Mendias, C.L., 2020. Single-cell transcriptomic analysis identifies extensive heterogeneity in the cellular composition of mouse Achilles tendons. Am. J. Physiol. - Cell Physiol. 319, C885–C894. https://doi.org/10.1152/ajpcell.00372.2020

Delabastita, T., Bogaerts, S., Vanwanseele, B., 2019. Age-related changes in achilles tendon stiffness and impact on functional activities: A systematic review and meta-analysis. J. Aging Phys. Act. 27, 116–127. https://doi.org/10.1123/japa.2017-0359

Derwin, K.A., Soslowsky, L.J., Kimura, J.H., Plaas, A.H., 2001. Proteoglycans and glycosaminoglycan fine structure in the mouse tail tendon fascicle. J. Orthop. Res. 19, 269–277. https://doi.org/10.1016/S0736-0266(00)00032-2

Dex, S., Lin, D., Shukunami, C., Docheva, D., 2016. TENOgenic MODULating INsider factor: systematic assessment on the functions of tenomodulin gene. Gene 587, 1–17. https://doi.org/10.1016/j.gene.2016.04.051

Di Martino, A., Cescon, M., D'Agostino, C., Schilardi, F., Sabatelli, P., Merlini, L., Faldini, C., 2023. Collagen VI in the Musculoskeletal System. Int. J. Mol. Sci. 24, 5095. https://doi.org/10.3390/ijms24065095

Disser, N.P., Yu, J.S., Yao, V.J.H., Rodeo, S.A., 2023. Pharmacological Therapies for Connective Tissue Fibrosis in Orthopaedics. Am. J. Sports Med. 51, 2766–2773. https://doi.org/10.1177/03635465221116358

Docheva, D., Hunziker, E.B., Fässler, R., Brandau, O., 2005. Tenomodulin Is Necessary for Tenocyte Proliferation and Tendon Maturation. Mol. Cell. Biol. 25, 699–705. https://doi.org/10.1128/mcb.25.2.699-705.2005

Dourte, L.M., Pathmanathan, L., Mienaltowski, M.J., Jawad, A.F., Birk, D.E., Soslowsky, L.J., 2013. Mechanical, Compositional, and Structural Properties of the Mouse Patellar Tendon with Changes in Biglycan Gene Expression. J. Orthop. Res. Off. Publ. Orthop. Res. Soc. 31, 1430–1437. https://doi.org/10.1002/jor.22372

Dunkman, A.A., Buckley, M.R., Mienaltowski, M.J., Adams, S.M., Thomas, S.J., Satchell, L., Kumar, A., Pathmanathan, L., Beason, D.P., Iozzo, R.V., Birk, D.E., Soslowsky, L.J., 2014. The Tendon Injury Response Is Influenced by Decorin and Biglycan. Ann. Biomed. Eng. 42, 619–630. https://doi.org/10.1007/s10439-013-0915-2

Durcan, L., Coole, A., McCarthy, E., Johnston, C., Webb, M.J., O'Shea, F.D., Gissane, C., Wilson, F., 2014. The prevalence of patellar tendinopathy in elite academy rugby: A clinical and imaging study. J. Sci. Med. Sport 17, 173–176. https://doi.org/10.1016/j.jsams.2013.05.014

Dy, P., Smits, P., Silvester, A., Penzo-Méndez, A., Dumitriu, B., Han, Y., la Motte, C.A. de, Kingsley, D.M., Lefebvre, V., 2010. Synovial joint morphogenesis requires the chondrogenic action of *Sox5* and *Sox6* in growth plate and articular cartilage. Dev. Biol. 341, 346–359. https://doi.org/10.1016/j.ydbio.2010.02.024

Dyment, N.A., Breidenbach, A.P., Schwartz, A.G., Russell, R.P., Aschbacher-Smith, L., Liu, H., Hagiwara, Y., Jiang, R., Thomopoulos, S., Butler, D.L., Rowe, D.W., 2015. Gdf5 progenitors give rise to fibrocartilage cells that mineralize via hedgehog signaling to form the zonal enthesis. Dev. Biol. 405, 96–107. https://doi.org/10.1016/J.YDBIO.2015.06.020

Dyment, N.A., Galloway, J.L., 2015. Regenerative Biology of Tendon: Mechanisms for Renewal and Repair. Curr. Mol. Biol. Rep. 1, 124–131. https://doi.org/10.1007/s40610-015-0021-3

Dyment, N.A., Liu, C.-F., Kazemi, N., Aschbacher-Smith, L.E., Kenter, K., Breidenbach, A.P., Shearn, J.T., Wylie, C., Rowe, D.W., Butler, D.L., 2013. The Paratenon Contributes to Scleraxis-Expressing Cells during Patellar Tendon Healing. PLOS ONE 8, e59944. https://doi.org/10.1371/journal.pone.0059944

Edom-Vovard, F., Duprez, D., 2004. Signals Regulating Tendon Formation During Chick Embryonic Development, Developmental Dynamics. https://doi.org/10.1002/dvdy.10481

Edom-Vovard, F., Schuler, B., Bonnin, M.A., Teillet, M.A., Duprez, D., 2002. Fgf4 positively regulates scleraxis and tenascin expression in chick limb tendons. Dev. Biol. 247, 351–366. https://doi.org/10.1006/dbio.2002.0707

Eekhoff, J.D., Fang, F., Kahan, L.G., Espinosa, G., Cocciolone, A.J., Wagenseil, J.E., Mecham, R.P., Lake, S.P., 2017. Functionally Distinct Tendons From Elastin Haploinsufficient Mice Exhibit Mild Stiffening and Tendon-Specific Structural Alteration. J. Biomech. Eng. 139, 1110031–1110039. https://doi.org/10.1115/1.4037932

Ellingson, A.J., Pancheri, N.M., Schiele, N.R., 2022. REGULATORS OF COLLAGEN CROSSLINKING IN DEVELOPING AND ADULT TENDONS. Eur. Cell. Mater. 43, 130–152. https://doi.org/10.22203/eCM.v043a11

Epelman, S., Lavine, K.J., Randolph, G.J., 2014. Origin and Functions of Tissue Macrophages. Immunity 41, 21–35. https://doi.org/10.1016/j.immuni.2014.06.013

Esteves de Lima, J., Blavet, C., Bonnin, M.-A., Hirsinger, E., Comai, G., Yvernogeau, L., Delfini, M.-C., Bellenger, L., Mella, S., Nassari, S., Robin, C., Schweitzer, R., Fournier-Thibault, C., Jaffredo, T., Tajbakhsh, S., Relaix, F., Duprez, D., 2021. Unexpected contribution of fibroblasts to muscle lineage as a mechanism for limb muscle patterning. Nat. Commun. 12, 3851. https://doi.org/10.1038/s41467-021-24157-x

Evans, R.A., Tian, Y. a C., Steadman, R., Phillips, A.O., 2003. TGF-β1-mediated fibroblast–myofibroblast terminal differentiation—the role of smad proteins. Exp. Cell Res. 282, 90–100. https://doi.org/10.1016/S0014-4827(02)00015-0

Exposito, J.-Y., Valcourt, U., Cluzel, C., Lethias, C., 2010. The Fibrillar Collagen Family. Int. J. Mol. Sci. 11, 407–426. https://doi.org/10.3390/ijms11020407

Eyal, S., Kult, S., Rubin, S., Krief, S., Felsenthal, N., Pineault, K.M., Leshkowitz, D., Salame, T.-M., Addadi, Y., Wellik, D.M., Zelzer, E., 2019. Bone morphology is regulated modularly by global and regional genetic programs. Dev. Camb. Engl. 146, dev167882. https://doi.org/10.1242/dev.167882

Eyre, D.R., Weis, M.A., Wu, J.-J., 2008. Advances in collagen cross-link analysis. Methods San Diego Calif 45, 65–74. https://doi.org/10.1016/j.ymeth.2008.01.002

Ezura, Y., Chakravarti, S., Oldberg, Å., Chervoneva, I., Birk, D.E., 2000. Differential Expression of Lumican and Fibromodulin Regulate Collagen Fibrillogenesis in Developing Mouse Tendons. J. Cell Biol. 151, 779–788.

Fan, R., Yan, X., Zhang, W., 2022. Relationship between asporin and extracellular matrix behavior: A literature review. Medicine (Baltimore) 101, e32490. https://doi.org/10.1097/MD.0000000000032490

Fang, F., Sup, M., Luzzi, A., Ferrer, X., Thomopoulos, S., 2022a. Hedgehog signaling underlying tendon and enthesis development and pathology. Matrix Biol. J. Int. Soc. Matrix Biol. 105, 87–103. https://doi.org/10.1016/j.matbio.2021.12.001

Fang, F., Xiao, Y., Zelzer, E., Leong, K.W., Thomopoulos, S., 2022b. A mineralizing pool of Gli1-expressing progenitors builds the tendon enthesis and demonstrates therapeutic potential. Cell Stem Cell 29, 1669-1684.e6. https://doi.org/10.1016/j.stem.2022.11.007

Fässler, R., Schnegelsberg, P.N., Dausman, J., Shinya, T., Muragaki, Y., McCarthy, M.T., Olsen, B.R., Jaenisch, R., 1994. Mice lacking alpha 1 (IX) collagen develop noninflammatory degenerative joint disease. Proc. Natl. Acad. Sci. 91, 5070–5074. https://doi.org/10.1073/pnas.91.11.5070

Favata, M., Beredjiklian, P.K., Zgonis, M.H., Beason, D.P., Crombleholme, T.M., Jawad, A.F., Soslowsky, L.J., 2006. Regenerative properties of fetal sheep tendon are not adversely affected by transplantation into an adult environment. J. Orthop. Res. 24, 2124–2132. https://doi.org/10.1002/jor.20271

Fearon, A., Dahlstrom, J.E., Twin, J., Cook, J., Scott, A., 2014. The Bonar score revisited: Region of evaluation significantly influences the standardized assessment of tendon degeneration. J. Sci. Med. Sport 17, 346–350. https://doi.org/10.1016/j.jsams.2013.07.008

Felsenthal, N., Rubin, S., Stern, T., Krief, S., Pal, D., Pryce, B.A., Schweitzer, R., Zelzer, E., 2018. Development of migrating tendon-bone attachments involves replacement of progenitor populations. Dev. Camb. 145. https://doi.org/10.1242/dev.165381

Felsenthal, N., Zelzer, E., 2017. Mechanical regulation of musculoskeletal system development. Dev. Camb. Engl. 144, 4271–4283. https://doi.org/10.1242/dev.151266

Fenwick, S.A., Hazleman, B.L., Riley, G.P., 2002. The vasculature and its role in the damaged and healing tendon. Arthritis Res. 4, 252–260.

Fessel, G., Li, Y., Diederich, V., Guizar-Sicairos, M., Schneider, P., Sell, D.R., Monnier, V.M., Snedeker, J.G., 2014. Advanced Glycation End-Products Reduce Collagen Molecular Sliding to Affect Collagen Fibril Damage Mechanisms but Not Stiffness. PLOS ONE 9, e110948. https://doi.org/10.1371/journal.pone.0110948

Fleming, S.J., Chaffin, M.D., Arduini, A., Akkad, A.-D., Banks, E., Marioni, J.C., Philippakis, A.A., Ellinor, P.T., Babadi, M., 2023. Unsupervised removal of systematic background noise from droplet-based single-cell

experiments using CellBender. Nat. Methods 20, 1323–1335. https://doi.org/10.1038/s41592-023-01943-7

Folestad, E., Kunath, A., Wågsäter, D., 2018. PDGF-C and PDGF-D signaling in vascular diseases and animal models. Mol. Aspects Med., Special issue PDGF 62, 1–11. https://doi.org/10.1016/j.mam.2018.01.005

Franchi, M., Torricelli, P., Giavaresi, G., Fini, M., 2013. Role of moderate exercising on Achilles tendon collagen crimping patterns and proteoglycans. Connect. Tissue Res. 54, 267–274. https://doi.org/10.3109/03008207.2013.807808

Franchi, M., Trirè, A., Quaranta, M., Orsini, E., Ottani, V., 2007. Collagen Structure of Tendon Relates to Function. Sci. World J. 7, 404–420. https://doi.org/10.1100/tsw.2007.92

Frizziero, A., Vittadini, F., Bigliardi, D., Costantino, C., 2022. Low Molecular Weight Hyaluronic Acid (500–730 Kda) Injections in Tendinopathies—A Narrative Review. J. Funct. Morphol. Kinesiol. 7, 3. https://doi.org/10.3390/jfmk7010003

Frizziero, A., Vittadini, F., Bigliardi, D., Costantino, C., 2020. The Role of Hyaluronic Acid Injection for the Treatment of Tendinopathy. Muscle Ligaments Tendons J. 10, 548. https://doi.org/10.32098/mltj.04.2020.01

Frolova, E.G., Drazba, J., Krukovets, I., Kostenko, V., Blech, L., Harry, C., Vasanji, A., Drumm, C., Sul, P., Jenniskens, G.J., Plow, E.F., Stenina-Adognravi, O., 2014. Control of Organization and Function of Muscle and Tendon by Thrombospondin-4. Matrix Biol. J. Int. Soc. Matrix Biol. 37, 35–48. https://doi.org/10.1016/j.matbio.2014.02.003

Fu, W., Yang, R., Li, J., 2023. Single-cell and spatial transcriptomics reveal changes in cell heterogeneity during progression of human tendinopathy. BMC Biol. 21, 132. https://doi.org/10.1186/s12915-023-01613-2

Fukuta, S., Oyama, M., Kavalkovich, K., Fu, F.H., Niyibizi, C., 1998. Identification of types II, IX and X collagens at the insertion site of the bovine achilles tendon. Matrix Biol. 17, 65–73. https://doi.org/10.1016/S0945-053X(98)90125-1

Funakoshi, T., Schmid, T., Hsu, H.-P., Spector, M., 2008. Lubricin Distribution in the Goat Infraspinatus Tendon: A Basis for Interfascicular Lubrication. JBJS 90, 803. https://doi.org/10.2106/JBJS.G.00627

Funderburgh, J.L., Caterson, B., Conrad, G.W., 1987. Distribution of proteoglycans antigenically related to corneal keratan sulfate proteoglycan. J. Biol. Chem. 262, 11634–11640. https://doi.org/10.1016/S0021-9258(18)60856-7

Fung, A., Sun, M., Soslowsky, L.J., Birk, D.E., 2022. Targeted conditional collagen XII deletion alters tendon function. Matrix Biol. Plus 16, 100123. https://doi.org/10.1016/j.mbplus.2022.100123

Furumatsu, T., Ozaki, T., Asahara, H., 2009. Smad3 activates the Sox9-dependent transcription on chromatin. Int. J. Biochem. Cell Biol. 41, 1198–1204. https://doi.org/10.1016/j.biocel.2008.10.032

Gaida, J.E., Alfredson, H., Kiss, Z.S., Bass, S.L., Cook, J.L., 2010. Asymptomatic Achilles tendon pathology is associated with a central fat distribution in men and a peripheral fat distribution in women: a cross sectional study of 298 individuals. BMC Musculoskelet. Disord. 11, 41. https://doi.org/10.1186/1471-2474-11-41

Galatz, L.M., Ball, C.M., Teefey, S.A., Middleton, W.D., Yamaguchi, K., 2004. The outcome and repair integrity of completely arthroscopically repaired large and massive rotator cuff tears. J. Bone Joint Surg. Am. 86, 219–224. https://doi.org/10.2106/00004623-200402000-00002

Gao, C.-H., Chen, C., Akyol, T., Dusa, A., Yu, G., Cao, B., Cai, P., 2024. ggVennDiagram: Intuitive Venn diagram software extended. iMeta 3, e177. https://doi.org/10.1002/imt2.177

Garcia-Melchor, E., Cafaro, G., MacDonald, L., Crowe, L.A.N., Sood, S., McLean, M., Fazzi, U.G., McInnes, I.B., Akbar, M., Millar, N.L., 2021. Novel self-amplificatory loop between T cells and tenocytes as a driver of chronicity in tendon disease. Ann. Rheum. Dis. 80, 1075–1085. https://doi.org/10.1136/annrheumdis-2020-219335

Garner, W.L., McDonald, J.A., Koo, M., Kuhn, C., Weeks, P.M., 1989. Identification of the collagen-producing cells in healing flexor tendons. Plast. Reconstr. Surg. 83, 875–879. https://doi.org/10.1097/00006534-198905000-00018

Gayoso, A., Lopez, R., Xing, G., Boyeau, P., Valiollah Pour Amiri, V., Hong, J., Wu, K., Jayasuriya, M., Mehlman, E., Langevin, M., Liu, Y., Samaran, J., Misrachi, G., Nazaret, A., Clivio, O., Xu, C., Ashuach, T., Gabitto, M., Lotfollahi, M., Svensson, V., da Veiga Beltrame, E., Kleshchevnikov, V., Talavera-López, C., Pachter, L., Theis, F.J., Streets, A., Jordan, M.I., Regier, J., Yosef, N., 2022. A Python library for probabilistic analysis of single-cell omics data. Nat. Biotechnol. 40, 163–166. https://doi.org/10.1038/s41587-021-01206-w

Geetha-Loganathan, P., Nimmagadda, S., Scaal, M., 2008. Wnt signaling in limb organogenesis. Organogenesis 4, 109–115.

Godinho, M.S.C., Thorpe, C.T., Greenwald, S.E., Screen, H.R.C., 2017. Elastin is Localised to the Interfascicular Matrix of Energy Storing Tendons and Becomes Increasingly Disorganised With Ageing. Sci. Rep. 7, 9713. https://doi.org/10.1038/s41598-017-09995-4

Goodman, S.A., May, S.A., Heinegård, D., Smith, R.K.W., 2004. Tenocyte response to cyclical strain and transforming growth factor beta is dependent upon age and site of origin. Biorheology 41, 613–628.

Griffith, J.F., Hu, M., Yeung, D.K.W., Guo, P., Lam, S.L., Xiao, F., Wang, D., Tomlinson, B., 2017. Achilles Tendon Xanthomas: Fat-Water Separation at Baseline and after Treatment. Radiology 285, 876–884. https://doi.org/10.1148/radiol.2017161435

Grimaldi, A., Comai, G., Mella, S., Tajbakhsh, S., 2022. Identification of bipotent progenitors that give rise to myogenic and connective tissues in mouse. eLife 11, e70235. https://doi.org/10.7554/eLife.70235

Grinstein, M., Dingwall, H.L., O'Connor, L.D., Zou, K., Capellini, T.D., Galloway, J.L., 2019. A distinct transition from cell growth to physiological homeostasis in the tendon. eLife 8. https://doi.org/10.7554/eLife.48689

Grinstein, M., Dingwall, H.L., Shah, R.R., Capellini, T.D., Galloway, J.L., 2018. A robust method for RNA extraction and purification from a single adult mouse tendon. PeerJ 6, e4664. https://doi.org/10.7717/peerj.4664

Grinstein, M., Tsai, S.L., Montoro, D., Dingwall, H.L., Zou, K., Sade-Feldman, M., Tanaka, M.J., Capellini, T.D., Rajagopal, J., Galloway, J.L., 2022. A quiescent resident progenitor pool is the central organizer of tendon healing. bioRxiv 2022.02.02.478533. https://doi.org/10.1101/2022.02.02.478533

Gros, J., Tabin, C.J., 2014. Vertebrate Limb bud formation is initiated by localized Epithelial to Mesenchymal Transition. Science 343, 1253. https://doi.org/10.1126/science.1248228

Guerquin, M.J., Charvet, B., Nourissat, G., Havis, E., Ronsin, O., Bonnin, M.A., Ruggiu, M., Olivera-Martinez, I., Robert, N., Lu, Y., Kadler, K.E., Baumberger, T., Doursounian, L., Berenbaum, F., Duprez, D., 2013. Transcription factor EGR1 directs tendon differentiation and promotes tendon repair. J. Clin. Invest. 123, 3564–3576. https://doi.org/10.1172/JCI67521

Hannafin, J.A., Arnoczky, S.P., 1994. Effect of cyclic and static tensile loading on water content and solute diffusion in canine flexor tendons: An in Vitro study. J. Orthop. Res. 12, 350–356. https://doi.org/10.1002/jor.1100120307

Harvey, T., Flamenco, S., Fan, C.M., 2019. A Tppp3+Pdgfra+ tendon stem cell population contributes to regeneration and reveals a shared role for PDGF signalling in regeneration and fibrosis. Nat. Cell Biol. 21, 1490. https://doi.org/10.1038/S41556-019-0417-Z

Havis, E., Bonnin, M.A., Olivera-Martinez, I., Nazaret, N., Ruggiu, M., Weibel, J., Durand, C., Guerquin, M.J., Bonod-Bidaud, C., Ruggiero, F., Schweitzer, R., Duprez, D., 2014. Transcriptomic analysis of mouse limb tendon cells during development. Dev. Camb. 141, 3683–3696. https://doi.org/10.1242/dev.108654

Hayashi, M., Zhao, C., Thoreson, A.R., Chikenji, T., Jay, G.D., An, K.-N., Amadio, P.C., 2013. The Effect of Lubricin on the Gliding Resistance of Mouse Intrasynovial Tendon. PLOS ONE 8, e83836. https://doi.org/10.1371/journal.pone.0083836

Hayashida, Y., Akama, T.O., Beecher, N., Lewis, P., Young, R.D., Meek, K.M., Kerr, B., Hughes, C.E., Caterson, B., Tanigami, A., Nakayama, J., Fukada, M.N., Tano, Y., Nishida, K., Quantock, A.J., 2006. Matrix morphogenesis in cornea is mediated by the modification of keratan sulfate by GlcNAc 6-O-sulfotransferase. Proc. Natl. Acad. Sci. U. S. A. 103, 13333–13338. https://doi.org/10.1073/pnas.0605441103

He, P., Ruan, D., Huang, Z., Wang, C., Xu, Y., Cai, H., Liu, H., Fei, Y., Heng, B.C., Chen, W., Shen, W., 2022. Comparison of Tendon Development Versus Tendon Healing and Regeneration. Front. Cell Dev. Biol. 10.

Heinemeier, K.M., Schjerling, P., Heinemeier, J., Magnusson, S.P., Kjaer, M., 2013. Lack of tissue renewal in human adult Achilles tendon is revealed by nuclear bomb 14C. FASEB J. 27, 2074–2079. https://doi.org/10.1096/fj.12-225599

Heinemeier, K.M., Schjerling, P., Øhlenschlæger, T.F., Eismark, C., Olsen, J., Kjær, M., 2018. Carbon-14 bomb pulse dating shows that tendinopathy is preceded by years of abnormally high collagen turnover. FASEB J. 32, 4763–4775. https://doi.org/10.1096/FJ.201701569R

Henry, S.P., Takanosu, M., Boyd, T.C., Mayne, P.M., Eberspaecher, H., Zhou, W., de Crombrugghe, B., Höök, M., Mayne, R., 2001. Expression Pattern and Gene Characterization of*Asporin*. J. Biol. Chem. 276, 12212–12221. https://doi.org/10.1074/jbc.M011290200

Herchenhan, A., Kalson, N.S., Holmes, D.F., Hill, P., Kadler, K.E., Margetts, L., 2012. Tenocyte contraction induces crimp formation in tendon-like tissue. Biomech. Model. Mechanobiol. 11, 449–459. https://doi.org/10.1007/s10237-011-0324-0

Herod, T.W., Chambers, N.C., Veres, S.P., 2016. Collagen fibrils in functionally distinct tendons have differing structural responses to tendon rupture and fatigue loading. Acta Biomater. 42, 296–307. https://doi.org/10.1016/j.actbio.2016.06.017

Heumos, L., Schaar, A.C., Lance, C., Litinetskaya, A., Drost, F., Zappia, L., Lücken, M.D., Strobl, D.C., Henao, J., Curion, F., Schiller, H.B., Theis, F.J., 2023. Best practices for single-cell analysis across modalities. Nat. Rev. Genet. 1–23. https://doi.org/10.1038/s41576-023-00586-w

Higuchi, T., Suzuki, D., Watanabe, T., Fanhchaksai, K., Ota, K., Yokoo, K., Furukawa, H., Watanabe, H., 2021. Versican contributes to ligament formation of knee joints. PLOS ONE 16, e0250366. https://doi.org/10.1371/journal.pone.0250366

Hilario, J.D., Rodino-Klapac, L.R., Wang, C., Beattie, C.E., 2009. Semaphorin 5A is a bifunctional axon guidance cue for axial motoneurons *in vivo*. Dev. Biol. 326, 190–200. https://doi.org/10.1016/j.ydbio.2008.11.007

Hildebrand, A., Romarís, M., Rasmussen, L.M., Heinegård, D., Twardzik, D.R., Border, W.A., Ruoslahti, E., 1994. Interaction of the small interstitial proteoglycans biglycan, decorin and fibromodulin with transforming growth factor beta. Biochem. J. 302 (Pt 2), 527–534. https://doi.org/10.1042/bj3020527

Himes, B.E., Jiang, X., Wagner, P., Hu, R., Wang, Q., Klanderman, B., Whitaker, R.M., Duan, Q., Lasky-Su, J., Nikolos, C., Jester, W., Johnson, M., Panettieri, R.A., Tantisira, K.G., Weiss, S.T., Lu, Q., 2014. RNA-Seq Transcriptome Profiling Identifies CRISPLD2 as a Glucocorticoid Responsive Gene that Modulates Cytokine Function in Airway Smooth Muscle Cells. PLoS ONE 9, e99625. https://doi.org/10.1371/journal.pone.0099625

Hinz, B., Gabbiani, G., Chaponnier, C., 2002. The NH2-terminal peptide of α–smooth muscle actin inhibits force generation by the myofibroblast in vitro and in vivo. J. Cell Biol. 157, 657–663. https://doi.org/10.1083/jcb.200201049

Ho, K.-Y., Kulig, K., 2016. Changes in water content in response to an acute bout of eccentric loading in a patellar tendon with a history of tendinopathy: A case report. Physiother. Theory Pract. 32, 566–570. https://doi.org/10.1080/09593985.2016.1206646

Honda, H., Gotoh, M., Kanazawa, T., Ohzono, H., Nakamura, H., Ohta, K., Nakamura, K., Fukuda, K., Teramura, T., Hashimoto, T., Shichijo, S., Shiba, N., 2017. Hyaluronic Acid Accelerates Tendon-to-Bone Healing After Rotator Cuff Repair. Am. J. Sports Med. 45, 3322–3330. https://doi.org/10.1177/0363546517720199

Hope, M., Saxby, T.S., 2007. Tendon Healing. Foot Ankle Clin. 12, 553–567. https://doi.org/10.1016/j.fcl.2007.07.003

Hopkins, C., Fu, S.-C., Chua, E., Hu, X., Rolf, C., Mattila, V.M., Qin, L., Yung, P.S.-H., Chan, K.-M., 2016. Critical review on the socio-economic impact of tendinopathy. Asia-Pac. J. Sports Med. Arthrosc. Rehabil. Technol. 4, 9–20. https://doi.org/10.1016/j.asmart.2016.01.002

Hou, J., Yang, R., Vuong, I., Li, F., Kong, J., Mao, H.-Q., 2021. Biomaterials strategies to balance inflammation and tenogenesis for tendon repair. Acta Biomater. 130, 1–16. https://doi.org/10.1016/j.actbio.2021.05.043

Howell, K., Chien, C., Laudier, D., Huang, A., Bell, R., Andarawis-Puri, N., Tufa, S., Keene, D., 2017. Novel Model of Tendon Regeneration Reveals Distinct Cell Mechanisms Underlying Regenerative and Fibrotic Tendon Healing. Sci. Rep. 7. https://doi.org/10.1038/srep45238

Howell, K.L., Kaji, D.A., Li, T.M., Montero, A., Yeoh, K., Nasser, P., Huang, A.H., 2021. Macrophage depletion impairs neonatal tendon regeneration. FASEB J. Off. Publ. Fed. Am. Soc. Exp. Biol. 35, e21618. https://doi.org/10.1096/fj.202100049R

Huang, A.H., 2017. Coordinated development of the limb musculoskeletal system: Tendon and muscle patterning and integration with the skeleton. Dev. Biol. 429, 420–428. https://doi.org/10.1016/j.ydbio.2017.03.028

Huang, A.H., Lu, H.H., Schweitzer, R., 2015a. Molecular regulation of tendon cell fate during development. J. Orthop. Res. 33, 800–812. https://doi.org/10.1002/jor.22834

Huang, A.H., Riordan, T.J., Pryce, B., Weibel, J.L., Watson, S.S., Long, F., Lefebvre, V., Harfe, B.D., Stadler, H.S., Akiyama, H., Tufa, S.F., Keene, D.R., Schweitzer, R., 2015b. Musculoskeletal integration at the wrist underlies the modular development of limb tendons. Dev. Camb. 142, 2431–2441. https://doi.org/10.1242/dev.122374

Huang, A.H., Watson, S.S., Wang, L., Baker, B.M., Akiyama, H., Brigande, J.V., Schweitzer, R., 2019. Requirement for scleraxis in the recruitment of mesenchymal progenitors during embryonic tendon elongation. Dev. Camb. Engl. 146, dev182782. https://doi.org/10.1242/dev.182782

Huang, Y., He, B., Wang, L., Yuan, B., Shu, H., Zhang, F., Sun, L., 2020. Bone marrow mesenchymal stem cell-derived exosomes promote rotator cuff tendon-bone healing by promoting angiogenesis and regulating M1 macrophages in rats. Stem Cell Res. Ther. 11, 496. https://doi.org/10.1186/s13287-020-02005-x

Huang, Z., Yin, Z., Xu, J., Fei, Y., Heng, B.C., Jiang, X., Chen, W., Shen, W., 2021. Tendon Stem/Progenitor Cell Subpopulations and Their Implications in Tendon Biology. Front. Cell Dev. Biol. 9, 631272. https://doi.org/10.3389/fcell.2021.631272

Hudson, D.M., Archer, M., Rai, J., Weis, M., Fernandes, R.J., Eyre, D.R., 2021. Age-related type I collagen modifications reveal tissue-defining differences between ligament and tendon. Matrix Biol. Plus 12, 100070. https://doi.org/10.1016/j.mbplus.2021.100070

Hudson, D.M., Weis, M., Rai, J., Joeng, K.S., Dimori, M., Lee, B.H., Morello, R., Eyre, D.R., 2017. P3h3-null and Sc65-null Mice Phenocopy the Collagen Lysine Under-hydroxylation and Cross-linking Abnormality of Ehlers-Danlos Syndrome Type VIA. J. Biol. Chem. 292, 3877–3887. https://doi.org/10.1074/jbc.M116.762245

Huijing, P.A., Voermans, N.C., Baan, G.C., Busé, T.E., van Engelen, B.G.M., de Haan, A., 2010. Muscle characteristics and altered myofascial force transmission in tenascin-X-deficient mice, a mouse model of Ehlers-

Danlos syndrome. J. Appl. Physiol. 109, 986–995. https://doi.org/10.1152/japplphysiol.00723.2009

Humphries, S.M., Lu, Y., Canty, E.G., Kadler, K.E., 2008. Active Negative Control of Collagen Fibrillogenesis in Vivo: INTRACELLULAR CLEAVAGE OF THE TYPE I PROCOLLAGEN PROPEPTIDES IN TENDON FIBROBLASTS WITHOUT INTRACELLULAR FIBRILS *. J. Biol. Chem. 283, 12129–12135. https://doi.org/10.1074/jbc.M708198200

Hurle, J.M., Ros, M.A., Gafian, Y., Macias, D., Critchlow, M., Hinchliffe, J.R., 1990. Experimental analysis of the role of ECM in the patterning of the distal tendons of the developing limb bud, Cell Differentiation and Development.

Iozzo, R.V., Schaefer, L., 2015. Proteoglycan form and function: A comprehensive nomenclature of proteoglycans. Matrix Biol. 42, 11–55. https://doi.org/10.1016/j.matbio.2015.02.003

Ippolito, E., Natali, P.G., Postacchini, F., Accinni, L., De Martino, C., 1980. Morphological, immunochemical, and biochemical study of rabbit Achilles tendon at various ages. J. Bone Jt. Surg. - Ser. A 62, 583–598. https://doi.org/10.2106/00004623-198062040-00014

Ito, Y., Toriuchi, N., Yoshitaka, T., Ueno-Kudoh, H., Sato, T., Yokoyama, S., Nishida, K., Akimoto, T., Takahashi, M., Miyaki, S., Asahara, H., 2010. The Mohawk homeobox gene is a critical regulator of tendon differentiation. Proc. Natl. Acad. Sci. U. S. A. 107, 10538–10542. https://doi.org/10.1073/pnas.1000525107

Izu, Y., Adams, S.M., Connizzo, B.K., Beason, D.P., Soslowsky, L.J., Koch, M., Birk, D.E., 2021. Collagen XII mediated cellular and extracellular mechanisms regulate establishment of tendon structure and function. Matrix Biol. J. Int. Soc. Matrix Biol. 95, 52. https://doi.org/10.1016/J.MATBIO.2020.10.004

Izu, Y., Ansorge, H.L., Zhang, G., Soslowsky, L.J., Bonaldo, P., Chu, M.-L., Birk, D.E., 2011. Dysfunctional Tendon Collagen Fibrillogenesis in Collagen VI Null Mice. Matrix Biol. J. Int. Soc. Matrix Biol. 30, 53–61. https://doi.org/10.1016/j.matbio.2010.10.001

Jakobsen, J.R., Krogsgaard, M.R., 2021. The Myotendinous Junction—A Vulnerable Companion in Sports. A Narrative Review. Front. Physiol. 12, 635561. https://doi.org/10.3389/fphys.2021.635561

Jakobsen, J.R., Mackey, A.L., Knudsen, A.B., Koch, M., Kjaer, M., Krogsgaard, M.R., 2017. Composition and adaptation of human myotendinous junction and neighboring muscle fibers to heavy resistance training. Scand. J. Med. Sci. Sports 27, 1547–1559. https://doi.org/10.1111/sms.12794

Jakobsen, J.R., Schjerling, P., Svensson, R.B., Buhl, R., Carstensen, H., Koch, M., Krogsgaard, M.R., Kjær, M., Mackey, A.L., 2021. RNA sequencing and immunofluorescence of the myotendinous junction of mature horses and humans. Am. J. Physiol.-Cell Physiol. 321, C453–C470. https://doi.org/10.1152/ajpcell.00218.2021

James, S.L., Abate, D., Abate, K.H., Abay, S.M., Abbafati, C., Abbasi, N., Abbastabar, H., Abd-Allah, F., Abdela, J., Abdelalim, A., Abdollahpour, I., Abdulkader, R.S., Abebe, Z., Abera, S.F., Abil, O.Z., Abraha, H.N., Abu-Raddad, L.J., Abu-Rmeileh, N.M.E., Accrombessi, M.M.K., Acharya, D., Acharya, P., Ackerman, I.N., Adamu, A.A., Adebayo, O.M., Adekanmbi, V., Adetokunboh, O.O., Adib, M.G., Adsuar, J.C., Afanvi, K.A., Afarideh, M., Afshin, A., Agarwal, G., Agesa, K.M., Aggarwal, R., Aghayan, S.A., Agrawal, S., Ahmadi, A., Ahmadi, M., Ahmadieh, H., Ahmed, M.B., Aichour, A.N., Aichour, I., Aichour, M.T.E., Akinyemiju, T., Akseer, N., Al-Aly, Z., Al-Eyadhy, A., Al-Mekhlafi, H.M., Al-Raddadi, R.M., Alahdab, F., Alam, K., Alam, T., Alashi, A., Alavian, S.M., Alene, K.A., Alijanzadeh, M., Alizadeh-Navaei, R., Aljunid, S.M., Alkerwi, A., Alla, F., Allebeck, P., Alouani, M.M.L., Altirkawi, K., Alvis-Guzman, N., Amare, A.T., Aminde, L.N., Ammar, W., Amoako, Y.A., Anber, N.H., Andrei, C.L., Androudi, S., Animut, M.D., Anjomshoa, M., Ansha, M.G., Antonio, C.A.T., Anwari, P., Arabloo, J., Arauz, A., Aremu, O., Ariani, F., Armoon, B., Ärnlöv, J., Arora, A., Artaman, A., Aryal, K.K., Asayesh, H., Asghar, R.J., Ataro, Z., Atre, S.R., Ausloos, M., Avila-Burgos, L., Avokpaho, E.F.G.A., Awasthi, A., Ayala Quintanilla, B.P., Ayer, R., Azzopardi, P.S., Babazadeh, A., Badali, H., Badawi, A., Bali, A.G., Ballesteros, K.E., Ballew, S.H., Banach, M., Banoub, J.A.M., Banstola, A., Barac, A., Barboza, M.A., Barker-Collo, S.L., Bärnighausen, T.W., Barrero, L.H., Baune, B.T., Bazargan-Hejazi, S., Bedi, N., Beghi, E., Behzadifar, Masoud, Behzadifar, Meysam, Béjot, Y., Belachew, A.B., Belay, Y.A., Bell, M.L., Bello, A.K., Bensenor, I.M., Bernabe, E., Bernstein, R.S., Beuran, M., Beyranvand, T., Bhala, N., Bhattarai, S., Bhaumik, S., Bhutta, Z.A., Biadgo, B., Bijani, A., Bikbov, B., Bilano, V., Bililign, N., Bin Sayeed, M.S., Bisanzio, D., Blacker, B.F., Blyth, F.M., Bou-Orm, I.R., Boufous, S., Bourne, R., Brady, O.J., Brainin, M., Brant, L.C., Brazinova, A., Breitborde, N.J.K., Brenner, H., Briant, P.S., Briggs, A.M., Briko, A.N., Britton, G., Brugha, T., Buchbinder, R., Busse, R., Butt, Z.A., Cahuana-Hurtado, L., Cano, J., Cárdenas, R., Carrero, J.J., Carter, A., Carvalho, F., Castañeda-Orjuela, C.A., Castillo Rivas, J., Castro, F., Catalá-López, F., Cercy, K.M., Cerin, E., Chaiah, Y., Chang, A.R., Chang, H.Y., Chang, J.C., Charlson, F.J., Chattopadhyay, A., Chattu, V.K., Chaturvedi, P., Chiang, P.P.C., Chin, K.L., Chitheer, A., Choi, J.Y.J., Chowdhury, R., Christensen, H., Christopher, D.J., Cicuttini, F.M., Ciobanu, L.G., Cirillo, M., Claro, R.M., Collado-Mateo, D., Cooper, C., Coresh, J., Cortesi, P.A., Cortinovis, M., Costa, M., Cousin, E., Criqui, M.H., Cromwell, E.A.,

Cross, M., Crump, J.A., Dadi, A.F., Dandona, L., Dandona, R., Dargan, P.I., Daryani, A., Das Gupta, R., Das Neves, J., Dasa, T.T., Davey, G., Davis, A.C., Davitoiu, D.V., De Courten, B., De La Hoz, F.P., De Leo, D., De Neve, J.W., Degefa, M.G., Degenhardt, L., Deiparine, S., Dellavalle, R.P., Demoz, G.T., Deribe, K., Dervenis, N., Des Jarlais, D.C., Dessie, G.A., Dey, S., Dharmaratne, S.D., Dinberu, M.T., Dirac, M.A., Djalalinia, S., Doan, L., Dokova, K., Doku, D.T., Dorsey, E.R., Doyle, K.E., Driscoll, T.R., Dubey, M., Dubljanin, E., Duken, E.E., Duncan, B.B., Duraes, A.R., Ebrahimi, H., Ebrahimpour, S., Echko, M.M., Edvardsson, D., Effiong, A., Ehrlich, J.R., El Bcheraoui, C., El Sayed Zaki, M., El-Khatib, Z., Elkout, H., Elyazar, I.R.F., Enayati, A., Endries, A.Y., Er, B., Erskine, H.E., Eshrati, B., Eskandarieh, S., Esteghamati, A., Esteghamati, S., Fakhim, H., Fallah Omrani, V., Faramarzi, M., Fareed, M., Farhadi, F., Farid, T.A., Farinha, C.S.E., Farioli, A., Faro, A., Farvid, M.S., Farzadfar, F., Feigin, V.L., Fentahun, N., Fereshtehnejad, S.M., Fernandes, E., Fernandes, J.C., Ferrari, A.J., Feyissa, G.T., Filip, I., Fischer, F., Fitzmaurice, C., Foigt, N.A., Foreman, K.J., Fox, J., Frank, T.D., Fukumoto, T., Fullman, N., Fürst, T., Furtado, J.M., Futran, N.D., Gall, S., Ganji, M., Gankpe, F.G., Garcia-Basteiro, A.L., Gardner, W.M., Gebre, A.K., Gebremedhin, A.T., Gebremichael, T.G., Gelano, T.F., Geleijnse, J.M., Genova-Maleras, R., Geramo, Y.C.D., Gething, P.W., Gezae, K.E., Ghadiri, K., Ghasemi Falavarjani, K., Ghasemi-Kasman, M., Ghimire, M., Ghosh, R., Ghoshal, A.G., Giampaoli, S., Gill, P.S., Gill, T.K., Ginawi, I.A., Giussani, G., Gnedovskaya, E.V., Goldberg, E.M., Goli, S., Gómez-Dantés, H., Gona, P.N., Gopalani, S.V., Gorman, T.M., Goulart, A.C., Goulart, B.N.G., Grada, A., Grams, M.E., Grosso, G., Gugnani, H.C., Guo, Y., Gupta, P.C., Gupta, Rahul, Gupta, Rajeev, Gupta, T., Gyawali, B., Haagsma, J.A., Hachinski, V., Hafezi-Nejad, N., Haghparast Bidgoli, H., Hagos, T.B., Hailu, G.B., Haj-Mirzaian, Arvin, Haj-Mirzaian, Arya, Hamadeh, R.R., Hamidi, S., Handal, A.J., Hankey, G.J., Hao, Y., Harb, H.L., Harikrishnan, S., Haro, J.M., Hasan, M., Hassankhani, H., Hassen, H.Y., Havmoeller, R., Hawley, C.N., Hay, R.J., Hay, S.I., Hedayatizadeh-Omran, A., Heibati, B., Hendrie, D., Henok, A., Herteliu, C., Heydarpour, S., Hibstu, D.T., Hoang, H.T., Hoek, H.W., Hoffman, H.J., Hole, M.K., Homaie Rad, E., Hoogar, P., Hosgood, H.D., Hosseini, S.M., Hosseinzadeh, M., Hostiuc, M., Hostiuc, S., Hotez, P.J., Hoy, D.G., Hsairi, M., Htet, A.S., Hu, G., Huang, J.J., Huynh, C.K., Iburg, K.M., Ikeda, C.T., Ileanu, B., Ilesanmi, O.S., Iqbal, U., Irvani, S.S.N., Irvine, C.M.S., Mohammed, Sheikh, Islam, S., Islami, F., Jacobsen, K.H., Jahangiry, L., Jahanmehr, N., Jain, S.K., Jakovljevic, M., Javanbakht, M., Jayatilleke, A.U., Jeemon, P., Jha, R.P., Jha, V., Ji, J.S., Johnson, C.O., Jonas, J.B., Jozwiak, J.J., Jungari, S.B., Jürisson, M., Kabir, Z., Kadel, R., Kahsay, A., Kalani, R., Kanchan, T., Karami, M., Karami Matin, B., Karch, A., Karema, C., Karimi, N., Karimi, S.M., Kasaeian, A., Kassa, D.H., Kassa, G.M., Kassa, T.D., Kassebaum, N.J., Katikireddi, S.V.,

Kawakami, N., Kazemi Karyani, A., Keighobadi, M.M., Keiyoro, P.N., Kemmer, L., Kemp, G.R., Kengne, A.P., Keren, A., Khader, Y.S., Khafaei, B., Khafaie, M.A., Khajavi, A., Khalil, I.A., Khan, E.A., Khan, M.S., Khan, M.A., Khang, Y.H., Khazaei, M., Khoja, A.T., Khosravi, A., Khosravi, M.H., Kiadaliri, A.A., Kiirithio, D.N., Kim, C.I., Kim, D., Kim, P., Kim, Y.E., Kim, Y.J., Kimokoti, R.W., Kinfu, Y., Kisa, A., Kissimova-Skarbek, K., Kivimäki, M., Knudsen, A.K.S., Kocarnik, J.M., Kochhar, S., Kokubo, Y., Kolola, T., Kopec, J.A., Kosen, S., Kotsakis, G.A., Koul, P.A., Koyanagi, A., Kravchenko, M.A., Krishan, K., Krohn, K.J., Kuate Defo, B., Kucuk Bicer, B., Kumar, G.A., Kumar, M., Kyu, H.H., Lad, D.P., Lad, S.D., Lafranconi, A., Lalloo, R., Lallukka, T., Lami, F.H., Lansingh, V.C., Latifi, A., Lau, K.M.M., Lazarus, J.V., Leasher, J.L., Ledesma, J.R., Lee, P.H., Leigh, J., Leung, J., Levi, M., Lewycka, S., Li, S., Li, Y., Liao, Y., Liben, M.L., Lim, L.L., Lim, S.S., Liu, S., Lodha, R., Looker, K.J., Lopez, A.D., Lorkowski, S., Lotufo, P.A., Low, N., Lozano, R., Lucas, T.C.D., Lucchesi, L.R., Lunevicius, R., Lyons, R.A., Ma, S., Macarayan, E.R.K., Mackay, M.T., Madotto, F., Magdy Abd El Razek, H., Magdy Abd El Razek, M., Maghavani, D.P., Mahotra, N.B., Mai, H.T., Majdan, M., Majdzadeh, R., Majeed, A., Malekzadeh, R., Malta, D.C., Mamun, A.A., Manda, A.L., Manguerra, H., Manhertz, T., Mansournia, M.A., Mantovani, L.G., Mapoma, C.C., Maravilla, J.C., Marcenes, W., Marks, A., Martins-Melo, F.R., Martopullo, I., März, W., Marzan, M.B., Mashamba-Thompson, T.P., Massenburg, B.B., Mathur, M.R., Matsushita, K., Maulik, P.K., Mazidi, M., McAlinden, C., McGrath, J.J., McKee, M., Mehndiratta, M.M., Mehrotra, R., Mehta, K.M., Mehta, V., Mejia-Rodriguez, F., Mekonen, T., Melese, A., Melku, M., Meltzer, M., Memiah, P.T.N., Memish, Z.A., Mendoza, W., Mengistu, D.T., Mengistu, G., Mensah, G.A., Mereta, S.T., Meretoja, A., Meretoja, T.J., Mestrovic, T., Mezerji, N.M.G., Miazgowski, B., Miazgowski, T., Millear, A.I., Miller, T.R., Miltz, B., Mini, G.K., Mirarefin, M., Mirrakhimov, E.M., Misganaw, A.T., Mitchell, P.B., Mitiku, H., Moazen, B., Mohajer, B., Mohammad, K.A., Mohammadifard, N., Mohammadnia-Afrouzi, M., Mohammed, M.A., Mohammed, Shafiu, Mohebi, F., Moitra, M., Mokdad, A.H., Molokhia, M., Monasta, L., Moodley, Y., Moosazadeh, M., Moradi, G., Moradi-Lakeh, M., Moradinazar, M., Moraga, P., Morawska, L., Moreno Velásquez, I., Morgado-Da-Costa, J., Morrison, S.D., Moschos, M.M., Mousavi, S.M., Mruts, K.B., Muche, A.A., Muchie, K.F., Mueller, U.O., Muhammed, O.S., Mukhopadhyay, S., Muller, K., Mumford, J.E., Murhekar, M., Musa, J., Musa, K.I., Mustafa, G., Nabhan, A.F., Nagata, C., Naghavi, M., Naheed, A., Nahvijou, A., Naik, G., Naik, N., Najafi, F., Naldi, L., Nam, H.S., Nangia, V., Nansseu, J.R., Nascimento, B.R., Natarajan, G., Neamati, N., Negoi, I., Negoi, R.I., Neupane, S., Newton, C.R.J., Ngunjiri, J.W., Nguyen, A.Q., Nguyen, Ha Thu, Nguyen, H.L.T., Nguyen, Huong Thanh, Nguyen, L.H., Nguyen, M., Nguyen, N.B., Nguyen, S.H., Nichols, E., Ningrum, D.N.A., Nixon, M.R., Nolutshungu, N., Nomura, S., Norheim,

O.F., Noroozi, M., Norrving, B., Noubiap, J.J., Nouri, H.R., Nourollahpour Shiadeh, M., Nowroozi, M.R., Nsoesie, E.O., Nyasulu, P.S., Odell, C.M., Ofori-Asenso, R., Ogbo, F.A., Oh, I.H., Oladimeji, O., Olagunju, A.T., Olagunju, T.O., Olivares, P.R., Olsen, H.E., Olusanya, B.O., Ong, K.L., Ong, S.K., Oren, E., Ortiz, A., Ota, E., Otstavnov, S.S., øverland, S., Owolabi, M.O., Mahesh, P.A., Pacella, R., Pakpour, A.H., Pana, A., Panda-Jonas, S., Parisi, A., Park, E.K., Parry, C.D.H., Patel, S., Pati, S., Patil, S.T., Patle, A., Patton, G.C., Paturi, V.R., Paulson, K.R., Pearce, N., Pereira, D.M., Perico, N., Pesudovs, K., Pham, H.Q., Phillips, M.R., Pigott, D.M., Pillay, J.D., Piradov, M.A., Pirsaheb, M., Pishgar, F., Plana-Ripoll, O., Plass, D., Polinder, S., Popova, S., Postma, M.J., Pourshams, A., Poustchi, H., Prabhakaran, D., Prakash, S., Prakash, V., Purcell, C.A., Purwar, M.B., Qorbani, M., Quistberg, D.A., Radfar, A., Rafay, A., Rafiei, A., Rahim, F., Rahimi, K., Rahimi-Movaghar, A., Rahimi-Movaghar, V., Rahman, M., Ur Rahman, M.H., Rahman, M.A., Rahman, S.U., Rai, R.K., Rajati, F., Ram, U., Ranjan, P., Ranta, A., Rao, P.C., Rawaf, D.L., Rawaf, S., Reddy, K.S., Reiner, R.C., Reinig, N., Reitsma, M.B., Remuzzi, G., Renzaho, A.M.N., Resnikoff, S., Rezaei, S., Rezai, M.S., Ribeiro, A.L.P., Robinson, S.R., Roever, L., Ronfani, L., Roshandel, G., Rostami, A., Roth, G.A., Roy, A., Rubagotti, E., Sachdev, P.S., Sadat, N., Saddik, B., Sadeghi, E., Saeedi Moghaddam, S., Safari, H., Safari, Y., Safari-Faramani, R., Safdarian, M., Safi, S., Safiri, S., Sagar, R., Sahebkar, A., Sahraian, M.A., Sajadi, H.S., Salam, N., Salama, J.S., Salamati, P., Saleem, K., Saleem, Z., Salimi, Y., Salomon, J.A., Salvi, S.S., Salz, I., Samy, A.M., Sanabria, J., Sang, Y., Santomauro, D.F., Santos, I.S., Santos, J.V., Santric Milicevic, M.M., Sao Jose, B.P., Sardana, M., Sarker, A.R., Sarrafzadegan, N., Sartorius, B., Sarvi, S., Sathian, B., Satpathy, M., Sawant, A.R., Sawhney, M., Saxena, S., Saylan, M., Schaeffner, E., Schmidt, M.I., Schneider, I.J.C., Schöttker, B., Schwebel, D.C., Schwendicke, F., Scott, J.G., Sekerija, M., Sepanlou, S.G., Serván-Mori, E., Seyedmousavi, S., Shabaninejad, H., Shafieesabet, A., Shahbazi, M., Shaheen, A.A., Shaikh, M.A., Shams-Beyranvand, M., Shamsi, M., Shamsizadeh, M., Sharafi, H., Sharafi, K., Sharif, M., Sharif-Alhoseini, M., Sharma, M., Sharma, R., She, J., Sheikh, A., Shi, P., Shibuya, K., Shigematsu, M., Shiri, R., Shirkoohi, R., Shishani, K., Shiue, I., Shokraneh, F., Shoman, H., Shrime, M.G., Si, S., Siabani, S., Siddiqi, T.J., Sigfusdottir, I.D., Sigurvinsdottir, R., Silva, J.P., Silveira, D.G.A., Singam, N.S.V., Singh, J.A., Singh, N.P., Singh, V., Sinha, D.N., Skiadaresi, E., Slepak, E.L.N., Sliwa, K., Smith, D.L., Smith, M., Soares Filho, A.M., Sobaih, B.H., Sobhani, S., Sobngwi, E., Soneji, S.S., Soofi, M., Soosaraei, M., Sorensen, R.J.D., Soriano, J.B., Soyiri, I.N., Sposato, L.A., Sreeramareddy, C.T., Srinivasan, V., Stanaway, J.D., Stein, D.J., Steiner, C., Steiner, T.J., Stokes, M.A., Stovner, L.J., Subart, M.L., Sudaryanto, A., Sufiyan, M.B., Sunguya, B.F., Sur, P.J., Sutradhar, I., Sykes, B.L., Sylte, D.O., Tabarés-Seisdedos, R., Tadakamadla, S.K.,

Tadesse, B.T., Tandon, N., Tassew, S.G., Tavakkoli, M., Taveira, N., Taylor, H.R., Tehrani-Banihashemi, A., Tekalign, T.G., Tekelemedhin, S.W., Tekle, M.G., Temesgen, H., Temsah, M.H., Temsah, O., Terkawi, A.S., Teweldemedhin, M., Thankappan, K.R., Thomas, N., Tilahun, B., To, Q.G., Tonelli, M., Topor-Madry, R., Topouzis, F., Torre, A.E., Tortajada-Girbés, M., Touvier, M., Tovani-Palone, M.R., Towbin, J.A., Tran, B.X., Tran, K.B., Troeger, C.E., Truelsen, T.C., Tsilimbaris, M.K., Tsoi, D., Tudor Car, L., Tuzcu, E.M., Ukwaja, K.N., Ullah, I., Undurraga, E.A., Unutzer, J., Updike, R.L., Usman, M.S., Uthman, O.A., Vaduganathan, M., Vaezi, A., Valdez, P.R., Varughese, S., Vasankari, T.J., Venketasubramanian, N., Villafaina, S., Violante, F.S., Vladimirov, S.K., Vlassov, V., Vollset, S.E., Vosoughi, K., Vujcic, I.S., Wagnew, F.S., Waheed, Y., Waller, S.G., Wang, Y., Wang, Y.P., Weiderpass, E., Weintraub, R.G., Weiss, D.J., Weldegebreal, F., Weldegwergs, K.G., Werdecker, A., West, T.E., Whiteford, H.A., Widecka, J., Wijeratne, T., Wilner, L.B., Wilson, S., Winkler, A.S., Wiyeh, A.B., Wiysonge, C.S., Wolfe, C.D.A., Woolf, A.D., Wu, S., Wu, Y.C., Wyper, G.M.A., Xavier, D., Xu, G., Yadgir, S., Yadollahpour, A., Yahyazadeh Jabbari, S.H., Yamada, T., Yan, L.L., Yano, Y., Yaseri, M., Yasin, Y.J., Yeshaneh, A., Yimer, E.M., Yip, P., Yisma, E., Yonemoto, N., Yoon, S.J., Yotebieng, M., Younis, M.Z., Yousefifard, M., Yu, C., Zadnik, V., Zaidi, Z., Zaman, S.B., Zamani, M., Zare, Z., Zeleke, A.J., Zenebe, Z.M., Zhang, K., Zhao, Z., Zhou, M., Zodpey, S., Zucker, I., Vos, T., Murray, C.J.L., 2018. Global, regional, and national incidence, prevalence, and years lived with disability for 354 Diseases and Injuries for 195 countries and territories, 1990-2017: A systematic analysis for the Global Burden of Disease Study 2017. The Lancet 392, 1789–1858. https://doi.org/10.1016/S0140-6736(18)32279-7

Järvinen, M., Józsa, L., Kannus, P., Järvinen, T.L.N., Kvist, M., Leadbetter, W., 1997. Histopathological findings in chronic tendon disorders. Scand. J. Med. Sci. Sports 7, 86–95. https://doi.org/10.1111/j.1600-0838.1997.tb00124.x

Järvinen, T.A., 2020. Neovascularisation in tendinopathy: from eradication to stabilisation? Br. J. Sports Med. 54, 1–2. https://doi.org/10.1136/bjsports-2019-100608

Jarvinen, T.A., Jarvinen, T.L., Kannus, P., Jozsa, L., Jarvinen, M., 2004. Collagen fibres of the spontaneously ruptured human tendons display decreased thickness and crimp angle. J. Orthop. Res. 22, 1303–1304. https://doi.org/10.1016/j.orthres.2004.04.003

Jelinsky, S.A., Rodeo, S.A., Li, J., Gulotta, L.V., Archambault, J.M., Seeherman, H.J., 2011. Regulation of gene expression in human tendinopathy. BMC Musculoskelet. Disord. 12, 86. https://doi.org/10.1186/1471-2474-12-86

Jenkins, E., Moss, J.B., Pace, J.M., Bridgewater, L.C., 2005. The new collagen gene COL27A1 contains SOX9-responsive enhancer elements. Matrix Biol. J. Int. Soc. Matrix Biol. 24, 177–184. https://doi.org/10.1016/j.matbio.2005.02.004

Jepsen, K.J., Wu, F., Peragallo, J.H., Paul, J., Roberts, L., Ezura, Y., Oldberg, A., Birk, D.E., Chakravarti, S., 2002. A syndrome of joint laxity and impaired tendon integrity in lumican- and fibromodulin-deficient mice. J. Biol. Chem. 277, 35532–35540. https://doi.org/10.1074/jbc.M205398200

Jiang, D., Liang, J., Noble, P.W., 2007. Hyaluronan in tissue injury and repair. Annu. Rev. Cell Dev. Biol. 23, 435–461. https://doi.org/10.1146/annurev.cellbio.23.090506.123337

Jin, L., Wu, J., Bellusci, S., Zhang, J.-S., 2019. Fibroblast Growth Factor 10 and Vertebrate Limb Development. Front. Genet. 9, 705. https://doi.org/10.3389/fgene.2018.00705

Johnston, J.M., Connizzo, B.K., Shetye, S.S., Robinson, K.A., Huegel, J., Rodriguez, A.B., Sun, M., Adams, S.M., Birk, D.E., Soslowsky, L.J., 2017. Collagen V haploinsufficiency in a murine model of classic Ehlers–Danlos syndrome is associated with deficient structural and mechanical healing in tendons. J. Orthop. Res. 35, 2707–2715. https://doi.org/10.1002/jor.23571

Jomaa, G., Kwan, C.-K., Fu, S.-C., Ling, S.K.-K., Chan, K.-M., Yung, P.S.-H., Rolf, C., 2020. A systematic review of inflammatory cells and markers in human tendinopathy. BMC Musculoskelet. Disord. 21, 78. https://doi.org/10.1186/s12891-020-3094-y

Jozsa, L., Kannus, P., Järvinen, T. a. H., Balint, J., Järvinen, M., 1996. Number and Morphology of Mechanoreceptors in the Myotendinous Junction of Paralysed Human Muscle. J. Pathol. 178, 195–200. https://doi.org/10.1002/(SICI)1096-9896(199602)178:2<195::AID-PATH453>3.0.CO;2-1

Kagan, H.M., Li, W., 2003. Lysyl oxidase: Properties, specificity, and biological roles inside and outside of the cell. J. Cell. Biochem. 88, 660–672. https://doi.org/10.1002/jcb.10413

Kague, E., Bessling, S.L., Lee, J., Hu, G., Passos-Bueno, M.R., Fisher, S., 2010. Functionally conserved cis-regulatory elements of *COL18A1* identified through zebrafish transgenesis. Dev. Biol. 337, 496–505. https://doi.org/10.1016/j.ydbio.2009.10.028

Kaji, D.A., Howell, K.L., Balic, Z., Hubmacher, D., Huang, A.H., 2020. Tgfβ signaling is required for tenocyte recruitment and functional neonatal tendon regeneration. eLife 9, 1–19. https://doi.org/10.7554/elife.51779

Kalamajski, S., Aspberg, A., Lindblom, K., Heinegård, D., Oldberg, Å., 2009. Asporin competes with decorin for collagen binding, binds calcium and

promotes osteoblast collagen mineralization. Biochem. J. 423, 53–59. https://doi.org/10.1042/BJ20090542

Kalamajski, S., Bihan, D., Bonna, A., Rubin, K., Farndale, R.W., 2016. Fibromodulin Interacts with Collagen Cross-linking Sites and Activates Lysyl Oxidase. J. Biol. Chem. 291, 7951–7960. https://doi.org/10.1074/jbc.M115.693408

Kalluri, R., Weinberg, R.A., 2009. The basics of epithelial-mesenchymal transition. J. Clin. Invest. 119, 1420–1428. https://doi.org/10.1172/JCI39104

Kalson, N.S., Lu, Y., Taylor, S.H., Holmes, D.F., Kadler, K.E., 2015. A structure-based extracellular matrix expansion mechanism of fibrous tissue growth. eLife 4, 1–22. https://doi.org/10.7554/eLife.05958

Kannus, P., 2000. Structure of the tendon connective tissue. Scand. J. Med. Sci. Sports 10, 312–320. https://doi.org/10.1034/j.1600-0838.2000.010006312.x

Kannus, P., Józsa, L., 1991. Histopathological changes preceding spontaneous rupture of a tendon. A controlled study of 891 patients. J. Bone Joint Surg. Am. 73, 1507–1525.

Kannus, P., Paavola, M., Józsa, L., 2005. Aging and Degeneration of Tendons, in: Maffulli, N., Renström, P., Leadbetter, W.B. (Eds.), Tendon Injuries: Basic Science and Clinical Medicine. Springer, p. 25. https://doi.org/10.1007/1-84628-050-8_4

Kapacee, Z., Richardson, S.H., Lu, Y., Starborg, T., Holmes, D.F., Baar, K., Kadler, K.E., 2008. Tension is required for fibripositor formation. Matrix Biol. 27, 371–375. https://doi.org/10.1016/j.matbio.2007.11.006

Kardon, G., 1998. Muscle and tendon morphogenesis in the avian hind limb. Development 125.

Karlsen, A., Gonzalez-Franquesa, A., Jakobsen, J.R., Krogsgaard, M.R., Koch, M., Kjaer, M., Schiaffino, S., Mackey, A.L., Deshmukh, A.S., 2022. The proteomic profile of the human myotendinous junction. iScience 25, 103836. https://doi.org/10.1016/j.isci.2022.103836

Kendal, A.R., Layton, T., Al-Mossawi, H., Appleton, L., Dakin, S., Brown, R., Loizou, C., Rogers, M., Sharp, R., Carr, A., 2020. Multi-omic single cell analysis resolves novel stromal cell populations in healthy and diseased human tendon. Sci. Rep. 10, 1–14. https://doi.org/10.1038/s41598-020-70786-5

Khan, K.M., Cook, J.L., Bonar, F., Harcourt, P., Åstrom, M., 1999. Histopathology of Common Tendinopathies. Sports Med. 27, 393–408. https://doi.org/10.2165/00007256-199927060-00004

Khatau, S.B., Kusuma, S., Hanjaya-Putra, D., Mali, P., Cheng, L., Lee, J.S.H., Gerecht, S., Wirtz, D., 2012. The Differential Formation of the LINC-Mediated Perinuclear Actin Cap in Pluripotent and Somatic Cells. PLoS ONE 7, e36689. https://doi.org/10.1371/journal.pone.0036689

Kieny, M., Chevallier, A., 1979. Autonomy of tendon development in the embryonic chick wing. Development 49.

Killian, M.L., 2022. Growth and mechanobiology of the tendon-bone enthesis. Semin. Cell Dev. Biol., Special issue: Musculoskeletal Physiology by Ryan Riddle / Special issue : Chromothripsis by Karen Crasta 123, 64–73. https://doi.org/10.1016/j.semcdb.2021.07.015

Killian, M.L., Cavinatto, L., Galatz, L.M., Thomopoulos, S., 2012. THE ROLE OF MECHANOBIOLOGY IN TENDON HEALING. J. Shoulder Elbow Surg. 21, 228–237. https://doi.org/10.1016/j.jse.2011.11.002

Kim, J.S., Jeon, H., Lee, H., Ko, J.M., Kim, Y., Choi, M., Nishimura, G., Kim, O.-H., Cho, T.-J., 2021. Biallelic novel mutations of the COL27A1 gene in a patient with Steel syndrome. Hum. Genome Var. 8, 17. https://doi.org/10.1038/s41439-021-00149-7

Kim, Y.I., Ryu, J.-S., Yeo, J.E., Choi, Y.J., Kim, Y.S., Ko, K., Koh, Y.-G., 2014. Overexpression of TGF-β1 enhances chondrogenic differentiation and proliferation of human synovium-derived stem cells. Biochem. Biophys. Res. Commun. 450, 1593–1599. https://doi.org/10.1016/j.bbrc.2014.07.045

Kinsella, M.G., Bressler, S.L., Wight, T.N., 2004. The regulated synthesis of versican, decorin, and biglycan: extracellular matrix proteoglycans that influence cellular phenotype. Crit. Rev. Eukaryot. Gene Expr. 14, 203–234. https://doi.org/10.1615/critreveukaryotgeneexpr.v14.i3.40

Klein, D., Palla, G., Lange, M., Klein, M., Piran, Z., Gander, M., Meng-Papaxanthos, L., Sterr, M., Bastidas-Ponce, A., Tarquis-Medina, M., Lickert, H., Bakhti, M., Nitzan, M., Cuturi, M., Theis, F.J., 2023. Mapping cells through time and space with moscot. https://doi.org/10.1101/2023.05.11.540374

Kleshchevnikov, V., Shmatko, A., Dann, E., Aivazidis, A., King, H.W., Li, T., Elmentaite, R., Lomakin, A., Kedlian, V., Gayoso, A., Jain, M.S., Park, J.S., Ramona, L., Tuck, E., Arutyunyan, A., Vento-Tormo, R., Gerstung, M., James, L., Stegle, O., Bayraktar, O.A., 2022. Cell2location maps fine-grained cell types in spatial transcriptomics. Nat. Biotechnol. 40, 661–671. https://doi.org/10.1038/s41587-021-01139-4

Knudsen, A.B., Larsen, M., Mackey, A.L., Hjort, M., Hansen, K.K., Qvortrup, K., Kjær, M., Krogsgaard, M.R., 2015. The human myotendinous junction: An ultrastructural and 3D analysis study. Scand. J. Med. Sci. Sports 25, e116–e123. https://doi.org/10.1111/sms.12221

Koch, M., Schulze, J., Hansen, U., Ashwodt, T., Keene, D.R., Brunken, W.J., Burgeson, R.E., Bruckner, P., Bruckner-Tuderman, L., 2004. A novel marker of tissue junctions, collagen XXII. J. Biol. Chem. 279, 22514–22521. https://doi.org/10.1074/jbc.M400536200

Kohler, J., Popov, C., Klotz, B., Alberton, P., Prall, W.C., Haasters, F., Müller-Deubert, S., Ebert, R., Klein-Hitpass, L., Jakob, F., Schieker, M., Docheva, D., 2013. Uncovering the cellular and molecular changes in tendon stem/progenitor cells attributed to tendon aging and degeneration. Aging Cell 12, 988–999. https://doi.org/10.1111/acel.12124

Kohrs, R.T., Zhao, C., Sun, Y.-L., Jay, G.D., Zhang, L., Warman, M.L., An, K.-N., Amadio, P.C., 2011. Tendon fascicle gliding in wild type, heterozygous, and lubricin knockout mice. J. Orthop. Res. 29, 384–389. https://doi.org/10.1002/jor.21247

Kolb, M., Margetts, P.J., Sime, P.J., Gauldie, J., 2001. Proteoglycans decorin and biglycan differentially modulate TGF-β-mediated fibrotic responses in the lung. Am. J. Physiol.-Lung Cell. Mol. Physiol. 280, L1327–L1334. https://doi.org/10.1152/ajplung.2001.280.6.L1327

Kondratko-Mittnacht, J., Duenwald-Kuehl, S., Lakes, R., Vanderby, R., 2015. Shear load transfer in high and low stress tendons. J. Mech. Behav. Biomed. Mater. 45, 109–120. https://doi.org/10.1016/j.jmbbm.2015.01.021

Kong, D., Wang, Z., Sarkar, S.H., Li, Y., Banerjee, S., Saliganan, A., Kim, H.-R.C., Cher, M.L., Sarkar, F.H., 2008. Platelet-Derived Growth Factor-D Overexpression Contributes to Epithelial-Mesenchymal Transition of PC3 Prostate Cancer Cells. Stem Cells 26, 1425–1435. https://doi.org/10.1634/stemcells.2007-1076

Korcari, A., Przybelski, S.J., Gingery, A., Loiselle, A.E., 2023. Impact of aging on tendon homeostasis, tendinopathy development, and impaired healing. Connect. Tissue Res. 64, 1–13. https://doi.org/10.1080/03008207.2022.2102004

Kosher, R.A., Savage, M.P., 1981. Glycosaminoglycan synthesis by the apical ectodermal ridge of chick limb bud. Nature 291, 231–232. https://doi.org/10.1038/291231a0

Kotabagi, S., Shah, H., Shukla, A., Girisha, K. m., 2017. Second family provides further evidence for causation of Steel syndrome by biallelic mutations in COL27A1. Clin. Genet. 92, 323–326. https://doi.org/10.1111/cge.13006

Krenn, V., Brand-Saberi, B., Wachtler, F., 1991. Hyaluronic acid influences the migration of myoblasts within the avian embryonic wing bud. Am. J. Anat. 192, 400–406. https://doi.org/10.1002/aja.1001920407

Kult, S., Olender, T., Osterwalder, M., Markman, S., Leshkowitz, D., Krief, S., Blecher-Gonen, R., Ben-Moshe, S., Farack, L., Keren-Shaul, H., Salame, T.-M., Capellini, T.D., Itzkovitz, S., Amit, I., Visel, A., Zelzer, E., 2021. Bi-fated tendon-to-bone attachment cells are regulated by shared enhancers and KLF transcription factors. eLife 10, e55361. https://doi.org/10.7554/eLife.55361

Kuo, C.K., Petersen, B.C., Tuan, R.S., 2008. Spatiotemporal protein distribution of TGF-betas, their receptors, and extracellular matrix molecules during embryonic tendon development. Dev. Dyn. Off. Publ. Am. Assoc. Anat. 237, 1477–1489. https://doi.org/10.1002/dvdy.21547

Kwan, K.Y.C., Ng, K.W.K., Rao, Y., Zhu, C., Qi, S., Tuan, R.S., Ker, D.F.E., Wang, D.M., 2023. Effect of Aging on Tendon Biology, Biomechanics and Implications for Treatment Approaches. Int. J. Mol. Sci. 24, 15183. https://doi.org/10.3390/ijms242015183

La Manno, G., Soldatov, R., Zeisel, A., Braun, E., Hochgerner, H., Petukhov, V., Lidschreiber, K., Kastriti, M.E., Lönnerberg, P., Furlan, A., Fan, J., Borm, L.E., Liu, Z., van Bruggen, D., Guo, J., He, X., Barker, R., Sundström, E., Castelo-Branco, G., Cramer, P., Adameyko, I., Linnarsson, S., Kharchenko, P.V., 2018. RNA velocity of single cells. Nature 560, 494–498. https://doi.org/10.1038/s41586-018-0414-6

Labelle-Dumais, C., Schuitema, V., Hayashi, G., Hoff, K., Gong, W., Dao, D.Q., Ullian, E.M., Oishi, P., Margeta, M., Gould, D.B., 2019. *COL4A1* Mutations Cause Neuromuscular Disease with Tissue-Specific Mechanistic Heterogeneity. Am. J. Hum. Genet. 104, 847–860. https://doi.org/10.1016/j.ajhg.2019.03.007

Lagemann, K., Lagemann, C., Taschler, B., Mukherjee, S., 2023. Deep learning of causal structures in high dimensions under data limitations. Nat. Mach. Intell. 5, 1306–1316. https://doi.org/10.1038/s42256-023-00744-z

Langberg, H., Olesen, J., Skovgaard, D., Kjaer, M., 2001. Age related blood flow around the Achilles tendon during exercise in humans. Eur. J. Appl. Physiol. 84, 246–248. https://doi.org/10.1007/s004210170013

Langhauser, M., Ustinova, J., Rivera-Milla, E., Ivannikov, D., Seidl, C., Slomka, C., Finne, J., Yoshihara, Y., Bastmeyer, M., Bentrop, J., 2012. Ncam1a and Ncam1b: Two carriers of polysialic acid with different functions in the developing zebrafish nervous system. Glycobiology 22, 196–209. https://doi.org/10.1093/glycob/cwr129

Lataillade, J.-J., Clay, D., Dupuy, C., Rigal, S., Jasmin, C., Bourin, P., Bousse-Kerdilès, M.-C.L., 2000. Chemokine SDF-1 enhances circulating CD34+ cell proliferation in synergy with cytokines: possible role in progenitor survival. Blood 95, 756–768. https://doi.org/10.1182/blood.V95.3.756

Lavagnino, M., Brooks, A.E., Oslapas, A.N., Gardner, K.L., Arnoczky, S.P., 2017. Crimp length decreases in lax tendons due to cytoskeletal tension, but is restored with tensional homeostasis. J. Orthop. Res. 35, 573–579. https://doi.org/10.1002/jor.23489

Leahy, T.P., Fung, A.K., Weiss, S.N., Dyment, N.A., Soslowsky, L.J., 2023. Investigating the temporal roles of decorin and biglycan in tendon healing. J. Orthop. Res. 41, 2238–2249. https://doi.org/10.1002/jor.25590

Lee, C., 2021. Tendon physiology and repair. Orthop. Trauma 35, 274–281. https://doi.org/10.1016/j.mporth.2021.07.003

Lee, M.-H., Tsai, H.-P., Lavy, C., Mouthuy, P.-A., Czernuszka, J., 2023. Time-dependent extracellular matrix alterations of young tendons in response to stress relaxation: a model for the Ponseti method. J. R. Soc. Interface 20, 20220712. https://doi.org/10.1098/rsif.2022.0712

Lefebvre, V., Behringer, R.R., de Crombrugghe, B., 2001. L-Sox5, Sox6 and Sox9 control essential steps of the chondrocyte differentiation pathway. Osteoarthritis Cartilage 9, S69–S75. https://doi.org/10.1053/joca.2001.0447

Legerlotz, K., Dorn, J., Richter, J., Rausch, M., Leupin, O., 2014. Age-dependent regulation of tendon crimp structure, cell length and gap width with strain. Acta Biomater. 10, 4447–4455. https://doi.org/10.1016/j.actbio.2014.05.029

Leiphart, Ryan J., Pham, H., Harvey, T., Komori, T., Kilts, T.M., Shetye, S.S., Weiss, S.N., Adams, S.M., Birk, D.E., Soslowsky, L.J., Young, M.F., 2022. Coordinate roles for collagen VI and biglycan in regulating tendon collagen fibril structure and function. Matrix Biol. Plus 13, 100099. https://doi.org/10.1016/j.mbplus.2021.100099

Leiphart, R. J., Weiss, S.N., DiStefano, M.S., Mavridis, A.A., Adams, S.A., Dyment, N.A., Soslowsky, L.J., 2022. Collagen V deficiency during murine tendon healing results in distinct healing outcomes based on knockdown severity. J. Biomech. 144, 111315. https://doi.org/10.1016/j.jbiomech.2022.111315

Lejard, V., Blais, F., Guerquin, M.J., Bonnet, A., Bonnin, M.A., Havis, E., Malbouyres, M., Bidaud, C.B., Maro, G., Gilardi-Hebenstreit, P., Rossert, J., Ruggiero, F., Duprez, D., 2011. EGR1 and EGR2 involvement in vertebrate tendon differentiation. J. Biol. Chem. 286, 5855–5867. https://doi.org/10.1074/jbc.M110.153106

Lemaître, G., Nogueira, F., Aridas, C.K., 2017. Imbalanced-learn: A Python Toolbox to Tackle the Curse of Imbalanced Datasets in Machine Learning. J. Mach. Learn. Res. 18, 1–5.

Leonardi, E.A., Xiao, M., Murray, I.R., Robinson, W.H., Abrams, G.D., 2021. Tendon-Derived Progenitor Cells With Multilineage Potential Are Present

Within Human Patellar Tendon. Orthop. J. Sports Med. 9, 23259671211023452. https://doi.org/10.1177/23259671211023452

Li, O., Vasudevan, D., Davey, C.A., Dröge, P., 2006. High-level expression of DNA architectural factor HMGA2 and its association with nucleosomes in human embryonic stem cells. Genes. N. Y. N 2000 44, 523–529. https://doi.org/10.1002/dvg.20242

Li, Y., Toole, B.P., Dealy, C.N., Kosher, R.A., 2007. Hyaluronan in Limb Morphogenesis. Dev. Biol. 305, 411–420. https://doi.org/10.1016/j.ydbio.2007.02.023

Lian, O.B., Engebretsen, L., Bahr, R., 2005. Prevalence of jumper's knee among elite athletes from different sports: a cross-sectional study. Am. J. Sports Med. 33, 561–567. https://doi.org/10.1177/0363546504270454

Lieberman, A., Barrett, R., Kim, J., Zhang, K.L., Avery, D., Monslow, J., Kim, H., Kim, B.-J., Pure, E., Ryeom, S., 2019. Deletion of calcineurin promotes a pro-tumorigenic fibroblast phenotype. Cancer Res. 79, 3928. https://doi.org/10.1158/0008-5472.CAN-19-0056

Lieberthal, K., Paterson, K.L., Cook, J., Kiss, Z., Girdwood, M., Bradshaw, E.J., 2019. Prevalence and factors associated with asymptomatic Achilles tendon pathology in male distance runners. Phys. Ther. Sport Off. J. Assoc. Chart. Physiother. Sports Med. 39, 64–68. https://doi.org/10.1016/j.ptsp.2019.06.006

Lin, A.H., Allan, A.N., Zitnay, J.L., Kessler, J.L., Yu, S.M., Weiss, J.A., 2020. Collagen Denaturation is Initiated Upon Tissue Yield in both Positional and Energy-Storing Tendons. Acta Biomater. 118, 153–160. https://doi.org/10.1016/j.actbio.2020.09.056

Lin, C.-S., Ning, H., Lin, G., Lue, T.F., 2012. Is CD34 truly a negative marker for mesenchymal stromal cells? Cytotherapy 14, 1159–1163. https://doi.org/10.3109/14653249.2012.729817

Lipp, S.N., Jacobson, K.R., Colling, H.A., Tuttle, T.G., Miles, D.T., McCreery, K.P., Calve, S., 2023. Mechanical loading is required for initiation of extracellular matrix deposition at the developing murine myotendinous junction. Matrix Biol. 116, 28–48. https://doi.org/10.1016/j.matbio.2023.01.003

Little, M.H., Kairath, P., 2017. Does Renal Repair Recapitulate Kidney Development? J. Am. Soc. Nephrol. 28, 34. https://doi.org/10.1681/ASN.2016070748

Littlewood, C., May, S., Walters, S., 2013. Epidemiology of Rotator Cuff Tendinopathy: A Systematic Review. Shoulder Elb. 5, 256–265. https://doi.org/10.1111/sae.12028

Liu, C.-F., Breidenbach, A., Aschbacher-Smith, L., Butler, D., Wylie, C., 2013. A Role for Hedgehog Signaling in the Differentiation of the Insertion Site of

the Patellar Tendon in the Mouse. PLoS ONE 8, e65411. https://doi.org/10.1371/journal.pone.0065411

Liu, C.-Y., Birk, D.E., Hassell, J.R., Kane, B., Kao, W.W.-Y., 2003. Keratocan-deficient mice display alterations in corneal structure. J. Biol. Chem. 278, 21672–21677. https://doi.org/10.1074/jbc.M301169200

Liu, H., Shalev, I., Manuel, J., He, W., Leung, E., Crookshank, J., Liu, M.F., Diao, J., Cattral, M., Clark, D.A., Isenman, D.E., Gorczynski, R.M., Grant, D.R., Zhang, L., Phillips, M.J., Cybulsky, M.I., Levy, G.A., 2008. The FGL2-FcγRIIB pathway: A novel mechanism leading to immunosuppression. Eur. J. Immunol. 38, 3114–3126. https://doi.org/10.1002/eji.200838338

Liu, H., Xu, J., Liu, C.-F., Lan, Y., Wylie, C., Jiang, R., 2015. Whole transcriptome expression profiling of mouse limb tendon development by using RNA-seq. J. Orthop. Res. Off. Publ. Orthop. Res. Soc. 33, 840–848. https://doi.org/10.1002/jor.22886

Liu, W., Watson, S.S., Lan, Y., Keene, D.R., Ovitt, C.E., Liu, H., Schweitzer, R., Jiang, R., 2010. The Atypical Homeodomain Transcription Factor Mohawk Controls Tendon Morphogenesis. Mol. Cell. Biol. 30, 4797–4807. https://doi.org/10.1128/mcb.00207-10

Logan, C., Hornbruch, A., Campbell, I., Lumsden, A., 1997. The role of Engrailed in establishing the dorsoventral axis of the chick limb. Development 124, 2317–2324. https://doi.org/10.1242/dev.124.12.2317

Longaker, M.T., Chiu, E.S., Adzick, N.S., Stern, M., Harrison, M.R., Stern, R., 1991. Studies in Fetal Wound Healing V. A Prolonged Presence of Hyaluronic Acid Characterizes Fetal Wound Fluid. Ann. Surg. 213, 292.

Longaker, M.T., Chiu, E.S., Harrison, M.R., Crombleholme, T.M., Langer, J.C., Duncan, B.W., Adzick, N.S., Verrier, E.D., Stern, R., 1989. Studies in Fetal Wound Healing IV. Hyaluronic Acid-Stimulating Activity Distinguishes Fetal Wound Fluid from Adult Wound Fluid. Ann. Surg. 210, 667.

Longaker, M.T., Whitby, D.J., Ferguson, M.W., Lorenz, H.P., Harrison, M.R., Adzick, N.S., 1994. Adult skin wounds in the fetal environment heal with scar formation. Ann. Surg. 219, 65–72. https://doi.org/10.1097/00000658-199401000-00011

Longo, U.G., Ronga, M., Maffulli, N., 2018. Achilles Tendinopathy. Sports Med. Arthrosc. Rev. 26, 16–30. https://doi.org/10.1097/JSA.0000000000000185

Lorda-Diez, C.I., García-Porrero, J.A., Hurlé, J.M., Montero, J.A., 2014. Decorin gene expression in the differentiation of the skeletal connective tissues of the developing limb. Gene Expr. Patterns 15, 52–60. https://doi.org/10.1016/j.gep.2014.04.003

Lorenzo, P., Aspberg, A., Önnerfjord, P., Bayliss, M.T., Neame, P.J., Heinegård, D., 2001. Identification and Characterization of Asporin: A NOVEL MEMBER OF THE LEUCINE-RICH REPEAT PROTEIN FAMILY CLOSELY RELATED TO DECORIN AND BIGLYCAN*. J. Biol. Chem. 276, 12201–12211. https://doi.org/10.1074/jbc.M010932200

Lui, P.P.Y., Chan, K.M., 2011. Tendon-Derived Stem Cells (TDSCs): From Basic Science to Potential Roles in Tendon Pathology and Tissue Engineering Applications. Stem Cell Rev. Rep. 7, 883–897. https://doi.org/10.1007/s12015-011-9276-0

Lui, P.P.-Y., Chan, L.-S., Lee, Y.-W., Fu, S.C., Chan, K.-M., 2010. Sustained expression of proteoglycans and collagen type III/type I ratio in a calcified tendinopathy model. Rheumatology 49, 231–239. https://doi.org/10.1093/rheumatology/kep384

Lui, P.P.Y., Cheuk, Y.C., Lee, Y.W., Chan, K.M., 2012. Ectopic chondro-ossification and erroneous extracellular matrix deposition in a tendon window injury model. J. Orthop. Res. 30, 37–46. https://doi.org/10.1002/jor.21495

Lui, P.P.Y., Wong, C.M., 2020. Biology of Tendon Stem Cells and Tendon in Aging, Frontiers in Genetics. Frontiers Media S.A. https://doi.org/10.3389/fgene.2019.01338

Luime, J.J., Koes, B.W., Hendriksen, I.J.M., Burdorf, A., Verhagen, A.P., Miedema, H.S., Verhaar, J.A.N., 2004. Prevalence and incidence of shoulder pain in the general population; a systematic review. Scand. J. Rheumatol. 33, 73–81. https://doi.org/10.1080/03009740310004667

Lundborg, G., Holm, S., Myrhage, R., 1980. The role of the synovial fluid and tendon sheath for flexor tendon nutrition. An experimental tracer study on diffusional pathways in dogs. Scand. J. Plast. Reconstr. Surg. 14, 99–107. https://doi.org/10.3109/02844318009105739

Ma, S.K.Y., Chan, A.S.F., Rubab, A., Chan, W.C.W., Chan, D., 2020. Extracellular Matrix and Cellular Plasticity in Musculoskeletal Development. Front. Cell Dev. Biol. 8, 567065. https://doi.org/10.3389/fcell.2020.00781

Maccarana, M., Svensson, R.B., Knutsson, A., Giannopoulos, A., Pelkonen, M., Weis, M., Eyre, D., Warman, M., Kalamajski, S., 2017. Asporin-deficient mice have tougher skin and altered skin glycosaminoglycan content and structure. PLOS ONE 12, e0184028. https://doi.org/10.1371/journal.pone.0184028

Maeda, T., Sakabe, T., Sunaga, A., Sakai, K., Rivera, A.L., Keene, D.R., Sasaki, T., Stavnezer, E., Iannotti, J., Schweitzer, R., Ilic, D., Baskaran, H., Sakai, T., 2011. Conversion of Mechanical Force into TGF-β-

Mediated Biochemical Signals. Curr. Biol. 21, 933–941. https://doi.org/10.1016/j.cub.2011.04.007

Maffulli, N., Barrass, V., Ewen, S.W., 2000. Light microscopic histology of achilles tendon ruptures. A comparison with unruptured tendons. Am. J. Sports Med. 28, 857–863. https://doi.org/10.1177/03635465000280061401

Maffulli, Nicola, Ewen, S.W.B., Waterston, S.W., Reaper, J., Barrass, V., 2000. Tenocytes from Ruptured and Tendinopathic Achilles Tendons Produce Greater Quantities of Type III Collagen than Tenocytes from Normal Achilles Tendons: An in Vitro Model of Human Tendon Healing. Am. J. Sports Med. 28, 499–505. https://doi.org/10.1177/03635465000280040901

Maffulli, N., Giai Via, A., Oliva, F., 2017. Revision Surgery for Failed Patellar Tendinopathy Exploration. Sports Med. Arthrosc. Rev. 25, 36. https://doi.org/10.1097/JSA.0000000000000141

Maffulli, N., Longo, U.G., Franceschi, F., Rabitti, C., Denaro, V., 2008. Movin and Bonar Scores Assess the Same Characteristics of Tendon Histology. Clin. Orthop. 466, 1605–1611. https://doi.org/10.1007/s11999-008-0261-0

Maffulli, N., Oliva, F., Maffulli, G.D., Migliorini, F., 2021. Failed Surgery for Patellar Tendinopathy in Athletes: Midterm Results of Further Surgical Management. Orthop. J. Sports Med. 9, 2325967121994550. https://doi.org/10.1177/2325967121994550

Maffulli, N., Sharma, P., Luscombe, K.L., 2004. Achilles tendinopathy: aetiology and management. J. R. Soc. Med. 97, 472–476. https://doi.org/10.1177/0141076809701004

Magnusson, S.P., Langberg, H., Kjaer, M., 2010. The pathogenesis of tendinopathy: balancing the response to loading. Nat. Rev. Rheumatol. 6, 262–268. https://doi.org/10.1038/nrrheum.2010.43

Maharjan, A.S., Pilling, D., Gomer, R.H., 2011. High and Low Molecular Weight Hyaluronic Acid Differentially Regulate Human Fibrocyte Differentiation. PLOS ONE 6, e26078. https://doi.org/10.1371/journal.pone.0026078

Makris, E.A., Responte, D.J., Paschos, N.K., Hu, J.C., Athanasiou, K.A., 2014. Developing functional musculoskeletal tissues through hypoxia and lysyl oxidase-induced collagen cross-linking. Proc. Natl. Acad. Sci. U. S. A. 111, E4832-4841. https://doi.org/10.1073/pnas.1414271111

Malfait, F., Coucke, P., Symoens, S., Loeys, B., Nuytinck, L., De Paepe, A., 2005. The molecular basis of classic Ehlers-Danlos syndrome: a comprehensive study of biochemical and molecular findings in 48 unrelated patients. Hum. Mutat. 25, 28–37. https://doi.org/10.1002/humu.20107

Malliaras, P., Barton, C.J., Reeves, N.D., Langberg, H., 2013. Achilles and Patellar Tendinopathy Loading Programmes. Sports Med. 43, 267–286. https://doi.org/10.1007/s40279-013-0019-z

Manske, P.R., Bridwell, K., Whiteside, L.A., Lesker, P.A., 1978. Nutrition of Flexor Tendons in Monkeys. Clin. Orthop. Relat. Res. 294.

Manske, P.R., Lesker, P.A., 1983. Nutrient Pathways to Extensor Tendons within the Extensor Retinacular Compartments: An Experimental Study in Dogs. Clin. Orthop. Relat. Res. 181, 234.

Marini, J.C., Forlino, A., Cabral, W.A., Barnes, A.M., San Antonio, J.D., Milgrom, S., Hyland, J.C., Körkkö, J., Prockop, D.J., De Paepe, A., Coucke, P., Symoens, S., Glorieux, F.H., Roughley, P.J., Lund, A.M., Kuurila-Svahn, K., Hartikka, H., Cohn, D.H., Krakow, D., Mottes, M., Schwarze, U., Chen, D., Yang, K., Kuslich, C., Troendle, J., Dalgleish, R., Byers, P.H., 2007. Consortium for osteogenesis imperfecta mutations in the helical domain of type I collagen: regions rich in lethal mutations align with collagen binding sites for integrins and proteoglycans. Hum. Mutat. 28, 209–221. https://doi.org/10.1002/humu.20429

Markova, D.Z., Pan, T.-C., Zhang, R.-Z., Zhang, G., Sasaki, T., Arita, M., Birk, D.E., Chu, M.-L., 2016. Forelimb contractures and abnormal tendon collagen fibrillogenesis in fibulin-4 null mice. Cell Tissue Res. 364, 637–646. https://doi.org/10.1007/s00441-015-2346-x

Márquez-Arabia, W.H., Gómez-Hoyos, J., Gómez, M., Flórez, I., Gallo, J.A., Monsalve, F., Arias, L.F., Martin, H.D., 2017. Influence of Aging on Microvascular Supply of the Gluteus Medius Tendon: A Cadaveric and Histologic Study. Arthrosc. J. Arthrosc. Relat. Surg. Off. Publ. Arthrosc. Assoc. N. Am. Int. Arthrosc. Assoc. 33, 1354–1360. https://doi.org/10.1016/j.arthro.2017.01.036

Marturano, J.E., Arena, J.D., Schiller, Z.A., Georgakoudi, I., Kuo, C.K., 2013. Characterization of mechanical and biochemical properties of developing embryonic tendon. Proc. Natl. Acad. Sci. U. S. A. 110, 6370–6375. https://doi.org/10.1073/pnas.1300135110

Marturano, J.E., Xylas, J.F., Sridharan, G.V., Georgakoudi, I., Kuo, C.K., 2014. Lysyl oxidase-mediated collagen crosslinks may be assessed as markers of functional properties of tendon tissue formation. Acta Biomater. 10, 1370–1379. https://doi.org/10.1016/j.actbio.2013.11.024

Masic, A., Bertinetti, L., Schuetz, R., Chang, S.W., Metzger, T.H., Buehler, M.J., Fratzl, P., 2015. Osmotic pressure induced tensile forces in tendon collagen. Nat. Commun. 6. https://doi.org/10.1038/ncomms6942

Mast, B.A., Flood, L.C., Haynes, J.H., Depalma, R.L., Cohen, I.K., Diegelmann, R.F., Krummel, T.M., 1991. Hyaluronic Acid is a Major Component of the Matrix of Fetal Rabbit Skin and Wounds: Implications for Healing by

Regeneration. Matrix 11, 63–68. https://doi.org/10.1016/S0934-8832(11)80228-3

Matsubayashi, Y., Millard, T.H., 2013. Developmental Models for Wound Healing, in: eLS. John Wiley & Sons, Ltd. https://doi.org/10.1002/9780470015902.a0021306

Mattei, D., Ivanov, A., van Oostrum, M., Pantelyushin, S., Richetto, J., Mueller, F., Beffinger, M., Schellhammer, L., vom Berg, J., Wollscheid, B., Beule, D., Paolicelli, R.C., Meyer, U., 2020. Enzymatic Dissociation Induces Transcriptional and Proteotype Bias in Brain Cell Populations. Int. J. Mol. Sci. 21, 7944. https://doi.org/10.3390/ijms21217944

McBride, D.J., Hahn, R.A., Silver, F.H., 1985. Morphological characterization of tendon development during chick embryogenesis: measurement of birefringence retardation. Int. J. Biol. Macromol. 7, 71–76. https://doi.org/10.1016/0141-8130(85)90034-0

McBride, D.J., Trelstad, R.L., Silver, F.H., 1988. Structural and mechanical assessment of developing chick tendon. Int. J. Biol. Macromol. 10, 194–200. https://doi.org/10.1016/0141-8130(88)90048-7

McMahon, P.J., Prasad, A., Francis, K.A., 2014. What Is the Prevalence of Senior-athlete Rotator Cuff Injuries and Are They Associated With Pain and Dysfunction? Clin. Orthop. Relat. Res. 472, 2427. https://doi.org/10.1007/s11999-014-3560-7

McNeilly, C.M., Banes, A.J., Benjamin, M., Ralphs, J.R., 1996. Tendon cells in vivo form a three dimensional network of cell processes linked by gap junctions. J. Anat. 189 (Pt 3), 593–600.

Meller, R., Schiborra, F., Brandes, G., Knobloch, K., Tschernig, T., Hankemeier, S., Haasper, C., Schmiedl, A., Jagodzinski, M., Krettek, C., Willbold, E., 2009. Postnatal maturation of tendon, cruciate ligament, meniscus and articular cartilage: A histological study in sheep. Ann. Anat. - Anat. Anz. 191, 575–585. https://doi.org/10.1016/j.aanat.2009.08.005

Meng, C., Jiang, B., Liu, M., Kang, F., Kong, L., Zhang, T., Wang, C., Wang, J., Han, C., Ren, Y., 2023. Repair of rotator cuff tears in patients aged 75 years and older: Does it make sense? A systematic review. Front. Public Health 10, 1060700. https://doi.org/10.3389/fpubh.2022.1060700

Meran, S., Luo, D.D., Simpson, R., Martin, J., Wells, A., Steadman, R., Phillips, A.O., 2011. Hyaluronan Facilitates Transforming Growth Factor-β1-dependent Proliferation via CD44 and Epidermal Growth Factor Receptor Interaction. J. Biol. Chem. 286, 17618–17630. https://doi.org/10.1074/jbc.M111.226563

Mezu-Ndubuisi, O.J., Maheshwari, A., 2021. Role of macrophages in fetal development and perinatal disorders. Pediatr. Res. 90, 513–523. https://doi.org/10.1038/s41390-020-01209-4

Midgley, A.C., Rogers, M., Hallett, M.B., Clayton, A., Bowen, T., Phillips, A.O., Steadman, R., 2013. Transforming Growth Factor-β1 (TGF-β1)-stimulated Fibroblast to Myofibroblast Differentiation Is Mediated by Hyaluronan (HA)-facilitated Epidermal Growth Factor Receptor (EGFR) and CD44 Co-localization in Lipid Rafts. J. Biol. Chem. 288, 14824–14838. https://doi.org/10.1074/jbc.M113.451336

Midwood, K.S., Chiquet, M., Tucker, R.P., Orend, G., 2016. Tenascin-C at a glance. J. Cell Sci. 129, 4321–4327. https://doi.org/10.1242/jcs.190546

Mienaltowski, M.J., Adams, S.M., Birk, D.E., 2013. Regional Differences in Stem Cell/Progenitor Cell Populations from the Mouse Achilles Tendon. Tissue Eng. Part A 19, 199–210. https://doi.org/10.1089/ten.tea.2012.0182

Millar, N.L., Murrell, G.A.C., Mcinnes, I.B., 2017. Inflammatory mechanisms in tendinopathy - towards translation. Nat. Rev. Rheumatol. 13, 110–122. https://doi.org/10.1038/nrrheum.2016.213

Millar, N.L., Silbernagel, K.G., Thorborg, K., Kirwan, P.D., Galatz, L.M., Abrams, G.D., Murrell, G.A.C., McInnes, I.B., Rodeo, S.A., 2021. Tendinopathy. Nat. Rev. Dis. Primer 7, 1–21. https://doi.org/10.1038/s41572-020-00234-1

Mills, F.B., Williams, K., Chu, C.H., Bornemann, P., Jackson, J.B., 2020. Prevalence of Abnormal Ultrasound Findings in Asymptomatic Posterior Tibial Tendons. Foot Ankle Int. 41, 1049–1055. https://doi.org/10.1177/1071100720931085

Mimpen, J., Paul, C., Network, T.S., Cribbs, A., Snelling, S., 2021. Nuclei isolation from snap-frozen tendon tissue for single nucleus RNA Sequencing. Protocols.io. https://dx.doi.org/10.17504/protocols.io.bc6xizfn

Mimpen, J.Y., Ramos-Mucci, L., Paul, C., Kurjan, A., Hulley, P., Ikwuanusi, C., Gwilym, S., Baldwin, M.J., Cribbs, A.P., Snelling, S.J.B., 2022. Single nucleus and spatial transcriptomic profiling of human healthy hamstring tendon. https://doi.org/10.1101/2022.12.19.521110

Minagawa, H., Yamamoto, N., Abe, H., Fukuda, M., Seki, N., Kikuchi, K., Kijima, H., Itoi, E., 2013. Prevalence of symptomatic and asymptomatic rotator cuff tears in the general population: From mass-screening in one village. J. Orthop. 10, 8–12. https://doi.org/10.1016/j.jor.2013.01.008

Miranda, H., Viikari-Juntura, E., Heistaro, S., Heliövaara, M., Riihimäki, H., 2005. A population study on differences in the determinants of a specific shoulder disorder versus nonspecific shoulder pain without clinical findings. Am. J. Epidemiol. 161, 847–855. https://doi.org/10.1093/aje/kwi112

Mizumoto, S., Yamada, S., 2023. Histories of Dermatan Sulfate Epimerase and Dermatan 4-O-Sulfotransferase from Discovery of Their Enzymes and Genes to Musculocontractural Ehlers-Danlos Syndrome. Genes 14, 509. https://doi.org/10.3390/genes14020509

Mizumoto, S., Yamada, S., 2021. An Overview of in vivo Functions of Chondroitin Sulfate and Dermatan Sulfate Revealed by Their Deficient Mice. Front. Cell Dev. Biol. 9, 764781. https://doi.org/10.3389/fcell.2021.764781

Mohammadi, Y., Tavangar, S.M., Saidijam, M., Amini, R., Etemadi, K., Karimi Dermani, F., Najafi, R., 2018. DCLK1 plays an important role in colorectal cancer tumorgenesis through the regulation of miR-200c. Biomed. Pharmacother. 103, 301–307. https://doi.org/10.1016/j.biopha.2018.04.042

Mohebbi, R., Rezasoltani, Z., Mir, M., Mohebbi, M., Vatandoost, S., Esmaily, H., 2021. High- Versus Low-Molecular-Weight Hyaluronic Acid for the Treatment of Rotator Cuff Tendinopathy: A Triple-Blind Randomized Comparative Trial. Ann. Pharmacother. 55, 1203–1214. https://doi.org/10.1177/1060028021994297

Moncayo-Arlandi, J., López-García, A., Fernández, M.C., Durán, A.C., Fernández, B., 2014. Osteoglycin deficiency does not affect atherosclerosis in mice. Atherosclerosis 237, 418–425. https://doi.org/10.1016/j.atherosclerosis.2014.09.016

Morelli, L., Giansanti, V., Cittaro, D., 2021. Nested Stochastic Block Models applied to the analysis of single cell data. BMC Bioinformatics 22, 576. https://doi.org/10.1186/s12859-021-04489-7

Moreth, K., Iozzo, R.V., Schaefer, L., 2012. Small leucine-rich proteoglycans orchestrate receptor crosstalk during inflammation. Cell Cycle Georget. Tex 11, 2084–2091. https://doi.org/10.4161/cc.20316

Moser, H.L., Abraham, A.C., Howell, K., Laudier, D., Zumstein, M.A., Galatz, L.M., Huang, A.H., 2021. Cell lineage tracing and functional assessment of supraspinatus tendon healing in an acute repair murine model. J. Orthop. Res. 39, 1789–1799. https://doi.org/10.1002/jor.24769

Moser, H.L., Doe, A.Ph., Meier, K., Garnier, S., Laudier, D., Akiyama, H., Zumstein, M.A., Galatz, L.M., Huang, A.H., 2018. Genetic Lineage Tracing of Targeted Cell Populations During Enthesis Healing. J. Orthop. Res. Off. Publ. Orthop. Res. Soc. 36, 3275–3284. https://doi.org/10.1002/jor.24122

Muhl, L., Genové, G., Leptidis, S., Liu, J., He, L., Mocci, G., Sun, Y., Gustafsson, S., Buyandelger, B., Chivukula, I.V., Segerstolpe, Å., Raschperger, E., Hansson, E.M., Björkegren, J.L.M., Peng, X.-R., Vanlandewijck, M., Lendahl, U., Betsholtz, C., 2020. Single-cell analysis

uncovers fibroblast heterogeneity and criteria for fibroblast and mural cell identification and discrimination. Nat. Commun. 2020 111 11, 1–18. https://doi.org/10.1038/s41467-020-17740-1

Munezane, H., Oizumi, H., Wakabayashi, T., Nishio, S., Hirasawa, T., Sato, T., Harada, A., Yoshida, T., Eguchi, T., Yamanashi, Y., Hashimoto, T., Iwatsubo, T., 2019. Roles of Collagen XXV and Its Putative Receptors PTPσ/δ in Intramuscular Motor Innervation and Congenital Cranial Dysinnervation Disorder. Cell Rep. 29, 4362-4376.e6. https://doi.org/10.1016/j.celrep.2019.11.112

Murchison, N.D., Price, B.A., Conner, D.A., Keene, D.R., Olson, E.N., Tabin, C.J., Schweitzer, R., 2007. Regulation of tendon differentiation by scleraxis distinguishes force-transmitting tendons from muscle-anchoring tendons. Development 134, 2697–2708. https://doi.org/10.1242/dev.001933

Murphy, M., Kardon, G., 2011. Origin of vertebrate limb muscle: The role of progenitor and myoblast populations, Current Topics in Developmental Biology. Academic Press. https://doi.org/10.1016/B978-0-12-385940-2.00001-2

Muscat, S., Nichols, A.E.C., Gira, E., Loiselle, A.E., 2022. CCR2 is expressed by tendon resident macrophage and T cells, while CCR2 deficiency impairs tendon healing via blunted involvement of tendon-resident and circulating monocytes/macrophages. FASEB J. 36, e22607. https://doi.org/10.1096/fj.202201162R

Myhrvold, S.B., Brouwer, E.F., Andresen, T.K.M., Rydevik, K., Amundsen, M., Grün, W., Butt, F., Valberg, M., Ulstein, S., Hoelsbrekken, S.E., 2022. Nonoperative or Surgical Treatment of Acute Achilles' Tendon Rupture. N. Engl. J. Med. 386, 1409–1420. https://doi.org/10.1056/NEJMoa2108447

Nakagawa, Y., Majima, T., Nagashima, K., 1994. Effect of ageing on ultrastructure of slow and fast skeletal muscle tendon in rabbit Achilles tendons. Acta Physiol. Scand. 152, 307–313. https://doi.org/10.1111/j.1748-1716.1994.tb09810.x

Nakamichi, R., Asahara, H., 2021. Regulation of tendon and ligament differentiation. Bone 143, 115609. https://doi.org/10.1016/j.bone.2020.115609

Narayanan, N., Calve, S., 2021. Extracellular matrix at the muscle – tendon interface: functional roles, techniques to explore and implications for regenerative medicine. Connect. Tissue Res. 62, 53–71. https://doi.org/10.1080/03008207.2020.1814263

Nassari, S., Blavet, C., Bonnin, M.-A., Stricker, S., Duprez, D., Fournier-Thibault, C., 2017. The chemokines CXCL12 and CXCL14 differentially

regulate connective tissue markers during limb development. Sci. Rep. 7, 17279. https://doi.org/10.1038/s41598-017-17490-z

Ng, L.J., Wheatley, S., Muscat, G.E., Conway-Campbell, J., Bowles, J., Wright, E., Bell, D.M., Tam, P.P., Cheah, K.S., Koopman, P., 1997. SOX9 binds DNA, activates transcription, and coexpresses with type II collagen during chondrogenesis in the mouse. Dev. Biol. 183, 108–121. https://doi.org/10.1006/dbio.1996.8487

Nichols, A.E.C., Wagner, N.W., Ketonis, C., Loiselle, A.E., 2023. Epitenon-derived cells comprise a distinct progenitor population that contributes to both tendon fibrosis and regeneration following acute injury. bioRxiv 2023.01.30.526242. https://doi.org/10.1101/2023.01.30.526242

Nie, D., Zhou, Y., Wang, W., Zhang, J., Wang, J.H.-C., 2021. Mechanical Overloading Induced-Activation of mTOR Signaling in Tendon Stem/Progenitor Cells Contributes to Tendinopathy Development. Front. Cell Dev. Biol. 9, 687856. https://doi.org/10.3389/fcell.2021.687856

Nishimoto, S., Wilde, S.M., Wood, S., Logan, M.P.O., 2015. RA Acts in a Coherent Feed-Forward Mechanism with Tbx5 to Control Limb Bud Induction and Initiation. Cell Rep. 12, 879–891. https://doi.org/10.1016/j.celrep.2015.06.068

Noah, A.C., Li, T.M., Martinez, L.M., Wada, S., Swanson, J.B., Disser, N.P., Sugg, K.B., Rodeo, S.A., Lu, T.T., Mendias, C.L., 2020. Adaptive and innate immune cell responses in tendons and lymph nodes after tendon injury and repair. J. Appl. Physiol. 128, 473–482. https://doi.org/10.1152/japplphysiol.00682.2019

Noback, P.C., Freibott, C.E., Tantigate, D., Jang, E., Greisberg, J.K., Wong, T., Vosseller, J.T., 2018. Prevalence of Asymptomatic Achilles Tendinosis. Foot Ankle Int. 39, 1205–1209. https://doi.org/10.1177/1071100718778592

Noonan, T.J., Garrett, W.E., 1992. Injuries at the myotendinous junction. Clin. Sports Med. 11, 783–806.

Norris, R.A., Damon, B., Mironov, V., Kasyanov, V., Ramamurthi, A., Moreno-Rodriguez, R., Trusk, T., Potts, J.D., Goodwin, R.L., Davis, J., Hoffman, S., Wen, X., Sugi, Y., Kern, C.B., Mjaatvedt, C.H., Turner, D.K., Oka, T., Conway, S.J., Molkentin, J.D., Forgacs, G., Markwald, R.R., 2007. Periostin regulates collagen fibrillogenesis and the biomechanical properties of connective tissues. J. Cell. Biochem. 101, 695–711. https://doi.org/10.1002/jcb.21224

Nourissat, G., Diop, A., Maurel, N., Salvat, C., Dumont, S., Pigenet, A., Gosset, M., Houard, X., Berenbaum, F., 2010. Mesenchymal Stem Cell Therapy Regenerates the Native Bone-Tendon Junction after Surgical Repair in a

Degenerative Rat Model. PLOS ONE 5, e12248. https://doi.org/10.1371/journal.pone.0012248

Nowotschin, S., Setty, M., Kuo, Y.-Y., Liu, V., Garg, V., Sharma, R., Simon, C.S., Saiz, N., Gardner, R., Boutet, S.C., Church, D.M., Hoodless, P.A., Hadjantonakis, A.-K., Pe'er, D., 2019. The emergent landscape of the mouse gut endoderm at single-cell resolution. Nature 569, 361–367. https://doi.org/10.1038/s41586-019-1127-1

Nutarelli, S., da Lodi, C.M.T., Cook, J.L., Deabate, L., Filardo, G., 2023. Epidemiology of Patellar Tendinopathy in Athletes and the General Population: A Systematic Review and Meta-analysis. Orthop. J. Sports Med. 11, 23259671231173659. https://doi.org/10.1177/23259671231173659

Ohuchi, H., Nakagawa, T., Yamamoto, A., Araga, A., Ohata, T., Ishimaru, Y., Yoshioka, H., Kuwana, T., Nohno, T., Yamasaki, M., Itoh, N., Noji, S., 1997. The mesenchymal factor, FGF10, initiates and maintains the outgrowth of the chick limb bud through interaction with FGF8, an apical ectodermal factor. Development 124, 2235–2244.

Oldfield, S.F., Evans, D.J.R., 2003. Tendon morphogenesis in the developing avian limb: Plasticity of fetal tendon fibroblasts. J. Anat. 202, 153–164. https://doi.org/10.1046/j.1469-7580.2003.00145.x

Oliva, F., Marsilio, E., Asparago, G., Frizziero, A., Berardi, A.C., Maffulli, N., 2021. The Impact of Hyaluronic Acid on Tendon Physiology and Its Clinical Application in Tendinopathies. Cells 10, 3081. https://doi.org/10.3390/cells10113081

Oliveros, J.C., 2015. Venny. An interactive tool for comparing lists with Venn's diagrams.

Orchard, J., Seward, H., 2002. Epidemiology of injuries in the Australian Football League, seasons 1997–2000. Br. J. Sports Med. 36, 39–44. https://doi.org/10.1136/bjsm.36.1.39

Oshiro, W., Lou, J., Xing, X., Tu, Y., Manske, P.R., 2003. Flexor tendon healing in the rat: A histologic and gene expression study. J. Hand Surg. 28, 814–823. https://doi.org/10.1016/S0363-5023(03)00366-6

Ostner, J., Carcy, S., Müller, C.L., 2021. tascCODA: Bayesian Tree-Aggregated Analysis of Compositional Amplicon and Single-Cell Data. Front. Genet. 12.

Pace, J.M., Corrado, M., Missero, C., Byers, P.H., 2003. Identification, characterization and expression analysis of a new fibrillar collagen gene, COL27A1. Matrix Biol. J. Int. Soc. Matrix Biol. 22, 3–14. https://doi.org/10.1016/s0945-053x(03)00007-6

Pakshir, P., Hinz, B., 2018. The big five in fibrosis: Macrophages, myofibroblasts, matrix, mechanics, and miscommunication. Matrix Biol. 68–69, 81–93. https://doi.org/10.1016/j.matbio.2018.01.019

Palla, G., Spitzer, H., Klein, M., Fischer, D., Schaar, A.C., Kuemmerle, L.B., Rybakov, S., Ibarra, I.L., Holmberg, O., Virshup, I., Lotfollahi, M., Richter, S., Theis, F.J., 2022. Squidpy: a scalable framework for spatial omics analysis. Nat. Methods 19, 171–178. https://doi.org/10.1038/s41592-021-01358-2

Pan, X.S., Li, J., Brown, E.B., Kuo, C.K., 2018. Embryo movements regulate tendon mechanical property development. Philos. Trans. R. Soc. Lond. B. Biol. Sci. 373, 20170325. https://doi.org/10.1098/rstb.2017.0325

Panni, A.S., Tartarone, M., Maffulli, N., 2000. Patellar Tendinopathy in Athletes: Outcome of Nonoperative and Operative Management. Am. J. Sports Med. 28, 392–397. https://doi.org/10.1177/03635465000280031901

Parisi, S., Piscitelli, S., Passaro, F., Russo, T., 2020. HMGA Proteins in Stemness and Differentiation of Embryonic and Adult Stem Cells. Int. J. Mol. Sci. 21, 362. https://doi.org/10.3390/ijms21010362

Park, S.-H., Lee, H.S., Young, K.W., Seo, S.G., 2020. Treatment of Acute Achilles Tendon Rupture. Clin. Orthop. Surg. 12, 1–8. https://doi.org/10.4055/cios.2020.12.1.1

Parker, M.W., Rossi, D., Peterson, M., Smith, K., Sikström, K., White, E.S., Connett, J.E., Henke, C.A., Larsson, O., Bitterman, P.B., 2014. Fibrotic extracellular matrix activates a profibrotic positive feedback loop. J. Clin. Invest. 124, 1622–1635. https://doi.org/10.1172/JCI71386

Pedregosa, F., Varoquaux, G., Gramfort, A., Michel, V., Thirion, B., Grisel, O., Blondel, M., Prettenhofer, P., Weiss, R., Dubourg, V., Vanderplas, J., Passos, A., Cournapeau, D., Brucher, M., Perrot, M., Duchesnay, É., 2011. Scikit-learn: Machine Learning in Python. J. Mach. Learn. Res. 12, 2825–2830.

Peffers, M.J., Fang, Y., Cheung, K., Wei, T.K.J., Clegg, P.D., Birch, H.L., 2015. Transcriptome analysis of ageing in uninjured human Achilles tendon. Arthritis Res. Ther. 17, 1–18. https://doi.org/10.1186/s13075-015-0544-2

Peffers, M.J., Thorpe, C.T., Collins, J.A., Eong, R., Wei, T.K.J., Screen, H.R.C., Clegg, P.D., 2014. Proteomic Analysis Reveals Age-related Changes in Tendon Matrix Composition, with Age- and Injury-specific Matrix Fragmentation*. J. Biol. Chem. 289, 25867–25878. https://doi.org/10.1074/jbc.M114.566554

Perucca Orfei, C., Bowles, A.C., Kouroupis, D., Willman, M.A., Ragni, E., Kaplan, L.D., Best, T.M., Correa, D., de Girolamo, L., 2021. Human Tendon Stem/Progenitor Cell Features and Functionality Are Highly

Influenced by in vitro Culture Conditions. Front. Bioeng. Biotechnol. 9. https://doi.org/10.3389/fbioe.2021.711964

Plaas, A., Sandy, J.D., Liu, H., Diaz, M.A., Schenkman, D., Magnus, R.P., Bolam-Bretl, C., Kopesky, P.W., Wang, V.M., Galante, J.O., 2011. Biochemical identification and immunolocalizaton of aggrecan, ADAMTS5 and inter-alpha-trypsin–inhibitor in equine degenerative suspensory ligament desmitis. J. Orthop. Res. 29, 900–906. https://doi.org/10.1002/jor.21332

Pokidysheva, E., Zientek, K.D., Ishikawa, Y., Mizuno, K., Vranka, J.A., Montgomery, N.T., Keene, D.R., Kawaguchi, T., Okuyama, K., Bächinger, H.P., 2013. Posttranslational Modifications in Type I Collagen from Different Tissues Extracted from Wild Type and Prolyl 3-Hydroxylase 1 Null Mice. J. Biol. Chem. 288, 24742–24752. https://doi.org/10.1074/jbc.M113.464156

Pöschl, E., Schlötzer-Schrehardt, U., Brachvogel, B., Saito, K., Ninomiya, Y., Mayer, U., 2004. Collagen IV is essential for basement membrane stability but dispensable for initiation of its assembly during early development. Dev. Camb. Engl. 131, 1619–1628. https://doi.org/10.1242/dev.01037

Posey, K.L., Hankenson, K., Veerisetty, A.C., Bornstein, P., Lawler, J., Hecht, J.T., 2008. Skeletal Abnormalities in Mice Lacking Extracellular Matrix Proteins, Thrombospondin-1, Thrombospondin-3, Thrombospondin-5, and Type IX Collagen. Am. J. Pathol. 172, 1664–1674. https://doi.org/10.2353/ajpath.2008.071094

Powers, R.M., Hevner, R.F., Halpain, S., 2023. The Neuron Navigators: Structure, function, and evolutionary history. Front. Mol. Neurosci. 15. https://doi.org/10.3389/fnmol.2022.1099554

Provenzano, P.P., Vanderby, R., 2006. Collagen fibril morphology and organization: implications for force transmission in ligament and tendon. Matrix Biol. J. Int. Soc. Matrix Biol. 25, 71–84. https://doi.org/10.1016/j.matbio.2005.09.005

Pryce, B.A., Brent, A.E., Murchison, N.D., Tabin, C.J., Schweitzer, R., 2007. Generation of transgenic tendon reporters, ScxGFP and ScxAP, using regulatory elements of the scleraxis gene. Dev. Dyn. 236, 1677–1682. https://doi.org/10.1002/dvdy.21179

Pryce, B.A., Watson, S.S., Murchison, N.D., Staverosky, J.A., Dünker, N., Schweitzer, R., 2009. Recruitment and maintenance of tendon progenitors by TGFB signaling are essential for tendon formation. Development 136, 1351–1361. https://doi.org/10.1242/dev.027342

Pufe, T., Petersen, W., Tillmann, B., Mentlein, R., 2001. The angiogenic peptide vascular endothelial growth factor is expressed in foetal and ruptured

tendons. Virchows Arch. 439, 579–585. https://doi.org/10.1007/s004280100422

Pufe, T., Petersen, W.J., Mentlein, R., Tillmann, B.N., 2005. The role of vasculature and angiogenesis for the pathogenesis of degenerative tendons disease. Scand. J. Med. Sci. Sports 15, 211–222. https://doi.org/10.1111/j.1600-0838.2005.00465.x

Puri, S., Coulson-Thomas, Y.M., Gesteira, T.F., Coulson-Thomas, V.J., 2020. Distribution and Function of Glycosaminoglycans and Proteoglycans in the Development, Homeostasis and Pathology of the Ocular Surface. Front. Cell Dev. Biol. 8. https://doi.org/10.3389/fcell.2020.00731

Qiu, C., Cao, J., Martin, B.K., Li, T., Welsh, I.C., Srivatsan, S., Huang, X., Calderon, D., Noble, W.S., Disteche, C.M., Murray, S.A., Spielmann, M., Moens, C.B., Trapnell, C., Shendure, J., 2022. Systematic reconstruction of cellular trajectories across mouse embryogenesis. Nat. Genet. 54, 328–341. https://doi.org/10.1038/s41588-022-01018-x

Qiu, C., Martin, B.K., Welsh, I.C., Daza, R.M., Le, T.-M., Huang, X., Nichols, E.K., Taylor, M.L., Fulton, O., O'Day, D.R., Gomes, A.R., Ilcisin, S., Srivatsan, S., Deng, X., Disteche, C.M., Noble, W.S., Hamazaki, N., Moens, C.B., Kimelman, D., Cao, J., Schier, A.F., Spielmann, M., Murray, S.A., Trapnell, C., Shendure, J., 2024. A single-cell time-lapse of mouse prenatal development from gastrula to birth. Nature 626, 1084–1093. https://doi.org/10.1038/s41586-024-07069-w

Quigley, A.S., Bancelin, S., Deska-Gauthier, D., Légaré, F., Kreplak, L., Veres, S.P., 2018. In tendons, differing physiological requirements lead to functionally distinct nanostructures. Sci. Rep. 8, 4409. https://doi.org/10.1038/s41598-018-22741-8

Rajpar, I., Tomlinson, R.E., 2022. Function of peripheral nerves in the development and healing of tendon and bone. Semin. Cell Dev. Biol., Special issue: Musculoskeletal Physiology by Ryan Riddle / Special issue : Chromothripsis by Karen Crasta 123, 48–56. https://doi.org/10.1016/j.semcdb.2021.05.001

Ramos-Mucci, L., Sarmiento, P., Little, D., Snelling, S., 2022. Research perspectives—Pipelines to human tendon transcriptomics. J. Orthop. Res. 40, 993–1005. https://doi.org/10.1002/jor.25315

Raudvere, U., Kolberg, L., Kuzmin, I., Arak, T., Adler, P., Peterson, H., Vilo, J., 2019. g:Profiler: a web server for functional enrichment analysis and conversions of gene lists (2019 update). Nucleic Acids Res. 47, W191–W198. https://doi.org/10.1093/nar/gkz369

Rayahin, J.E., Buhrman, J.S., Zhang, Y., Koh, T.J., Gemeinhart, R.A., 2015. High and low molecular weight hyaluronic acid differentially influence

macrophage activation. ACS Biomater. Sci. Eng. 1, 481–493. https://doi.org/10.1021/acsbiomaterials.5b00181

Rees, S.G., Davies, J.R., Tudor, D., Flannery, C.R., Hughes, C.E., Dent, C.M., Caterson, B., 2002. Immunolocalisation and expression of proteoglycan 4 (cartilage superficial zone proteoglycan) in tendon. Matrix Biol. 21, 593–602. https://doi.org/10.1016/S0945-053X(02)00056-2

Rees, S.G., Waggett, A.D., Kerr, B.C., Probert, J., Gealy, E.C., Dent, C.M., Caterson, B., Hughes, C.E., 2009. Immunolocalisation and expression of keratocan in tendon. Osteoarthritis Cartilage 17, 276–279. https://doi.org/10.1016/j.joca.2008.07.007

Reuvers, J., Thoreson, A.R., Zhao, C., Zhang, L., Jay, G.D., An, K.-N., Warman, M.L., Amadio, P.C., 2011. The mechanical properties of tail tendon fascicles from lubricin knockout, wild type and heterozygous mice. J. Struct. Biol. 176, 41–45. https://doi.org/10.1016/j.jsb.2011.07.013

Riasat, K., Bardell, D., Goljanek-Whysall, K., Clegg, P.D., Peffers, M.J., 2020. Epigenetic mechanisms in Tendon Ageing. Br. Med. Bull. 135, 90. https://doi.org/10.1093/bmb/ldaa023

Ribitsch, I., Bileck, A., Aldoshin, A.D., Kańduła, M.M., Mayer, R.L., Egerbacher, M., Gabner, S., Auer, U., Gültekin, S., Huber, J., Kreil, D.P., Gerner, C., Jenner, F., 2021. Molecular Mechanisms of Fetal Tendon Regeneration Versus Adult Fibrous Repair. Int. J. Mol. Sci. 22, 5619. https://doi.org/10.3390/ijms22115619

Ricard-Blum, S., 2011. The Collagen Family. Cold Spring Harb. Perspect. Biol. 3, a004978. https://doi.org/10.1101/cshperspect.a004978

Richardson, L., Venkataraman, S., Stevenson, P., Yang, Y., Moss, J., Graham, L., Burton, N., Hill, B., Rao, J., Baldock, R.A., Armit, C., 2014. EMAGE mouse embryo spatial gene expression database: 2014 update. Nucleic Acids Res. 42, D835–D844. https://doi.org/10.1093/nar/gkt1155

Richardson, S.H., Starborg, T., Lu, Y., Humphries, S.M., Meadows, R.S., Kadler, K.E., 2007. Tendon Development Requires Regulation of Cell Condensation and Cell Shape via Cadherin-11-Mediated Cell-Cell Junctions. Mol. Cell. Biol. 27, 6218–6228. https://doi.org/10.1128/MCB.00261-07

Riddle, R.D., Johnson, R.L., Laufer, E., Tabin, C., 1993. Sonic hedgehog mediates the polarizing activity of the ZPA. Cell 75, 1401–1416. https://doi.org/10.1016/0092-8674(93)90626-2

Riel, H., Lindstrøm, C.F., Rathleff, M.S., Jensen, M.B., Olesen, J.L., 2019. Prevalence and incidence rate of lower-extremity tendinopathies in a Danish general practice: a registry-based study. BMC Musculoskelet. Disord. 20, 239. https://doi.org/10.1186/s12891-019-2629-6

Riggin, C.N., Schultz, S.M., Sehgal, C.M., Soslowsky, L.J., 2019. Ultrasound Evaluation of Anti-Vascular Endothelial Growth Factor–Induced Changes in Vascular Response Following Tendon Injury. Ultrasound Med. Biol. 45, 1841–1849. https://doi.org/10.1016/j.ultrasmedbio.2019.03.002

Riggin, C.N., Weiss, S.N., Rodriguez, A.B., Raja, H., Chen, M., Schultz, S.M., Sehgal, C.M., Soslowsky, L.J., 2022. Increasing Vascular Response to Injury Improves Tendon Early Healing Outcome in Aged Rats. Ann. Biomed. Eng. 50, 587–600. https://doi.org/10.1007/s10439-022-02948-7

Riley, G., 2004. The pathogenesis of tendinopathy. A molecular perspective. Rheumatology 43, 131–142. https://doi.org/10.1093/rheumatology/keg448

Rio, E., Moseley, L., Purdam, C., Samiric, T., Kidgell, D., Pearce, A.J., Jaberzadeh, S., Cook, J., 2014. The pain of tendinopathy: physiological or pathophysiological? Sports Med. Auckl. NZ 44, 9–23. https://doi.org/10.1007/s40279-013-0096-z

Rio, E.K., Ellis, R.F., Henry, J.M., Falconer, V.R., Kiss, Z.S., Girdwood, M.A., Cook, J.L., Gaida, J.E., 2018. Don't Assume the Control Group Is Normal—People with Asymptomatic Tendon Pathology Have Higher Pressure Pain Thresholds. Pain Med. 19, 2267–2273. https://doi.org/10.1093/pm/pny117

Robinson, K.A., Sun, M., Barnum, C.E., Weiss, S.N., Huegel, J., Shetye, S.S., Lin, L., Saez, D., Adams, S.M., Iozzo, R.V., Soslowsky, L.J., Birk, D.E., 2017. Decorin and biglycan are necessary for maintaining collagen fibril structure, fiber realignment, and mechanical properties of mature tendons. Matrix Biol. 64, 81–93. https://doi.org/10.1016/j.matbio.2017.08.004

Robinson, P.S., Huang, T.-F., Kazam, E., Iozzo, R.V., Birk, D.E., Soslowsky, L.J., 2005. Influence of Decorin and Biglycan on Mechanical Properties of Multiple Tendons in Knockout Mice. J. Biomech. Eng. 127, 181–185. https://doi.org/10.1115/1.1835363

Rolfe, K.J., Grobbelaar, A.O., 2012. A Review of Fetal Scarless Healing. ISRN Dermatol. 2012, 1–9. https://doi.org/10.5402/2012/698034

Rolnick, K.I., Choe, J.A., Leiferman, E.M., Kondratko-Mittnacht, J., Clements, A.E.B., Baer, G.S., Jiang, P., Vanderby, R., Chamberlain, C.S., 2022. Periostin modulates extracellular matrix behavior in tendons. Matrix Biol. Plus 16, 100124. https://doi.org/10.1016/j.mbplus.2022.100124

Ros, M.A., Rivero, F.B., Hinchliffe, J.R., Hurle, J.M., 1995. Immunohistological and ultrastructural study of the developing tendons of the avian foot. Anat. Embryol. (Berl.) 192, 483–496. https://doi.org/10.1007/BF00187179

Rosini, S., Pugh, N., Bonna, A.M., Hulmes, D.J.S., Farndale, R.W., Adams, J.C., 2018. Thrombospondin-1 promotes matrix homeostasis by interacting with collagen and lysyl oxidase precursors and collagen cross-linking sites. Sci. Signal. 11, eaar2566. https://doi.org/10.1126/scisignal.aar2566

Rozario, T., DeSimone, D.W., 2010. The extracellular matrix in development and morphogenesis: A dynamic view. Dev. Biol., Special Section: Morphogenesis 341, 126–140. https://doi.org/10.1016/j.ydbio.2009.10.026

Ruggiu, M., Herbst, R., Kim, N., Jevsek, M., Fak, J.J., Mann, M.A., Fischbach, G., Burden, S.J., Darnell, R.B., 2009. Rescuing Z+ agrin splicing in Nova null mice restores synapse formation and unmasks a physiologic defect in motor neuron firing. Proc. Natl. Acad. Sci. 106, 3513–3518. https://doi.org/10.1073/pnas.0813112106

Russo, V., Khatib, M.E., Prencipe, G., Citeroni, M.R., Faydaver, M., Mauro, A., Berardinelli, P., Cerveró-Varona, A., Haidar-Montes, A.A., Turriani, M., Giacinto, O.D., Raspa, M., Scavizzi, F., Bonaventura, F., Stöckl, J., Barboni, B., 2022. Tendon Immune Regeneration: Insights on the Synergetic Role of Stem and Immune Cells during Tendon Regeneration. Cells 11, 434. https://doi.org/10.3390/CELLS11030434

Ruzzini, L., Abbruzzese, F., Rainer, A., Longo, U.G., Trombetta, M., Maffulli, N., Denaro, V., 2014. Characterization of age-related changes of tendon stem cells from adult human tendons. Knee Surg. Sports Traumatol. Arthrosc. 22, 2856–2866. https://doi.org/10.1007/s00167-013-2457-4

Sager, B., Gates, S., Collett, G., Chhabra, A., Khazzam, M., 2019. Innervation of the subscapularis: an anatomic study. JSES Open Access 3, 65–69. https://doi.org/10.1016/j.jses.2019.02.001

Sajithlal, G.B., Chithra, P., Chandrakasan, G., 1998. Advanced glycation end products induce crosslinking of collagen in vitro. Biochim. Biophys. Acta BBA - Mol. Basis Dis. 1407, 215–224. https://doi.org/10.1016/S0925-4439(98)00043-X

Sakabe, T., Sakai, K., Maeda, T., Sunaga, A., Furuta, N., Schweitzer, R., Sasaki, T., Sakai, T., 2018. Transcription factor scleraxis vitally contributes to progenitor lineage direction in wound healing of adult tendon in mice. J. Biol. Chem. 293, 5766–5780. https://doi.org/10.1074/jbc.RA118.001987

Salo, A.M., Myllyharju, J., 2021. Prolyl and lysyl hydroxylases in collagen synthesis. Exp. Dermatol. 30, 38–49. https://doi.org/10.1111/exd.14197

Sanders, T.L., Maradit Kremers, H., Bryan, A.J., Ransom, J.E., Smith, J., Morrey, B.F., 2015. The Epidemiology and Health Care Burden of Tennis

Elbow: A Population-Based Study. Am. J. Sports Med. 43, 1066–1071. https://doi.org/10.1177/0363546514568087

Sasaki, T., Stoop, R., Sakai, T., Hess, A., Deutzmann, R., Schlötzer-Schrehardt, U., Chu, M.-L., von der Mark, K., 2016. Loss of fibulin-4 results in abnormal collagen fibril assembly in bone, caused by impaired lysyl oxidase processing and collagen cross-linking. Matrix Biol. J. Int. Soc. Matrix Biol. 50, 53–66. https://doi.org/10.1016/j.matbio.2015.12.002

Schaar, A.C., Heumos, L., 2023. 7. Normalization, in: Single-Cell Best Practices.

Scheibner, K.A., Lutz, M.A., Boodoo, S., Fenton, M.J., Powell, J.D., Horton, M.R., 2006. Hyaluronan fragments act as an endogenous danger signal by engaging TLR2. J. Immunol. Baltim. Md 1950 177, 1272–1281. https://doi.org/10.4049/jimmunol.177.2.1272

Schiele, N.R., von Flotow, F., Tochka, Z.L., Hockaday, L.A., Marturano, J.E., Thibodeau, J.J., Kuo, C.K., 2015. Actin cytoskeleton contributes to the elastic modulus of embryonic tendon during early development. J. Orthop. Res. 33, 874–881. https://doi.org/10.1002/jor.22880

Schwartz, A.G., Lipner, J.H., Pasteris, J.D., Genin, G.M., Thomopoulos, S., 2013. Muscle loading is necessary for the formation of a functional tendon enthesis. Bone 55, 44–51. https://doi.org/10.1016/j.bone.2013.03.010

Schwartz, A.G., Long, F., Thomopoulos, S., 2015. Enthesis fibrocartilage cells originate from a population of Hedgehog-responsive cells modulated by the loading environment. Development 142, 196–206. https://doi.org/10.1242/dev.112714

Schweitzer, R., Chyung, J.H., Murtaugh, L.C., Brent, A.E., Rosen, V., Olson, E.N., Lassar, A., Tabin, C.J., 2001. Analysis of the tendon cell fate using Scleraxis, a specific marker for tendons and ligaments. Dev. Camb. Engl. 128, 3855–3866.

Scott, A., Lian, Ø., Roberts, C., Cook, J., Handley, C., Bahr, R., Samiric, T., Ilic, M., Parkinson, J., Hart, D., Duronio, V., Khan, K., 2008. Increased versican content is associated with tendinosis pathology in the patellar tendon of athletes with jumper's knee. Scand. J. Med. Sci. Sports 18, 427–435. https://doi.org/10.1111/j.1600-0838.2007.00735.x

Scott, J.E., Hughes, E.W., 1986. Proteoglycan-collagen relationships in developing chick and bovine tendons. Influence of the physiological environment. Connect. Tissue Res. 14, 267–278. https://doi.org/10.3109/03008208609017470

Selvanetti, A., Cipolla, M., Puddu, G., 1997. Overuse tendon injuries: Basic science and classification. Oper. Tech. Sports Med., Surgical Treatment

of Overuse Tendon Injuries 5, 110–117. https://doi.org/10.1016/S1060-1872(97)80031-7

Sethi, A., Mao, W., Wordinger, R.J., Clark, A.F., 2011. Transforming Growth Factor–β Induces Extracellular Matrix Protein Cross-Linking Lysyl Oxidase (LOX) Genes in Human Trabecular Meshwork Cells. Invest. Ophthalmol. Vis. Sci. 52, 5240–5250. https://doi.org/10.1167/iovs.11-7287

Setty, M., Kiseliovas, V., Levine, J., Gayoso, A., Mazutis, L., Pe'er, D., 2019. Characterization of cell fate probabilities in single-cell data with Palantir. Nat. Biotechnol. 37, 451–460. https://doi.org/10.1038/s41587-019-0068-4

Shah, J.S., Palacios, E., Palacios, L., 1982. Development of crimp morphology and cellular changes in chick tendons. Dev. Biol. 94, 499–504. https://doi.org/10.1016/0012-1606(82)90366-9

Shao, X., Taha, I.N., Clauser, K.R., Gao, Y. (Tom), Naba, A., 2020. MatrisomeDB: the ECM-protein knowledge database. Nucleic Acids Res. 48, D1136–D1144. https://doi.org/10.1093/nar/gkz849

Sharif, F., Ahmad, A., Shabbir, A., 2023. Does the ultrasound imaging predict lower limb tendinopathy in athletes: a systematic review. BMC Med. Imaging 23, 217. https://doi.org/10.1186/s12880-023-01181-5

Sharma, P., Maffulli, N., 2006. Biology of tendon injury: healing, modeling and remodeling. J. Musculoskelet. Neuronal Interact. 6, 181–190.

Shen, H., Yoneda, S., Sakiyama-Elbert, S.E., Zhang, Q., Thomopoulos, S., Gelberman, R.H., 2021. Flexor Tendon Injury and Repair: The Influence of Synovial Environment on the Early Healing Response in a Canine Model. JBJS 103, e36. https://doi.org/10.2106/JBJS.20.01253

Shiri, R., Varonen, H., Heliövaara, M., Viikari-Juntura, E., 2007. Hand dominance in upper extremity musculoskeletal disorders. J. Rheumatol. 34, 1076–1082.

Shukunami, C., Takimoto, A., Nishizaki, Y., Yoshimoto, Y., Tanaka, S., Miura, S., Watanabe, H., Sakuma, T., Yamamoto, T., Kondoh, G., Hiraki, Y., 2018. Scleraxis is a transcriptional activator that regulates the expression of Tenomodulin, a marker of mature tenocytes and ligamentocytes. Sci. Rep. 8, 3155. https://doi.org/10.1038/s41598-018-21194-3

Shukunami, C., Takimoto, A., Oro, M., Hiraki, Y., 2006. Scleraxis positively regulates the expression of tenomodulin, a differentiation marker of tenocytes. Dev. Biol. 298, 234–247. https://doi.org/10.1016/j.ydbio.2006.06.036

Sim, D., Jiang, J., Leong, N.L., 2022. Fibrosis and Adipogenesis in Injured or Diseased Tendon. Curr. Tissue Microenviron. Rep. 3, 61–66. https://doi.org/10.1007/s43152-022-00035-6

Simpson, M., Rio, E., Cook, J., 2016. At What Age Do Children and Adolescents Develop Lower Limb Tendon Pathology or Tendinopathy? A Systematic Review and Meta-analysis. Sports Med. 46, 545–557. https://doi.org/10.1007/s40279-015-0438-0

Simpson, R.M.L., Meran, S., Thomas, D., Stephens, P., Bowen, T., Steadman, R., Phillips, A., 2009. Age-Related Changes in Pericellular Hyaluronan Organization Leads to Impaired Dermal Fibroblast to Myofibroblast Differentiation. Am. J. Pathol. 175, 1915–1928. https://doi.org/10.2353/ajpath.2009.090045

Singh, K., Loreth, D., Pöttker, B., Hefti, K., Innos, J., Schwald, K., Hengstler, H., Menzel, L., Sommer, C.J., Radyushkin, K., Kretz, O., Philips, M.-A., Haas, C.A., Frauenknecht, K., Lilleväli, K., Heimrich, B., Vasar, E., Schäfer, M.K.E., 2018. Neuronal Growth and Behavioral Alterations in Mice Deficient for the Psychiatric Disease-Associated Negr1 Gene. Front. Mol. Neurosci. 11. https://doi.org/10.3389/fnmol.2018.00030

Singh, M.K., Petry, M., Haenig, B., Lescher, B., Leitges, M., Kispert, A., 2005. The T-box transcription factor *Tbx15* is required for skeletal development. Mech. Dev. 122, 131–144. https://doi.org/10.1016/j.mod.2004.10.011

Smith, S.M., Zhang, G., Birk, D.E., 2014. Collagen V localizes to pericellular sites during tendon collagen fibrillogenesis. Matrix Biol. 33, 47–53. https://doi.org/10.1016/j.matbio.2013.08.003

Snedeker, J.G., Foolen, J., 2017. Tendon injury and repair – A perspective on the basic mechanisms of tendon disease and future clinical therapy. Acta Biomater. 63, 18–36. https://doi.org/10.1016/j.actbio.2017.08.032

Snow, H.E., Riccio, L.M., Mjaatvedt, C.H., Hoffman, S., Capehart, A.A., 2005. Versican expression during skeletal/joint morphogenesis and patterning of muscle and nerve in the embryonic mouse limb. Anat. Rec. A. Discov. Mol. Cell. Evol. Biol. 282A, 95–105. https://doi.org/10.1002/ar.a.20151

Soares da Costa, D., Reis, R.L., Pashkuleva, I., 2017. Sulfation of Glycosaminoglycans and Its Implications in Human Health and Disorders. Annu. Rev. Biomed. Eng. 19, 1–26. https://doi.org/10.1146/annurev-bioeng-071516-044610

Soeda, T., Deng, J.M., de Crombrugghe, B., Behringer, R.R., Nakamura, T., Akiyama, H., 2010. Sox9-expressing precursors are the cellular origin of the cruciate ligament of the knee joint and the limb tendons. genesis 48, 635–644. https://doi.org/10.1002/dvg.20667

Sorg, H., Tilkorn, D.J., Mirastschijski, U., Hauser, J., Kraemer, R., 2018. Panta Rhei: Neovascularization, Angiogenesis and Nutritive Perfusion in Wound Healing. Eur. Surg. Res. 59, 232–241. https://doi.org/10.1159/000492410

Spiesz, E.M., Thorpe, C.T., Chaudhry, S., Riley, G.P., Birch, H.L., Clegg, P.D., Screen, H.R.C., 2015. Tendon extracellular matrix damage, degradation and inflammation in response to in vitro overload exercise. J. Orthop. Res. 33, 889–897. https://doi.org/10.1002/jor.22879

Spiesz, E.M., Thorpe, C.T., Thurner, P.J., Screen, H.R.C., 2018. Structure and collagen crimp patterns of functionally distinct equine tendons, revealed by quantitative polarised light microscopy (qPLM). Acta Biomater. 70, 281–292. https://doi.org/10.1016/j.actbio.2018.01.034

Splittgerber, L.E., Ihm, J.M., 2019. Significance of Asymptomatic Tendon Pathology in Athletes. Curr. Sports Med. Rep. 18, 192–200. https://doi.org/10.1249/JSR.0000000000000600

Squair, J.W., Gautier, M., Kathe, C., Anderson, M.A., James, N.D., Hutson, T.H., Hudelle, R., Qaiser, T., Matson, K.J.E., Barraud, Q., Levine, A.J., La Manno, G., Skinnider, M.A., Courtine, G., 2021. Confronting false discoveries in single-cell differential expression. Nat. Commun. 12, 5692. https://doi.org/10.1038/s41467-021-25960-2

Ståhl, P.L., Salmén, F., Vickovic, S., Lundmark, A., Navarro, J.F., Magnusson, J., Giacomello, S., Asp, M., Westholm, J.O., Huss, M., Mollbrink, A., Linnarsson, S., Codeluppi, S., Borg, Å., Pontén, F., Costea, P.I., Sahlén, P., Mulder, J., Bergmann, O., Lundeberg, J., Frisén, J., 2016. Visualization and analysis of gene expression in tissue sections by spatial transcriptomics. Science 353, 78–82. https://doi.org/10.1126/science.aaf2403

Stammers, M., Ivanova, I.M., Niewczas, I.S., Segonds-Pichon, A., Streeter, M., Spiegel, D.A., Clark, J., 2020. Age-related changes in the physical properties, cross-linking, and glycation of collagen from mouse tail tendon. J. Biol. Chem. 295, 10562–10571. https://doi.org/10.1074/jbc.RA119.011031

Staverosky, J.A., Pryce, B.A., Watson, S.S., Schweitzer, R., 2009. Tubulin polymerization-promoting protein family member 3, Tppp3, is a specific marker of the differentiating tendon sheath and synovial joints. Dev. Dyn. 238, 685–692. https://doi.org/10.1002/dvdy.21865

Steffen, D., Avey, A., Mienaltowski, M.J., Baar, K., 2023a. The rat Achilles and patellar tendons have similar increases in mechanical properties but become transcriptionally divergent during postnatal development. J. Physiol. 601, 3869–3884. https://doi.org/10.1113/JP284393

Steffen, D., Mienaltowski, M., Baar, K., 2023b. Spatial gene expression in the adult rat patellar tendon. Matrix Biol. Plus 19–20, 100138. https://doi.org/10.1016/j.mbplus.2023.100138

Stowe, E.J., Keller, M.R., Connizzo, B.K., 2023. Cellular Senescence Impairs Tendon Extracellular Matrix Remodeling in Response to Mechanical Unloading. https://doi.org/10.1101/2023.12.22.572594

Stricker, S., Mathia, S., Haupt, J., Seemann, P., Meier, J., Mundlos, S., 2012. Odd-skipped related genes regulate differentiation of embryonic limb mesenchyme and bone marrow mesenchymal stromal cells. Stem Cells Dev. 21, 623–633. https://doi.org/10.1089/scd.2011.0154

Strocchi, R., De Pasquale, V., Guizzardi, S., Govoni, P., Facchini, A., Raspanti, M., Girolami, M., Giannini, S., 1991. Human achilles tendon: Morphological and morphometric variations as a function of age. Foot Ankle 12, 100–104. https://doi.org/10.1177/107110079101200207

Subramanian, A., Kanzaki, L.F., Galloway, J.L., Schilling, T.F., 2018. Mechanical force regulates tendon extracellular matrix organization and tenocyte morphogenesis through TGFbeta signaling. eLife 7, e38069. https://doi.org/10.7554/eLife.38069

Subramanian, A., Schilling, T.F., 2015. Tendon development and musculoskeletal assembly: Emerging roles for the extracellular matrix. Dev. Camb. 142, 4191–4204. https://doi.org/10.1242/dev.114777

Subramanian, A., Schilling, T.F., 2014. Thrombospondin-4 controls matrix assembly during development and repair of myotendinous junctions. eLife 3, e02372. https://doi.org/10.7554/eLife.02372

Subramanian, A., Wayburn, B., Bunch, T., Volk, T., 2007. Thrombospondin-mediated adhesion is essential for the formation of the myotendinous junction in Drosophila. Development 134, 1269–1278. https://doi.org/10.1242/dev.000406

Sugimoto, Y., Takimoto, A., Akiyama, H., Kist, R., Scherer, G., Nakamura, T., Hiraki, Y., Shukunami, C., 2013. Scx+/Sox9+ progenitors contribute to the establishment of the junction between cartilage and tendon/ligament. Development 140, 2280–2288. https://doi.org/10.1242/dev.096354

Sun, M., Chen, S., Adams, S.M., Florer, J.B., Liu, H., Kao, W.W.-Y., Wenstrup, R.J., Birk, D.E., 2011. Collagen V is a dominant regulator of collagen fibrillogenesis: dysfunctional regulation of structure and function in a corneal-stroma-specific Col5a1-null mouse model. J. Cell Sci. 124, 4096–4105. https://doi.org/10.1242/jcs.091363

Sun, M., Luo, E.Y., Adams, S.M., Adams, T., Ye, Y., Shetye, S.S., Soslowsky, L.J., Birk, D.E., 2020. Collagen XI regulates the acquisition of collagen fibril structure, organization and functional properties in tendon. Matrix Biol. J. Int. Soc. Matrix Biol. 94, 77–94. https://doi.org/10.1016/j.matbio.2020.09.001

Sun, Y., Berger, E.J., Zhao, C., Jay, G.D., An, K.-N., Amadio, P.C., 2006. Expression and mapping of lubricin in canine flexor tendon. J. Orthop. Res. 24, 1861–1868. https://doi.org/10.1002/jor.20239

Sun, Y.-L., Wei, Z., Zhao, C., Jay, G.D., Schmid, T.M., Amadio, P.C., An, K.-N., 2015. Lubricin in human achilles tendon: The evidence of intratendinous sliding motion and shear force in achilles tendon. J. Orthop. Res. 33, 932–937. https://doi.org/10.1002/jor.22897

Sunwoo, J.Y., Eliasberg, C.D., Carballo, C.B., Rodeo, S.A., 2020. The role of the macrophage in tendinopathy and tendon healing. J. Orthop. Res. 38, 1666–1675. https://doi.org/10.1002/jor.24667

Suzuki, A., Yabu, A., Nakamura, H., 2022. Advanced glycation end products in musculoskeletal system and disorders. Methods 203, 179–186. https://doi.org/10.1016/j.ymeth.2020.09.012

Svärd, A., Hammerman, M., Eliasson, P., 2020. Elastin levels are higher in healing tendons than in intact tendons and influence tissue compliance. FASEB J. 34, 13409–13418. https://doi.org/10.1096/fj.202001255R

Svensson, L., Aszódi, A., Reinholt, F.P., Fässler, R., Heinegård, D., Oldberg, Å., 1999. Fibromodulin-null Mice Have Abnormal Collagen Fibrils, Tissue Organization, and Altered Lumican Deposition in Tendon*. J. Biol. Chem. 274, 9636–9647. https://doi.org/10.1074/jbc.274.14.9636

Svensson, R.B., Smith, S.T., Moyer, P.J., Magnusson, S.P., 2018. Effects of maturation and advanced glycation on tensile mechanics of collagen fibrils from rat tail and Achilles tendons. Acta Biomater. 70, 270–280. https://doi.org/10.1016/j.actbio.2018.02.005

Sylva, M., 2014. On the connective tissue regulator Follistatin-like 1.

Szklarczyk, D., Kirsch, R., Koutrouli, M., Nastou, K., Mehryary, F., Hachilif, R., Gable, A.L., Fang, T., Doncheva, N.T., Pyysalo, S., Bork, P., Jensen, L.J., von Mering, C., 2023. The STRING database in 2023: protein–protein association networks and functional enrichment analyses for any sequenced genome of interest. Nucleic Acids Res. 51, D638–D646. https://doi.org/10.1093/nar/gkac1000

Tan, Q., Lui, P.P.Y., Lee, Y.W., 2013. In Vivo Identity of Tendon Stem Cells and the Roles of Stem Cells in Tendon Healing. Stem Cells Dev. 22, 3128–3140. https://doi.org/10.1089/scd.2013.0073

Tang, C., Chen, Y., Huang, J., Zhao, K., Chen, X., Yin, Z., Heng, B.C., Chen, W., Shen, W., 2018. The roles of inflammatory mediators and immunocytes in tendinopathy. J. Orthop. Transl. 14, 23–33. https://doi.org/10.1016/j.jot.2018.03.003

Tasheva, E.S., Koester, A., Paulsen, A.Q., Garrett, A.S., Boyle, D.L., Davidson, H.J., Song, M., Fox, N., Conrad, G.W., 2002. Mimecan/osteoglycin-deficient mice have collagen fibril abnormalities. Mol. Vis. 8, 407–415.

Taylor, S.H., Al-Youha, S., Van Agtmael, T., Lu, Y., Wong, J., McGrouther, D.A., Kadler, K.E., 2011. Tendon Is Covered by a Basement Membrane Epithelium That Is Required for Cell Retention and the Prevention of Adhesion Formation. PLoS ONE 6, e16337. https://doi.org/10.1371/journal.pone.0016337

Tempfer, H., Traweger, A., 2015. Tendon Vasculature in Health and Disease. Front. Physiol. 6. https://doi.org/10.3389/fphys.2015.00330

Thakkar, D., Grant, T.M., Hakimi, O., Carr, A.J., 2014. Distribution and expression of type VI collagen and elastic fibers in human rotator cuff tendon tears. Connect. Tissue Res. 55, 397–402. https://doi.org/10.3109/03008207.2014.959119

Thankam, F.G., Boosani, C.S., Dilisio, M.F., Agrawal, D.K., 2019. Epigenetic mechanisms and implications in tendon inflammation (Review). Int. J. Mol. Med. 43, 3–14. https://doi.org/10.3892/ijmm.2018.3961

Theodorou, A., Komnos, G., Hantes, M., 2023. Patellar tendinopathy: an overview of prevalence, risk factors, screening, diagnosis, treatment and prevention. Arch. Orthop. Trauma Surg. 143, 6695–6705. https://doi.org/10.1007/s00402-023-04998-5

Theodossiou, S.K., Murray, J.B., Schiele, N.R., 2020. Cell-cell junctions in developing and adult tendons. Tissue Barriers 8, 1695491. https://doi.org/10.1080/21688370.2019.1695491

Theodossiou, S.K., Schiele, N.R., 2019. Models of tendon development and injury. BMC Biomed. Eng. 1. https://doi.org/10.1186/s42490-019-0029-5

Thomas, P.E., Peters-Golden, M., White, E.S., Thannickal, V.J., Moore, B.B., 2007. PGE2 inhibition of TGF-β1-induced myofibroblast differentiation is Smad-independent but involves cell shape and adhesion-dependent signaling. Am. J. Physiol.-Lung Cell. Mol. Physiol. 293, L417–L428. https://doi.org/10.1152/ajplung.00489.2006

Thomopoulos, S., Kim, H.M., Rothermich, S.Y., Biederstadt, C., Das, R., Galatz, L.M., 2007. Decreased muscle loading delays maturation of the tendon enthesis during postnatal development. J. Orthop. Res. 25, 1154–1163. https://doi.org/10.1002/JOR.20418

Thomopoulos, S., Parks, W.C., Rifkin, D.B., Derwin, K.A., 2015. Mechanisms of tendon injury and repair, in: Journal of Orthopaedic Research. John Wiley and Sons Inc., pp. 832–839. https://doi.org/10.1002/jor.22806

Thomopoulos, S., Williams, G.R., Gimbel, J.A., Favata, M., Soslowsky, L.J., 2003. Variation of biomechanical, structural, and compositional properties along the tendon to bone insertion site. J. Orthop. Res. 21, 413–419. https://doi.org/10.1016/S0736-0266(03)0057-3

Thomson, J., Singh, M., Eckersley, A., Cain, S.A., Sherratt, M.J., Baldock, C., 2019. Fibrillin microfibrils and elastic fibre proteins: Functional

interactions and extracellular regulation of growth factors. Semin. Cell Dev. Biol. 89, 109–117. https://doi.org/10.1016/j.semcdb.2018.07.016

Thornton, G.M., Lemmex, D.B., Ono, Y., Beach, C.J., Reno, C.R., Hart, D.A., Lo, I.K.Y., 2015. Aging affects mechanical properties and lubricin/PRG4 gene expression in normal ligaments. J. Biomech. 48, 3306–3311. https://doi.org/10.1016/j.jbiomech.2015.06.005

Thornton, G.M., Shao, X., Chung, M., Sciore, P., Boorman, R.S., Hart, D.A., Lo, I.K.Y., 2010. Changes in mechanical loading lead to tendonspecific alterations in MMP and TIMP expression: influence of stress deprivation and intermittent cyclic hydrostatic compression on rat supraspinatus and Achilles tendons. Br. J. Sports Med. 44, 698–703. https://doi.org/10.1136/bjsm.2008.050575

Thorpe, Chavaunne T, Birch, H.L., Clegg, P.D., Screen, H.R., 2013. The role of the non-collagenous matrix in tendon function. Int. J. Exp. Pathol. 94, 248–259. https://doi.org/10.1111/iep.12027

Thorpe, Chavaunne T., Klemt, C., Riley, G.P., Birch, H.L., Clegg, P.D., Screen, H.R.C., 2013. Helical sub-structures in energy-storing tendons provide a possible mechanism for efficient energy storage and return. Acta Biomater. 9, 7948–7956. https://doi.org/10.1016/j.actbio.2013.05.004

Tickle, C., Towers, M., 2017. Sonic Hedgehog Signaling in Limb Development. Front. Cell Dev. Biol. 5, 14. https://doi.org/10.3389/fcell.2017.00014

Tidball, J.G., 1984. Myotendinous junction: morphological changes and mechanical failure associated with muscle cell atrophy. Exp. Mol. Pathol. 40, 1–12. https://doi.org/10.1016/0014-4800(84)90060-1

Tong, S., Sun, Y., Kuang, B., Wang, M., Chen, Z., Zhang, W., Chen, J., 2024. A Comprehensive Review of Muscle–Tendon Junction: Structure, Function, Injury and Repair. Biomedicines 12, 423. https://doi.org/10.3390/biomedicines12020423

Toole, B.P., 2001. Hyaluronan in morphogenesis. Semin. Cell Dev. Biol. 12, 79–87. https://doi.org/10.1006/scdb.2000.0244

Tozer, S., Duprez, D., 2005. Tendon and ligament: Development, repair and disease. Birth Defects Res. Part C - Embryo Today Rev. 75, 226–236. https://doi.org/10.1002/bdrc.20049

Tzircotis, G., Thorne, R.F., Isacke, C.M., 2005. Chemotaxis towards hyaluronan is dependent on CD44 expression and modulated by cell type variation in CD44-hyaluronan binding. J. Cell Sci. 118, 5119–5128. https://doi.org/10.1242/jcs.02629

Tzortzaki, E.G., Tischfield, J.A., Sahota, A., Siafakas, N.M., Gordon, M.K., Gerecke, D.R., 2003. Expression of FACIT collagens XII and XIV during bleomycin-induced pulmonary fibrosis in mice. Anat. Rec. A. Discov. Mol. Cell. Evol. Biol. 275A, 1073–1080. https://doi.org/10.1002/ar.a.10120

Uitto, J., Li, Q., Urban, Z., 2013. The complexity of elastic fiber biogenesis in the skin – a perspective to the clinical heterogeneity of cutis laxa. Exp. Dermatol. 22, 88–92. https://doi.org/10.1111/exd.12025

Valdivia, M., Vega-Macaya, F., Olguín, P., 2017. Mechanical control of myotendinous junction formation and tendon differentiation during development. Front. Cell Dev. Biol. 5, 26. https://doi.org/10.3389/fcell.2017.00026

Van Agtmael, T., Bailey, M.A., Schlötzer-Schrehardt, U., Craigie, E., Jackson, I.J., Brownstein, D.G., Megson, I.L., Mullins, J.J., 2010. Col4a1 mutation in mice causes defects in vascular function and low blood pressure associated with reduced red blood cell volume. Hum. Mol. Genet. 19, 1119–1128. https://doi.org/10.1093/hmg/ddp584

Vasta, S., Di Martino, A., Zampogna, B., Torre, G., Papalia, R., Denaro, V., 2016. Role of VEGF, Nitric Oxide, and Sympathetic Neurotransmitters in the Pathogenesis of Tendinopathy: A Review of the Current Evidences. Front. Aging Neurosci. 8. https://doi.org/10.3389/fnagi.2016.00186

Veit, G., Kobbe, B., Keene, D.R., Paulsson, M., Koch, M., Wagener, R., 2006. Collagen XXVIII, a novel von Willebrand factor A domain-containing protein with many imperfections in the collagenous domain. J. Biol. Chem. 281, 3494–3504. https://doi.org/10.1074/jbc.M509333200

Velasco, J., Li, J., DiPietro, L., Stepp, M.A., Sandy, J.D., Plaas, A., 2011. Adamts5 Deletion Blocks Murine Dermal Repair through CD44-mediated Aggrecan Accumulation and Modulation of Transforming Growth Factor β1 (TGFβ1) Signaling. J. Biol. Chem. 286, 26016–26027. https://doi.org/10.1074/jbc.M110.208694

Vijai, M., Baba, M., Ramalingam, S., Thiyagaraj, A., 2021. DCLK1 and its interaction partners: An effective therapeutic target for colorectal cancer. Oncol. Lett. 22, 850. https://doi.org/10.3892/ol.2021.13111

Vinestock, R.C., Felsenthal, N., Assaraf, E., Katz, E., Rubin, S., Heinemann-Yerushalmi, L., Krief, S., Dezorella, N., Levin-Zaidman, S., Tsoory, M., Thomopoulos, S., Zelzer, E., 2022. Neonatal Enthesis Healing Involves Noninflammatory Acellular Scar Formation through Extracellular Matrix Secretion by Resident Cells. Am. J. Pathol. 192, 1122–1135. https://doi.org/10.1016/j.ajpath.2022.05.008

Vogel, A., Rodriguez, C., Izpisúa-Belmonte, J.C., 1996. Involvement of FGF-8 in initiation, outgrowth and patterning of the vertebrate limb. Development 122, 1737–1750. https://doi.org/10.1016/0168-9525(96)81475-2

Voleti, P.B., Buckley, M.R., Soslowsky, L.J., 2012. Tendon Healing: Repair and Regeneration. Annu. Rev. Biomed. Eng. 14, 47–71. https://doi.org/10.1146/annurev-bioeng-071811-150122

Waggett, A.D., Ralphs, J.R., Kwan, A.P., Woodnutt, D., Benjamin, M., 1998. Characterization of collagens and proteoglycans at the insertion of the human Achilles tendon. Matrix Biol. J. Int. Soc. Matrix Biol. 16, 457–470. https://doi.org/10.1016/s0945-053x(98)90017-8

Wälchli, C., Koch, M., Chiquet, M., Odermatt, B.F., Trueb, B., 1994. Tissue-specific expression of the fibril-associated collagens XII and XIV. J. Cell Sci. 107 (Pt 2), 669–681. https://doi.org/10.1242/jcs.107.2.669

Walia, B., Li, T.M., Crosio, G., Montero, A.M., Huang, A.H., 2022. Axin2-lineage cells contribute to neonatal tendon regeneration. Httpsezproxy-Prdbodleianoxacuk2102101080030082072022036732 1–14. https://doi.org/10.1080/03008207.2022.2036732

Walker-Bone, K., Palmer, K.T., Reading, I., Coggon, D., Cooper, C., 2012. Occupation and epicondylitis: a population-based study. Rheumatology 51, 305–310. https://doi.org/10.1093/rheumatology/ker228

Wang, F., Flanagan, J., Su, N., Wang, L.-C., Bui, S., Nielson, A., Wu, X., Vo, H.-T., Ma, X.-J., Luo, Y., 2012. RNAscope. J. Mol. Diagn. JMD 14, 22–29. https://doi.org/10.1016/j.jmoldx.2011.08.002

Wang, N., Wang, H., Shen, L., Liu, X., Ma, Y., Wang, C., 2024. Aging-Related Rotator Cuff Tears: Molecular Mechanisms and Implications for Clinical Management. Adv. Biol. n/a, 2300331. https://doi.org/10.1002/adbi.202300331

Wang, V.M., Bell, R.M., Thakore, R., Eyre, D.R., Galante, J.O., Li, J., Sandy, J.D., Plaas, A., 2012. Murine tendon function is adversely affected by aggrecan accumulation due to the knockout of ADAMTS5. J. Orthop. Res. 30, 620–626. https://doi.org/10.1002/jor.21558

Wang, W., Olson, D., Liang, G., Franceschi, R.T., Li, C., Wang, B., Wang, S.S., Yang, S., 2012. Collagen XXIV (Col24α1) Promotes Osteoblastic Differentiation and Mineralization through TGF-β/Smads Signaling Pathway. Int. J. Biol. Sci. 8, 1310–1322. https://doi.org/10.7150/ijbs.5136

Waskom, M., 2021. seaborn: statistical data visualization. J. Open Source Softw. 6, 3021. https://doi.org/10.21105/joss.03021

Watanabe, T., Imamura, Y., Hosaka, Y., Ueda, H., Takehana, K., 2007. Graded Arrangement of Collagen Fibrils in the Equine Superficial Digital Flexor Tendon. Connect. Tissue Res. 48, 332–337. https://doi.org/10.1080/03008200701692800

Weis, M.A., Hudson, D.M., Kim, L., Scott, M., Wu, J.-J., Eyre, D.R., 2010. Location of 3-Hydroxyproline Residues in Collagen Types I, II, III, and V/XI Implies a Role in Fibril Supramolecular Assembly. J. Biol. Chem. 285, 2580–2590. https://doi.org/10.1074/jbc.M109.068726

Wenstrup, R.J., Florer, J.B., Brunskill, E.W., Bell, S.M., Chervoneva, I., Birk, D.E., 2004. Type V collagen controls the initiation of collagen fibril

assembly. J. Biol. Chem. 279, 53331–53337. https://doi.org/10.1074/jbc.M409622200

Wenstrup, R.J., Smith, S.M., Florer, J.B., Zhang, G., Beason, D.P., Seegmiller, R.E., Soslowsky, L.J., Birk, D.E., 2011. Regulation of Collagen Fibril Nucleation and Initial Fibril Assembly Involves Coordinate Interactions with Collagens V and XI in Developing Tendon. J. Biol. Chem. 286, 20455–20465. https://doi.org/10.1074/jbc.M111.223693

Wojciak, B., Crossan, J.F., 1993. The accumulation of inflammatory cells in synovial sheath and epitenon during adhesion formation in healing rat flexor tendons. Clin. Exp. Immunol. 93, 108–114. https://doi.org/10.1111/j.1365-2249.1993.tb06505.x

Wolman, M., Kasten, F.H., 1986. Polarized light microscopy in the study of the molecular structure of collagen and reticulin. Histochemistry 85, 41–49. https://doi.org/10.1007/BF00508652

Woods, E.L., Grigorieva, I.V., Midgley, A.C., Brown, C.V.M., Lu, Y., Phillips, A.O., Bowen, T., Meran, S., Steadman, R., 2021. CD147 mediates the CD44s-dependent differentiation of myofibroblasts driven by transforming growth factor-β1. J. Biol. Chem. 297. https://doi.org/10.1016/j.jbc.2021.100987

Wu, F., Nerlich, M., Docheva, D., 2017. Tendon injuries: Basic science and new repair proposals. EFORT Open Rev. 2, 332–342. https://doi.org/10.1302/2058-5241.2.160075

Wu, W., Huang, R., Wu, Q., Li, P., Chen, J., Li, B., Liu, H., 2014. The Role of Six1 in the Genesis of Muscle Cell and Skeletal Muscle Development. Int. J. Biol. Sci. 10, 983–989. https://doi.org/10.7150/ijbs.9442

Wynn, T.A., Chawla, A., Pollard, J.W., 2013. Origins and Hallmarks of Macrophages: Development, Homeostasis, and Disease. Nature 496, 445–455. https://doi.org/10.1038/nature12034

Xu, C., Prete, M., Webb, S., Jardine, L., Stewart, B.J., Hoo, R., He, P., Meyer, K.B., Teichmann, S.A., 2023. Automatic cell-type harmonization and integration across Human Cell Atlas datasets. Cell 186, 5876-5891.e20. https://doi.org/10.1016/j.cell.2023.11.026

Yamamoto, S., Uchida, Y., Ohtani, T., Nozaki, E., Yin, C., Gotoh, Y., Yakushiji-Kaminatsui, N., Higashiyama, T., Suzuki, T., Takemoto, T., Shiraishi, Y., Kuroiwa, A., 2019. Hoxa13 regulates expression of common Hox target genes involved in cartilage development to coordinate the expansion of the autopodal anlage. Dev. Growth Differ. 61, 228–251. https://doi.org/10.1111/dgd.12601

Yan, R., Zhang, H., Ma, Y., Lin, R., Zhou, B., Zhang, T., Fan, C., Zhang, Y., Wang, Z., Fang, T., Yin, Z., Cai, Y., Ouyang, H., Chen, X., 2022. Discovery of Muscle-Tendon Progenitor Subpopulation in Human

Myotendinous Junction at Single-Cell Resolution. Research 2022. https://doi.org/10.34133/2022/9760390

Yang, B., Guo, H., Zhang, Y., Chen, L., Ying, D., Dong, S., 2011. MicroRNA-145 Regulates Chondrogenic Differentiation of Mesenchymal Stem Cells by Targeting Sox9. PLOS ONE 6, e21679. https://doi.org/10.1371/journal.pone.0021679

Yang, Y., Wu, Y., Zhou, K., Wu, D., Yao, X., Heng, B.C., Zhou, J., Liu, H., Ouyang, H., 2021. Interplay of Forces and the Immune Response for Functional Tendon Regeneration. Front. Cell Dev. Biol. 9. https://doi.org/10.3389/fcell.2021.657621

Yaseen, W., Kraft-Sheleg, O., Zaffryar-Eilot, S., Melamed, S., Sun, C., Millay, D.P., Hasson, P., 2021. Fibroblast fusion to the muscle fiber regulates myotendinous junction formation. Nat. Commun. 12, 3852. https://doi.org/10.1038/s41467-021-24159-9

Yin, Z., Hu, J.J., Yang, L., Zheng, Z.F., An, C.R., Wu, B.B., Zhang, C., Shen, W.L., Liu, H.H., Chen, J.L., Heng, B.C., Guo, G.J., Chen, X., Ouyang, H.W., 2016. Single-cell analysis reveals a nestin+ tendon stem/progenitor cell population with strong tenogenic potentiality. Sci. Adv. 2, 1600874. https://doi.org/10.1126/sciadv.1600874

Yoon, J.H., Halper, J., 2005. Tendon proteoglycans: biochemistry and function. J. Musculoskelet. Neuronal Interact. 5, 22–34.

Yoshida, C.A., Yamamoto, H., Fujita, T., Furuichi, T., Ito, K., Inoue, K., Yamana, K., Zanma, A., Takada, K., Ito, Y., Komori, T., 2004. Runx2 and Runx3 are essential for chondrocyte maturation, and Runx2 regulates limb growth through induction of Indian hedgehog. Genes Dev. 18, 952–963. https://doi.org/10.1101/gad.1174704

Young, B.B., Gordon, M.K., Birk, D.E., 2000. Expression of type XIV collagen in developing chicken tendons: association with assembly and growth of collagen fibrils. Dev. Dyn. Off. Publ. Am. Assoc. Anat. 217, 430–439. https://doi.org/10.1002/(SICI)1097-0177(200004)217:4<430::AID-DVDY10>3.0.CO;2-5

Zabrzyńska, M., Grzanka, D., Zielińska, W., Jaworski, Ł., Pękala, P., Gagat, M., 2021. The Bonar Score in the Histopathological Assessment of Tendinopathy and Its Clinical Relevance—A Systematic Review. Medicina (Mex.) 57, 367. https://doi.org/10.3390/medicina57040367

Zelzer, E., Blitz, E., Killian, M.L., Thomopoulos, S., 2014. Tendon-to-bone attachment: From development to maturity. Birth Defects Res. Part C - Embryo Today Rev. 102, 101–112. https://doi.org/10.1002/bdrc.21056

Zhang, B., He, P., Lawrence, J.E.G., Wang, S., Tuck, E., Williams, B.A., Roberts, K., Kleshchevnikov, V., Mamanova, L., Bolt, L., Polanski, K., Li, T., Elmentaite, R., Fasouli, E.S., Prete, M., He, X., Yayon, N., Fu, Y.,

Yang, H., Liang, C., Zhang, Hui, Blain, R., Chedotal, A., FitzPatrick, D.R., Firth, H., Dean, A., Bayraktar, O.A., Marioni, J.C., Barker, R.A., Storer, M.A., Wold, B.J., Zhang, Hongbo, Teichmann, S.A., 2023. A human embryonic limb cell atlas resolved in space and time. Nature 1–11. https://doi.org/10.1038/s41586-023-06806-x

Zhang, C.-H., Gao, Y., Hung, H.-H., Zhuo, Z., Grodzinsky, A.J., Lassar, A.B., 2022. Creb5 coordinates synovial joint formation with the genesis of articular cartilage. Nat. Commun. 13, 7295. https://doi.org/10.1038/s41467-022-35010-0

Zhang, C.-H., Gao, Y., Jadhav, U., Hung, H.-H., Holton, K.M., Grodzinsky, A.J., Shivdasani, R.A., Lassar, A.B., 2021. Creb5 establishes the competence for Prg4 expression in articular cartilage. Commun. Biol. 4, 1–17. https://doi.org/10.1038/s42003-021-01857-0

Zhang, G., Ezura, Y., Chervoneva, I., Robinson, P.S., Beason, D.P., Carine, E.T., Soslowsky, L.J., Iozzo, R.V., Birk, D.E., 2006. Decorin regulates assembly of collagen fibrils and acquisition of biomechanical properties during tendon development. J. Cell. Biochem. 98, 1436–1449. https://doi.org/10.1002/jcb.20776

Zhang, G., Young, B.B., Birk, D.E., 2003. Differential expression of type XII collagen in developing chicken metatarsal tendons. J. Anat. 202, 411–420. https://doi.org/10.1046/j.1469-7580.2003.00174.x

Zhang, G., Young, B.B., Ezura, Y., Favata, M., Soslowsky, L.J., Chakravarti, S., Birk, D.E., 2005. Development of tendon structure and function: Regulation of collagen fibrillogenesis. J. Musculoskelet. Neuronal Interact. 5, 5–21.

Zhang, J., Li, F., Williamson, K.M., Tan, S., Scott, D., Onishi, K., Hogan, M.V., Wang, J.H.-C., 2021. Characterization of the structure, vascularity, and stem/progenitor cell populations in porcine Achilles tendon (PAT). Cell Tissue Res. 384, 367–387. https://doi.org/10.1007/s00441-020-03379-3

Zhang, J., Wang, J.H.-C., 2013. The Effects of Mechanical Loading on Tendons - An In Vivo and In Vitro Model Study. PLoS ONE 8, e71740. https://doi.org/10.1371/journal.pone.0071740

Zhang, S., Ju, W., Chen, Xiaoyi, Zhao, Y., Feng, L., Yin, Z., Chen, Xiao, 2021. Hierarchical ultrastructure: An overview of what is known about tendons and future perspective for tendon engineering. Bioact. Mater. 8, 124–139. https://doi.org/10.1016/j.bioactmat.2021.06.007

Zhang, Y., Mao, S., Mukherjee, S., Kannan, S., Seelig, G., 2023. UNCURL-App: Interactive database-driven analysis of scRNA-Seq data. https://doi.org/10.1101/2020.04.15.043737

Zhao, Q., Eberspaecher, H., Lefebvre, V., de Crombrugghe, B., 1997. Parallel expression of Sox9 and Col2a1 in cells undergoing chondrogenesis.

Dev. Dyn. 209, 377–386. https://doi.org/10.1002/(SICI)1097-0177(199708)209:4<377::AID-AJA5>3.0.CO;2-F

Zheng, G.X.Y., Terry, J.M., Belgrader, P., Ryvkin, P., Bent, Z.W., Wilson, R., Ziraldo, S.B., Wheeler, T.D., McDermott, G.P., Zhu, J., Gregory, M.T., Shuga, J., Montesclaros, L., Underwood, J.G., Masquelier, D.A., Nishimura, S.Y., Schnall-Levin, M., Wyatt, P.W., Hindson, C.M., Bharadwaj, R., Wong, A., Ness, K.D., Beppu, L.W., Deeg, H.J., McFarland, C., Loeb, K.R., Valente, W.J., Ericson, N.G., Stevens, E.A., Radich, J.P., Mikkelsen, T.S., Hindson, B.J., Bielas, J.H., 2017. Massively parallel digital transcriptional profiling of single cells. Nat. Commun. 8, 14049. https://doi.org/10.1038/ncomms14049

Zhou, G., Li, C., Cai, L., 2004. Advanced Glycation End-Products Induce Connective Tissue Growth Factor-Mediated Renal Fibrosis Predominantly through Transforming Growth Factor β-Independent Pathway. Am. J. Pathol. 165, 2033–2043. https://doi.org/10.1016/S0002-9440(10)63254-3

Zhu, M., Tao, H., Samani, M., Luo, M., Wang, X., Hopyan, S., Sun, Y., 2020. Spatial mapping of tissue properties in vivo reveals a 3D stiffness gradient in the mouse limb bud. Proc. Natl. Acad. Sci. 117, 4781–4791. https://doi.org/10.1073/pnas.1912656117

Ziegenhain, C., Vieth, B., Parekh, S., Reinius, B., Guillaumet-Adkins, A., Smets, M., Leonhardt, H., Heyn, H., Hellmann, I., Enard, W., 2017. Comparative Analysis of Single-Cell RNA Sequencing Methods. Mol. Cell 65, 631-643.e4. https://doi.org/10.1016/j.molcel.2017.01.023